Brine Extraction and Treatment Strategies to Enhance Pressure Management and Control of CO_2 Plumes in Deep Geologic Formations

Final Technical Report

September 1, 2015—March 31, 2017

Principal Investigator: Roland T. Okwen, Ph.D.
Co-Principal Investigators: Scott Frailey and Seyed Dastgheib
Illinois State Geological Survey
Prairie Research Institute
University of Illinois
(217) 244-2869
rokwen@illinois.edu

Report Issue Date: March 31, 2017

US DOE Award Number : DE-FE0026136

The Board of Trustees of the University of Illinois
David W. Richardson, AVCR-Director
c/o Office of Sponsored Programs & Research Administration
1901 S. First Street, Suite A
Champaign, Illinois 61820

DISCLAIMER

ACKNOWLEDGMENT

This material is based upon work supported by the Department of Energy Award Number DE-FE0026136.

ABSTRACT

The overall goal of the this project is to develop and validate pressure management and carbon dioxide (CO_2) plume control strategies that can address technical and economic barriers to commercial deployment of CO_2 storage technologies, based on computational and field demonstration work at the Archer Daniels Midland Company (ADM) facility where the Illinois Basin–Decatur Project (IBDP) and the Illinois-Industrial Carbon Capture and Storage (IL-ICCS) projects are located. To accomplish the overall goal, the ISGS designed a brine extraction storage test (BEST) that could be completed in two phases. The goal of BEST Phase I was to evaluate the feasibilities of extraction well(s) placement, the brine extraction to CO_2 injection rate ratio, extraction well completion, and brine treatment and handling. The goal of BEST Phase II would be to validate the brine extraction and treatment options deemed feasible in Phase I by (1) demonstrating the efficacy of brine extraction (BE) in managing pressure (i.e., formation) and the CO_2 plume, and (2) demonstrating treatment of extracted brine with high total dissolved solids (TDS; >200,000 mg/L) using multiple advanced treatment technologies. This report details work done in Phase I.

Several brine extraction and treatment scenarios were tested, simulated, and analyzed for their effectiveness in extracting brine. Initially a vertical well was studied; however, geologic modeling, reservoir modeling, and the existing facility and wellbore infrastructure dictated that the location of a vertical brine extraction well was limited to an area with no existing monitoring wells and where the well would be in relative proximity to an existing CO_2 plume. Consequently, a vertical well was excluded, and a horizontal brine extraction well placed above the existing CO_2 plume near two existing wells was studied. The horizontal well option allows the project to leverage the availability of cased-hole logs and cross-well tomography to monitor CO_2 saturation and plume distribution, respectively. Because of the proximity of the horizontal well option to two existing wells, no additional monitoring well (or caprock penetration) is required.

The recommended brine extraction pilot design options are (1) a horizontal extraction well at the base of the Middle Mt. Simon, which is 350–520 ft (107–158 m) above the CO_2 plume at CCS#1 and VW#1; or (2) a vertical extraction well 0.5 mi (0.8 km) from CCS#2 in a direction approximately southeast of CCS#2, perpendicular to the direction of high hydraulic connectivity. A horizontal extraction well has advantages over a vertical extraction well, including less risk of drilling into an existing CO_2 plume and it can be located between two other wells that can be used for monitoring. Thus, because the two existing wells can serve as monitoring wells, it eliminates the need for a third verification well and allows for a lower extraction rate to control the CO_2 plume and pressure.

Managing pressure and the CO_2 plume distribution via brine extraction creates the obvious and important challenge of handling and treating the extracted brine. There were three options for brine disposal: (1) underground injection control (UIC) disposal well, (2) brine treatment and industrial use, and (3) brine pretreatment and discharge into municipal wastewater system. The primary design elements were budget and permitting requirements. The disposal well would be a vertical well drilled and completed into the Potosi Dolomite. For the range of extraction rates anticipated, the cost of this well is relatively constant. The cost of brine treatment is highly depends on the extraction rate, which depends on the well orientation. If relatively high rates are required, the vertical disposal well option is more favorable; for relatively lower rates, the two brine treatment options have lower costs. Life-cycle-analysis studies on extracted brine handling options suggest that a UIC well has a lower environmental impact than brine treatment. Both brine disposal

options using brine treatment require removal of suspended solids from the extracted brine. The most suitable commercially available technology and the most promising emerging and innovative technology are recommended for implementation in Phase II.

Though the challenges of this project are written specific to Decatur, every CO_2 storage site considering the use of brine extraction integrated with CO_2 storage will have similar, if not identical, technical and logistical challenges.

TABLE OF CONTENTS

LIST OF TABLES

LIST OF FIGURES

CONTRIBUTORS

The following ISGS staff contributed to Task 2: Peter Berger, Seyed Dastgheib, Ruth Kaplan, Jiaxing Li, David Ruhter, and Hafiz Salih. The following Trimeric staff contributed to Task 2: Darryl Mamrosh, Ray McKaskle, and Brad Piggott. Seyed Dastgheib (ISGS), Hafiz Salih (ISGS), Jiaxing Li (ISGS), Peter Berger (ISGS), Ruth Kaplan (ISGS), Darryl Mamrosh (Trimeric), Ray Mckaskle (Trimeric) provided technical content and writing for Task 2. Seyed Dastgheib, Susan Krusemark (ISGS), and Ray McKaskle reviewed the report for Task 2.

Mansour Khosravi (ISGS), Oladipupo Babarinde, Yaghoob Lasemi (ISGS), and Zohreh Askari (ISGS) provided text and geologic characterization for Task 3. John Grube provided a technical review of the geologic characterization section. Hannes Leetaru provided input on the geologic characterization.

The following people contributed to Task 4: Fang Yang (ISGS) and Christopher Patterson (ISGS) provided reservoir modeling and text; Andrew Anderson (ISGS) provided geomechanical analysis and text; Roland Okwen (ISGS) conducted horizontal well simulations and generated some figures for Chris Korose to generate CO_2 plume maps on ARCGIS. Damon Garner provided Access Database support. Robert Will and Donald (Schlumberger) provided geomechanical modeling support.

Edward Mehnert (ISGS) and George El-kaseeh (Schlumberger) provided technical content and writing for Task 5.

Scott Frailey (ISGS) provided technical content and writing for Task 6. Trimeric provided Appendices 6-A–C. Nick Malkewicz (Schlumberger Carbon Services), William Graham Payne (Schlumberger Carbon Services), and Jim Kirksey (Loudon Technical Services LLC) provided Appendix 6-D.

Roland Okwen, Scott Frailey, and Steve Whittaker (ISGS) provided technical reviews of the report.

Daniel Klen (ISGS) and Susan Krusemark (ISGS) provided editing and formatting for the report.

INTRODUCTION

Deep saline geologic formations (storage units) are viewed as the best carbon dioxide (CO_2) storage candidates because they have the largest storage capacity and are widespread compared with depleted oil and gas reservoirs. Pressure is expected to inhibit commercial-scale CO_2 injection into storage units because of concerns such as (1) causing hydraulic fracturing, (2) exceeding the capillary pressure of seals, and (3) limiting storage in units with closed outer boundaries. The heterogeneous nature of storage units causes uneven CO_2 saturation distribution, which negatively affects utilization of pore space available for storage. Brine extraction from storage units is viewed as a strategy to mitigate pressure buildup and control CO_2 plumes. However, handling of extracted brine, geologic characterization, and reservoir and geomechanical modeling are required. Brine extraction and CO_2 storage with brine handling can serve as a method to reduce the carbon footprint of fossil-fueled industrial processes, risk of fracturing confining units because of excessive pressure buildup, and intrusion of CO_2 and brine into adjacent formations.

The goal of brine extraction storage test (BEST) Phase I was to evaluate the feasibilities of extraction well(s) placement, brine-extraction-to-CO_2-injection rate ratio, extraction well completion, and brine treatment and handling. This study includes computational and field demonstration work at the Archer Daniels Midland (ADM) facility where the Illinois Basin–Decatur Project (IBDP) and the Illinois Industrial Carbon Capture and Storage (IL-ICCS) projects are located. The ADM facility is located in Decatur, Illinois, USA.

Current and emerging technologies for treating and handling extracted brine were evaluated, including evaporative-crystallization, forward osmosis (FO), reverse osmosis (RO), membrane distillation, and the multi-effect evaporation (MEE). Factors used to evaluate different treatment technologies included total dissolved solids (TDS) limitations, energy consumption and requirements, purified water recovery percentages, technology readiness level, and cost. Two test-bed facilities were designed for testing advanced brine treatment technologies at the bench and pilot scale.

The geologic, petrophysical, and geophysical data for six geologic formations were analyzed, reviewed, and used to generate a geologic model. The formations studied include the Ironton Sandstone, Galesville Sandstone, Potosi Dolomite, St. Peter Sandstone, Eau Claire formation, Mt. Simon Sandstone, and Precambrian.

The geologic model served as input for reservoir modeling, which was performed to simulate brine extraction scenarios using horizontal or vertical wells. Differences in formation pressure changes (differential pressure, Δp), CO_2 saturation, the Δp index (DPI), and storage efficiency (E) between the simulated brine extraction scenarios and a baseline simulation (i.e., simulation case without brine extraction) were used to determine the optimal brine extraction scenario, which was considered the scenario that minimized the volume of extracted brine while reducing pressure buildup. Scenarios with different well location(s), well types, extraction rates, and pressure drawdown were evaluated with respect to the baseline to determine the scenario that optimally reduced pressure buildup in the subsurface. Geomechanical modeling was also conducted to ensure formation and well integrity during injection and extraction operations.

Permitting requirements were investigated for a brine extraction well and an underground injection control (UIC) disposal well.

TASK 2-0 ASSESSMENT OF BRINE TREATMENT OPTIONS

In this task, brine and brackish water treatment strategies were investigated. The objective was to evaluate technologies for treating extracted brine for beneficial uses, such as cooling or boiler feed water or for pre-treatment. This work assesses available technologies for treating high total dissolved solids (TDS) concentrations (i.e., brine) and low-TDS (i.e., brackish) water. Geochemical modeling, laboratory work to treat high-TDS and low-TDS water, a life-cycle assessment (LCA) accounting for safe handling of extracted and treated brines, and a cost estimation of selected brine treatment processes was performed. The high-TDS brine from the lower Mt. Simon Sandstone has a TDS concentration of approximately 230,000 mg/L (ppm). The brine extracted from the St. Peter Formation has a TDS concentration of 3,700 ppm (low TDS or brackish water). Treatment technologies were evaluated and brine treatment cost estimated to determine the most suitable technologies to propose for Phase II of the project.

Subtask 2-1 Assessment of High-TDS Brine Treatment Options

Work in Subtask 2-1 focused on screening technologies suitable for treatment of high-TDS brines with a concentration of about 230,000 ppm, such as water from the Mt. Simon Sandstone. Several important factors in the screening of technologies considered include applicability to treating high-TDS brine (TDS limitations), energy consumption and requirements, water recovery percentages, technology readiness level, cost, and other factors. The pros and cons of all the screened technologies were compared. The evaluation of emerging technologies included high-TDS treatment projects funded by the DOE (through FOA-0001095 and FOA-0001238) that provided descriptive information about their processes. However, for some of these DOE-funded projects, we were unable to find sufficient information about their proposed processes to perform a meaningful technical assessment of the technologies.

The evaporation-crystallization technology was selected as the most suitable commercially available technology. Some emerging technologies, including forward osmosis (FO), electrodialysis, membrane distillation, humidification-dehumidification, and multi-effect evaporation (MEE), were considered worthy of further study. Various laboratory experiments were performed to evaluate the performance of different pretreatment options for Mt. Simon brine. Furthermore, additional laboratory experiments were conducted to evaluate the performance of the direct contact membrane distillation (DCMD) process in desalinating pretreated Mt. Simon brine.

The Trimeric Corporation (Trimeric; Buda, TX) estimated the cost of pretreating (using coagulation, lime softening, sedimentation, and filtration) and desalinating (using the selected evaporation–crystallization technology) high-TDS brine at 2,000 gallon per minute (gpm) input capacity. Trimeric used scaling methods to extrapolate the results to cases of 500, 585, and 5,000 gpm. Cost estimations included capital, operation and maintenance, and the overall cost of water treatment.

Introduction to Water Treatment Technologies

A thorough evaluation and screening of different commercial and emerging water treatment technologies for treating extracted brine was performed. The objective was to treat brine for beneficial uses, such as cooling water (TDS <1,000 ppm) or boiler feed water (distilled water quality with TDS <10 ppm). Guidelines for water quality requirements were provided in a previous DOE report (Knutson et al., 2012).

Desalination was the most important portion of the overall water treatment process because sodium chloride (NaCl) is the primary dissolved solid in the extracted brines. However, suspended solids, scale-forming species, and other contaminants could interfere with desalination processes)

and must be removed. Therefore, pretreatment processes for the removal of different contaminants before desalination were also reviewed.

The first step was to identify and review commercially available and emerging desalination technologies. Four search engines and literature databases were primarily used to accomplish this task: Engineering Village, ScienceDirect, Scopus, and Google Scholar. Additionally, some information about commercially available technologies was extracted from websites of different companies that manufacture and sell desalination unit operations. References were saved and organized by using the RefWorks, a reference management tool. The resulting RefWorks database contained more than 1,200 references. The references were sorted according to the type of treatment technology. Most of the sources utilized in the literature review and technology screening process were published within the last 10 years.

Technologies were evaluated primarily based on salinity limitations, maturity, and energy consumption. Other factors, including capital costs, operating costs, pretreatment requirements, and capacity, were also considered. Table 2-1-1 presents a summary of desalination technologies. The advantages, challenges, research gaps, and applicability of each technology to high-salinity and low-salinity water treatment are discussed in Sections 2-1 and 2-2.

In Table 2-1-1, desalination technologies are identified, categorized, and numbered. A process description for each of the 21 unique technologies is provided, and some of the most prevalent process variations and configurations are listed. Each variation or configuration does not warrant its own description because the basic separation principle remained unchanged. For example, for Fractional Freeze Crystallization of Ice (#15), at least four possible methods of freezing exist (direct contact freezing, vacuum freezing, indirect contact freezing, and eutectic freeze crystallization), but the general method of desalination (freezing the feed solution to produce pure water crystals) was the same in each case. For each desalination technology, new variations and configurations will arise as researchers continue to develop, improve, and optimize the process for specific applications.

Other information presented in Table 2-1-1 includes examples of vendors or developers of the technology, an estimate of the type of pretreatment that may be required for the feed brine, and capacity limits. The list of vendors or developers for each technology is not intended to be comprehensive and provides only a few examples. The pretreatment requirements indicate how other common contaminants might be removed before desalination; typically, removal of most of the suspended solids and scale-forming species is recommended. Capacity limitations indicate the maximum typical throughput for the technology in commercial operation. Some industrial processes are designed to treat more than 100,000 m^3 (264 million gallons) of water per day, whereas others are more limited. Emerging brine treatment processes may currently be in operation at the bench scale only but have the potential to be scaled up.

Additional process notes, such as reported salinity limitations, current research, and challenges, are provided in the "Comments" row. These topics were further developed when each process was screened for suitability for high-TDS water treatment (Table 2-1-3).

The selected references listed in Table 2-1-1 provide key references for each topic investigated. These key references, derived from our database of more than 1,200 references, are listed at the end of this report. The numbered references shown in Table 2-1-1 are correlated to the reference list in Table 2-1-2.

A majority of desalination technologies can be classified as being based on "membrane" or "thermal" separation techniques. A membrane process uses a selective barrier across which the desired product (water) preferentially flows. In a conventional thermal process, a phase change of

the pure water product is achieved by boiling the feed solution. The main categories in Table 2-1-1 include membrane, evaporative concentration, evaporative crystallization, antisolvent crystallization, refrigerated crystallization, and supercritical desalination. Additional categories in Table 2-1-1, including capacitive deionization, extraction, ion exchange, and adsorption, rely on neither membranes nor phase change, but on some other means of removing dissolved salts.

Evaporative concentrators produce purified water by boiling the feed stream. The conventional evaporative concentration processes are multiple-effect distillation (MED) and multiple-stage flash (MSF), which are usually designed to increase brine concentration from approximately seawater concentrations (about 35,000 ppm of TDS) to about 80,000 ppm of TDS. Different evaporative processes might result in greater concentrations of the brine stream.

In an evaporative crystallization process, the feed is concentrated beyond its saturation point, resulting in the evaporation of water and the precipitation of salts. The crystallization of salts, water, or both might also be achieved by cooling (refrigerated crystallization) or by changing the saturation conditions of the solution (antisolvent addition and supercritical desalination).

Some desalination processes exhibit characteristics of multiple categories. For example, membrane distillation uses both thermal and membrane separation principles, but it is assigned to the "membrane" category because it uses a hydrophobic membrane to exclude saline solution from the product stream. Capacitive deionization is similar to electrodialysis, but no membrane is used. The selection of an appropriate desalination technology depends on location, feed water composition, and treatment objectives. A water treatment facility would be tailored for a specific application and might incorporate one or more of the desalination technologies listed in Table 2-1-1. For example, a reverse osmosis (RO) process and an evaporative crystallization process might be operated in series, with the RO waste stream (a concentrated brine) used as the feed for an evaporative crystallizer.

In general, membrane processes tend to be less energy intensive than processes that require heating, but they exhibit limitations caused by membrane clogging. A fouled membrane will reduce water flux and product purity. Pretreatment reduces membrane fouling, but if the salinity is too high, then salts will still precipitate at the membrane. Membranes also become less efficient as the salinity of the feed water increases because of the need to provide higher pressures to overcome higher osmotic pressures associated with high-salinity feeds.

Membrane performance is critical in membrane processes; a membrane must be highly selective and allow for adequate water flux. Researchers seek to determine the best materials and parameters when developing new membranes and membrane modules.

Crystallization processes may be designed to result in less (or even no) liquid waste compared with some other technologies, such as membrane processes or evaporative concentrators, which accomplish recovery of only a portion of the water from the feed. Common challenges in crystallization processes include their high energy demand and the expense of the equipment needed to separate solid precipitates from solution.

Processes based on adsorption principles are limited by adsorbent availability and capacity. Even in a process with a low-TDS feed stream, a high volume of adsorbents is needed, which creates issues related to sorbent regeneration and the high capital cost. These processes are more likely to be used as a polishing step (to remove any residual salts in the produced water from a previous desalination process) than as the primary desalination treatment step.

Table 2-1-1 Desalination technologies overview (continues to page 33).

Evaluation of desalination technologies	1	2	3	4	5	6
	Membrane	**Membrane**	**Membrane**	**Membrane**	**Membrane**	**Evaporative concentration**
	Reverse osmosis (RO)	**Forward osmosis (FO)**	**Membrane distillation (MD)**	**Membrane crystallization**	**Electrodialysis (ED) & electrodialysis reversal (EDR)**	**Conventional distillation: Multiple-effect distillation (MED) & multiple-stage flash (MSF)**
Description	Water is forced to permeate a membrane by feeding the brine to an RO unit at elevated pressure. The permeate stream should meet most product requirements.	A draw solution with higher osmotic pressure than the feed solution is used to draw water from the feed solution through a membrane. The water must then be recovered from the draw solution.	Separation by evaporation; steam permeates a hydrophobic membrane. The temperature difference creates a vapor pressure gradient across the membrane, which drives the separation process.	An RO or MD system is designed to allow for the formation of solids. It might include the use of seed crystals to induce scale formation on the seed crystals instead of on the membrane.	A combination of anion and cation exchange membranes between an anode and a cathode is used to produce concentrate and dilute product streams by transport of the salts from the dilute stream to the concentrate stream.	A distillation process whereby heat for reboiling is provided by a utility heat source. Multiple effects or multiple-stage flash strategies are used to increase efficiency. The distillate meets product requirements. Concentrate bottoms require disposal or further treatment.
Variations/ configurations	Many, including single stage, multiple stage, semi-batch, and closed circuit.		Air Gap MD, Direct Contact MD, Vacuum MD, Water Gap MD, and Electrically Conductive MD.	Slurry precipitation and recycle RO (SPARRO) is designed to precipitate and remove scale-forming species.	EDR is ED with cycling of the polarity of the electrode plates. It allows for flushing of precipitated solids out of the membranes.	In MED, preheated water evaporates at the heat exchanger surface. In MSF, preheated steam flashes into vapor when introduced to a low-pressure vessel. Both can be operated with vapor compression.
Examples of vendors/ developers	Many, e.g., Aquatech, GE Global Research, IDE Technologies, Poseidon Water, Desalitech, Evoqua, Doosan.	Oasys and Modern Water.	Pilot scale by Aquaver, Memsys, and RTI International.		GE Global Research, Saltworks, and PC Cell.	Many, e.g., Aquatech, Veolia, IDE Technologies, and Doosan.
Pretreatment required	Filtration for suspended solids removal is typically required. Other pretreatment may be required for components that could precipitate or foul membranes (e.g., water softening required for hard feed sources).	Filtration for solids removal is typically required. Other pretreatment may be required for components that could precipitate or foul membranes (e.g., water softening required for hard feed sources). The fouling potential with FO may be lower than that with RO.	Filtration for solids removal is typically required. Other pretreatment may be required for components that could precipitate or foul membranes.	Has potentially less stringent pretreatment requirements than conventional membrane processes.	Filtration for solids removal is typically required. Other pretreatment may be required for components that could precipitate or foul membranes.	Filtration for solids removal is typically required. Other pretreatment may be required for removal of components that might foul or corrode heat exchangers.
Capacity	Membranes are modular and allow for very large systems. Plants with a 100,000+ m^3/day capacity are in operation.	Current systems are at the pilot scale.	Membranes are modular, and very large systems might be practical. Current systems are at the pilot scale.		Very large plants (100,000+ m^3/day) have been built for potable water production and are in operation.	The unit capacity is typically up to 75,000 m^3/day. Very large plants (100,000+ m^3/day) are in operation.

Evaluation of desalination technologies	1	2	3	4	5	6
	Membrane	Membrane	Membrane	Membrane	Membrane	Evaporative concentration
	Reverse osmosis (RO)	Forward osmosis (FO)	Membrane distillation (MD)	Membrane crystallization	Electrodialysis (ED) & electrodialysis reversal (EDR)	Conventional distillation: Multiple-effect distillation (MED) & multiple-stage flash (MSF)
Comments	There are practical limits to the TDS level because of osmotic pressure and the high degree of water hardness associated with high TDS. Conventional systems cannot treat TDS >70,000 mg/L.	Various salinity ranges have been reported, up to at least 175,000 mg/L of TDS. Identification of the best draw solution is critical. Oasys reports the use of an ammonia/carbon dioxide draw solution to desalinate 103,000 mg/L of TDS feed, with a resulting brine of 241,000 mg/L of TDS.	Reported testing of vacuum membrane distillation up to 300 g/L, but flux was reduced. GE Global Research (2015) and Memsys (2016) reported use of membrane distillation to treat 150 to 230 g/L of TDS. Flux limitations at high TDS are caused by membrane fouling.	An emerging technology, with limited information available.	Tends to be very fouling resistant and can treat turbid water sources. Low-TDS (<10,000 ppm) applications are most typical, although technology may be feasible for higher salinity feeds. Saltworks advertises an EDR process for a feed stream with 80,000 ppm of TDS (resulting brine: 150,000 ppm of TDS). Laboratory-scale research on a multiple-stage ED for a 195,000 ppm NaCl feed is in progress.	Corrosion and fouling issues arise at high TDS.
Selected references (refer to Table 2-1-2)	1–11, 55–57	1, 6, 8, 12–16, 58–60	6, 7, 17, 18, 19, 61, 62	19	1, 5, 6, 10, 11, 16, 19, 20, 21, 63	1, 5, 11, 22–29, 56, 64, 65
Evaluation of desalination technologies	7	8	9	10	11	12
	Evaporative concentration	Evaporative concentration	Evaporative crystallization	Evaporative crystallization	Evaporative crystallization	Evaporative crystallization
	Standard brine concentrators	Humidification compression	Standard evaporative crystallizers	Spray drying	Natural evaporation	SAL-PROC
Description	Evaporators designed to concentrate brines to near saturation. Distillate meets product requirements. Concentrate bottoms require disposal or further treatment.	A gas stream (e.g., air) is used to strip water from the feed. The wet gas is then compressed and the water condensed.	Similar to other evaporative technologies, except that distillation is operated past the precipitation point of salts, and salts are continuously removed and filtered out. Can be zero liquid discharge (ZLD).	Brine is heated and sprayed into a tower and contacted with a hot gas. Water evaporates, leaving salt crystals. Water vapor could be condensed and recovered.	Use of solar heating, wind, etc., to evaporate water brine. Purified water product would typically not be recovered. Usually implemented as a conventional evaporation pond, but other intensified versions are also available.	Patented process involving precipitation of specific salts, and the use of natural evaporation (ponds) to treat high-TDS water.
Variations/ configurations	Many types of evaporators are possible, but falling film evaporators driven by mechanical vapor compression (MVC) are common. Thermal vapor compression and thermal multiple-effect evaporation processes are also used.	Humidification, dehumidification, dewvaporation.	Many variations: May be operated with or without vapor compression, at ambient pressure or under vacuum, multiple or single effect. Many types of crystallizers are available. Use of a forced-circulation crystallizer is common.		Evaporation ponds, solar stills, wind-aided intensified evaporation (WAIV), advanced solar dryer (ASD).	
Examples of vendors/ developers	Many, e.g., GE Global Research, 212 Resources, Fountain Quail, IDE Technologies, and Veolia.	Gradiant Technology (start-up company), Saltworks, Altela Inc.	Many, e.g., Veolia, 212 Resources, and GE Global Research.	AquaSonics International.	Lesico CleanTech, others.	Patented by Geo-Processors USA.

Evaluation of desalination technologies	1	2	3	4	5	6
	Membrane	Membrane	Membrane	Membrane	Membrane	Evaporative concentration
	Reverse osmosis (RO)	Forward osmosis (FO)	Membrane distillation (MD)	Membrane crystallization	Electrodialysis (ED) & electrodialysis reversal (EDR)	Conventional distillation: Multiple-effect distillation (MED) & multiple-stage flash (MSF)
Pretreatment required	Filtration for solids removal typically required. Other pretreatment may be required for removal of components that might foul or corrode heat exchangers.	Filtration for solids removal would be required. Softening or other pretreatment (e.g., pH adjustment, additives) would also be required to prevent fouling of contactor.	Additives or pretreatment may be required to prevent surface fouling.	Filtration would likely be required. Other pretreatment uncertain.	Probably minimal to no pretreatment required.	Filtration, lime treatment.
Capacity	Standalone MVC capacity is typically less than 5,000 m^3/day.	May be focused on smaller applications.		Low capacity, less than 2.3 m^3/h.	Limited by footprint versus available space.	May treat up to 8,000 m^3/day. Limited by footprint versus available space.
Comments	Corrosion and fouling issues at high TDS. Higher TDS feeds require a much higher compression ratio. Vapor recompression as a heat source is favored (compared with conventional heat sources) where power is cheap.	High water recovery. Potential applications include small-capacity brackish water and seawater desalination systems in remote regions. Emerging technology for high TDS. Gradiant Technology claims feed up to 140,000 mg/L of TDS may be treated, and in at least one study (Minier-Matar et al., 2016) humidification compression was used for crystallization	Only suited to high-TDS feed streams that are near the saturation limit.	Very energy intensive, with a low probability of efficient heat recovery. Most efficient for saturated solutions.	A simple technology in which water is not recovered. Limited applicability in very cold climates. Large land area requirements. Expensive evaporation pond liners are required to prevent contamination of the environment.	Based on older technologies, and could be a good technology for brine streams with relatively high concentrations of more valuable salts. Differs from traditional evaporation ponds in the selective recovery of salts. No water recovery.
Selected references (refer to Table 2-1-2)	5, 10, 11, 22, 23, 30–32, 64–66	8, 33–35, 61	1, 36, 37, 64–66	38, 39, 64	6, 40	6

Evaluation of desalination technologies	13	14	15	16	17	18
	Antisolvent crystallization	Refrigerated crystallization	Refrigerated crystallization	Refrigerated crystallization	Capacitive deionization	Supercritical desalination
	Antisolvent addition, with antisolvent recovery by distillation	Cooling crystallization of salt	Fractional freeze crystallization of ice	Multiple-phase turbo-expansion	Capacitive deionization	Supercritical desalination
Description	An antisolvent (reduces the solubility of salts in brine) is added, and precipitated salts are filtered out. Water is then recovered from the water–antisolvent mixture by distillation. Further treatment may be required.	Instead of evaporation, cooling is used to precipitate salts from solution, with the solids continuously removed and filtered out. Can be a very low discharge process. The mother liquor (ML) will likely need other treatment.	A solution is subjected to controlled freezing and melting, which can result in the separation of purified water from salts. Multiple freeze–melt cycles can be used.	Brine is atomized into a compressed air stream, and the mixture is then expanded in a turbo-expander capable of handling multiple phases. Cooling of the expansion results in the production of salt crystals and ice crystals, which are then separated.	Porous carbon electrodes are used to attract and store anions and cations from a feed brine stream, allowing purified water to exit. Occasionally, the polarity is reversed, and a concentrated brine solution is recovered.	Brine is heated above the critical point (374 °C, 220 bar), resulting in precipitation of most salts. In the power cogeneration process proposed by researchers at the University of Illinois, supercritical (SC) steam with only ~100 ppm of salt is polished by SC membrane distillation and used to generate power. Low-pressure steam is condensed as pure water. The salt product is continuously removed.

Variations/ configurations			Direct-contact freezing, vacuum freezing, indirect-contact freezing, eutectic freeze crystallization.			With or without continuous removal of salts; with or without cogeneration.
Examples of vendors/ developers			Crystal Solutions and BC Technologies.	GE Global Research.	Voltea and Enpar Technologies.	
Pretreatment required			Filtration would likely be required. Other pretreatment is uncertain.	Filtration would likely be required. Other pretreatment is uncertain.	Filtration for solids removal is typically required. Other pretreatment may be required for components that could precipitate or foul electrodes.	Filtration for solids removal is required. Other pretreatment may or may not be required, depending on the desired quality of the salt product.
Capacity					Modular units can theoretically be used at a large scale.	Depends on the design. The cogeneration process would be intentionally large scale because it would be coupled with power plants.
Comments	Antisolvent addition is commonly applied for precipitation of salts or organics in specialty chemical production. There seems no precedent for operation of such a scheme at a very large scale. The process and economics are very uncertain.	NaCl is the salt with the highest concentration; it has a low-solubility change with temperature. This results in severe limits to its applicability.	A highly debated technology; it may or may not be viable. The product water purity may not be high enough. Equipment may be complex. Has been successfully applied in other industries, but the feasibility of application to desalination is debatable. The process is similar to multiple-phase turbo-expansion.	An innovative technology, with claims to be more energy efficient than thermal crystallization. An early-stage project with optimistic predictions based on modeling, but more research is required.	A viable technology, which appears to be in the early phase of commercialization. Focused on brackish water. No very large scale applications are apparent; these might be prohibitive because of the capital expenditure.	An emerging technology with potential ZLD applications if integrated with a coal- or gas-fired or solar power plant. Produced water replaces the existing purified water supply at the plant. The plant produces both power and high-purity water with a high efficiency.
Selected references (refer to Table 2-1-2)	41	6	1, 42–46, 61, 67–70	47	48–50	71

Evaluation of desalination technologies	**19**	**20**	**21**
	Extraction	**Ion exchange**	**Adsorption**
	Solvent extraction	**Ion exchange**	**Adsorption**
Description	Nonaqueous solvent that extracts high-purity water from brine. Water is recovered from the solvent–water mixture by a temperature swing and phase separation, and then membrane treatment of water to remove residual solvent.	With a mixed bed of H^+ and OH^--loaded ion exchange (or cation and anion beds in series), salts can be adsorbed onto the resin and removed.	Reversibly adsorbs salts or water onto a solid adsorbent. The process would be cyclical, with the loaded adsorbent regenerated by the temperature swing, pressure swing, and solvent washes.
Variations/configurations			Water adsorption from the vapor phase is the primary example found.
Examples of vendors/developers	Research Triangle Institute.	Many, e.g., IDE Technologies, Dow, Saltworks, and more.	
Pretreatment required	Filtration for solids removal is required. Other pretreatment may be required.	Filtration for solids removal is required. Other pretreatment may be required.	
Capacity		Can be implemented on a large scale.	
Comments	An emerging technology. Limited information is available.	Uses a caustic and an acid for regeneration. High TDS levels and flow rates probably result in this technology not being applicable.	The reference example required waste heat for evaporating water.
Selected references (refer to Table 2-1-2)	51	1	52, 53

Table 2-1-2 Selected references as examples. Complete citations are found in the reference list at the end of this section. Brochures or articles taken from company websites are listed by article title rather than author name.

1	**2**	**3**	**4**	**5**	**6**	**7**	**8**	**9**
Ahmad and Williams, 2012	Aines et al., 2011	Bourcier et al., 2011	Elimelech and Phillip, 2011	Ifelebuegu et al., 2014	Morillo et al., 2014	Rahardianto et al., 2007	Subramani and Jacangelo, 2015	Greenlee et al., 2009
10	**11**	**12**	**13**	**14**	**15**	**16**	**17**	**18**
Mezher et al., 2011	Curcio et al., 2015	Coday et al., 2014	Shaffer et al., 2015	Qasim et al., 2015	McGinnis et al., 2013	Sethi et al., 2008	NETL, 2014a	"Technology of thermal membrane distillation," Memsys, 2016
19	**20**	**21**	**22**	**23**	**24**	**25**	**26**	**27**
Juby et al., 2008	"Electrochem; advanced EDR," Saltworks Technologies, 2015a	McGovern et al., 2014	Ettouney, 2009	Desware, 2002–2016	Igunnu and Chen, 2014	"Desalination by distillation," Sidem-Veolia	Al-Karaghouli and Kazmerski, 2013	Al-Sahali and Ettouney, 2007
28	**29**	**30**	**31**	**32**	**33**	**34**	**35**	**36**
Ghaffour et al., 2013	Miller et al., 2015	Das, 2012	Shaffer et al., 2013	Awerbuch and Weekes, 1990	Ghalavand et al., 2014	"HDH tackles brine disposal challenge," Gradiant Corp., 2014	"SaltMaker low temperature crystallizer," Saltworks Technologies, 2015b	Lozier et al., 2007
37	**38**	**39**	**40**	**41**	**42**	**43**	**44**	**45**
"Zero-liquid-discharge (ZLD) crystallizers," GE Power, 2016	Pereira et al., 2007	Collares-Pereira et al., 2004	"WAIV—Wind aided intensified evaporation," Lesico CleanTech	Zijlema et al., 2000	Fakhru'l-Razi et al., 2009	Williams et al., 2013	Williams et al., 2015	Guerra et al., 2011
46	**47**	**48**	**49**	**50**	**51**	**52**	**53**	**54**
Heist and Barron, 1983	"Water desalination using multi-phase turbo-expander," GE Global Research, 2015	Roelofs et al., 2015	"Capacitive deionization," TDA Research, Inc., 2004	Demirer et al., 2013	Bajpayee et al., 2012	"Adsorption desalination," Water Desalination and Reuse Center	Shkolnikov et al., 2012	Zhou et al., 2014
55	**56**	**57**	**58**	**59**	**60**	**61**	**62**	**63**
Alspach, 2014	Xu et al., 2013	Voutchkov, 2011	Chekli et al., 2016	Drioli et al., 2015	"Membrane distillation," Aquaver, 2014	Minier-Matar et al., 2016	Minier-Matar et al., 2014	"ElectroChem advanced EDR," Saltworks Technologies, 2015a
64	**65**	**66**	**67**	**68**	**69**	**70**	**71**	
Mickley, 2008	Zuback et al., 2014	Thiel et al., 2015	Rane and Padiya, 2011	Wiegandt and Von Berg, 1980	Fujioka et al., 2013	Gao et al., 2014	Odu et al., 2015	

Screening of Desalination Technologies for High-TDS Brine

Desalinating Mt. Simon brine is challenging because of its high salinity, about 230,000 ppm of TDS. Technologies were screened based on brine salinity and limitations of high-TDS brine treatment technologies. Water quality parameters of the Mt. Simon brine are presented in the next section. Despite the breadth of literature available on desalination (a search for "desalination" yielded more than 35,000 results on ScienceDirect and more than 40,000 results on Engineering Village), most papers on desalination deal with processes designed to treat brines with TDS less than 60,000 ppm, such as seawater. The vast majority of desalination processes are not designed to treat brines with TDS above 60,000 ppm. High-TDS brines are typically disposed of via deep well injection or discharge to the ocean. High-TDS brine treatment is commonly practiced only when environmental regulations mandate the implementation of a zero liquid discharge (ZLD) process to minimize or eliminate liquid waste. A literature review was conducted to identify desalination technologies and select the best for treating Mt. Simon brine. Table 2-1-1 presents an overview of desalination technologies. Besides technical feasibility, other factors that are of vital importance for technology selection include the energy consumption, capital cost, and total processing costs. Because desalination is rarely applied to high-TDS brines, limited energy consumption and cost data are available. Table 2-1-3 includes reported energy requirements for high-TDS desalination.

The pros and cons of applying each process to high-TDS brine are reported in Table 2-1-3. Pros and cons are indicative of the suitability of the technology of each application. A desalination method may be theoretically or technically feasible for high-TDS brines but might not be commercially viable or implemented at industrial scale for reasons such as high costs, limited data availability, research gaps, and process complexity.

The technology readiness level (TRL) indicates the maturity of a given process technology. Technology readiness level rankings are defined by the US DOE. A TRL of 9 indicates a technology has been successfully operated in industry. Laboratory-scale research (innovative technologies) are assigned TRLs ranging between 3 and 5, whereas emerging technologies operating at the pilot scale may be assigned a TRL of 6 or 7. Some innovative technologies appear promising but equipment is not likely to be commercially available in the near future. All these factors are taken into consideration before a preliminary ranking is assigned. In Table 2-1-3, the most promising technologies for treatment of high-TDS brine are assigned a 1, and those that are least likely to be applicable are assigned a 4.

Salinity limitations was used as a metric for screening high-TDS brine treatment technologies. The initial TDS concentration present in brine from the Mt. Simon (about 230,000 ppm of TDS, primarily from NaCl) is at least four times greater than the feed salinity that most desalination processes are designed to handle.

Conventional membrane processes are generally not applicable to the treatment of high-TDS brines because of ion concentration polarization effects; the ion concentration of the solution tends to be higher closer to the membrane, which may result in salt precipitation. Although salt precipitation is desirable in some processes, uncontrolled precipitation may clog membranes, making them less effective. If precipitation could be controlled and the crystals removed without membrane clogging (a scheme that membrane crystallization [#4] attempts to incorporate), then the salt precipitation would actually facilitate higher water recovery, but this technology requires further development.

Other factors limit membrane processes as well. The high osmotic pressure of high-TDS brines is a limitation for RO processes because available membrane modules cannot withstand the

pressures needed to overcome the high osmotic pressure. Forward osmosis and membrane distillation are more practical for high-TDS brines. However, with FO, the follow-up treatment of the draw solution might be impractical. Membrane distillation theoretically allows for total exclusion of salts, and researchers would need to resolve high water recovery issues, such as membrane fouling, before scaling up a membrane process. Forward osmosis and membrane distillation both show promise at the laboratory and pilot scales, and these technologies may prove to be technically feasible with further development.

Crystallization processes appear to be more promising because they are capable of precipitating and removing salts by design. The use of temperature reduction to precipitate salts from the brine was determined to be unsuitable for high-TDS brine treatment because the primary salt in the Mt. Simon brine is NaCl, and NaCl has a relatively low change in solubility in the temperature range usually considered for refrigerated crystallization. The established crystallization technology that is most applicable to the Mt. Simon brine is evaporative crystallization, and this technology was deemed the leading candidate among those that are commercially established. Variations in evaporative crystallization, such as the use of multiple stages or the use of vapor recompression instead of conventional heating, should be evaluated for Mt. Simon brine treatment.

Energy consumption is typically the greatest expense in a desalination plant, especially for high-TDS brines, because the minimum theoretical energy of separation increases with increasing feed salinity. Other process costs include infrastructure, labor, maintenance, and amortization of the capital cost. The theoretical minimum energy requirement for desalination resulting in the production of a purified water stream is directly related to the concentration of the feed brine; desalination of highly saline brines will necessarily be significantly more costly than desalination of seawater or brackish water. Still, the energy consumption of industrial crystallization processes is at least four times higher than the theoretical minimum energy of desalination of high-TDS brine (~10 kWh/m^3). Emerging technologies have the potential to significantly reduce desalination costs by lowering the energy demand closer to the theoretical minimum. Refrigerated freeze-crystallization processes appear to be a promising alternative because the energy requirements could be lower, but equipment and systems for handling ice or separating ice crystals from salt crystals, or both, need to be developed.

On the basis of energy consumption and the ability to produce a salt, the ISGS supercritical desalination treatment with a continuous salt and water production process is one of the promising emerging technologies. According to process simulations, this supercritical desalination process might approach the minimal theoretical separation energy when it is integrated with a power generation system. Furthermore, the input energy would be partially recovered as electrical power in the water–electricity cogeneration system. Continued investment in this treatment process is recommended to characterize it so that a more complete technical and economic analysis can be produced. It should be noted that other researchers (e.g., Lean et al., 2012; Research Partnership to Secure Energy for America, 2011) have also proposed the treatment of produced water or brine by supercritical precipitation; however, only a partial water recovery of ~10% for treatment of Mt. Simon brine by these processes is expected without the addition of a conventional crystallization unit. Furthermore, such an approach might not be energetically superior to existing thermal evaporators without a highly efficient heat recovery and integration system or integration with a power generation system. Many emerging technologies face challenges at high salinity; for example, high salinity might greatly reduce flux and water recovery for membrane distillation.

Table 2-1-3 Desalination technologies screening for Mt. Simon brine.

Evaluation of desalination technologies for Mt. Simon brine desalination	1	2	3	4	5	6
	Membrane	**Membrane**	**Membrane**	**Membrane**	**Membrane**	**Evaporative concentration**
	Reverse osmosis (RO)	**Forward osmosis (FO)**	**Membrane distillation (MD)**	**Membrane crystallization**	**Electrodialysis (ED) & electrodialysis reversal (EDR)**	**Conventional distillation: Multiple-effect distillation (MED) & multiple-stage flash (MSF)**
Can 230,000 ppm of TDS brine (Mt. Simon) be treated effectively?	No. Osmotic pressure is too high. Advanced membrane modules might treat 105,000 ppm of TDS feeds.	Not at this time, but recommend pursuing it as an emerging technology. Finding the best draw solution will be critical. Salt precipitation will inhibit flux and recovery.	Not at this time, but recommend pursuing it as an emerging technology. Likely to be technically feasible.	Not at this time, but recommend pursuing it as an emerging technology.	Not at this time, but recommend pursuing it as an emerging technology. Several claims have been made that ED/EDR is technically feasible for high TDS, but technology requires further development for high-TDS applications.	Yes, with proper adjustments to allow for the highly corrosive nature of the feed brine. Conventional thermal processes are limited to a maximum TDS in the range of 80,000 to 150,000 ppm, but multiple-effect evaporation may be applied to Mt. Simon brine if the appropriate materials of construction are selected. Fouling with solid precipitant will also occur at any reasonable recovery because of solubility limits.
Concentrated brine or solid product produced?	N/A	Concentrated brine.	Concentrated brine.	Slurry of salt and brine.	Concentrated brine.	Concentrated brine.
Characteristics of the brine or salt	N/A	Slightly more concentrated brine (~260,000 ppm).	Slightly more concentrated brine (~260,000 ppm).	Impure salt can be recovered. Higher NaCl purity by presoftening the feed.	Unknown.	Near saturation.
Expected recovery of treated water (%)	N/A	~10%–30%, based on avoiding salt precipitation.	~10%–30%, based on avoiding salt precipitation.	Very high.	Unknown.	Very high.
Purity of recovered water	N/A	Depends on the draw solution and draw solution recovery.	Good; should meet product requirements.	Should be able to recover high-purity water.	Should be able to recover high-purity water.	Good; should meet product requirements.
Energy consumption	N/A	Depends on the draw solution and draw solution recovery. Limited data are available. McGinnis et al. (2013) reported ~275 $kWh_{thermal}$ when the feed was 73,000 ppm of TDS and the draw solution was NH_3CO_2.	Limited data are available. Minier-Matar et al. (2016) reported ~260 $kWh_{thermal}/m^3$ for a 6.3 wt% feed brine.	Limited data are available.	Estimated as high as 176 kWh/m^3 by Ahmad and Williams (2012).	Estimated by Trimeric: 212 $kWh_{thermal}/m^3$ for 88% water recovery using a 6-stage MEE process. Additional electrical power (~1–2 kWh/m^3) is also needed.
Pros	N/A	With further development of draw solutions and recovery methods, FO might eventually be less energy intensive than thermal processes.	Theoretical 100% rejection of all ions. Can utilize low-quality heat sources.	Can be used for the ZLD approach.	May be technically feasible, with less scaling potential than RO.	Technology is readily available and might be further upgraded to handle high-TDS brines.
Cons	N/A	Currently impractical because of low water recovery, membrane fouling, and other operating issues associated with undesired precipitation of salts, even with softening pretreatment.	Further research required to resolve issues of precipitation of concentrated brine, low flux, and low water recovery.	Very high osmotic pressure might render the technology impractical.	Highly energy consumptive, although some researchers claim it will be competitive with MVC evaporation.	High capital costs and high energy requirements are predicted. Near-saturation liquid waste will still require further treatment or disposal.
Technology readiness level (TRL)	N/A	~6	~6	<5	~5	9
Preliminary ranking (1, 2, 3, 4)	N/A	2	2	2	2	1
Selected references (refer to Table 2-1-2)	1–11, 55–57	1, 6, 8, 12–16, 58–60	6, 7, 17, 18, 19, 61, 62	19	1, 5, 6, 10, 11, 16, 19, 20, 21, 63	1, 5, 11, 22–29, 56, 64, 65

Table 2-1-3 continued. Desalination technologies screening for Mt. Simon brine.

Evaluation of desalination technologies for Mt. Simon brine desalination	7	8	9	10	11	12
	Evaporative concentration	**Evaporative concentration**	**Evaporative crystallization**	**Evaporative crystallization**	**Evaporative crystallization**	**Evaporative crystallization**
	Standard brine concentrators	**Humidification compression**	**Standard evaporative crystallizers**	**Spray drying**	**Natural evaporation**	**SAL-PROC**
Can 230,000 ppm of TDS brine (Mt. Simon) be treated effectively?	Yes, for partial treatment. Brine concentration may be increased to near saturation.	Not at this time, but recommend pursuing as an emerging technology. Likely to be technically feasible.	Yes.	Yes, but capacity is limited.	Yes, if sufficient space is available and water recovery is not an issue.	Yes.
Concentrated brine or solid product produced?	Concentrated brine.	Probably concentrated brine, although Minier-Matar et al. report potential salt production with humidification compression.	Solid product is filtered out and dried.	Solid product is collected and dried.	Solid product.	Various purified salt products are possible.
Characteristics of the brine or salt	Near saturation.	Near saturation.	Salt will be impure. Might improve with pretreatment of brine or specialized crystallizer design.	Salt will be impure. Might improve with pretreatment of brine or specialized design.	Impure mixed salt sludge would occasionally be dug out from the pond and landfilled (or reprocessed).	Purified (salable) salt products
Expected recovery of treated water (%)	Very high.	Limited data available.	Very high.	Water can be recovered if needed.	Water not usually recovered.	Water not recovered.
Purity of recovered water	Should be able to recover high-purity water.	Should be able to recover high-purity water.	Should meet requirements.	Should meet requirements.	N/A	N/A
Energy consumption	20–50 $kWh_{electrical}/m^3$ or may be more than 200 $kWh_{thermal}/m^3$ for high-TDS feeds. Lower energy requirements for lower salinity feeds.	Limited data are available. Some estimate 200–300 $kWh_{thermal}/m^3$.	52–66 $kWh_{electrical}/m^3$ or ~200 $kWh_{thermal}/m^3$	Limited data are available.	Limited data are available.	Limited data are available.
Pros	Established technology is capable of handling high-TDS brines.	Low-grade heat sources and solar energy might be used.	Could be used for ZLD or near ZLD. A well-established commercial technology.	A simple process, which could be ZLD. Commercially proven.	A simple technology.	A combination of relatively simple technologies. Yields presumably salable salt products.
Cons	The capacity for most commercially available brine concentrators is low, <5,000 m^3/day. Expensive equipment may be required to minimize corrosion.	Potential corrosion of equipment at high TDS.	Energy intensive. Recovery of a salt stream with any value may be difficult.	Highly unlikely to be economically viable at a large scale. Recovery of water from outlet gas would be difficult and expensive.	No water recovery; produces a mixed salt sludge.	No water recovery. Large footprints. Many unit operations.
Technology readiness level (TRL)	9	~6	9	≤9	9	≤8
Preliminary ranking (1, 2, 3, 4)	2	2	1	3	3	3
Selected references (refer to Table 2-1-2)	5, 10, 11, 22, 23, 30–32, 64–66	8, 33–35, 61	1, 36, 37, 64–66	38, 39, 64	6, 40	6

Table 2-1-3 continued. Desalination technologies screening for Mt. Simon brine.

Evaluation of desalination technologies for Mt. Simon brine desalination	13	14	15	16	17	18
	Antisolvent crystallization	**Refrigerated crystallization**	**Refrigerated crystallization**	**Refrigerated crystallization**	**Capacitive deionization**	**Supercritical desalination**
	Antisolvent addition, with antisolvent recovery by distillation	**Cooling crystallization of salt**	**Fractional freeze crystallization of ice**	**Multiple-phase turbo-expansion**	**Capacitive deionization**	**Supercritical desalination**
Can 230,000 ppm of TDS brine (Mt. Simon) be treated effectively?	Some literature indicates that this is technically feasible, but the technology is not readily available and research is limited.	No. A small change in NaCl solubility with temperature.	Possibly. More research is required.	Not at this time. Possibly technically applicable, but economics not known. No data (even lab data) are available to demonstrate the concept.	No. TDS is too high for economic application.	Recommend pursuing the process. Includes power cogeneration as an emerging technology because brines with >50,000 ppm of TDS are the target.
Concentrated brine or solid product produced?	Solid product.	N/A	Concentrated brine.	Solid salt crystals are separated.	N/A	Solid salt product.
Characteristics of the brine or salt	Salt will be impure. Might improve with pretreatment of brine or specialized crystallizer design.	N/A		Salt will be impure. Might improve with pretreatment of brine or specialized crystallizer design.	N/A	Salt will be impure. Might improve with pretreatment or stage-wise salt precipitation.
Expected recovery of treated water (%)	Should be high.	N/A		Probably very high.	N/A	Very high.
Purity of recovered water	Uncertain; depends on separation of the antisolvent.	N/A	Ice may require further desalination.	Should meet requirements.	N/A	Product water should be of high purity.
Energy consumption	Limited data are available.	N/A	The enthalpy of freezing is 7× lower than the enthalpy of evaporation.	~40 kWh/m^3 of electrical energy consumption for any feed predicted by the manufacturer, which is reported to be 45% lower than complete recovery by crystallization but still energy intensive.	N/A	Depends on process design. The power cogeneration process might approach the thermodynamic limit (~10 kWh/m^3 for concentrated brine); other configurations might require higher energy consumption.
Pros	A relatively simple technology concept.	N/A	Theoretically lower energy requirements; less risk of scaling at low temperatures.	Could be used for ZLD.	N/A	Integration with a power plant could result in power generation and high-purity water production in a ZLD system.
Cons	Experimental technology. Uncertain if there is as much effort in developing compared with other emerging technologies. Probably poor economics compared with evaporation.	N/A	Low product purity; equipment is complex (difficulties in handling and melting ice).	An emerging technology. Few data are available. Could be competitive, particularly if solids recovery or handling is easier.	N/A	An emerging technology that is dependent on integration with power plants, so could not be implemented everywhere.
Technology readiness level (TRL)	<5	N/A	~5	3	N/A	5
Preliminary ranking (1, 2, 3, 4)	4	N/A	4	3	N/A	2
Selected references (refer to Table 2-1-2)	41	6	1, 42–46, 61, 67–70	47	48–50	71

Table 2-1-3 continued. Desalination technologies screening for Mt. Simon brine.

Evaluation of desalination technologies for Mt. Simon brine desalination	19	20	21
	Extraction	Ion exchange	Adsorption
	Solvent extraction	Ion exchange	Adsorption
Can 230,000 ppm of TDS brine (Mt. Simon) be treated effectively?	Potentially applicable, highly uncertain. Limited information was found.	No. TDS is too high.	TDS is too high. Not practical because of the need for a huge volume of adsorbent per volume of brine. Technology does not seem particularly promising.
Concentrated brine or solid product produced?		N/A	
Characteristics of the brine or salt		N/A	
Expected recovery of treated water (%)		N/A	
Purity of recovered water		N/A	
Energy consumption		N/A	
Pros		N/A	
Cons		N/A	
Technology readiness level (TRL)		N/A	<5
Preliminary ranking (1, 2, 3, 4)	4	N/A	4
Selected references (refer to Table 2-1-2)	51	1	52, 53

Major Research Gaps for Treating High-TDS Brine

The treatment of high-TDS brines is a relatively new research area. The salinity limitations of all the desalination technologies have not been fully explored. Processes that may be technically feasible, such as electrodialysis reversal (EDR) or membrane distillation, have not been adequately tested for high-TDS feeds. Optimal process parameters have not yet been determined, and appropriate equipment or materials are not commercially available. Energy consumption data are limited and, when provided, indicate a significant potential to reduce energy consumption for thermal processes. Therefore, it cannot be assumed that the design, performance, and economic parameters associated with most existing technologies, which are based on operation with low-TDS salinity brines, are necessarily applicable to the treatment of high-TDS brines. A preliminary summary of the major research gaps associated with each technology for treating high-TDS brine is presented in Table 2-1-4.

Pretreatment Technologies

Pretreatment may be required to remove contaminants that interfere with the desalination process. Pretreatment processes usually include a physical process to remove suspended solids and chemical additives to soften the water, adjust the pH, or remove some low-concentration soluble components that cause problems (such as fouling). For treating produced water in the petroleum industry, pretreatments that target hydrocarbons (oil and grease, various aromatic and aliphatic compounds) are critical, but these processes are not necessary for water recovered from saline formations like those from the Mt. Simon and St. Peter Formations. Common pretreatment processes and their anticipated applicability are summarized in Table 2-1-5. The pretreatment processes presented in Table 2-1-5 are categorized as physical separation, chemical treatment, or biological treatment.

Table 2-1-4 Major research gaps of desalination technologies.

Research gaps of desalination technologies	1	2	3	4	5	6
	Membrane	**Membrane**	**Membrane**	**Membrane**	**Membrane**	**Evaporative concentration**
	Reverse osmosis (RO)	**Forward osmosis (FO)**	**Membrane distillation (MD)**	**Membrane crystallization**	**Electrodialysis (ED) & electrodialysis reversal (EDR)**	**Conventional distillation: Multiple-effect distillation (MED) & multiple-stage flash (MSF)**
Research gaps	Requires the development of membrane materials and stronger membrane modules that can withstand the high pressure requirements for desalination of highly saline brines. Membrane scaling, mostly caused by ion concentration polarization, must be reduced.	Requires identification of the best draw solution, as well as the development of draw solution recovery procedures and the limitation of scaling caused by ion concentration polarization. Advanced high-flux fouling-resistive membranes need to be developed.	Membrane scaling and fouling must be decreased to improve flux at high salinity. Crystallization on the membrane surface must be prohibited. The best configuration must be determined.	Requires the development of a controlled crystallization procedure so that crystals can be collected and membrane fouling can be eliminated.	Requires further research for application of ED and EDR to highly saline brines before commercialization.	A mature technology, but energy consumption is significantly greater than the theoretical energy minimum, so there is space for a reduction in energy requirements. Current research is in using waste heat sources, in reducing scaling, and in cogeneration facilities.

Research gaps of desalination technologies	7	8	9	10	11	12
	Evaporative concentration	**Evaporative concentration**	**Evaporative crystallization**	**Evaporative crystallization**	**Evaporative crystallization**	**Evaporative crystallization**
	Standard brine concentrators	**Humidification compression**	**Standard evaporative crystallizers**	**Spray drying**	**Natural evaporation**	**SAL-PROC**
Research gaps	A mature technology, but energy consumption is significantly greater than the theoretical energy minimum, so there is space for a reduction in energy requirements. Current research is in using waste heat sources, in reducing scaling, and in cogeneration facilities.	An emerging technology, and more research is required before implementation at the commercial scale. Corrosion, fouling, and scaling of equipment are likely with high-TDS feed solutions.	A mature technology, but energy consumption is significantly greater than the theoretical energy minimum, so there is space for a reduction in energy requirements.	A mature technology, but it currently operates only at a small scale.	Current research is in the reduction of land area requirements and the rate of evaporation, improvements in water recovery, and application of the technology to cooler climates.	Precipitation of NaCl is unlikely.

Research gaps of desalination technologies	13	14	15	16	17	18
	Antisolvent crystallization	**Refrigerated crystallization**	**Refrigerated crystallization**	**Refrigerated crystallization**	**Capacitive deionization**	**Supercritical desalination**
	Antisolvent addition, with antisolvent recovery by distillation	**Cooling crystallization of salt**	**Fractional freeze crystallization of ice**	**Multiple-phase turbo-expansion**	**Capacitive deionization**	**Supercritical desalination**
Research gaps	This is only an experimental technology. Requires much more research.	Crystallization of NaCl by this method is unlikely.	Theoretically, salts are excluded in ice formation, but actually, the product ice does not meet water purity requirements without further treatment.	Separation of salt crystals from ice crystals may be challenging because the salt will be sticky.	Regeneration of the electrodes is challenging, and incomplete electrode regeneration results in a reduction in absorption capacity. Additionally, ion concentration and the shadow spacer effect (the spacer will cover or shadow the electrode) limit ionic transport.	Operation at very high temperatures and pressures can present practical design challenges. Membrane treatment of supercritical steam may also be challenging. This technology needs to be tested at a pilot scale.

Table 2-1-4 continued. Major research gaps of desalination technologies.

Research gaps of desalination technologies	19	20	21
	Extraction	Ion exchange	Adsorption
	Solvent extraction	Ion exchange	Adsorption
Research gaps	An emerging technology; requires extensive research before commercialization.	Resin will be overloaded quickly with a high inlet concentration.	Requires more research related to adsorbent selection and regeneration.

Some sort of physical separation to remove large particles, suspended solids, and hydrocarbons is a critical step in brine or water treatment. This is generally accomplished based on size exclusion (filtration), density differences, a gas to collect particulates (flotation), or a gas to strip volatile organic compounds from the water. Chemical treatments adjust the water chemistry to render a desalination process more effective, precipitate chemical species that must be removed before the desalination process, or both. Biological treatments are currently being evaluated as alternatives to standard pretreatments but are not yet commonly used in industry.

Standard pretreatment processes include coagulation, flocculation, lime softening, and media filtration. The addition of a coagulant helps break up colloidal particles, and the addition of a flocculant promotes the collection of those particles into flocs, which can then be removed by filtration or settling. Lime softening helps precipitate metal and compounds containing calcium (Ca). The removal of Ca reduces the risk of scaling during the desalination process. Media filters, especially walnut shell filters, are widely applied in produced water treatment.

Laboratory Testing of High-TDS Mt. Simon Brine

Sampling of Mt. Simon Brine

One barrel of Mt. Simon brine was collected according to the protocols of the ISGS Geochemistry Section (Figure 2-1-1). The sample was retrieved from the Archer Daniels Midland Company (ADM) facility at 1001 North Brush College Road in Decatur, Illinois, where the Illinois Basin–Decatur Project (IBDP) and the Illinois-Industrial Carbon Capture and Storage (IL-ICCS) projects are located.

This sample was drawn from Zone 2 of the Mt. Simon Sandstone at a depth of 6,700 ft. At the time of sampling, the density of the sample was measured as 1.132 g/cm^3 and the conductivity as 199.7 mS/cm. The pH of the sample was 7.08 and the turbidity was 599 nephelometric turbidity units (NTU). The dissolved oxygen content of the sample was measured as 0.0 mg/L. The TDS of the extracted brine was estimated, based on a rough correlation of density to TDS, as approximately 198,000 mg/L. The sample was transported to the ISGS laboratory and stored in a refrigerator at 4 °C for further characterization and treatment studies.

Table 2-1-5 Pretreatment technologies (continued to page 45).

Evaluation of pretreatment technologies	1 Physical separation Media filtration	2 Physical separation Gravity filtration	3 Physical separation Hydrocyclone	4 Physical separation Flotation	5 Physical separation Adsorption
Target contaminants	Suspended solids, oil, and grease.	Suspended solids, oil, and grease.	Hydrocarbons, including dispersed oil and grease; process removes 5- to 15-µm particles, but hydrocyclone will not remove soluble oils.	Organic chemicals and particulates, including natural organic matter (NOM), oil, and grease.	Mostly dissolved organics, but adsorption of heavy metals, Fe, and Mn is possible.
Process notes	Uses sand, gravel, anthracite, walnut shells, or other. Process is not affected by salinity.	Sand is usually used as the filtration medium.	Separates oil from water based on density; can also separate solids.	Gas or mechanical shear propellers are used to generate bubbles that collect particulates.	Mainly organoclays and activated carbon for organics. May use zeolites and activated alumina adsorbents for metals. The process is best used as a polishing step because the adsorbent can easily be overloaded and regeneration can be costly.
Applicability to Mt. Simon brine	Yes, after initial coagulation and lime softening.	Yes, after initial coagulation and lime softening.	Might be applicable for removal of fine solids.	Not needed because no oil and grease are present.	Not needed because the level of organics is low.
Applicability to St. Peter brackish water	Yes, after initial coagulation and lime softening	Yes, after initial coagulation and lime softening	Might be applicable for the removal of fine solids.	Not needed because no oil and grease are present.	Not needed because the level of organics is low.
Selected references as examples	Igunnu and Chen, 2014; Fakhru'l-Razi et al., 2009; Guerra et al., 2011				

Evaluation of pretreatment technologies	6 Physical separation Clarifier	7 Physical separation Settling ponds	8 Physical separation Air stripping	9 Physical separation Ion exchange
Target contaminants	Suspended solids.	Large particulates.	Organic chemicals and particulates (volatile organic compounds), such as benzene, toluene, ethylbenzene, xylene and vinyl chloride. Also removes odor and oxidizing contaminants such as Fe and Mn.	Scaling and fouling contaminants.
Process notes	A sloped-bottom tank or basin is used to separate liquid from suspended solid particles.	A pond or basin is used to remove particulates by gravity settling.	Air is brought into contact with the water in a packed column and contaminants are	Water is softened by an ion exchange resin. The resin will require regeneration.

Evaluation of pretreatment technologies	1	2	3	4	5
	Physical separation	**Physical separation**	**Physical separation**	**Physical separation**	**Physical separation**
	Media filtration	**Gravity filtration**	**Hydrocyclone**	**Flotation**	**Adsorption**
				transferred to the gas phase.	
Applicability to Mt. Simon brine	Might be necessary after coagulation.		Might be necessary to remove suspended solids.	Not needed because the level of organics is low.	Not applicable for high-TDS feed.
Applicability to St. Peter brackish water	Might be necessary after coagulation.		Likely not necessary.	Not needed because the level of organics is low.	Likely not necessary.
Selected references as examples	Igunnu and Chen, 2014; Fakhru'l-Razi et al., 2009; Guerra et al., 2011				

Evaluation of pretreatment technologies	10	11	12	13
	Chemical treatment	**Chemical treatment**	**Chemical treatment**	**Chemical treatment**
	Coagulation and flocculation	**Lime softening, sodium hydroxide, and other antiscalants**	**Chemical oxidation**	**pH adjustment**
Target contaminants	Colloidal particles.	Scale-forming contaminants, including Ca and metals.	Organic chemical and particulate removal, chemical oxygen demand (COD), biological oxygen demand (BOD), and some inorganics, including Fe, Mn, and S.	N/A
Process notes	A coagulant breaks up colloidal particles and a flocculent promotes the collection of those particles into flocs.	Addition of calcium hydroxide [$Ca(OH)_2$] to cause precipitation of scale-forming contaminants, especially Ca. Addition of sodium hydroxide (NaOH) to increase silica solubility and reduce scaling. Other antiscalants may be used instead of $Ca(OH)_2$.	An oxidant (usually ozone, peroxide, permanganate, oxygen, or chlorine) is mixed in.	May require pH adjustment by chemical addition for some processes.
Applicability to Mt. Simon brine	Needed.	Needed.	Not needed because the level of organics is low.	Possibly.
Applicability to St. Peter brackish water	Needed.	Needed.	Not needed because the level of organics is low.	Possibly.
Selected references as examples	Igunnu and Chen, 2014; Fakhru'l-Razi et al., 2009; Guerra et al., 2011			

Evaluation of pretreatment technologies	14	15
	Biological treatment	**Biological treatment**
	Biological aerated filters	**Membrane bioreactors**

Evaluation of pretreatment technologies	1	2	3	4	5
	Physical separation	Physical separation	Physical separation	Physical separation	Physical separation
	Media filtration	Gravity filtration	Hydrocyclone	Flotation	Adsorption
Target contaminants	Oil, suspended solids, ammonia, nitrogen, COD, BOD, Fe, Mn, heavy metals, dissolved and soluble organics, and hydrogen sulfide (H_2S).			COD, oil, and gas	
Process notes	Permeable media, such as rocks, gravel, or a plastic medium, facilitate the biochemical oxidation or removal of organic constituents, but this aerobic process is not effective when salinity exceeds 100,000 mg/L.			Bench- and pilot-scale studies for oil and gas removal.	
Applicability to Mt. Simon brine	Not applicable for high-TDS feed.			Not needed because no oil and gas are present.	
Applicability to St. Peter brackish water	Not needed.			Not needed because no oil and gas are present.	
Selected references as examples	Igunnu and Chen, 2014; Fakhru'l-Razi et al., 2009; Guerra et al., 2011				

Characterization of Mt. Simon Brine

Representative samples of Mt. Simon brine were characterized for various water quality parameters, including concentrations of anions, cations, trace elements, alkalinity, total suspended solids (TSS), TDS, total organic carbon (TOC), particle size distribution (PSD) of suspended solids, and radioactivity. The cation composition and radioactivity tests were conducted by Activation Laboratories Ltd. (Actlabs) in Ancaster, Ontario, Canada (Tables 2-1-6 and 2-1-7). Data obtained from the ISGS Geochemistry Section, including concentrations of ammonia, various anions, and alkalinity, were based on methods described by Labotka et al. (2015) and Locke et al. (2013; Table 2-1-6).

Figure 2-1-1 Mt. Simon brine sample collection during well swabbing.

Table 2-1-6 Water chemistry of Mt. Simon samples (continued on next page).

Constituent	Laboratory or source	Method	Concentration (mg/L)
Ag	Actlabs	ICP-OES[1]	<0.05
Alkalinity ($CaCO_3$-equiv.)	ISGS Geochemistry	Titration	21
Al	Actlabs	ICP-OES	3.2
As	Actlabs	ICP-OES	<0.3
B	ISGS Geochemistry	IC[2]	18.2
Ba	Actlabs	ICP-OES	3.290
Be	Actlabs	ICP-OES	<0.02
Bi	Actlabs	ICP-OES	<0.2
Br	ISGS Geochemistry	IC	650
Ca	Actlabs	ICP-OES	20,800
Cd	Actlabs	ICP-OES	<0.02
Ce	Actlabs	ICP-OES	<0.3
Cl	ISGS Geochemistry	IC	120,000
Co	Actlabs	ICP-OES	<0.02
Cr	Actlabs	ICP-OES	<0.2
Cs	Actlabs	ICP-MS[3]	0.173
Cu	Actlabs	ICP-OES	0.109
Dy	Actlabs	ICP-MS	0.00122
Er	Actlabs	ICP-MS	0.00066
Eu	Actlabs	ICP-MS	0.000307
F	ISGS Geochemistry	IC	<25
Fe	Actlabs	ICP-OES	68.6
Ga	Actlabs	ICP-MS	<0.0002
Gd	Actlabs	ICP-MS	0.00117
Ge	Actlabs	ICP-MS	0.00059
Hf	Actlabs	ICP-MS	0.000151
Hg	Actlabs	ICP-MS	0.253
Ho	Actlabs	ICP-MS	0.000117
In	Actlabs	ICP-MS	0.000111
K	Actlabs	ICP-OES	1,930
La	Actlabs	ICP-MS	<0.00002
Li	Actlabs	ICP-OES	13.7
Lu	Actlabs	ICP-MS	<0.00002
Mg	Actlabs	ICP-OES	1,980
Mn	Actlabs	ICP-OES	53.6
Mo	Actlabs	ICP-OES	<0.05
Na	Actlabs	ICP-OES	45,300
Nb	Actlabs	ICP-MS	<0.0001
Nd	Actlabs	ICP-MS	0.00637
NH_3	ISGS Geochemistry	IC	7.88
Ni	Actlabs	ICP-OES	<0.05
NO_3	ISGS Geochemistry	IC	<2

Constituent	Laboratory or source	Method	Concentration (mg/L)
P	Actlabs	ICP-OES	0.38
Pb	Actlabs	ICP-OES	<0.1
Pr	Actlabs	ICP-MS	0.00184
Rb	Actlabs	ICP-MS	2.690
S	Actlabs	ICP-OES	354
Sb	Actlabs	ICP-OES	<0.1
Sc	Actlabs	ICP-MS	<0.02
Se	Actlabs	ICP-OES	<0.2
Si	Actlabs	ICP-OES	15.4
Sm	Actlabs	ICP-MS	0.00134
Sn	Actlabs	ICP-OES	<0.1
SO_4	ISGS Geochemistry	ISGS	290
Sr	Actlabs	ICP-OES	781
Ta	Actlabs	ICP-MS	<0.00002
Tb	Actlabs	ICP-MS	0.000134
Te	Actlabs	ICP-OES	<0.1
Th	Actlabs	ICP-MS	0.00037
Ti	Actlabs	ICP-OES	<0.1
Tl	Actlabs	ICP-OES	<0.1
Tm	Actlabs	ICP-MS	<0.00002
U	Actlabs	ICP-OES	<0.5
V	Actlabs	ICP-OES	<0.1
W	Actlabs	ICP-OES	<0.1
Y	Actlabs	ICP-OES	<0.1
Yb	Actlabs	ICP-MS	0.000522
Zn	Actlabs	ICP-OES	2.800
Zr	Actlabs	ICP-MS	0.00107

[1]Inductively coupled plasma–optical emission spectroscopy.
[2]Ion chromatography.
[3]Inductively coupled plasma–mass spectrometry.

The TDS and TSS of the Mt. Simon sample were measured at our laboratory by using standard method 2540 C (Clesceri et al., 1998). The Mt. Simon sample had high levels of TSS (2,831 ± 129 mg/L) and TDS (224,667 ± 2,606 mg/L). Water chemistry data suggested that the majority of dissolved solids were sodium (Na) and Ca salts (45,300 mg/L of Na^+, 120,000 mg/L of Cl^-, and 20,800 mg/L of Ca^{2+}). Other cations with lower but considerable concentrations included Mg^{2+}, K^+, Ba^{2+}, Sr^{2+}, Mn^{2+}, and Fe^{3+}. In addition to the dominant chloride anion, sulfate and bromide were detected at concentrations of 290 mg/L and 650 mg/L, respectively, in the Mt. Simon brine. The concentration of sulfide species was 354 mg/L. Other species with concentrations between 1 and 20 mg/L included Al, B, Ba, Li, N, and Zn. Several other trace elements with concentrations below 1 mg/L were also detected in the tested sample (Table 2-1-6).

Suspended solids removal is an essential stage in treatment or handing scenarios, and both TSS concentration and the PSD of suspended solids are important factors for process design. The average size of suspended solids in the Mt. Simon brine and PSD of particles were measured by using a Horiba LA-950 laser diffraction particle size analyzer. Samples were treated by ultrasonic

vibration for 2 min to enhance particle dispersion before particle size analysis. The mean particle size was calculated based on the PSD data obtained from three replicate runs. Figure 2-1-2 illustrates the PSD, shown as q (%; volume percentage of each size) versus particle size (µm). The PSD of suspended particles in Mt. Simon brine ranged from 1 to 20 µm, with an average size of ~6 µm (Figure 2-1-2).

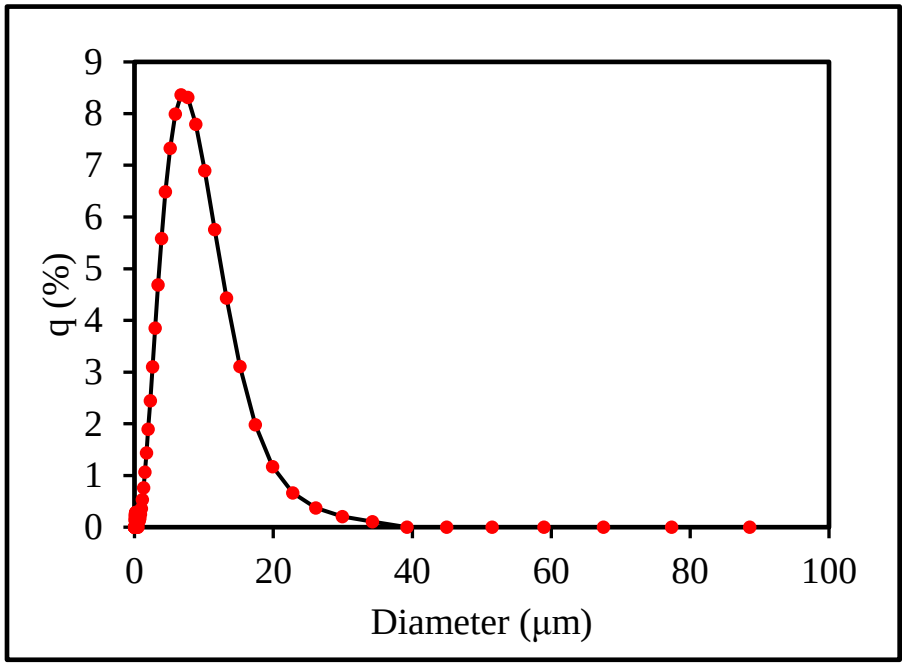

Figure 2-1-2 Size distribution of suspended solids in the Mt. Simon brine.

Mt. Simon brine samples were sent to Midwest Laboratories (Omaha, Nebraska) for measurement of concentration of TOC by Standard Method 5310B (Standard Methods Online, 2011). In this method, a sample is injected into a calibrated instrument that first removes the inorganic carbon by acid addition and purging, and then sends the sample to the combustion tube to oxidize organic carbon to CO_2. An infrared detector is used to measure the CO_2 level. The concentration of TOC in the sample is calculated based on the amount of CO_2 released from the sample. The TOC concentration of the Mt. Simon brine was 58 mg/L, which is relatively high. It is likely that the majority of organic species in the sampled Mt. Simon brine originated from drilling fluids because the Mt. Simon Sandstone, unlike the petroleum-producing formations, is not expected to contain significant amounts of organic compounds. Long operation of wells drilled into the Mt. Simon Sandstone is expected to generate brines with low TOC concentrations.

Naturally occurring radioactive materials (NORM) are commonly found in produced water as ^{40}K, ^{238}U, ^{232}Th, and their decay products. These primary radioactive minerals have a half-life of over a billion years and thus are not very radioactive. Furthermore, U and Th are insoluble in water. However, ^{238}U decays to ^{226}Ra and ^{232}Th decays to ^{228}Ra, which are more soluble, with half-lives of 1,600 and 5.75 years, respectively. Because of their relative solubility over a long period, ^{226}Ra and ^{228}Ra are the primary radioisotopes of concern in produced water.

The radionuclides in the extracted brine from the Mt. Simon Sandstone and the coagulated dried filtrate removed from the brine were quantified in a gamma-ray spectrometer by analysis of the gamma-ray energy spectrum produced. Actlabs completed the following radiochemical test

packages: (1) equivalent uranium (eU), (2) gross alpha and gross beta counting, and (3) a gamma scan. Table 2-1-7 presents the concentrations of selected radionuclides along with gross alpha and gross beta counts are presented. The Mt. Simon brine sample exhibited levels of gross beta activities greater than the US Environmental Protection Agency (USEPA) limits for drinking water (Table 2-1-8). Table 2-1-8 presents some of the regulations and guides for handling water, sludge, and solid waste containing NORM. According to the regulation guidelines shown, the Mt. Simon brine can be disposed of—without removal of suspended solids—as nonradioactive waste. Furthermore, the distilled or purified water and salt obtained from proper treatment of the Mt. Simon brine might potentially be utilized for beneficial uses (e.g., salts for road application and purified water as boiler feed water) if all regulations can be met.

Table 2-1-7 Concentration of radionuclides in Mt. Simon brine.

Radionuclides	As received Mt. Simon Brine (pCi/L)	Coagulated Mt. Simon solids filtrate (pCi/g)
Gross alpha	52.16	9.19
Gross beta	437.84	83.51
^{238}U	310.81	4.86
^{232}Th	94.86	156.49
^{210}Pb	<2.7	<2.7
^{226}Ra	38.65	<2.7
^{212}Pb	59.95	55.60
^{214}Pb	35.57	<2.7
^{208}Ti	25.09	14.88
^{212}Bi	<1.35	65.92
^{214}Bi	24.60	3.07
^{228}Ac	446.39	18.34
^{40}K	609.98	18.80

Table 2-1-8 Regulations and guidance for handling water and waste containing NORM.

Regulations	Radionuclides	Level
U.S. Environmental Protection Agency (USEPA) drinking water limits—maximum contaminant levels (Guerra et al., 2011)	Gross beta	50 pCi/L
	Gross alpha	15 pCi/L
	^{226}Ra	5 pCi/L
USEPA (1990) guides for liquid waste disposal into sewer	^{226}Ra	<400 pCi/L
USEPA (1990) guides for solid waste disposal to landfill with no need for long-term institutional control (dried)	^{226}Ra	<3 pCi/g
	^{210}Pb	<3 pCi/g
	U	<30 pCi/g
State of Illinois permitting requirements exemption for sludge resulting from the treatment of water or sewage and containing naturally occurring radioactive materials (dry weight basis; Title 32, Illinois Emergency Management Agency, 2016)	Sum of ^{226}Ra and ^{228}Ra	<200 pCi/g

Pretreatment of Mt. Simon Brine, Stage 1

Pretreatment of the Mt. Simon brine sample was conducted in two stages. The first stage included coagulation, flocculation, sedimentation, and sand filtration to remove suspended solids and reduce the concentration of scale-forming species. The second stage was focused on the reduction of total hardness by nanofiltration (NF), ion exchange, and precipitative softening, in addition to TOC adsorption by activated carbon. Limited desalination experiments were also performed by DCMD.

Alum and Lime Coagulation

Several chemicals can be used as coagulants in water treatment. Alum [aluminum sulfate, $Al_2(SO_4)_3$], ferric chloride, lime (calcium oxide, CaO), and polymer polyelectrolytes are the most common coagulants in the water treatment industry. The application of alum coagulant in a range of 0–100 mg/L for pretreatment of Mt. Simon brine was investigated. To increase the efficiency of coagulation, lime was added in a dose range of 70–500 mg/L. Preliminary tests indicated that the addition of lime was necessary for coagulation of the Mt. Simon brine because Mt. Simon brine becomes acidic (pH ~4.5–5.0) after prolonged exposure to air, and it cannot be treated with alum alone without any pH adjustment. Mixing of alum and lime with the brine induces the coagulation and flocculation of precipitates and suspended particles, which can then be separated out by settling and filtration.

Three sets of jar test experiments were conducted to determine effective dosages of coagulant and lime, and to determine the effectiveness of coagulation, flocculation, lime softening, sedimentation, and filtration in reducing turbidity.

Experiment 1 was conducted to determine the effectiveness of alum addition without pH adjustment. Alum coagulant was added in the specified dose range (0–100 mg/L) without lime addition.

Experiment 2 was conducted to determine the optimal alum dose when the pH of the water was increased to 8.5. Alum coagulant was added in the specified dose range (0–100 mg/L) with a lime dose of 285 mg/L. This lime dose was selected to increase the sample pH to 8.5.

Experiment 3 was conducted to test the impact of different lime doses on the coagulation process. The optimal alum dose (obtained in experiment 2) was added with a lime dose range of 0–500 mg/L.

The following procedure was applied in each experiment:

1. A 200-mL quantity of Mt. Simon brine was added to a beaker in a Phipps & Bird Jar Tester stirrer system.
2. Initial turbidity, conductivity, and pH were measured.
3. Alum coagulant and lime were added (the dosage varied according to the experimental design).
4. Rapid mixing at 300 rpm for 1 min was applied, followed by slow mixing at 30 rpm for 15 min.
5. Beaker contents were allowed 1 h to settle. Turbidity was measured at various intervals during the settling process (after 3 min, 15 min, 30 min, and 1 h).
6. Conductivity and pH were measured again after the 1-h settling period.
7. To mimic sand filtration, the supernatant liquid was passed through a 0.45-μm filter.
8. Coagulated and filtered water samples were collected and analyzed for water chemistry characterization.

Tables 2-1-9 to 2-1-11 show the Mt. Simon brine jar test results, including tests with alum only, alum with a fixed dose of lime, and various doses of lime with a fixed dose of alum. The experiments were conducted using a Phipps & Bird Jar Tester stirrer system (Figure 2-1-3).

The first series of results indicate that alum treatment alone, even at high doses, could not significantly change water turbidity. It was necessary to increase the pH, which is a critical parameter for water treatment.

Table 2-1-9 Mt. Simon brine jar test results for experiment 1 (varied alum dose, no lime).

	Alum dose (mg/L)					
Turbidity (NTU)	**0**	**20**	**40**	**60**	**80**	**100**
Initial	603	603	603	603	603	603
After 3 min	598	569	562	567	557	557
After 30 min	559	548	565	573	557	546
After 60 min	559	518	546	555	546	538

Hydrolytic dissociation of coagulant in water causes changes in pH. For instance, when alum is added to water, it undergoes the reaction below. The alum reacts with bicarbonate to form aluminum hydroxide, a precipitate:

$$Al_2(SO_4)_3 + 3Ca(HCO_3)_2 \rightarrow 2Al(OH)_3 + 6CO_2 + 3CaSO_4. \quad \text{(Reaction 2-1-1)}$$

Additional aluminum hydroxide precipitation may occur because of the pH change. The solubility product of aluminum hydroxide, $Al(OH)_3$, is

$$K_{sp} = [Al]\,[OH^-]^3/[Al(OH)_3] = 1.26 \times 10^{-33}. \quad \text{(Equation 2-1-1)}$$

In the second set of experiments, a lime dose of 285 mg/L was used to increase the pH to 8.5, and an optimal alum dose of 100 mg/L was determined. After an hour, water turbidity reduced from 599 to 4 NTU and pH dropped from 8.5 to 8.0 (Table 2-1-10).

Table 2-1-10 Mt. Simon brine jar test results for experiment 2 (varied alum dose, 285 mg/L of lime).

Turbidity and pH	**Alum dose (mg/L)**					
	0	**20**	**40**	**60**	**80**	**100**
Initial Turbidity (NTU)	599	599	599	599	599	599
Turbidity after 3 min (NTU)	37.7	44.9	40.4	28.3	36.1	14.1
Turbidity after 15 min (NTU)	42.2	46.8	36.6	23.3	23.1	7.4
Turbidity after 30 min (NTU)	46.9	50.1	37.6	24.7	18.8	4.7
Turbidity after 60 min (NTU)	53.9	54.5	36.5	23.2	19.1	3.9
pH	8.52	8.48	8.39	8.13	8.10	7.95

The third series of results suggests that the appropriate dose of lime to reduce turbidity to ~4 NTU was ~143 mg/L. Therefore, the recommended dosages of lime and alum were 143 mg/L and 100 mg/L, respectively. The addition of ~143 mg/L of lime with 100 mg/L of alum increased the brine pH to 6.81. A significantly larger dose of 499 mg/L of lime resulted in a higher turbidity value of 23 NTU, compared with 4.5 NTU when a lime dose of ~143 mg/L was used (Table 2-1-11).

Table 2-1-11 Mt. Simon brine jar test results for experiment 3 (100 mg/L of alum, varied lime dose).

Turbidity and pH	**Lime dose (mg/L)**					
	71.25	**142.5**	**213.75**	**356.25**	**427.5**	**498.75**
Initial Turbidity (NTU)	533	533	533	533	533	533
Turbidity after 3 min (NTU)	22.4	20.3	34.8	40.4	33.9	36
Turbidity after 15 min (NTU)	11.6	8.8	40.4	24	22.1	23.1
Turbidity after 30 min (NTU)	8.8	4.3	33.9	17.6	21.9	21.9
Turbidity after 60 min (NTU)	7.4	4.5	36	15.6	21.4	23
pH	6.02	6.81	7.38	8.43	8.53	8.34

Sand Filtration

Sand filtration experiments were conducted to investigate their effectiveness in removing residual turbidity following coagulation, flocculation, and settling. The sand filtration experiments were conducted with a bench-scale column test performed with a 1.1-cm inner diameter (I.D.) × 30-cm chromatography column obtained from Ace Glass (Vineland, NJ). The Phipps & Bird Jar Tester stirrer connected to a Phipps & Bird column filtration system used for sand filtration is illustrated in Figure 2-1-3.

The empty bed contact time and other parameters of the sand column are listed in Table 2-1-12

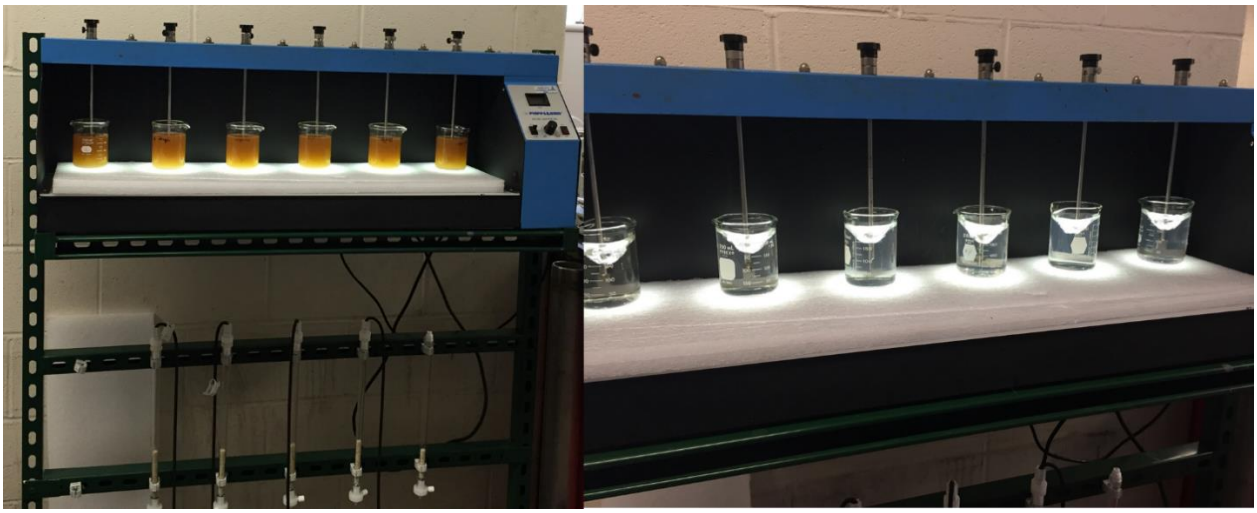

Figure 2-1-3 The jar test and sand filtration setup with beakers filled with Mt. Simon brine (left) and St. Peter water (right).

Table 2-1-12 Sand filter parameters.

Parameter	Study filter
Depth	10 cm
Surface area	36.5 cm^2
Empty bed contact time	5.6 min
Flow rate	1.5 mL/min
Sand size	0.45–0.55 mm

Mt. Simon brine that was coagulated —using 143 mg/L of lime and 100 mg/L of alum— and settled was pumped through the packed columns at a preset flow rate of 1.5 mL/min by using a Masterflex peristaltic pump. Effluent samples were collected at the outlet of columns at selected time intervals. Turbidity and conductivity were monitored at the outlets of the columns. Treatment design parameters, such as removal efficiency and breakthrough time, were recorded.

Figure 2-1-4 shows the effectiveness of the sand filter in reducing the turbidity of Mt. Simon brine from 13 to 0.01 NTU. A high ratio of $turbidity_{out}/turbidity_{in}$ was observed for up to ~90 bed volumes. The effluent turbidity after sand filtration then decreased to 0.01 NTU and later <0.001 NTU after 200 bed volumes. This may have been due to the ripening effect normally observed in newly packed sand filters. A filter with a newly installed medium typically has a ripening period, during which the captured particles gradually provide a better collector surface and improve the overall efficiency of the filter. Filtration through 0.45-µm filters was found to have a similar impact on turbidity, compared with filtration through the sand filters.

The sand filtration experiment was stopped after about 300 bed volumes were treated. Slow sand filters are typically never allowed to reach breakthrough and are always backwashed when the head loss reaches the maximum acceptable head in the system.

Polyelectrolyte Polymer Coagulation

Polyelectrolyte polymer coagulation was evaluated as an alternative to alum coagulation. Mt. Simon brine samples were pretreated by coagulation and sedimentation using several types of commercially available liquid cationic and anionic polymer coagulants with differing molecular weights. The screened polymers included AQ 109, AQ 110, AQ 194, AQ 200, AQ 314, and AQ 587 obtained from Aquamark Inc. (Chesterland, OH). The jar testing procedures described in the alum and lime-softening coagulation section were followed. Initial tests were conducted with polymer doses ranging from 10 to 100 mg/L without using any lime. We then investigated coagulation with multiple polymers, in which the primary polymer dose ranged from 10 to 100 mg/L and a secondary polymer, as a coagulation aid or flocculent, was dosed at 10 mg/L. From the preliminary screening, AQ 314 was selected as the primary polymer coagulant, whereas AQ 587 was tested as both a coagulant and flocculent. Polymer AQ 314 is a predominantly anionic polymer, whereas AQ587 is 60% cationic. Tables 2-1-13 to 2-1-16 present polymer dosages and resulting reductions in turbidity, along with the measured pH and conductivity values.

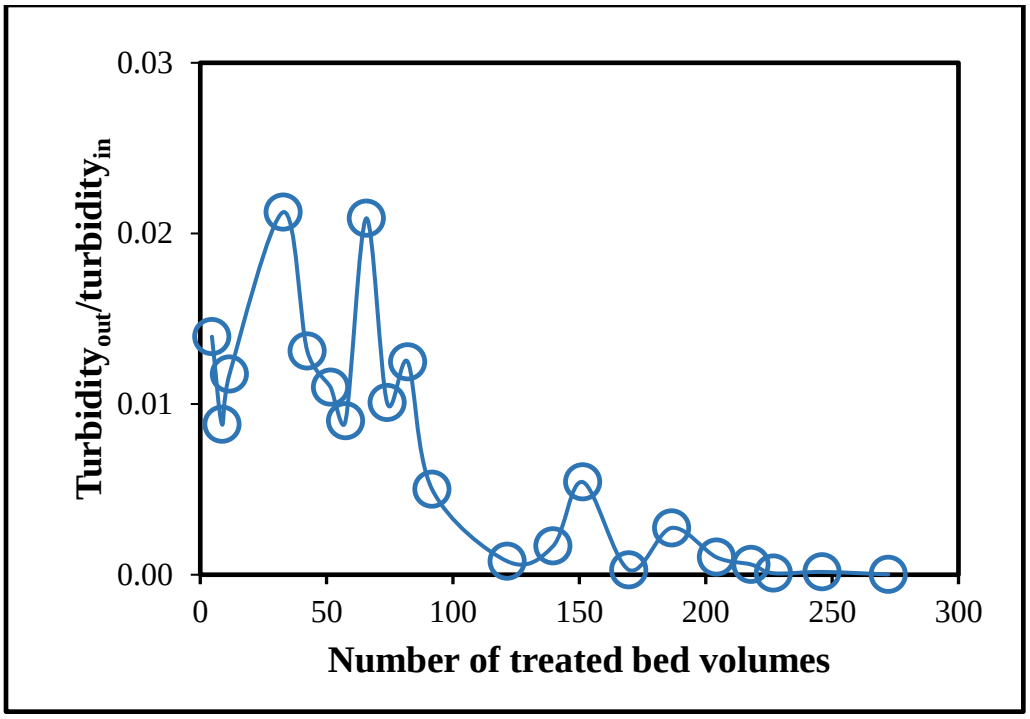

Figure 2-1-4 Effectiveness of sand filtration in removing residual turbidity from the coagulated and settled Mt. Simon brine.

Table 2-1-13 Jar test results for high-dose polymer coagulation with AQ 314. The initial pH was 4.69 and the initial conductivity was 193.6 mS/cm.

Turbidity, pH, and conductivity	AQ 314 dose (mg/L)					
	10	20	40	60	80	100
Initial turbidity (NTU)	502	502	502	502	502	502
Turbidity after 15 min (NTU)	30.1	37.3	46.4	53.4	59.3	63.6
Turbidity after 30 min (NTU)	28.9	35.6	46.8	52.3	57.6	62.4
Turbidity after 60 min (NTU)	29.7	34.5	45.1	51.7	54.3	64
Final pH	4.38	4.52	4.54	4.59	4.61	4.7
Final conductivity (mS/cm)	191.1	193.3	193	192.8	193.1	192.2

Table 2-1-14 Jar test results for high-dose polymer coagulation with AQ 587. The initial pH was 4.44 and the initial conductivity was 195.2 mS/cm.

Turbidity, pH, and conductivity	AQ 587 dose (mg/L)					
	10	20	40	60	80	100
Initial turbidity (NTU)	630	630	630	630	630	630
Turbidity after 15 min (NTU)	70.3	70.9	82.7	106	121	132
Turbidity after 30 min (NTU)	68.5	69.3	80.8	103	115	128
Turbidity after 60 min (NTU)	65.4	67	77	98.2	107	121
Final pH	4.24	4.32	4.38	4.40	4.40	4.43
Final conductivity (mS/cm)	192.2	192.2	191.6	191.3	190.7	191.3

Table 2-1-15 Jar test results for high-dose polymer coagulation with AQ 314 as the primary coagulant and AQ 587 as the flocculation aid. The initial pH was 4.58 and the initial conductivity was 200.6 mS/cm.

Turbidity (NTU)	AQ 314 dose/AQ 587 dose (mg/L)					
	10/10	20/10	40/10	60/10	80/10	100/10
Initial	542	542	542	542	542	542
After 15 min	33	36.1	43.9	50.4	55.1	65.7
After 30 min	31.9	34.8	43.1	50	54.9	63.6

Table 2-1-16 Jar test results for low-dose polymer coagulation with AQ 314 and AQ587 with no lime addition. The initial pH was 4.5 and the initial conductivity was 197.2 mS/cm.

Turbidity (NTU)	AQ314 dose/AQ587 dose (mg/L)					
	10/7.5	10/15	10/20	10/25	10/30	10/40
Initial	536	536	536	536	536	536
After 15 min	22.1	22.2	24.2	20.7	19.6	21.9
After 30 min	21.9	22.0	25	20.7	19.5	21.6

Experimental results of polymer coagulation in the 10–100 mg/L dose range indicate that the highest turbidity reduction (from 542 to 33 NTU) was achieved when an ~10 mg/L dose of AQ 314 was applied. The effluent turbidity could be further reduced to 22 NTU by a combination of 10 mg/L of AQ 314 and 7.5 mg/L of AQ 587. The results also suggest that the application of a lower polymer dose (10 mg/L or lower) might result in better turbidity removal. The addition of more polymer coagulant beyond 10 mg/L might result in coagulant overdosing, which causes charge reversal (from positive to negative or vice versa), resulting in restabilization of the suspended colloids and thus deteriorating the coagulation process and increasing the turbidity. Therefore, additional experiments were conducted to further investigate the impact of lower coagulant doses on brine turbidity and to find the optimal polymer dose.

The selected polymer coagulants were applied at lower dosage levels (0–10 mg/L) in the absence and presence of a fixed dose of lime (150 mg/L) to increase the pH of the brine sample to ~7.5. The pH change was not necessary for most polymer coagulants but it might be beneficial for precipitating metals during the coagulation stage or might be needed for the main stage desalination treatment. For each polymer used, experimental data were analyzed, and the effectiveness of each dose was evaluated. Experimental conditions, including types of selected polymers or polymer mixtures, polymer doses, and lime dose (if any), and results of the coagulation experiments are presented in Tables 2-1-17 to 2-1-22. The data confirmed that a lower polymer concentration between 0.5 and 8.5 mg/L without lime addition resulted in the best turbidity reduction in the polymer concentration ranges tested.

Table 2-1-17 Jar test results for low-dose polymer coagulation with AQ 314 and no lime addition. The initial pH was 4.5 and the initial conductivity was 195.4 mS/cm.

Turbidity (NTU)	AQ dose 314 (mg/L)					
	0.5	1	2	3.5	6.5	8.5
Initial	551	551	551	551	551	551
After 15 min	20.6	30.7	26.1	23.5	20.8	20.8
After 30 min	20.3	29.7	25.8	23.5	20.8	20.7

Table 2-1-18 Jar test results for low-dose polymer coagulation with AQ 314 and AQ 587 with no lime added. The initial pH was 4.5 and the initial conductivity was 197.2 mS/cm.

Turbidity (NTU)	AQ 314 dose/AQ 587 dose (mg/L)					
	5/5	10/5	15/5	5/10	10/10	15/10
Initial	616	616	616	616	616	616
After 15 min	20.3	21.0	21.9	23	19.2	22.3
After 30 min	20.6	20.5	21.4	22.9	19.6	21.8

Table 2-1-19 Jar test results for low-dose polymer coagulation with AQ 314 and with the addition of 150 mg/L of lime. The initial pH was 4.5 and the initial conductivity was 195.4 mS/cm. Lime addition increased the pH to >8.

Turbidity, pH, and conductivity	AQ dose 314/lime (mg/L)					
	0.25/150	0.5/150	1/150	2/150	7/150	10/150
Initial turbidity (NTU)	551	551	551	551	551	551
Turbidity after 15 min (NTU)	62.0	54.7	55.1	66.4	33.8	32.2
Turbidity after 30 min (NTU)	58	48.2	45.9	60.1	22.1	23.1
Final pH	8.39	8.48	8.58	8.56	8.58	8.63
Final conductivity (mS/cm)	186.8	189.5	190.9	190.7	190.8	191.1

Table 2-1-20 Jar test results for low-dose polymer coagulation with multiple polymers. No lime was added.

Turbidity (NTU)	AQ 314 dose/AQ 587 dose (mg/L)					
	5/5	10/5	15/5	5/10	10/10	15/10
Initial	551	551	551	551	551	551
After 15 min	20.6	30.7	26.1	23.5	20.8	20.8
After 30 min	20.3	29.7	25.8	23.5	20.8	20.7

Table 2-1-21 Jar test results for low-dose polymer coagulation with AQ 200 and with lime addition. The initial pH was 4.83 and the initial conductivity was 191.6 mS/cm. Lime addition increased the pH to >8.

Turbidity, pH, and conductivity	AQ 200 dose/lime (mg/L)					
	0/150	1/150	2/150	4/150	6/150	10/150
Initial turbidity (NTU)	620	620	620	620	620	620
Turbidity after 15 min (NTU)	89.4	89.3	101	86.8	104	66.6
Turbidity after 30 min (NTU)	92.3	89.8	104	87	105	67.9
Final pH	8.75	8.66	8.55	8.58	8.69	8.73
Final conductivity (mS/cm)	190.6	190.7	190.6	190.5	190	188.3

Table 2-1-22 Jar test results for low-dose polymer coagulation with AQ 587 and with lime addition. The initial pH was 4.83 and the initial conductivity was 191.6 mS/cm.

	AQ 587 dose/lime (mg/L)					
Turbidity (NTU)	**0/150**	**1/150**	**2/150**	**4/150**	**6/150**	**10/150**
Initial	613	613	613	613	613	613
After 15 min	100.5	242	229	212	213	209
After 30 min	102.1	240	229	209	209	205

The addition of the different polymers to the brine samples, without lime addition, had no significant impact on pH or conductivity. Polymer AQ 314 showed superior performance in reducing turbidity of the Mt. Simon brine sample in the presence and absence of the coagulation aid and lime. The turbidity of the brine sample was reduced from ~599 to 20.3 NTU with the addition of a small dose (0.5 mg/L) of AQ 314 with no lime addition. A relatively larger dose (7.0 mg/L) of the same polymer coagulant was needed to achieve the same turbidity level when lime was added. However, this dose was 20 times less than the required alum dose of 100 mg/L, which resulted in a significant reduction in sludge production. Polymer coagulants are known for their low effective dosages and the production of denser sludge. These properties usually result in substantial economic benefits. In general, polymer coagulation requires lower doses; however, relatively better turbidity reduction was achieved with alum and lime at significantly higher doses.

Pretreatment of Mt. Simon Brine, Stage 2

Stage 2 pretreatment experiments were conducted on samples that had already passed through the selected Stage 1 pretreatment process: alum coagulation, flocculation, lime softening, settling, and filtration through a 0.45-µm filter. In Stage 2, potential additional pretreatments were examined that might further reduce the concentrations of scale-forming species or dissolved organic carbon (DOC). Stage 2 pretreatment tests, which were conducted in parallel, included NF, ion exchange, and precipitative softening to further reduce the concentrations of scale-forming species, as well as adsorption with activated carbon to reduce the concentration of DOC.

Ion Exchange

The objective of the ion exchange treatment was to reduce the concentrations of scale-forming species, including Ca and Mg, which can cause a scaling problem during the desalination process. The following two ion exchange resins that are widely used in the water treatment industry were tested: a DOWEX MAC-3 weak acid resin and a DOWEX Marathon C strong acid resin, both manufactured by Dow Water & Process Solutions (Midland, MI) and obtained from Sigma-Aldrich (St. Louis, MO). The main characteristics of the two resins are listed in Table 2-1-23. The MAC-3 resin was treated with a 2 N NaOH solution to transform the resin from the H-form to the Na-form, and then washed extensively with deionized water.

Table 2-1-23 Characteristics of the ion exchange resins used for the Mt. Simon brine.

Characteristic	**MAC-3**	**Marathon C**
Type	Weak acid cation	Strong acid cation
Total exchange capacity, min (equiv/L)	3.8	2.0
Water content (%)	44–50	42–48
Particle density (g/mL)	1.18	1.28
Particle size	300–1,200 µm	585 ± 50 µm

The ion exchange equilibrium tests were conducted at about 23 °C (73.4 °F) by using the bottle-point technique, where each bottle provided one data point for the adsorption isotherm. Experiments were conducted by using varied amounts of ion exchange resins placed in 250-mL amber glass bottles with Teflon-lined closures. The bottles were tumbled for 3 days to ensure they reached equilibrium (Figure 2-1-5). At equilibrium, samples were filtered through a 0.45-µm filter and analyzed for Ca, Mg, and total hardness by inductive coupled plasma–optical emission spectroscopy (ICP-OES) method. Results are presented in Table 2-1-24. The maximum resin dose was calculated based on having enough ion exchange capacity in the added resin for 80%–90% removal of divalent cations. Mt. Simon brine contained about 1.22 equiv/L of divalent cations, which translated to a resin dose of up to 600 mg/L.

Figure 2-1-5 Ion exchange equilibrium test conducted by using a rotating tumbler.

Table 2-1-24 Results of the ion exchange experiments for Mt. Simon produced water.

Resin	**Dose (g/L)**	**Mg^{2+} (mg/L)**	**Ca^{2+} (mg/L)**	**Total hardness (mg/L of $CaCO_3$)**
Blank	0	1,940	21,708	12,462
MAC-3	342	1,357	12,663	7,457
MAC-3	264	1,508	14,573	8,543
MAC-3	291	1,648	16,583	9,628
MAC-3	113	1,769	18,794	10,854
Marathon C	583	1,045	7,065	4,392
Marathon C	440	1,296	10,352	6,221
Marathon C	325	1,467	12,764	7,588
Marathon C	230	1,628	15,276	8,965

The ion exchange results showed that the introduction of a high dose of the Marathon C resin (583 g/L) to the Mt. Simon brine sample resulted in Ca^{2+} and Mg^{2+} reductions of 67% and 46%, respectively, and a 65% reduction in total hardness (Table 2-1-24). When the MAC-3 resin was used at a dose of 342 g/L, the concentrations of Ca^{2+} and Mg^{2+} in the Mt. Simon brine sample were reduced by only 42% and 30%, respectively, corresponding to a total hardness reduction of 40%. These results were obtained when an unrealistically high dose of 583 g/L of Marathon C and 342 g/L of MAC-3 were applied. These results indicated that cation exchange resins, even when applied in very high doses, were inefficient for softening high-TDS Mt. Simon brine. This result was mainly due to the high TDS concentration (i.e., ~230,000 mg/L) and high Na content of the brine. In the ion exchange softening process, divalent cations in the water were exchanged with Na ions in the resin, and the high Na background of the high-TDS produced water limited the effectiveness of the ion exchange process.

Adsorption uptakes of Ca and Mg were calculated from Equation 2-1-2, where C_0 is the blank concentration, C_e the equilibrium concentration, v is the solution volume, and m is the resin mass:

$$q_e = \frac{(C_0 - C_e)v}{m} \qquad \text{(Equation 2-1-2)}$$

The Ca^{2+} and Mg^{2+} adsorption equilibrium data were fitted to the Langmuir adsorption model:

$$q_e = q_{max} \frac{b\,C_e}{1 + b\,C_e} \qquad \text{(Equation 2-1-3)}$$

where b is the equilibrium constant for distribution of the adsorbate between the surface and the aqueous phase and q_{max} is the maximum monolayer coverage.

Fitting the ion exchange isotherm data into adsorption models is useful for comparing the adsorption performance of different resins and predicting the adsorption uptake at other equilibrium concentrations, in the absence of experimental data. As an example, Figure 2-1-6 illustrates the linear fit of the Ca^{2+} and Mg^{2+} ion exchange adsorption data for the Mt. Simon brine to the Langmuir adsorption model.

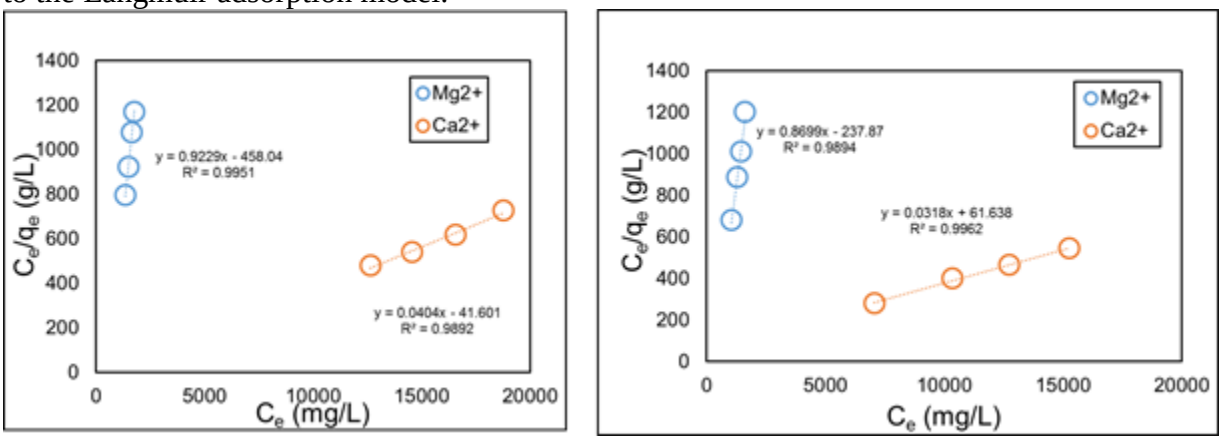

Figure 2-1-6 Langmuir isotherm fit for the adsorption of Mg^{2+} and Ca^{2+} from Mt. Simon produced water onto ion exchange resins (left, MAC-3; right, Marathon C).

Precipitative Softening

Chemical precipitation is the most common softening method used in water treatment. It involves addition of lime and soda ash (sodium carbonate, Na_2CO_3) to reduce water hardness. The main objective of the precipitative softening work was to assess the impact of lime and soda ash addition on the precipitation of divalent cations, namely Ca^{2+} and Mg^{+2}, and the reduction of total hardness. Carbonated hardness is usually due to the presence of bicarbonates of Ca and Mg, whereas noncarbonated hardness is due to the presence of chlorides and sulfates of Ca and Mg. When lime is added, it reacts with dissolved CO_2 and divalent cations until all available bicarbonates are consumed:

$$CO_2 + CaO \leftrightarrow CaCO_3, \quad \text{(Reaction 2-1-2)}$$

$$Ca^{2+} + 2HCO_3^- + Ca(OH)_2 \leftrightarrow 2CaCO_3 + 2H_2O, \quad \text{(Reaction 2-1-3)}$$

$$Mg^{2+} + 2HCO_3^- + 2Ca(OH)_2 \leftrightarrow Mg(OH)_2 + 2CaCO_3 + 2H_2O, \quad \text{(Reaction 2-1-4)}$$

$$MgCO_3 + CaO + H_2O \leftrightarrow Mg(OH)_2 + CaCO_3. \quad \text{(Reaction 2-1-5)}$$

The Ca^{2+} and Mg^{2+} concentrations are significantly higher than the bicarbonate concentration in Mt. Simon brine; thus, lime addition alone would not be effective in reducing the concentration of Ca^{2+}. A high dose of soda ash was needed for a significant reduction in Ca concentration. Soda ash is assumed to react with Ca^{2+} according to the following reactions:

$$Ca^{2+} + SO_4^{2-} + Na_2CO_3 \leftrightarrow CaCO_3 + 2Na^+ + SO_4^{2-}, \quad \text{(Reaction 2-1-6)}$$

$$Ca^{2+} + 2Cl^- + Na_2CO_3 \leftrightarrow CaCO_3 + 2Na^+ + 2Cl^-. \quad \text{(Reaction 2-1-7)}$$

To evaluate the performance of lime–soda ash softening, seven jar tests were carried out using Mt. Simon brine in the presence of different lime doses (20–1,200 mg/L) and a fixed dose of 13,800 mg/L of soda ash. One jar test was used as a blank and was treated like the other jars with no lime or soda ash added. The jar test experiments for a single-stage softening process were conducted using a procedure similar to that described in Stage 1 experiments, except that rapid mixing was applied for 10 min and no slow mixing was applied. The filtered supernatant liquid was sent to Actlabs for Ca and Mg concentration measurement and hardness analysis.

The moles of lime needed to precipitate each mole of carbonate hardness can be determined according to Reactions 2-1-2 to 2-1-5. On the basis of Reactions 2-1-2 and 2-1-3, each mole (mol) of CaO can remove 1 mol of carbonate hardness or 1 mol of carbonic acid (H_2CO_3). Furthermore, 2 mol of CaO is needed to remove 1 mol of magnesium carbonate ($MgCO_3$) hardness. The same approach can be used to calculate the required soda ash dose. The molar ratio of $NaCO_3$ to hardness is determined from Reactions 2-1-6 and 2-1-7, assuming that the Mt. Simon brine contains $CaSO_4$ and $CaCl_2$. For both reactions, 1 mol of soda ash is needed for each mole of noncarbonate hardness removal. Jar test results confirmed that chemical precipitation was effective in hardness removal from Mt. Simon brine (Table 2-1-25).

Table 2-1-25 Impact of lime soda ash softening on scale-forming species in Mt. Simon brine.

Lime dose (mg/L)	Soda ash dose (mg/L)	Final pH	Mg (mg/L)	Ca (mg/L)	Hardness (mg/L)	Mg removal (%)	Ca removal (%)	Hardness reduction (%)
0	0	5	1,990	21,708	57,200	N/A	N/A	N/A
1,200	13,800	11.44	<10	12,599.5	28,300	>99	42	51
600	13,800	11.10	<10	12,376.5	27,700	>99	43	52
300	13,800	10.83	<10	12,153.5	27,200	>99	44	53
100	13,800	10.57	35.68	12,265	27,500	98	44	52
50	13,800	10.50	49.06	12,265	27,500	97	44	52
20	13,800	10.70	50.96	12,376.5	27,800	97	43	51

The concentration of Mg^{2+} in Mt. Simon brine was ~2,000 mg/L and could be reduced to <10 mg/L when a lime dose of ~300 mg/L was used (>99% removal). However, the initial Ca^{2+} concentration was very high (~ 22,000 mg/L). Moreover, the alkalinity value of Mt. Simon brine was low (21 mg/L), which indicated that the concentration of the carbonated hardness was very low (~21 mg/L) compared with the noncarbonated hardness (~57,200 mg/L). To overcome this obstacle, a high dose of soda ash (13,800 mg/L) was added to increase the carbonate concentration and precipitate more calcium carbonate ($CaCO_3$). This dose resulted in 44% Ca removal. These results suggest that the addition of lime was not necessary for the removal of hardness from the Mt. Simon sample; however, an elevated dose of soda ash was required.

We also conducted an experiment using only caustic soda (NaOH) with no additional chemical additives to investigate the impact of pH change on softening. The Mt. Simon brine sample was mixed for 10 min after the addition of a premeasured amount of 10 N NaOH to increase the sample pH to 11.4. Precipitates were allowed to settle for 15 min, and then the supernatant liquid was filtered through a 0.45-μm filter and analyzed. As expected, the pH increase of the Mt. Simon brine sample to 11.4 resulted in a significant reduction in Mg^{2+} concentration from 1,990 to <10 mg/L. A slight decrease in concentration of other divalent cations was also observed: Ca^{2+} concentration reduced from 19,700 to 17,500 mg/L and Sr^{2+} reduced from 751 to 620 mg/L. Total hardness was reduced by 24% (from 57,400 to 43,700 mg/L), compared with a 51% reduction by the soda ash treatment at the same pH of 11.4 (Table 2-1-25). These results indicated that although pH adjustment was sufficient for near-complete precipitation of Mg, soda ash treatment was needed for a more effective reduction of Ca^{2+} ions in the Mt. Simon brine.

From a practical point of view, a two-stage softening process may be needed for large-scale Mt. Simon brine softening. Caustic soda can be added at the first stage to remove Mg^{2+}, followed by recarbonation by bubbling CO_2 gas to increase brine alkalinity, which is needed for Ca^{2+} precipitation. A smaller soda ash dose can then be applied in the second stage for Ca^{2+} precipitation, followed by recarbonation for pH adjustment.

Nanofiltration

Nanofiltration was evaluated as an alternative method for water softening. Nanofiltration treatment was conducted using a laboratory scale, 316 stainless steel (316SS), and SEPA CF II cross-flow filtration unit obtained from Sterlitech Corporation (Kent, WA). The system is depicted in Figure 2-1-7. The active cross-sectional area of the membranes is 139 cm^2 (54.8 in.), and the maximum operating pressure of the system is 69 bar (1,000 psia). The pump and control valve regulate pressure across the membrane. A membrane sheet was cut to fit the membrane holder and

then soaked in ultrapure water for at least 24 h. The membrane was then compacted with ultrapure water at the operating pressure for 3 h for the produced water experiment. Pretreated brine (with doses of 143 mg/L of lime and 100 mg/L of alum, settled and filtered) with turbidity less than 0.02 NTU was then pumped through the system for 1 min to flush out the residual water. After the residual water was fully removed, the pressure and flow rate were increased to operating conditions of 50–200 psi. The feed to the NF system was operated in a closed-loop configuration. Permeate was either removed from the system (standard mode) or returned to the feed tank (recycle mode). At the conclusion of each experiment, final feed loop and permeate concentrations of Ca, Mg, and total hardness were measured (Table 2-1-26). The membrane filtration system was cleaned thoroughly with tap water after each experiment, followed by a dilute phosphoric acid (H_3PO_4) solution wash and a final rinse with ultrapure water until the conductivity of the outlet was equal to that of the inlet.

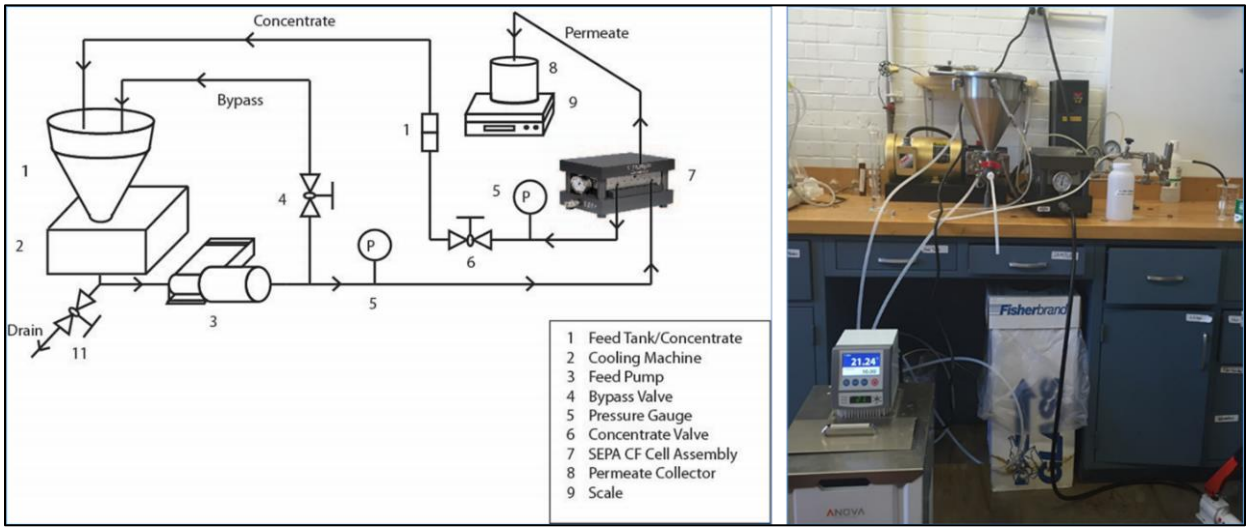

Figure 2-1-7 Schematic diagram and photograph of the NF bench-scale setup.

Two types of NF membranes were tested for pretreating Mt. Simon brine: a Dow FILMTEC™ NF270 flat sheet membrane and a Dow FILMTEC™ NF90 membrane. The NF90 membrane was designed and manufactured to achieve a high removal of salts, nitrate, iron, and organic compounds from feed water. The NF270 membrane is designed to remove a high percentage of large molecular weight species while allowing passage of a medium to high percentage of salt (NaCl and KCl) and a medium percentage of hardness (divalent cations). The NF90, on the other hand, is designed for high salt rejection.

The permeate flow rate and conductivity were monitored. A 100-mL quantity of permeate was collected and subjected to hardness species analysis. Salt rejection was calculated based on conductivity according to the following equation:

$$Salt\ rejection = 1 - \frac{conductivity_{out}}{conductivity_{in}}. \quad \text{(Equation 2-1-4)}$$

A low flux of about 0.22 L/m^2/h was observed when the high-rejection NF90 membrane was used at the highest operating pressure of 200 psi (Figure 2-1-8). The salt rejection was very

low, at 14.45% (Figure 2-1-9). The highest flux obtained with the NF270 membrane was 10 L/m^2/h, with salt rejection of 8.5%. As expected for the Mt. Simon brine with a high TDS value of about 230,000 mg/L, the low flux observed for the NF90 membrane was due to the high osmotic pressure, which exceeded the operating pressure of 200 psi. The low salt rejection was likely due to the concentration polarization phenomenon. Table 2-1-26 illustrates the effectiveness of the two selected membranes in removing divalent cations. The NF270 membrane at an operating pressure of 200 psi removed ~44% Mg and ~20% Ca from the permeate, which resulted in a 22% total hardness reduction. The removal of Ca was further enhanced to 98% when the NF90 membrane was used; however, the rejection of Mg was reduced to 35%. The experimental data also showed that the total hardness of the Mt. Simon brine could be reduced by 55% by NF when using an NF90 membrane at 200 psi.

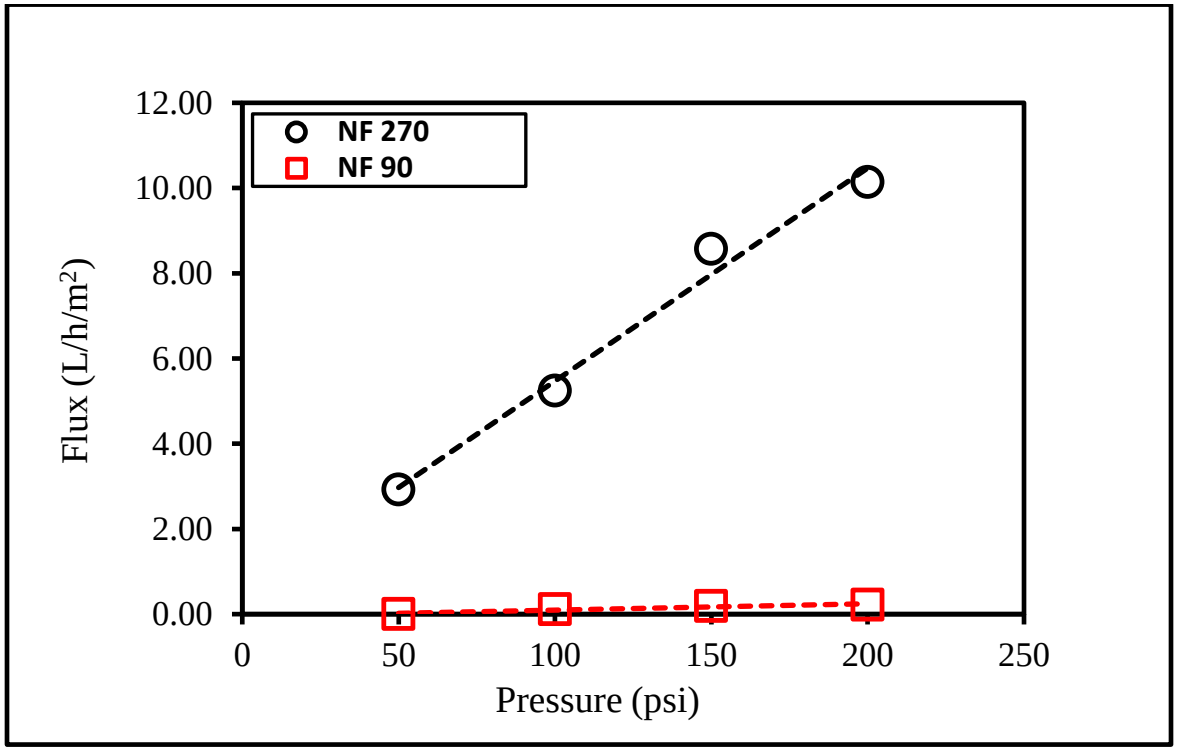

Figure 2-1-8 Water flux of the NF experiments with the Mt. Simon brine feed.

Dissolved Organic Carbon Adsorption by Activated Carbon

Adsorption with activated carbon was investigated as a means of reducing dissolved organic carbon (DOC) concentration in brine. Adsorption isotherms of DOC uptake from Mt. Simon brine (after Stage 1 pretreatments with coagulation/flocculation, sedimentation, and filtration) were measured using 0.04–10 g/L of activated carbon at 22°C (68°F). The activated carbon samples used were F400 (obtained from Calgon Carbon Corporation, Pittsburgh, PA) and AC (obtained from Carbon Enterprises, Inc., Circleville, OH). Both activated carbons are coal based, but F-400 is a microporous activated carbon with a surface area of ~900 m^2/g (9688.5 ft^2/g) that is widely used for drinking water treatment, and AC is a mesoporous activated carbon with surface area of ~300 m^2/g (3229.5 ft^2/g) and is recommended for treatment of oilfield produced water. Both activated carbons had similar particle sizes (20 × 50 mesh or 0.30–0.84 mm).

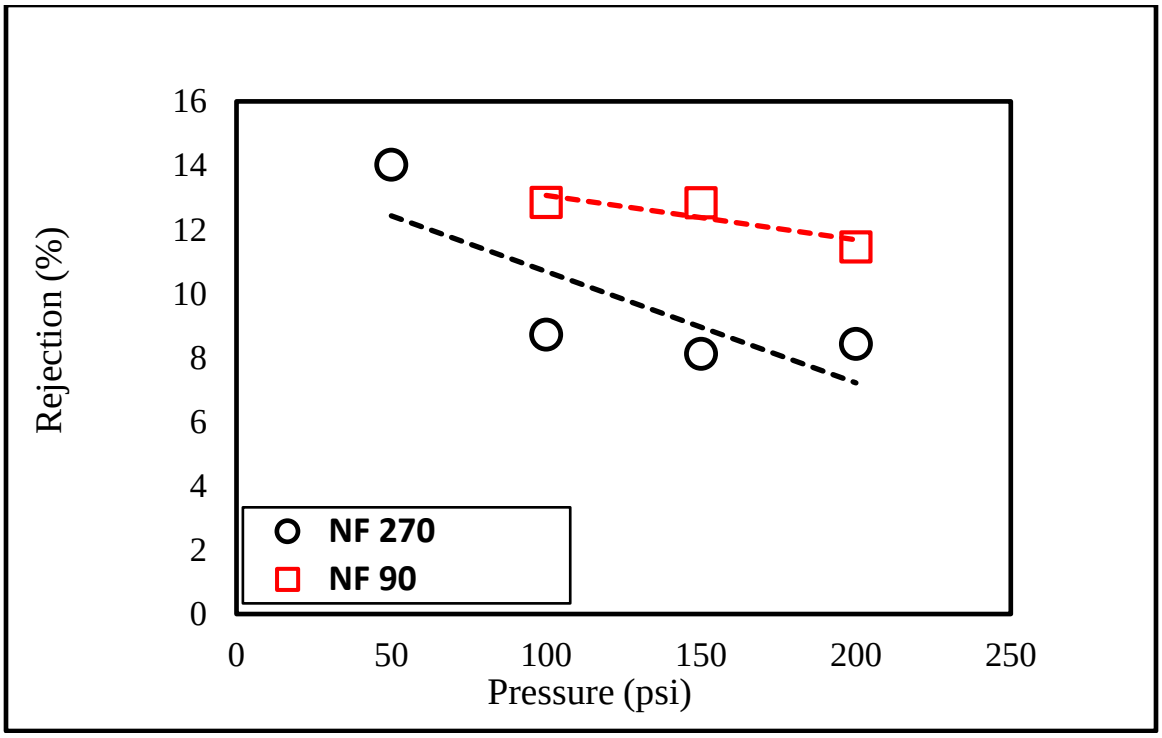

Figure 2-1-9 Salt rejection of the NF experiments with the Mt. Simon brine feed.

Table 2-1-26 Mg, Ca, and total hardness removal from Mt. Simon brine by NF based on differences in their respective concentrations in the feed loop and the permeate at the conclusion of the NF experiment.

Membrane	Mg (mg/L)	Ca (mg/L)	Total hardness (mg/L of $CaCO_3$)	Removal (%)		
				Mg	Ca	Hardness
NF270-permeate	837.42	15,400	42,738	44	20	22
NF270-feed	1,499.40	19,000	54,468	N/A		
NF90-permeate	693.35	368	25,235	35	98	55
NF90-feed	1,060.80	16,700	46,920	N/A		

Adsorption isotherms of DOC uptake from the Mt. Simon are shown in Figure 2-1-10. As indicated by the low initial slopes of the isotherms, both tested activated carbons did not have a high affinity for the removal of dissolved organics from the Mt. Simon brine. This is unlike the typical isotherms for DOC removal from drinking water sources (e.g., surface water or groundwater), which exhibit a high initial slope and high adsorption affinity. The high salt background of the produced water samples and molecular characteristics of DOC species in the Mt. Simon brine might significantly affect interaction of DOC species with the activated carbon surface and control the adsorption phenomenon. Both tested activated carbons had similar uptakes up to the equilibrium concentration of ~30 mg/L, after which there was a significant increase in the adsorption uptake by the AC carbon at higher concentrations. This might have been due to the larger pores of the AC carbon being more accessible to large molecules.

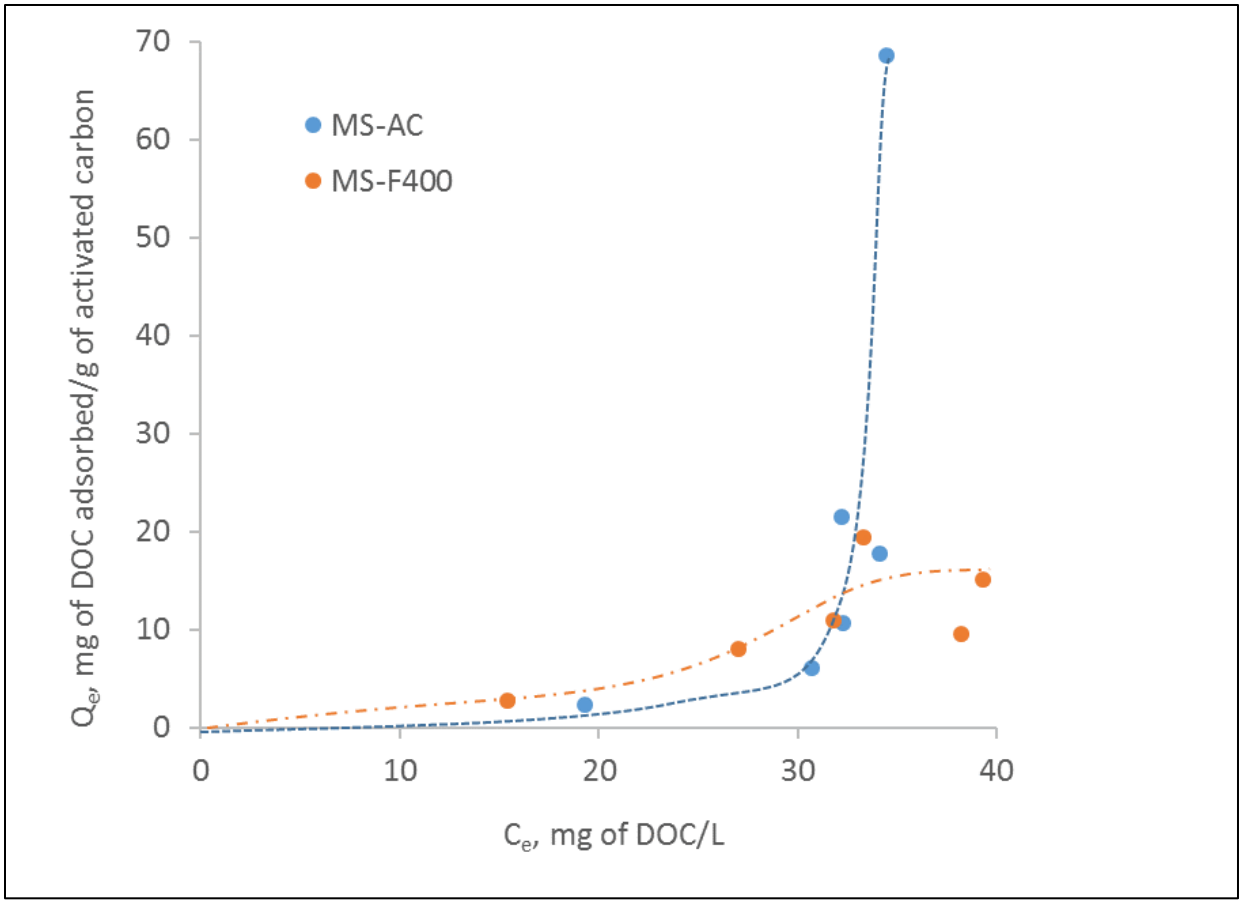

Figure 2-1-10 Adsorption isotherms of dissolved organic carbon (DOC) from coagulated and filtered Mt. Simon brine by the F400 and AC activated carbons. MS, Mt. Simon brine.

Desalination of Mt. Simon Brine by Direct Contact Membrane Distillation

We investigated the treatment of the pretreated Mt. Simon brine by the direct contact membrane distillation (DCMD) technology, using a commercial polymeric (Teflon) membrane, TF200, obtained from the Pall Corporation (Cortland, NY). Membrane distillation is an emerging technology, and it is promising for desalting highly saline waters. This technology is a thermally driven separation process in which only vapor passes through the hydrophobic membrane pores. Mass transfer of water vapor through the membrane is driven by the vapor pressure difference resulting mainly from the temperature difference across the membrane (i.e., the feed and permeate sides). Direct-contact membrane distillation has a configuration in which liquids are in direct contact with both sides of the membrane. Figure 2-1-11 shows a schematic diagram of the bench-scale DCMD experimental setup used in this investigation.

The membrane holder, illustrated in Figure 2-1-11, is designed for testing 1-in.-diameter membranes and consists of two stainless steel compartments. The top and bottom compartments are separated by the tested membrane. Each 1-in.-diameter membrane has an effective area of 2.8 cm^2 (1.1 in) and is sealed in the membrane holder by using proper O-rings. Feed and permeate solutions were circulated at a fixed cross-flow rate of 100 mL/min by using peristaltic pumps. The feed solution contained pretreated Mt. Simon brine (coagulated and filtered) at ~70 ± 2°C (158°F ± 2°F), and a premeasured amount of deionized water at ~5 ± 1°C (41°F ± 1°F) was used as a

permeate solution. The salt concentration was measured by a Thermo Scientific Orion STAR A322 conductivity meter (Thermo Scientific, Waltham, MA) equipped with a Thermo Scientific Orion conductivity cell. To promote mixing of the solutions and prevent concentration and heat polarization, stainless steel membrane spacers were used in the feed and permeate solution channels.

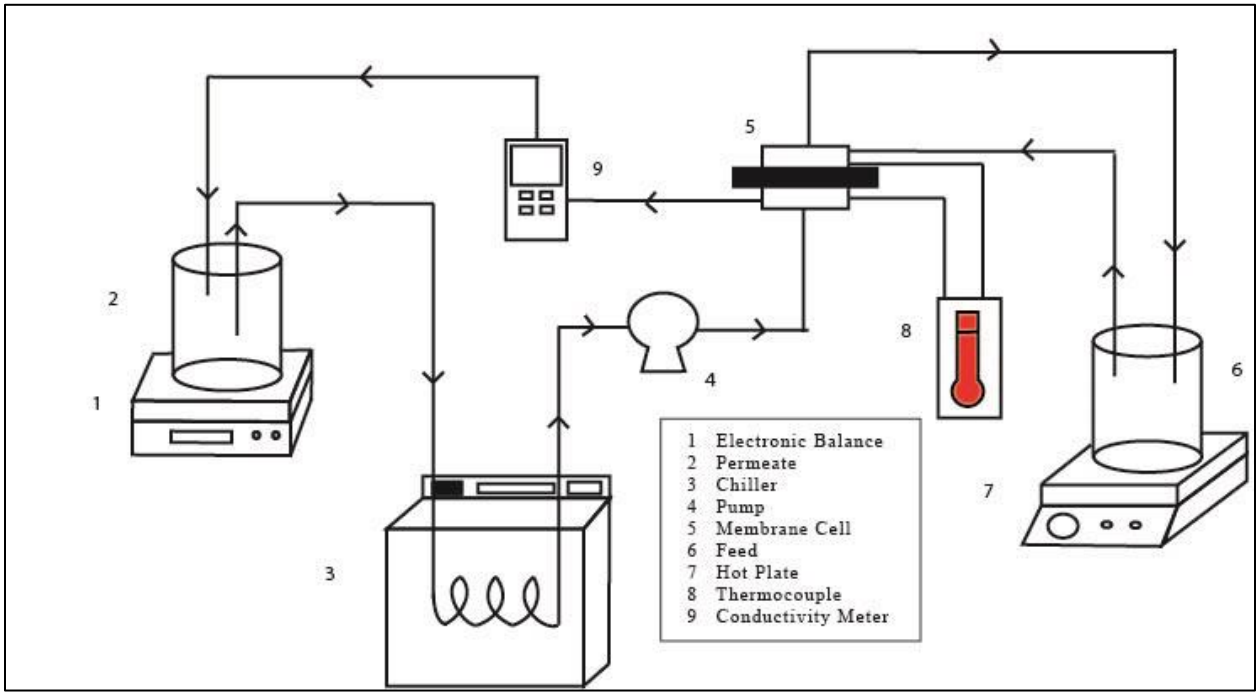

Figure 2-1-11 Bench-scale DCMD experimental setup.

Water flux was obtained by measuring the increase in weight of permeate solutions with an electronic balance. The reported flux values were averaged over the entire duration of the experiments. The water flux, J_w (kg/m^2/h), through the membrane was calculated by

$$J_w = \frac{\frac{\Delta M}{\rho}}{A\,\Delta t}, \qquad \text{(Equation 2-1-5)}$$

where ΔM refers to the change in mass of the feed solution with time Δt, ρ is the density of water (assumed as 1.0 g/cm^3), and A is the effective area of the membrane. The NaCl rejection fraction (R) was calculated by

$$R = 1 - \frac{\Delta C \cdot Df}{Ct}, \qquad \text{(Equation 2-1-6)}$$

where ΔC refers to the change in salt concentration (or conductivity) of the permeate solution, Df is the dilution factor on the permeate side, and Ct is the final salt concentration of the feed.

The DCMD experiments were conducted in triplicate to ensure the reproducibility of the results. Figure 2-1-12 presents the average flux and permeate conductivity values obtained from the DCMD experiments conducted with pretreated Mt. Simon brine (Stage 1 pretreatments with 143 mg/L of lime and 100 mg/L of alum applied) with an initial conductivity of ~193 mS/cm.

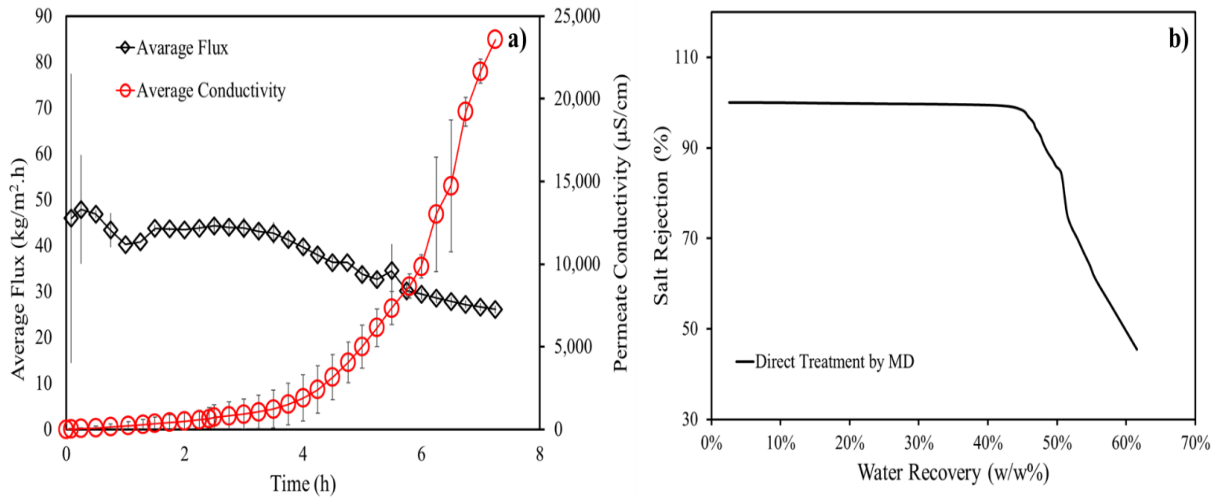

Figure 2-1-12 Average flux and permeate conductivity values in the DCMD treatment of pretreated Mt. Simon brine (left) and salt rejection vs. water recovery (right).

Membrane distillation results showed a high salt rejection of more than 99% during the first 3 hours of the tests. However, the salt rejection and the average flux declined continuously with time. This adverse effect may be attributed to the increase in feed concentration with time. When the TDS concentration of the feed brine was near the saturation level, salt crystals could have been deposited on the surface of the membrane. A more concentrated brine could also result in the formation of a concentration boundary layer (concentration polarization), which would change the water activity and viscosity. A scanning electron microscopy (SEM) instrument equipped with energy-dispersive X-ray spectroscopy (EDS) instrument was used to examine the used TF200 membranes. Figure 2-1-13 presents a comparison between the SEM image of the new, as-received TF200 membrane (a), and the SEM image of the TF200 membrane used to treat the Mt. Simon brine sample (b). The SEM images clearly show that membrane fouling resulted from the deposition of salts on the surface of the used membrane. This result was further investigated by elemental analysis using the SEM-EDS technique. The SEM-EDS analysis indicated that the deposited salts consisted of several elements (Figure 2-1-13, panels c and d); however, iron and manganese were dominant.

Cost Estimations for High-TDS Brine Treatment

Trimeric performed cost estimations for the high-TDS brine treatment. The company estimated the cost of brine pretreatment, partial water recovery by mechanical vapor recompression (MVR), evaporation, and a near-zero liquid discharge (near-ZLD) process by multiple-effect evaporation (MEE) with 88% water recovery. The brine composition data used for the Trimeric treatment simulation were based on a Mt. Simon brine sample similar to that described in Table 2-1-6.

Brine Pretreatment Process

Figure 2-1-14 shows a process flow diagram (PFD) of a proposed system to treat 2,000 gpm (7.6 m^3/min) of Mt. Simon brine for TSS removal, and the corresponding material flows are displayed in Figure 2-1-15. The system includes lime addition, at the rate of 143 mg/L of feed

water, to raise the pH slightly (to about 8), precipitate some of the metals, and encourage solids coagulation. The addition of a polymer flocculant at a rate of 5 mg/L is also included to enhance solids flocculation, settling, and removal by filtration. The primary equipment in the system is a conventional flocculation and clarification vessel. Construction primarily of 316SS is assumed because of the corrosive nature of the brine. This material selection is preliminary, and further work will be required to confirm the proper material of construction for this application as the design of the project advances. More expensive alloys may be required in some sections of the process; conversely, it may be possible to use less expense coated carbon steel or fiberglass in some parts of the process. Detailed consideration of materials of construction, possibly including corrosion tests, should be considered in the future to determine the proper choices for materials.

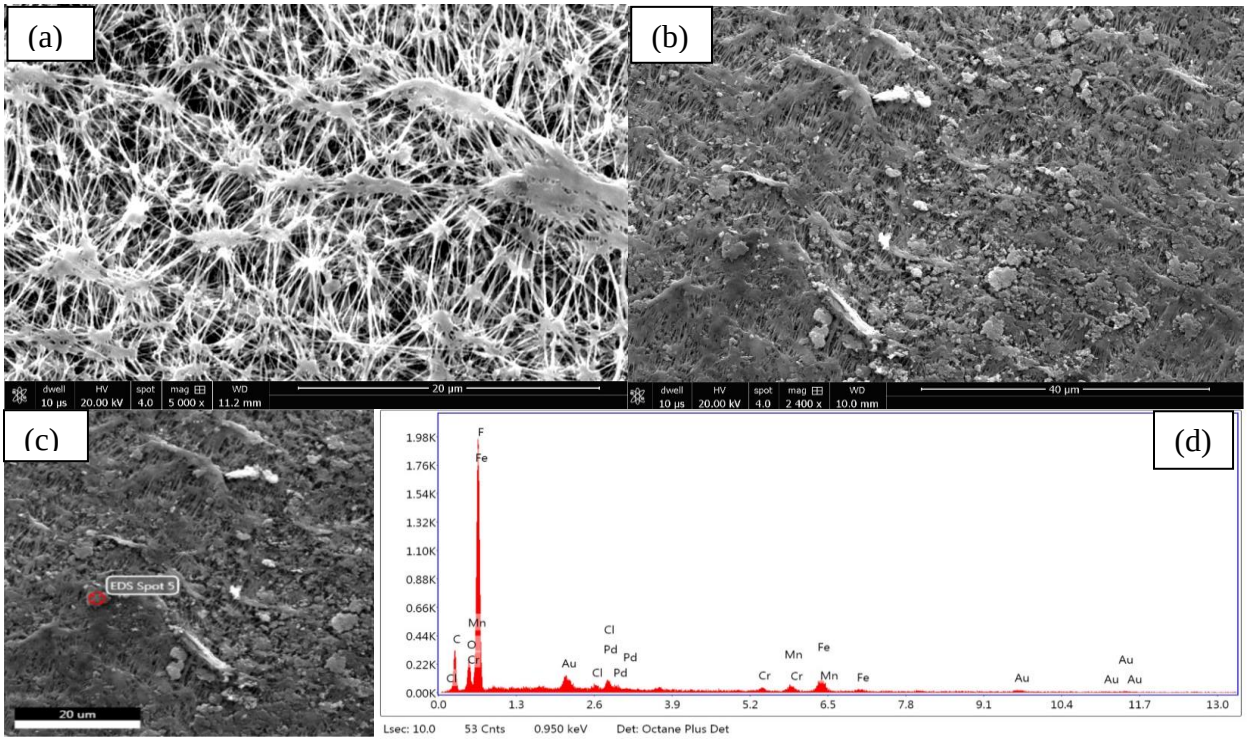

Figure 2-1-13 Scanning electron microscopy (SEM) images of the new (a) and used (b) TF200 membranes along with an energy-dispersive X-ray spectroscopy (EDS) elemental analysis (c and d).

The system includes a lime slurry preparation system, which includes lime storage bins, conveyor feeders, and a slurry mix tank. The lime slurry and a small amount of flocculant are fed to the flocculation and clarification vessel. The sludge from the underflow of the clarification vessel is fed to a rotary vacuum drum filter, with the wet cake collected in bins for landfill disposal. The overflow from the flocculation and clarification vessel is pumped through a hydrocyclone to remove the majority of suspended solids that were not removed in the clarification vessel. The slurry underflow from the hydrocyclone is returned to the clarification vessel.

The hydrocyclone overflow is referred to as “pretreated brine” and is mostly free of suspended solids. This pretreated brine could be the feed material to other processing systems focused on recovering water and salts from the brine or otherwise disposing of the water, such as by injection.

It is assumed that the complete softening of the brine (e.g., the removal of all the Ca and Mg from the feed) is not required. Although the moderate lime addition rate (143 mg/L) results in enhanced clarification and precipitation of some metals, the pretreated brine contains very high concentrations of Ca. The laboratory work discussed earlier in this report demonstrates that the use of ion exchange and NF are not practical options for the removal of Ca and Mg from the brine. The use of additional lime and soda ash to increase the pH to >10 can complete the softening process.

The presence of large amounts of Ca cation has an effect on the desalination processes. For example, the solubility of calcium chloride ($CaCl_2$) and its saturation boiling temperature are much higher than that of NaCl. As a result, the presence of large amounts of Ca in the brine practically reduces the effectiveness of evaporative crystallization processes for very high water recovery, or ZLD, because of the high temperatures and low pressures required for $CaCl_2$ evaporative crystallization. The removal of Ca during the pretreatment stage could be used to more easily achieve ZLD in an evaporative crystallization process, as well as to produce a purer NaCl salt product.

Cost estimation data for the pretreatment system are shown in Figure 2-1-16. Capital cost estimates were derived primarily from Aspen Capital Cost Estimator software. The costs are based on the first quarter of 2015.

The largest capital cost item is the flocculation and clarification vessel (T-1210). This is a standard open-top clarifier with a mixed flocculation section. Other technology options are available for completing this task with smaller footprint equipment, such as systems that use vanes to enhance particle settling in a smaller area. Further testing of the brine would be required to determine the suitability of different equipment configurations for this application.

Figure 2-1-17 gives the capital and operating costs for the 2,000 gpm case, based on the purchase cost of the necessary equipment for the pretreatment. Additionally, the design and cost information generated for the 2,000 gpm case were used to estimate the costs of three other cases: 500, 585, and 5,000 gpm of feed. The information for these alternate cases is also shown in Table 2-1-27.

Brine Treatment with MVR to Recover 10% of Water

Figure 2-1-18 presents a schematic diagram of a proposed system to recover approximately 10% of the water from a 2,000 gpm pretreated brine stream as a purified product. An approximate material balance is shown in Figure 2-1-19. The system uses a single-stage MVR system to distill water from the brine. Approximately 233 gpm of purified water is recovered.

Mt. Simon brine, containing approximately 20 wt% TDS, is first subjected to pretreatment to remove TSS (discussed previously). The brine is then pumped to an MVR package unit after first going through an exchanger (E-2110) to preheat the feed. The heated feed is then separated from any noncondensable gases in a separator drum (D-2101) and sent to a recirculating evaporator vessel (EV-2201). In the evaporator vessel, the feed brine is partially evaporated by exchanging heat with condensing water vapor from the compressor. Concentrated brine is pumped from the evaporator back through the E-2110 and exits the MVR package unit. Vapor, which is primarily water with a small amount (roughly 350 ppmv) of hydrogen sulfide (H_2S), exiting the evaporator will be treated for H_2S removal in a caustic scrubber column (V-2301); the H_2S must be removed from the vapor because it would otherwise become a contaminant in the recovered water.

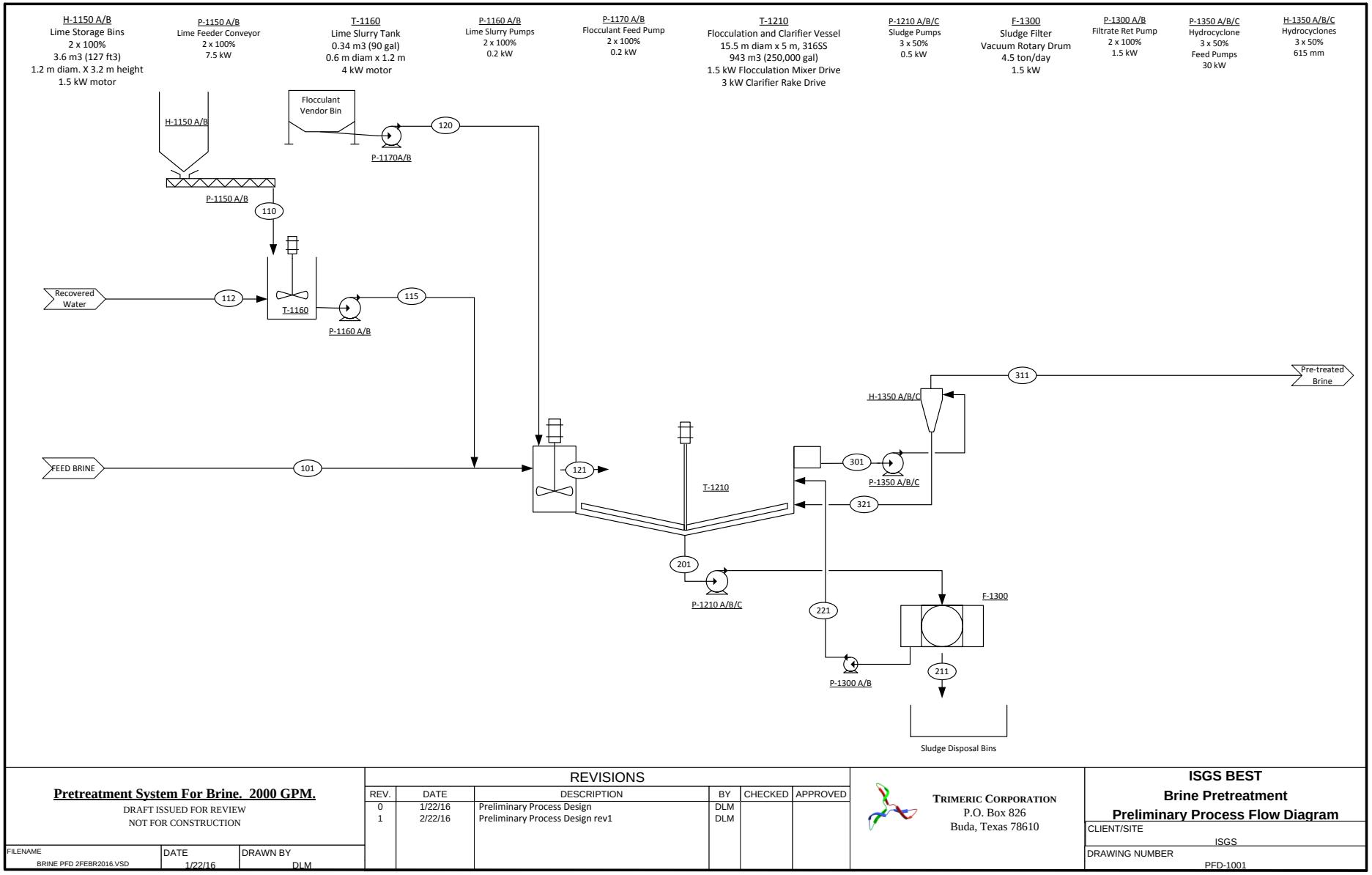

Pretreatment System For Brine. 2000 GPM.
DRAFT ISSUED FOR REVIEW
NOT FOR CONSTRUCTION

FILENAME	DATE	DRAWN BY
BRINE PFD 2FEBR2016.VSD	1/22/16	DLM

REVISIONS

REV.	DATE	DESCRIPTION	BY	CHECKED	APPROVED
0	1/22/16	Preliminary Process Design	DLM		
1	2/22/16	Preliminary Process Design rev1	DLM		

TRIMERIC CORPORATION
P.O. Box 826
Buda, Texas 78610

ISGS BEST
Brine Pretreatment
Preliminary Process Flow Diagram

CLIENT/SITE: ISGS
DRAWING NUMBER: PFD-1001

Figure 2-1-14 PFD for the brine pretreatment system.

APPROXIMATE PROCESS MATERIAL BALANCE **ISGS BEST**
BRINE PRETREATMENT SECTION **REV 2. 26 SEPTEMBER 2016**

MAIN PROCESS STREAMS

Stream Number		101		121		311	
Stream Name		Feed		Lime-Treated Feed		Clarified, Lime-Treated Feed	
	Phase	Liquid (thin slurry)		Liquid (thin slurry)		Liquid	
Temperature	C	32		32		32	
Pressure	bar(a)	1.1		1.01		1.01	
Flowrate	lpm	7,571		7,575		7,548	
Flowrate	gpm	2,000		2,001		1,994	
Flowrate	kg/h	513,302		513,574		511,756	
Liq Density	g/mL	1.13		1.13		1.13	
pH		6.4		8		8	
TSS	mg/L	2,831		2,831		28	
	kg/h	1,286		1,286		13	
TDS	mg/L	197,079		197,142		197,142	
	kg/h	89,523		89,599		89,504	
Water by diff	wt%	82.3		82.3		82.5	
	kg/h	422,493		422,689		422,239	
Cationic species	MW	mmol/L	mg/L	mmol/L	mg/L	mmol/L	mg/L
Na+	22.99	2088	48,000	2088	48,000	2,088	48,000
Ca++	40.08	549	22,000	553	22,150	553	22,150
K+	39.10	90	3,500	90	3,500	90	3,500
Mg++	24.31	61.72	1,500	61.72	1,500	61.72	1,500
Fe+++	55.85	0.91	50.8	0.91	51	0.91	51
NH4+	18.04	0.73	13.2	0.73	13.2	0.73	13.2
Mn++	54.94	1.31	72.0	1.31	72.0	1.31	72.0
Al+++	26.98	0.02	0.54	0.02	0.54	0.02	0.54
Zn++	65.39	0.03	2.0	0.03	2.0	0.03	2.0
Li+	6.94	3.30	22.9	3.30	22.9	3.30	22.9
B+++	10.81	1.54	16.6	1.54	16.6	1.54	16.6
Ba++	137.33	0.02	2.7	0.02	2.7	0.02	2.7
Sr++	87.62	9.03	791	9.03	791	9.03	791
sum of cations		2,805	75,972	2,809	76,122	2,809	76,122
Anionic species	MW	mmol/L	mg/L	mmol/L	mg/L	mmol/L	mg/L
Cl-	35.45	3,380	119,830	3,380	119,830	3,380	119,830
SO4--	96.06	3.8	360.2	3.8	360.2	3.8	360.2
CO3--	60.01	0.92	55.21	low	low	low	low
Br-	79.90	8.26	660	8.26	660	8.26	660
NO3-	62.00	0.06	3.72	0.06	3.72	0.06	3.72
S--	32.07	5.15	165.14	5.15	165.14	5.15	165
Se--	78.96	0.0003	0.02	0.0003	0.02	0.0003	0.02
sum of anions		3,398	121,074	3,397	121,019	3,397	121,019

ADDITIVE STREAMS

Stream Number	110	112	115	120
Stream Name	Lime	Recovered Water	Lime Slurry	Flocculant
Phase	Solid	Liquid	Liquid (thick slurry)	Liquid
Flowrate, kg/h	65.0	195	260	2.3
SG		1	1.2	1
Composition	CaO	Water	25% Ca(OH)2 in water	Polymer solution
Comment	Dosage: 143 mg/L	Lime Slurry	25% slurry	Dosage: 5 mg/L

SLUDGE REMOVAL STREAMS

Stream Number		201	211	221
Stream Name		Sludge Slurry to Filter	Sludge Cake	Centrate Return
	Phase	Liquid (heavy slurry)	Solid (sludge cake)	Liquid (slurry)
Flowrate	kg/h	7,073	1,819	5,254
Solids	wt%	20	70	2.7
Solids	kg/h	1,415	1,273	141
Liquid	kg/h	5,658	546	5,113
Water	kg/h	4,670	450	4,220
TDS	kg/h	988	95	892

Pretreatment System For Brine. 2000 GPM.
DRAFT ISSUED FOR REVIEW
NOT FOR CONSTRUCTION

FILENAME: BRINE PFD 10OCT2016.VSD | DATE: 1/22/16 | DRAWN BY: DLM

REVISIONS

REV.	DATE	DESCRIPTION	BY	CHECKED	APPROVED
0	1/22/16	Preliminary Process Design 1st draft	DLM		
1	2/24/16	Preliminary Process Design 2nd draft	DLM		
2	9/26/16	Revise lime and flocculant rates	DLM		

TRIMERIC CORPORATION
P.O. Box 826
Buda, Texas 78610

ISGS BEST
Brine Pretreatment
Preliminary Process Flow Diagram
CLIENT/SITE: ISGS
DRAWING NUMBER: PFD-1002

Figure 2-1-15 Approximate material balance for the brine pretreatment.

PROJECT: ISGS BEST **Brine Pretreatment Facility, including Lime Addition and Flocculation**
Brine Pretreatment SECTION 1000 2,000 gpm, 20 w% brine
TRIMERIC CORPORATION 3/2/2016 Version 2.
Early Phase Conceptual Capital Cost Estimate

#	Item	Equipment Name	Tag #	Quantity	Purchased Equipment Cost (total)	Installed Cost (total)	Design Parameters
1	Solids Storage Vessel	Lime Storage Bins	H-1150 A/B	2 x 100%	$ 50,200	$ 91,400	3.6 m3 (127 ft3) storage per unit (4 days total). 1.2 m diam x 3.2 m. Cone bottom with vibrators (1.5 kW).
2	Conveyor	Lime Feeder Conveyor	P-1150 A/B	2 x 100%	$ 29,000	$ 43,600	Conveyor type solid feeder, one for each lime storage bin. 30 m (100 ft) length. 7.5 kW drive.
3	Agitated Vessel	Lime Slurry Mixing Tank	T-1160	1	$ 64,100	$ 141,700	0.34 m3 (90 gal) tank. 0.6 m diam x 1.2 m. 316ss. 4 kW drive for mixer.
4	Pump	Lime Slurry Pump	P-1160 A/B	2 x 100%	$ 7,000	$ 35,500	6 L/min (1.6 gpm), 23 m (75 ft) head, slurry pump. 316SS. 0.2 kW drive.
5	Pump	Flocculant Feed Pump	P-1170 A/B	2 x 100%	$ 11,000	$ 27,300	0.4 L/min (0.1 gpm), 30 m (98 ft) head, diaphragm metering pump. 316SS. 0.2 kW drive.
6	Vessel	Flocculation & Clarification Vessel	T-1210	1	$ 727,900	$ 1,362,900	15.5 m (51 ft) diam x 5 m (16.4 ft) flocculation & clarification vessel. 316SS. 1.5 kW flocculation mixer, 3 kW main rake.
7	Pump	Sludge Pumps	P-1210 A/B/C	3 x 50%	$ 50,100	$ 108,500	96 L/min (25 gpm), 15 m (50 ft) head, slurry pump. 316SS slurry. 0.5 kW drive.
8	Filter	Sludge Filter	F-1300	1	$ 124,300	$ 198,900	4.5 tpd vacuum rotary drum filter. 316SS. 1.5 kW drive.
9	Pump	Filtrate Return Pump	P-1300 A/B	2 x 100%	$ 11,600	$ 78,200	175 L/min (46 gpm), 15 m (50 ft) centrifugal pump. 316SS. 1.5 kW drive.
10	Pump	Hydrocyclone Feed Pump	P-1350 A/B/C	3 x 50%	$ 99,000	$ 387,400	4550 L/min (1200 gpm), 45 m (148 ft) head centrifugal pump. 316SS. 30 kW drive.
11	Hydrocyclone	Clarified Liquid Hydrocyclone	H-1350 A/B/C	3 x 50%	$ 110,700	$ 196,900	615 mm (24 inch) hydrocyclone. 316SS liner.

Major Equpiment Cost (MEC)	$ 1,284,900		
Installation Cost (IC)	$ 1,387,400		
Installed Equipment Cost (IEC)		$ 2,672,300	
Tax (8% of MEC + 2.5% of IC)	$ 137,500		
Freight (1.6% of MEC)	$ 20,600		
Contractor Fees (30% of IC)	$ 416,200		
SUBTOTAL		$ 3,246,600	
Engineering & Procurement (15% of Subtotal)	$ 487,000		
Contingency (20% of Subtotal)	$ 649,300		
Early Phase Capital Cost Estimate		**$ 4,383,000**	*1Q2015 basis.*

Figure 2-1-16 Cost estimate data for the pretreatment system.

PROJECT: ISGS BEST **Brine Pretreatment Facility, including Lime Addition and Flocculation**
Brine Pretreatment SECTION 1000
TRIMERIC CORPORATION 9/26/2016 Version 3
Early Phase Operating Cost Estimate

Operating Cost Factor	Usage Rate	Unit Cost	Cost (rate)	
			$/h	k$/y
Electrical Power	100 kW	0.08 $/kW-h	8.0	68
Lime	65 kg/h	0.15 $/kg	9.8	83
Flocculant	2.3 kg/h	3 $/kg	6.9	59
Sludge Disposal (Landfill)	1820 kg/h	40 $/ton	80.2	684
Labor	2 FTE	100 K$/FTE/y	23.5	200
Maintenance + G&A		4.5 % CAPEX/y	23.1	197
SUBTOTAL OPERATING COST			151.5	1,291
Capital Amortization		5 % CAPEX/y	25.7	219
TOTAL OPERATING COST INCLUDING CAPITAL AMORTIZATION			**177.2**	**1,510**
TOTAL UNIT COST FOR WATER TREATMENT		**1.48** $ / 1000 gal		

Assumptions:

Operating days/year	355	
Flowrate	2000	gpm (20 w% brine)
Capital Amortization	20	year, straight-line, no interest
Maintenance & G&A	4.5	pct of CAPEX/year

Figure 2-1-17 Brine pretreatment facility costs for a 2,000 gpm facility.

Table 2-1-27 Capital and operating costs for brine pretreatment at a feed rate of 2,000 gpm and extrapolation to feed rates of 500, 585, and 5,000 gpm.

Case (gpm)	Capital cost ($)	Annual operating cost ($, including capital amortization)	Cost for pretreated water ($/1,000 gal)
2,000 (base)	4,383,000	1,510,000	1.48
500	1,908,000	555,000	2.17
585	2,096,000	611,000	2.04
5,000	7,595,000	3,205,000	1.25

The presence of H_2S in the condensing water can result in corrosion issues. Fresh 20 wt% caustic is fed to the scrubber via a heat recovery exchanger (E-2301) that serves to preheat the caustic. The column operates at the temperature of the steam, so there is no significant condensation of water vapor into the caustic liquid phase. The majority of the caustic is recirculated to the top of the column, and a portion is purged through the heat recovery exchanger (E-2301).

The vapor that has been subjected to H_2S removal is then compressed (C-2400) and condensed in the evaporator. The condensate is pumped through the heat recovery exchanger (E-

2110) before leaving the MVR package unit. The condensate, which is recovered purified water, is collected in a tank (T-2701) and pumped to users. The blowdown from the caustic scrubber (containing excess NaOH and sodium salts of sulfide [Na_2S and NaHS]) is mixed with the concentrated brine and pumped from the unit. It is assumed, but not known, that the spent caustic could be disposed of with the concentrated brine. This will need to be confirmed as the design of the project advances.

The capital cost estimate for the equipment shown in the PFD is given in Figure 2-1-20. The capital cost for the MVR package system was derived (with various adjustments) from data published in the *Desalting Handbook for Planners*, 3rd edition (U.S. Department of the Interior, 2003). The rest of the capital costs were estimated by using the Aspen Capital Cost Estimator (v.8.7.1). All costs are on a first quarter of 2015 basis.

The capital and operating cost estimates for this process also include pumps sized for the concentrated brine discharge to flow through a 1-mi (1.6-km) pipeline and to arrive at the injection well inlet with a pressure of 150 psig, as well as the costs of the pipeline. In this case, the pipeline was estimated to have a diameter of 12 in. and constructed of 316SS. The brine has high viscosity (relative to water), and this results in a larger pipeline diameter requirement for a reasonable pressure drop. The material selection for the pipeline is preliminary, and further work will be required to confirm the proper material of construction for this application as the design of the project advances. Corrosion tests should be considered in the future to determine if this metal alloy is a suitable material of construction.

Figures 2-1-21 and 2-1-22 summarize the total capital and operating costs for this process, based on treating 2,000 gpm of feed brine with and without accounting for the value for the recovered purified water. The 2,000 gpm design and cost estimate information was used to estimate the costs for cases of 500 gpm of feed (~58 gpm of recovered water), 585 gpm of feed (68 gpm of recovered water), and 5,000 gpm of feed (~583 gpm of recovered water). The total capital and operating cost estimates for these cases are also given in Tables 2-1-28 and 2-1-29, with and without including a value for the recovered purified water.

It should be noted that a significant improvement to the process shown in the PFD may be possible. The need to scrub a very small amount of H_2S from the steam results in the need for equipment that represents a significant portion of the capital cost (roughly 20%). Although the caustic scrubber process is not complex, the operation of caustic scrubbing of H_2S at ~106 °C results in the need for the system to be constructed of alloys more expensive than 316SS; the use of AL-6XN (and similar high-alloy steels) is assumed in the cost estimate. This material selection is preliminary, and further work will be required to confirm the proper material of construction for this application. Corrosion tests should be considered in the future to determine whether this metal alloy is a suitable material of construction. Potential approaches for reducing the cost associated with dealing with the H_2S include the following: (1) operate the evaporator under vacuum to lower the scrubbing temperature to allow for the use of lower cost metals, or (2) avoid the need to scrub H_2S by converting the H_2S to a nonvolatile species before evaporation. Regarding option 2, there are various ways of chemically converting H_2S, including the use of iron redox chemistry to convert the sulfide to sulfur, and other oxidation chemistries. This topic could be considered part of further studies.

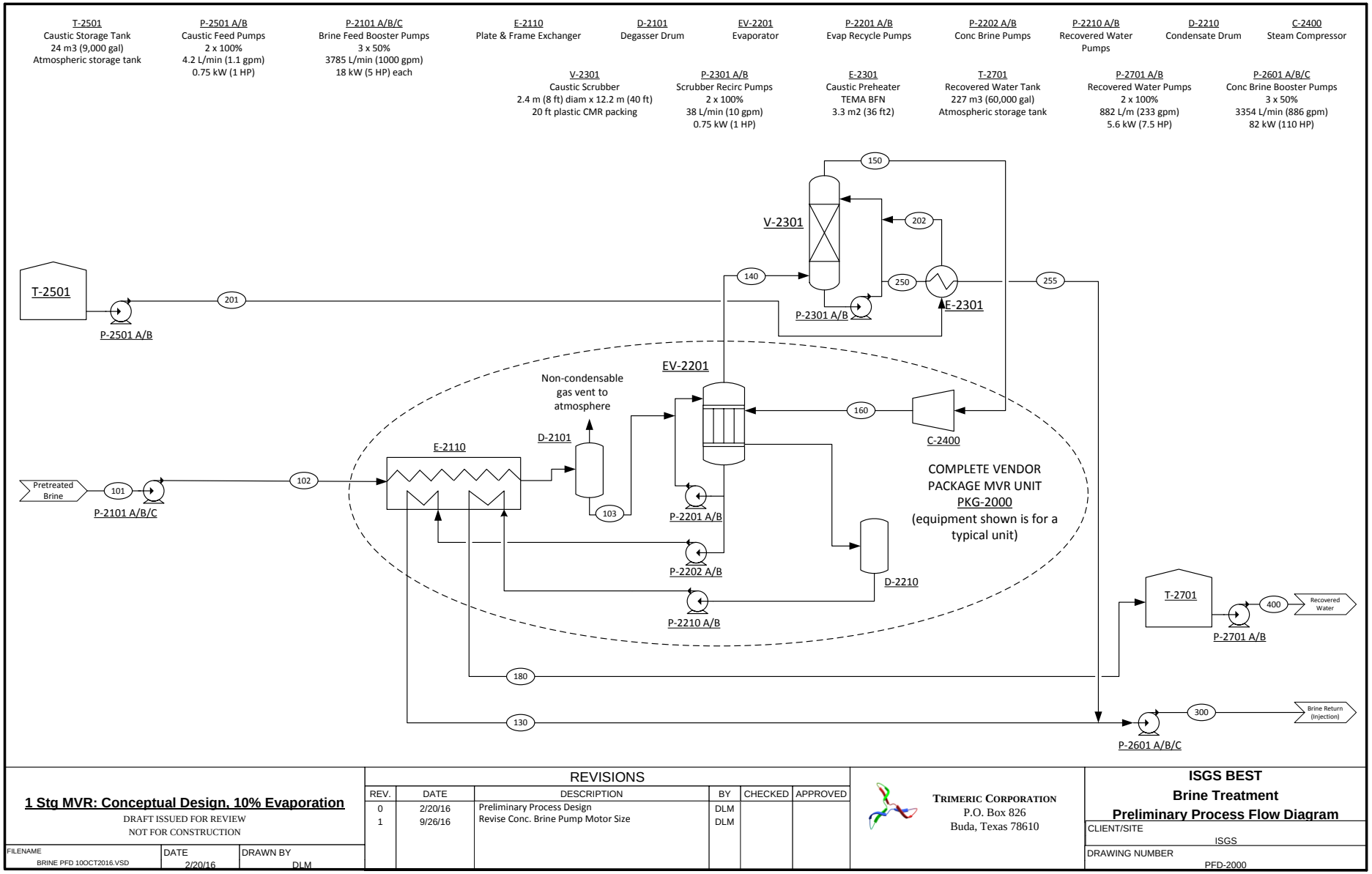

Figure 2-1-18 PFD for 10% recovery of Mt. Simon brine.

APPROXIMATE PROCESS MATERIAL BALANCE **ISGS BEST**
1 Stg MVR: 10% Evaporation **REV 2. 26 September 2016.**

MAIN PROCESS STREAMS ***Approximate Material Balance***

Stream Number		**101**		**102**		**103**		**130**		**140**		**150**		**160**		**180**		**201**		**202**		**250**		**255**		**300**		**400**	
Stream Name		**Pretreated Brine**		**Pretreated Brine from Pump**		**Heated Brine**		**Residual Concentrated Brine**		**Vapor from Evaporator**		**Vapor from Scrubber**		**Vapor from Compressor**		**Recovered Water**		**Caustic Feed**		**Preheated Caustic Feed**		**Scrubber Blowdown**		**Cooled Scrubber Blowdown**		**Residual Concentrated Brine**		**Recovered Water**	
Phase		Liquid		Liquid		Liquid		Liquid		Vapor		Vapor		Vapor		Liquid		Liquid		Liquid		Liquid		Liquid		Liquid		Liquid	
Temperature	C	32		32		104		35		107		107		181		45		35		91		105		42		35		45	
Pressure	bar(a)	1.05		3		2		1.1		1.1		1.05		1.9		1.1		5		4		2.6		2		12.8		3	
Flowrate	lpm	7,571		7,571		7,571		6,660		1,380,000 (actual)		1,400,000 (actual)		955,300 (actual)		882		4.1		4.1		4.6		4.6		6,665		882	
	gpm	2,000		2,000		2,000		1,760								233		1.1		1.1		1.2		1.2		1,761		233	
	kg/h	513,302		513,302		513,302		460,896		52,406		52,371		52,371		52,371		304		304		331		331		461,227		52,371	
Liq Density	g/mL	1.13		1.13		1.13		1.15								1.0		1.23		1.23		1.20		1.20		1.15		1.0	
Approximate pH		8		8		8		8										15		15		11		11		10			
TDS	mg/L	197,046		197,046		197,046		223,906								~0		258,332		258,332		255,756		255,756		223,970		~0	
	kg/h	89,508		89,508		89,508		89,473										61		61		71		71		89,560			
Water by diff	wt%	82.6		82.6		82.6		80.7		99.9		100.0		100.0		100.0		80.0		80.0		80.0		80.0		80.7		100.0	
	kg/h	423,987		423,987		423,987		371,713		52,371		52,371		52,371		52,371		243		243		265		265		372,210		52,371	
Major Cationic species		**mmol/L**	**mg/L**	**mmol/L**	**mg/L**	**mmol/L**	**mg/L**	**mmol/L**	**mg/L**	**mmol/L**	**mg/L**	**mmol/L**	**mg/L**	**mmol/L**	**mg/L**	**mmol/L**	**mg/L**	**mmol/L**	**mg/L**	**mmol/L**	**mg/L**	**mmol/L**	**mg/L**	**mmol/L**	**mg/L**	**mmol/L**	**mg/L**	**mmol/L**	**mg/L**
Na+	22.99	2088	48,000	2088	48,000	2,088	48,000	2373	54,565									6459	148,482	6459	148,482	6,459	148,482	6,459	148,482	2,376	54,629		
Ca++	40.08	549	22,000	549	22,000	549	22,000	624	25,009																	624	25,009		
K+	39.10	90	3,500	90	3,500	90	3,500	102	3,979																	102	3,979		
Sr++	87.62	9.03	791	9.030	791	9.03	791.2	10.265	899																	10	899		
others		70	1,681	70.000	1,681	70	1681.0	79.573	1,911																	80	1,911		
sum of cations		2,805	75,972	2,805	75,972	2,805	75,972	3,189	86,362									6,459	148,482	6,459	148,482	6,459	148,482	6,459	148,482	3,192	86,427		
Major Anionic species		**mmol/L**	**mg/L**	**mmol/L**	**mg/L**	**mmol/L**	**mg/L**	**mmol/L**	**mg/L**	**mmol/L**	**mg/L**	**mmol/L**	**mg/L**	**mmol/L**	**mg/L**	**mmol/L**	**mg/L**	**mmol/L**	**mg/L**	**mmol/L**	**mg/L**	**mmol/L**	**mg/L**	**mmol/L**	**mg/L**	**mmol/L**	**mg/L**	**mmol/L**	**mg/L**
Cl-	35.45	3,380	119,830	3380	119,830	3,380	119,830	3842	136,218																	3,842	136,218		
SO4--	96.06	3.8	360.2	3.75	360	3.8	360.2	4.26	410																	4.26	410		
Br-	79.90	8.26	660.01	8.26	660	8.26	660	9.39	750																	9.39	750		
S--	32.07	5.15	165.14	5.15	165	5.15	165	3.12	100													3,345	107,274	3,345	107,274	5.15	165		
OH-	17.01																	6459	109,850	6459	109,850								
others		1	58.00	1	58	1	58	1	66																				
sum of anions		3,398	121,074	3398	121,074	3,398	121,074	3860	137,544									6,459	109,850	6,459	109,850	3,345	107,274	3,345	107,274	3,861	137,543		
Vapor Phase Species										**mol%**	**wt %**	**mol%**	**wt %**	**mol%**	**wt %**														
H2O	18.01528									99.96	99.93	100	100	100	100														
H2S	34.1									351 ppm	664 ppm	< 10 ppm	< 10 ppm	< 10 ppm	< 10 ppm														

1 Stg MVR: Conceptual Design, 10% Evaporation
DRAFT ISSUED FOR REVIEW
NOT FOR CONSTRUCTION

FILENAME	DATE	DRAWN BY
BRINE PFD 10OCT2016.VSD	2/20/16	DLM

REVISIONS

REV.	DATE	DESCRIPTION	BY	CHECKED	APPROVED
0	2/20/16	Preliminary Process Design	DLM		
2	9/26/16	Increase Residual Brine Discharge Pump Pressure	DLM		

TRIMERIC CORPORATION
P.O. Box 826
Buda, Texas 78610

ISGS BEST
Brine Treatment
Preliminary Process Flow Diagram
CLIENT/SITE: ISGS
DRAWING NUMBER: PFD-2000

Figure 2-1-19 Approximate material balance for 10% recovery of Mt. Simon brine.

PROJECT: ISGS BEST **Water Recovery from Brine by Single Stage MVR. 10% Water Recovery Basis.**
Brine Pretreatment SECTION 2000 2,000 gpm, 20 wt. % brine, recover ~233 gpm water.
TRIMERIC CORPORATION 9/26/2016 Version 2
Early Phase Conceptual Capital Cost Estimate

#	Item	Equipment Name	Tag #	Quantity	Purchased Equipment Cost (total)	Installed Cost (total)	Design Information
1	Pump	Brine Feed Booster Pump	P-2101 A/B/C	3 x 50%	$ 57,600	$ 192,300	3785 L/min (1000 gpm), 2 bar (29 psi) head, centrifugal pump. 18 kW (25 HP) per unit. 316SS.
2	Pump	Caustic Feed Pump	P-2501 A/B	2 x 100%	$ 6,800	$ 49,400	4.2 L/min (1.1 gpm), 4 bar (58 psi) head, gear pump. 316SS. 0.75 kW (1 HP). CS.
3	Tank	20% Caustic Tank	T-2501	1	$ 26,300	$ 68,400	24.1 m3 (9,000 gal). 3 m (10 ft) diam x 5 m (16 ft). Atmospheric storage tank. CS.
4	Absorber Tower	Caustic Scrubber	V-2301	1	$ 601,800	$ 938,100	2.4 m (8 ft) diam x 12.2 (40 ft) packed tower. #3 Plastic CMR packing. 6.1 m (20 ft) packed height. AL-6XN.
5	Pump	Caustic Recirculation Pump	P-2301 A/B	2 x 100%	$ 36,600	$ 86,200	38 L/min (10 gpm), 1.5 bar (22 psi) head ANSI mag drive pump. 0.75 kW (1 HP). AL-6XN.
6	Heat Exchanger	Caustic Preheater	E-2301	1	$ 16,900	$ 90,900	TEMA BFN exchanger, 3.3 m2 (36 ft2) heat transfer area. 100 kPag des pressure, 150 C des temperature. AL-6XN.
7	Tank	Recovered Water Tank	T-2701	1	$ 76,000	$ 162,200	227 m3 (60,000 gal). 5.5 m (18 ft) diam x 9.8 m (32 ft). Atmospheric storage tank. CS.
8	Pump	Recovered Water Pump	P-2701 A/B	2 x 100%	$ 12,400	$ 48,600	882 L/m (233 gpm), 20 m (67 ft) head single-stage centrifugal pump. 5.6 kW (7.5 HP). CS.
9	Pump	Brine Return Pump	P-2601 A/B/C	3 x 50%	$ 160,200	$ 721,400	3354 L/min (886 gpm), 11.7 bar (169 psi) head, centrifugal pump. 82 kW (110 HP) per unit. 316SS.
10	Pipeline	Brine Return Pipeline	Pipeline	1 mile	$ 325,149	$ 632,722	1 mile of 12" pipe. 316SS.
11	Package	MVR Package Distillation Unit	PKG-2000	1	$ 1,558,200	$ 4,674,700	1270 m3/day (233 gpm) water production, single stage MVR, package unit.
					Major Equpiment Cost (MEC)	$ 2,877,949	
					Installation Cost (IC)	$ 4,786,973	
					Installed Equipment Cost (IEC)	$ 7,664,922	
					Tax (8% of MEC + 2.5% of IC)	$ 349,900	
					Freight (1.6% of MEC)	$ 46,000	
					Construction OH, Contractor Fees (30% of IC)	$ 1,436,100	
					Subtotal	$ 9,496,922	
					Engineering & Procurement (15% of Subtotal)	$ 1,424,500	
					Contingency (20% of Subtotal)	$ 1,899,400	
					Early Phase Capital Cost Estimate	**$12,821,000**	*1Q15 basis. NOTE: Excludes cost of pre-treatment for TSS removal. 2,000 gpm Feed Basis, with ~233 gpm Recovered Water.*

Figure 2-1-20 The 10% brine recovery facility costs for a 2,000 gpm facility.

PROJECT: ISGS BEST **Water Recovery from Brine by Single Stage MVR. 10% Water Recovery Basis.**
Brine Pretreatment SECTION 2000 2,000 gpm, 20 wt. % brine, recover ~233 gpm water.
TRIMERIC CORPORATION 9/26/2016 Version 3
Early Phase Conceptual Operating Cost Estimate

Operating Cost Factor	Usage Rate	Unit Cost	Cost (rate)	
			$/h	k$/y
Electrical Power	2444 kW	0.08 $/kW-h	195.5	1666
Caustic (dry basis)	64 kg/h	500 $/MT	32.0	273
Water Product	233 gpm	-2 $/kgal	-28.0	-238
Labor	6 FTE	100 K$/FTE/y	70.4	600
Maintenance + G&A		4.5 % CAPEX/y	67.7	577
SUBTOTAL OPERATING COST			337.7	2,877
Capital Amortization		5 % CAPEX/y	75.2	641
TOTAL OPERATING COST INCLUDING CAPITAL AMORTIZATION			**412.9**	**3,518**

NET UNIT COST FOR TREATING BRINE - $/1000 GAL	**3.4**
NET UNIT COST FOR PRODUCT WATER - $/1000 GAL	**29.5**

Assumptions:

Operating days/year	355	
Flowrate	2,000	gpm (20 w% brine), ~10% water recovery
Capital Amortization	20	year, straight-line, no interest
Maintenance & G&A	4.5	pct of CAPEX/year

A positive value for net unit cost indicates the process costs money to operate, a negative value indicates the process generates a profit.

Figure 2-1-21 The 10% brine recovery operating costs for a 2,000 gpm facility, including a value for recovered purified water.

PROJECT: ISGS BEST **Water Recovery from Brine by Single Stage MVR. 10% Water Recovery Basis.**
Brine Pretreatment SECTION 2000 2,000 gpm, 20 wt. % brine, recover ~233 gpm water.
TRIMERIC CORPORATION 9/26/2016 Version 3
Early Phase Conceptual Operating Cost Estimate

Operating Cost Factor	Usage Rate	Unit Cost	Cost (rate)	
			$/h	k$/y
Electrical Power	2444 kW	0.08 $/kW-h	195.5	1666
Caustic (dry basis)	64 kg/h	500 $/MT	32.0	273
Labor	6 FTE	100 K$/FTE/y	70.4	600
Maintenance + G&A		4.5 % CAPEX/y	67.7	577
SUBTOTAL OPERATING COST			365.7	3,115
Capital Amortization		5 % CAPEX/y	75.2	641
TOTAL OPERATING COST INCLUDING CAPITAL AMORTIZATION			**440.9**	**3,756**

NET UNIT COST FOR TREATING BRINE - $/1000 GAL	**3.7**
NET UNIT COST FOR PRODUCT WATER - $/1000 GAL	**31.5**

Assumptions:

Operating days/year	355	
Flowrate	2,000	gpm (20 w% brine), ~10% water recovery
Capital Amortization	20	year, straight-line, no interest
Maintenance & G&A	4.5	pct of CAPEX/year

A positive value for net unit cost indicates the process costs money to operate, a negative value indicates the process generates a profit.

Figure 2-1-22 The 10% brine recovery operating costs for a 2,000 gpm facility, without including a value for recovered purified water.

Table 2-1-28 Capital and operating costs for the MVR process at a feed rate of 2,000 gpm (~10% water recovery), and extrapolation to cases of 500, 585, and 5,000 gpm of feed, including a value for recovered purified water.

Case (gpm)	Capital cost ($)	Annual operating cost ($, including capital amortization)	Cost for recovered water ($/1,000 gal)
2,000 (base)	12,821,000	3,518,000	29.54
500	5,581,000	1,455,000	48.87
585	6,132,000	1,580,000	45.35
5,000	22,217,000	7,061,000	23.71

Table 2-1-29 Capital and operating costs for the MVR process at a feed rate of 2,000 gpm (~10% water recovery), and extrapolation to cases of 500, 585, and 5,000 gpm of feed, without including a value for recovered purified water.

Case (gpm)	Capital cost ($)	Annual operating cost ($, including capital amortization)	Cost for recovered water ($/1,000 gal)
2,000 (base)	12,821,000	3,756,000	31.54
500	5,581,000	1,515,000	50.87
585	6,132,000	1,650,000	47.35
5,000	22,217,000	7,657,000	25.71

Brine Treatment by Multiple-Effect Evaporation to Recover 88% of Water

Figure 2-1-23 shows a schematic diagram of a proposed system to recover the majority of the water (~88%) from a 2,000 gpm pretreated brine stream as a purified product. The approximate material balance of the system is shown in Figure 2-1-24. The process uses a six-stage multiple-effect evaporator (MEE) system to separate water from the brine. A salt product, consisting primarily of NaCl but also containing some $CaCl_2$, potassium chloride (KCl), and calcium sulfate dihydrate ($CaSO_4 \cdot 2H_2O$) is also produced.

Mt. Simon brine, containing approximately 20 wt% TDS, is first subjected to pretreatment for TSS removal (as discussed previously). The brine is pumped through a plate cross-exchanger (E-6100), where it is preheated by water condensate streams from the first five MEE stages. The preheated feed is further heated in the first evaporator (EV-6001) by steam (produced by a boiler), evaporating a portion of the water from the brine. The steam produced by the first evaporator is then used to provide heat to the second evaporator, steam produced in the second evaporator is used to provide heat to the third evaporator, and so on. The steam from the last (sixth) evaporator is condensed via cooling. The key to this process concept is to operate the evaporators at consecutively lower pressures so that the boiling temperature of the brine (despite its becoming more concentrated in dissolved salts) is reduced from one evaporator to the next; the lower boiling temperature of an evaporator allows for the steam from the previous evaporator to transfer heat to the next evaporator during condensation.

The first evaporator operates at 38 psig/293 °F (3.6 bar/145 °C), and the sixth evaporator (EV-6006) operates at −12.5 psig/156 °F (0.15 bar/69 °C); the PFD shows the approximate temperature and pressure of each evaporator. The steam produced in each stage (except for the last) is condensed by evaporating brine in the next evaporator in the sequence; the condensed hot

water is then further cooled by transferring heat to the feed brine in E-6100. A vacuum pump (VP-6401) provides a vacuum on the final condenser separator drum (D-6401), which allows the last three evaporator stages to operate under vacuum conditions.

The first four evaporator stages will simply concentrate the brine, without the precipitation of salts occurring to a significant extent. The brine exiting the fourth stage will be at the solubility limit of salts, and salt precipitation will occur in the fifth and sixth evaporation stages. The design and cost of the last two evaporator units are therefore different to accommodate the bulk salt crystallization that occurs.

The recovered water (about 1,660 gpm) is collected in a storage tank and pumped to users. In the evaporative crystallizers (EVC-6005, EVC-6006), salts are precipitated as water is evaporated, resulting in a liquid phase that is a slurry of solid salt particles and brine. Evaporative crystallizers are equipped with thickening and clarification sections, such that in EVC-6005, thickened slurry is collected from the bottom of the vessel and a clarified brine is collected from a different part of the vessel. The clarified liquid from EVC-6005 is fed to EVC-6006. In EVC-6006, it is assumed that the slurry is not thickened, and instead the entire liquid slurry product from this final stage is combined with the thickened slurry from EVC-6005. The combined slurry stream, roughly 378 gpm containing about 40 wt% solids, is cooled and filtered. The solids collected from the filters are then dried.

There are four parallel trains of filtration and drying equipment. Each train consists of a rotary vacuum drum filter (F-6301 A/B/C/D), and the wet solids are dumped into a continuous rotary dryer (D-6201 A/B/C/D). The rotary dryer uses direct contact of the wet solids with combustion gases from burning natural gas (note that for simplicity, the material balance does not show the combustion gases added to the dryer); extra combustion air can be added to control the temperature. The dried solid product is dumped into bins, and the combustion gases from the dryer are sent to a baghouse to filter out entrained solids before venting to the atmosphere. Salt is produced at a rate of about 60 MT/h and contains less than 1 wt% moisture; the dry mass composition of the salt is 89% NaCl, 8.1% $CaCl_2$, 2.1% KCl, and 0.7% $CaSO_4 \cdot 2H_2O$. All the minor species in the Mt. Simon brine composition could not be included in the material balance; it is likely that additional small-concentration components (e.g., metals) will be present in this salt, some of which might be important in the consideration of its disposition.

The filtrate streams from F-6301 A/B/C/D are combined and stored in a tank. This concentrated brine, at a flow rate of approximately 230 gpm, containing roughly 50 wt% TDS (mostly $CaCl_2$), is pumped from the tank for use or disposal; as the brine cools during storage, some additional $CaCl_2$ may precipitate from solution. Accommodations for the precipitation of the added salt may need to be added to the design later.

The concentrated brine pumps are sized for the concentrated brine discharge to flow through a 1-mi (1.6-km) pipeline and to arrive at the injection well inlet with a pressure of 150 psig. In this case, the pipeline was estimated to be 8 in. in diameter and assumed to be constructed of 316SS. The concentrated brine has a high viscosity (relative to water), and this results in a larger pipeline diameter requirement for a reasonable pressure drop. The material selection for the pipeline is preliminary and further work will be required to confirm the proper material of construction for this application as the design of the project advances. Corrosion tests should be considered in the future to determine whether this metal alloy is a suitable material of construction.

One issue not directly addressed in this design is H_2S. During the distillation process, H_2S is formed in the brine from soluble sulfide salts, and a portion of the H_2S is stripped into the vapor (steam) phase. As a result, water recovered from each MEE stage is predicted to contain some

H_2S, with the combined recovered water stream containing roughly 205 ppmw of H_2S unless measures are taken to prevent it. In the design of a different system (10% water recovery from brine by single-stage MVR), the H_2S in the steam is removed before condensing by scrubbing with hot caustic in a packed tower. Although that approach could also be used in this process, a separate scrubber would probably be required for all six evaporation stages; this would result in an increase in the capital cost estimate by, very roughly, $10 million. Although the material balance shows the presence of H_2S in the recovered water, the design and economic basis for this process includes the assumption that the H_2S will be handled in some other, not currently defined, more economical method than hot caustic scrubbing. There are various means of chemically converting H_2S to a nonvolatile product that could be used to prevent the H_2S problem, including the use of iron redox chemistry to convert the sulfide to sulfur, and other oxidation chemistries. Treatment of the condensed water could also be done. This topic can be investigated later, and laboratory studies should be considered. If it is preferred to assume that the H_2S would be handled by caustic scrubbing, then an additional $10 million should be added to the capital cost estimate.

The capital cost estimate for the equipment shown in the PFD is given in Figure 2-1-25. Figures 2-1-26 and 2-1-27 summarize the total capital and operating costs for this process based on treating 2,000 gpm of feed brine with and without including values for the recovered purified water and for the produced salt, respectively. Capital costs were estimated using the Aspen Capital Cost Estimator (v.8.7.1), with various adjustments made based on experience, comparison with other data and the literature, and so forth. All costs are on a first quarter of 2015 basis. Three utility systems are included in the cost estimate but are not shown on the PFD: a package steam boiler to provide steam to the first MEE stage, a power transformer, and a water cooling tower system. These utility systems are required for the MEE process, as shown in the PFD.

Figure 2-1-26 indicates that the process generates a profit when the values for recovered purified water and (predominantly) produced salt are included in the operating cost estimate. However, a number of factors are not accounted for in this cost estimate that could significantly affect the economics of the overall process. Some of these are as follows:

- Pretreatment is not included. (It is a separate module, with separately calculated costs.)
- It is assumed that the product salts would be acceptable for road use as is. It is not known whether environmental or other issues would require further treatment of this salt, which would result in increased capital and operational expenditures.
- This design does not include a process to prevent or deal with H_2S from vaporizing with the steam in the evaporators–crystallizers. This is a recognized limitation to the process that will have to be addressed (cost not determined).
- This design does not include produced salt storage or loading facilities. This could be a substantial capital cost because of the likely need to store significant amounts of salt.
- The cost of production and injection wells is not included.
- Market saturation is not included.
- Seasonal variation (mild winters) is not included.

The 2,000 gpm design and cost estimate information were used, along with standard cost escalation methodologies, to estimate the costs of the cases with 500 gpm of feed (~415 gpm of recovered water), 585 gpm of feed (~486 gpm of recovered water), and 5,000 gpm of feed (~4,510 gpm of recovered water). The total capital and operating cost estimates for these cases are also given in Tables 2-1-30 and 2-1-31, with and without including values for the recovered purified water and for the produced salts, respectively. A positive value for the net unit cost indicates the process costs money to operate; a negative value indicates the process generates a profit.

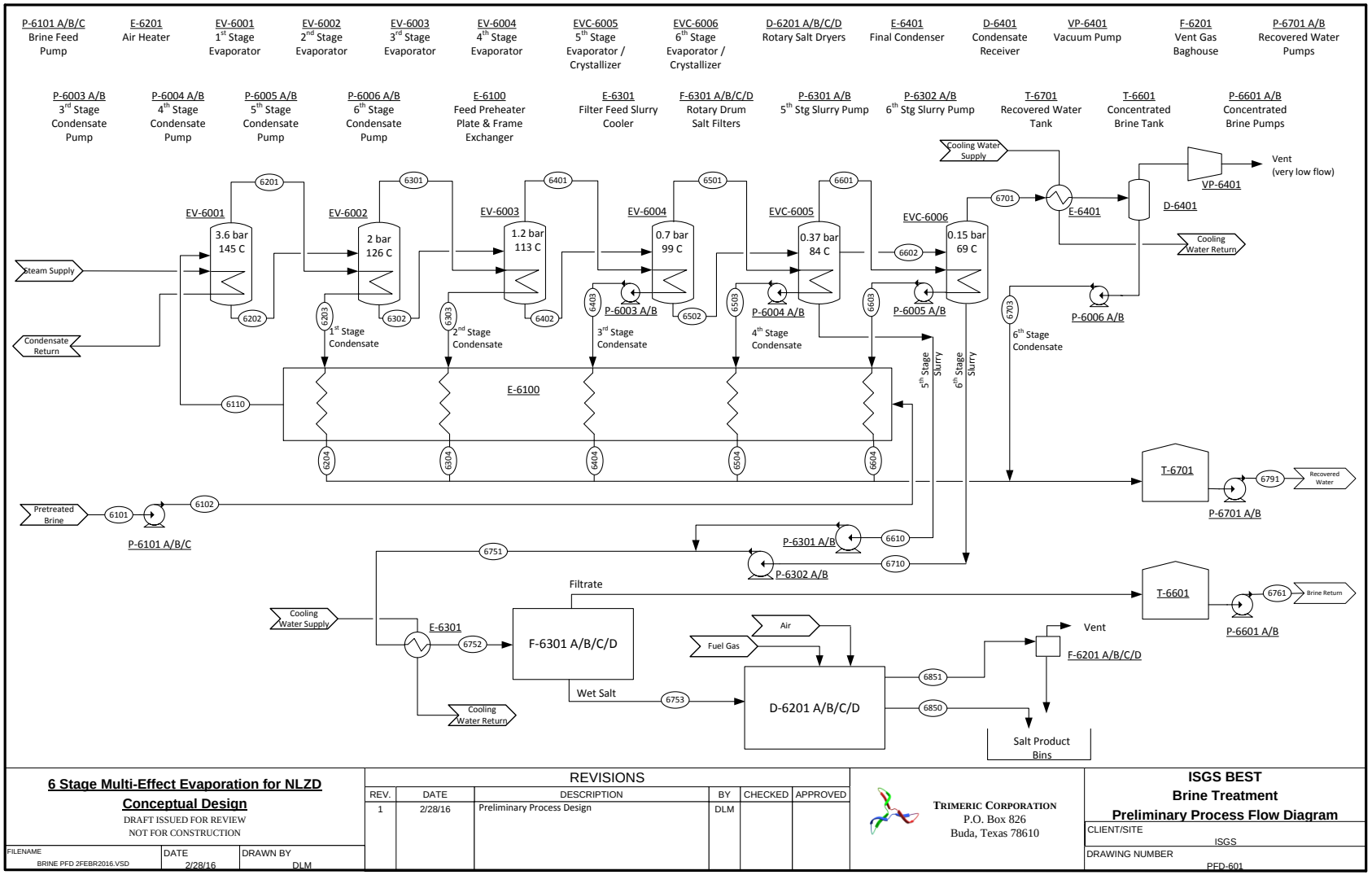

Figure 2-1-23 PFD for near-ZLD treatment of the brine by MEE.

ISGS BEST: Treatment of 2,000 gpm of brine using Mulit-Effect Evaporation and recovery of water (NLZD)

APPROXIMATE MATERIAL BALANCE Version 2 9/27/2016

	Units	6101	6102	6201	6202	6203	6204	6301	6302	6303	6304	6401	6402	6403	6404	6501	6502	6503	6504	6601	6602	6603	6604	6610	6701	6703	6710	6751	6752	6761	6791	6850	6851
Temperature	C	32.0	32.1	145.0	145.0	133.3	45.0	125.8	125.8	117.7	45.0	112.7	112.7	105.8	45.0	99.0	99.0	89.9	45.0	83.5	83.5	74.2	45.0	83.5	68.5	53.7	68.5	72.4	50.0	45.0	46.3	150.0	150.0
Pressure	BAR	1.01	5.00	3.60	3.60	3.60	3.60	2.00	2.00	2.00	2.00	1.24	1.24	2.00	9.00	0.70	0.70	2.00	0.70	0.37	0.61	2.00	0.37	0.61	0.14	2.00	0.14	3.00	3.00	13.20	3.00	1.01	1.01
Mass Flow	KG/HR	515,184	515,184	39,549	475,635	39,549	39,549	53,664	421,972	53,664	53,664	61,575	360,396	61,575	61,575	68,056	292,341	68,056	68,056	73,807	176,038	73,807	73,807	42,495	77,117	77,246	98,921	141,416	141,416	75,451	373,768	60,210	15,775
Mole Flow	KMOL/HR	26,437	26,437	2,194	24,243	2,194	2,194	2,978	21,264	2,978	2,978	3,418	17,846	3,418	3,418	3,777	14,066	3,778	3,777	4,097	8,244	4,097	4,097	1,252	4,281	4,288	3,540	4,786	4,771	3,323	20,745	982	678
Vol Flow (actual)	L/MN	7,565	7,564	346,270	7,460	1,044	666	815,554	6,380	1,745	903	1,457,766	5,256	1,076	1,036	2,778,243	4,009	1,175	1,145	5,417,969	2,314	1,261	1,242	423	14,389,920	1,305	1,019	1,442	1,430	875	6,294	440	392,683
Vapor Fraction		0	0	1	0	0.001	0	1	0	0.001	0	1	0	0	0	1	0	0	0	1	0	0	0	0	1	0	0	0	0	0	0	0	0	1
Liquid Fraction		1	1	0	1	0.999	1	0	1	0.999	1	0	1	1	1	0	0.9999447	1	1	0	0.9942836	1	1	0.661159	0	1	0.8671304	0.8120244	0.8081122	0.999148	1	0.023486	0
Solid Fraction		0	0	0	0	0	0	0	0	0	0	0	0	0	0	0	5.53E-05	0	0	0	0.0057164	0	0	0.338841	0	0	0.1328696	0.1879756	0.1918878	0.000852	0	0.976514	0
Average MW		19.5	19.5	18.0	19.6	18.0	18.0	18.0	19.8	18.0	18.0	18.0	20.2	18.0	18.0	18.0	20.8	18.0	18.0	18.0	21.4	18.0	18.0	33.9	18.0	18.0	27.9	29.5	29.6	22.7	18.0	61.3	23.3
Mass Density	KG/CUM	1,135.0	1,135.2	1.9	1,062.7	631.4	990.1	1.1	1,102.4	512.6	990.2	0.7	1,147.2	953.9	990.6	0.4	1,215.3	985.3	990.2	0.2	1,268.0	975.3	990.2	1,675.7	0.1	986.4	1,618.4	1,634.8	1,647.8	1,437.4	989.8	2,278.6	0.7
Enthalpy Flow	MJ/HR	-7,393,163	-7,392,921	-522,196	-6,586,736	-609,222	-624,002	-710,761	-5,788,949	-830,716	-847,224	-817,067	-4,851,926	-956,682	-972,216	-904,775	-3,807,439	-1,061,952	-1,074,646	-983,378	-2,264,084	-1,156,551	-1,165,523	-402,742	-1,029,624	-1,217,077	-1,061,318	-1,464,028	-1,469,387	-941,059	-5,899,444	-431,718	-74,916
Mass Enthalpy	KJ/KG	-14,351	-14,350	-13,204	-13,848	-15,404	-15,778	-13,245	-13,719	-15,480	-15,788	-13,269	-13,463	-15,537	-15,789	-13,295	-13,024	-15,604	-15,791	-13,324	-12,861	-15,670	-15,791	-9,477	-13,351	-15,756	-10,729	-10,353	-10,391	-12,476	-15,784	-7,170	-4,749
pH		7.0	7.0		8.0	4.1	4.2		8.5	4.4	4.4		8.9	6.1	4.5		9.2	6.2	4.6		9.5	6.4	4.8	9.5		6.6	9.8	9.7	10.3	10.5	4.5	9.7		
Component Mass Fraction																																	
H2O		0.8262058	0.8262058	0.999059	0.8118575	0.999058	0.999058	0.999698	0.787949	0.999697	0.999697	0.9998352	0.7517324	1	0.999835	0.999894	0.6938522	1	0.9998931	0.9999436	0.6655393	1	0.9999433	0.278439	0.9999739	1	0.4046589	0.3667226	0.3667212	0.593154	0.9997984	0.002696	0.366077
H2S		3.00E-05	3.00E-05	0.000941	5.25E-07	0.000938	0.000938	0.000302	9.46E-08	0.000801	0.000901	0.0001648	3.04E-08	0	0.000164	0.000106	1.01E-08	0	0.0001057	5.64E-05	2.75E-09	0	5.58E-05	1.15E-09	2.61E-05	0	2.39E-10	4.58E-10	2.16E-10	2.95E-10	0.0002048	4.48E-13	3.01E-06
CA++		0.0215393	0.0215393	0	0.0232751	0	0	0	0.0261928	0	0	0	0.0306334	0	0	0	0.0376245	0	0	0	0.0564766	0	0	0.023628	0	0	0.1003085	0.0772545	0.0772538	0.124954	0	0.003023	0
CAOH+		1.36E-08	1.36E-08	0	7.00E-05	0	0	0	0.00013907	0	0	0	0.0002122	0	0	0	0.0003095	0	0	0	0.0005045	0	0	0.000211	0	0	0.0009441	0.0007235	0.0007221	0.001168	0	0.000236	0
H3O+		3.15E-09	3.16E-09	0	2.96E-10	1.50E-06	1.33E-06	0	6.78E-11	7.77E-07	7.51E-07	0	2.52E-11	1.58E-08	5.54E-07	0	8.83E-12	1.17E-08	4.45E-07	0	3.17E-12	8.36E-09	3.23E-07	1.33E-12	0	4.91E-09	4.41E-13	5.92E-13	1.31E-13	1.49E-13	6.28E-07	4.89E-15	0
K+		0.0031002	0.0031003	0	0.0033572	0	0	0	0.0037841	0	0	0	0.0044307	0	0	0	0.0054622	0	0	0	0.0082388	0	0	0.003447	0	0	0.0083455	0.0108708	0.0077103	0.011423	0	2.46E-05	0
NA+		0.0423928	0.0423928	0	0.0459059	0	0	0	0.051744	0	0	0	0.0605846	0	0	0	0.0746886	0	0	0	0.0969766	0	0	0.023837	0	0	0.0068609	0.0087764	0.008082	0.012826	0	1.06E-05	0
HS-		0.0001656	0.0001166	0	8.09E-05	2.60E-06	2.31E-06	0	5.45E-05	1.35E-06	1.31E-06	0	3.68E-05	0	9.63E-07	0	2.16E-05	0	7.73E-07	0	1.18E-05	0	5.61E-07	4.93E-06	0	0	1.28E-06	2.38E-06	2.38E-06	3.85E-06	1.09E-06	2.19E-09	0
HSO4-		6.48E-10	6.49E-10	0	1.20E-09	0	0	0	2.40E-10	0	0	0	9.71E-11	0	0	0	3.18E-11	0	0	0	4.79E-12	0	0	2.00E-12	0	0	2.36E-13	3.61E-13	4.00E-14	3.83E-14	0	3.00E-13	0
CL-		0.1055766	0.1055766	0	0.1143257	1.25E-10	1.25E-10	0	0.1288649	2.31E-11	2.31E-11	0	0.1508821	0	1.02E-11	0	0.1860069	0	6.10E-12	0	0.1948947	0	2.00E-12	0.081454	0	0	0.1949608	0.1595642	0.1556274	0.250389	2.05E-11	0.00523	0
OH-		1.55E-09	1.55E-09	0	1.97E-06	3.45E-10	9.85E-12	0	3.31E-06	4.27E-10	1.74E-11	0	3.29E-06	1.41E-08	2.35E-11	0	2.22E-06	1.05E-08	2.92E-11	0	2.87E-06	7.47E-09	4.02E-11	1.20E-06	0	4.39E-09	1.52E-06	1.51E-06	1.92E-06	3.27E-06	2.24E-11	1.50E-08	0
BR-		0.0008815	0.0008815	0	0.0006297	0	0	0	0.00070978	0	0	0	0.0008311	0	0	0	0.0010245	0	0	0	0.0015453	0	0	0.000647	0	0	0.00275	0.0021179	0.0021179	0.003426	0	0.000683	0
SO4--		0.0004570	0.0004571	0	0.0004949	0	0	0	0.00055787	0	0	0	0.0006532	0	0	0	0.0005497	0	0	0	0.0002363	0	0	9.89E-05	0	0	1.65E-05	2.09E-05	1.69E-05	2.59E-05	0	8.96E-07	0
S--		1.69E-11	1.69E-11	0	4.42E-07	7.35E-14	2.08E-16	0	3.41E-07	3.13E-14	2.06E-16	0	2.07E-07	0	2.05E-16	0	8.64E-08	0	2.04E-16	0	3.28E-08	0	2.03E-16	1.37E-08	0	0	1.39E-09	3.17E-09	2.04E-09	3.01E-09	2.28E-16	1.84E-10	0
KCL(S)		0	0	0	0	0	0	0	0	0	0	0	0	0	0	0	0	0	0	0	0	0	0	0	0	0	0.0120432	0.0008021	0.0068287	0.001998	0	0.020731	0
CACL2(S)		0	0	0	0	0	0	0	0	0	0	0	0	0	0	0	0	0	0	0	0	0	0	0	0	0	0	0	0	0	0	0.080251	0
CASO4.2H2O(S)		0	0	0	0	0	0	0	0	0	0	0	0	0	0	0	0.0004579	0	0	0	0.0001093	0	0	0.007197	0	0	0.0010677	0.002946	0.0029532	2.49E-06	0	0.006944	0
NACL(S)		0	0	0	0	0	0	0	0	0	0	0	0	0	0	0	0	0	0	0	0.01558	0	0	0.581037	0	0	0.2680461	0.3701197	0.3719622	0.000627	0	0.880231	0
Air		0	0	0	0	0	0	0	0	0	0	0	0	0	0	0	0	0	0	0	0	0	0	0	0	0	0	0	0	0	0	1.05E-08	0.63392
Component Mass Flow																																	
H2O	KG/HR	425648	425648	39511.38	386148	39511.32	39511.33	53647.5	332492	53647.46	53647.46	61565.18	270922	61575	61565.15	68048.68	202841	68056	68048.65	73803.28	117160	73807	73803.25	11832.23	77114.85	77246	40029.35	51860.51	51860.3	44742.4	375691	158.7012	5774.813
H2S	KG/HR	15.47288	15.47289	37.19849	0.2495419	37.09245	37.10426	16.21737	0.0399023	16.14267	16.14513	10.14534	0.0109473	0	10.08425	7.24535	0.0029443	0	7.191152	4.161184	0.0004848	0	4.118507	4.90E-05	2.015532	0	2.36E-05	6.47E-05	3.05E-05	2.23E-05	76.56242	2.70E-08	0.047533
CA++	KG/HR	11096.7	11096.7	0	11070.46	0	0	0	11052.65	0	0	0	11040.17	0	0	0	10999.16	0	0	0	9942.033	0	0	1004.064	0	0	9922.145	10925.04	10924.94	9425.468	0	181.9972	0
CAOH+	KG/HR	0.0069697	0.0070184	0	33.30525	0	0	0	58.68495	0	0	0	76.4615	0	0	0	90.47763	0	0	0	88.81473	0	0	8.969565	0	0	93.39101	102.3152	102.1233	88.06751	0	14.21857	0
H3O+	KG/HR	0.0016245	0.0016262	0	0.0001408	0.059204	0.052596	0	2.86E-05	0.041719	0.04032	0	9.07E-06	0.000973	0.034099	0	2.58E-06	0.00079915	0.0302527	0	5.58E-07	0.00061676	0.0238231	5.63E-08	0	0.0003795	4.37E-08	8.36E-08	1.86E-08	1.12E-08	0.2349062	2.95E-10	0
K+	KG/HR	1597.219	1597.219	0	1596.807	0	0	0	1596.807	0	0	0	1596.807	0	0	0	1596.807	0	0	0	1450.335	0	0	146.472	0	0	825.5509	1537.322	1090.359	861.6548	0	1.48281	0
NA+	KG/HR	21840.13	21840.13	0	21834.5	0	0	0	21834.5	0	0	0	21834.5	0	0	0	21834.5	0	0	0	10030.06	0	0	1012.954	0	0	678.6859	1241.126	1142.93	967.4581	0	0.638004	0
HS-	KG/HR	60.04874	60.04872	0	38.48576	0.102906	0.091443	0	23.02062	0.072491	0.070101	0	13.27472	0	0.059284	0	6.302378	0	0.0525958	0	2.076321	0	0.041415	0.209692	0	0	0.1266279	0.3366085	0.3368059	0.290606	0.4084051	0.000132	0
HSO4-	KG/HR	0.0003302	0.0003342	0	0.0005706	0	0	0	0.00010118	0	0	0	3.50E-05	0	0	0	9.23E-06	0	0	0	8.44E-07	0	0	8.52E-08	0	0	2.33E-08	5.10E-08	5.66E-09	2.89E-09	0	1.81E-08	0
CL-	KG/HR	54391.38	54391.38	0	54377.36	4.95E-06	4.95E-06	0	54377.36	1.24E-06	1.24E-06	0	54377.36	0	6.28E-07	0	54377.36	0	4.15E-07	0	34273.69	0	1.48E-07	3461.364	0	0	19285.76	22564.96	22008.22	18887.21	7.67E-06	314.8785	0
OH-	KG/HR	0.0007980	0.0007997	0	0.9352705	1.37E-05	3.89E-07	0	1.396971	2.29E-05	9.32E-07	0	1.185709	0.00087	1.45E-06	0	0.6476475	0.00071451	1.99E-06	0	0.5050538	0.00055144	2.97E-06	0.051006	0	0.0003395	0.1501652	0.2148319	0.2720751	0.246456	8.37E-06	0.000901	0
BR-	KG/HR	299.5861	299.5861	0	299.5089	0	0	0	299.5089	0	0	0	299.5089	0	0	0	299.5089	0	0	0	272.0355	0	0	27.47337	0	0	272.0355	299.5089	299.5089	258.4012	0	41.10775	0
SO4--	KG/HR	235.4654	235.4654	0	235.4045	0	0	0	235.405	0	0	0	235.405	0	0	0	160.7085	0	0	0	41.60483	0	0	4.201751	0	0	1.632573	2.951665	2.386998	1.954494	0	0.053975	0
S--	KG/HR	8.70E-06	8.73E-06	0	0.2104119	2.91E-09	8.21E-12	0	0.144064	1.68E-09	1.10E-11	0	0.0747792	0	1.26E-11	0	0.0252487	0	1.39E-11	0	0.0057765	0	1.50E-11	0.000583	0	0	0.0001375	0.000448	0.0002888	0.000227	8.52E-11	1.11E-05	0
KCL(S)	KG/HR	0	0	0	0	0	0	0	0	0	0	0	0	0	0	0	0	0	0	0	0	0	0	0	0	0	1191.329	113.4252	965.688	150.7345	0	1248.215	0
CACL2(S)	KG/HR	0	0	0	0	0	0	0	0	0	0	0	0	0	0	0	0	0	0	0	0	0	0	0	0	0	0	0	0	0	0	4851.88	0
CASO4.2H2O(S)	KG/HR	0	0	0	0	0	0	0	0	0	0	0	0	0	0	0	133.8751	0	0	0	33.97498	0	0	305.8333	0	0	105.6153	416.6151	417.6271	0.187986	0	418.1175	0
NACL(S)	KG/HR	0	0	0	0	0	0	0	0	0	0	0	0	0	0	0	0	0	0	0	2742.687	0	0	24691.11	0	0	26515.45	52351.84	52601.47	47.29471	0	52998.63	0
AIR	KG/HR	0	0	0	0	0	0	0	0	0	0	0	0	0	0	0	0	0	0	0	0	0	0	0	0	0	0	0	0	0	0	0.000634	9999.999

6 Stage Multi-Effect Evaporation for NLZD
Conceptual Design
DRAFT ISSUED FOR REVIEW
NOT FOR CONSTRUCTION

FILENAME	DATE	DRAWN BY
BRINE PFD 10OCT2016.VSD	2/28/16	DLM

REVISIONS

REV.	DATE	DESCRIPTION	BY	CHECKED	APPROVED
1	2/28/16	Preliminary Process Design	DLM		
2	9/27/16	Revise Conc. Brine Pump Discharge Pressure	DLM		

TRIMERIC CORPORATION
P.O. Box 826
Buda, Texas 78610

ISGS BEST
Brine Treatment
Preliminary Process Flow Diagram

CLIENT/SITE: ISGS
DRAWING NUMBER: PFD-602

Figure 2-1-24 Approximate material flows for near-ZLD treatment of the brine by MEE.

PROJECT: ISGS BEST		Water Recovery from Brine by Multi-Effect Evaporator. Near-ZLD basis.						
Brine NZLD by MEE		SECTION 6000	2,000 gpm, 20 wt. % brine, recover ~1,660 gpm water.					
TRIMERIC CORPORATION		9/27/2016	Version 2					
Early Phase Conceptual Capital Cost Estimate								
#	**Item**	**Equipment Name**	**Tag #**	**Quantity**	**Purchased Equipment Cost (total)**	**Installed Cost (total)**	**Power Use (kW)**	**Design Information**
1	Pump	Brine Feed Pumps	P-6101 A/B/C	3 x 50%	$ 64,800	$ 202,000	69.2	3,785 L/min (,1000 gpm) each, 4 bar (58 psi) head, centrifugal pump. 37.5 kW (50 hp) drive. 316SS.
2	Evaporator	1st Stage Evaporator	EV-6001	1	$ 2,369,000	$ 3,662,600	0.0	Horizontal tube evaporator. Approx 3,100 m2 (33,400 ft2) surface area.
3	Evaporator	2nd Stage Evaporator	EV-6002	1	$ 2,369,000	$ 3,662,600	0.0	Horizontal tube evaporator. Approx 3,100 m2 (33,400 ft2) surface area.
4	Evaporator	3rd Stage Evaporator	EV-6003	1	$ 2,369,000	$ 3,662,600	0.0	Horizontal tube evaporator. Approx 3,100 m2 (33,400 ft2) surface area.
5	Evaporator	4th Stage Evaporator	EV-6004	1	$ 2,369,000	$ 3,662,600	0.0	Horizontal tube evaporator. Approx 3,100 m2 (33,400 ft2) surface area.
6	Crystallizer	5th Stage Evaporator / Crystallizer	EVC-6005	1	$ 4,475,800	$ 5,445,400	0.0	Oslo-type crystallizer. 15 tonne/hr solids capacity.
7	Crystallizer	6th Stage Evaporator / Crystallizer	EVC-6006	1	$ 4,475,800	$ 5,445,400	0.0	Oslo-type crystallizer. 15 tonne/hr solids capacity.
8	Pump	3rd stage Condensate Pump	P-6003 A/B	2 x 100%	$ 12,600	$ 55,000	1.8	1,076 L/min (284 gpm), 0.8 bar (11.6 psi) head, centrifual pump. 2.2 kW (3 hp) drive. CS.
9	Pump	4th Stage Condensate Pump	P-6004 A/B	2 x 100%	$ 13,400	$ 56,000	3.5	1,175 L/min (310 gpm), 1.3 bar (19 psi) head, centrigual pump. 4 kW (5.4 hp) drive. CS.
10	Pump	5th Stage Condensate Pump	P-6005 A/B	2 x 100%	$ 14,000	$ 56,800	4.7	1,261 L/min (333 gpm), 1.6 bar (23.2 psi) head, centrifugal pump. 5.5 kW (7.4 hp) drive. CS.
11	Pump	6th Stage Condensate Pump	P-6006 A/B	2 x 100%	$ 14,500	$ 58,000	5.5	1,305 L/min (345 gpm), 1.9 bar (28 psi) head, centrifugal pump. 6 kW (8 hp) drive. CS.
12	Heat Exchanger	Feed Preheater Plate & Frame Exchanger	E-6100	1	$ 121,800	$ 409,300	0.0	Plate & frame heat exchanger, 5 condensate streams with feed brine. 675 m2 (7,263 ft2). 316SS.
13	Heat Exchanger	Final Condenser	E-6401	1	$ 307,100	$ 555,100	0.0	Shell & tube heat exchanger, cooling water on shell side. 1,213 m2 (13,062 ft2) area. TEMA BEM. 316SS tube, CS shell.
14	Vessel	Condensate Receiver	D-6401	1	$ 52,900	$ 220,200	0.0	Vertical vessel. 1.5 m (4.9 ft) diam x 4.5 m (15 ft). 316 SS.
15	Vacuum Pump	Vacuum Pump	VP-6401	1	$ 41,200	$ 70,700	11.0	Oil-sealed single stage vacuum pump. 500 m3/h flowrate assumed. 316SS.
16	Pump	5th Stage Slurry Pump	P-6301 A/B	2 x 100%	$ 18,200	$ 109,500	2.3	423 L/min (112 gpm), 2.4 bar (35 psi) head, slurry pump. 3 kW (4 hp) drive. 316SS.
17	Pump	6th Stage Slurry Pump	P-6302 A/B	2 x 100%	$ 21,200	$ 131,500	6.7	1,019 L/min (269 gpm), 2.8 bar (41 psi) head, slurry pump. 7 kW (9.4 hp) drive. 316SS.
18	Heat Exchanger	Filter Feed Slurry Cooler	E-6301	1	$ 41,500	$ 166,600	0.0	Shell & tube heat exchanger, cooling water on shell side. 101 m2 (1,088 ft2) area. TEMA BEM. 316SS tube, CS shell.
19	Dryer	Salt Dryers	D-6201 A/B/C/D	4 x 25%	$ 2,712,400	$ 3,471,100	40.0	Direct heated (natural gas) rotary dryers. 2.1 MW heat duty (7.3 MMBTU/h) each. 10 kW (13.4 hp) drive.
20	Filter	Salt Filters	F-6301 A/B/C/D	4 x 25%	$ 859,600	$ 1,203,800	22.0	Rotary Drum filters. 71 m2 filtration area each. 5.5 kW (7.4 hp) drive.
21	Filter	Dryer Vent Baghouses	F-6201 A/B/C/D	4 x 25%	$ 72,400	$ 144,200	0.0	Air vent baghouse filters, with shakers. 4200 m3/h (15,000 ft3/h) capacity.
22	Tank	Concentrated Brine Tank	T-6601	1	$ 229,600	$ 361,200	0.0	Low pressure (API-type) storage tank. 7.5 m (25 ft) diam x 9.75 m (32 ft). 420 m3 (111,000 gal). 316SS.
23	Pump	Concentrated Brine Return Pump	P-6601 A/B	2 x 100%	$ 46,800	$ 193,100	22.3	916 L/min (242 gpm), 12.1 bar (175 psi) head, centrigual pump. 22.3 kW (30 hp) drive. 316SS.
24	Pipeline	Concentrated Brine Return Pipeline	Pipeline	1 mile	$ 199,200	$ 387,700	0.0	1 mile of 8" pipe. 316SS.
25	Tank	Recovered Water Tank	T-6701	1	$ 359,000	$ 491,600	0.0	Low pressure (API-type) storage tank. 18 m (59 ft) diam x 12.2 m (40 ft). 3,028 m3 (798,000 gal). CS
26	Pump	Recovered Water Pump	P-6701 A/B	2 x 100%	$ 28,800	$ 96,600	28.7	6294 L/min (1663 gpm), 2 bar (29 psi) head, centrigual pump. 30 kW (40 hp) drive. CS.
27	Boiler	Package Steam Boiler		1	$ 847,000	$ 1,319,500	0.0	Natural gas fired stream boiler. 103,000 kg/h stream production at 6 bar.
28	Power	Power Transformer with Panel		1	$ 72,200	$ 72,200	0.0	Power Transformer and panel. 890 kVA.
29	Cooling Tower	Complete Cooling Tower System		1	$ 778,100	$ 1,156,400	484.0	75,720 L/min (20,000 gpm) Cooling tower (field erected) system. 190 kW (255 hp) pumps (2), 75 kW (100 hp) fans (3).
				Major Equpiment Cost (MEC)	$25,355,900		701.7	
				Installation Cost (IC)	$11,173,400			
				Installed Equipment Cost (IEC)		$ 36,529,300		
				Tax (8% of MEC + 2.5% of IC)	$ 2,307,800			
				Freight (1.6% of MEC)	$ 405,700			
				Contractor Fees (30% of IC)	$ 3,352,000			
				Subtotal		$ 42,594,800		
				Engineering & Procurement (15% of Subtotal)	$ 6,389,200			
				Contingency (20% of Subtotal)	$ 8,519,000			
				Early Phase Capital Cost Estimate		**$57,503,000**		*1Q15 basis. NOTE: Does not include feed brine pretreatment.*

Figure 2-1-25 Capital costs for near-ZLD treatment of the brine by MEE.

PROJECT: ISGS BEST **Water Recovery from Brine by Multi-Effect Evaporator. Near-ZLD basis.**
Brine NZLD by MEE SECTION 6000 2,000 gpm, 20 wt. % brine, recover ~1,660 gpm water.
TRIMERIC CORPORATION 9/27/2016 Version 2
Early Phase Operating Cost Estimate

Operating Cost Factor	Usage Rate	Unit Cost	Cost (rate) $/h	Cost (rate) k$/y
Electrical Power	736 kW	0.08 $/kW-h	59	502
Natural Gas	317 MMBTU/h	4 $/MMBTU	1,268	10,803
Water Product	1,660 gpm	-2 $/kgal	-199	-1,697
Salt Product	65 ton/h	-42 $/ton (dry)	-2,730	-23,260
Labor	12 FTE	100 K$/FTE/y	141	1,200
Maintenance + G&A		4.5 % CAPEX/y	304	2,588
SUBTOTAL OPERATING COST			-1,158	-9,864
Capital Amortization		5 % CAPEX/y	337	2,875
TOTAL OPERATING COST INCLUDING CAPITAL AMORTIZATION			**-820**	**-6,989**
NET UNIT COST FOR TREATING BRINE - $/1000 GAL		**-6.84**		
NET UNIT COST FOR PRODUCT WATER - $/1000 GAL		**-8.24**		

Assumptions:

Operating days/year	355	
Flowrate	2000	GPM
Capital Amortization	20	year, straight-line, no interest
Maintenance & G&A	4.5	pct of CAPEX/year

A positive value for net unit cost indicates the process costs money to operate, a negative value indicates the process generates a profit.

Figure 2-1-26 Operating costs for near-ZLD treatment of the brine by MEE, including values for recovered purified water and produced salt.

PROJECT: ISGS BEST **Water Recovery from Brine by Multi-Effect Evaporator. Near-ZLD basis.**
Brine NZLD by MEE SECTION 6000 2,000 gpm, 20 wt. % brine, recover ~1,660 gpm water.
TRIMERIC CORPORATION 9/27/2016 Version 2
Early Phase Operating Cost Estimate

Operating Cost Factor	Usage Rate	Unit Cost	Cost (rate) $/h	Cost (rate) k$/y
Electrical Power	736 kW	0.08 $/kW-h	59	502
Natural Gas	317 MMBTU/h	4 $/MMBTU	1,268	10,803
Labor	12 FTE	100 K$/FTE/y	141	1,200
Maintenance + G&A		4.5 % CAPEX/y	304	2,588
SUBTOTAL OPERATING COST			1,771	15,093
Capital Amortization		5 % CAPEX/y	337	2,875
TOTAL OPERATING COST INCLUDING CAPITAL AMORTIZATION			**2,109**	**17,968**
NET UNIT COST FOR TREATING BRINE - $/1000 GAL		**17.57**		
NET UNIT COST FOR PRODUCT WATER - $/1000 GAL		**21.17**		

Assumptions:

Operating days/year	355	
Flowrate	2000	GPM
Capital Amortization	20	year, straight-line, no interest
Maintenance & G&A	4.5	pct of CAPEX/year

A positive value for net unit cost indicates the process costs money to operate, a negative value indicates the process generates a profit.

Figure 2-1-27 Operating costs for near-ZLD treatment of the brine by MEE without including values for recovered purified water and produced salt.

Table 2-1-30 Capital and operating costs for MEE at a feed rate of 2,000 gpm (~88% water recovery), and extrapolation to cases of 500, 585, and 5,000 gpm of feed, including values for recovered purified water and produced salt.

Case (gpm)	Capital cost ($)	Annual operating cost ($, including capital amortization)	Net cost for recovered water ($/1,000 gal)
2,000 (base)	57,503,000	−6,989,000	−8.24
500	25,030,000	−35,000	−0.17
585	27,502,000	−280,000	−1.13
5,000	99,645,000	−23,263,000	−10.97

Table 2-1-31 Capital and operating costs for MEE at a feed rate of 2,000 gpm (~88% water recovery), and extrapolation to cases of 500, 585, and 5,000 gpm of feed, without including values for recovered purified water and produced salt.

Case (gpm)	Capital cost ($)	Annual operating cost ($, including capital amortization)	Cost for recovered water ($/1,000 gal)
2,000 (base)	57,503,000	17,968,000	21.17
500	25,030,000	6,204,000	29.24
585	27,502,000	7,019,000	28.28
5,000	99,645,000	39,129,000	18.44

Subtask 2-2 Assessment of Low-TDS Water Treatment Options

An assessment of different desalination and pretreatment technologies for high-salinity brine and an identification of research gaps for each technology are presented under Subtask 2-1. In Subtask 2-2, we focus on screening technologies suitable for treatment of low-TDS water, specifically for brackish water with a TDS of about 3,700 ppm, as in the St. Peter Formation. The best available technologies selected were reverse osmosis and electrodialysis. A series of experiments were conducted to evaluate the performance of different pretreatment and membrane treatment options. Trimeric performed cost estimations for water treatment (using the selected RO technology) for a 2,000 gpm input capacity and used scaling methods for the 500 and 5,000 gpm cases. Cost estimations included capital, operation and maintenance, and the overall cost of water treatment.

Screening of Desalination Technologies for Low-TDS Water

Brackish water desalination is a well-established industrial process. Treatment options with applicability to water from the St. Peter Formation are significantly more abundant than for water from the Mt. Simon Sandstone. The brackish water stream is amenable to conventional treatment processes that result in the recovery of a purified water stream and a higher TDS residual water stream. The initial concentration of NaCl in the brackish water is low enough that the stream can be concentrated significantly before solubility or osmotic pressure limitations are reached. The basis for selecting a technology for brackish water treatment is to concentrate the feed stream as much as practically possible while recovering water. The precipitation of most of the salts (NaCl) in the feed stream would be avoided, although precipitation of minor components might occur.

The technologies identified in Table 2-1-1 for the high-TDS brine treatment assessment were also evaluated for their applicability to brackish water. Unlike with the high-TDS brine treatment screening, most processes were not eliminated based on salinity limitations. The other screening parameters, especially water recovery, energy consumption, treatment costs, and maturity of the technology, were utilized to determine the best treatment option. The results are

summarized in Table 2-2-1. The screening process for low-TDS brackish water was identical to that applied to high-TDS brine. The first question addressed was whether a given technology was technically capable of treating 3,700 ppm of TDS brackish water. Most desalination processes could treat brackish water effectively. The product outlets, including salt waste and recovered water, were then evaluated. Treatment processes having high water recovery and high product purity are desired.

Additional screening considerations were applied; many desalination technologies may be effective at separating salt from low-TDS water, but our goal was to select the best process for St. Peter Formation water treatment based on technical and economic parameters. In some cases, treatment cost data were available from the literature, which might include energy, equipment, labor, maintenance, and other costs. Although a technology with the lowest overall cost is desired—with the overall cost consisting of the combined operating and capital cost—it is considered likely that the most energy-efficient processes will also have lower overall costs. The predicted energy consumption, which is typically the largest expense in desalination processes, and total treatment cost estimates are reported in Table 2-2-1. The values reported here are based on information published by other researchers; thus, the results will not be identical when treating St. Peter Formation water, but the values reported below provide a rough estimate that is useful in selecting a desalination process. For cases in which data for brackish water (TDS <10,000 ppm) were not available, data for seawater desalination (TDS ~35,000 ppm) were used. A seawater desalination cost provides an optimistic estimate because brackish water desalination should generally be less expensive than seawater desalination.

The overall process pros, cons, and assigned TRL values are summarized in Table 2-2-1. These are the specific advantages and challenges expected if a technology is used to treat St. Peter Formation water. A high TRL value (9) indicates that a process is mature and used in industry, whereas lower values indicate that a process is an emerging technology and that further research may be required before applying the process to St. Peter Formation water.

All the screening parameters discussed (potential application of the process to low-TDS brackish water, characteristics of the product, water recovery, energy consumption, treatment costs, pros, cons, and process maturity) were analyzed to assign a preliminary ranking to each technology. A score of 1 is the best possible preliminary ranking.

The most promising treatment technology identified was RO, followed by EDR and combinations of EDR and RO. Membrane processes were generally more energy efficient than evaporative processes, and because of the lower salinity of the St. Peter Formation brackish water. In contrast, the membrane processes were not well suited for the high-salinity Mt. Simon brine.

Reverse osmosis is recommended for this application because it is a relatively simple and less expensive commercially available process that has a proven track record in the desalination industry. Reverse osmosis is more mature than FO, membrane distillation, and membrane crystallization, which do not exhibit any substantial advantages over RO for this application.

Electrodialysis reversal is the most promising alternative to RO. It is also commercially available and exhibits many of the same advantages as RO, but typically with slightly higher costs and slightly less pure product water. The EDR configuration allows for regular purging of scales from the membrane, which would be necessary considering the relatively high water hardness of St. Peter water. This unique part of EDR may result in EDR having an advantage for this application compared with conventional electrodialysis.

Table 2-2-1 Desalination technology screening for St. Peter Formation brackish water.

Evaluation of desalination technologies for desalination of St. Peter water	1	2	3	4	5	6
	Membrane	Membrane	Membrane	Membrane	Membrane	Evaporative concentration
	Reverse osmosis (RO)	Forward osmosis (FO)	Membrane distillation (MD)	Membrane crystallization	Electrodialysis (ED) & electrodialysis reversal (EDR)	Conventional distillation: Multiple-effect distillation (MED) & multiple-stage flash (MSF)
Can 3,700 ppm of TDS brackish water (St. Peter) be treated effectively?	Yes, with the appropriate pretreatment.	Yes, with the appropriate pretreatment.	Yes, with the appropriate pretreatment. Does not seem to have an advantage over conventional evaporation–distillation.	Yes. Can probably be used to recover water with RO without the need for a softening pretreatment.	Yes. Softening or another pretreatment would likely be required. Product water may not be as pure as RO.	Yes. Pretreatment (e.g., softening, pH adjustment) may be required.
Does technology produce a concentrated brine or a solid product?	Concentrated brine.	Concentrated brine.	Concentrated brine.	Concentrated brine. The ZLD approach may not be practical because of the high osmotic pressure.	Concentrated brine.	Concentrated brine.
Characteristics of the recovered brine or salt	Concentrated brine on the order of ~30,000 ppm of TDS.	Brine concentrations >100,000 ppm of TDS have been reported.		Probably similar to conventional RO.		Concentrated brine >30,000 ppm of TDS.
Expected recovery of treated water (%)	Up to 90%.			Probably similar to conventional RO.	Up to 90% for brackish water.	50%–90%
Capability to achieve required purity for recovered water	Good; should meet product requirements.		Good; should meet product requirements.	Probably similar to conventional RO.	Typically not as good as RO water. Can be combined with an RO unit to produce higher purity water.	High-quality water can be recovered.
Energy consumption	Brackish water: 0.5–3 $kWh_{electrical}/m^3$.	Pressure is expected to be lower than RO. Total energy consumption depends on the draw solution recovery step.	Higher than RO for brackish water sources.	Limited data available.	Brackish water: 1.5–7 $kWh_{electrical}/m^3$. Seawater: 17 $kWh_{electrical}/m^3$.	Seawater: 5.5–28 $kW_{elec\ equiv}/m^3$
Treatment cost	\$0.30–\$0.70/m^3				\$0.50–\$1.00/m^3	Seawater: \$0.50–\$1.50/m^3
Pros	Simple, economically proven, well-established technology that is typically economically favored for brackish water.	Probably technically feasible.	Technically feasible. Pervaporation (in other applications) is proven industrially.	Can possibly remove the need for presoftening of feed water.	Well-established technology that has been commercially implemented successfully. Can be less prone to fouling than RO, especially in an EDR configuration.	Well-established, commercially viable technology. Applied at a large scale for treatment of produced and sea waters. Good for locations with waste heat available.
Cons	Source water is hard. Conventional membrane technology will require softening or other additives (pH adjustment, antiscaling).	Advantages versus conventional RO seem minimal. Probably not worth using as a stand-alone process, but may save money by using in hybrid with RO.	Significant pretreatment requirements. No clear advantage versus conventional evaporation–distillation.	Emerging technology. ZLD is probably not practical. The economic advantage compared with conventional RO plus softening is not clear.	Source water is hard and may require softening or other pretreatment. Product water purity may be low.	Various pretreatments are required to prevent solids from fouling heat transfer surfaces. Costs are typically higher than for RO.
Technology readiness level (TRL)	9	~6	~6	<5	9	9
Preliminary ranking (1, 2, 3, 4)	1	4	4	4	2	2. Would be better if waste heat were available.
Selected references (refer to Table 2-1-2)	1–11, 55–57	1, 6, 8, 12–16, 59–60	6, 7, 17, 18, 19, 61, 62	19	1, 5, 6, 10, 11, 16, 19, 20, 21, 63	1, 5, 11, 22–29, 56, 64, 65

Table 2-2-1 continued. Desalination technology screening for St. Peter Formation brackish water.

Evaluation of desalination technologies for desalination of St. Peter water	7	8	9	10	11	12
	Evaporative concentration	**Evaporative concentration**	**Evaporative crystallization**	**Evaporative crystallization**	**Evaporative crystallization**	**Evaporative crystallization**
	Standard brine concentrators	**Humidification compression**	**Standard evaporative crystallizers**	**Spray drying**	**Natural evaporation**	**SAL-PROC**
Can 3,700 ppm of TDS brackish water (St. Peter) be treated effectively?	Yes. Pretreatment (e.g., softening, pH adjustment) may be required.	Yes. Pretreatment (e.g., softening, pH adjustment) may be required.	Can be applied, but not economically. Would be used only in combination with another technology to concentrate the feed.	No. TDS is too low.	Yes, provided that sufficient space is available and water recovery is not an issue.	No. TDS is too low.
Does technology produce a concentrated brine or a solid product?	Concentrated brine.	Concentrated brine.	N/A	N/A	Solid product.	N/A
Characteristics of the recovered brine or salt	Concentrated brine >30,000 ppm of TDS.	Concentrated brine.	N/A	N/A	Impure mixed salt sludge would occasionally be dug out from the pond & landfilled.	N/A
Expected recovery of treated water (%)	50%–90%	Possibly up to 97.5%.	N/A	N/A	Water is not typically recovered.	N/A
Capability to achieve required purity for recovered water	High-quality water can be recovered.	Recovered water should be acceptable.	N/A	N/A	N/A	N/A
Energy consumption	Seawater: 7–12 $kWh_{electrical}/m^3$.		N/A	N/A	N/A	N/A
Treatment cost	\$0.50–\$1.90/m^3		N/A	N/A	N/A	N/A
Pros	A well-established, commercially viable technology. Applied at a large scale for treatment of produced water and seawater. Good for locations with low-cost electric power.	Relatively simple process; may reduce energy consumption with the use of low-grade heat sources.	N/A	N/A	A simple technology.	N/A
Cons	Various pretreatments are required to prevent solids from fouling heat transfer surfaces. Costs are typically higher than for RO.	An emerging technology. Appears to be focused on smaller scale applications.	N/A	N/A	No water recovery; produces a mixed salt sludge.	N/A
Technology readiness level (TRL)	9	~6	N/A	N/A	9	N/A
Preliminary ranking (1, 2, 3, 4)	3	4	N/A	N/A	4	N/A
Selected references (refer to Table 2-1-2)	5, 10, 11, 22, 23, 30–32, 64–66	8, 33–35, 61	1, 36, 37, 64–66	38, 39, 64	6, 40	6

Table 2-2-1 continued. Desalination technology screening for St. Peter Formation brackish water.

Evaluation of desalination technologies for desalination of St. Peter water	13	14	15	16	17	18
	Antisolvent crystallization	**Refrigerated crystallization**	**Refrigerated crystallization**	**Refrigerated crystallization**	**Capacitive deionization**	**Supercritical desalination**
	Antisolvent addition, with antisolvent recovery by distillation	**Cooling crystallization of salt**	**Fractional freeze crystallization of ice**	**Multiple-phase turbo-expansion**	**Capacitive deionization**	**Supercritical desalination**
Can 3,700 ppm of TDS brackish water (St. Peter) be treated effectively?	No. TDS is too low for this to be practical.	No. TDS is too low for crystallization.	Technically feasible, but not economically relevant at low TDS levels	No. Targets higher salinity applications.	Yes.	Not at this time, but technology is under development for seawater desalination applications.
Does technology produce a concentrated brine or a solid product?	N/A	N/A	N/A	N/A	Concentrated brine.	Concentrated brine.
Characteristics of the recovered brine or salt	N/A	N/A	N/A	N/A	Probably similar to conventional RO brine.	
Expected recovery of treated water (%)	N/A	N/A	N/A	N/A	80–90%.	Limited information is available.
Capability to achieve required purity for recovered water	N/A	N/A	N/A	N/A	Good water quality can be obtained directly from capacitive deionization.	Should meet product requirements.
Energy consumption	N/A	N/A	N/A	N/A		Limited information is available. Odu et al. (2015) reported ~125 $kWh_{thermal}/m^3$ for seawater desalination.
Treatment cost	N/A	N/A	N/A	N/A		N/A
Pros	N/A	N/A	N/A	N/A	A relatively simple technology, with high recovery of water possible. Appears to be further in development (some commercial applications) compared with other emerging technologies.	Not likely to be advantageous for low-salinity applications.
Cons	N/A	N/A	N/A	N/A	Most commercial applications appear fairly small scale. It is not clear that it has significant advantages over existing technologies.	Technology is still in the experimental stages and is probably best applied to higher salinity feeds.
Technology readiness level (TRL)	N/A	N/A	N/A	N/A	7–9	N/A
Preliminary ranking (1, 2, 3, 4)	N/A	N/A	N/A	N/A	3	N/A
Selected references (refer to Table 2-1-2)	41	6	1, 42–46, 61, 67–70	47	48–50	71

Table 2-2-1 continued. Desalination technology screening for St. Peter Formation brackish water.

Evaluation of desalination technologies for desalination of St. Peter water	19	20	21
	Extraction	Ion exchange	Adsorption
	Solvent extraction	Ion exchange	Adsorption
Can 3,700 ppm of TDS brackish water (St. Peter) be treated effectively?	No. Solvent extraction would likely be focused on high-TDS water streams.	No. TDS is too high (typical applications are 500 ppm maximum).	Possibly. Technology does not seem particularly promising.
Does technology produce a concentrated brine or a solid product?	N/A	N/A	
Characteristics of the recovered brine or salt	N/A	N/A	
Expected recovery of treated water (%)	N/A	N/A	
Capability to achieve required purity for recovered water	N/A	N/A	
Energy consumption	N/A	N/A	
Treatment cost	N/A	N/A	
Pros	N/A	N/A	
Cons	N/A	N/A	
Technology readiness level (TRL)	N/A	N/A	<5
Preliminary ranking (1, 2, 3, 4)	N/A	N/A	4
Selected references (refer to Table 2-1-2)	51	1	52, 53

Treatment of the brackish water stream by an evaporation technology is technically feasible but would probably be economical only if a large quantity of waste heat or low-cost fuel were available. Similarly, capacitive deionization (no. 17) and adsorption (no. 21) should be possible for low-TDS water, but they do not appear advantageous when compared with RO.

Several technologies, including refrigeration processes, crystallization technologies, and extraction technologies, are likely not practical for such low-TDS water, because salt recovery is not required or desired. These processes target high-TDS applications or cases in which salt recovery is desired, or both.

The TDS level in the brackish water stream is in an optimal range for treatment with RO membranes intended for brackish water treatment. Barring other factors gaining unforeseen prominence (e.g., the fate of small-concentration components, dealing with hardness components, energy sources, or integration with other facilities), RO would likely be the most economical method for concentrating brackish water and recovering a usable water product.

Pretreatment Technologies

Reverse osmosis is not the only unit operation that would be required to treat brackish water. Additional unit operations might include pretreatment of the feed to the RO unit, such as

filtration, carbon treatment, softening, pH adjustment, or the addition of antifouling chemicals. A chemical precipitation step might possibly also be desired. Following the RO treatment, the concentrated stream might need to be subjected to further filtration, pH adjustment, or both before being disposed of (presumably by subsurface injection). Further treatment requirements for the recovered water would likely be minimal.

Pretreatment will focus on removing only suspended solids and scale-forming species because brackish water from the St. Peter Formation contains negligible amounts of oil or other contaminants. Refer back to Table 2-1-5 (Subtask 2-1) for a summary of available pretreatment technologies and their potential applicability to low-TDS water extracted from the St. Peter Formation.

Cost Estimations for Low-TDS Brackish Water Treatment

The ISGS evaluated the recovery of purified water from a subsurface brackish water stream to be pumped from the St. Peter Formation. The recovered water would be suitable for service water use at the ADM facility (Decatur, IL), and the water reject stream could be disposed by subsurface injection or possibly in the ADM wastewater treatment facility. Trimeric estimated the cost of an RO unit to treat this stream, developed a basic PFD, and estimated a preliminary material balance for the process. The PFD and material balance are presented in Figures 2-2-1 and 2-2-2. Assumptions for developing the RO unit design are as follows:

1. The feed stream contains negligible concentrations of hydrocarbon. A typical TOC limit for RO units is 3 ppm. An activated carbon filter would likely be required if the TOC in feed water exceeds 3 ppm. This estimate has provided no cost for TOC treatment. A full analysis of the feed stream, including hydrocarbon contaminants is required in a demonstration or industrial-scale project.
2. The feed stream turbidity and salt density index (SDI) can be adequately treated with multimedia filter beds. This assumes that the suspended solids in the feed stream are larger than 15–20 µm in diameter or that a coagulant chemical may be injected into the feed stream to agglomerate small particles into large enough particles for the multimedia filter beds to remove them. The SDI for the feed stream entering the RO should be less than 5 µm and ideally less than 3 µm. Trimeric strongly recommends completing an SDI test on the feed stream if this project moves forward into the next phase.
3. The RO portion of the new facility will be divided into individual modular treating units that are "off the shelf." For this project, the cost estimation of the RO modules was provided by a vendor.
4. The RO unit will have a relatively small storage tank volume to reduce exposure of the water stream to oxygen, which could result in the precipitation of otherwise soluble species. A small storage volume will minimize the cost of the RO unit. The permeate (product) water tank was sized for 8 h of storage capacity at 2,000 gpm of feed water.
5. The RO units will be installed in a building that will be near the extraction well. The permeate storage tank will be installed in close proximity to the RO units.

Brackish water is assumed to be available from a well (the cost of the well and well pump are not included in this estimate) at a low pressure; a pump is used to boost the pressure of the water to send it through a pretreatment system, which is intended to remove a small amount of TSS (18.5 mg/L). The pretreatment consists of a coarse filter (or screen), followed by multimedia filters (primarily sand). Small amounts of chemicals, such as coagulants, flocculants, or antiscaling additives, may be required to enhance filtration and avoid fouling of the membranes.

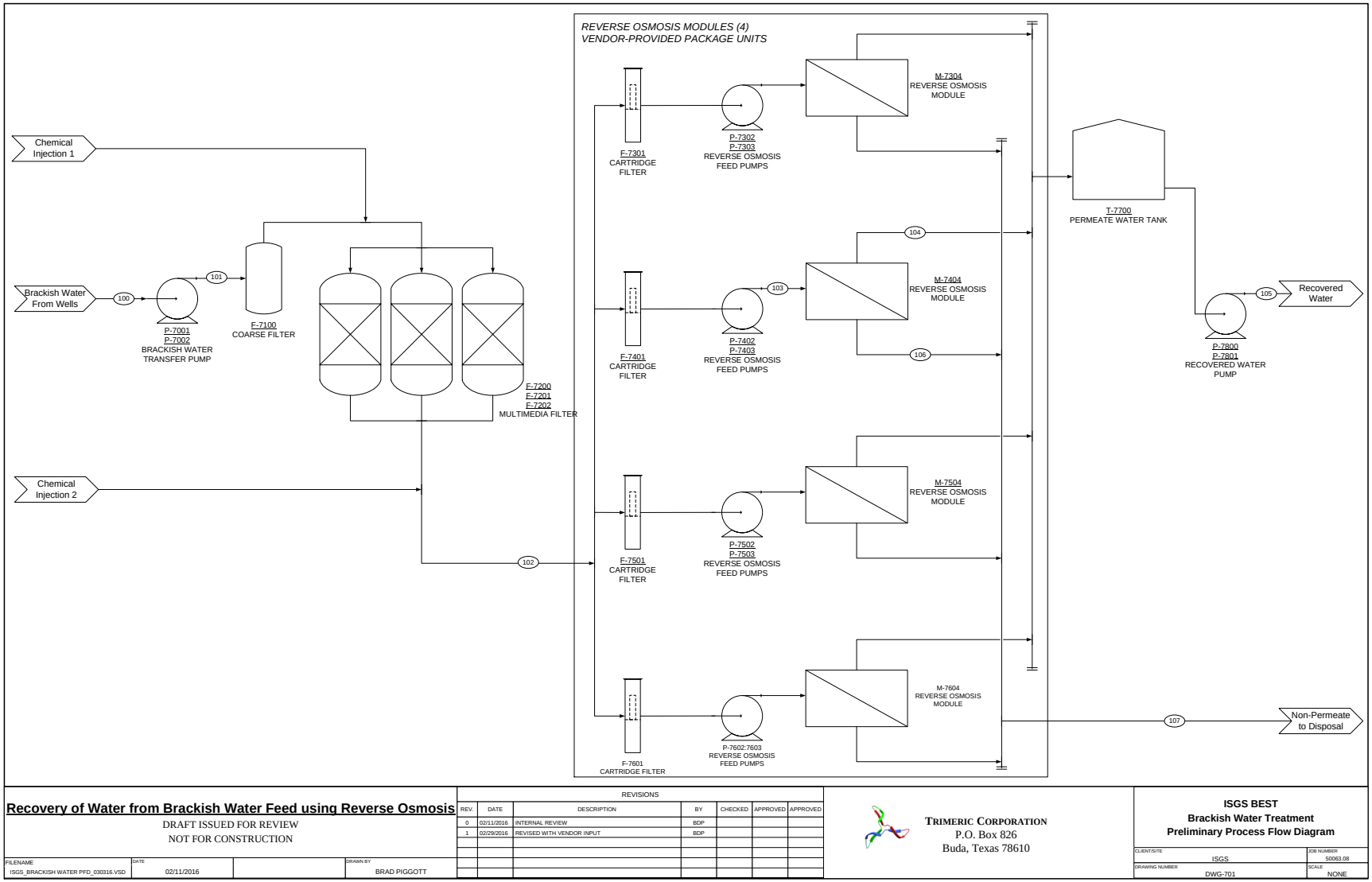

Figure 2-2-1 PFD for brackish water treatment by RO.

Stream Number		100	101	102	103	104	105	106	107
Stream Name	Units	Raw Water Feed	Feed Pump Discharge	Feed to RO System	RO Pump Discharge	Permeate Stream	Recovered Water	Reject Stream	Reject to Outfall
Temperature	°C	25	25	25	25	25	25	25	25
Pressure	bara	1	10	3.9	17.7	1.7	3.0	16.7	16.7
Flow Rate	gpm	2,000	2,000	2,000	500	425	1,700	75	300
	L/min	7,570	7,570	7,570	1,893	1,609	6,435	284	1,136
pH		7.70	7.70	7.70	7.70				
TSS	mg/L	18.50	18.50						
Turbidity	NTU	9.50	9.50	< 1	< 1				
TDS	mg/L	3,692.50	3,692.50	3692.5	3692.5	217	217	23,386	23,386
Cationic Species	MW (g/gmol)	mg/L	mg/L	mg/L	mg/L	mg/L	mg/L	mg/L	mg/L
Na^{+}	22.99	1,130.25	1,130.25	1,130.25	1,130.25	66.49	66.49	7,158.25	7,158.25
Ca^{2+}	40.08	69.55	69.55	69.55	69.55	4.09	4.09	440.48	440.48
K^{+}	39.10	42.43	42.43	42.43	42.43	2.50	2.50	268.74	268.74
Mg^{2+}	24.31	27.88	27.88	27.88	27.88	1.64	1.64	176.54	176.54
Fe^{3+}	55.85	0.58	0.58	0.58	0.58	0.03	0.03	3.67	3.67
Mn^{2+}	54.94	0.17	0.17	0.17	0.17	0.01	0.01	1.07	1.07
Ba^{2+}	137.33	0.06	0.06	0.06	0.06	0.00	0.00	0.39	0.39
Sum of Cations		1,270.92	1,270.92	1,270.92	1,270.92	74.76	74.76	8,049.14	8,049.14
Anionic Species	MW (g/gmol)	mg/L	mg/L	mg/L	mg/L	mg/L	mg/L	mg/L	mg/L
Cl^{-}	35.45	1,874.75	1,874.75	1,874.75	1874.75	110.28	110.28	11,873.42	11,873.42
$SO4^{2-}$	96.06	222.25	222.25	222.25	222.25	13.07	13.07	1,407.58	1,407.58
CO_3^{2-}	60.01	233.75	233.75	233.75	233.75	13.75	13.75	1,480.42	1,480.42
Br^{-}	79.90	8.22	8.22	8.22	8.22	0.48	0.48	52.06	52.06
F^{-}	19.00	3.29	3.29	3.29	3.29	0.19	0.19	20.85	20.85
Sum of Anions		2,342.26	2,342.26	2,342.26	2,342.26	137.78	137.78	14,834.33	14,834.33
Neutral Species	MW (g/gmol)	mg/L	mg/L	mg/L	mg/L	mg/L		mg/L	mg/L
SiO_2	60.08	6.16	6.16	6.16	6.16	0.36	0.36	38.98	38.98

Recovery of Water from Brackish Water Feed using Reverse Osmosis

DRAFT ISSUED FOR REVIEW
NOT FOR CONSTRUCTION

FILENAME: ISGS_BRACKISH WATER PFD_030316.VSD | DATE: 02/11/2016 | DRAWN BY: BRAD PIGGOTT

REVISIONS

REV.	DATE	DESCRIPTION	BY	CHECKED	APPROVED	APPROVED
0	02/11/2016	INTERNAL REVIEW	BDP			
1	02/29/2016	REVISED WITH VENDOR INPUT	BDP			

TRIMERIC CORPORATION
P.O. Box 826
Buda, Texas 78610

ISGS BEST
Brackish Water Treatment
Preliminary Process Flow Diagram

CLIENT/SITE: ISGS | JOB NUMBER: 50063.08
DRAWING NUMBER: DWG-702 | SCALE: NONE

Figure 2-2-2 Approximate material balance for brackish water treatment by RO.

The filtered water would then enter the membrane skids (four 500-gpm units in parallel). Pumps on the skids would boost the pressure of the water to approximately 242 psig (17.7 bar) before it enters the membrane modules.

The permeate from the membrane modules would be the recovered product water, which would be stored in a tank and pumped to users. Approximately 85% (1,700 gpm) of the water fed to the system would be recovered as product purified water. The reject (nonpermeate) stream is the concentrated brine stream, which is assumed to flow, at its remaining line pressure ≥ 150 psi, through a 1-mi (1.6-km) pipeline to the disposal location (injection well). In this case, the pipeline was designed to have a diameter of 6 in. and constructed using 316SS. The material selection for the pipeline is preliminary, and further work will be required to confirm the proper material of construction for this application as the design of the project advances. Corrosion tests should be considered in the future to determine whether this metal alloy is a suitable material of construction.

The capital cost estimate for the 2,000-gpm RO unit is provided in Figure 2-2-3. Figures 2-2-4 and 2-2-5 summarize the total capital and operating costs for this process based on treating 2,000 gpm of brackish water, with and without a value for the recovered purified water. Capital costs were estimated with the Aspen Capital Cost Estimator (v.8.7.1) based on vendor budgetary estimates for the membrane skids and Trimeric estimates for the remaining equipment. The data for the 2,000-gpm-capacity unit and typical cost-scaling methodologies were used to estimate the capital and operating costs for 500- and 5,000-gpm-capacity units. These data are shown in Tables 2-2-2 and 2-2-3, with and without a value for the recovered purified water.

PROJECT: ISGS BEST **Brackish Water Treatment System**
BRACKISH WATER RO PLANT SECTION 7000 2,000 gpm St. Peter's Formation Feed
TRIMERIC CORPORATION 9/27/2016 Version 2
Early Phase Conceptual Capital Cost Estimate

#	Item	Equipment Name	Tag #	Quantity	Purchased Equipment Cost (total)	Installed Cost (total)	Electrical Power (kW)	Design Information
1	Pump	Brackish Water Transfer Pump	P-7001, P-7002	2 x 100%	$ 145,800	$ 239,300	159	7,570 L/min (2000 gpm), 92 m (302 ft) head, centifugal pump. 186 kW (250 hp). CS.
2	Filter	Coarse Filter	F-7100	1	$ 102,500	$ 276,800	0	4.3 m (14 ft) diam x 6.1 m (20 ft) coarse filter vessel. CS.
3	Filter	Multimedia Filter	F-7200, F-7201, F-7202	3 x 33%	$ 393,900	$ 890,800	0	4.3 m (14 ft) diam x 6.1 m (20 ft) layered sand-type filter vessel, vertical, downflow. CS.
4	Package System	Reverse Osmosis Module	M-7300, M-7400, M-7500, M-7600	4 x 25%	$1,100,000	$ 1,650,000	313	Module includes cartridge filtes, RO pumps, and RO membranes. 17.7 bar (256 psi) operating pressure.
5	Tank	Permeate Water Tank	T-7700	1	$ 406,200	$ 532,100	0	2,452 m3 (912,000 gal). 24.4 m (80 ft) diam x 6.6 m (21.7 ft), low pressure (API-type) storage tank. 8 hr storage. CS.
6	Pump	Permeate Water Pump	P-7800, P-7801	2 x 100%	$ 32,600	$ 101,300	26	6,435 L/min (1,700 gpm), 20.4 m (67 ft) head, centifugal pump. 29.8 kW (40 hp). CS.
7	Pipeline	Reject Pipeline to Reinjection	Pipeline	1 mile	$ 163,400	$ 317,900	0	6" x 1 mile pipeline. 316SS.
8	Power	Power Transformer with Panel			$ 60,200	$ 60,200		653 kVA power transformer with panel.
9	Building	Building for System			$ 300,000	$ 300,000		14 m (46 ft) W x 18.3 m (60 ft) L x 7.6 m (25 ft) H building. Contains modules, MM Filter, Inlet Filter.

Major Equpiment Cost (MEC)	$2,704,600		
Installation Cost (IC)	$1,663,800		
Installed Equipment Cost (IEC)		$ 4,368,400	
Tax (8% of MEC + 2.5% of IC)	$ 258,000		
Freight (1.6% of MEC)	$ 43,300		
Contractor Fees (30% of IC)	$ 499,100		
SUBTOTAL		$ 5,168,800	
Engineering & Procurement (15% of Subtotal)	$ 775,300		
Contingency (20% of Subtotal)	$1,033,800		
Early Phase Capital Cost Estimate		**$6,978,000**	*2,000 gpm feed, 1,700 gpm water recovered. 1Q15 Capital Cost Basis. Does not include well, well pump, or other downhole equipment*

Figure 2-2-3 Facility costs for brackish water treatment by RO.

PROJECT: ISGS BEST **Brackish Water Treatment System**
BRACKISH WATER RO PLANT SECTION 7000 2,000 gpm St. Peter's Formation Feed
TRIMERIC CORPORATION 9/27/2016 Version 2
Early Phase Operating Cost Estimate

Operating Cost Factor	Usage Rate	Unit Cost	Cost (rate)	
			$/h	k$/y
Electrical Power	522 kW	0.08 $/kW-h	41.8	356
Antiscalant	1 kg/h	3.23 $/kg	3.2	28
Other Chemicals	1 kg/h	3 $/kg	3.0	26
Membrane Replacement	86.4 membranes/yr	600 $/membrane	5.9	52
Water Product	1,700 gpm	-2 $/kgal	-204.0	-1738
Labor	2 FTE	100 K$/FTE/y	23.5	200
Maintenance + G&A		3.5 % CAPEX/y	28.7	244
SUBTOTAL OPERATING COST			-98.0	-833
Capital Amortization		5 % CAPEX/y	41.0	349
TOTAL OPERATING COST INCLUDING CAPITAL AMORTIZATION			**-57.0**	**-484**

NET UNIT COST FOR TREATING BRACKISH WATER - $/1000 GAL	**-0.48**
NET UNIT COST FOR PRODUCT WATER - $/1000 GAL	**-0.56**

Assumptions:

Operating days/year	355	
Flowrate	2000	GPM
Capital Amortization	20	year, straight-line, no interest
Maintenance & G&A	3.5	pct of CAPEX/year (excludes membranes)

A positive value for net unit cost indicates the process costs money to operate, a negative value indicates the process generates a profit.

Figure 2-2-4 Operating costs for brackish water treatment by RO, including a value for recovered purified water.

PROJECT: ISGS BEST **Brackish Water Treatment System**
BRACKISH WATER RO PLANT SECTION 7000 2,000 gpm St. Peter's Formation Feed
TRIMERIC CORPORATION 9/27/2016 Version 2
Early Phase Operating Cost Estimate

Operating Cost Factor	Usage Rate	Unit Cost	Cost (rate)	
			$/h	k$/y
Electrical Power	522 kW	0.08 $/kW-h	41.8	356
Antiscalant	1 kg/h	3.23 $/kg	3.2	28
Other Chemicals	1 kg/h	3 $/kg	3.0	26
Membrane Replacement	86.4 membranes/yr	600 $/membrane	5.9	52
Labor	2 FTE	100 K$/FTE/y	23.5	200
Maintenance + G&A		3.5 % CAPEX/y	28.7	244
SUBTOTAL OPERATING COST			106.0	905
Capital Amortization		5 % CAPEX/y	41.0	349
TOTAL OPERATING COST INCLUDING CAPITAL AMORTIZATION			**147.0**	**1,254**

NET UNIT COST FOR TREATING BRACKISH WATER - $/1000 GAL	**1.22**
NET UNIT COST FOR PRODUCT WATER - $/1000 GAL	**1.44**

Assumptions:

Operating days/year	355	
Flowrate	2000	GPM
Capital Amortization	20	year, straight-line, no interest
Maintenance & G&A	3.5	pct of CAPEX/year (excludes membranes)

A positive value for net unit cost indicates the process costs money to operate, a negative value indicates the process generates a profit.

Figure 2-2-5 Operating costs for brackish water treatment by RO, without including a value for recovered purified water.

Table 2-2-2 Capital and operating costs for an RO unit at a feed rate of 2,000 gpm and extrapolation to cases of 500 and 5,000 gpm of feed, including a value for recovered purified water.

Case (gpm)	Capital cost ($)	Annual operating cost ($, including capital amortization)	Net cost for recovered water ($/1,000 gal)[1]
2,000 (base)	6,460,000	−484,000	−0.56
500	2,131,000	76,000	0.35
5,000	13,446,000	−1,370,000	−0.64

[1]A positive value for the net unit cost indicates the process costs money to operate; a negative value indicates the process generates a profit.

Table 2-2-3 Capital and operating costs for an RO unit at a feed rate of 2,000 gpm and extrapolation to cases of 500 and 5,000 gpm feed, without including a value for recovered purified water.

Case (gpm)	Capital cost ($)	Annual operating cost ($, including capital amortization)	Cost for recovered water ($/1,000 gal)
2,000 (base)	6,460,000	1,254,000	1.44
500	2,131,000	511,000	2.35
5,000	13,446,000	2,975,000	1.36

Subtask 2-3 Geochemical Modeling

Four geochemical simulation scenarios were performed to evaluate the scaling potential and compatibility between brines from the Mt. Simon Sandstone and Potosi Dolomite. Scenarios 1 and 2 simulated the cooling and exposure of Mt. Simon brine to air. Both represent relatively simple processes that were modeled as batch reactions. These scenarios were initially modeled using the modeling software Phreeqc (Parkhurst and Appelo, 1999) and then revised to run using React (Bethke, 2008); only the final models are discussed here. Scenarios 3 and 4 simulated one-dimensional radial flow of air-equilibrated brine and pretreated brine injected into the Potosi Dolomite using using X1t software (Bethke, 2008).

Simulation results suggest that the likelihood of scale formation caused by the short transit time and slow kinetics of silicate precipitation would be low. When results of the extraction model were then fed into a simulation of extracted brine interacting with air, oxides formed that aided in the removal of trace metals. The results of the injection models demonstrate the importance of understanding formation petrology in determining the extent of the injection plume.

Scenario 1: Cooling Brine

The most basic scenario was the extraction of brine from the Mt. Simon, with the brine cooling down to surface temperature during transport. The modeled temperature decrease from 122 °F (50 °C) to 77 °F (25 °C) was considered a reasonable approximation of an average surface temperature. The pressure decrease was omitted from the model because pressure had little impact on the mineral saturation states. The cooling model was run twice, once with an extended Debye-Hückel thermodynamic database (Wolery, 1992) and once with a Pitzer database (Harvie et al., 1984). The Pitzer database was more accurate in modeling highly saline solutions such as the

brines in this study; however, it is a smaller database that considers fewer aqueous species and does not allow for redox reactions.

The brine modeled is the sample described in Table 2-3-1. All minerals were considered to be at equilibrium with the water. This assumption allowed precipitation to occur, which would equate to potential well scale formation. Several minerals were excluded from the equilibrium calculations, such as muscovite and other well-ordered crystalline materials; because it was kinetically unlikely they would form during brine extraction. Some oxides were also excluded because they clearly did not form during the sampling process, as evidenced by the presence of trace uranium and vanadium concentrations. The final modeling script is listed in Appendix A.

Table 2-3-1 Measured concentrations (µg/L) of elements in a Mt. Simon brine sample.

Al	As	Ba	Ca	Co	Cr	Cs
2,790	4.58	3,450	2.3×10^7	4.71	32.40	173
Cu	**Fe**	**K**	**Li**	**Mg**	**Mn**	**Na**
95	70,800	1430,000	16,100	1,830,000	57,300	3.7×10^7
Si	**Sn**	**Sr**	**U**	**V**	**Zn**	**pH**
18,500	21.20	644,000	2.59	20.20	3,000	5.37

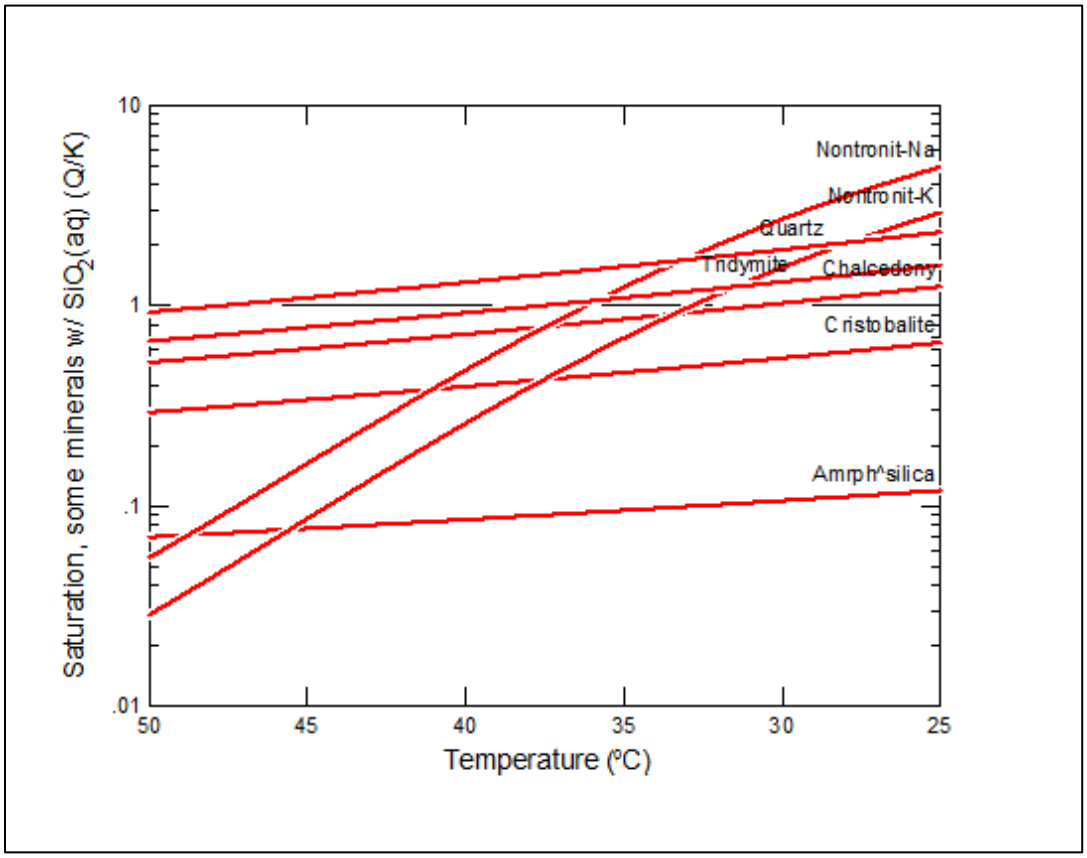

Figure 2-3-1 Changes in the mineral saturation state as brine cools during extraction when quartz is not allowed to precipitate.

Figure 2-3-1 shows the results of the first extraction scenario. There is no mineral precipitation; however, several of the quartz polymorphs are oversaturated in the cooled brine alone, whereas amorphous silica is undersaturated. This result is somewhat ambiguous because of the uncertainty of equilibrium constants for the amorphous phases. Therefore, a silica phase has some potential to precipitate, up to 4.12 mg/kg of brine, if quartz precipitates. However, this is a maximum estimate and any precipitation would likely be limited by kinetics. Some clay minerals are also oversaturated in the final brine, but allowing for some silica precipitation keeps these minerals from becoming saturated (Figure 2-3-2).

The results of the model using Pitzer equations also yielded no mineral precipitation. However, the silica and aluminum phases were omitted because of limitations of the thermodynamic database. This was the only scenario run using the Pitzer equations; the others involved redox reactions for which the database did not have coefficients.

For this scenario, the model calculations show that the chances of scale formation are minute because the kinetics of silicate precipitation are too slow to be of interest during the short cooling time.

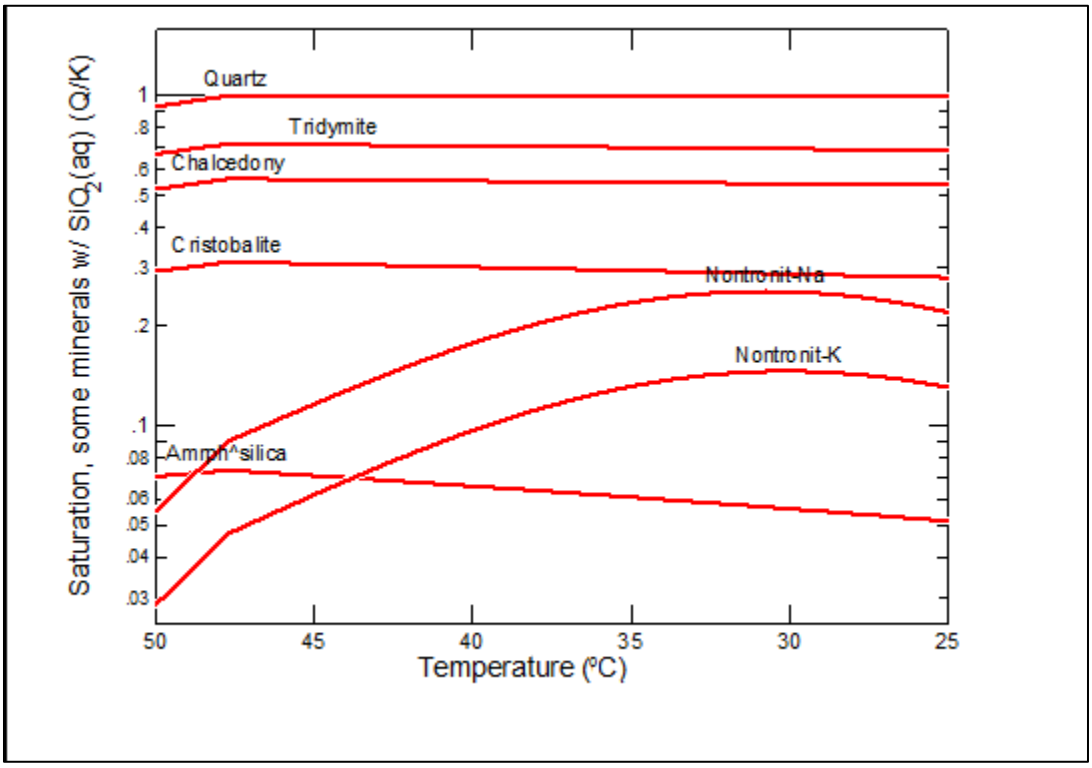

Figure 2-3-2. Changes in the mineral saturation state as brine cools during extraction when quartz is allowed to precipitate.

Scenario 2: Exposure of Brine to Air

The model for this scenario was built on the results of the previous scenario. The chemical composition from the cooling model was used as input Scenario 2. Given the initial brine chemistry, the fugacity of O_2 and CO_2 was increased to 0.2 and 0.0032 bar, respectively, to simulate the exposure of the brine to air at ambient pressure and the attainment of equilibrium. The model used the same Debye-Hückel thermodynamic database as the previous model and had the

same limitations on mineral precipitation. An additional database of two-layer surface sorption on iron oxides (Dzombak and Morel, 1990) was added to account for potential changes in trace metals as iron oxidized and dropped out of solution. A listing of the modeling script is provided in Appendix A.

The precipitation of iron and manganese oxides increased as the fugacity of O_2 increased, as shown in Figure 2-3-3. The initial precipitation of $Fe(OH)_3$ was very rapid, but birnessite ($Mn_8O_{19}H_{10}$) eventually outcompeted $Fe(OH)_3$ for O_2 and re-reduced some of the iron. The precipitation of iron oxide also drove the removal of metals from solution as they sorbed onto the newly formed mineral surface (Figure 2-3-4). As the reaction continued, the amount of metals on the surface appeared to decrease; however, this was because birnessite was precipitating, which caused $Fe(OH)_3$ to dissolve. In reality, there would also be sorption onto the birnessite surface, but we lacked a database to model these reactions. The concentration of CO_2 in solution decreased when exposed to the atmosphere, so this did not drive precipitation.

The reaction of brine with the atmosphere was favorable because it caused the removal of trace metals via sorption and co-precipitation, although given the large flow rates of brine that will be extracted, the attainment of equilibrium of the trace metals with air, if desired, might represent a significant unit operation. The amount of sorption calculated by the model was a minimum because the model could be improved by the creation and incorporation of further thermodynamic data.

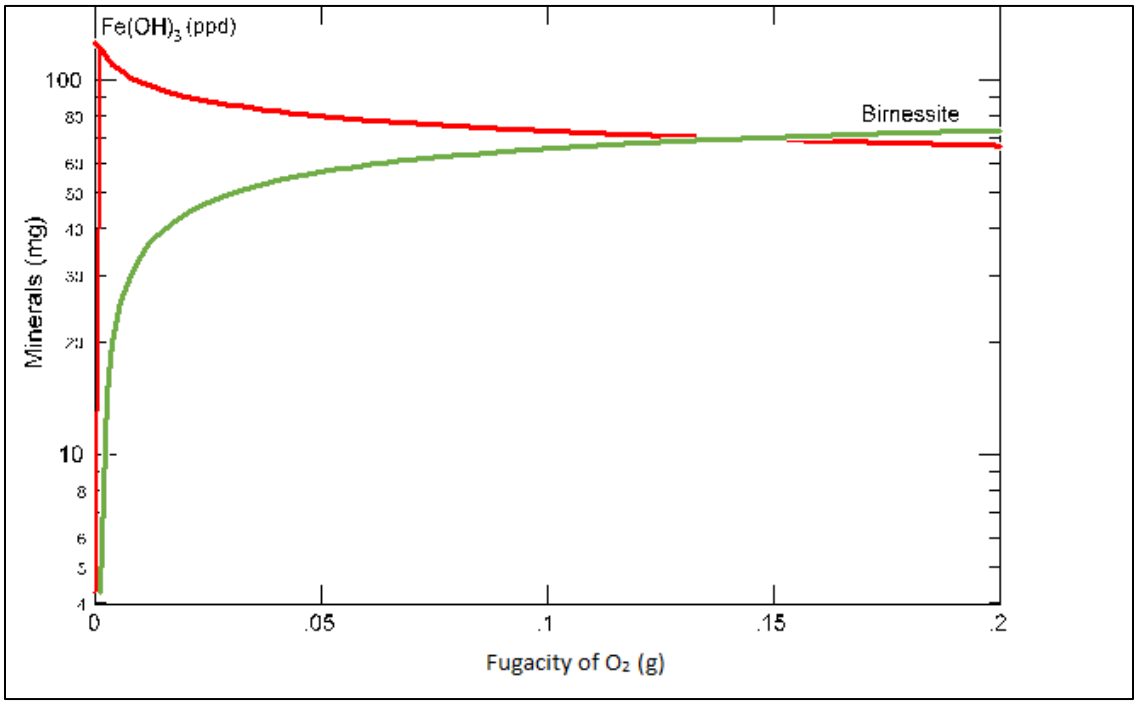

Figure 2-3-3 Modeled precipitation of oxides when Mt. Simon brine equilibrates with air.

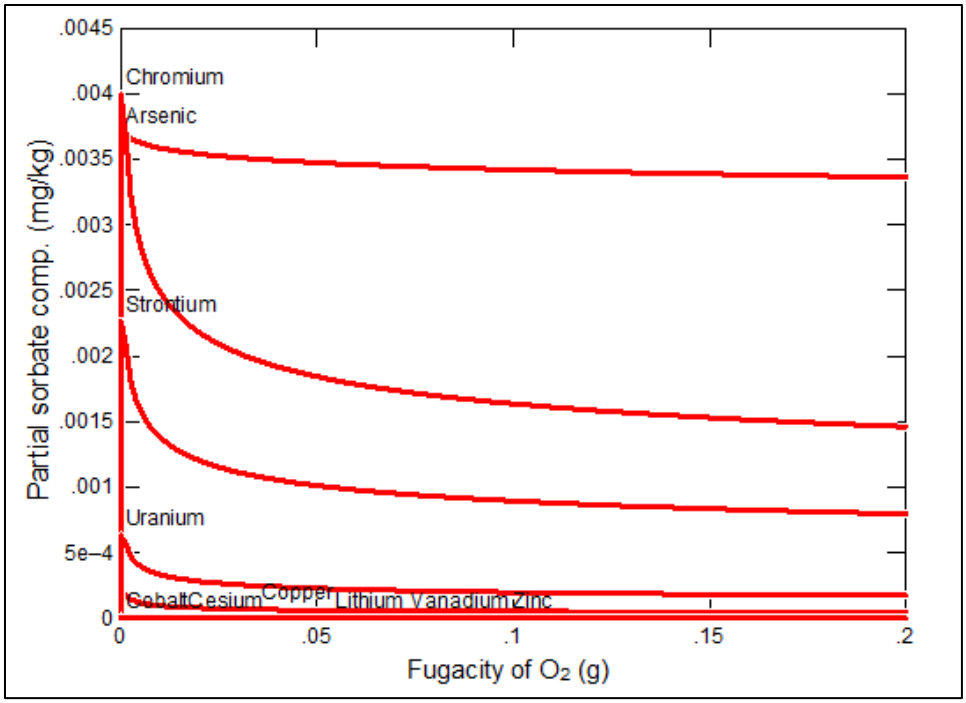

Figure 2-3-4 Sorption of trace metals onto iron oxides while Mt. Simon brine equilibrates with air. The initial spike is due to the fast precipitation of $Fe(OH)_3$ and the slow decrease is due to the formation of birnessite.

Scenario 3: Injecting Oxidized Brine

This scenario was again built on the results of the previous one. The input chemistry was the composition of the brine after the precipitation of oxides and sorption reactions in the air exposure model (Scenario 2). The Scenario 3 model took this base brine, increased the temperature to 109 °F (43 °C), and simulated the injection of this fluid into the Potosi Dolomite. This formation had high permeability because of its karstic morphology. This morphology resulted in a dual-porosity system in which the formation had large, approximately 0.9-ft (0.3-m) openings, as well as smaller and less contiguous matrix porosity. Further complicating the system, quartz coated the inside of the large vugs and potentially isolated the conductive open channels from the rest of the formation (Freiburg and Leetaru, 2012).

To simulate the injection, a one-dimensional radial grid model was created to simulate brine injection at 20,000 bbl/day into a 30.3-ft (10-m) injection zone. In X1t, dual porosity was modeled as a free-flowing zone connected to stagnant zones with diffusive exchange between the two. It is this exchange that the quartz linings might inhibit. To evaluate the impact of these linings, we ran the model with free diffusion between the different zones and with inhibited diffusion (a lower set diffusion coefficient). Table 2-3-2 shows the initial mineralogy of the system, Table 2-3-3 shows the brine composition, and Table A-3 (in Appendix A) contains the input script. The simulation assumed all minerals initially present in the system maintained equilibrium with the fluid, except quartz, which had a low kinetic reaction set.

Both model results showed minor amounts of mineral dissolution and precipitation. The main differences between the two results are the distance traveled and the shape of the displacing fluid front as it moves away from the injection well (Figures 2-3-5 and 2-3-6). The high-salinity Mt. Simon brine (displacing fluid) displaced the lower salinity Potosi brine (displaced fluid). The

high-salinity brine plume in the freely diffusing model was sharper and the plume traveled less than half the distance it covered in the isolated channel model because exchange with formation matrix retarded its movement.

The same pattern was evident in the plots of trace metals (Figures 2-3-7 and 2-3-8). However, the trace metal concentrations did not show a concentration front at the same location as the dissolved solids. The amount of retardation that occurred for each component depended on the amount of transfer between the free-flowing and stagnant zones. Therefore, a component with similar concentrations in both zones would experience less diffusion between zones and therefore less retardation. The dissolved solids plot was dominated by Na^+ and Cl^-, which showed a large difference between the injected and native brines and were therefore more retarded. The concentration difference for the trace metals was lower, which led to less retardation.

Overall, there was no evidence of significant mineral precipitation. In addition, these results emphasized the importance of developing a further understanding of the Potosi Dolomite and that the petrology of the unit plays a vital role in understanding fluid flow through the formation.

Table 2-3-2 Mineral composition of the Potosi Dolomite by volume. Results are an average of two XRD analyses of samples from a depth of 1,379 m (4,524 ft).

	Dolomite	Calcite	Siderite	Quartz	Clay	Pyrite
Volume (%)	82.30	0.67	1.33	13.00	2.00	0.67

Table 2-3-3 Potosi brine composition used in the models (µg/L).[1]

Al	As	Ba	Ca	Co	Cr	Cs
20	1.00×10^{-3}	235	5,135,000	1.00×10^{-3}	1.00×10^{-3}	1.00×10^{-3}
Cu	**Fe**	**K**	**Li**	**Mg**	**Mn**	**Na**
1.00×10^{-3}	*	482,000	8,600	*	1.7×10^{7}	**
Si	**Sn**	**Sr**	**U**	**V**	**Zn**	**pH**
*	1.00×10^{-3}	138,900	1.00×10^{-3}	1.00×10^{-3}	1.00×10^{-3}	7

[1]A single asterisk (*) indicates the concentration of these elements was not explicitly set. They were considered at equilibrium with various minerals. See the model input listing for details. Double asterisks (**) indicate the concentration of Na was set according to charge balance needs.

Scenario 4: Injecting Pretreated Brine

The setup for this scenario was identical to the one used for injecting air-saturated brine (scenario 2). The only difference was the composition of the injected fluid, which was pretreated brine (Table 2-3-4). Several species, such as SiO_2, were present in the formation waters but not in the injected brine. Concentrations of these species were set to an arbitrarily low value of 1.0×10^{-6} mg/L. The CO_2 and O_2 concentrations of the injected brine were also set at equilibrium with the atmosphere (Appendix A). Simulations were completed for both the freely exchanging and isolated channel configurations.

The results of these models paralleled those of the air-saturated brine injection. The greatest differences were the lower concentrations or absence of some components, such as vanadium, and the lower overall dissolved solids (Figures 2-3-9 to 2-3-12). The low concentration of Si in the injected brine could cause dissolution of the quartz lining the vugs that isolates the main flow

channel from the matrix; however, the slow kinetics of quartz dissolution (Palandri and Kharaka, 2004, and references therein) mean this would potentially only happen over hundreds of years.

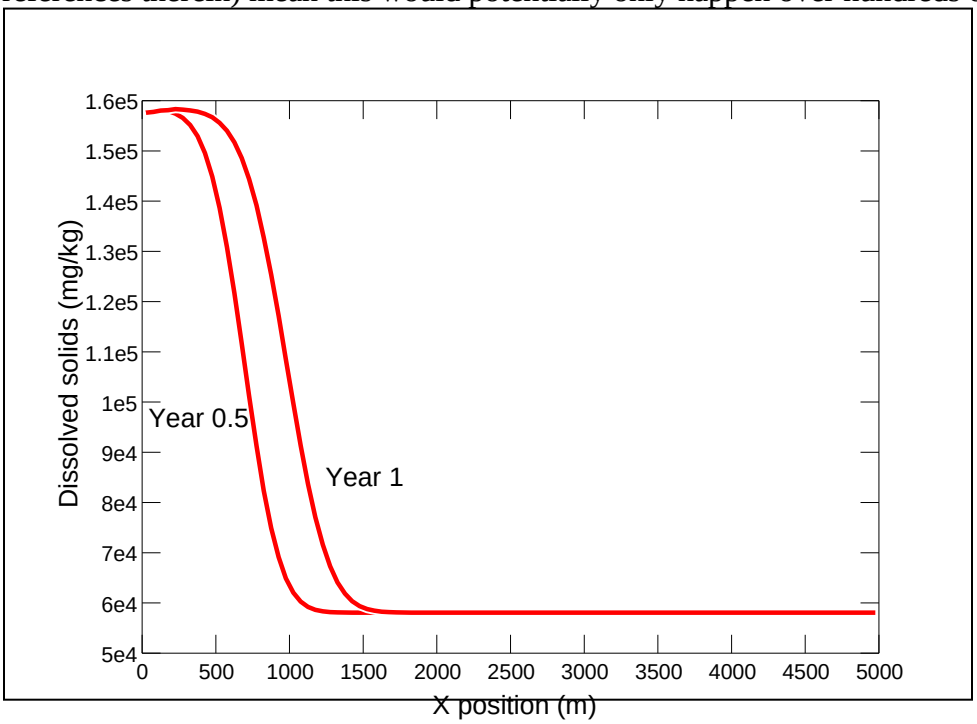

Figure 2-3-5 Total dissolved solids distribution at different times in a model of air-saturated brine injection in which brine in vuggy porosity can freely exchange with the matrix.

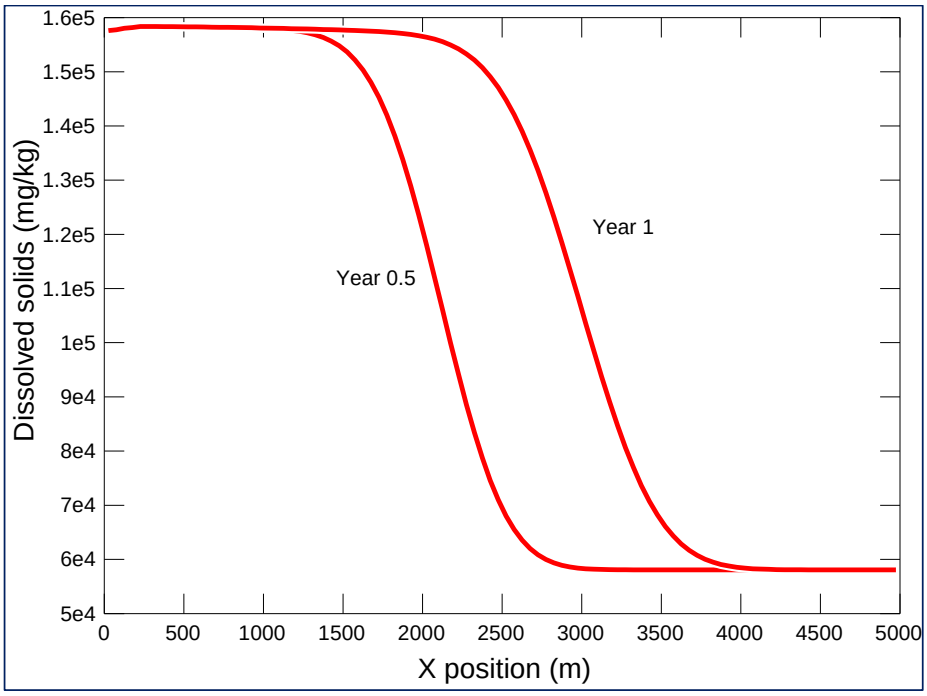

Figure 2-3-6 Total dissolved solids distribution at different times in a model of air-saturated brine injection in which brine exchange between vuggy porosity and the matrix is inhibited.

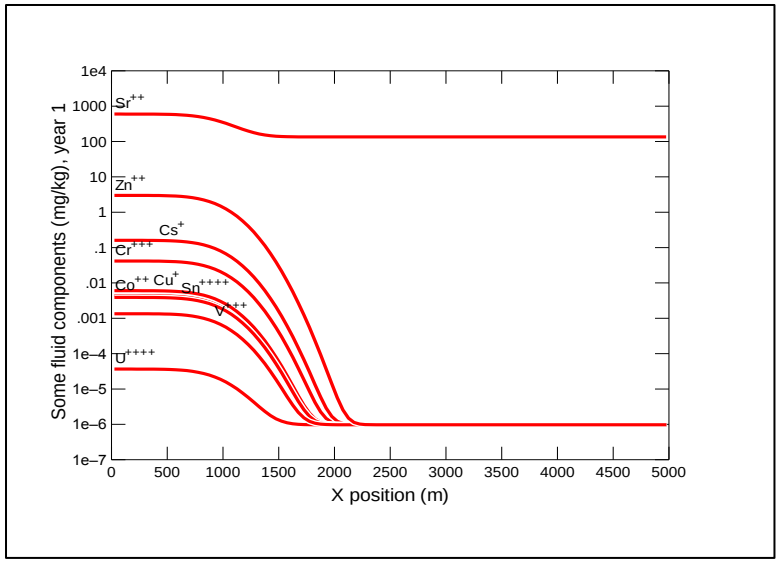

Figure 2-3-7 Trace metal distribution at different times in a model of air-saturated brine injection in which brine in vuggy porosity can freely exchange with the matrix.

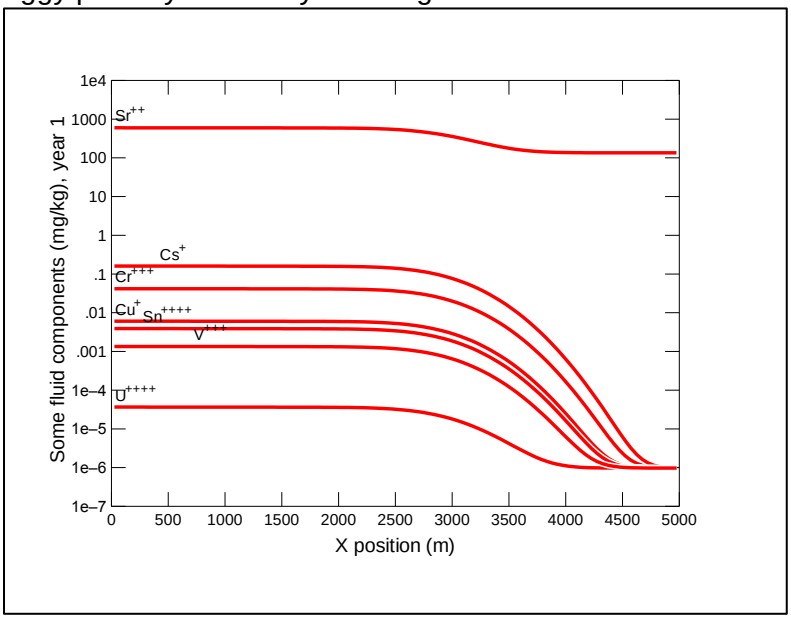

Figure 2-3-8 Trace metal distribution at different times in a model of air-saturated brine injection in which brine exchange between vuggy porosity and the matrix is inhibited.

Table 2-3-4 Measured concentrations of elements in pretreated Mt. Simon brine (µg/L).

Al	As	Ba	Ca	Co	Cr	Cs
232	<3	2,360	2×10^7	2.01	<50	168
Cu	**Fe**	**K**	**Li**	**Mg**	**Mn**	**Na**
48.2	4,490	1,420,000	16,000	1,690,000	39,900	2.9×10^7
Si	**Sn**	**Sr**	**U**	**V**	**Zn**	**pH**
<20,000	<10	492,000	0.164	<10	333	7

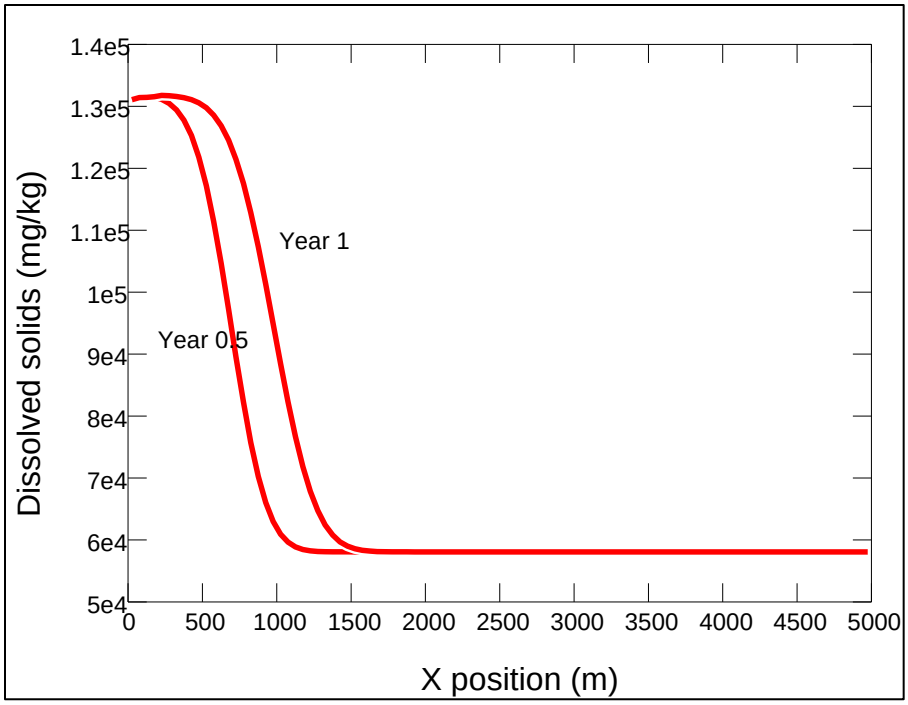

Figure 2-3-9 Total dissolved solids distribution at different times in a model of pretreated brine injection in which brine in vuggy porosity can freely exchange with the matrix.

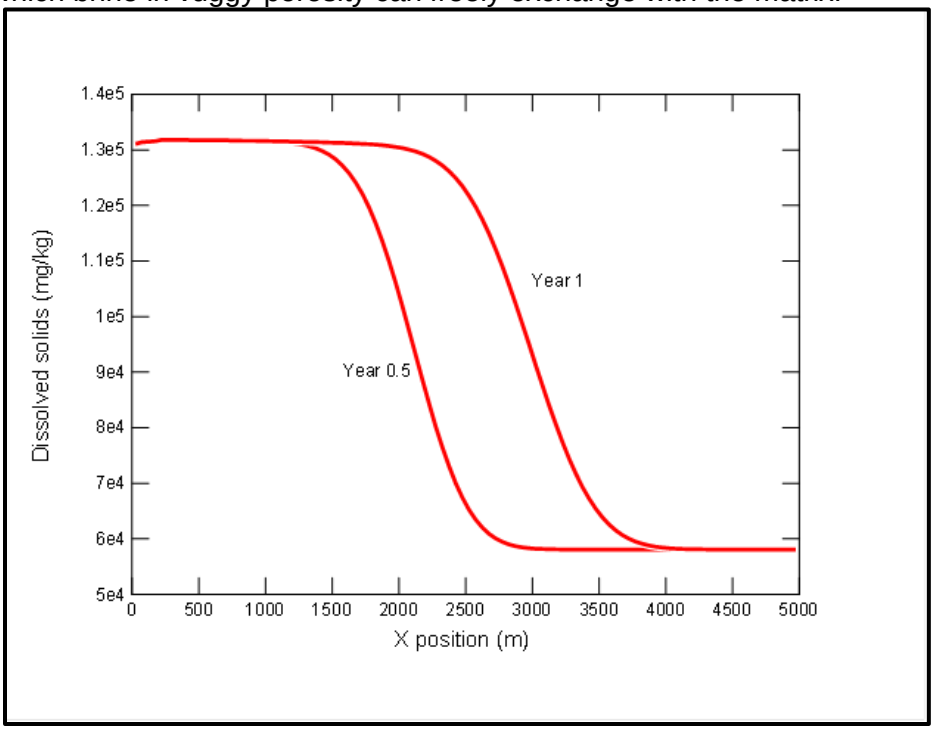

Figure 2-3-10 Total dissolved solids distribution at different times in a model of pretreated brine injection in which brine exchange between vuggy porosity and the matrix is inhibited.

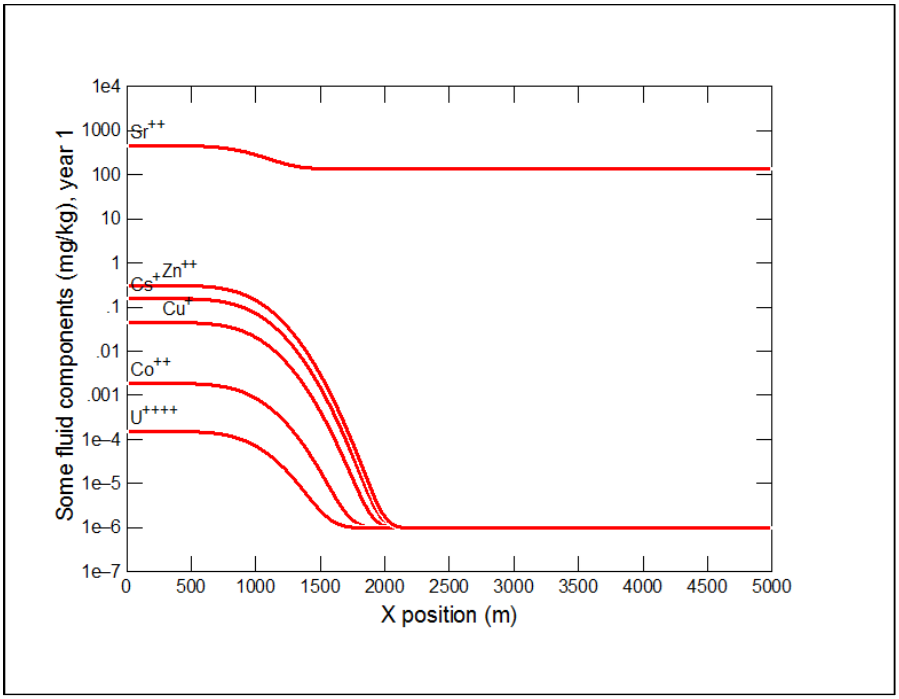

Figure 2-3-11 Trace metal distribution at different times in a model of pretreated brine injection in which brine in vuggy porosity can freely exchange with the matrix.

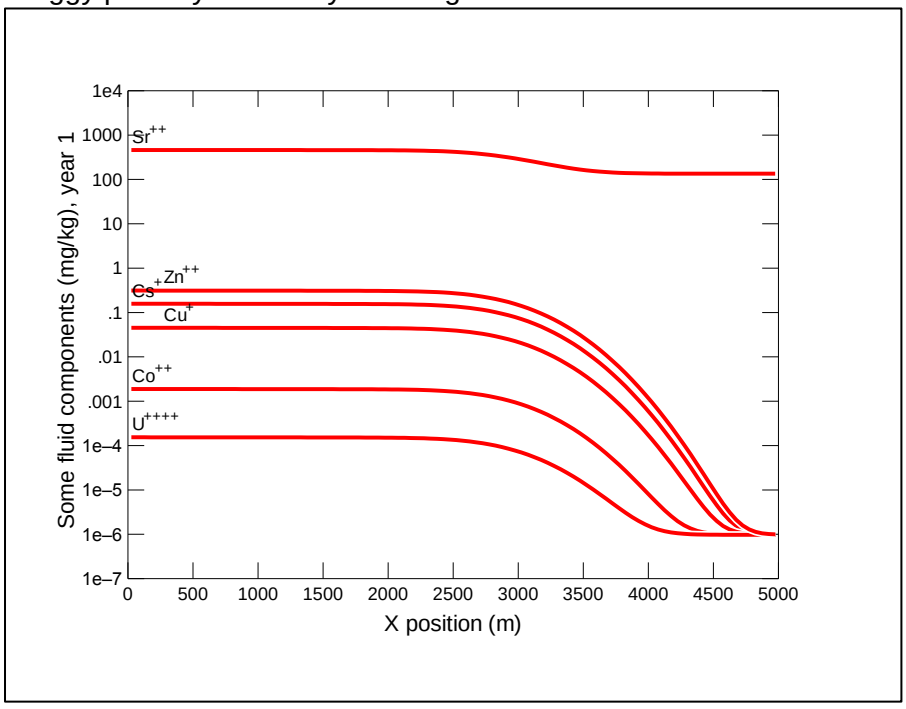

Figure 2-3-12 Trace metal distribution at different times in a model of pretreated brine injection in which brine exchange between vuggy porosity and the matrix is inhibited.

Appendix 2-A Geochemical Modeling Scripts

The following tables present the geochemical modeling scripts for Subtask 2-3.

Table 2-A-1 Script for modeling Scenario 1, extraction and cooling of Mt. Simon brine.

data = thermo.dat verify
temperature initial = 50 °C, final = 25 °C
H_2O = 1 free kg
Al^{3+} = .001 mg/L
$As(OH)_4^-$ = 8.492 ug/L
Ba^{2+} = 2.417 mg/L
Ca^{2+} = 23300 mg/L
Co^{2+} = 4.71 ug/L
$Cr3^+$ = 32.4 ug/L
Cs^+ = 173 ug/L
Cu^+ = 95 ug/L
swap Fe^{3+} for Fe^{2+}
Fe^{3+} = 70.8 mg/L
K^+ = 1430 mg/L
Li^+ = 16.1 mg/L
Mg^{2+} = 1830 mg/L
Mn^{2+} = 57.3 mg/L
Na^+ = 36700 mg/L
$SiO_2(aq)$ = 6.55 mg/L
Sn^{4+} = 21.2 ug/L
Sr^{2+} = 644 mg/L
U^{4+} = 2.59 ug/L
V^{3+} = 20.2 ug/L
Zn^{2+} = 3 mg/kg
Cl^- = 93.73 mg/kg
balance on Cl^-
HCO_3^- = 343 mg/kg
SO_4^{2-} = 343 mg/kg
pH = 5.37
swap e^- for $O_2(aq)$

Eh = –55.5 mV

suppress Uranophane Bornite Uraninite Coffinite
suppress $ZnCr_2O_4$ $U4O_9(c)$ Barite $V_3O_5(c)$
suppress $V_2O_3(c)$ Strontianite Cr_2O_3 $FeCr_2O_4$
suppress SnO_2 $Co(FeO_2)_2$ $MgCr_2O_4$ $V_4O_7(c)$
suppress $V_2O_4(c)$ $V_2O_5(c)$ Quartz Chalcedony
suppress Tridymite Mordenite-K Muscovite Nontronit-Ca
suppress Nontronit-K Nontronit-Mg Clinoptil-K Nontronit-Na

Table 2-A-2 Script for modeling Scenario 2, exposure of Mt. Simon brine to air.

```
# React script, exposure of Mt. Simon brine to air
data = thermo.dat verify
surface_data      = FeOH+.dat
temperature       = 25 °C
H2O               = .999999998202 free kg
Al+3              = 4.084790043849 × 10-8 mol
As(OH)4-          = 6.547254522037 × 10-8 mol
Ba+2              = 1.939755800825 × 10-5 mol
Ca+2              = .6407137394806 mol
Co+2              = 8.808393599804 × 10-8 mol
Cr+3              = 6.867693490285 × 10-7 mol
Cs+               = 1.434628007913 × 10-6 mol
Cu+               = 1.647673723598 × 10-6 mol
O2(aq)            = 4.921389625024 × 10-65 activity
K+                = .04031011079062 mol
Li+               = .002556463877464 mol
Mg+2              = .08298341308361 mol
Mn+2              = .001149522843051 mol
Na+               = 1.759408557818 mol
SiO2(aq)          = .0001201478830279 mol
Sn+4              = 5.758063035574 × 10-28 free molal
Sr+2              = .008100623498505 mol
U+4               = 3.364550447691 × 10-22 free molal
V+3               = 4.370351038403 × 10-7 mol
Zn+2              = 5.446346203559 × 10-5 mol
Cl-               = 3.260761413191 mol
balance on Cl-
HCO3-             = .006672236983428 mol
SO4-2             = .004238296097775 mol
pH                = 5.418426842932
Fe+2              = .001397234299036 mol

slide fugacity of O2(g) .2
slide log fugacity of CO2(g) to −2.5
suppress  Uranophane Bornite Uraninite Coffinite
suppress  ZnCr2O4 U4O9(c) Barite V3O5(c)
suppress  V2O3(c) Strontianite Cr2O3 FeCr2O4
suppress  SnO2 Co(FeO2)2 MgCr2O4 V4O7(c)
suppress  V2O4(c) V2O5(c) Quartz Chalcedony
suppress  Tridymite Mordenite-K Muscovite Nontronit-Ca
suppress  Nontronit-K Nontronit-Mg Clinoptil-K Nontronit-Na
suppress  Hematite Goethite Jarosite-K Pyrolusite
suppress  Ferrite-Ca Ferrite-Cu Magnetite Ferrite-Zn
```

Table 2-A-3 Script for modeling Scenario 3, injection of air saturated Mt. Simon brine (continued on next page).

```
# X1t script, model for the injection of air saturated Mt. Simon brine
data = thermo.dat verify
time start = 0 day, end = 1 yr
radial r1 = 1 m  r2 = 5000 m  angle = 360 degrees
left = inlet
right = outlet
height = 10 m
Nx = 100
discharge = 50.6 m3/m2/day
#set the diffusion coefficient to 10-10 for the low diffusion model
dual_porosity volfrac = .6, geometry = blocks, half-width = 1 m, diff_length = 2 cm, Nsubnode = 2, retardation = 1, porosity = .95, diff_coef = 1 × 10-5 cm2/s
porosity = .3
temperature initial = 43 °C, inlet = 43 °C, constant = on
decouple HS-
scope = initial
  H2O          = 1 free kg
  Al3+         = 20 ug/L
  As(OH)4-     = 1 × 10-6 mmol/kg
  Ba2+         = .235 mg/L
  Ca2+         = 5135 mg/L
  swap e- for O2(aq)
  Eh           = -.1277 V
  K+           = 482.7 mg/L
  Li+          = 8.6 mg/L
  swap Dolomite for Mg2+
  Dolomite     = 82.3 free volume%
  Mn2+         = .00014952 mmol/kg
  Na+          = 16570 mg/L
  balance on Na+
  swap Amrph^silica for SiO2(aq)
  Amrph^silica = 1 free volume%
  Sr2+         = 138.9 mg/L
  Cl-          = 35290 mg/L
  swap Calcite for HCO3-
  Calcite      = .67 free volume%
  SO42-        = 1220 mg/L
  pH           = 6.94
  swap Siderite for Fe2+
  Siderite     = 1.33 free volume%
  Br-          = 177 mg/L
  swap Pyrite for HS-
  Pyrite       = .67 free volume%
```

Co^{2+} = 1×10^{-6} mg/L
Cr^{3+} = 1×10^{-6} mg/L
Cs^{+} = 1×10^{-6} mg/L
Cu+ = 1×10^{-6} mg/L
Sn^{4+} = 1×10^{-6} mg/L
U^{4+} = 1×10^{-6} mg/L
V^{3+} = 1×10^{-6} mg/L
Zn^{2+} = 1×10^{-6} mg/L
scope = inlet
H_2O = .999983 free kg
Al^{3+} = 4.08479×10^{-8} mol
$As(OH)_4^-$ = 1.13198×10^{-37} free molal
Ba^{2+} = 1.93974×10^{-5} mol
Ca^{2+} = .640713 mol
swap $O_2(g)$ for $O_2(aq)$
$O_2(g)$ = .2 fugacity
K^{+} = .0403101 mol
Li^{+} = .00255646 mol
Mg^{2+} = .0829834 mol
Mn^{2+} = .00114952 mol
Na^{+} = 1.75941 mol
$SiO_2(aq)$ = .000120148 mol
Sr^{2+} = .00810059 mol
Cl^- = 3.26076 mol
balance on Cl^-
swap $CO_2(g)$ for HCO_3^-
$CO_2(g)$ = .00316228 fugacity
$SO4^{2-}$ = .0042277 mol
H^{+} = .000349041 mol
Fe^{2+} = .000221557 mol
Br^- = .00905471 mol
HS^- = 1×10^{-6} mol
Co^{2+} = 8.80839×10^{-8} mol
Cr^{3+} = 4.20506×10^{-17} free molal
Cs^{+} = 1.43463×10^{-6} mol
Cu+ = 3.96879×10^{-21} free molal
Sn^{4+} = 4.44963×10^{-22} free molal
U^{4+} = 8.08155×10^{-48} free molal
V^{3+} = 4.039×10^{-32} free molal
Zn^{2+} = 5.44634×10^{-5} mol
kinetic Quartz 13 volume% rate_con = 1.02×10^{-18} surface = 100

suppress ALL
unsuppress Amrph^silica Calcite Dolomite Pyrite
unsuppress Siderite

Table 2-A-4 Script for modeling Scenario 4, injection of pretreated Mt. Simon brine (continued on next page).

```
# X1t script, model for the injection of pretreated Mt. Simon brine
data = thermo.dat verify
time start = 0 day, end = 1 yr
radial r1 = 1 m  r2 = 5000 m  angle = 360o
left = inlet
right = outlet
height = 10 m
Nx = 100
discharge = 50.6 m3/m2/day
#set the diffusion coefficient to 10-10 for the low diffusion model
dual_porosity volfrac = .6, geometry = blocks, half-width = 1 m, diff_length = 2 cm, Nsubnode = 2, retardation
= 1, porosity = .95, diff_coef = 10-10 cm2/s
porosity = .3
temperature initial = 43 oC, inlet = 43 oC, constant = on
decouple HS–
scope = initial
  H2O           = 1 free kg
  Al3+          = 20 ug/L
  As(OH)4–      = 1 × 10-6 mmol/kg
  Ba2+          = .235 mg/L
  Ca2+          = 5135 mg/L
  swap e– for O2(aq)
  Eh            = –.1277 V
  K+            = 482.7 mg/L
  Li+           = 8.6 mg/L
  swap Dolomite for Mg2+
  Dolomite      = 82.3 free volume%
  Mn2+          = .00014952 mmol/kg
  Na+           = 16570 mg/L
  balance on Na+
  swap Amrph^silica for SiO2(aq)
  Amrph^silica = 1 free volume%
  Sr2+          = 138.9 mg/L
  Cl–           = 35290 mg/L
  swap Calcite for HCO3–
  Calcite       = .67 free volume%
  SO42–         = 1220 mg/L
  pH            = 6.94
  swap Siderite for Fe2+
  Siderite      = 1.33 free volume%
  Br–           = 177 mg/L
  swap Pyrite for HS–
```

```
   Pyrite          = .67 free volume%
   Co+2            = 1 × 10-6 mg/L
   Cr3+            = 1 × 10-6 mg/L
   Cs+             = 1 × 10-6  mg/L
   Cu+             = 1 × 10-6 mg/L
   Sn+4            = 1 × 10-6 mg/L
   U+4             = 1 × 10-6 mg/L
   V+3             = 1 × 10-6 mg/L
   Zn+2            = 1 × 10-6 mg/L
scope = inlet
   H2O             = 1 free kg
   Al+3            = 232 ug/L
   As(OH)4-        = 1 × 10-6 mg/kg
   Ba+2            = 2360 ug/L
   Ca+2            = 20.2 g/L
   swap O2(g) for O2(aq)
   O2(g)           = .2 fugacity
   K+              = 1420 mg/L
   Li+             = 16 mg/L
   Mg+2            = 1690 mg/L
   Mn+2            = 39.9 mg/L
   Na+             = 28.7 g/L
   SiO2(aq)        = 1 × 10-6 mol
   Sr+2            = 492 mg/L
   balance on Cl-
   swap CO2(g) for HCO3-
   CO2(g)          = .00316228 fugacity
   SO4-2           = 1 × 10-6 mg/L
   pH              = 7
   Fe+2            = 4.49 mg/L
   Br-             = .00905471 mol
   HS-             = 1 × 10-6 mg/L
   Co+2            = 2.01 ug/L
   Cr+3            = 1 × 10-6 mg/L
   Cs+             = 168 ug/L
   Cu+             = 48.2 ug/L
   Sn+4            = 1 × 10-6 mg/L
   U+4             = .164 ug/L
   V+3             = 1 × 10-6 mg/L
   Zn+2            = 333 ug/L
kinetic Quartz 13 volume% rate_con = 1.02 × 10-18 surface = 100
suppress ALL
unsuppress  Amrph^silica Calcite Dolomite Illite
unsuppress  Pyrite Siderite
```

Subtask 2-4 Life Cycle Assessment of Brine Extraction, Treatment, and Handling

Introduction to LCA

Life cycle assessment (LCA) is a tool used to quantify the total environmental impact of a process. The "cradle-to-grave" LCA methodology set forth in the International Standards for Life Cycle Assessment (ISO 14040 and ISO 14044) evaluates the impact of a process over its entire life span, from extraction of raw materials to the disposal of materials at process termination. In the case of desalination, operation is typically the most significant segment of the life cycle.

An LCA consists of four phases: goal and scope, life cycle inventory (LCI), life cycle impact analysis (LCIA), and interpretation. Zhou et al. (2014) summarized the LCA methodology in a figure, which is presented in Figure 2-4-1 with some modifications for this study.

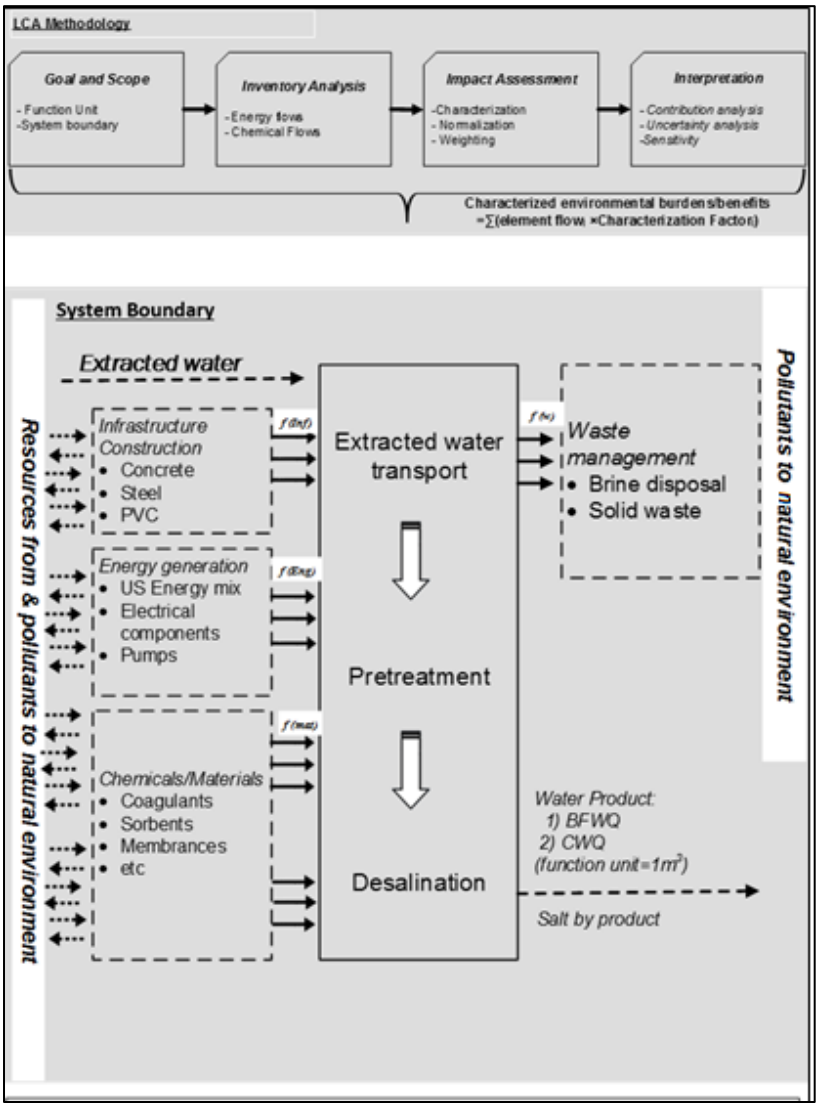

Figure 2-4-1 LCA methodology used to assess the potential environmental impacts of the extracted water treatment (adapted from Zhou et al., 2014, with some modifications for this study).

The goal and scope phase, where the purpose and parameters of the LCA are stated, should provide insight into the objectives, method, and results of the LCA. Authors may list assumptions, justify the inclusion or exclusion of certain impact categories, explore the limitations and challenges of the LCA, and more. The goal and scope phase necessitates a defined functional unit for the system and system boundaries. The functional unit describes the primary purpose of a system; the functional unit for a water treatment process might be 1 unit of the inlet raw water or product water, regardless of the treatment technologies selected for water treatment. The system boundary identifies the processes included in the LCA.

The LCI is the data-collection phase, in which all the system inlet and outlet flows are identified and quantified. The inventory should be as comprehensive as possible because it will be used to calculate the total environmental impact of the system.

The potential environmental impact of the system is evaluated in the LCIA phase. The LCIA requires a characterization step, in which impact categories (e.g., fossil fuel resources, human toxicity, climate change, etc.) are defined and all system inflows and outflows (previously quantified in the LCI phase) are assessed for their contributions to each impact category. Normalization and weighting steps are optional components of the LCIA. The LCIA results for each impact category may have different units, but normalization (division by a reference value) allows for comparison. Weighting is the assignment of a subjective valuation to each impact category. After normalization and weighting, the results for each impact category may be totaled for a final LCA score.

An LCA is usually conducted with an LCA software package, from which a predefined LCIA approach may be selected. The software contains libraries with energy consumption, emission, and materials data to which many of the inputs and outputs identified in the LCI can be linked. The software will amass data and report LCA results by impact category. For example, if alum is used as a coagulant in the coagulation process, the alum inflow quantity recorded in the LCI will be linked to a library containing data about greenhouse gas emissions resulting from alum production. Alum production emissions will be tallied with greenhouse gas emissions from other system processes, and the total greenhouse gas emissions value will then be converted to a CO_2 equivalent. If a global warming impact category is included in the LCIA, the result will then be reported in terms of kilograms of CO_2 emissions.

The final step of an LCA is the interpretation phase, which usually includes the utilization of software tools to confirm the LCA results. In the interpretation phase, selected process parameters may be adjusted to determine their influence on the LCA results. The interpretation allows for a better understanding and application of LCA results.

LCA Methodology and Results

The goal of this study was to examine and compare the environmental impact of various water-handling options for water extracted from the Mt. Simon Sandstone and St. Peter Formation. Following pretreatment steps for removal of suspended solids (referred to as TSS) and scale-forming species, potential pathways considered for the high-TDS Mt. Simon brine handling included treatment for beneficial use or disposal by injection into the Potosi Dolomite. Low-TDS brackish water extracted from the St. Peter Formation should be treated for beneficial use. Waste brine generated from low-TDS brackish treatment could then be treated by a high-TDS treatment facility or disposed of by deep injection. For each handling option, pretreatment was excluded from the system boundaries; the inlet stream was assumed to be pretreated water and the environmental impacts of pretreatment processes were evaluated separately. This research includes

several LCA studies: pretreatment LCAs for both high- and low-TDS feeds, and comparative LCA cases for high- and low-TDS handling options.

GaBi version 6.0 commercial software was used to perform LCA studies. Eight environmental impact categories from the U.S. EPA Impact Assessment Method (TRACI 2.1) were selected for analysis. Within each impact category, results were normalized by using TRACI 2.1 (USA, 2008), including biogenic carbon (person equivalents) normalization factors provided by the software. Weighting was applied with the Thinkstep LCIA Survey 2012, North America, TRACI 2.1, including "biogenic carbon (person equiv. weighted)" weights provided by the software, and weighted scores were totaled for a total impact score for each handling option (PE International, 2016). Water depletion was also evaluated for each handling option, which is an additional impact category not included in TRACI 2.1. Water depletion was evaluated with the ReCiPe method using the GaBi software. Table 2.4.1 presents key results for each LCA study. Table 2.4.2 presents analysis of each LCA study. Detailed inventory analyses and results for each handling option and scenario analysis are presented in Appendix B. Water balances are also included in Appendix B.

Pretreatment

The pretreatment processes applied to Mt. Simon brine and St. Peter brackish water were identical: treatment began with rapid mixing with lime and alum for 1 min (coagulation), followed by slow mixing for 30 min (flocculation), then 30 min of settling (sedimentation), and finally sand filtration, resulting in pretreated water and waste sludge. The design basis was 8 million gallons per day (MGD) of feed water. The functional unit was 1 m^3 output of pretreated St. Peter brackish water or pretreated Mt. Simon brine. Detailed LCI and LCIA results are presented in Appendix B. We concluded that, among the pretreatment processes for both high- and low-TDS feeds, coagulation had the greatest environmental impact because it requires production of pretreatment chemicals (i.e., lime and alum production). Landfill disposal of sludge also had a high environmental impact, and the overall environmental impact could be improved significantly if alternative methods of sludge handling (such as beneficial industrial uses) were considered. The total environmental impact score for pretreatment was 0.0166 for Mt. Simon brine and 0.0122 for St. Peter water. Potential future studies might include investigation of the environmental impact of alternative pretreatments, such as the use of a different coagulant that requires lower coagulant doses, leading to the generation of less solid waste.

High-TDS Brine-Handling Options

Four cases were considered for high-TDS brine handling, as described in Table 2-4-1. As with pretreatment, the design basis for each case was 8 MGD of brine extracted from the Mt. Simon over a process lifetime of 20 years. Because the primary purpose in each case was to safely handle brine extracted from the Mt. Simon, a functional unit of 1 m^3 of pretreated Mt. Simon brine was selected, which is the inlet to the system. In a conventional desalination LCA, the goal of the system would be to produce purified water, so the functional unit would be 1 m^3 of outlet desalinated water. For comparison, we conducted additional LCAs with the conventional functional unit of 1 m^3 of desalinated water in all cases that had a desalinated water outlet stream (Cases 2–4).

The inventory data were based on experimental data, modeling values, and bibliographic data obtained from the relevant literature. For example, the thermal energy requirements for the evaporative processes were estimated by an Aspen simulation conducted by Trimeric as 212 $kWh_{thermal}/m^3$ of outlet desalinated water, with an additional 34 $kWh_{thermal}/m^3$ required for salt drying in Case 3. The energy estimations by Trimeric were based on processes designed with MEE units,

but infrastructure data for MEE were unavailable in the GaBi professional databases. A hot water tank was selected from the Ecoinvent inventory to model the MEE equipment. The hot water tank data set covered the production of a chrome steel tank, including a heat exchanger and boiler. The maximum capacity of each tank was 600 L; thus, a large number of hot water tanks were used in the LCI. Our model was limited because the environmental impact of the production of a real, large-scale evaporator might not match the impact of the production of many hot water tanks. Detailed data collection sources and inventories are presented in Appendix B.

Table 2-4-1 High-TDS brine-handling cases.

Case	Description
Case 1: Deep well injection (DWI)	Pretreated Mt. Simon brine is conveyed via pipeline to Class II injection wells, where it is injected without further treatment. The LCA explores the environmental impact of the drilling and construction of the injection wells and the energy consumption for transporting and injecting the pretreated brine. The impact of the injected brine on the receiving geological formation is not addressed in this study.
Case 2: Partial evaporation (partial)	Pretreated Mt. Simon brine is treated by partial evaporation. 10 wt% of the brine is recovered as desalinated water, and the remaining concentrated brine is transported to injection wells. The LCA explores the environmental impact of recovery of 10% of the pretreated Mt. Simon brine in addition to the impact of deep well injection (see Case 1) of the remaining waste brine.
Case 3: Evaporation + crystallization with valuable products (ZLD_Val)	Pretreated Mt. Simon brine is treated by evaporation and crystallization processes, resulting in 88 wt% water recovery, which is nearly zero-liquid discharge (ZLD). Other products include concentrated residual brine and valuable salt crystals, which could be used in road deicing applications. There is no waste to dispose of by deep well injection. The LCA explores the environmental impact of treating pretreated Mt. Simon brine through evaporation and crystallization and the energy consumption for salt drying, but it does not include any transportation requirements for the by-products.
Case 4: Evaporation + crystallization with disposal (ZLD_Dis)	Pretreated Mt. Simon brine is treated by evaporation and crystallization processes, resulting in 88 wt% water recovery. The residual brine is disposed of by deep injection, and salt crystals are transported to a landfill. The LCA examines the environmental impact of treating Mt. Simon brine through evaporation and crystallization processes and the disposal of residual waste in a landfill or deep well.

A comparison of the results for each handling option is presented below. The environmental impact of pretreatment of the high-TDS brine extracted from the Mt. Simon Sandstone is also presented. Tables 2-4-2 and 2-4-3 present the LCIA results before normalization

and weighting of each impact category evaluated with the TRACI 2.1 method, including resources (fossil fuels), global warming, smog, ozone depletion, human toxicity, eutrophication, ecotoxicity, and acidification. Further breakdown of the results, including the contribution of each component of the LCI (infrastructure, operation, etc.), is presented in Appendix B. Water depletion was evaluated separately, and the results are presented later in this report.

Table 2-4-2 Environmental impact of high-TDS brine-handling options by impact categories when the functional unit is 1 m^3 of pretreated Mt. Simon brine that is the outlet of the pretreatment case and inlet of Cases 1–4. Results are not normalized or weighted.

Environmental impact categories	Pretreatment	Case 1: Deep well injection	Case 2: Partial evaporation	Case 3: Evaporation + crystallization with valuable products	Case 4: Evaporation + crystallization with disposal
Fossil fuels (MJ surplus energy)	6.36×10^{-1}	1.85×10^{0}	1.60×10^{1}	1.37×10^{2}	1.30×10^{2}
Global warming (kg CO_2-equiv)	4.41×10^{0}	2.47×10^{0}	8.04×10^{0}	5.55×10^{1}	1.65×10^{2}
Smog (kg O_3-equiv)	4.46×10^{-2}	9.14×10^{-2}	2.07×10^{-1}	1.18×10^{0}	1.95×10^{0}
Ozone depletion (kg CFC 11-equiv)	1.42×10^{-8}	2.65×10^{-8}	2.69×10^{-8}	6.03 × 10-9	1.06×10^{-8}
Human toxicity, cancer (CTUh)	5.47×10^{-8}	2.75×10^{-8}	3.65×10^{-8}	4.13×10^{-8}	6.70×10^{-8}
Eutrophication (kg N-equiv)	1.85×10^{-3}	7.77×10^{-4}	1.14×10^{-3}	2.93×10^{-3}	4.20×10^{-2}
Ecotoxicity (CTUe)	1.45×10^{0}	1.20×10^{0}	1.90×10^{0}	3.01×10^{0}	3.90×10^{0}
Acidification (kg SO_2-equiv)	4.40×10^{-3}	7.79×10^{-3}	1.12×10^{-2}	4.06×10^{-2}	1.24×10^{-1}

Each impact category in Tables 2-4-2 and 2-4-3 has distinct units, but after the normalization and weighting steps, a total impact score was determined for each case. Weighted environmental scores for each case are presented in Figure 2-4-2. Further details are available in Appendix B.

In an LCA study, a lower environmental impact score is indicative of a lower negative impact on the environment. The goal is to determine which treatment or handling case has the least impact on the environment. Case 1, in which the pretreated brine is disposed of by deep injection without any further treatment, has the lowest environmental impact because no energy is consumed by the treatment processes. Major contributors to the environmental impact of this process include

electrical energy for brine pumping (transportation and injection) and materials for the drilling and construction of disposal wells. The drilling and construction of disposal wells consist of several activities that may result in the release of drilling fluid and various pollutants that are emitted during the manufacturing of materials (e.g., cement, chemicals) used for well construction. The impact of the injected brine on the receiving geological formation is not addressed in this study because of the lack of available data.

Table 2-4-3 Environmental impact of high-TDS brine-handling options by impact categories when the functional unit is 1 m^3 of desalinated water. Results are not normalized or weighted.

Environmental impact categories	Case 2: Partial evaporation	Case 3: Evaporation + crystallization with valuable products	Case 4: Evaporation + crystallization with disposal
Fossil fuels (MJ surplus energy)	1.60×10^{2}	1.67×10^{2}	1.59×10^{2}
Global warming (kg CO_2-equiv)	8.00×10^{1}	6.78×10^{1}	2.02×10^{2}
Smog (kg O_3-equiv)	2.06×10^{0}	1.44×10^{0}	2.38×10^{0}
Ozone depletion (kg CFC 11-equiv)	2.67×10^{-7}	7.36 × 10-9	1.30×10^{-8}
Human toxicity, cancer (CTUh)	3.63×10^{-7}	5.03×10^{-8}	8.18×10^{-8}
Eutrophication (kg N-equiv)	1.13×10^{-2}	3.57×10^{-3}	5.13×10^{-2}
Ecotoxicity (CTUe)	1.89×10^{1}	3.67×10^{0}	4.75×10^{0}
Acidification (kg SO_2-equiv)	1.12×10^{-1}	4.95×10^{-2}	1.51×10^{-1}

In Case 2, the importance of the functional unit is most apparent. Because the water recovery in Case 2 is so low (only 10% water recovery), producing 1 m^3 of purified water requires an input of about 10 m^3 of pretreated brine, resulting in an environmental impact about 10 times greater than when the functional unit is 1 m^3 of feed.

In Cases 3 and 4, the total impact score is high because energy consumption for high-TDS brine desalination is extremely high, more than 200 $kWh_{thermal}/m^3$ of water recovered. Furthermore, in Case 4 additional energy and infrastructure are needed for salt and brine disposal, which leads to additional environmental impacts. Treatment of landfill gas, leachate, and sludge makes the landfill disposal process a major contributor to the overall environmental impact.

Overall, if safe handling of the brine (as a waste stream) is the main objective, then Case 1, deep well injection, has the lowest environmental impact. Case 3 is the most attractive if the objective is to produce purified water. At this point, the environmental impacts of brine disposal

have not yet been considered beyond transportation and injection. Further investigation of the impact of deep well injection on the underground aquifers is recommended.

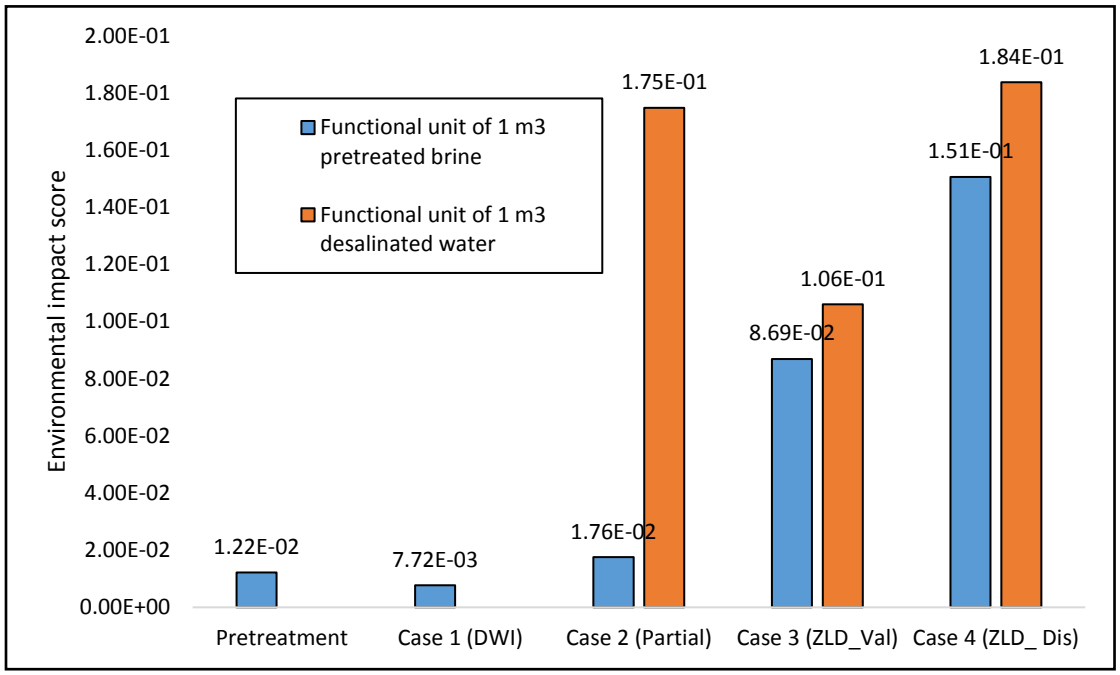

Figure 2-4-2 Total weighted environmental impact scores of high-TDS brine-handling options. See Table 2-4-1 for a description of each case.

Low-TDS Brackish Water-Handling Options

Six cases are considered for low-TDS brackish water handling. In each case, the inlet is pretreated brackish water extracted from the St. Peter Formation. The pretreated brackish water is treated by a desalination technology, resulting in concentrated brine and desalinated water. The concentrated brine is disposed of by deep injection, and the desalinated water is collected as the product. The cases differ only in the selected desalination technology, as listed in Table 2-4-4.

The design basis for each case is the same as for the high-TDS-handling cases: 8 MGD, with a lifetime of 20 years. In each case, a water recovery ratio of 95% was assumed, which should be feasible because the inlet salinity is less than 4,000 ppm of TDS. Because water recovery is consistent in each case and because most of the water is recovered, the conventional functional unit of 1 m^3 of purified water is used in each low-TDS brackish water treatment LCA. Most of the infrastructure data for RO, FO, and NF were adapted from supplementary material provided in the LCA study by Coday et al. (2015). It was assumed that membranes for RO, FO and NF would be replaced every 5 years. For evaporative processes (Cases 4–6), limited information was available about materials for commercial equipment, so the inventory was simplified in the same way that the high-TDS MEE equipment was simplified: 600-L hot water tanks with heat exchangers and boilers were used as a conceptual model for evaporative equipment. Detailed inventories are presented in Appendix B.

The same environmental impact categories analyzed for the high-TDS treatment LCAs were also selected for analyzing the low-TDS cases. The LCIA results are presented in Table 2-4-5, and further details are available in Appendix B. In each case, the operation phase has a significantly higher effect on the total environmental impact score than the building phase; that is, energy consumption contributes more to LCIA results than infrastructure construction. A

comparison of the total impact score for each case is presented in Figure 2-4-3, with the environmental impacts of the pretreatments.

Table 2-4-4 Low-TDS brackish water-handling cases.

Case	Description
Case 1: Reverse osmosis (RO)	RO is utilized for desalination of pretreated St. Peter brackish water. Energy consumption is assumed to be 2 $kWh_{electrical}/m^3$ of desalinated water (Tarnacki et al., 2012).
Case 2: Forward osmosis with magnesium sulfate (FO_DS1)	Pretreated St. Peter water is desalinated by an FO process with a 20 wt% $MgSO_4$ draw solution. Energy consumption of FO here is assumed to be 30% less than with the RO process, based on the operation of FO at a significantly lower pressure than the typical RO pressure. Regeneration of the draw solution is accomplished by NF, with an energy requirement of 0.5 $kWh_{electrical}/m^3$ (Coday et al., 2015).
Case 3: Forward osmosis with ammonium bicarbonate (FO_DS2)	Case 3 is similar to Case 2, except that the draw solution is 1 M NH_4HCO_3 and is recovered by a thermal process requiring 0.1 $kWh_{electrical}/m^3$ (Qin and He, 2014) or a total process energy requirement of ~1.5 $kWh_{electrical}/m^3$ (McGinnis and Elimelech, 2007).
Case 4: Multiple-stage flash (MSF)	MSF is utilized for desalination of pretreated St. Peter brackish water. Energy consumption is assumed to be 4.25 $kWh_{electrical}/m^3$ and 76.4 $kWh_{thermal}/m^3$ of desalinated water (Fath et al., 2011).
Case 5: Multiple-effect evaporation (MEE)	MEE is utilized for desalination of pretreated St. Peter brackish water. Energy consumption is assumed to be 1 $kWh_{electrical}/m^3$ and 51.4 $kWh_{thermal}/m^3$ of desalinated water (Fath et al., 2011).
Case 6: Vapor compression (VC)	A mechanical VC process is utilized for desalination of pretreated St. Peter brackish water. Energy consumption is assumed to be 10.4 $kWh_{electrical}/m^3$ of desalinated water (Shaffer et al., 2013).

Energy consumption was the greatest contributor to the environmental impact of each process, and the total scores roughly corresponded to the energy requirements. Lower energy membrane processes, such as RO or FO, had the lowest environmental impacts for brackish water treatment. With FO, the draw solution regeneration step was a critical step for the recovery of pure water. However, it might have had a significant impact on the overall environmental impact of the process, mainly because of the energy demand of the regeneration step. It should be noted that the energy demand for both steps of the FO process in the FO inventories was based on pilot-scale studies, and the LCA results might not closely match an industrial-scale case. Among the thermal desalination processes (Cases 4–6), Case 6 (VC) had the lowest environmental impact, mainly because of the higher efficiency of the VC desalination technology.

Table 2-4-5 Environmental impact of low-TDS brackish water-handling options by impact category when the functional unit is 1 m^3 of purified water. Results are not normalized or weighted.

Impact category	Pretreatment	Case 1: RO	Case 2: FO_DS1	Case 3: FO_DS2	Case 4: MSF	Case 5: MED	Case 6: VC
Fossil fuels (MJ surplus energy)	5.38×10^{-1}	1.14×10^{0}	1.13×10^{0}	1.55×10^{0}	5.37×10^{1}	3.52×10^{1}	5.16×10^{0}
Global warming (kg CO_2-equiv)	3.49×10^{0}	1.52×10^{0}	1.44×10^{0}	1.76×10^{0}	2.38×10^{1}	1.48×10^{1}	7.35×10^{0}
Smog (kg O_3-equiv)	3.74×10^{-2}	4.52×10^{-2}	4.15×10^{-2}	6.72×10^{-2}	5.25×10^{-1}	3.22×10^{-1}	2.02×10^{-1}
Ozone depletion (kg CFC 11-equiv)	1.41×10^{-8}	6.55 × 10-9	4.18 × 10-9	3.50×10^{-8}	5.23 × 10-9	4.36 × 10-9	6.89 × 10-9
Human toxicity, cancer (CTUh)	5.43×10^{-8}	3.31 × 10-9	3.82 × 10-9	3.37×10^{-8}	1.38×10^{-8}	1.28×10^{-8}	1.31×10^{-8}
Eutrophication (kg N-equiv)	1.54×10^{-3}	3.29×10^{-4}	2.87×10^{-4}	1.16×10^{-3}	1.53×10^{-3}	9.35×10^{-4}	1.14×10^{-3}
Ecotoxicity (CTUe)	1.43×10^{0}	2.29×10^{-1}	1.56×10^{-1}	2.27×10^{0}	1.41×10^{0}	1.14×10^{0}	8.50×10^{-1}
Acidification (kg SO_2-equiv)	3.71×10^{-3}	4.80×10^{-3}	4.32×10^{-3}	5.96×10^{-3}	2.34×10^{-2}	1.27×10^{-2}	2.11×10^{-2}

Pretreatment of the St. Peter brackish water had a relatively high environmental impact, even higher than the impact of the RO and FO processes (Figure 2-4-3). We based our pretreatment LCA study on laboratory tests that used an alum coagulant with lime softening (Subtask 2-1). Relatively high doses of pretreatment chemicals were required to reduce the TSS concentration to the desired level, and production of these chemicals has a high environmental impact. Other pretreatment options were explored later (Subtask 2-1), and we determined that if polymer coagulants were used, lower dosages would be required. We recommend investigating the environmental impact of alternative pretreatment options. Future work may also include an analysis of the water depletion value for pretreatment.

Water Depletion

One presumed advantage of the treatment of extracted waters from the Mt. Simon Sandstone and St. Peter Formation is the production of fresh water, a valuable resource. However, treatment processes will require some water input associated with energy generation or material or infrastructure production, so we investigated the net water loss or gain by each treatment option. Water depletion values were evaluated by the ReCiPe method and are depicted in Figures 2-4-4 and 2-4-5. This method was selected because of its availability in the GaBi software. Negative scores indicate net water gains, and positive scores indicate net water losses.

For the high-TDS treatment, every case resulted in a total water depletion score greater than 0, indicating that the water requirements for treating water were greater than the quantity of fresh water that would be produced (Figure 2-4-4). For the low-TDS treatment, RO, FO with magnesium sulfate ($MgSO_4$) as the draw solution, and MED resulted in net water gains of only 0.03 to 0.06 m^3, whereas other treatment options resulted in net water losses (Figure 2-4-5).

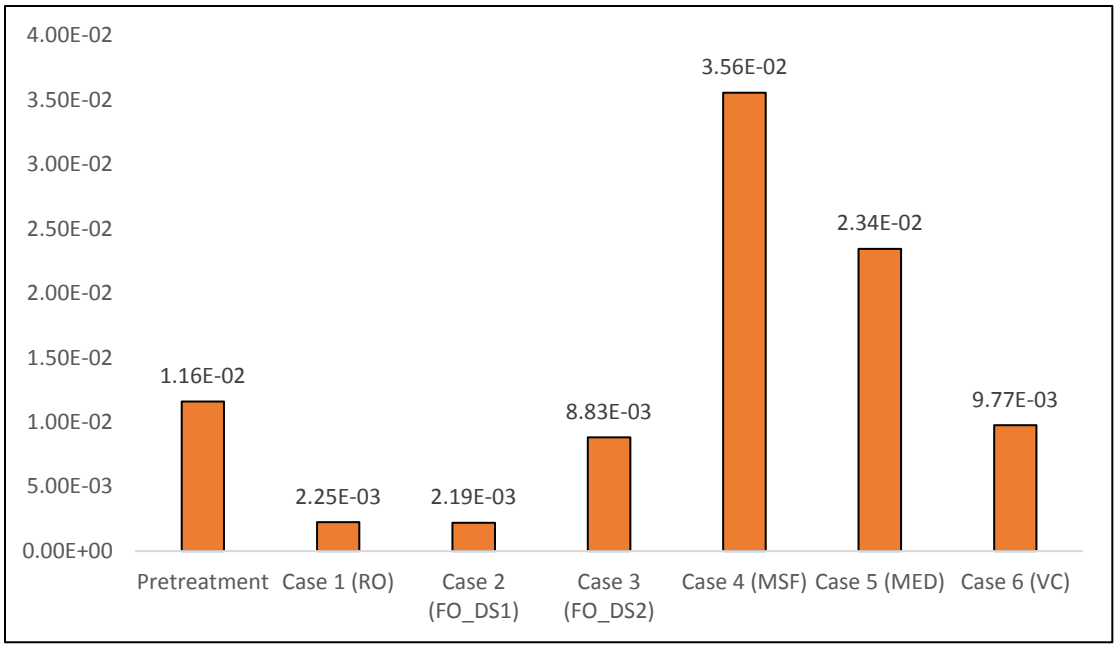

Figure 2-4-3 Total weighted environmental impact scores of low-TDS brackish water desalination options. Refer to Table 2-4-4 for a description of each case.

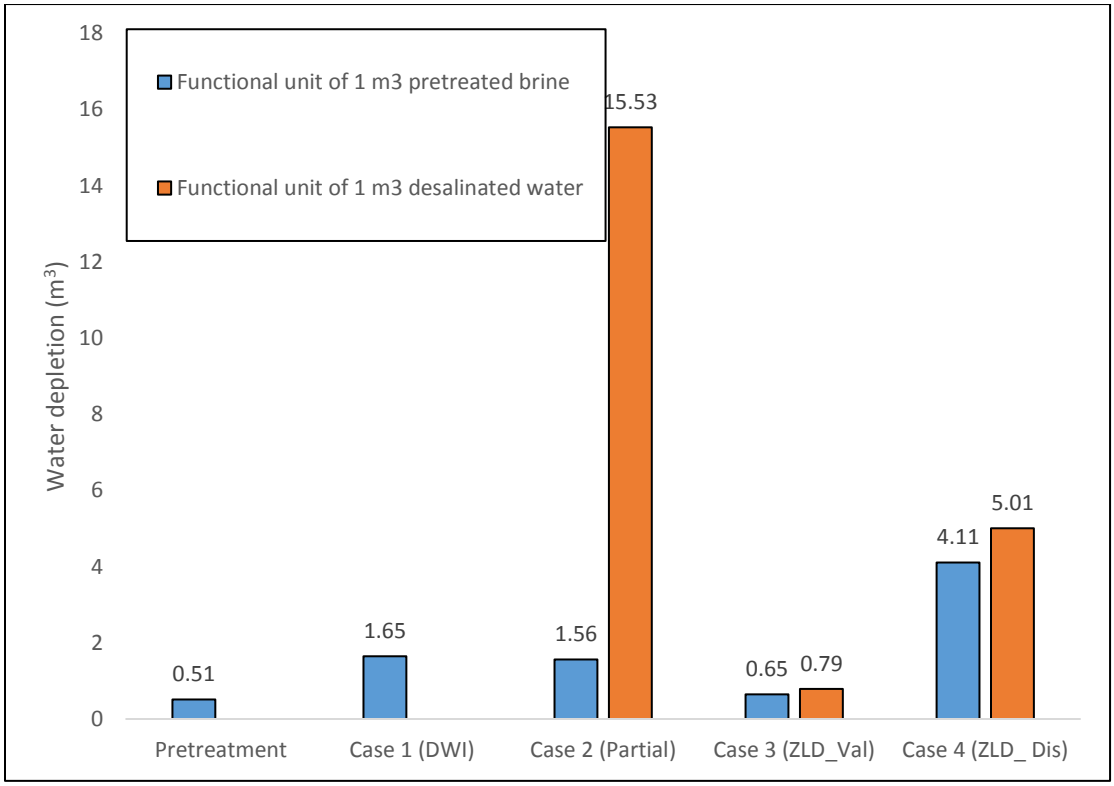

Figure 2-4-4 Water depletion for high-TDS handling of Mt. Simon brine based on ReCiPe water consumption assumptions.

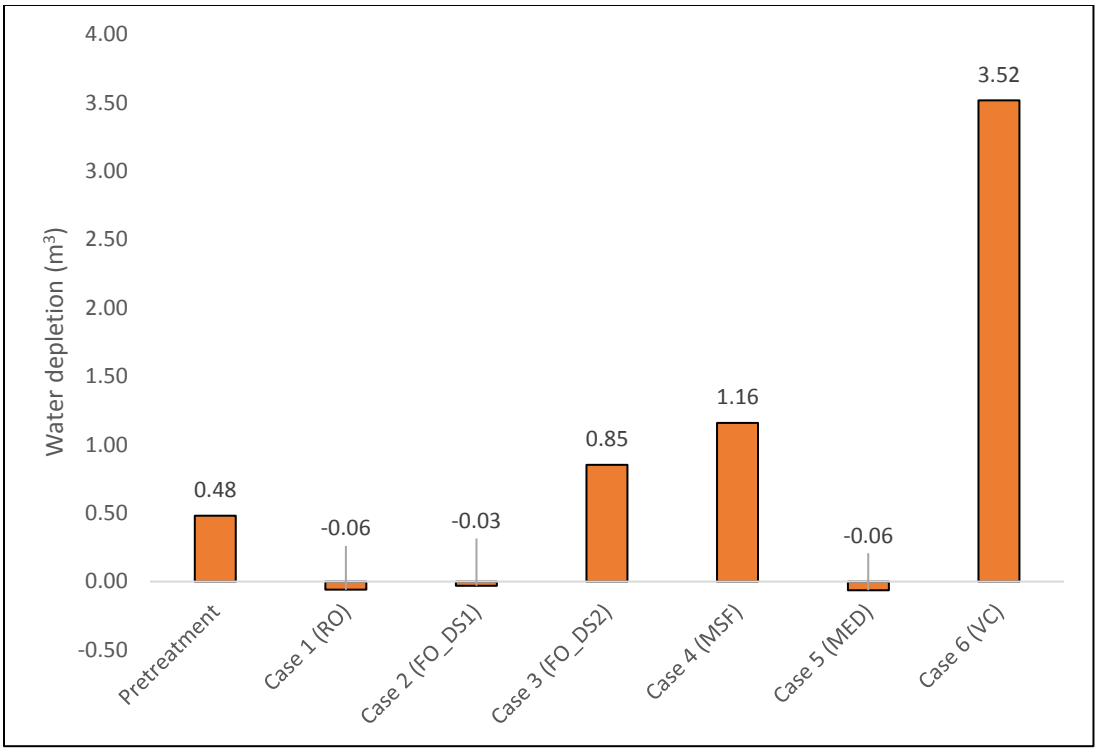

Figure 2-4-5 Water depletion for low-TDS desalination of St. Peter Formation water based on ReCiPe water consumption assumptions and a functional unit of 1 m^3 of desalinated water.

Water depletion scores were much higher than expected, and the unpromising results were most likely due to the ReCiPe approach, which evaluates water usage (the total water requirements of the process) rather than water consumption (water lost in the process, primarily by evaporation; Flury et al., 2012). Appendix B presents the contribution of each process component to its total water depletion value. In most scenarios, the majority of the water depletion modeled with GaBi was due to water used for electricity generation, deep injection, hot water tank production, or landfill disposal. The GaBi software did not provide a breakdown for water depletion values with hot water tank production, but a closer examination revealed that 84% of the water depletion contribution from deep well injection was due to electrical energy for piping and injection. The ReCiPe method assigns a water depletion score of approximately 0.4 m^3 (~106 gallons) for every kilowatt hour of electricity produced, based on the U.S. Electricity Mix available in GaBi. The electricity composition in GaBi is about 42.5% hard coal, 23.5% natural gas, 20.2% nuclear, 6.8% hydro, and the remainder from other sources. The water withdrawal for each energy source agreed with values reported in the literature (Macknick et al., 2011), but the majority of water withdrawal for thermoelectric power production was used for cooling water and was not consumed in the process. Calculations were performed to roughly estimate the water depletion scores if water depletion for electricity generation were based on water consumption rather than water withdrawal. On the basis of data provided by Macknick et al. (2011), and using a similar distribution for electricity composition as suggested in the U.S. Electricity Mix available in GaBi, we estimated that about 1 gallon (0.0038 m^3) of water might be consumed for each kilowatt hour of electricity produced (Macknick et al., 2011), which is only a fraction (slightly less than 0.1%) of the water depletion estimated by the ReCiPe method. Our adjusted results are detailed in Appendix B and summarized in Figures 2-4-6 and 2-4-7.

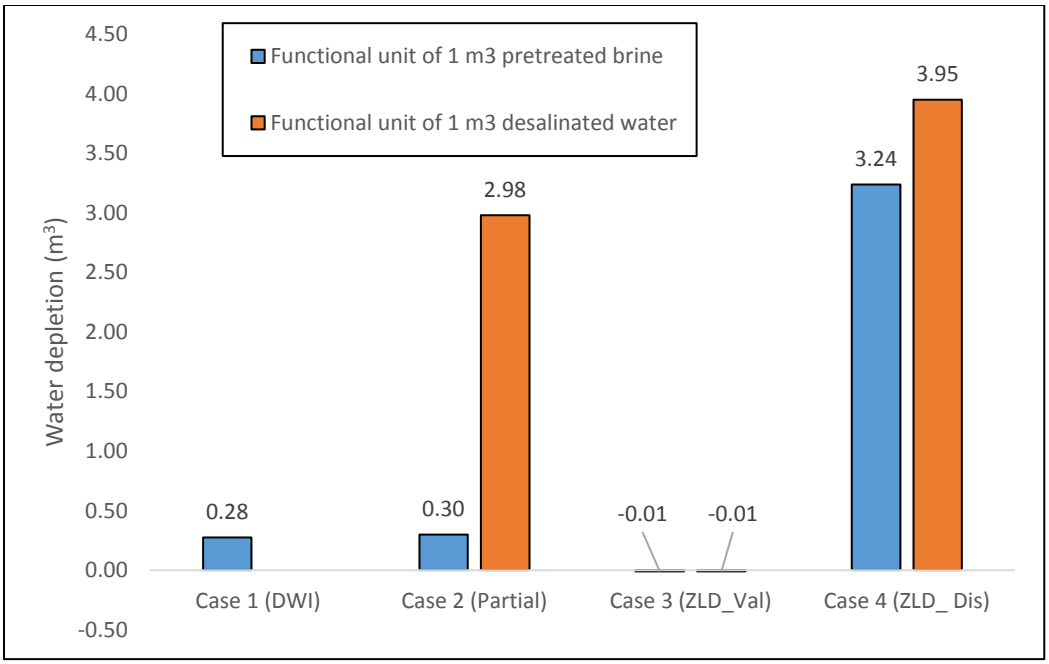

Figure 2-4-6 Adjusted water depletion results for high-TDS handling of Mt. Simon brine.

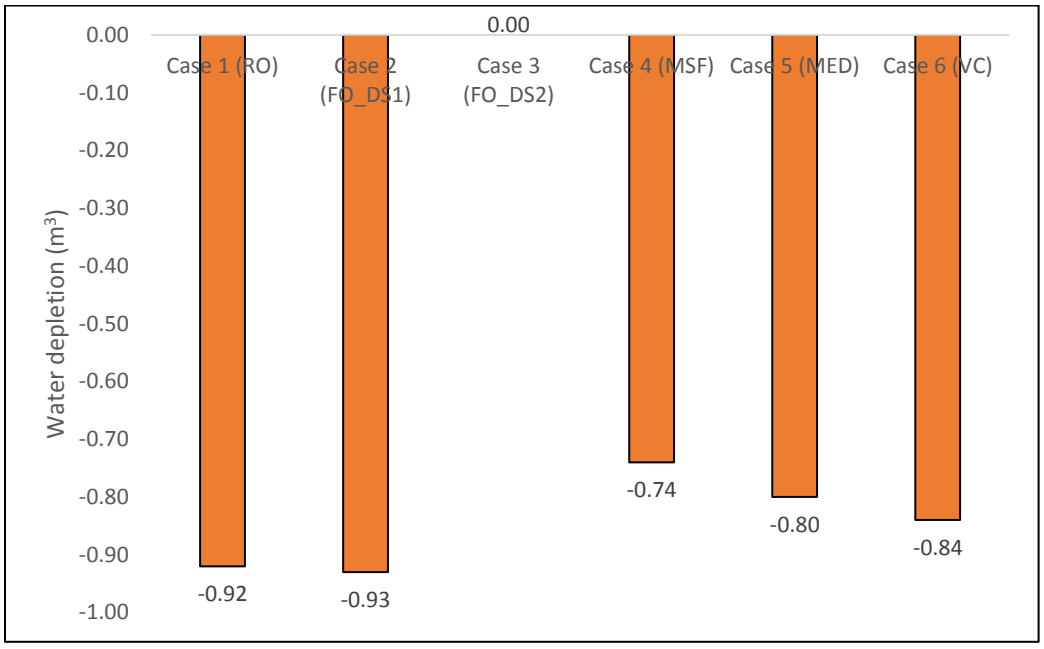

Figure 2-4-7 Adjusted water depletion results for low-TDS desalination of St. Peter Formation water. A functional unit of 1 m^3 of desalinated water is assumed.

Even with the adjusted values, high-TDS brine-management options mostly resulted in a net water loss, except for Case 3, which showed some minimal net water gain. For water extracted from the St. Peter, every treatment option except FO with ammonium bicarbonate as the draw solution yielded some net water gain. The greatest contributor to water depletion in the FO case was ammonium bicarbonate production, which might be overestimated by the ReCiPe method because water usage was evaluated rather than water consumption. Every other low-TDS

desalination case yielded at least 0.74 m^3 of net water gain for each 1 m^3 of desalinated water produced.

Our adjusted water depletion values were limited because the ReCiPe method evaluated water usage rather than water consumption for every contributor to water depletion; we were able to estimate adjusted water depletion values only for the contributions to electricity generation defined in our inventory. Our estimates do not serve as a conclusive analysis of water depletion based on water consumption, but merely a demonstration that water depletion values based on water consumption would be significantly lower than those obtained when water usage or water withdrawal is the basis for assessment. Further investigation of water depletion by each process is recommended, possibly with the use of different software or methods. Further investigation of water depletion related to pretreatment processes is also recommended because this was not explored thoroughly in this work.

Scenario Analysis

Scenario analyses create a comprehensive picture of the environmental impact of each process, including analyses of extreme process conditions. The impact of adjusting a single inventory item on the environmental impact of the process was evaluated.

Mt. Simon Brine-Handling Scenario Analyses

Table 2-4-6 provides a summary of the parameter adjustments for a scenario analysis of Mt. Simon brine-handling options. Because the composition of extracted brine depends greatly on the geological environment and operation conditions, scenarios were investigated in which the impact of the sludge disposal was reduced. The TSS concentration was reduced by approximately 90%, from the observed value of 2,830 to 300 mg/L, and the distance to the landfill was reduced by 90%, from 5 to 0.5 mi (8 to 0.8 km).

For Case 1, disposal by deep injection, increasing the distance by 10 times was investigated in the event that the disposal well had to be placed 10 mi (16 km) from the brine extraction site. For Cases 2–4, in which energy consumption had the highest contribution to the total environmental impact score but energy consumption values were based on modeling rather than industrial data, the thermal energy required by evaporation and crystallization processes was varied by ±50% to allow for a broad range of energy requirements. Because information was limited regarding the thermal energy requirements for high-TDS evaporative processes, investigating a broad energy range was necessary to confirm the LCA results. For all scenario analyses, the functional unit used was 1 m^3 of pretreated brine inlet to the system. The total weighted environmental impact values of new scenarios are summarized in Figures 2-4-8 to 2-4-10. In all cases, Scenario A is the baseline scenario described previously (see Table 2-4-1). Detailed results are presented in Appendix B.

Table 2-4-6 Adjusted parameters for a scenario analysis of high-TDS brine-management options.

Pretreatment or treatment cases	Scenario B	Scenario C
Pretreatment	Decrease TSS to 300 mg/L	Decrease landfill transportation distance to 0.5 mi (0.8 km)
Case 1	Increase pipeline to 10 mi (16 km)	N/A
Cases 2–4	Energy ↓ 50%	Energy ↑ 50%

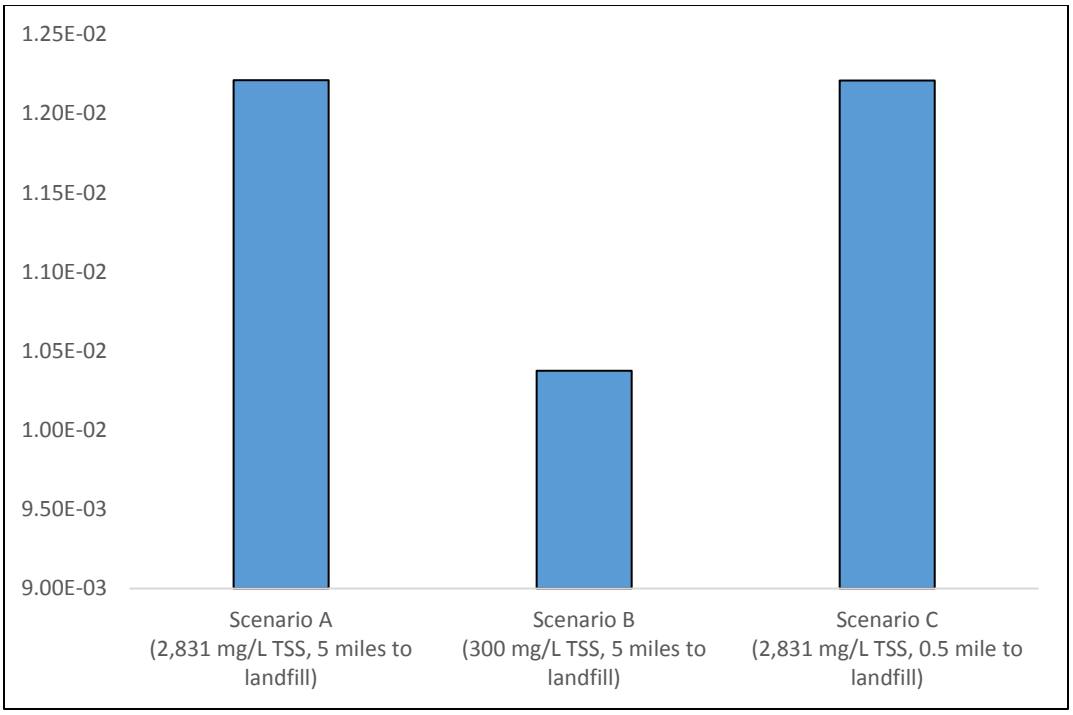

Figure 2-4-8 Environmental impact score results of a scenario analysis for pretreatment of high-TDS brine. The functional unit is 1 m^3 of pretreated Mt. Simon brine outlet from the system.

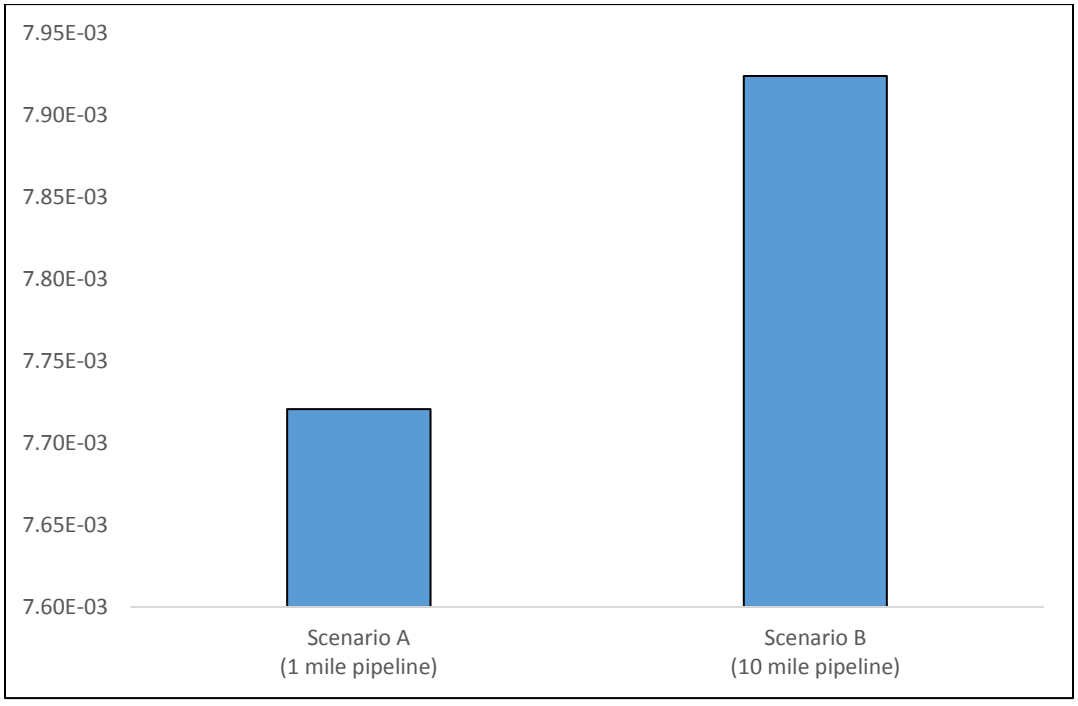

Figure 2-4-9 Environmental impact score results of a scenario analysis for handling high-TDS brine by deep well injection (Case 1). The functional unit is 1 m^3 of pretreated Mt. Simon brine inlet to the system.

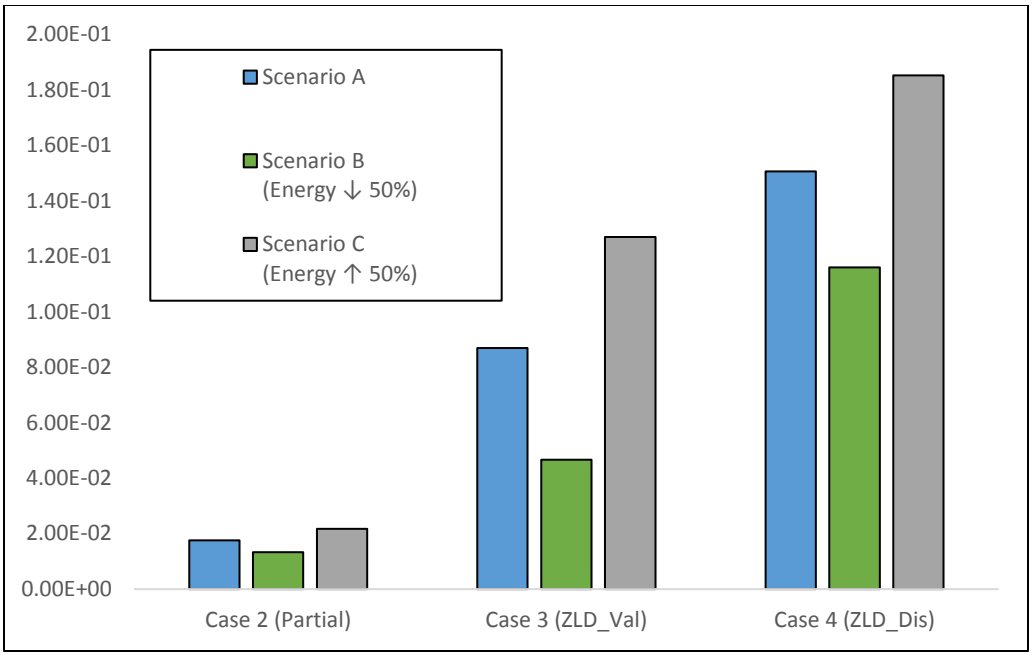

Figure 2-4-10 Environmental impact score results of a scenario analysis for treatment of high-TDS brine. The functional unit is 1 m^3 of pretreated Mt. Simon brine inlet to the system.

Scenario analysis results indicated that the distance for sludge disposal was not as significant as the TSS value. A change in pipeline distance did not affect the environmental impact results significantly in the deep injection case, indicating the pipeline distance accounted for only a small proportion of the overall impact. Energy consumption, in both electrical and thermal forms, contributed the most to the total impacts in every case. For Cases 2–4, changing energy usage would affect almost all the impact categories.

St. Peter Brackish Water-Handling Scenario Analyses

Because pretreatment processes for St. Peter brackish water and Mt. Simon brine were identical, a scenario analysis was not conducted on the pretreatment of St. Peter water. For the various St. Peter brackish water desalination options, energy consumption and water recovery rate were found to have the greatest impacts on LCA results, so these parameters were changed to observe the environmental impacts in extreme scenarios. The LCA results were investigated in the event that energy consumption was decreased by 50% (Scenario B) or increased by 50% (Scenario C), or that water recovery was reduced to 50% (Scenario D). For RO (Scenario B), energy was doubled rather than increased by 50% to account for an energy range up to 4 kWh/m^3, which was predicted to be a high estimate for energy consumption for RO. A detailed inventory based on these adjustments is presented in Appendix B. Energy consumption could decrease if significant technological improvements are made, whereas energy consumption could increase or recovery could decrease if a process is inefficient. It is important to note that because the functional unit was 1 m^3 of desalinated water in every case, adjusting the water recovery rate to 50% required a corresponding adjustment of the total energy consumption in the inventory. Detailed results are presented in Appendix B. The results for the total impact score and water depletion values are compared in Figure 2-4-11.

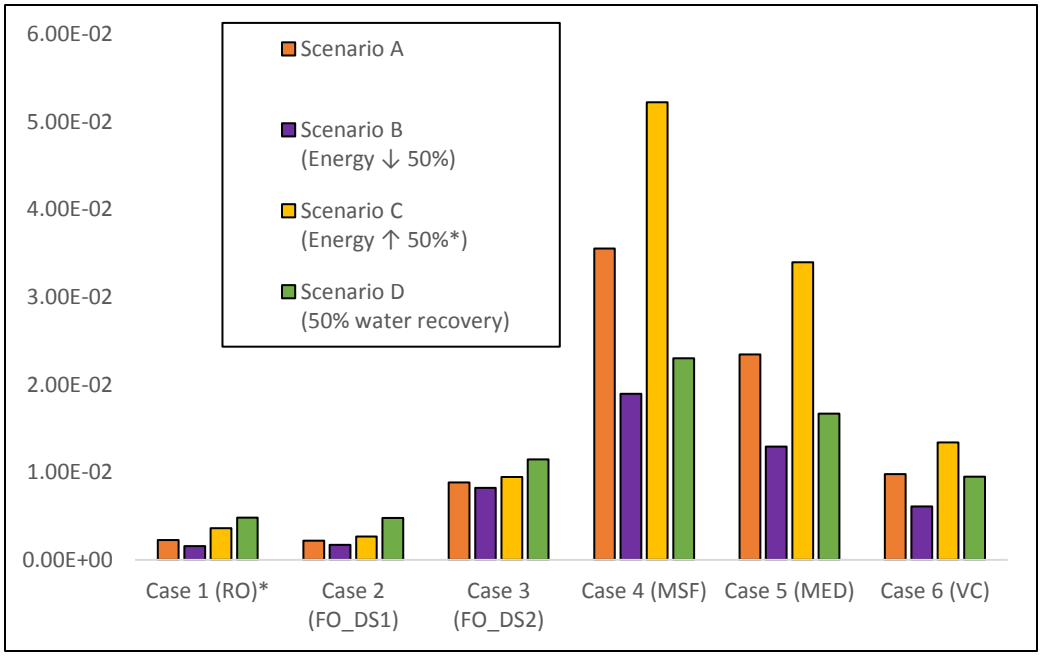

Figure 2-4-11 Environmental impact results of a scenario analysis for treatment of high-TDS brine. An asterisk (*) indicates energy increased by 100% instead of 50% for Case 1, Scenario B.

Comparison of Results with the Literature

Every LCA study is unique. The inventory analysis in each LCA is tailored to a particular process with specified feed water chemistry, product and waste stream compositions, energy source, materials of construction, process efficiency, life span, and more. Investigators may make assumptions in the LCI or choose to exclude certain inlets and outlets based on the goal and scope of the LCA. Additionally, investigators use varied software, methods, impact categories, and weighting standards. Because LCA parameters can vary so dramatically, the results of our LCA were compared only with similar studies. The majority of published desalination LCAs have investigated the environmental impact of RO, so our comparison was focused on conventional RO processes with brackish water or seawater inlets. The results for global warming and acidification potential, the most commonly studied impact categories, are summarized in Figures 2-4-12 and 2-4-13. Appendix B provides further details for each study presented here. For the global warming impact, literature results ranged from 0.62 to 4.61 kg of CO_2-equiv and our result, 1.52 kg of CO_2-equiv, fell within that range. For the impact of acidification, our result of 4.80×10^{-3} kg of SO_2-equivalent was lower than the impacts in other studies, which ranged from 6.1×10^{-3} to 2.7 × 10-2 kg of SO_2-equivalent.

Raluy et al. (2006) did not confine their study to RO desalination, but used an LCA to compare MSF, MED, and RO for the desalination of seawater. The authors selected 45,500 m^3/day of desalinated water as the functional unit. Raluy et al. (2006) used data from currently operating desalination plants designed to operate for 25 years to build the LCI. The system boundaries for each case included the desalination plant components, infrastructure, operation and maintenance, and disassembly at the end of plant life. Similar to the present study, Raluy et al. (2006) concluded that RO had a significantly lower environmental impact than did thermal processes. They also determined that the operation phase of each desalination process had the highest environmental impact, at least 88.6% of the total score, which confirms our assumption that using a simplified model for the infrastructure had a negligible effect on the final results (Raluy et al., 2006). A

comparison of our MSF and MED LCA results with those from Raluy et al. (2006) for global warming, eutrophication, and acidification are presented in Figures 2-4-14 to 2-4-16, and further details are presented in Appendix B.

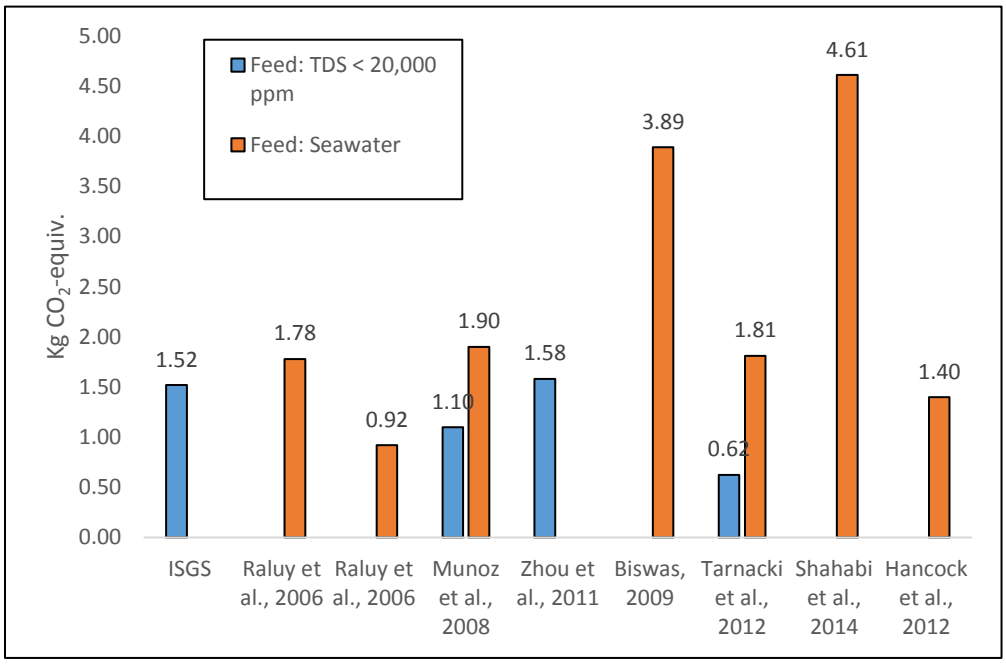

Figure 2-4-12 Global warming impact of RO as determined by various LCA studies. ISGS results refer to the current study.

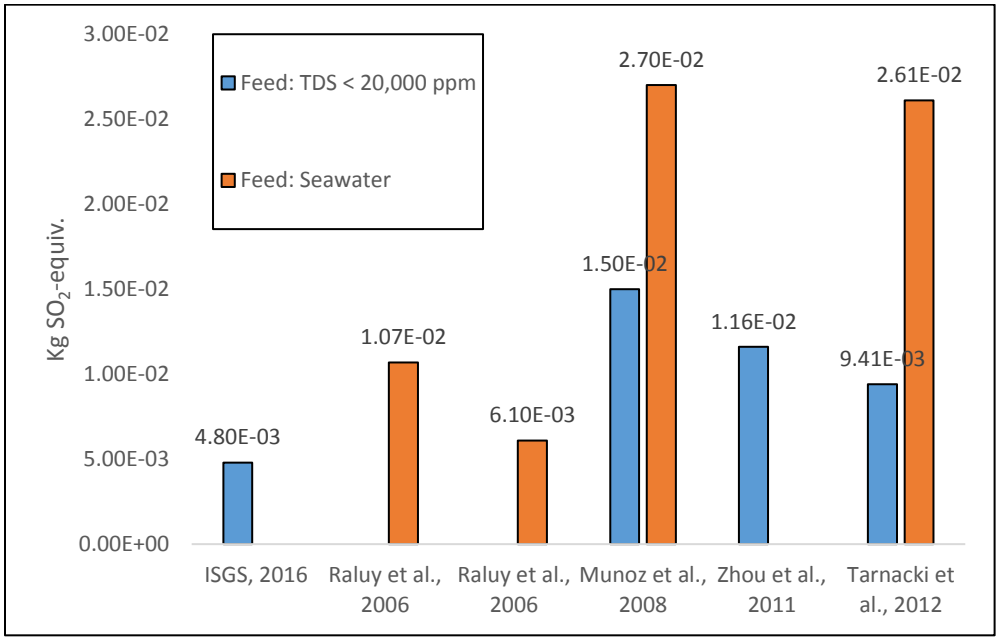

Figure 2-4-13 Acidification impact of RO as determined by various LCA studies. ISGS results refer to the current study.

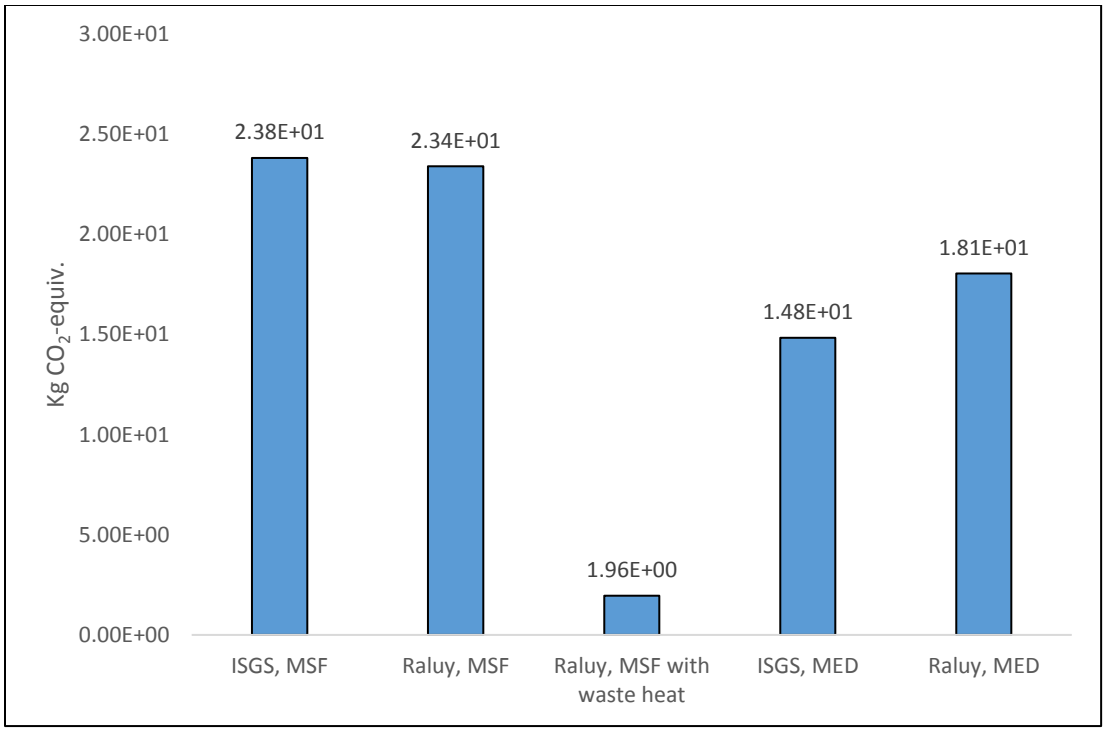

Figure 2-4-14 Global warming impact of MSF and MED as determined by various LCA studies. ISGS results refer to the current study. Raluy results refer to those from Raluy et al. (2006).

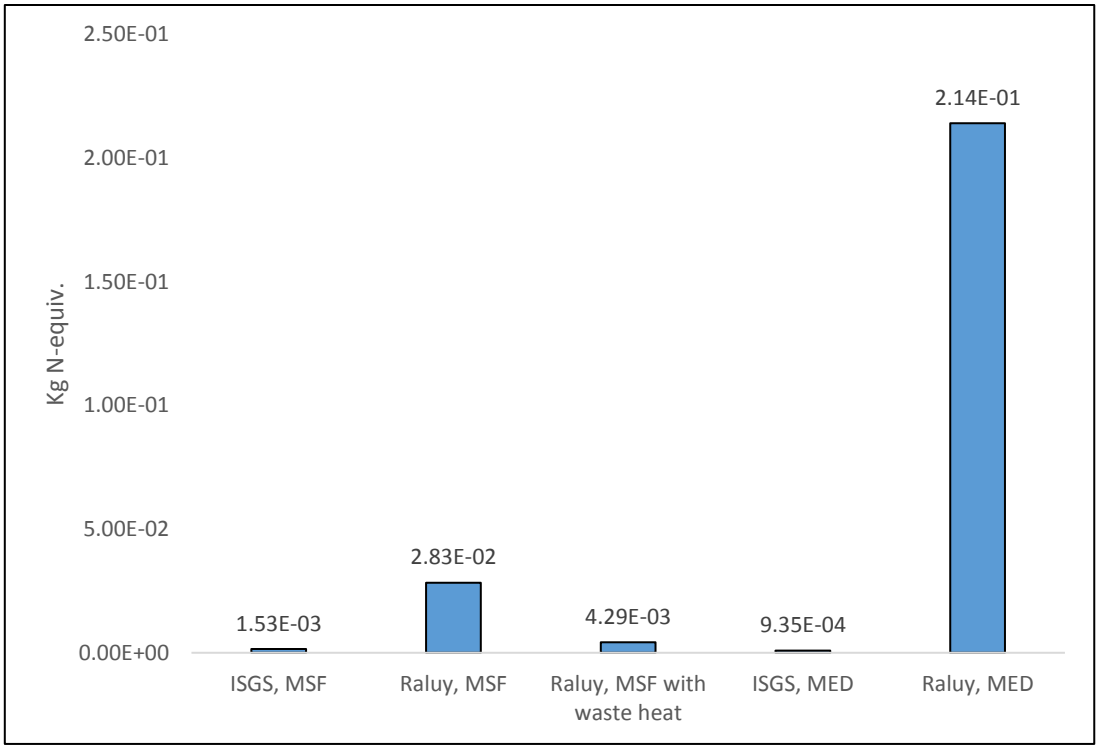

Figure 2-4-15 Eutrophication impact of MSF and MED as determined by various LCA studies. ISGS results refer to the current study.

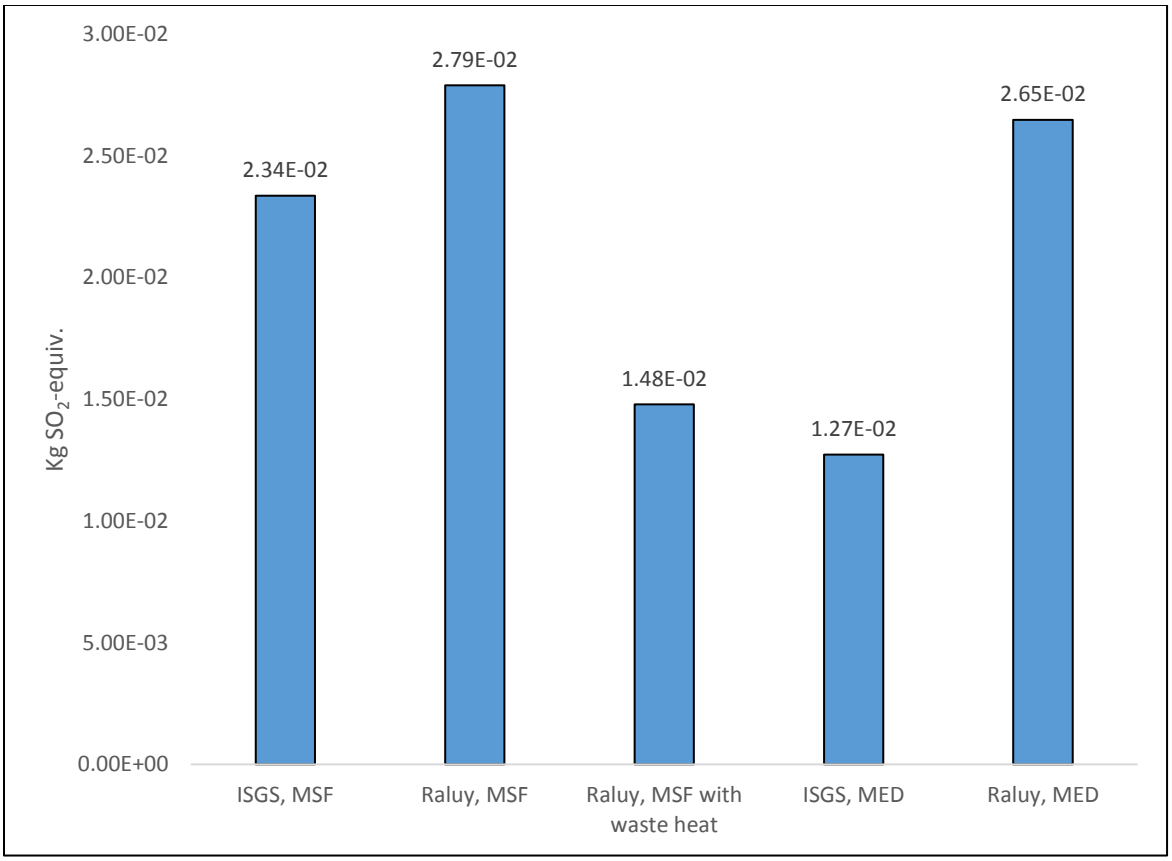

Figure 2-4-16 Acidification impact of MSF and MED as determined by various LCA studies. ISGS results refer to the current study.

Our results for global warming and acidification categories are comparable to the results of Raluy et al. (2006). Differences were mostly due to the LCI databases used for the LCA modeling. Raluy et al. (2006) conducted their studies using databases specifically built for European countries, whereas the GaBi professional database was built for North America and the Ecoinvent databases were either applicable worldwide or specific to North America. Raluy et al. (2006) also indicated that the high environmental impact of thermal desalination processes might be mitigated by integrating them with other processes. This is most clearly seen in the low global warming impact resulting from MSF with a waste heat source instead of fossil fuels.

Appendix 2-B Detailed LCA Inventory and Results

Data Collection for LCI

All inventory data are based on a process flow rate of 8 million gallons per day (MGD) of feed water over a process life span of 20 years. Chemical doses were based on laboratory experiments, in which the optimal doses were 150 mg/L of lime and 100 mg/L of alum. Sludge removed from pretreatment is expected to be 80 wt% solids. Waste designated for landfill disposal is assumed to be transported by trucks with a 24.7 metric ton capacity over a distance of 8 km. Brine designated for disposal by deep well injection is assumed to be conveyed for 1.6 km via pipeline. Additional data used to calculate the input values for certain infrastructure and energy inputs in this study were collected from various sources, as described below. Detailed inventories are then presented in the following tables.

Infrastructure—Concrete, steel, pipe, and sand

Pretreatment infrastructure data were estimated by using the U.S. Environmental Protection Agency (USEPA) report on estimating water treatment costs (Gumerman et al., 1979), which presents cost curves for the construction, operation, and maintenance of numerous process units. The USEPA report presents the cost of construction materials, such as concrete, according to the velocity gradient (G) of mixing and the total basin volume. Infrastructure data in the pretreatment case were projected from the 1979 material prices in the USEPA case study to 2015 estimated prices, and then divided by the unit price in 2015 to calculate the required quantity, as shown in the equation below:

$$Material\ quantity = \frac{Price\ in\ year\ 1979}{Price\ index(1979\ to\ 2015)} \times \frac{1}{Unit\ price}.$$

To determine the prices in 1979, design parameters had to be defined. For rapid mixing, the desired range for G was between 700 and 1,000 s^{-1}, and the mixing or retention time was 20 to 60 s (Wang et al., 2005). In the design for coagulation, G was 900, the basin volume was 1,000 ft^3, the retention time was set at 1 min, and the flow rate was 8 MGD. For the flocculation process, G was 20 (Wang et al., 2005), the basin volume was 2,500 ft^3, the retention time was set at 15 min, and the flow rate was 8 MGD. Clarifier information was selected based on a basin area of 2,240 ft^2, with the retention time set as 30 min. Cost information in the USEPA report was estimated for clarifiers that had a 12-ft sidewall depth. Sand filtration criteria were a sand volume of 2,800 ft^3 with a 5-min retention time. For each pretreatment process, corresponding construction information, such as costs for concrete and steel, were selected from the report and used to project the current cost. By using unit prices from online resources (Quandl, 2015; Statista, 2015; ICIS, 2012; PetroChemWire, 2013), we could obtain material quantities for concrete, steel, and piping. Gravity filtration data in the USEPA report were also used to determine the total media requirement for sand filtration; the density of sand was assumed to be 1700 kg/m^3 (Washington State Department of Health, 2002).

Infrastructure—Pump stations, deep wells, and evaporation equipment

For the purposes of this study, pump station capacity is 644,546 m^3 per year (Wernet et al., 2016), with quantity doubled because an extra set is always assumed to be on standby. Disposal well capacity is assumed to be similar to production well capacity, which is 583 gpm (McCurdy, 2011). Disposal well depth is 4,800 ft. Evaporation equipment is modeled with a volume of 600 L each, including the heat exchanger and boiler (Wernet et al., 2016).

Energy

Energy consumption in the pretreatment case was calculated from data in the USEPA report based on the same design and process parameters as for the construction materials. Energy requirements for pumping water into disposal wells were based on an estimated 0.54 kWh electricity required per barrel (1 barrel = 42 gallons; Coday et al., 2015). Energy consumption for high-TDS desalination cases, including electrical and thermal energy requirements, were estimated by Trimeric and reported in the inventory tables below. Energy requirements for low-TDS desalination were approximated based on values reported in the literature and are presented in the inventory tables.

Normalization and Weighting Factors

For every LCA case, the initial LCIA results were normalized using TRACI 2.1, USA 2008, including biogenic carbon (person equivalents) normalization factors and weighted using

the Thinkstep LCIA Survey 2012, North-America, TRACI 2.1, including biogenic carbon (person equiv. weighted) weights provided by GaBi software and detailed in Table A-1 (PE International, 2016).

Table 2-B-1 Normalization and weighting factors.

Impact category	Normalization factor	Weighting factor
Resources, fossil fuels	5.78×10^{-5}	6.2
Global warming	4.13×10^{-5}	8.9
Smog	7.19×10^{-4}	6.9
Ozone depletion	6.21×10^{0}	5.2
Human toxicity	1.97×10^{4}	7.8
Eutrophication	4.63×10^{-2}	6.6
Ecotoxicity	9.01×10^{-5}	6.7
Acidification	1.10×10^{-2}	5.8

Pretreatment of High-TDS Brine

Inventory data, a water balance, LCIA results, and scenario analysis results for pretreatment of Mt. Simon brine by coagulation, flocculation, clarification, sedimentation, and sand filtration are provided in this section.

Table 2-B-2 LCI inputs for pretreatment of Mt. Simon brine for the lifetime of the plant (continued on next page).

Treatment process	Product flow		Equivalent value	Unit	Source
Coagulation	Infrastructure	Concrete	39	metric ton	Estimates based on data provided in the U.S. Environmental Protection Agency (USEPA) report
		Steel	28	metric ton	
		Pump station	36	pcs	Wernet et al. (2016)
	Chemical	Lime	3.32×10^{7}	kg	Based on design parameters
		Alum	2.21×10^{7}	kg	
	Energy	Electricity	6.79×10^{6}	kWh	Estimates based on data provided in the USEPA report
	Feed water	Mt. Simon brine-1	2.49×10^{11}	kg	Based on design parameters
Flocculation	Infrastructure	Concrete	385	metric ton	Estimates based on data provided in the USEPA report
		Steel	284	metric ton	
	Energy	Electricity	98,000	kWh	
	Feed water	Mt. Simon brine-2	2.49×10^{11}	kg	Based on design parameters
Clarification	Infrastructure	Concrete	388	metric ton	

Treatment process	Product flow		Equivalent value	Unit	Source
		Steel	454	metric ton	Estimates based on data provided in the USEPA report
		Pipe	3.11×10^4	kg	
	Energy	Electricity	218,800	kWh	
	Feed water	Mt. Simon brine-3	2.49×10^{11}	kg	Based on design parameters
Sand filtration	Infrastructure	Concrete	1,259	metric ton	Estimates based on data provided in the USEPA report
		Steel	419	metric ton	
		Pipe	3.34×10^5	kg	
		Pump station[1]	2	pcs	Wernet et al. (2016)
		Sand	149	metric ton	Estimates based on data provided in the USEPA report
	Energy	Electricity	6,250,200	kWh	
	Feed water	Mt. Simon brine-4	2.49×10^{11}	kg	Based on design parameters
Landfill	Feed to landfill	Sludge	8.53×10^8	kg	Based on design parameters
	Transportation	Pipeline	8	km	

[1]The frequency of assumed use was once every 2 weeks for backwashing.

Table 2-B-3 LCI outputs for pretreatment of Mt. Simon brine for the lifetime of the plant.

Treatment process	Product flow	Output value	Unit
Coagulation	Mt. Simon brine-2	2.4942×10^{11}	kg
Flocculation	Mt. Simon brine-3	2.4942×10^{11}	kg
Clarification	Mt. Simon brine-4	2.4869×10^{11}	kg
	Sludge (80% solids)	7.3501×10^8	kg
Sand filtration	Pretreated Mt. Simon brine	2.4857×10^{11}	kg
	Sludge (80% solids)	1.1750×10^8	kg

Table 2-B-4 Process water balance for pretreatment of Mt. Simon brine for the lifetime of the plant.

Water input	Amount	Unit
Raw Mt. Simon brine	2.4937×10^{11}	kg
Water output	**Amount**	**Unit**
Pretreated Mt. Simon brine	2.4857×10^{11}	kg
Difference	7.9718×10^8	kg
Reason	Caused by the removal of TSS	

Table 2-B-5 Environmental impact results for pretreatment of Mt. Simon brine with a functional unit of 1 m^3 of pretreated Mt. Simon brine.

Impact category	Total	Diesel	Transportation	Landfill	Sand filtration	Flocculation	Coagulation	Clarification
Resources, fossil fuels (MJ surplus energy)	6.36×10^{-1}	3.52×10^{-3}	0.00×10^{0}	4.26×10^{-1}	2.65×10^{-2}	1.26×10^{-3}	1.75×10^{-1}	3.52×10^{-3}
Global warming (kg CO_2-equiv)	4.41×10^{0}	3.03×10^{-4}	1.59×10^{-3}	4.06×10^{0}	2.87×10^{-2}	2.08×10^{-3}	3.19×10^{-1}	4.35×10^{-3}
Smog (kg O_3-equiv)	4.46×10^{-2}	2.41×10^{-5}	1.47×10^{-5}	3.18×10^{-2}	9.19×10^{-4}	7.63×10^{-5}	1.17×10^{-2}	1.53×10^{-4}
Ozone depletion (kg CFC 11-equiv)	1.42×10^{-8}	1.59×10^{-14}	0.00×10^{0}	1.07×10^{-11}	1.74×10^{-10}	1.58×10^{-11}	1.39×10^{-8}	2.85×10^{-11}
Human toxicity (CTUh)	5.47×10^{-8}	8.05×10^{-13}	2.10×10^{-16}	7.62×10^{-10}	1.42×10^{-9}	1.16×10^{-12}	5.24×10^{-8}	1.08×10^{-10}
Eutrophication (kg N-equiv)	1.85×10^{-3}	3.51×10^{-7}	4.03×10^{-8}	1.36×10^{-3}	1.28×10^{-5}	2.74×10^{-7}	4.74×10^{-4}	6.98×10^{-7}
Ecotoxicity (CTUe)	1.45×10^{0}	1.88×10^{-4}	4.52×10^{-11}	3.24×10^{-2}	3.28×10^{-2}	3.94×10^{-4}	1.38×10^{0}	7.34×10^{-4}
Acidification (kg SO_2-equiv)	4.40×10^{-3}	1.61×10^{-6}	6.40×10^{-7}	3.02×10^{-3}	9.27×10^{-5}	5.90×10^{-6}	1.27×10^{-3}	1.32×10^{-5}

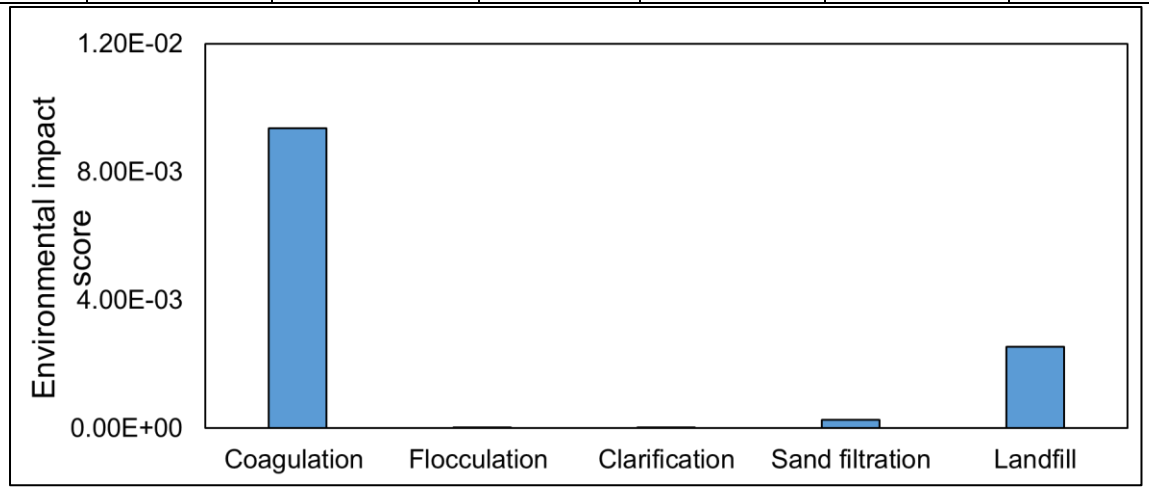

Figure 2-B-1 Weighted impact scores for pretreatment of Mt. Simon brine with a functional unit of 1 m^3 of pretreated Mt. Simon brine.

Table 2-B-6 Water depletion for pretreatment of Mt. Simon brine with a functional unit of 1 m^3 of pretreated Mt. Simon brine.

Water depletion (m^3)	Total	Coagulation	Flocculation	Clarification	Sand filtration	Landfill	Diesel
GaBi result	0.51	0.07	0	0	0.02	0.11	0
Adjusted result	N/A						

Table 2-B-7 Scenario analysis for pretreatment of Mt. Simon brine with a functional unit of 1 m^3 of pretreated Mt. Simon brine.

Impact category	Scenario A Baseline	Scenario B TSS ↓ 90%	Scenario C Distance ↓ 90%
Resources, fossil fuels (MJ surplus energy)	6.36×10^{-1}	3.31×10^{-1}	6.32×10^{-1}
Global warming (kg CO_2-equiv)	4.41×10^{0}	1.53×10^{0}	4.41×10^{0}
Smog (kg O_3-equiv)	4.46×10^{-2}	2.20×10^{-2}	4.46×10^{-2}
Ozone depletion (kg CFC 11-equiv)	1.42×10^{-8}	1.41×10^{-8}	1.42×10^{-8}
Human toxicity (CTUh)	5.47×10^{-8}	5.40×10^{-8}	5.47×10^{-8}
Eutrophication (kg N-equiv)	1.85×10^{-3}	8.83×10^{-4}	1.85×10^{-3}
Ecotoxicity (CTUe)	1.45×10^{0}	1.42×10^{0}	1.45×10^{0}
Acidification (kg SO_2-equiv)	4.40×10^{-3}	2.25×10^{-3}	4.40×10^{-3}

Pretreatment of Low-TDS Brackish Water

Inventory data, a water balance, LCIA results, and scenario analysis results for pretreatment of St. Peter brackish water by coagulation, flocculation, clarification, sedimentation, and sand filtration are provided in this section.

Table 2-B-8 LCI inputs for pretreatment of low-TDS brackish water for the lifetime of the plant (continued on next page).

Treatment process	Product flow		Equivalent value	Unit	Source
Coagulation	Infrastructure	Concrete	39	metric ton	Estimates based on data provided in the U.S. Environmental Protection Agency (EPA) report
		Steel	28	metric ton	
		Pump station	36	pcs	Wernet et al. (2016)
	Chemical	Lime	3.32×10^{7}	kg	Based on design parameters
		Alum	2.21×10^{7}	kg	
	Energy	Electricity	6.79×10^{6}	kWh	Estimates based on data provided in the USEPA report
	Feed water	St. Peter water-1	2.21×10^{11}	kg	Based on design parameters

Treatment process	Product flow		Equivalent value	Unit	Source
Flocculation	Infrastructure	Concrete	385	metric ton	Estimates based on data provided in the USEPA report
		Steel	284	metric ton	
	Energy	Electricity	98,000	kWh	
	Feed water	St. Peter water-2	2.21×10^{11}	kg	Based on design parameters
Clarification	Infrastructure	Concrete	388	metric ton	Estimates based on data provided in the USEPA report
		Steel	454	metric ton	
		Pipe	3.11×10^{4}	kg	
	Energy	Electricity	218,800	kWh	
	Feed water	St. Peter water-3	2.21^{11}	kg	Based on design parameters
Sand filtration	Infrastructure	Concrete	1,259	metric ton	Estimates based on data provided in the USEPA report
		Steel	419	metric ton	
		Pipe	3.34×10^{5}	kg	
		Pump station[1]	2	pcs	Wernet et al. (2016)
		Sand	149	metric ton	Estimates based on data provided in the EPA report
	Energy	Electricity	6,250,200	kWh	
	Feed water	St. Peter water-4	2.21×10^{11}	kg	Based on design parameters
Landfill	Feed to landfill	Sludge	7.43×10^{7}	kg	Based on design parameters
	Transportation	Pipeline	8	km	

[1]The frequency of assumed use was once every 2 weeks for backwashing.

Table 2-B-9 LCI outputs for pretreatment of low-TDS brackish water for the lifetime of the plant.

Treatment process	Product flow	Output value	Unit
Coagulation	St. Peter water-2	2.214223×10^{11}	kg
Flocculation	St. Peter water-3	2.214223×10^{11}	kg
Clarification	St. Peter water-4	2.213488×10^{11}	kg
	Sludge (80% solids)	7.35×10^{7}	kg
Sand filtration	Pretreated St. Peter water	2.213480×10^{11}	kg
	Sludge (80% solids)	7.68×10^{5}	kg

Table 2-B-10 Process water balance for pretreatment of low-TDS brackish water for the lifetime of the plant.

Water input	Amount	Unit
Raw St. Peter water	2.2137×10^{11}	kg
Water output	**Amount**	**Unit**
Pretreated St. Peter water	2.2135×10^{11}	kg
Difference	1.8952×10^{7}	kg
Reason	Caused by the removal of TSS	

Table 2-B-11 Environmental results for pretreatment of low-TDS brackish water with a functional unit of 1 m^3 of pretreated St. Peter brackish water.

Impact category	Total	Diesel	Transportation	Landfill	Sand filtration	Flocculation	Coagulation	Clarification
Resources, fossil fuels (MJ surplus energy)	5.38×10^{-1}	2.73×10^{-3}	0.00×10^{0}	3.30×10^{-1}	2.68×10^{-2}	1.26×10^{-3}	1.74×10^{-1}	3.09×10^{-3}
Global warming (kg CO_2-equiv)	3.49×10^{0}	2.34×10^{-4}	1.23×10^{-3}	3.14×10^{0}	2.87×10^{-2}	2.06×10^{-3}	3.18×10^{-1}	3.84×10^{-3}
Smog (kg O_3-equiv)	3.74×10^{-2}	1.86×10^{-5}	1.14×10^{-5}	2.46×10^{-2}	9.19×10^{-4}	7.59×10^{-5}	1.16×10^{-2}	1.34×10^{-4}
Ozone depletion (kg CFC 11-equiv)	1.41×10^{-8}	1.23×10^{-14}	0.00×10^{0}	8.25×10^{-12}	1.73×10^{-10}	1.57×10^{-11}	1.39×10^{-8}	2.51×10^{-11}
Human toxicity (CTUh)	5.43×10^{-8}	6.23×10^{-13}	1.63×10^{-16}	5.90×10^{-10}	1.46×10^{-9}	1.16×10^{-12}	5.21×10^{-8}	9.34×10^{-11}
Eutrophication (kg N-equiv)	1.54×10^{-3}	2.72×10^{-7}	3.12×10^{-8}	1.05×10^{-3}	1.28×10^{-5}	2.73×10^{-7}	4.72×10^{-4}	6.13×10^{-7}
Ecotoxicity (CTUe)	1.43×10^{0}	1.46×10^{-4}	3.50×10^{-11}	2.51×10^{-2}	3.26×10^{-2}	3.92×10^{-4}	1.38×10^{0}	6.48×10^{-4}
Acidification (kg SO_2-equiv)	3.71×10^{-3}	1.24×10^{-6}	4.95×10^{-7}	2.34×10^{-3}	9.31×10^{-5}	5.87×10^{-6}	1.26×10^{-3}	1.16×10^{-5}

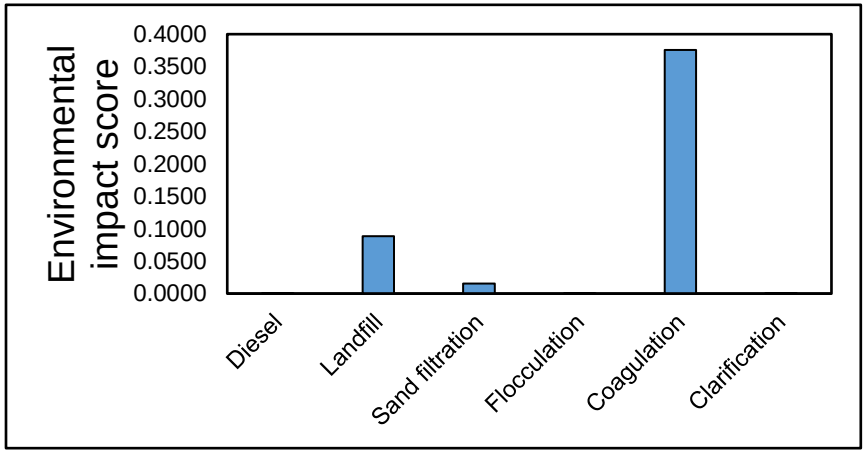

Figure 2-B-2 Weighted impact scores for pretreatment of low-TDS brackish water with a functional unit of 1 m^3 of pretreated St. Peter brackish water.

Table 2-B-12 Water depletion for pretreatment of low-TDS brackish water with a functional unit of 1 m^3 of pretreated St. Peter brackish water.

Water depletion (m^3)	Total	Diesel	Landfill	Sand filtration	Flocculation	Coagulation	Clarification
GaBi result	0.48	0.0001	0.09	0.02	0.0002	0.38	0.0005
Adjusted result	N/A						

High-TDS Brine Handling, Case 1

Inventory data, a water balance, LCIA results, and scenario analysis results for the disposal of Mt. Simon brine by deep well injection are provided in this section.

Table 2B-13 LCI inputs for high-TDS handling by deep well injection (Case 1) for the lifetime of the plant.

Product flow		Equivalent value	Unit	Source
Infrastructure	Deep well	10	pcs	McCurdy (2011)
	Pump station	36	pcs	Wernet et al. (2016)
Energy	Electricity	7.49×10^8	kWh	Coday et al. (2015)
Brine	Pretreated Mt. Simon brine	2.49×10^{11}	kg	Based on design parameters
Transportation	Pipeline	1.6	km	Based on design parameters

Table 2-B-14 Process water balance for pretreatment of Mt. Simon brine for the lifetime of the plant.

Water input	**Amount**	**Unit**
Pretreated Mt. Simon brine	2.4857×10^{11}	kg
Water output	**Amount**	**Unit**
Injected Mt. Simon brine	2.4857×10^{11}	kg
Difference	0	kg

Table 2-B-15 Environmental impact results for high-TDS handling by deep well injection (Case 1) with a functional unit of 1 m^3 of pretreated Mt. Simon brine.

Impact category	Total	Pump station	Onshore well	Electrical energy for transportation	Electric energy for injection
Resources, fossil fuels (MJ surplus energy)	1.85×10^0	2.34×10^{-2}	2.12×10^{-1}	1.56×10^{-2}	1.60×10^0
Global warming (kg CO_2-equiv)	2.47×10^0	3.56×10^{-2}	1.31×10^{-1}	2.22×10^{-2}	2.28×10^0
Smog (kg O_3-equiv)	9.14×10^{-2}	2.34×10^{-3}	2.66×10^{-2}	6.03×10^{-4}	6.19×10^{-2}
Ozone depletion (kg CFC 11-equiv)	2.65×10^{-8}	2.48×10^{-9}	2.31×10^{-8}	8.71×10^{-12}	8.95×10^{-10}
Human toxicity (CTUh)	2.75×10^{-8}	7.90×10^{-9}	1.92×10^{-8}	3.87×10^{-12}	3.97×10^{-10}
Eutrophication (kg N-equiv)	7.77×10^{-4}	1.49×10^{-4}	3.29×10^{-4}	2.88×10^{-6}	2.96×10^{-4}
Ecotoxicity (CTUe)	1.20×10^0	5.44×10^{-1}	6.04×10^{-1}	5.35×10^{-4}	5.50×10^{-2}
Acidification (kg SO_2-equiv)	7.79×10^{-3}	1.75×10^{-4}	1.05×10^{-3}	6.33×10^{-5}	6.50×10^{-3}

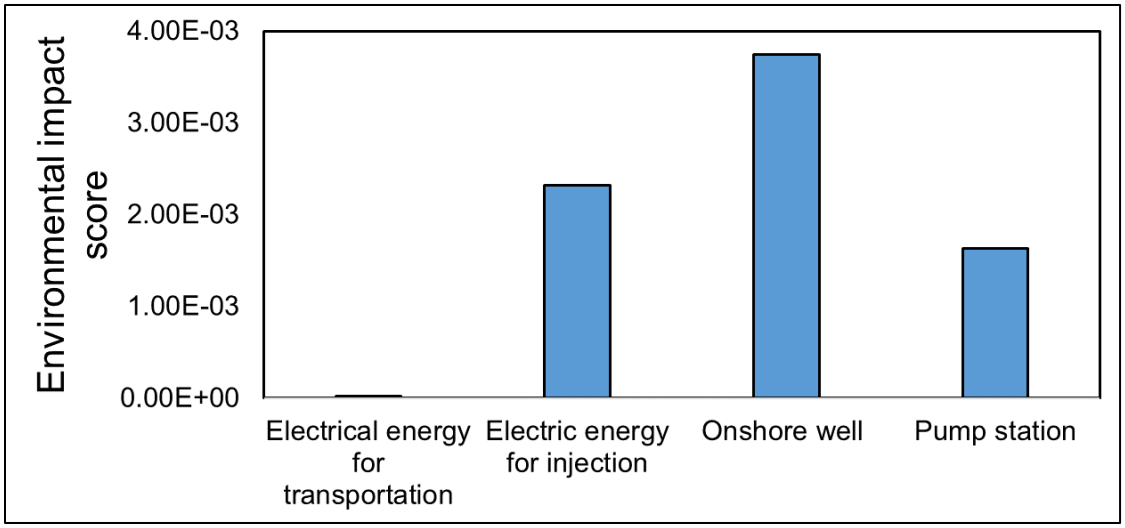

Figure 2-B-3 Weighted impact scores for high-TDS handling by deep well injection (Case 1) with a functional unit of 1 m^3 of pretreated Mt. Simon brine.

Table 2-B-16 Water depletion for high-TDS handling by deep well injection (Case 1) with a functional unit of 1 m^3 of pretreated Mt. Simon brine.

Water depletion (m^3)	Total	Pump station construction	Onshore well production	Electric energy for piping	Electric energy for injection
GaBi result	1.65	0.07	0.19	0.01	1.37
Adjusted result	0.28	0.07	0.19	0.00	0.01

Table 2-B-17 Scenario analysis for high-TDS handling by deep well injection (Case 1) with a functional unit of 1 m^3 of pretreated Mt. Simon brine.

Impact category	Scenario A Baseline	Scenario B Distance ↑ 10×
Resources, fossil fuels (MJ surplus energy)	1.85×10^{0}	1.99×10^{0}
Global warming (kg CO_2-equiv)	2.47×10^{0}	2.67×10^{0}
Smog (kg O_3-equiv)	9.14×10^{-2}	9.68×10^{-2}
Ozone depletion (kg CFC 11-equiv)	2.65×10^{-8}	2.66×10^{-8}
Human toxicity (CTUh)	2.75×10^{-8}	2.75×10^{-8}
Eutrophication (kg N-equiv)	7.77×10^{-4}	8.03×10^{-4}
Ecotoxicity (CTUe)	1.20×10^{0}	1.21×10^{0}
Acidification (kg SO_2-equiv)	7.79×10^{-3}	8.36×10^{-3}
Water depletion (m^3)	1.65	1.77

High-TDS Brine Handling, Case 2

Inventory data, a water balance, LCIA results, and scenario analysis results for partial treatment (10% recovery) of Mt. Simon brine by evaporation are provided in this section.

Table 2-B

-18 LCI inputs for high-TDS handling by evaporation (Case 2) for the lifetime of the plant, evaporation step.

Product flow		**Value**	**Unit**	**Source**
Infrastructure	Hot water tank	1,225	pcs	PE International (2016)
	Pump station	36	pcs	Wernet et al. (2016)
Energy	Thermal energy from natural gas	4.68×10^9	kWh	212 kWh/m^3 of desalinated water estimated thermal energy usage (Trimeric Corp.)
	Electricity	8.26×10^6	kWh	0.374 kWh/m^3 of desalinated water estimated electrical energy usage (Trimeric Corp.)
Brine	Pretreated Mt. Simon brine	2.49×10^{11}	kg	Based on design parameters

Table 2-B-19 LCI inputs for high-TDS handling by evaporation (Case 2) for the lifetime of the plant, deep well injection step.

Product flow		**Equivalent value**	**Unit**	**Source**
Infrastructure	Deep well	10	pcs	McCurdy (2011)
	Pump station	36	pcs	Wernet et al. (2016)
Energy	Electricity	$6.83^0 8$	kWh	Coday et al. (2015)
Brine	Concentrated Mt. Simon brine	2.27×10^{11}	kg	Based on design parameters
Transportation	Pipeline	1.6	km	Based on design parameters

Table 2-B-20 Process water balance for pretreatment of Mt. Simon brine for the lifetime of the plant.

Water input	**Amount**	**Unit**
Pretreated Mt. Simon brine	2.4857×10^{11}	kg
Water output	**Amount**	**Unit**
Concentrated Mt. Simon brine	2.2651×10^{11}	kg
Desalinated water	2.2063×10	kg
Difference	0	kg

Table 2-B-21 Environmental impact results for high-TDS handling by evaporation (Case 2), with a functional unit of 1 m^3 of pretreated Mt. Simon brine.

Impact category	Total	Thermal energy	Pump station	Hot water tank production	Electricity	Deep well injection
Resources, fossil fuels (MJ surplus energy)	1.60×10^{1}	1.43×10^{1}	2.33×10^{-2}	3.79×10^{-3}	1.76×10^{-2}	1.68×10^{0}
Global warming (kg CO_2-equiv)	8.04×10^{0}	5.73×10^{0}	3.54×10^{-2}	4.21×10^{-3}	2.51×10^{-2}	2.24×10^{0}
Smog (kg O_3-equiv)	2.07×10^{-1}	1.21×10^{-1}	2.33×10^{-3}	3.04×10^{-4}	6.80×10^{-4}	8.29×10^{-2}
Ozone depletion (kg CFC 11-equiv)	2.69×10^{-8}	3.15×10^{-12}	2.47×10^{-9}	3.45×10^{-10}	9.82×10^{-12}	2.40×10^{-8}
Human toxicity (CTUh)	3.65×10^{-8}	5.45×10^{-10}	7.86×10^{-9}	3.11×10^{-9}	4.36×10^{-12}	2.50×10^{-8}
Eutrophication (kg N-equiv)	1.14×10^{-3}	2.57×10^{-4}	1.48×10^{-4}	2.20×10^{-5}	3.25×10^{-6}	7.05×10^{-4}
Ecotoxicity (CTUe)	1.90×10^{0}	1.87×10^{-1}	5.42×10^{-1}	7.36×10^{-2}	6.04×10^{-4}	1.09×10^{0}
Acidification (kg SO_2-equiv)	1.12×10^{-2}	3.91×10^{-3}	1.74×10^{-4}	2.66×10^{-5}	7.14×10^{-5}	7.06×10^{-3}

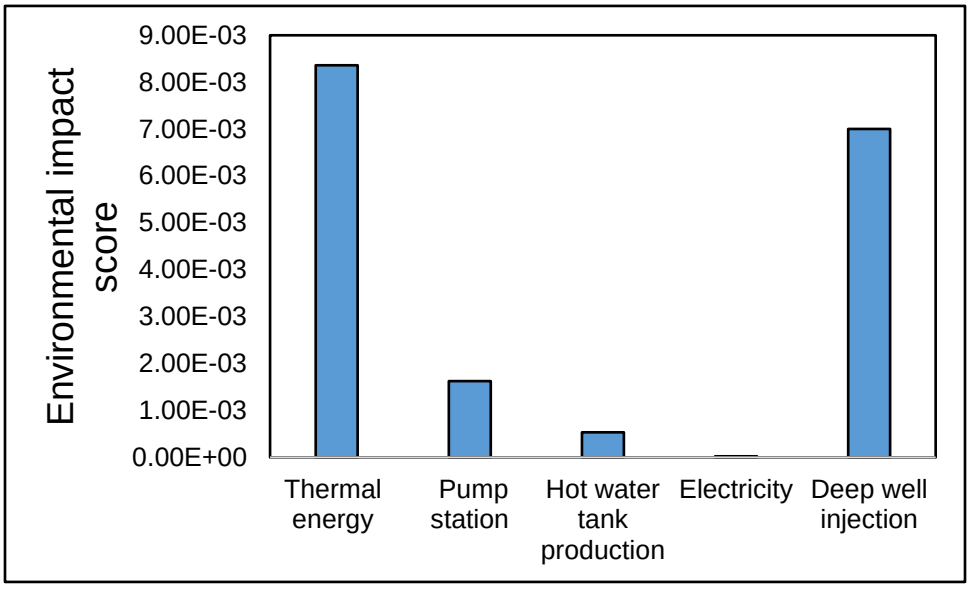

Figure 2-B-4 Weighted environmental impact scores for high-TDS handling by evaporation (Case 2) with a functional unit of 1 m^3 of pretreated Mt. Simon brine.

Table 2-B-22 Environmental impact results for high-TDS handling by evaporation (Case 2), with a functional unit of 1 m^3 of desalinated water.

Impact category	Total	Thermal energy	Pump station	Hot water tank production	Electricity	Deep well injection
Resources, fossil fuels (MJ surplus energy)	1.60×10^{2}	1.42×10^{2}	2.32×10^{-1}	3.77×10^{-2}	1.75×10^{-1}	1.67×10^{1}
Global warming (kg CO_2-equiv)	8.00×10^{1}	5.70×10^{1}	3.53×10^{-1}	4.19×10^{-2}	2.49×10^{-1}	2.23×10^{1}
Smog (kg O_3-equiv)	2.06×10^{0}	1.20×10^{0}	2.32×10^{-2}	3.03×10^{-3}	6.76×10^{-3}	8.25×10^{-1}
Ozone depletion (kg CFC 11-equiv)	2.67×10^{-7}	3.14×10^{-11}	2.46×10^{-8}	3.43×10^{-9}	9.78×10^{-11}	2.39×10^{-7}
Human toxicity (CTUh)	3.63×10^{-7}	5.43×10^{-9}	7.83×10^{-8}	3.10×10^{-8}	4.34×10^{-11}	2.48×10^{-7}
Eutrophication (kg N-equiv)	1.13×10^{-2}	2.56×10^{-3}	1.48×10^{-3}	2.19×10^{-4}	3.23×10^{-5}	7.01×10^{-3}
Ecotoxicity (CTUe)	1.89×10^{1}	1.87×10^{0}	5.39×10^{0}	7.33×10^{-1}	6.01×10^{-3}	1.09×10^{1}
Acidification (kg SO_2-equiv)	1.12×10^{-1}	3.89×10^{-2}	1.73×10^{-3}	2.64×10^{-4}	7.11×10^{-4}	7.03×10^{-2}

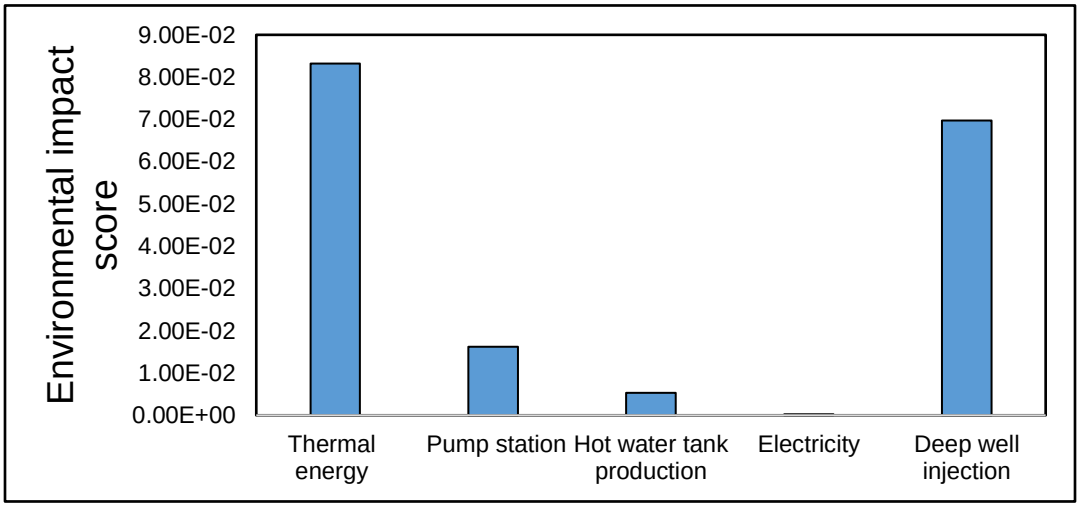

Figure 2-B-5 Weighted environmental impact scores for high-TDS handling by evaporation (Case 2) with a functional unit of 1 m^3 of desalinated water.

Table 2-B-23 Water depletion for high-TDS handling by evaporation (Case 2).

Water depletion (m^3)		Total	Thermal energy	Pump station	Hot water tank production	Evaporation	Electricity	Deep well injection
Functional unit of 1 m^3 of pretreated brine	**GaBi result**	1.56	0.04	0.07	0.04	−0.10	0.02	1.50
	Adjusted result	0.30	0.04	0.07	0.04	−0.10	0.00	0.25
Functional unit of 1 m^3 of desalinated water	**GaBi result**	15.53	0.35	0.68	0.44	−1.00	0.15	14.90
	Adjusted result	2.98	0.35	0.68	0.44	−1.00	0.00	2.50

Table 2-B-24 Scenario analysis for high-TDS handling by evaporation (Case 2), with a functional unit of 1 m^3 of pretreated brine.

Impact category	Scenario A Baseline	Scenario B Energy ↓ 50%	Scenario C Energy ↑ 50%
Resources, fossil fuels (MJ surplus energy)	1.60×10^{1}	8.87×10^{0}	2.32×10^{1}
Global warming (kg CO_2-equiv)	8.04	5.16	10.92
Smog (kg O_3-equiv)	2.07×10^{-1}	1.46×10^{-1}	2.68×10^{-1}
Ozone depletion (kg CFC 11-equiv)	2.69×10^{-8}	2.69×10^{-8}	2.69×10^{-8}
Human toxicity (CTUh)	3.65×10^{-8}	3.62×10^{-8}	3.68×10^{-8}
Eutrophication (kg N-equiv)	1.14×10^{-3}	1.01×10^{-3}	1.27×10^{-3}
Ecotoxicity (CTUe)	1.90	1.80	1.99
Acidification (kg SO_2-equiv)	1.12×10^{-2}	9.25×10^{-3}	1.32×10^{-2}
Water depletion (m^3)	1.56	1.54	1.59

High-TDS Brine Handling, Case 3

Inventory data, a water balance, LCIA results, and scenario analysis results for near-ZLD treatment of Mt. Simon brine by evaporation, in the case in which salt crystals are retained for beneficial use, are provided in this section.

Table 2-B-25 LCI inputs for high-TDS handling by evaporation + crystallization with valuable products (Case 3) for the lifetime of the plant.

Product flow		Value	Unit	Source
Infrastructure	Evaporation equipment	11,025	pcs	PE International (2016)
	Pump station	36	pcs	Wernet et al. (2016)
Energy	Thermal energy from natural gas	4.44×10	kWh	246 kWh/m^3 of desalinated water estimated thermal energy usage (Trimeric Corp.)
	Electricity	3.61×10^8	kWh	2 kWh/m^3 of desalinated water estimated electricity usage (Trimeric Corp.)
Water	Pretreated Mt. Simon brine	2.4857×10^{11}	kg	Based on design parameters

Table 2-B-26 Process water balance for high-TDS handling by evaporation + crystallization with valuable products (Case 3) for the lifetime of the plant.

Water input	**Amount**	**Unit**
Pretreated Mt. Simon brine	2.49×10^{11}	kg
Water output	**Amount**	**Unit**
Concentrated Mt. Simon brine	4.0889×10	kg
Desalinated water	1.80×10^{11}	kg
Difference	2.73×10^{10}	kg
Reason	Caused by the generation of salt crystals	

Table B-27 Environmental impact results for high-TDS handling by evaporation + crystallization with valuable products (Case 3), with a functional unit of 1 m^3 of pretreated Mt. Simon brine.

Impact category	Total	Thermal energy	Pump station	Evaporation equipment	Electricity
Resources, fossil fuels (MJ surplus energy)	1.37×10^2	1.36×10^2	2.33×10^{-2}	3.41×10^{-2}	7.68×10^{-1}
Global warming (kg CO_2-equiv)	5.55×10^1	5.44×10^1	3.54×10^{-2}	3.79×10^{-2}	1.10×10^0
Smog (kg O_3-equiv)	1.18×10^0	1.15×10^0	2.33×10^{-3}	2.74×10^{-3}	2.97×10^{-2}
Ozone depletion (kg CFC 11-equiv)	6.03×10^{-9}	2.99×10^{-11}	2.47×10^{-9}	3.10×10^{-9}	4.29×10^{-10}
Human toxicity (CTUh)	4.13×10^{-8}	5.17×10^{-9}	7.86×10^{-9}	2.80×10^{-8}	1.91×10^{-10}
Eutrophication (kg N-equiv)	2.93×10^{-3}	2.44×10^{-3}	1.48×10^{-4}	1.98×10^{-4}	1.42×10^{-4}
Ecotoxicity (CTUe)	3.01×10^0	1.78×10^0	5.42×10^{-1}	6.63×10^{-1}	2.64×10^{-2}
Acidification (kg SO_2-equiv)	4.06×10^{-2}	3.71×10^{-2}	1.74×10^{-4}	2.39×10^{-4}	3.12×10^{-3}

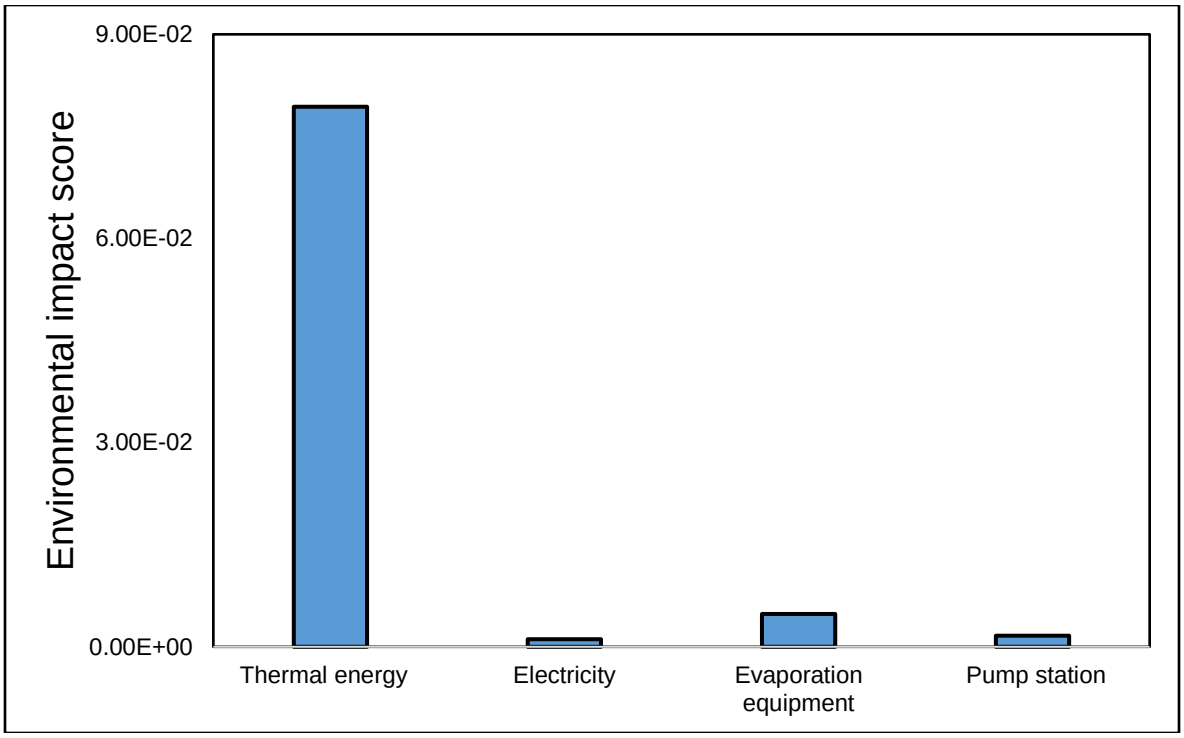

Figure 2-B-6 Weighted environmental impact scores for high-TDS handling by evaporation + crystallization with valuable products (Case 3), with a functional unit of 1 m^3 of pretreated Mt. Simon brine.

Table 2-B-28 Environmental impact results for high-TDS handling by evaporation + crystallization with valuable products (Case 3), with a functional unit of 1 m^3 of desalinated water.

Impact category	Total	Thermal energy	Pump station	Evaporation equipment	Electricity
Resources, fossil fuels (MJ surplus energy)	1.67×10^{2}	1.66×10^{2}	2.84×10^{-2}	4.16×10^{-2}	9.37×10^{-1}
Global warming (kg CO_2-equiv)	6.78×10^{1}	6.63×10^{1}	4.32×10^{-2}	4.62×10^{-2}	1.34×10^{0}
Smog (kg O_3-equiv)	1.44×10^{0}	1.40×10^{0}	2.85×10^{-3}	3.34×10^{-3}	3.62×10^{-2}
Ozone depletion (kg CFC 11-equiv)	7.36×10^{-9}	3.65×10^{-11}	3.01×10^{-9}	3.78×10^{-9}	5.24×10^{-10}
Human toxicity (CTUh)	5.03×10^{-8}	6.31×10^{-9}	9.59×10^{-9}	3.42×10^{-8}	2.32×10^{-10}
Eutrophication (kg N-equiv)	3.57×10^{-3}	2.98×10^{-3}	1.81×10^{-4}	2.42×10^{-4}	1.73×10^{-4}
Ecotoxicity (CTUe)	3.67×10^{0}	2.17×10^{0}	6.61×10^{-1}	8.08×10^{-1}	3.22×10^{-2}
Acidification (kg SO_2-equiv)	4.95×10^{-2}	4.52×10^{-2}	2.12×10^{-4}	2.92×10^{-4}	3.81×10^{-3}

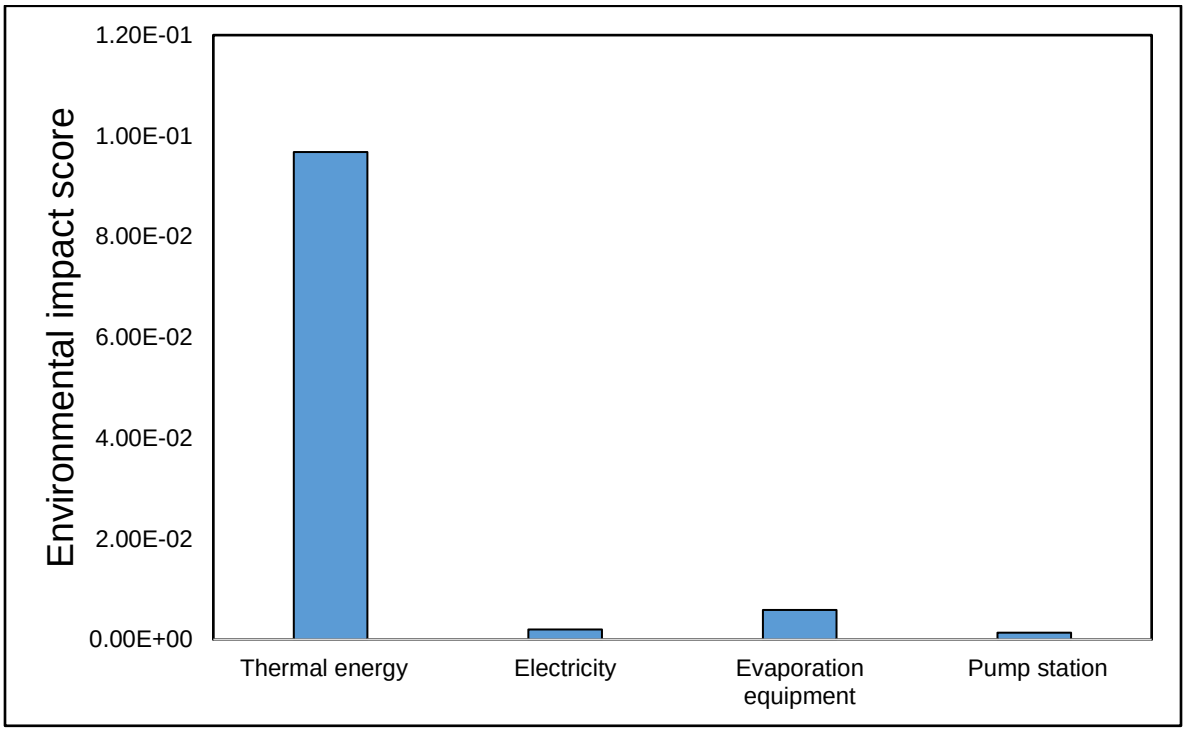

Figure 2-B-7 Weighted impact scores for high-TDS handling by evaporation + crystallization with valuable products (Case 3), with a functional unit of 1 m^3 of desalinated water.

Table 2-B-29 Water depletion for high-TDS handling by evaporation + crystallization with valuable products (Case 3).

Water depletion (m^3)		**Total**	**Thermal energy**	**Pump station**	**Hot water tank production**	**Evaporation + crystallization**	**Electricity**
Functional unit of 1 m^3 of pretreated brine	**GaBi result**	0.65	0.33	0.07	0.40	−0.82	0.66
	Adjusted result	−0.01	0.33	0.07	0.40	−0.82	0.01
Functional unit of 1 m^3 of desalinated water	**GaBi result**	0.79	0.41	0.09	0.49	−1.00	0.80
	Adjusted result	−0.01	0.41	0.09	0.49	−1.00	0.01

Table 2-B-30 Scenario analysis for high-TDS handling by evaporation + crystallization with valuable products (Case 3), with a functional unit of 1 m^3 of pretreated Mt. Simon brine.

Impact category	Scenario A Baseline	Scenario B Energy ↓ 50%	Scenario C Energy ↑ 50%
Resources, fossil fuels (MJ surplus energy)	1.37×10^{2}	6.83×10^{1}	2.05×10^{2}
Global warming (kg CO_2-equiv)	5.55×10^{1}	2.78×10^{1}	8.32×10^{1}
Smog (kg O_3-equiv)	1.18×10^{0}	5.94×10^{-1}	1.77×10^{0}
Ozone depletion (kg CFC 11-equiv)	6.03×10^{-9}	5.80×10^{-9}	6.26×10^{-9}
Human toxicity (CTUh)	4.13×10^{-8}	3.86×10^{-8}	4.39×10^{-8}
Eutrophication (kg N-equiv)	2.93×10^{-3}	1.64×10^{-3}	4.21×10^{-3}
Ecotoxicity (CTUe)	3.01×10^{0}	2.11×10^{0}	3.91×10^{0}
Acidification (kg SO_2-equiv)	4.06×10^{-2}	2.05×10^{-2}	6.06×10^{-2}
Water depletion (m^3)	0.65	0.15	1.14

High-TDS Brine Handling, Case 4

Inventory data, a water balance, LCIA results, and scenario analysis results for near-ZLD treatment of Mt. Simon brine by evaporation, for the case in which residual salt sludge is handled by landfill disposal, are provided in this section.

Table B-31 LCI inputs for high-TDS handling by evaporation + crystallization with disposal (Case 4) for the lifetime of the plant, evaporation and crystallization steps.

Product flow		Value	Unit	Source
Infrastructure	Evaporation equipment	11,025	pcs	PE International (2016)
	Pump station	36	pcs	Wernet et al. (2016)
Energy	Thermal energy from natural gas	3.82×10^{10}	kWh	212 kWh/m^3 of desalinated water estimated thermal energy usage (Trimeric Corp.)
	Electricity	3.26×10^{8}	kWh	1.806 kWh/m^3 of desalinated water estimated electricity usage (Trimeric Corp.)
Water	Pretreated Mt. Simon brine	2.49×10^{11}	kg	Based on design parameters

Table B-32 LCI inputs for high-TDS handling by evaporation + crystallization with disposal (Case 4) for the lifetime of the plant, disposal.

Product flow		Equivalent value	Unit	Source
Infrastructure	Deep well	2	pcs	McCurdy (2011)
	Pump station	8	pcs	Wernet et al. (2016)
Energy	Electricity	1.32×10^{8}	kWh	Coday et al. (2015)
Brine	Concentrated residual brine	4.09×10^{10}	kg	Based on design parameters
Transportation	Pipeline	1.6	km	Based on design parameters
Waste	Salt slurry	2.73×10^{10}	kg	Based on design parameters
Transportation	Truck distance	8	km	

Table 2-B-33 Process water depletion for high-TDS handling by evaporation + crystallization with disposal (Case 4) for the lifetime of the plant, evaporation and crystallization steps.

Water input	**Amount**	**Unit**
Pretreated Mt. Simon brine	2.49×10^{11}	kg
Water output	**Amount**	**Unit**
Injected Mt. Simon brine	4.0889×10^{10}	kg
Desalinated water	1.80×10^{11}	kg
Difference	2.73×10^{10}	kg
Reason	Caused by the generation of salt crystals	

Table 2-B-34 Environmental impact results for high-TDS handling by evaporation + crystallization with disposal (Case 4), with a functional unit of 1 m^3 of pretreated Mt. Simon brine.

Impact category	**Total**	**Thermal energy**	**Diesel**	**Pump station**	**Evaporation equipment**	**Truck**	**Landfill**	**Electricity**	**Deep well injection**
Resources, fossil fuels (MJ surplus energy)	1.30×10^{2}	1.17×10^{2}	1.02×10^{-1}	2.33×10^{-2}	3.41×10^{-2}	0.00×10^{0}	1.23×10^{1}	6.93×10^{-1}	3.03×10^{-1}
Global warming (kg CO_2-equiv)	1.65×10^{2}	4.68×10^{1}	8.74×10^{-3}	3.54×10^{-2}	3.79×10^{-2}	4.58×10^{-2}	1.17×10^{2}	9.89×10^{-1}	4.05×10^{-1}
Smog (kg O_3-equiv)	1.95×10^{0}	9.87×10^{-1}	6.95×10^{-4}	2.33×10^{-3}	2.74×10^{-3}	4.24×10^{-4}	9.17×10^{-1}	2.68×10^{-2}	1.50×10^{-2}
Ozone depletion (kg CFC 11-equiv)	1.06×10^{-8}	2.57×10^{-11}	4.58×10^{-13}	2.47×10^{-9}	3.10×10^{-9}	0.00×10^{0}	3.08×10^{-10}	3.88×10^{-10}	4.34×10^{-9}
Human toxicity (CTUh)	6.70×10^{-8}	4.45×10^{-9}	2.32×10^{-11}	7.86×10^{-9}	2.80×10^{-8}	6.06×10^{-15}	2.20×10^{-8}	1.72×10^{-10}	4.51×10^{-9}
Eutrophication (kg N-equiv)	4.20×10^{-2}	2.10×10^{-3}	1.01×10^{-5}	1.48×10^{-4}	1.98×10^{-4}	1.16×10^{-6}	3.93×10^{-2}	1.28×10^{-4}	1.27×10^{-4}
Ecotoxicity (CTUe)	3.90×10^{0}	1.53×10^{0}	5.44×10^{-3}	5.42×10^{-1}	6.63×10^{-1}	1.31×10^{-9}	9.36×10^{-1}	2.38×10^{-2}	1.97×10^{-1}
Acidification (kg SO_2-equiv)	1.24×10^{-1}	3.19×10^{-2}	4.64×10^{-5}	1.74×10^{-4}	2.39×10^{-4}	1.85×10^{-5}	8.71×10^{-2}	2.82×10^{-3}	1.28×10^{-3}

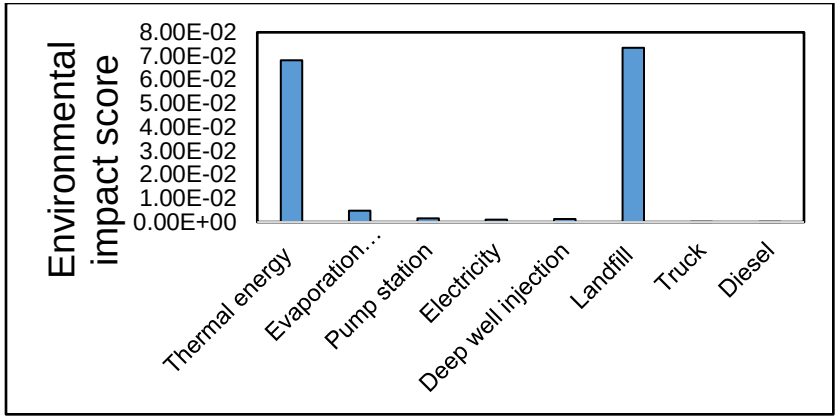

Figure 2-B-8 Weighted environmental impact scores for high-TDS handling by evaporation + crystallization with disposal (Case 4), with a functional unit of 1 m^3 of pretreated Mt. Simon brine.

Table B-35 Environmental impact results for high-TDS handling by evaporation + crystallization with disposal (Case 4), with a functional unit of 1 m^3 of desalinated water.

Impact category	Total	Thermal energy	Diesel	Pump station	Evaporation equipment	Truck	Landfill	Electricity	Deep well injection
Resources, fossil fuels (MJ surplus energy)	1.59×10^{2}	1.42×10^{2}	1.24×10^{-1}	2.84×10^{-2}	4.16×10^{-2}	0.00×10^{0}	1.50×10^{1}	8.46×10^{-1}	3.70×10^{-1}
Global warming (kg CO_2-equiv)	2.02×10^{2}	5.71×10^{1}	1.07×10^{-2}	4.32×10^{-2}	4.62×10^{-2}	5.59×10^{-2}	1.43×10^{2}	1.21×10^{0}	4.94×10^{-1}
Smog (kg O_3-equiv)	2.38×10^{0}	1.20×10^{0}	8.48×10^{-4}	2.85×10^{-3}	3.34×10^{-3}	5.17×10^{-4}	1.12×10^{0}	3.27×10^{-2}	1.83×10^{-2}
Ozone depletion (kg CFC 11-equiv)	1.30×10^{-8}	3.14×10^{-11}	5.59×10^{-13}	3.01×10^{-9}	3.78×10^{-9}	0.00×10^{0}	3.75×10^{-10}	4.73×10^{-10}	5.30×10^{-9}
Human toxicity (CTUh)	8.18×10^{-8}	5.43×10^{-9}	2.83×10^{-11}	9.59×10^{-9}	3.42×10^{-8}	7.39×10^{-15}	2.68×10^{-8}	2.10×10^{-10}	5.50×10^{-9}
Eutrophication (kg N-equiv)	5.13×10^{-2}	2.56×10^{-3}	1.24×10^{-5}	1.81×10^{-4}	2.42×10^{-4}	1.42×10^{-6}	4.80×10^{-2}	1.56×10^{-4}	1.55×10^{-4}
Ecotoxicity (CTUe)	4.75×10^{0}	1.87×10^{0}	6.64×10^{-3}	6.61×10^{-1}	8.08×10^{-1}	1.59×10^{-9}	1.14×10^{0}	2.91×10^{-2}	2.40×10^{-1}
Acidification (kg SO_2-equiv)	1.51×10^{-1}	3.89×10^{-2}	5.66×10^{-5}	2.12×10^{-4}	2.92×10^{-4}	2.25×10^{-5}	1.06×10^{-1}	3.44×10^{-3}	1.56×10^{-3}

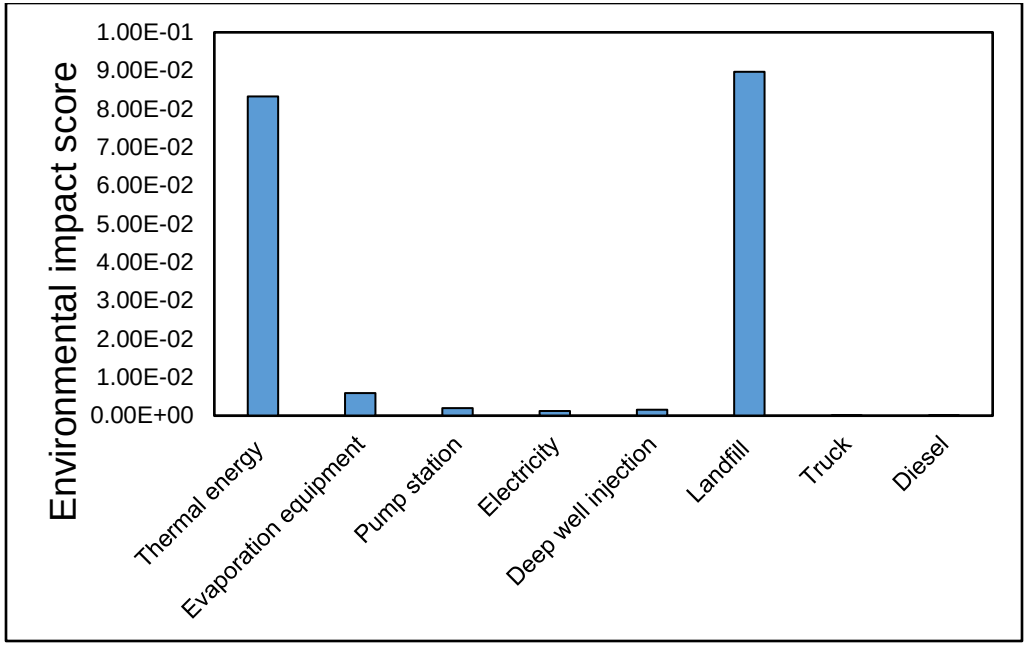

Figure 2-B-9 Weighted environmental impact scores for high-TDS handling by evaporation + crystallization with disposal (Case 4), with a functional unit of 1 m^3 of desalinated water.

Table 2-B-36 Water depletion for high-TDS handling by evaporation + crystallization with disposal (Case 4).

Water depletion (m^3)		Total	Thermal energy	Diesel	Pump station	Evaporation equipment	Evaporation + crystallization	Landfill	Electricity	Deep well injection
Functional unit of 1 m^3 of pretreated brine	**GaBi result**	4.11	0.29	0.00	0.07	0.40	−0.82	3.30	0.60	0.27
	Adjusted result	3.24	0.29	0.00	0.07	0.40	−0.82	3.30	0.01	0.05
Functional unit of 1 m^3 of desalinated water	**GaBi result**	5.01	0.35	0.00	0.09	0.49	−1.00	4.02	0.73	0.33
	Adjusted result	3.95	0.35	0.00	0.09	0.49	−1.00	4.02	0.01	0.06

Table 2-B-37 Scenario analysis for high-TDS handling by evaporation + crystallization with disposal (Case 4), with a functional unit of 1 m^3 of pretreated Mt. Simon brine.

Impact category	Scenario A Baseline	Scenario B Energy ↓ 50%	Scenario C Energy ↑ 50%
Resources, fossil fuels (MJ surplus energy)	1.30×10^{2}	7.15×10^{1}	1.89×10^{2}
Global warming (kg CO_2-equiv)	1.65×10^{2}	1.41×10^{2}	1.89×10^{2}
Smog (kg O_3-equiv)	1.95×10^{0}	1.45×10^{0}	2.46×10^{0}
Ozone depletion (kg CFC 11-equiv)	1.06×10^{-8}	1.04×10^{-8}	1.08×10^{-8}
Human toxicity (CTUh)	6.70×10^{-8}	6.47×10^{-8}	6.93×10^{-8}
Eutrophication (kg N-equiv)	4.20×10^{-2}	4.09×10^{-2}	4.31×10^{-2}
Ecotoxicity (CTUe)	3.90×10^{0}	3.12×10^{0}	4.67×10^{0}
Acidification (kg SO_2-equiv)	1.24×10^{-1}	1.06×10^{-1}	1.41×10^{-1}
Water depletion (m^3)	4.11	3.67	4.55

Low-TDS Brackish Water Treatment, Case 1

Inventory data, a water balance, LCIA results, and scenario analysis results for treatment of St. Peter brackish water by RO are provided in this section.

Table 2-B-38 LCI inputs for low-TDS handling by RO (Case 1) for the lifetime of the plant, RO step (Tarnacki et al., 2012).

Product flow		Equivalent value	Unit	Source
Infrastructure	PVC pipe E	5.69×10^{4}	kg	Coday et al. (2015)
	Glass fiber reinforced plastic	8.66×10^{5}	kg	
	Hot rolled sheet, steel	2.24×10^{6}	kg	
	Stainless steel hot rolled coil	3.43×10^{4}	kg	
	Galvanized steel sheet	6.73×10^{4}	kg	
Energy	Electricity	4.21×10^{8}	kWh	
Membrane materials	Polyamide	2.04×10^{5}	kg	
	Epoxy	4.05×10^{0}	kg	
	Polypropylene	2.82×10^{5}	kg	
	PVC Pipe	4.92×10^{4}	kg	
	PVC injection molding	4.55×10^{4}	kg	
	Glass fiber reinforced plastic	1.97×10^{5}	kg	
Water	Pretreated St. Peter water	2.21×10^{11}	kg	Based on design parameters
Chemical	Polycarboxylates	5.19×10^{5}	kg	Coday et al. (2015)

Table 2-B-39 LCI inputs for low-TDS handling by RO (Case 1) for the lifetime of the plant, deep well injection step.

Product flow		Equivalent value	Unit	Source
Infrastructure	Deep well	1	pcs	McCurdy (2011)
	Pump station	2	pcs	Wernet et al. (2016)
Energy	Electricity	3.77×10^{7}	kWh	Tarnacki et al. (2012)
Brine	Concentrated St. Peter water	1.11×10^{10}	kg	Based on design parameters
Transportation	Pipeline	1.6	km	Based on design parameters

Table 2-B-40 Process water balance for low-TDS handling by RO (Case 1) for the lifetime of the plant.

Water input	**Amount**	**Unit**
Pretreated St. Peter water	2.21×10^{11}	kg
Water output	**Amount**	**Unit**
Concentrated St. Peter water	1.11×10^{10}	kg
Desalinated water	2.10×10^{11}	kg
Difference	0	Kg

Table 2-B-41 Environmental impact results for low-TDS handling by RO (Case 1), with a functional unit of 1 m^3 of desalinated water.

Impact category	Total	Antiscalant	Electricity	Membrane materials (RO)	Infrastructure (RO)	Deep well injection
Resources, fossil fuels (MJ surplus energy)	1.14×10^{0}	8.01×10^{-3}	9.36×10^{-1}	4.58×10^{-2}	6.41×10^{-2}	8.60×10^{-2}
Global warming (kg CO_2-equiv)	1.52×10^{0}	3.09×10^{-3}	1.34×10^{0}	1.80×10^{-2}	5.19×10^{-2}	1.15×10^{-1}
Smog (kg O_3-equiv)	4.52×10^{-2}	1.34×10^{-4}	3.62×10^{-2}	8.80×10^{-4}	3.74×10^{-3}	4.25×10^{-3}
Ozone depletion (kg CFC 11-equiv)	6.55×10^{-9}	4.46×10^{-10}	5.23×10^{-10}	4.25×10^{-10}	3.93×10^{-9}	1.23×10^{-9}
Human toxicity (CTUh)	3.31×10^{-9}	1.43×10^{-10}	2.32×10^{-10}	4.77×10^{-10}	1.18×10^{-9}	1.28×10^{-9}
Eutrophication (kg N-equiv)	3.29×10^{-4}	7.13×10^{-6}	1.73×10^{-4}	1.31×10^{-5}	1.00×10^{-4}	3.61×10^{-5}
Ecotoxicity (CTUe)	2.29×10^{-1}	1.35×10^{-2}	3.22×10^{-2}	1.30×10^{-2}	1.15×10^{-1}	5.59×10^{-2}
Acidification (kg SO_2-equiv)	4.80×10^{-3}	1.23×10^{-5}	3.80×10^{-3}	6.16×10^{-5}	5.56×10^{-4}	3.62×10^{-4}

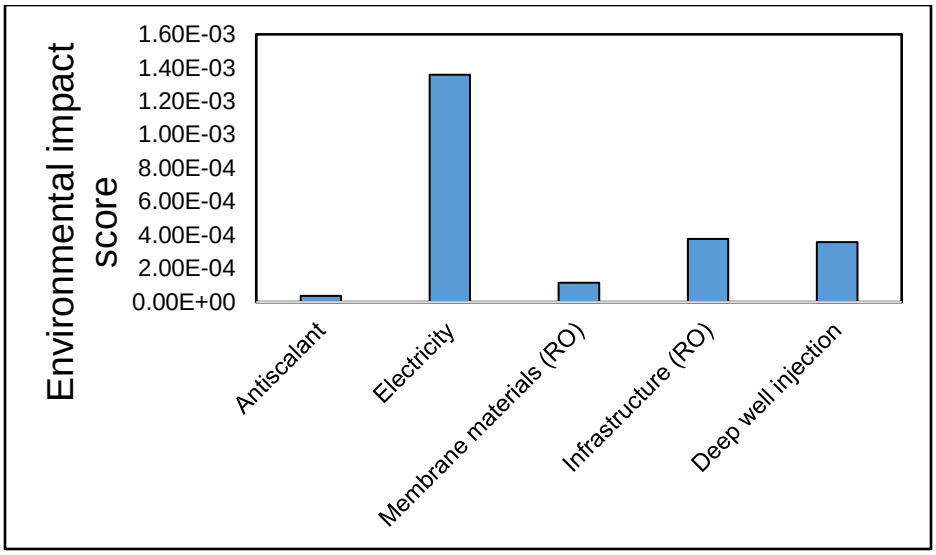

Figure 2-B-10 Weighted environmental impact scores for low-TDS handling by RO (Case 1), with a functional unit of 1 m^3 desalinated water.

Table 2-B-42 Water depletion for low-TDS handling by RO (Case 1), functional unit 1 m^3 desalinated water.

Water depletion (m^3)	Total	Antiscalant	RO	Electricity	Membrane materials (RO)	Infrastructure (RO)	Deep well injection
GaBi result	−0.06	0.01	−1.00	0.80	0.02	0.04	0.08
Adjusted result	−0.92	0.01	−1.00	0.01	0.02	0.04	0.01

Table 2-B-43 Scenario analysis for low-TDS handling by RO (Case 1), with a functional unit of 1 m^3 of desalinated water.

Impact category	Scenario A Baseline	Scenario B Energy ↓ 50%	Scenario C Energy ↑ 2×	Scenario D 50% water recovery
Resources, fossil fuels (MJ surplus energy)	1.14×10^{0}	6.71×10^{-1}	2.07×10^{0}	1.47×10^{0}
Global warming (kg CO_2-equiv)	1.52×10^{0}	8.54×10^{-1}	2.86×10^{0}	1.92×10^{0}
Smog (kg O_3-equiv)	4.52×10^{-2}	2.71×10^{-2}	8.14×10^{-2}	6.61×10^{-2}
Ozone depletion (kg CFC 11-equiv)	6.55×10^{-9}	6.29×10^{-9}	7.08×10^{-9}	1.74×10^{-8}
Human toxicity (CTUh)	3.31×10^{-9}	3.19×10^{-9}	3.54×10^{-9}	1.47×10^{-8}
Eutrophication (kg N-equiv)	3.29×10^{-4}	2.43×10^{-4}	5.02×10^{-4}	5.71×10^{-4}
Ecotoxicity (CTUe)	2.29×10^{-1}	2.13×10^{-1}	2.61×10^{-1}	7.16×10^{-1}
Acidification (kg SO_2-equiv)	4.80×10^{-3}	2.89×10^{-3}	8.59×10^{-3}	6.24×10^{-3}
Water depletion (m^3)	−0.06	−0.46	0.74	0.72

Low-TDS Brackish Water Treatment, Case 2

Inventory data, a water balance, LCIA results, and scenario analysis results for treatment of St. Peter brackish water by FO with a $MgSO_4$ draw solution are provided in this section.

Table 2-B-44 LCI inputs for low-TDS handling by FO_DS1 (Case 2) for the lifetime of the plant, FO/NF steps.

Product flow		Equivalent value	Unit	Source
Infrastructure - FO	PVC pipe	1.04×10^5	kg	Coday et al. (2015)
	PVC injection molding E	7.94×10^3	kg	
	Acrylonitrile-butadiene-styrene copolymer	4.69×10^3	kg	
	Polyethylene, HDPE[1]	7.37×10^5	kg	
	Glass fiber reinforced plastic	7.74×10^5	kg	
	Hot rolled sheet, steel	1.58×10^6	kg	
	Stainless steel hot rolled coil	2.77×10^4	kg	
	Galvanized steel sheet	3.20×10^4	kg	
Infrastructure - NF	Aluminum framing	6.40×10^4	kg	
	PVC pipe	1.46×10^4	kg	
	Stainless steel hot rolled coil	2.67×10^4	kg	
	Polypropylene	5.20×10^4	kg	
Energy	Electricity (FO)	2.94×10^8	kWh	
	Electricity (NF)	1.05×10^8	kWh	
Membrane materials	Acrylonitrile-butadiene-styrene copolymer	1.78×10^5	kg	
	Viscose fibers	5.12×10^4	kg	
	Polypropylene film	1.06×10^5	kg	
	PVC pipe	3.02×10^5	kg	
	Glass fiber reinforced plastic	2.64×10^5	kg	
	Polystyrene	7.41×10^5	kg	
	Polyurethane, flexible foam	4.59×10^5	kg	
	Polyvinylchloride, suspension polymerized	3.24×10^4	kg	
Water	Pretreated St. Peter water	2.21348×10^{11}	kg	Based on design parameters
Chemical	$MgSO_4$	5.86×10^5	kg	Based on design parameters

[1]HDPE, high-density polyethylene.

Table 2-B-45 LCI inputs for low-TDS handling by FO_DS1 (Case 2) for the lifetime of the plant, deep well injection steps.

Product flow		Equivalent value	Unit	Source
Infrastructure	Deep well	1	pcs	McCurdy (2011)
	Pump station	2	pcs	Wernet et al. (2016)
Energy	Electricity	3.77×10^7	kWh	Coday et al. (2015)
Brine	Concentrated St. Peter water	1.11×10^{10}	kg	Based on design parameters
Transportation	Pipeline	1.6	km	Based on design parameters

Table 2-B-46 Process water balance for low-TDS handling by FO_DS1 (Case 2) for the lifetime of the plant.

Water input	**Amount**	**Unit**
Pretreated St. Peter water	2.21×10^{11}	kg
Water output	**Amount**	**Unit**
Concentrated St. Peter water	1.11×10^{10}	kg
Desalinated water	2.10×10^{11}	kg
Difference	0	kg

Table 2-B-47 Environmental impact results for low-TDS handling by FO_DS1 (Case 2), with a functional unit of 1 m^3 of desalinated water.

Impact category	**Total**	**Magnesium sulfate production**	**Electricity**	**NF**	**Membrane materials (FO)**	**Infrastructure (FO)**	**Deep well injection**
Resources, fossil fuels (MJ surplus energy)	1.13×10^{0}	9.16×10^{-4}	6.54×10^{-1}	2.39×10^{-1}	8.73×10^{-2}	6.67×10^{-2}	8.61×10^{-2}
Global warming (kg CO_2-equiv)	1.44×10^{0}	1.25×10^{-3}	9.33×10^{-1}	3.23×10^{-1}	3.01×10^{-2}	3.90×10^{-2}	1.15×10^{-1}
Smog (kg O_3-equiv)	4.15×10^{-2}	8.48×10^{-5}	2.53×10^{-2}	8.87×10^{-3}	1.25×10^{-3}	1.74×10^{-3}	4.25×10^{-3}
Ozone depletion (kg CFC 11-equiv)	4.18×10^{-9}	8.53×10^{-11}	3.66×10^{-10}	1.48×10^{-10}	6.28×10^{-10}	1.72×10^{-9}	1.23×10^{-9}
Human toxicity (CTUh)	3.82×10^{-9}	4.28×10^{-11}	1.62×10^{-10}	1.06×10^{-10}	1.19×10^{-9}	1.04×10^{-9}	1.28×10^{-9}
Eutrophication (kg N-equiv)	2.87×10^{-4}	3.52×10^{-6}	1.21×10^{-4}	4.15×10^{-5}	3.87×10^{-5}	4.60×10^{-5}	3.61×10^{-5}
Ecotoxicity (CTUe)	1.56×10^{-1}	2.60×10^{-3}	2.25×10^{-2}	8.57×10^{-3}	1.69×10^{-2}	4.93×10^{-2}	5.60×10^{-2}
Acidification (kg SO_2-equiv)	4.32×10^{-3}	8.81×10^{-6}	2.66×10^{-3}	1.02×10^{-3}	1.22×10^{-4}	1.52×10^{-4}	3.62×10^{-4}

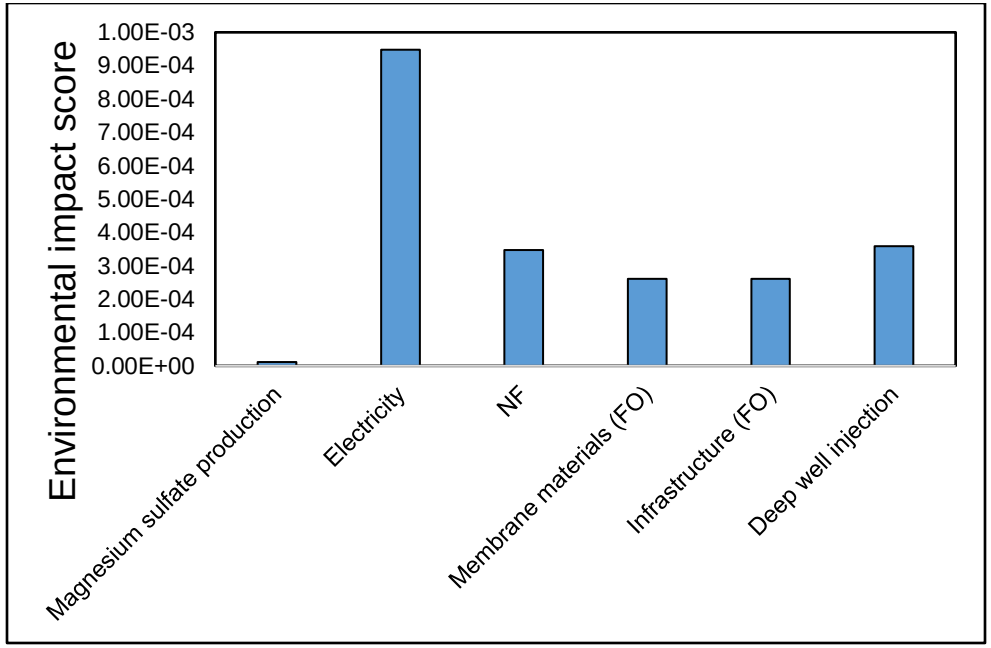

Figure 2-B-11 Weighted environmental impact scores for low-TDS handling by FO_DS1 (Case 2), with a functional unit of 1 m^3 of desalinated water.

Table 2-B-48 Water depletion for low-TDS handling by FO_DS1 (Case 2), with a functional unit of 1 m^3 of desalinated water.

Water depletion	Total	Magnesium sulfate production	Electricity (FO)	NF	Membrane materials (FO)	Infra-structure (FO)	Deep well injection	Infra-structure (NF)	Electricity (NF)
GaBi result	−0.03	0.01	0.56	−1.00	0.01	0.03	0.08	0.03	0.25
Adjusted result	−0.93	0.01	0.01	−1.00	0.01	0.03	0.01	0.03	0.00

Table 2-B-49 Scenario analysis for low-TDS handling by FO_DS1 (Case 2), functional unit 1 m^3 desalinated water.

Impact category	Scenario A Baseline	Scenario B Energy ↓ 50%	Scenario C Energy ↑ 50%	Scenario D 50% water recovery
Resources, fossil fuels (MJ surplus energy)	1.13×10^{0}	8.06×10^{-1}	1.46×10^{0}	1.48×10^{0}
Global warming (kg CO_2-equiv)	1.44×10^{0}	9.74×10^{-1}	1.91×10^{0}	1.88×10^{0}
Smog (kg O_3-equiv)	4.15×10^{-2}	2.88×10^{-2}	5.42×10^{-2}	6.34×10^{-2}
Ozone depletion (kg CFC 11-equiv)	4.18×10^{-9}	4.00×10^{-9}	4.37×10^{-9}	1.50×10^{-8}
Human toxicity (CTUh)	3.82×10^{-9}	3.74×10^{-9}	3.90×10^{-9}	1.52×10^{-8}
Eutrophication (kg N-equiv)	2.87×10^{-4}	2.26×10^{-4}	3.48×10^{-4}	5.34×10^{-4}
Ecotoxicity (CTUe)	1.56×10^{-1}	1.45×10^{-1}	1.67×10^{-1}	6.43×10^{-1}
Acidification (kg SO_2-equiv)	4.32×10^{-3}	2.99×10^{-3}	5.66×10^{-3}	5.83×10^{-3}
Water depletion (m^3)	–0.03	–0.31	0.25	0.73

Low-TDS Brackish Water Treatment, Case 3

Inventory data, a water balance, LCIA results, and scenario analysis results for treatment of St. Peter brackish water by FO with a NH_4HCO_3 draw solution are provided in this section.

Table 2-B-50 LCI inputs for low-TDS handling by FO_DS2 (Case 3) for the lifetime of the plant, FO steps.

Product flow		Equivalent value	Unit	Source
Infrastructure–FO	PVC pipe	1.04×10^5	kg	Coday et al., (2015)
	PVC injection molding E	7.94×10^3	kg	
	Acrylonitrile-butadiene-styrene copolymer	4.69×10^3	kg	
	Polyethylene, HDPE[1]	7.37×10^5	kg	
	Glass fiber reinforced plastic	7.74×10^5	kg	
	Hot rolled sheet, steel	1.58×10^6	kg	
	Stainless steel hot rolled coil	2.77×10^4	kg	
	Galvanized steel sheet	3.20×10^4	kg	
	Pump station	36	pcs	Wernet et al., (2016)
Infrastructure–DS recovery	Hot water tank	4.21×10^3	pcs	
Energy	Electricity (FO)	2.94×10^8	kWh	Coday et al., (2015)
	Electricity (DS recovery)	2.10×10^7	kWh	Qin and He (2014)
	Electricity (pumping)	7.86×10^7	kWh	Estimated by Trimeric Corp.
Membrane materials	Acrylonitrile-butadiene-styrene copolymer	1.78×10^5	kg	Coday et al., (2015)
	Viscose fibers	5.12×10^4	kg	
	Polypropylene film	1.06×10^5	kg	
	PVC pipe	3.02×10^5	kg	
	Glass fiber reinforced plastic	2.64×10^5	kg	
	Polystyrene	7.41×10^5	kg	
	Polyurethane, flexible foam	4.59×10^5	kg	
	Polyvinylchloride, suspension polymerized	3.24×10^4	kg	
Water	Pretreated St. Peter water	2.21×10^{11}	kg	Based on design parameters
Chemical	NH_4HCO_3	4.36×10^7	kg	Maneechan et al. (2014)

[1]HDPE, high-density polyethylene.

Table 2-B-51 LCI inputs for low-TDS handling by FO_DS2 (Case 3) for the lifetime of the plant, deep well injection steps.

Product flow		Equivalent value	Unit	Source
Infrastructure	Deep well	1	pcs	McCurdy (2011)
	Pump station	2	pcs	Wernet et al. (2016)
Energy	Electricity	3.77×10^7	kWh	Coday et al. (2015); Qin and He (2014)
Brine	Concentrated St. Peter water	1.11×10^{10}	kg	Based on design parameters
Transportation	Pipeline	1.6	km	Based on design parameters

Table 2-B-52 Process water balance for low-TDS handling by FO_DS2 (Case 3) for the lifetime of the plant.

Water input	**Amount**	**Unit**
Pretreated St. Peter water	2.21×10^{11}	kg
Water output	**Amount**	**Unit**
Concentrated St. Peter water	1.11×10^{10}	kg
Desalinated water	2.10×10^{11}	kg
Difference	0	kg

Table 2-B-53 Environmental impact results for low-TDS handling by FO_DS2 (Case 3), with a functional unit of 1 m^3 of desalinated water.

Impact category	**Total**	**Pump station**	**Hot water tank production**	**Ammonium bicarbonate**	**Electricity**	**Membrane materials (FO)**	**Infrastructure (FO)**	**Deep well injection**
Resources, fossil fuels (MJ surplus energy)	1.55×10^{0}	2.44×10^{-2}	1.36×10^{-2}	3.96×10^{-1}	8.76×10^{-1}	8.73×10^{-2}	6.67×10^{-2}	8.58×10^{-2}
Global warming (kg CO_2-equiv)	1.76×10^{0}	3.70×10^{-2}	1.51×10^{-2}	2.74×10^{-1}	1.25×10^{0}	3.01×10^{-2}	3.90×10^{-2}	1.15×10^{-1}
Smog (kg O_3-equiv)	6.72×10^{-2}	2.44×10^{-3}	1.09×10^{-3}	2.26×10^{-2}	3.39×10^{-2}	1.25×10^{-3}	1.74×10^{-3}	4.24×10^{-3}
Ozone depletion (kg CFC 11-equiv)	3.50×10^{-8}	2.58×10^{-9}	1.24×10^{-9}	2.71×10^{-8}	4.90×10^{-10}	6.28×10^{-10}	1.72×10^{-9}	1.23×10^{-9}
Human toxicity (CTUh)	3.37×10^{-8}	8.22×10^{-9}	1.12×10^{-8}	1.06×10^{-8}	2.17×10^{-10}	1.19×10^{-9}	1.04×10^{-9}	1.28×10^{-9}
Eutrophication (kg N-equiv)	1.16×10^{-3}	1.55×10^{-4}	7.92×10^{-5}	6.40×10^{-4}	1.62×10^{-4}	3.87×10^{-5}	4.60×10^{-5}	3.60×10^{-5}
Ecotoxicity (CTUe)	2.27×10^{0}	5.67×10^{-1}	2.65×10^{-1}	1.29×10^{0}	3.01×10^{-2}	1.69×10^{-2}	4.93×10^{-2}	5.58×10^{-2}
Acidification (kg SO_2-equiv)	5.96×10^{-3}	1.82×10^{-4}	9.55×10^{-5}	1.49×10^{-3}	3.56×10^{-3}	1.22×10^{-4}	1.52×10^{-4}	3.61×10^{-4}

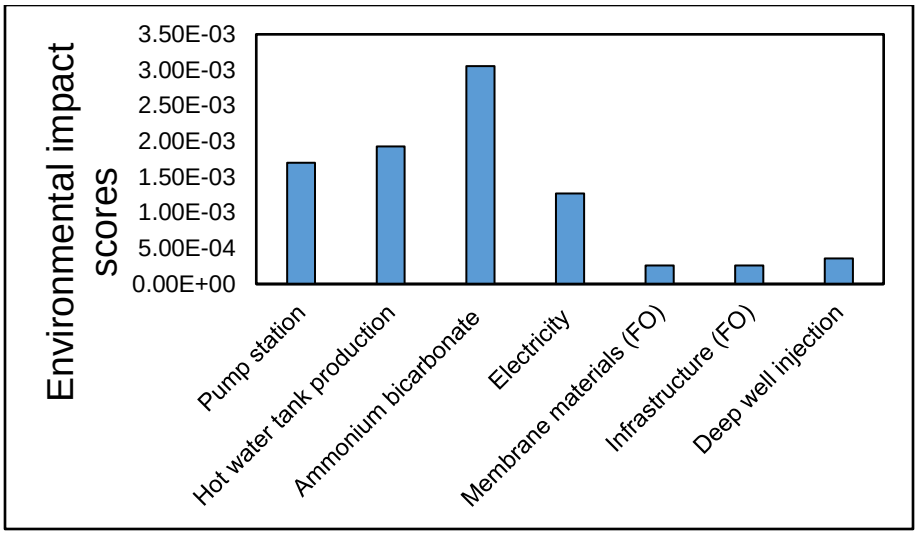

Figure 2-B-12 Weighted environmental impact scores for low-TDS handling by FO_DS2 (Case 3), with a functional unit of 1 m^3 of desalinated water.

Table 2-B-54 Water depletion for low-TDS handling by FO_DS2 (Case 3), with a functional unit of 1 m^3 of desalinated water.

Water depletion	Total	Pump station	Hot water tank production	Ammonium bicarbonate	FO	Electricity	Membrane materials (FO)	Infrastructure (FO)	Deep well injection
GaBi result	0.85	0.07	0.16	0.74	–1.00	0.75	0.01	0.03	0.08
Adjusted result	0.00	0.07	0.16	0.74	–1.00	0.01	0.01	0.03	0.01

Table 2-B-55 Scenario analysis for low-TDS handling by FO_DS2 (Case 3), functional unit 1 m^3 desalinated water.

Impact category	Scenario A Baseline	Scenario C Energy ↓ 50%	Scenario B Energy ↑ 50%	Scenario D 50% water recovery
Resources, fossil fuels (MJ surplus energy)	1.55×10^{0}	1.11×10^{0}	1.99×10^{0}	1.91×10^{0}
Global warming (kg CO_2-equiv)	1.76×10^{0}	1.14×10^{0}	2.39×10^{0}	2.20×10^{0}
Smog (kg O_3-equiv)	6.72×10^{-2}	5.03×10^{-2}	8.42×10^{-2}	8.93×10^{-2}
Ozone depletion (kg CFC 11-equiv)	3.50×10^{-8}	3.48×10^{-8}	3.53×10^{-8}	4.58×10^{-8}
Human toxicity (CTUh)	3.37×10^{-8}	3.36×10^{-8}	3.38×10^{-8}	4.51×10^{-8}
Eutrophication (kg N-equiv)	1.16×10^{-3}	1.08×10^{-3}	1.24×10^{-3}	1.40×10^{-3}
Ecotoxicity (CTUe)	2.27×10^{0}	2.26×10^{0}	2.29×10^{0}	2.76×10^{0}
Acidification (kg SO_2-equiv)	5.96×10^{-3}	4.18×10^{-3}	7.74×10^{-3}	7.52×10^{-3}
Water depletion (m^3)	0.85	0.48	1.23	1.66

Low-TDS Brackish Water Treatment, Case 4

Inventory data, a water balance, LCIA results, and scenario analysis results for treatment of St. Peter brackish water by MSF are provided in this section.

Table 2-B-56 LCI inputs for low-TDS handling by MSF (Case 4) for the lifetime of the plant, MSF step.

Product flow		Equivalent value	Unit	Source
Infrastructure	Hot water tank	702	pcs	PE International (2016)
	Pump station	36	pcs	Wernet et al. (2016)
Brackish water	Pretreated St. Peter water	2.21×10^{11}	kg	Based on design parameters
Energy	Electricity for MSF	8.94×10^{8}	kWh	Mezher et al. (2011)
	Electricity for pumping	7.86×10^{7}	kWh	Estimated by Trimeric Corp.
	Thermal energy	1.61×10^{10}	kWh	Mezher et al.(2011)

Table 2-B-57 LCI inputs for low-TDS handling by MSF (Case 4) for the lifetime of the plant, deep well injection step.

Product flow		Equivalent value	Unit	Source
Infrastructure	Deep well	1	pcs	McCurdy (2011)
	Pump station	2	pcs	Wernet et al. (2016)
Energy	Electricity	3.77×10^{7}	kWh	Coday et al. (2015)
Brine	Concentrated St. Peter water	1.11×10^{10}	kg	Based on design parameters
Transportation	Pipeline	1.6	km	Based on design parameters

Table 2-B-58 Process water balance for low-TDS handling by MSF (Case 4) for the lifetime of the plant.

Water input	**Amount**	**Unit**
Pretreated St. Peter water	2.21×10^{11}	kg
Water output	**Amount**	**Unit**
Concentrated St. Peter water	1.11×10^{10}	kg
Desalinated water	2.10×10^{11}	kg
Difference	0	kg

Table 2-B-59 Environmental impact results for low-TDS handling by MSF (Case 4), with a functional unit of 1 m^3 of desalinated water.

Impact category	Total	Thermal energy	Pump Station	Hot water tank	Electricity	Deep well injection
Resources, fossil fuels (MJ surplus energy)	5.37×10^{1}	5.14×10^{1}	2.43×10^{-2}	2.27×10^{-3}	2.16×10^{0}	8.59×10^{-2}
Global warming (kg CO_2-equiv)	2.38×10^{1}	2.06×10^{1}	3.70×10^{-2}	2.52×10^{-3}	3.08×10^{0}	1.15×10^{-1}
Smog (kg O_3-equiv)	5.25×10^{-1}	4.35×10^{-1}	2.44×10^{-3}	1.82×10^{-4}	8.35×10^{-2}	4.24×10^{-3}
Ozone depletion (kg CFC 11-equiv)	5.23×10^{-9}	1.13×10^{-11}	2.58×10^{-9}	2.06×10^{-10}	1.21×10^{-9}	1.23×10^{-9}
Human toxicity (CTUh)	1.38×10^{-8}	1.96×10^{-9}	8.21×10^{-9}	1.86×10^{-9}	5.36×10^{-10}	1.28×10^{-9}
Eutrophication (kg N-equiv)	1.53×10^{-3}	9.24×10^{-4}	1.55×10^{-4}	1.32×10^{-5}	3.99×10^{-4}	3.61×10^{-5}
Ecotoxicity (CTUe)	1.41×10^{0}	6.74×10^{-1}	5.66×10^{-1}	4.41×10^{-2}	7.42×10^{-2}	5.59×10^{-2}
Acidification (kg SO_2-equiv)	2.34×10^{-2}	1.40×10^{-2}	1.82×10^{-4}	1.59×10^{-5}	8.78×10^{-3}	3.61×10^{-4}

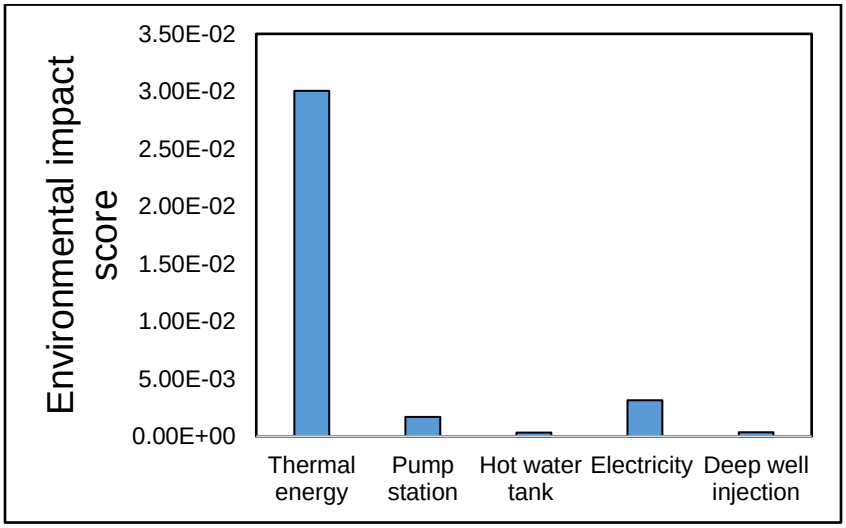

Figure 2-B-13 Weighted environmental impact scores for low-TDS handling by MSF (Case 4), with a functional unit of 1 m^3 of desalinated water.

Table 2-B-60 Water depletion for low-TDS handling by MSF (Case 4), with a functional unit of 1 m^3 of desalinated water.

Water depletion	Total	Thermal energy	Pump station	Hot water tank	MSF	Electricity	Deep well injection
GaBi result	1.16	0.13	0.07	0.03	−1.00	1.86	0.08
Adjusted result	−0.74	0.13	0.07	0.03	−1.00	0.02	0.01

Table 2-B-61 Scenario analysis for low-TDS handling by MSF (Case 4), functional unit 1 m^3 desalinated water.

Impact category	Scenario A Baseline	Scenario B Energy ↓ 50%	Scenario C Energy ↑ 50%	Scenario D 50% water recovery
Resources, fossil fuels (MJ surplus energy)	5.37×10^{1}	2.69×10^{1}	8.06×10^{1}	2.90×10^{1}
Global warming (kg CO_2-equiv)	2.38×10^{1}	1.20×10^{1}	3.57×10^{1}	1.36×10^{1}
Smog (kg O_3-equiv)	5.25×10^{-1}	2.66×10^{-1}	7.86×10^{-1}	3.17×10^{-1}
Ozone depletion (kg CFC 11-equiv)	5.23×10^{-9}	4.62×10^{-9}	5.85×10^{-9}	1.57×10^{-8}
Human toxicity (CTUh)	1.38×10^{-8}	1.26×10^{-8}	1.51×10^{-8}	2.41×10^{-8}
Eutrophication (kg N-equiv)	1.53×10^{-3}	8.65×10^{-4}	2.19×10^{-3}	1.22×10^{-3}
Ecotoxicity (CTUe)	1.41×10^{0}	1.04×10^{0}	1.79×10^{0}	1.56×10^{0}
Acidification (kg SO_2-equiv)	2.34×10^{-2}	1.20×10^{-2}	3.48×10^{-2}	1.58×10^{-2}
Water depletion (m^3)	1.16	0.17	2.15	1.38

Low-TDS Brackish Water Treatment, Case 5

Inventory data, a water balance, LCIA results, and scenario analysis results for treatment of St. Peter brackish water by MED are provided in this section.

Table 2-B-62 LCI inputs for low-TDS handling by MED (Case 5) for the lifetime of the plant, MED step.

Product flow		Equivalent value	Unit	Source
Infrastructure	Hot water tank	702	pcs	PE International (2016)
	Pump station	36	pcs	Wernet et al. (2016)
Brackish water	Pretreated St. Peter water	2.21×10^{11}	kg	Based on design parameters
Energy	Electricity for MED	2.10×10^{8}	kWh	Mezher et al.(2011)
	Electricity for pumping	7.86×10^{7}	kWh	Estimated by Trimeric Corp.
	Thermal energy	1.08×10^{10}	kWh	Mezher et al. (2011)

Table 2-B-63 LCI inputs for low-TDS handling by MED (Case 5) for the lifetime of the plant, deep well injection step.

Product flow		Equivalent value	Unit	Source
Infrastructure	Deep well	1	pcs	McCurdy (2011)
	Pump station	2	pcs	Wernet et al. (2016)
Energy	Electricity	3.77×10^{7}	kWh	Coday et al. (2015)
Brine	Concentrated St. Peter water	1.11×10^{10}	kg	Based on design parameters

Transportation	Pipeline	1.6	km	Based on design parameters

Table 2-B-64 Process water balance for low-TDS handling by MED (Case 5) for the lifetime of the plant.

Water input	**Amount**	**Unit**
Pretreated St. Peter water	2.21×10^{11}	kg
Water output	**Amount**	**Unit**
Concentrated St. Peter water	1.11×10^{10}	kg
Desalinated water	2.10×10^{11}	kg
Difference	0	kg

Table 2-B-65 Environmental impact results for low-TDS handling by MED (Case 5), with a functional unit of 1 m^3 of desalinated water.

Impact category	**Total**	**Thermal energy**	**Electricity**	**Pump station**	**Hot water tank**	**Deep well injection**
Resources, fossil fuels (MJ surplus energy)	3.52×10^{1}	3.45×10^{1}	6.39×10^{-1}	2.43×10^{-2}	2.27×10^{-3}	8.59×10^{-2}
Global warming (kg CO_2-equiv)	1.48×10^{1}	1.38×10^{1}	8.77×10^{-1}	3.70×10^{-2}	2.52×10^{-3}	1.15×10^{-1}
Smog (kg O_3-equiv)	3.22×10^{-1}	2.92×10^{-1}	2.39×10^{-2}	2.44×10^{-3}	1.82×10^{-4}	4.24×10^{-3}
Ozone depletion (kg CFC 11-equiv)	4.36×10^{-9}	7.60×10^{-12}	3.35×10^{-10}	2.58×10^{-9}	2.06×10^{-10}	1.23×10^{-9}
Human toxicity (CTUh)	1.28×10^{-8}	1.31×10^{-9}	1.52×10^{-10}	8.21×10^{-9}	1.86×10^{-9}	1.28×10^{-9}
Eutrophication (kg N-equiv)	9.35×10^{-4}	6.20×10^{-4}	1.11×10^{-4}	1.55×10^{-4}	1.32×10^{-5}	3.61×10^{-5}
Ecotoxicity (CTUe)	1.14×10^{0}	4.52×10^{-1}	2.11×10^{-2}	5.66×10^{-1}	4.41×10^{-2}	5.59×10^{-2}
Acidification (kg SO_2-equiv)	1.27×10^{-2}	9.42×10^{-3}	2.75×10^{-3}	1.82×10^{-4}	1.59×10^{-5}	3.61×10^{-4}

Table 2-B-66 Water depletion for low-TDS handling by MED (Case 5), with a functional unit of 1 m^3 of desalinated water.

Water depletion	**Total**	**Thermal energy**	**Electricity**	**Pump station**	**Hot water tank**	**MED**	**Deep well injection**
GaBi result	−0.06	0.09	0.67	0.07	0.03	−1.00	0.08
Adjusted result	−0.80	0.09	0.01	0.07	0.03	−1.00	0.01

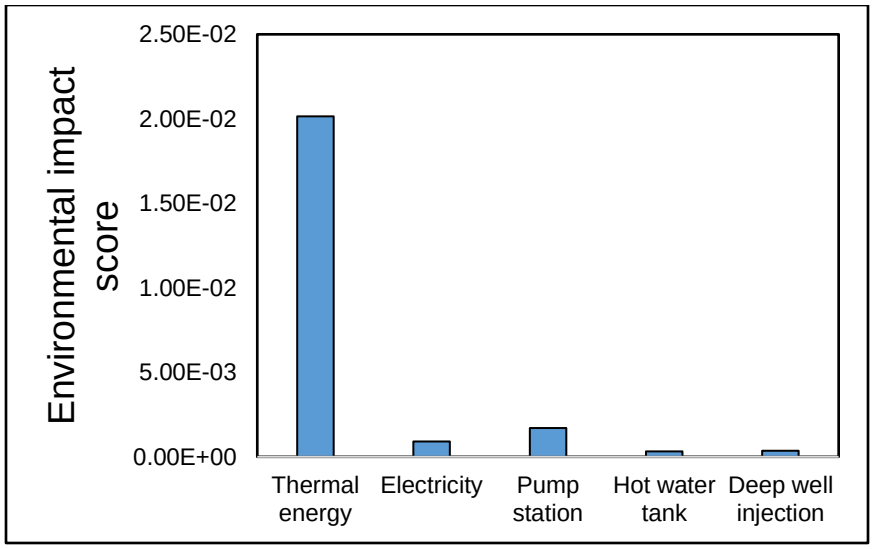

Figure 2-B-14 Weighted environmental impact scores for low-TDS handling by MED (Case 5), with a functional unit of 1 m^3 of desalinated water.

Table 2-B-67 Scenario analysis for low-TDS handling by MED (Case 5), with a functional unit of 1 m^3 of desalinated water.

Impact category	Scenario A Baseline	Scenario B Energy ↓ 50%	Scenario C Energy ↑ 50%	Scenario D 50% water recovery
Resources, fossil fuels (MJ surplus energy)	3.52×10^{1}	1.77×10^{1}	5.28×10^{1}	1.94×10^{1}
Global warming (kg CO_2-equiv)	1.48×10^{1}	7.50×10^{0}	2.22×10^{1}	8.92×10^{0}
Smog (kg O_3-equiv)	3.22×10^{-1}	1.65×10^{-1}	4.80×10^{-1}	2.11×10^{-1}
Ozone depletion (kg CFC 11-equiv)	4.36×10^{-9}	4.19×10^{-9}	4.53×10^{-9}	1.52×10^{-8}
Human toxicity (CTUh)	1.28×10^{-8}	1.21×10^{-8}	1.36×10^{-8}	2.36×10^{-8}
Eutrophication (kg N-equiv)	9.35×10^{-4}	5.69×10^{-4}	1.30×10^{-3}	9.12×10^{-4}
Ecotoxicity (CTUe)	1.14×10^{0}	9.02×10^{-1}	1.38×10^{0}	1.42×10^{0}
Acidification (kg SO_2-equiv)	1.27×10^{-2}	6.64×10^{-3}	1.88×10^{-2}	1.02×10^{-2}
Water depletion (m^3)	–0.06	–0.44	0.31	0.74

Low-TDS Brackish Water Treatment, Case 6

Inventory data, a water balance, LCIA results, and scenario analysis results for treatment of St. Peter brackish water by VC are provided in this section.

Table 2-B-68 LCI inputs for low-TDS handling by VC (Case 6) for the lifetime of the plant, VC step.

Product flow		Equivalent value	Unit	Source
Infrastructure	Hot water tank	878	pcs	PE International (2016)
	Pump station	36	pcs	Wernet et al. (2016)
Brackish water	Pretreated St. Peter water	2.21×10^{11}	kg	Based on design parameters
Energy	Electricity for VC	2.19×10^{9}	kWh	Shaffer et al. (2013)
	Electricity for pumping	7.86×10^{7}	kWh	Estimated by Trimeric Corp.

Table 2-B-69 LCI inputs for low-TDS handling by VC (Case 6) for the lifetime of the plant, deep well injection step.

Product flow		Equivalent value	Unit	Source
Infrastructure	Deep well	1	pcs	McCurdy (2011)
	Pump station	2	pcs	Wernet et al. (2016)
Energy	Electricity	3.77×10^{7}	kWh	Coday et al. (2015)
Brine	Concentrated St. Peter water	1.11×10^{10}	kg	Based on design parameters
Transportation	Pipeline	1.6	km	Based on design parameters

Table 2-B-70 Process water balance for low-TDS handling by VC (Case 6) for the lifetime of the plant.

Water input	**Amount**	**Unit**
Pretreated St. Peter water	2.21×10^{11}	kg
Water output	**Amount**	**Unit**
Concentrated St. Peter water	1.11×10^{10}	kg
Desalinated water	2.10×10^{11}	kg
Difference	0	kg

Table B-71 Environmental impact results for low-TDS handling by VC (Case 6), with a functional unit of 1 m^3 of desalinated water.

Impact category	Total	Pump station	Hot water tank production	Electricity	Deep well injection
Resources, fossil fuels (MJ surplus energy)	5.16×10^{0}	2.43×10^{-2}	2.84×10^{-3}	5.04×10^{0}	8.59×10^{-2}
Global warming (kg CO_2-equiv)	7.35×10^{0}	3.70×10^{-2}	3.15×10^{-3}	7.19×10^{0}	1.15×10^{-1}
Smog (kg O_3-equiv)	2.02×10^{-1}	2.44×10^{-3}	2.28×10^{-4}	1.95×10^{-1}	4.24×10^{-3}
Ozone depletion (kg CFC 11-equiv)	6.89×10^{-9}	2.58×10^{-9}	2.58×10^{-10}	2.82×10^{-9}	1.23×10^{-9}
Human toxicity (CTUh)	1.31×10^{-8}	8.21×10^{-9}	2.33×10^{-9}	1.25×10^{-9}	1.28×10^{-9}
Eutrophication (kg N-equiv)	1.14×10^{-3}	1.55×10^{-4}	1.65×10^{-5}	9.32×10^{-4}	3.61×10^{-5}
Ecotoxicity (CTUe)	8.50×10^{-1}	5.66×10^{-1}	5.51×10^{-2}	1.73×10^{-1}	5.59×10^{-2}
Acidification (kg SO_2-equiv)	2.11×10^{-2}	1.82×10^{-4}	1.99×10^{-5}	2.05×10^{-2}	3.61×10^{-4}

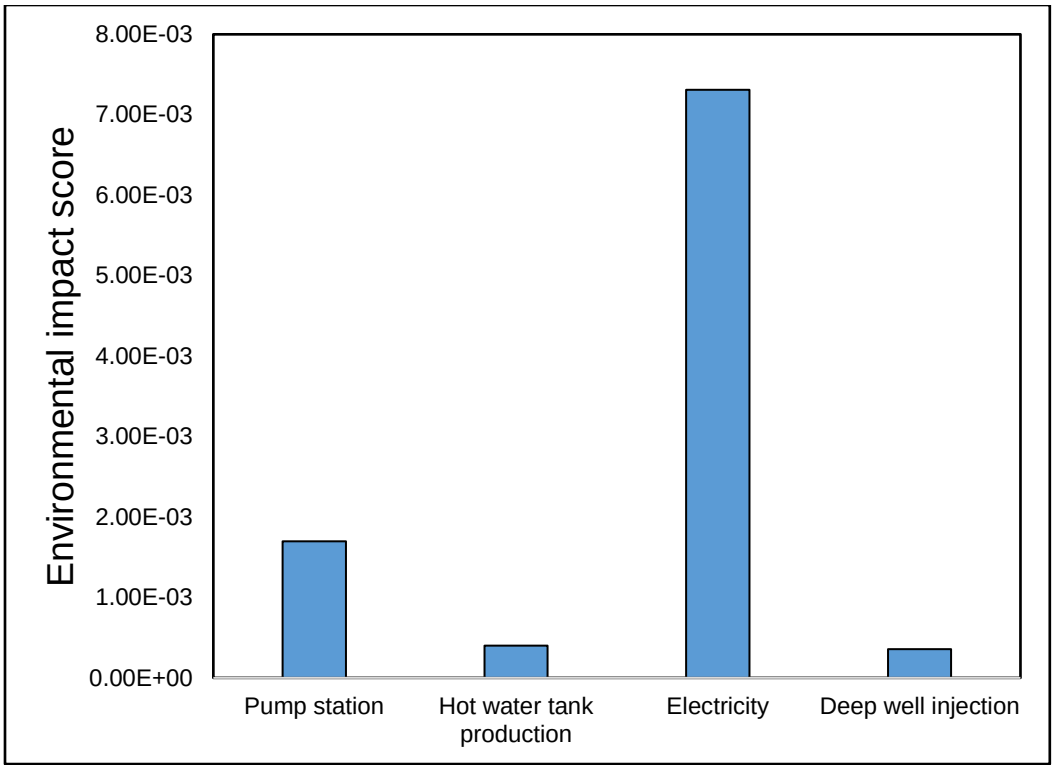

Figure 2-B-15 Weighted environmental impact scores for low-TDS handling by VC (Case 6), with a functional unit of 1 m^3 of desalinated water.

Table 2-B-72 Water depletion for low-TDS handling by VC (Case 6), with a functional unit of 1 m^3 of desalinated water.

Water depletion	Total	VC	Pump station	Hot water tank	Electricity	Deep well injection
GaBi result	3.52	−1.00	0.07	0.03	4.33	0.08
Adjusted result	−0.84	−1.00	0.07	0.03	0.04	0.01

Table 2-B-73 Scenario analysis for low-TDS handling by VC (Case 6), with a functional unit of 1 m^3 of desalinated water (continued on next page).

Impact category	Scenario A Baseline	Scenario B Energy↓ 50%	Scenario C Energy ↑ 50%	Scenario D 50% water recovery
Resources, fossil fuels (MJ surplus energy)	5.16×10^{0}	2.62×10^{0}	7.67×10^{0}	3.53×10^{0}
Global warming (kg CO_2-equiv)	7.35×10^{0}	3.74×10^{0}	1.09×10^{1}	4.96×10^{0}
Smog (kg O_3-equiv)	2.02×10^{-1}	1.04×10^{-1}	2.99×10^{-1}	1.47×10^{-1}
Ozone depletion (kg CFC 11-equiv)	6.89×10^{-9}	5.47×10^{-9}	8.29×10^{-9}	1.66×10^{-8}
Human toxicity (CTUh)	1.31×10^{-8}	1.24×10^{-8}	1.37×10^{-8}	2.39×10^{-8}

Impact category	Scenario A Baseline	Scenario B Energy↓ 50%	Scenario C Energy ↑ 50%	Scenario D 50% water recovery
Eutrophication (kg N-equiv)	1.14×10^{-3}	6.72×10^{-4}	1.60×10^{-3}	1.02×10^{-3}
Ecotoxicity (CTUe)	8.50×10^{-1}	7.63×10^{-1}	9.37×10^{-1}	1.27×10^{0}
Acidification (kg SO_2-equiv)	2.11×10^{-2}	1.08×10^{-2}	3.13×10^{-2}	1.45×10^{-2}
Water depletion (m^3)	3.52	1.34	5.67	2.62

Comparison of Results with the Literature

Table 2-B-74 Comparison of LCA results with the literature for low-TDS desalination by RO (continued on next page).

	Reference							
LCA results	**ISGS, 2016 (this work)**	**Raluy et al., 2006**	**Raluy et al., 2006**	**Muñoz and Fernández-Alba, 2008**	**Muñoz and Fernández-Alba, 2008**	**Zhou et al., 2011**	**Zhou et al., 2011**	**Biswas, 2009**
Feed water	3,933 ppm TDS	seawater	seawater	15,300 ppm TDS	seawater	15,000 ppm TDS	15,000 ppm TDS	seawater
Energy consumption	2 kWh/m^3	4 kWh/m^3	2 kWh/m^3	2 kWh/m^3	not reported	2 kWh/m^3	2 kWh/m^3	not reported
Recovery (%)	95	not reported	not reported	~65	~65	not reported	not reported	not reported
Software/method	GaBi 6.110, TRACI 2.1	SimaPro 6	SimaPro 6	SimaPro 7	SimaPro 7	SimaPro 7, CML2	SimaPro 7, TRACI	SimaPro 7, Australian Greenhouse Gas
Fossil fuels (MJ)	1.14×10^{0}	—	—	2.30×10^{1}	4.20×10^{1}	—	—	—
Global warming (kg CO_2-equiv)	1.52×10^{0}	1.78×10^{0}	9.20×10^{-1}	1.10×10^{0}	1.90×10^{0}	1.58×10^{0}	1.58×10^{0}	3.89×10^{0}
Ozone depletion (kg CFC 11-equiv)	6.55×10^{-9}	—	—	—	—	4.30×10^{-8}	4.34×10^{-8}	—
Eutrophication (kg N-equiv)	3.29×10^{-4}	3.87×10^{-3}	2.03×10^{-3}	—	—	—	7.66×10^{-4}	—
Acidification (kg SO_2-equiv)	4.80×10^{-3}	1.07×10^{-2}	6.10×10^{-3}	1.50×10^{-2}	2.70×10^{-2}	1.16×10^{-2}	—	—
LCA results	**Tarnacki et al., 2012**	**Tarnacki et al., 2012**	**Tarnacki et al., 2012**	**Shahabi et al., 2014**	**Shahabi et al., 2014**	**Shahabi et al., 2014**	**Hancock et al., 2011**	
Feed water	seawater	2% TDS	>5% TDS industrial wastewater	seawater	seawater	seawater	seawater	
Energy consumption	3 kWh/m^3	1 kWhm^3	5 kWh/m^3	3.5 kWh/m^3	wind energy	92% wind, 8% photo-voltaic solar	4.0 kWh	
Recovery (%)	42.5	not reported	not reported	not reported	not reported	not reported	50%	

LCA results	Reference							
	ISGS, 2016 (this work)	Raluy et al., 2006	Raluy et al., 2006	Muñoz and Fernández-Alba, 2008	Muñoz and Fernández-Alba, 2008	Zhou et al., 2011	Zhou et al., 2011	Biswas, 2009
Software/method	CML 2001	CML 2001	CML 2001	SimaPro 7.3.3, IPCC 2007	SimaPro 7.3.3, IPCC 2007	SimaPro 7.3.3, IPCC 2007	SimaPro, CML 2011	
Fossil fuels (MJ)	—	—	—	—			—	
Global warming (kg CO_2-equiv)	1.81×10^{0}	6.24×10^{-1}	2.99×10^{0}	4.61×10^{0}	4.46×10^{-1}	4.91×10^{-1}	1.40×10^{0}	
Ozone depletion (kg CFC 11-equiv)	—	—	—	—			—	
Eutrophication (kg N-equiv)	—	—	—	—			—	
Acidification (kg SO_2-equiv)	2.61×10^{-2}	9.41×10^{-3}	4.27×10^{-2}	—			—	

Table 2-B-75 Comparison of LCA results to literature for low-TDS desalination by MSF and MED.

LCA results	Reference				
	ISGS, 2016 (this work)	Raluy et al., 2006	Raluy et al., 2006	ISGS, 2016 (this work)	Raluy et al., 2006
Desalination technology	MSF	MSF driven by fossil fuels	MSF driven by waste heat	MED	MED driven by fossil fuels
Feed water	3,933 ppm TDS	seawater	seawater	3,933 ppm TDS	seawater
Energy consumption	76.4 kWh thermal + 4.25 kWh electric	333 MJ/m^3 thermal + 4 kWh/m^3 mechanical	51.4 kWh thermal + 1 kWh electric	263 MJ/m^3 thermal + 2 kWh/m^3 mechanical	263 MJ/m3 thermal + 2 kWh/m^3 mechanical
Software/method	Gabi 6.110, TRACI 2.1	SimaPro 6	SimaPro 6	Gabi 6.110, TRACI 2.1	SimaPro 6
Global warming (kg CO_2-equiv)	2.38×10^{1}	2.34×10^{1}	1.96×10^{0}	1.48×10^{1}	1.81×10^{1}
Eutrophication (kg N-equiv)	1.53×10^{-3}	2.83×10^{-2}	4.29×10^{-3}	9.35×10^{-4}	2.14×10^{-1}
Acidification (kg SO_2-equiv)	2.34×10^{-2}	2.79×10^{-2}	1.48×10^{-2}	1.27×10^{-2}	2.65×10^{-2}

Appendix 2-B References

Biswas, W.K., 2009, Life cycle assessment of seawater desalinization in Western Australia: International Journal of Environmental, Chemical, Ecological, Geological and Geophysical Engineering, v. 3, p. 231–237.

Coday, B.D., L. Miller-Robbie, E.G. Beaudry, J. Munakata-Marr, T.Y. Cath, 2015, Life cycle and economic assessments of engineered osmosis and osmotic dilution for desalination of Haynesville shale pit water: Desalination v. 369, p. 188–200.

Gumerman, R., R. Culp, and S. Hansen, 1979, Estimating water treatment costs, volume 2: Cost curves applicable to 1 to 200 mgd treatment plants: Cincinati, Ohio, U.S. Environmental Protection Agency, Municipal Environmental Research Laboratory, EPA-600/2-79-162b.

Hancock, N.T., N.D. Black, and T.Y. Cath, 2011, A comparative life cycle assessment of hybrid osmotic dilution desalination and established seawater desalination and wastewater

reclamation processes: Water Research, v. 46, p. 1145–1154.
ICIS, 2012, US PVC contract prices rise 3 cents/lb for September: London, ICIS, October 13, http://www.icis.com/resources/news/2012/10/13/9603736/us-pvc-contract-prices-rise-3-cents-lb-for-september/ (accessed March 15, 2016).
Maneechan, M., P. Punyapalakul, and A. Wongrueng, 2014, Utilization of ammonium bicarbonate as draw solution in forward osmosis process: A case study of cooling water reuse: International Conference on Agricultural, Environmental and Biological Sciences (AEBS-2014), Phuket, Thailand, p. 55–59, http://dx.doi.org/10.15242/IICBE.C414047.
McCurdy, R., 2011, Underground injection wells for produced water disposal: Oklahoma City, Oklahoma, Chesapeake Energy Corporation, http://www.epa.gov/sites/production/files/documents/21_McCurdy_-_UIC_Disposal_508.pdf (accessed March 15, 2016).
Mezher, T., H. Fath, Z. Abbas, and A. Khaled, 2011, Techno-economic assessment and environmental impacts of desalination technologies: Desalination, v. 266, p. 263–273.
Muñoz, I., and. A.R. Fernández-Alba, 2008, Reducing the environmental impacts of reverse osmosis desalination by using brackish groundwater resources: Water Research, v. 42, p. 801–811.
PE International, 2016, GaBi software, system and databases for life cycle engineering: Leinfelden-Echterdingen, Germany, Thinkstep, GaBi Professional Database, http://www.gabi-software.com/ (accessed May 19, 2016).
PetroChemWire, 2013. PVC & Pipe Report, https://www.petrochemwire.com/Sample_Issues/Images/PVC & Pipe Report.pdf (accessed March 10, 2016).
Qin, M., and Z. He, 2014, Self-supplied ammonium bicarbonate draw solute for achieving wastewater treatment and recovery in a microbial electrolysis cell- forward osmosis-coupled system: Environmental Science & Technology Letters, v. 1, p. 437–441.
Quandl, 2015. Industrial Metals Prices and Charts, https://www.quandl.com/collections/markets/industrial-metals (accessed March 15, 2016).
Raluy, G., L. Serra, and J. Uche, 2006, Life cycle assessment of MSF, MED and RO desalination technologies: Energy, v. 31, p. 2361–2372.
Shaffer, D.L., L.H. Arias Chavez, M. Ben-Sasson, S. Romero-Vargas Castrillón, N.Y. Yip, and M. Elimelech, 2013, Desalination and reuse of high-salinity shale gas produced water: Drivers, technologies, and future directions: Environmental Science and Technology, v. 47, p. 9569–9583
Shahabi, M.P., A. Mchugh, M. Anda, and G. Ho, 2014, Environmental life cycle assessment of seawater reverse osmosis desalination plant powered by renewable energy: Renewable Energy, v. 67, p. 53–58.
Shammas, N.K., 2005, Coagulation and flocculation, *in* K.L. Wang, Y. Huang, and N. Shammas, eds., Physicochemical treatment processhemical treatment processes: Toytoya, New Jersey, Humana Press, p. 103–138.
Statista, 2015, Statistics and facts about the U.S. cement market: New York, Statistica, https://www.statista.com/topics/1195/cement/ (accessed March 9, 2016).
Tarnacki, K., M. Meneses, T. Melin, J. van Medevoort, and A. Jansen, 2012, Environmental assessment of desalination processes: Reverse osmosis and Memstill®: Desalination, v. 296, p. 69–80.
Wang, K., L., Huang, Y.-T., K. Shammas, N., 2005. Coagulation and Flocculation, in:

Physicochemical Treatment Processshemical Treatment Processes. Humana Press.
Washington State Department of Health, 2002, Sand/media specifications: Tumwater, Washington State Department of Health, http://www.doh.wa.gov/portals/1/Documents/Pubs/337-104.pdf (accessed March 9, 2016).
Wernet, G., C. Bauer, B. Steubing, J. Reinhard, and B. Weidema, 2016, The ecoinvent database version 3 (part I): Overview and methodology: The International Journal of Life Cycle Assessment, http://link.springer.com/10.1007/s11367-016-1087-8 (accessed May 19, 2016).
Zhou, J., V.W.-C. Chang, and A.G. Fane, 2011. Environmental life cycle assessment of brackish water reverse osmosis desalination for different electricity production models: Energy &Environmental Sci. v. 4, p. 2267–2278.

Subtask 2-5 Laboratory Testing of Low-TDS Brackish Water Treatment by Membrane Technology

This subtask is aimed at collecting laboratory data for treating low-TDS St. Peter brackish water by different pretreatments (coagulation, lime softening, sand filtration, and ion exchange) and desalination methods (NF, RO, and FO). The laboratory data generated from these experiments can be useful for designing pilot- and large-scale water treatment plants.

Sampling of St. Peter Brackish Water

Following the protocols of the ISGS Geochemistry Section, one barrel of water was drawn from a depth of 3,455 ft (1,053 m) in the St. Peter Formation. The sample was collected from the ADM facility in Decatur, Illinois. The collected sample had a pH, dissolved oxygen content, turbidity, and density of 7.7, 0.7 mg/L, 9.5 NTU, and 1.0014 g/cm^3, respectively.

Characterization of St. Peter Brackish Water

St. Peter water was characterized by the same methods as the Mt. Simon brine in Subtask 2-1. Actlabs Corporation conducted cation composition and radioactivity tests. Data obtained from the ISGS Geochemistry Section included concentrations of various cations, anions, and alkalinity (Table 2-5-1). Water chemistry data suggest that Na^+ was the dominant cation, with a concentration of 1,150 mg/L, followed by Ca^{2+} (140 mg/L), and that chloride was the most abundant anion (1,875 mg/L). The data in Table 2-5-1 indicate that NaCl was the most dominant salt in the St. Peter water sample, whereas Ca ions were the dominant divalent cations that might contribute to scale formation. St. Peter water also had a relatively high level of alkalinity (i.e., 234 mg/L). Other species with concentrations above 1 mg/L were K^+ (46 mg/L), Mg^{2+} (27 mg/L), Sr^{2+} (3 mg/L), SO_4^{2-} (222 mg/L), F^- (3 mg/L), Br^- (8 mg/L), and Si (12 mg/L). Concentrations of some other elements (Ba, Fe, Li, Mn, and Zn) were at the 0.1–1 mg/L level. According to the measured water quality parameters, St. Peter brackish water could be a potential source of drinking water after appropriate treatments.

The TDS and TSS of the samples were measured at the ISGS Applied Research Laboratory by using standard method 254 ^{0}C (Clesceri et al., 1998). The St. Peter water had a TSS value of 18.5 ± 3.5 mg/L and a TDS value of 3,933 ± 258 mg/L.

Gross alpha and gross beta analyses along with equivalent uranium (eU) using a gamma-ray spectrometer were completed on untreated (as-received) samples (Table 2-5-2). The measured radioactivity level of the St. Peter brackish water is below the USEPA drinking water limits presented in Table 2-1-8 (Subtask 2-1).

Pretreatment and Desalination of St. Peter Brackish Water

The methods tested for treatment of St. Peter water are shown schematically in Figure 2-5-1. Many of the same pretreatment experiments conducted for the Mt. Simon brine (Subtask 2-1) were also conducted for the St. Peter water. These included jar test experiments to characterize the effects of different alum and lime dosage rates for coagulation/flocculation and sedimentation, experiments to simulate sand filtration, and ion exchange and NF experiments to evaluate these methods for water softening. Nanofiltration, RO, and FO were then considered for desalination processes.

Table 2-5-1 Water chemistry of the St. Peter brackish water sample (continued on next page).

Constituent	Laboratory	Method	Concentration (mg/L)
Ag	Actlabs	ICP-MS	<0.004
Alkalinity ($CaCO_3$-equiv)	ISGS Geochemistry	Titration	233.75
Al	Actlabs	ICP-MS	<0.04
As	Actlabs	ICP-MS	<0.0006
Ba	Actlabs	ICP-MS	0.499
Be	Actlabs	ICP-MS	<0.002
Bi	Actlabs	ICP-MS	<0.006
Br	ISGS Geochemistry	IC	8.22
Ca	Actlabs	ICP-MS	144
Cd	Actlabs	ICP-MS	<0.0002
Ce	Actlabs	ICP-MS	<0.00002
Cl	ISGS Geochemistry	IC	1,874.75
Co	Actlabs	ICP-MS	<0.0001
Cr	Actlabs	ICP-MS	<0.01
Cs	Actlabs	ICP-MS	0.000775
Cu	Actlabs	ICP-MS	0.0105
Dy	Actlabs	ICP-MS	<0.00002
Er	Actlabs	ICP-MS	<0.00002
Eu	Actlabs	ICP-MS	<0.00002
F	ISGS Geochemistry	IC	3.2925
Fe	Actlabs	ICP-MS	<0.2
Ga	Actlabs	ICP-MS	<0.0002
Gd	Actlabs	ICP-MS	<0.00002
Ge	Actlabs	ICP-MS	0.00098
Hf	Actlabs	ICP-MS	<0.00002
Hg	Actlabs	ICP-MS	0.0245
Ho	Actlabs	ICP-MS	<0.00002
In	Actlabs	ICP-MS	<0.00002
K	Actlabs	ICP-MS	46
La	Actlabs	ICP-MS	<0.00002
Li	Actlabs	ICP-MS	0.945
Lu	Actlabs	ICP-MS	<0.00002

Constituent	Laboratory	Method	Concentration (mg/L)
Mg	Actlabs	ICP-MS	27.3
Mn	Actlabs	ICP-MS	0.124
Mo	Actlabs	ICP-MS	<0.002
Na	Actlabs	ICP-MS	1,150
Nb	Actlabs	ICP-MS	<0.0001
Nd	Actlabs	ICP-MS	0.000123
Ni	Actlabs	ICP-MS	<0.006
NO_3	ISGS Geochemistry	IC	<0.155
Pb	Actlabs	ICP-MS	<0.0002
Pr	Actlabs	ICP-MS	0.000027
Rb	Actlabs	ICP-MS	0.0549
Sb	Actlabs	ICP-MS	<0.0002
Sc	Actlabs	ICP-MS	<0.02
Se	Actlabs	ICP-MS	<0.004
Si	Actlabs	ICP-MS	12.3
Sm	Actlabs	ICP-MS	<0.00002
Sn	Actlabs	ICP-MS	<0.002
SO_4	ISGS Geochemistry	IC	222.25
Sr	Actlabs	ICP-MS	3.39
Ta	Actlabs	ICP-MS	<0.00002
Tb	Actlabs	ICP-MS	<0.00002
Te	Actlabs	ICP-MS	<0.002
Th	Actlabs	ICP-MS	<0.00002
Ti	Actlabs	ICP-MS	<0.002
Tl	Actlabs	ICP-MS	<0.00002
Tm	Actlabs	ICP-MS	<0.00002
U	Actlabs	ICP-MS	0.000304
V	Actlabs	ICP-MS	<0.002
W	Actlabs	ICP-MS	0.0132
Y	Actlabs	ICP-MS	<0.00006
Yb	Actlabs	ICP-MS	<0.00002
Zn	Actlabs	ICP-MS	0.692
Zr	Actlabs	ICP-MS	<0.0002

[1]Inductively coupled plasma–mass spectrometry.
[2]Ion chromatography.

Table 2-5-2 Presence of radionuclides in St. Peter brackish water.

Analyte symbol	St. Peter water (pCi/L)
Gross alpha	5.95
Gross beta	16.76
K-40	<27.03
U-238	<2.703
Th-232	6.76

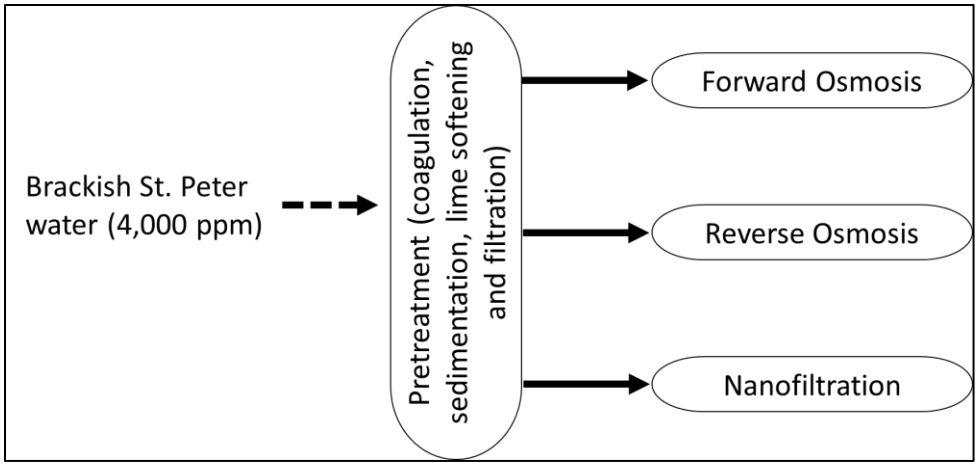

Figure 2-5-1 Treatments performed on St. Peter brackish water.

Alum Coagulation and Lime Softening

The same experimental procedures as described for the Mt. Simon jar test experiments in Subtask 2-1 were applied to St. Peter brackish water. The first series of experiments was conducted with an alum dose of 0–100 mg/L but without the addition of lime. In the second series of experiments, the same alum dose was applied with a constant lime dose of 285 mg/L. The third set of experiments was conducted using a constant alum dose of 100 mg/L and a varied lime dose of 71–500 mg/L (Tables 2-5-4 to 2-5-6).

Table 2-5-3 Jar test results for experiment 1 (varied alum dose, no lime) on St. Peter water.

	$Al_2(SO_4)_3$ dose (mg/L)					
Turbidity (NTU)	**0**	**20**	**40**	**60**	**80**	**100**
Initial	9.45	9.45	9.45	9.45	9.45	9.45
After 3 min	4.02	6.41	7.92	8.25	9.27	8.2
After 15 min	2.95	6.26	4.49	3.9	4.76	2.28
After 30 min	1.39	2.63	3.54	3.1	2.87	2.06
After 60 min	2.74	3.54	3.05	2.37	1.95	1.27

Table 2-5-4 Jar test results for experiment 2 (varied alum dose, 285 mg/L of lime) on St. Peter water.

	$Al_2(SO_4)_3$ dose (mg/L)					
Turbidity (NTU)	**0**	**20**	**40**	**60**	**80**	**100**
Initial	9.79	9.79	9.79	9.79	9.79	9.79
After 3 min	64.9	17.03	6.51	3.59	1.77	1.06
After 15 min	68.1	10.82	3.37	3.41	1.76	0.83
After 30 min	47	9.55	3.33	2.37	0.99	0.94
After 60 min	27.8	5.78	2.11	2.13	0.87	0.88

Table 2-5-5 Jar test results for experiment 3 (100 mg/L of alum, varied lime dose) on St. Peter water.

	Lime dose (mg/L)					
Turbidity (NTU)	**71.25**	**142.5**	**213.75**	**356.25**	**427.5**	**498.75**
Initial	9.56	9.56	9.56	9.56	9.56	9.56
After 3 min	15.87	3.6	1.5	5.29	6.93	3.45
After 15 min	4.98	1.83	1.45	3.86	5.9	3.73
After 30 min	4.92	1.46	0.89	5.89	7.51	3.79
After 60 min	2.09	0.67	0.59	2.53	7.9	2.93

Results indicated that a low turbidity level of 1.3 NTU was achievable by using an alum dose of 100 mg/L without any lime addition. Lime addition at a dose of 143 mg/L could further lower the turbidity to 0.6 NTU. Therefore, the optimal doses of alum and lime selected for pretreatment of St. Peter water were 100 mg/L and 143 mg/L, respectively.

The addition of 143 mg/L of lime to the St. Peter water sample in the presence of 100 mg/L of alum resulted in an increase in the pH value from 7.5 to 8.77. Under basic conditions, the precipitation of some metal species took place. Table 2-5-6 shows the impact of lime addition on the concentrations of major scale-forming species (Ca and Mg). The addition of 500 mg/L of lime resulted in 98% Mg removal; however, excessive lime addition contributed to an increase in Ca ions in the solution. The addition of 213 mg/L of lime resulted in a 47% reduction in the Ca concentration. It is possible to further lower the Ca concentration by adding Na_2CO_3, as discussed in the pretreatment of Mt. Simon brine.

Table 2-5-6 Impact of lime softening on scale-forming species in St. Peter brackish water.

Lime dose (mg/L)	Ca (mg/L)	Mg (mg/L)	Total hardness (mg/L of $CaCO_3$)
0.00	144	32.6	403
71	124	29.5	432
213	76.3	26.1	298
500	147	0.687	371

Sand Filtration Experiments

The sand filtration apparatus described in Subtask 2-1 was also used to filter pretreated St. Peter brackish water. The feed was first pretreated by coagulation/flocculation, lime softening, and settling, with doses of 100 mg/L of alum and 143 mg/L of lime. The sand filtration experiment was stopped after ~300 bed volumes were treated. Figure 2-5-2 shows the effectiveness of the sand filter in reducing the turbidity of the coagulated and settled St. Peter brackish water sample from ~1 to 0.001 NTU. The effluent turbidity showed the same trend as observed with Mt. Simon brine attributable to the ripening effect.

Ion Exchange

Ion exchange experiments were conducted using a method similar to the Mt. Simon brine test described in Subtask 2-1. The St. Peter feed was pretreated by coagulation/flocculation, lime softening, and settling, with doses of 100 mg/L of alum and 143 mg/L of lime, and then passed through a 0.45-μm filter before the ion exchange tests. The ion exchange resins (Table 2-5-7) showed better performance when used with the St. Peter water, compared with their performance with the Mt. Simon brine. The MAC-3 resin was more effective than the Marathon C resin for

softening St. Peter water. Total hardness was reduced by 58% when the MAC-3 was used at a dose of 0.8 g/L (Table 2-5-7). Using higher doses of resin in a batch system or a packed-bed continuous system with sufficient residence time would further reduce the Ca, Mg, and total hardness of the St. Peter water.

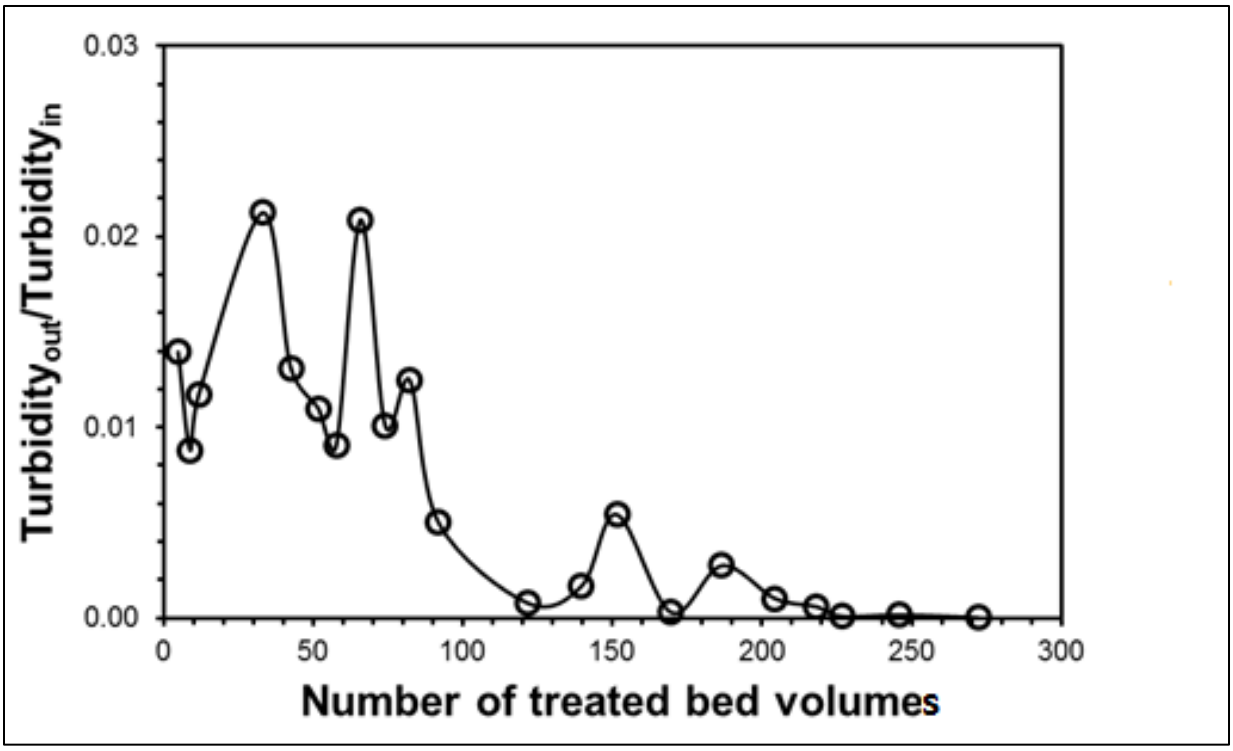

Figure 2-5-2 Effectiveness of sand filtration in removing residual turbidity from coagulated and settled St. Peter water.

Table 2-5-7 Results of preliminary ion exchange experiments for St. Peter brackish water.

Dissolved Ca, Mg, or hardness values	Resin type and dose (g/L)						
	Blank (no resin)	**Marathon C (1.07)**	**Marathon C (0.59)**	**Marathon C (0.14)**	**MAC-3 (0.8)**	**MAC-3 (0.4)**	**MAC-3 (0.1)**
Ca (mg/L)	92.8	104	<70	71.7	<70	<70	<70
Mg (mg/L)	32.6	21.3	22	29.5	16.2	21.6	26.1
Total hardness (mg/L of $CaCO_3$)	366	348	201	301	154	212	262

Nanofiltration

Nanofiltration (NF) was tested as a water-softening pretreatment for St. Peter brackish water and as a desalination treatment. As with the ion exchange experiments, the St. Peter feed was pretreated by coagulation/flocculation, lime softening, and settling, with doses of 100 mg/L of alum and 143 mg/L of lime, and then passed through a 0.45-μm filter before water softening by NF. The same NF methodology described for the Mt. Simon brine in Subtask 2-1 was applied to

the St. Peter feed. Operating pressures for each experiment were based on the manufacturers' guidelines and the typical practical pressure range used in the industry. For NF tests, the typical feed pressure range (50–200 psi) was used.

Nanofiltration is commonly used with low-TDS water for softening to remove scale-forming species and other species such as natural organic matter. However, according to the NF membrane characteristics, the process may also reduce the NaCl concentration and may be considered a primary treatment (desalination) process. Figures 2-5-3 and 2-5-4 show the performance of the NF90 and the NF270 membranes in removing TDS from the St. Peter water sample. Salt rejection was calculated based on the measured conductivity of feed and permeate samples. Sample conductivity correlated with the concentration of dissolved salts (mainly NaCl). The NF270 showed a very high flux of 126 L/m^2/h with a low salt rejection of 14% at an operating pressure of 200 psi. Thus, it might be suitable for pretreatment of the St. Peter brackish water to remove suspended particles and reduce total hardness, but not as a main-stage desalination process. For instance, the concentrations of Ca and Mg were reduced by 44% and 20%, respectively, in the permeate stream compared with the influent stream when NF270 was used as the NF membrane (Table 2-5-8); this translated into a 27% reduction in total hardness. On the other hand, the NF90 membrane showed a higher salt rejection of 79% and a water flux of approximately 6 L/m^2/h at an operating pressure of 200 psi, and might be considered for desalination. The water flux and salt rejection of the NF90 membrane could be further enhanced by increasing the operating pressure. The concentrations of Ca, Mg and total hardness in the pretreated St. Peter water sample were significantly reduced by 89%, 92%, and 90%, respectively, when the NF90 was used.

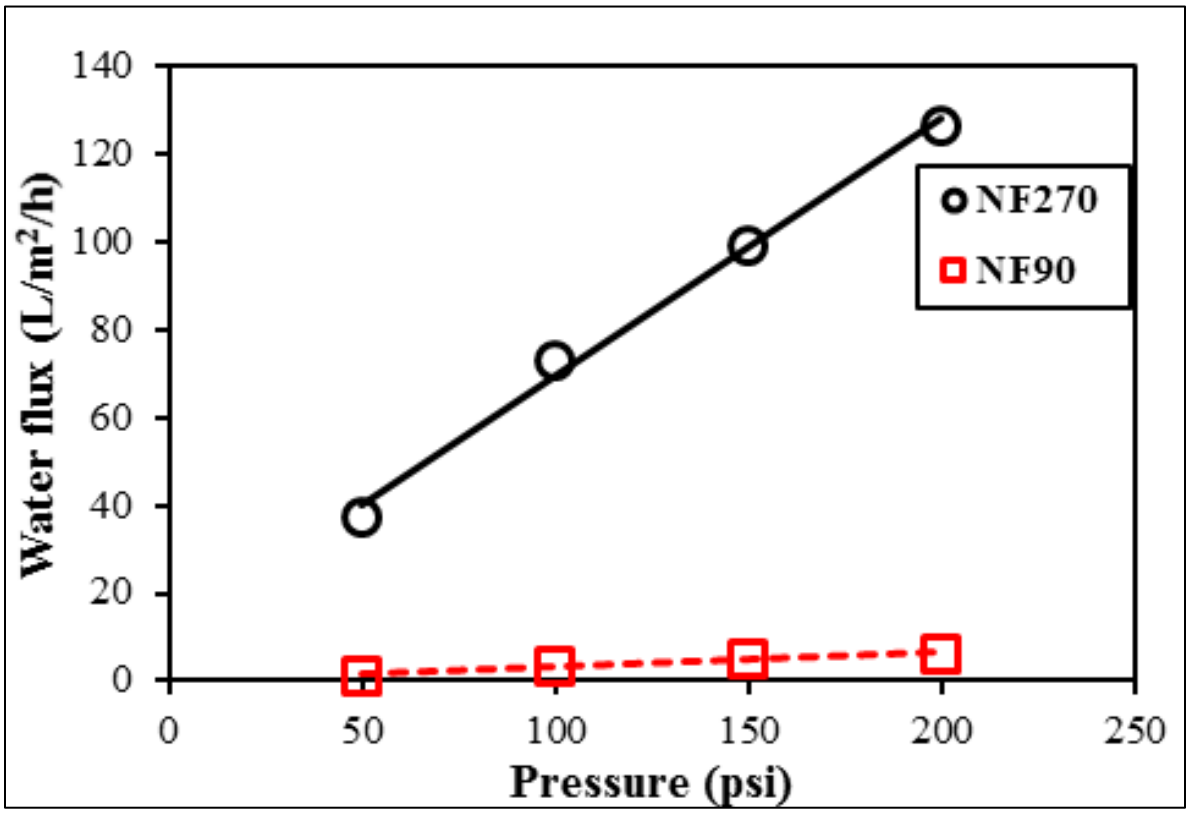

Figure 2-5-3 Water flux of the NF experiments with the St. Peter water feed.

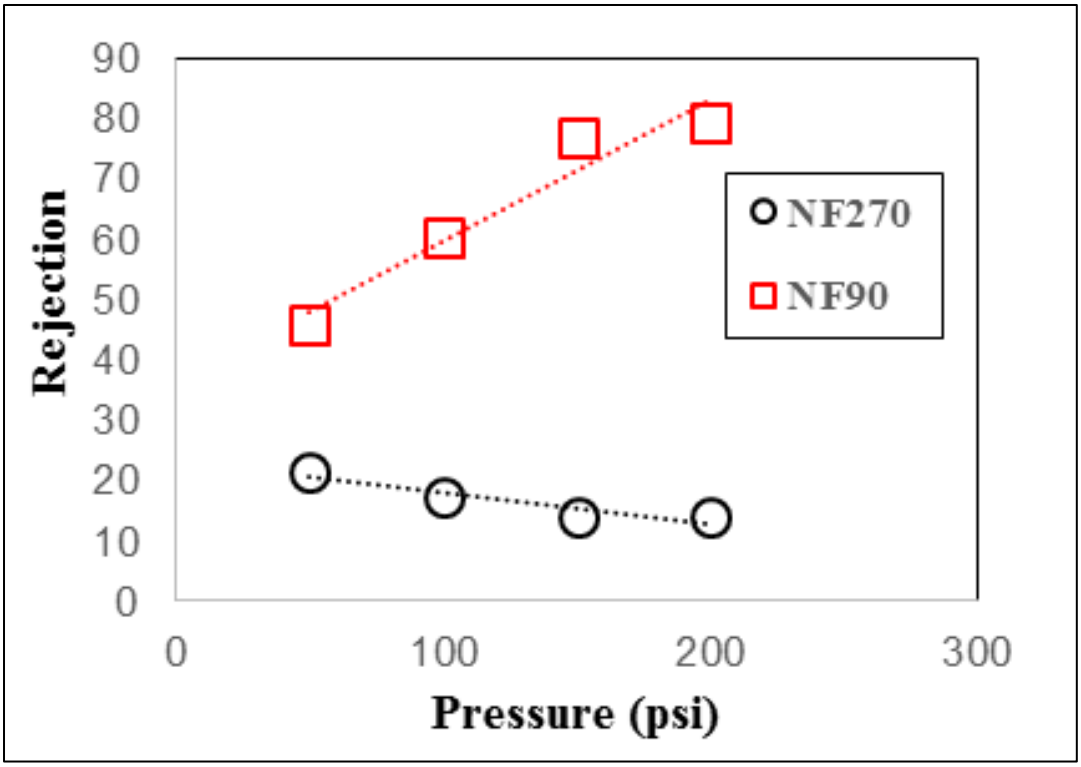

Figure 2-5-4 Salt rejection of the NF experiments with the St. Peter water feed.

Table 2-5-8 Impact of NF on St. Peter water hardness.

Membrane	Mg (mg/L)	Ca (mg/L)	Total hardness (mg/L of $CaCO_3$)	Removal (%)		
				Mg	Ca	Hardness
NF270–permeate	21.318	64.1	250.92	23	29	27
NF270–feed	27.54	90	342.72	N/A		
NF90–permeate	2.6316	<7	31.824	89	92	90
NF90–feed	24.276	82	309.06	N/A		

Reverse Osmosis

To obtain laboratory data that could potentially be used for designing pilot- and large-scale water treatment plants, a St. Peter brackish water sample was treated by using three commercially available RO membranes: Dow SW30HR, GE Osmonics AG, and GE Osmonics AK flat sheet membranes were tested in replicate manner, with three tests for each membrane. The same experimental system and a similar method as described in Subtask 2-1 for the NF experiments were applied to pretreated St. Peter water with the RO process. Samples that underwent RO treatment were first coagulated with doses of 100 mg/L of alum and 143 mg/L of lime and then filtered through 0.45-µm filters, resulting in turbidity values of less than 0.02 NTU. The RO tests were conducted at selected feed pressures ranging between 150 and 600 psi, as recommended by the manufacturer.

As shown in Figure 2-5-5, water flux across the membrane increased in direct proportion to increased feed water pressure. Increased feed water pressure also resulted in slightly increased salt rejection (Figure 2-5-6), although the relationship was less significant than for water flux.

Because RO membranes are imperfect barriers to dissolved salts in feed water, some salt always passes through the membrane. As feed water pressure was increased, this salt passage was increasingly overcome as water was pushed through the membrane at a faster rate than salt could be transported. The highest water flux across the membrane (79 L/m^2/h) was achieved by using the GE Osmonics AK membrane at an operating pressure of 600 psi with a salt rejection of 96%. At 600 psi, a water flux of 49 L/m^2/h and a 98% salt rejection were achieved with the GE Osmonics AG membrane, compared with 31 L/m^2/h and a salt rejection of 99% when the AW300HR membrane was used at the same operating pressure (Figure 2-5-5).

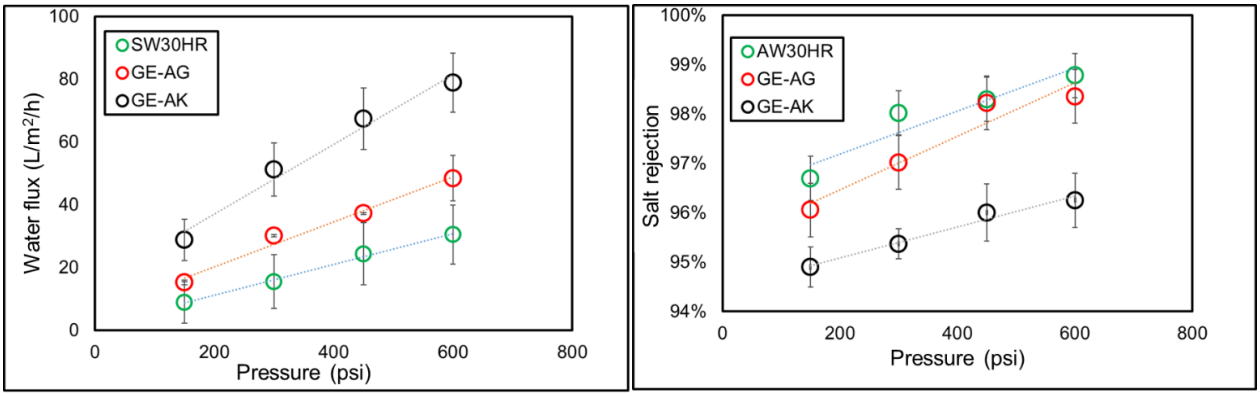

Figure 2-5-5 Water flux and salt rejection obtained for RO of St. Peter brackish water with three RO membranes: Dow SW300HR, GE Osmonics AG (GE-AG), and GE Osmonics AK (GE-AK).

Forward Osmosis

Forward osmosis was investigated as a potential desalination method for St. Peter brackish water. Two potential draw solutions were used: $MgSO_4$ and Mt. Simon brine. With the $MgSO_4$ draw solution, no laboratory-scale draw solution recovery was performed. With the Mt. Simon brine draw solution, desalination of ADM wastewater was tested, as well as desalination of St. Peter brackish water, and the DCMD method was used to recover fresh water from the diluted Mt. Simon brine. Figure 2-5-6 shows a schematic diagram of the bench-scale FO experimental system. Feed and draw solutions were circulated at a fixed cross-flow rate of 1.0 L/min. Each membrane was cut to an active area of 42 cm^2 and sealed in a Sterlitech Clear Cast Acrylic CF042-FO membrane cell. A commercially available Aquaporin flat sheet membrane (obtained from Sterlitech) was used for all the FO experiments. The membrane was oriented with the active layer facing the draw solution and the support layer facing the feed solution.

A 20 wt% $MgSO_4$ solution was used as the draw solution, and a feed solution of deionized water was used for the baseline experiments. The same procedure was then used for two feed solutions: (1) pretreated (coagulated and filtered) St. Peter brackish water, and (2) as-received ADM wastewater, collected from the discharge valve after the secondary treatment. The TDS and TSS concentrations of the ADM wastewater were 2,627 mg/L and 268 mg/L, respectively. The conductivity values of the draw and feed solutions were measured before and after the experiments with a conductivity meter. Conductivity values were used to calculate salt concentrations. Water flux (L/m^2/h) was obtained by measuring the weight change of the feed solutions with an electronic balance connected to a data logging system. The reported flux values were averaged over the entire experiment. Experiments were conducted over time spans of 1 to 20 h.

The water volumetric flux (J_w) in the system was calculated by the following equation:

$$J_w = \frac{\frac{\Delta M}{\rho}}{A \cdot \Delta t}, \qquad \text{(Equation 2-5-1)}$$

where ΔM refers to the change in mass of the feed solution over the time of the experiment, Δt (60 min), ρ is the density of the water (assumed as 1.0 g/cm^3), and A is the area of the membrane (0.0026 m^2). The salt reverse mass flux, J_s (g/m^2/h), was calculated by the following equation:

$$J_s = \frac{V_t \cdot C_t - V_0 \cdot C_0}{A \cdot \Delta t}, \qquad \text{(Equation 2-5-2)}$$

where V_0 and V_t are the initial and final feed volumes and C_0 and C_t are the initial and final salt concentrations in the feed solution.

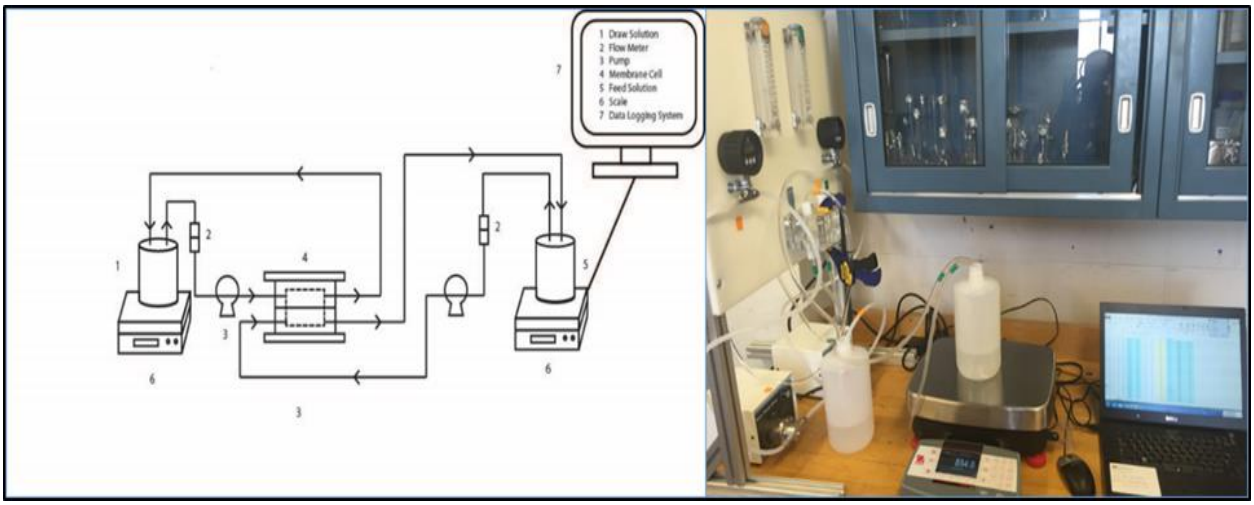

Figure 2-5-6 Schematic diagram and photograph of the FO bench-scale setup.

Figure 2-5-7 depicts a comparative illustration of the water flux for deionized water or St. Peter water when a 20% $MgSO_4$ draw solution was used in the FO treatment. The average fluxes obtained with the deionized water and St. Peter water sample were approximately 10 L/m^2/h and 6 L/m^2/h, respectively. These fluxes could be significantly increased by selecting a different membrane or draw solution.

Because of its high salinity, Mt. Simon brine might also be considered an effective potential draw solution. The pretreated Mt. Simon brine was used as the draw solution for the FO treatment of St. Peter water and ADM wastewater samples, and the water flux and reversed salt flux were compared with those obtained using the 20% $MgSO_4$ draw solution. In a series of baseline FO experiments using deionized water as a feed stream, the Mt. Simon draw solution was observed to create a higher osmotic pressure than the $MgSO_4$ draw solution. This resulted in a higher water flux through the membrane when Mt. Simon brine was used as the draw solution (Figures 2-5-8 and 2-5-9). However, the presence of monovalent ionic solutes in the Mt. Simon brine and the higher water flux resulted in a relatively higher reversed salt flux of 8.2 g/m^2/h compared with the 1.13 g/m^2/h observed when the $MgSO_4$ draw solution was used. Representative samples of the deionized water feed were collected and analyzed by ICP-OES to determine the extent of reversed salt flux (Table 2-5-9). The data in Table 2-5-9 show that Na, K, and Ca were the major contributors to the reversed salt flux when Mt. Simon brine was used as the draw solution.

Furthermore, the FO membrane used in these investigations showed a higher rejection of Mg (Table 2-5-9).

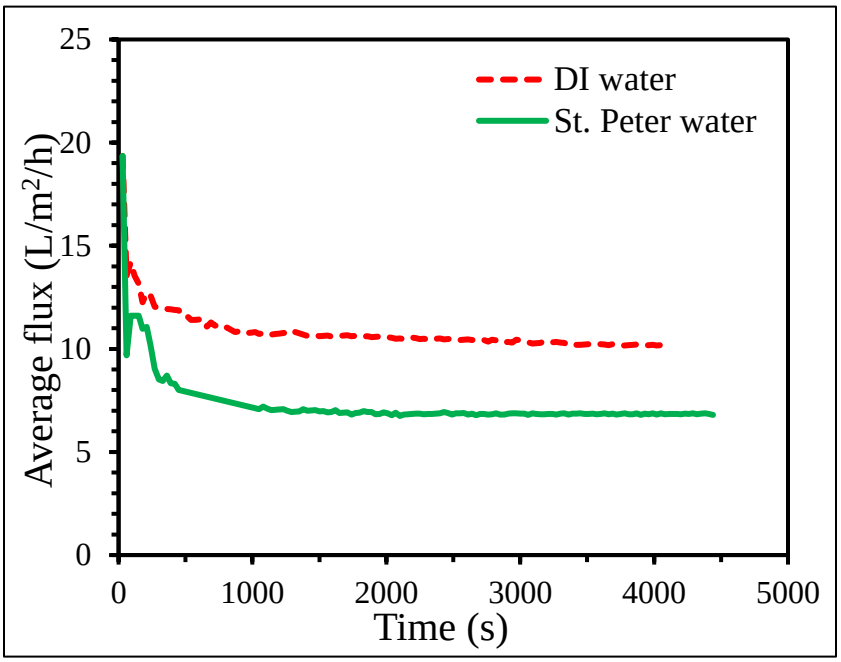

Figure 2-5-7 Water flux of the FO experiments using 20% $MgSO_4$ as a draw solution with the St. Peter water feed. DI water, deionized water. DI stands for deionized water.

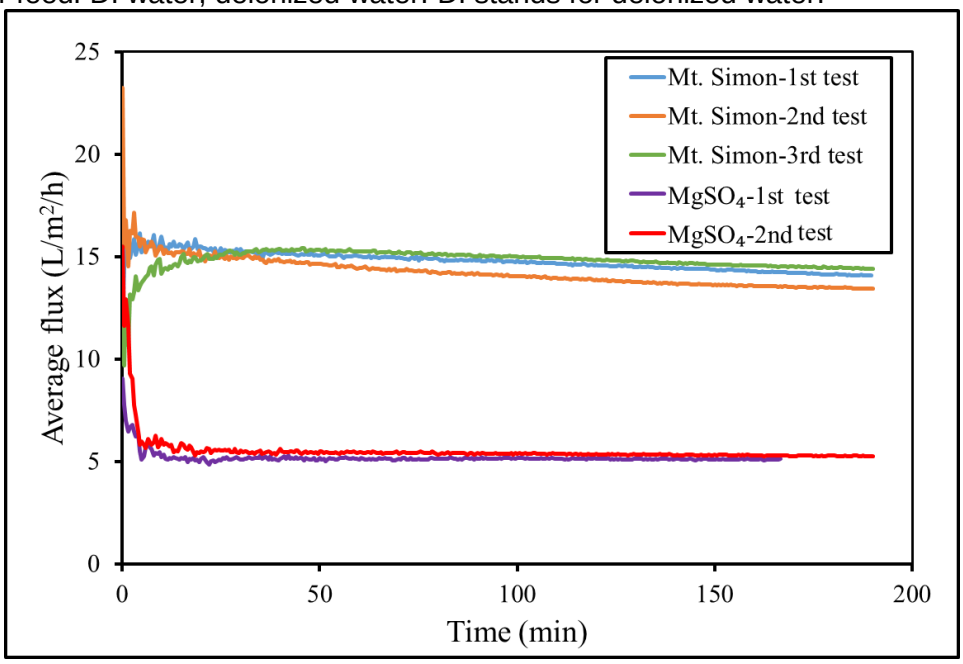

Figure 2-5-8 Flux values of different baseline FO experiments using deionized water as the feed and Mt. Simon brine or a 20% $MgSO_4$ solution as the draw solution.

Table 2-5-9 Passage of selected cations through the FO and MD membranes when Mt. Simon and $MgSO_4$ draw solutions were used with deionized (DI) water as the feed (for FO) or permeate (for MD), and when the pretreated Mt. Simon brine was desalinated by MD.

	Cation (mg/L)								
Analyte	**K**	**Mg**	**Mn**	**Si**	**Ca**	**Li**	**Na**	**S**	**Sr**
Initial concentration	1,930	1,980	53.60	15.4	20,800	13.70	45,300	354	781
FO (DI as feed), Mt. Simon draw solution	80.80	17.60	0.48	<0.1	205.60	<0.05	872	<1	0.88
FO (DI as feed), $MgSO_4$ draw solution	14.50	37.70	<0.01	<0.1	8.70	<0.05	23.20	<0.1	<10
MD permeate, pretreated Mt. Simon brine feed after 30 min	3.80	0.80	0.03	7.20	8.2	<0.05	23.8	<1	0.280
MD permeate, pretreated Mt. Simon brine feed after 360 min	1,245	816	8.97	4.20	9,900	4.23	37,000	36	360

Water flux values of the FO experiments for treatment of St. Peter water, ADM wastewater, and deionized water (as a baseline) when using $MgSO_4$ or Mt. Simon brine as draw solutions are compared in Figure 2-5-10. These results indicate that Mt. Simon brine had superior performance over the conventional $MgSO_4$ draw solution and could potentially be used as an effective draw solution for the FO water treatment process.

Several experiments were conducted for extended periods of time (up to 20 hours) to obtain preliminary information about the interaction between the membrane and the feed and draw solutions. These experiments were conducted to investigate the impact of the external concentration polarization and membrane fouling on the FO process. The extended experiments were conducted with a feed of either pretreated St. Peter water or ADM wastewater, using either the pretreated Mt. Simon brine or the $MgSO_4$ solution as the draw solution (Figures 2-5-11 and 2-5-12). The data in Figure 2-5-11 show that the average water flux was relatively stable when St. Peter water was used as the feed with the two draw solutions. However, in the case of the ADM wastewater feed, the impact of the fouling species (e.g., organic matter) adhering to the membrane surface resulted in a significant flux decline. The fouling had more impact on the water flux during the first 2,000 minutes of the experiments when the pretreated Mt. Simon brine was used as the draw solution. This result can be explained by the higher osmotic pressure of the Mt. Simon brine, which resulted in a higher driving force to push the wastewater feed solution, containing dissolved fouling species, to the membrane surface. The extent of membrane fouling was investigated by SEM to compare new and used FO membranes (Figure 2-5-12). Scanning electron microscopy images of the backing sides (facing the feed) of the new membrane (Figure 2-5-12, panel a) and membranes used to dewater wastewater with the Mt. Simon draw solution (Figure 2-5-12, panel c) or the 20% $MgSO_4$ draw solution (Figure 2-5-12, panel e) are shown, in addition to SEM images (Figure 2-5-12, panels b, d, and f) of the rejection sides (facing the draw solutions) of these membranes, respectively. Comparison of the SEM images of the backing of these membranes clearly shows the pore blockage and reduction of surface area resulting from wastewater species attaching on the surface of the membrane. Moreover, SEM images of the rejection sides of the membrane facing the Mt. Simon and $MgSO_4$ draw solutions (Figure 2-5-12, panels d and f, respectively) show possible salt deposition on the membrane surface.

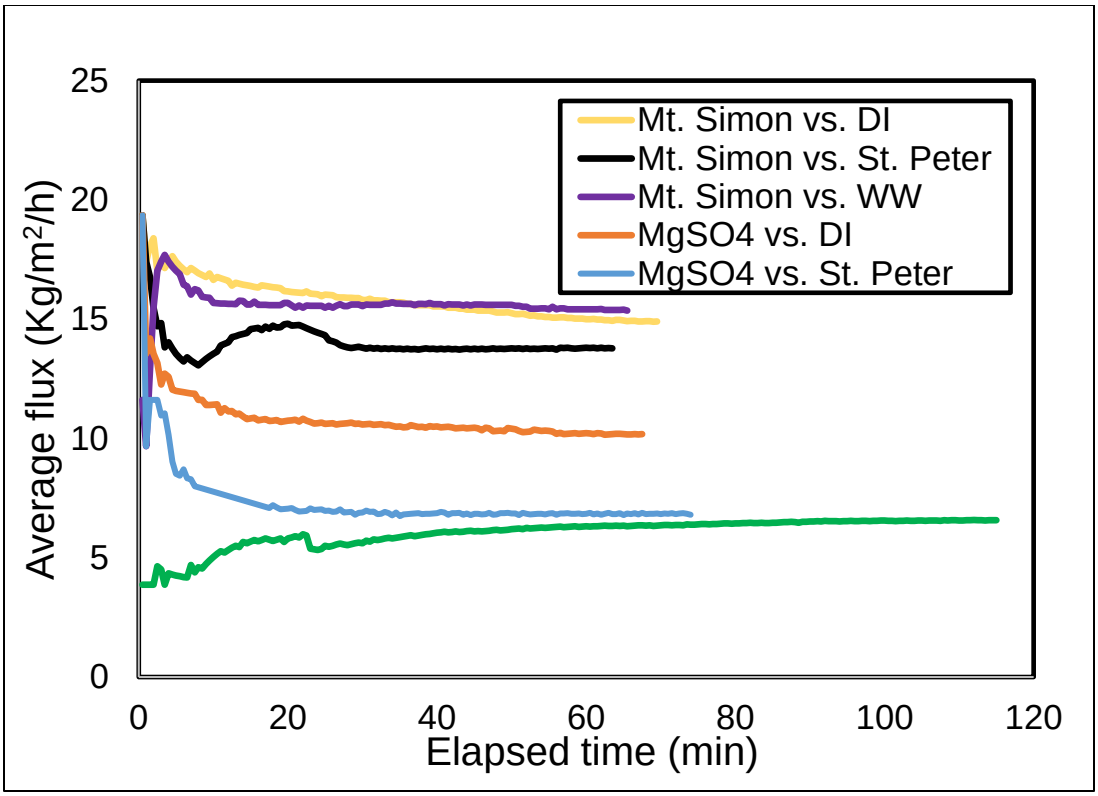

Figure 2-5-9 Water flux values of FO experiments for treatment of St. Peter water, ADM wastewater (WW), and deionized (DI) water (as a baseline) using $MgSO_4$ or Mt. Simon brine as the draw solutions.

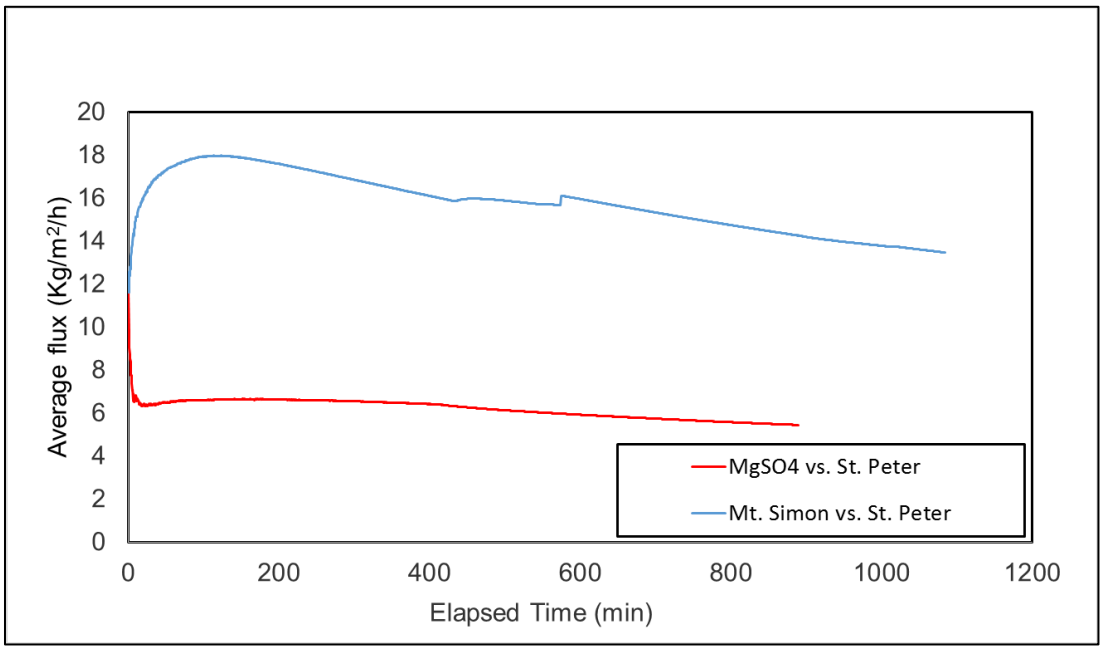

Figure 2-5-10 Extended tests of the treatment of St. Peter brackish water by FO.

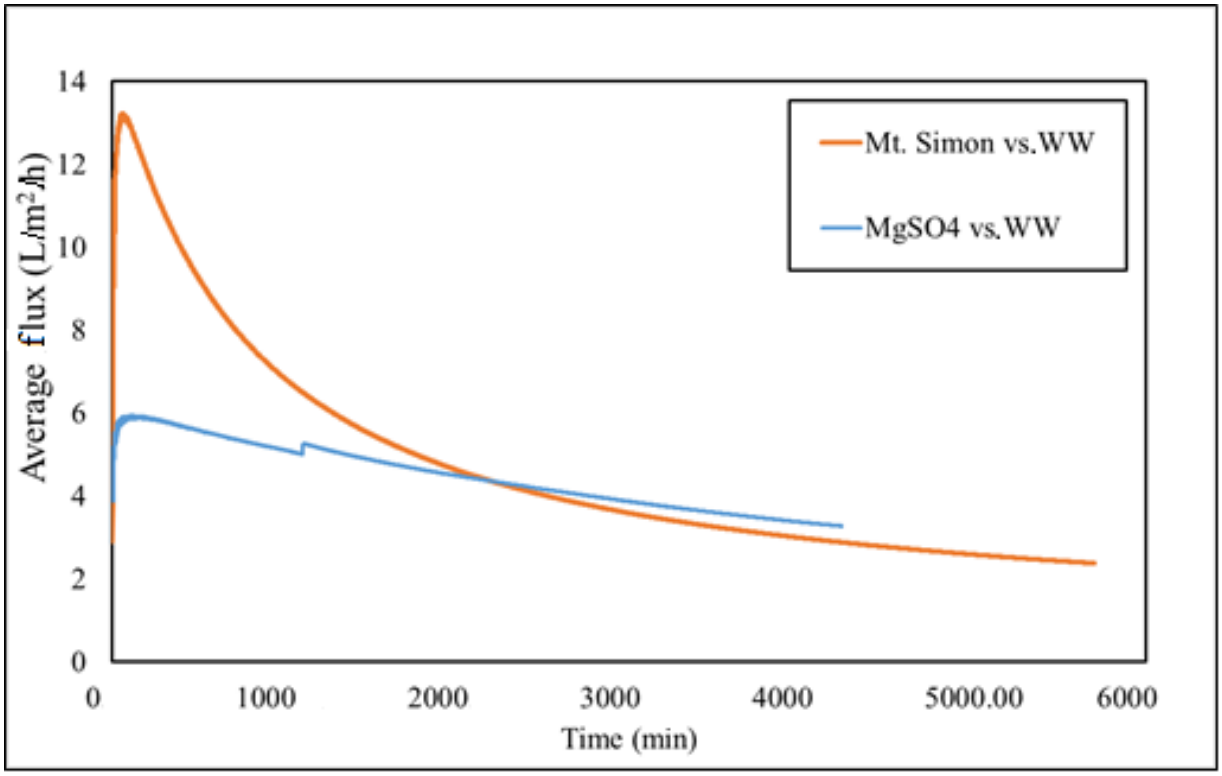

Figure 2-5-11 Extended tests of the treatment of ADM wastewater (WW) by FO.

Finally, experiments to regenerate the diluted Mt. Simon draw solutions by DCMD were performed. The diluted Mt. Simon brine resulted from FO treatment of the St. Peter water and ADM wastewater samples. Results of the DCMD experiments were compared with those obtained from DCMD treatment of the pretreated Mt. Simon brine with TDS of approximately 230,000 ppm and a conductivity of 193 mS/cm (Subtask 2-1). As shown in Figure 2-5-13, membrane distillation treatment of the diluted Mt. Simon brine provided a higher flux and better overall permeate quality compared with the membrane distillation treatment of the pretreated Mt. Simon brine. Membrane distillation results of both the pretreated Mt. Simon brine and diluted brine indicated a high salt rejection of more than 99% during the first 4 hours of the tests. However, a sharp increase in the permeate conductivity (or a significant reduction in salt rejection) was observed for the pretreated Mt. Simon brine after 4 hours of operation as the pretreated Mt. Simon brine approached the solution saturation and salt precipitation limit. Representative samples were collected from the permeate side of the membrane distillation setup at 30 and 360 minutes. These samples were analyzed by ICP-OES to investigate the selectivity of the TF200 membrane during the time span of the experiment. The data in Table 2-5-9 confirm that during the early stages of the experiment, the salt rejection was very high, with negligible amounts of Na^+ and K^+ (monovalent ions) passing through the membrane. However, when a significant amount of pure water was removed and brine concentration was further increased, the rejection of monovalent ions was dramatically decreased to less than 20%, and the rejection of divalent ions (Ca, Mg, and Sr) was greatly (~50%) reduced.

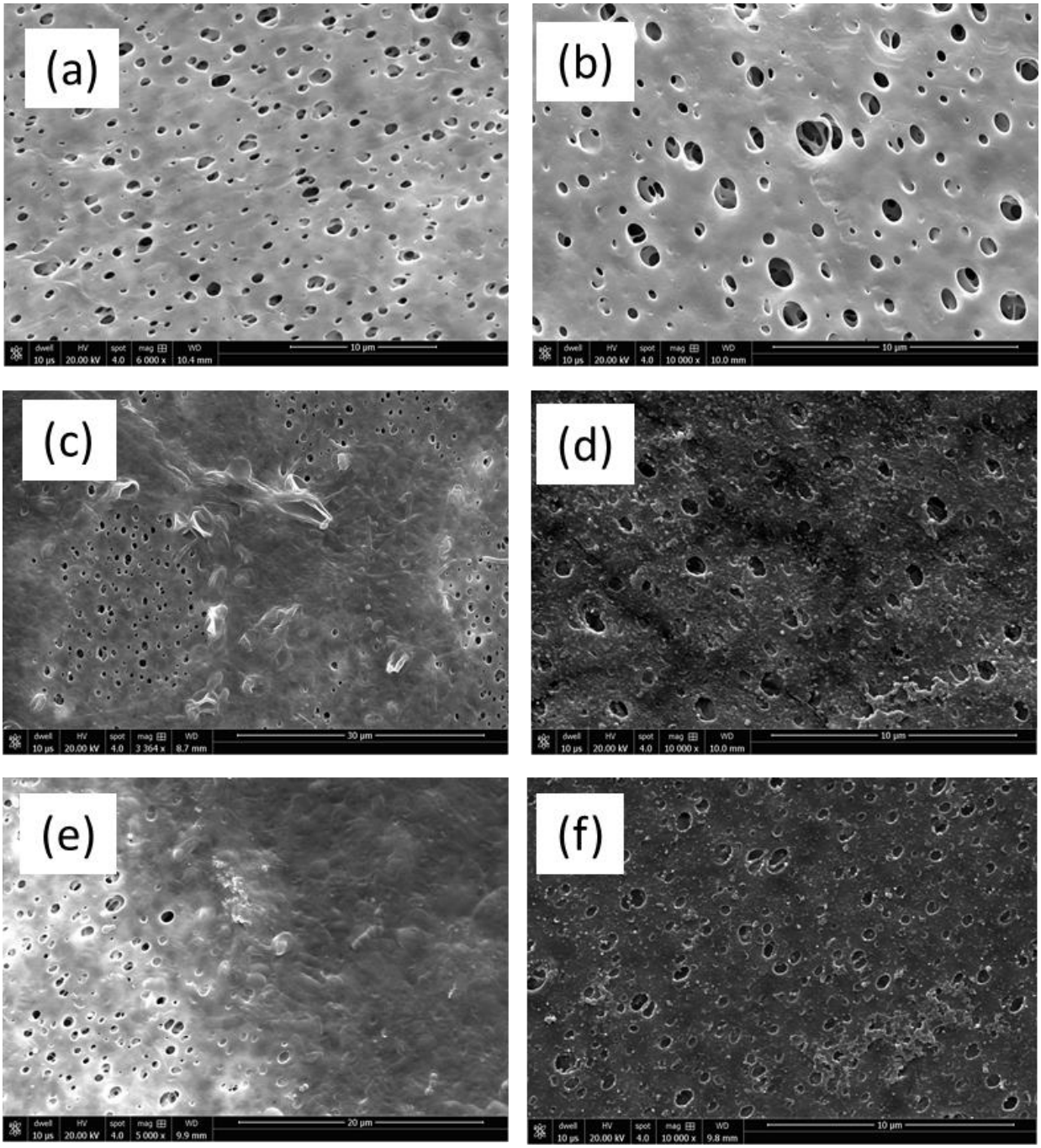

Figure 2-5-12 Scanning electron microscopy (SEM) images of the new FO membrane: (a) backing side, (b) rejection side, (c) backing side facing the wastewater feed, (d) rejection side facing the Mt. Simon draw solution, (e) backing side facing the wastewater feed, and (f) rejection side facing the $MgSO_4$ draw solution.

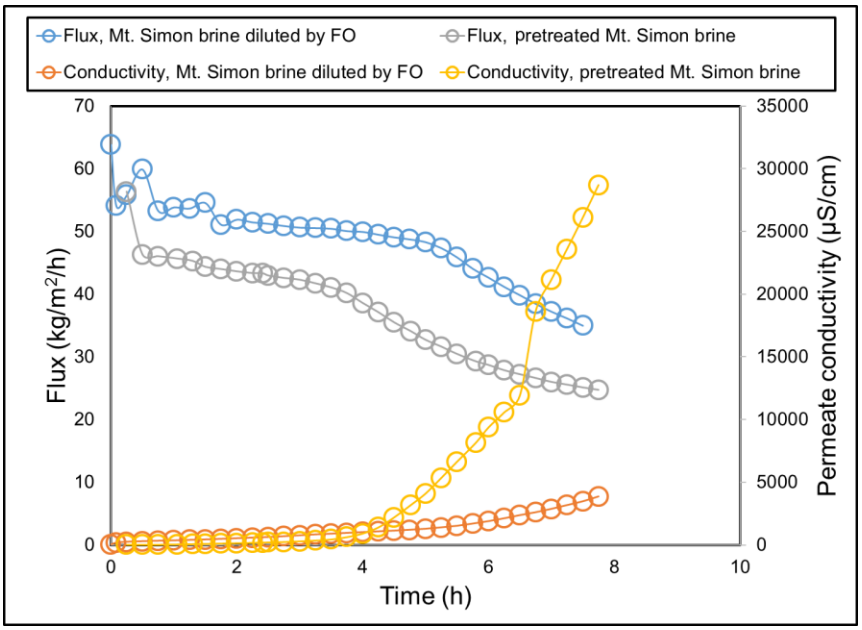

Figure 2-5-13 Treatment of pretreated Mt. Simon brine by the membrane distillation process. Treatment of diluted Mt. Simon brine (obtained from FO treatment of the ADM wastewater) is included for comparison.

Subtask 2-6 Assessment of Brine Treatment Options for Phase II

An assessment of options for the treatment of high-TDS Mt. Simon brine was presented in Subtask 2.1. The ISGS and Trimeric teams focused on screening technologies suitable for the treatment of high-TDS brine with a concentration of approximately 230,000 ppm, as in the Lower Mt. Simon Sandstone. Several factors, including applicability of the technology for high-TDS treatment (TDS limitations), energy consumption and requirements, water recovery percentages, technology readiness level, cost, and other factors, were discussed. The advantages and disadvantages of all the screened technologies were compared.

We recommend, based on our evaluation, the evaporation–crystallization technology as the most suitable commercially available technology for the treatment of Mt. Simon Brine because other commercially available desalination technologies are not well suited to treat highly saline brines. However, energy consumption costs for evaporative crystallizers are expected to be high. As a result, further investigation of emerging technologies at a test-bed facility is recommended. We recommend testing the evaporation–crystallization technology at the pilot scale in a test-bed facility to obtain baseline data for large-scale design and for comparison with other emerging and innovative technologies.

As is further described in Task 6, the proposed pilot plant test bed facility is designed to test multiple desalination technologies. We recommend testing all technologies in high-TDS treatment projects funded by the DOE through FOA-0001095 and FOA-0001238. We anticipate a test-bed facility that contains facilities for testing brine-treatment technologies at both the pilot (~5 gpm throughput) and mini-rig or bench (<1 gpm throughput) scale. The scale of operation to be tested would be determined by the readiness level of the technology. The relevant projects are described in Table 2-6-1 below. However, for some of the DOE-funded projects, we were unable to find enough detailed information on the proposed processes to perform technical assessments of those technologies.

Table 2-6-1 DOE-funded projects for treatment of high-TDS brine.

Performer, funding	Project title	Description
Ohio University, FOA-1238	Advanced Integrated Technologies for Treatment and Reutilization of Impaired Water in Fossil Fuel-Based Power Plant Systems (NETL, 2015a)	A precipitative supercritical process to remove salts. According to the limited information available, the goal of the project is partial water recovery with optimal heat recovery.
General Electric Company, FOA-1238 & FOA-1095	Project 1: Model-Based Extracted Water Desalination System for Carbon Sequestration (NETL, 2015a); Project 2: Water Desalination Using Multiple-Phase Turbo-Expander (NETL, 2015b)	Project 1: Details not provided. Project 2: Brine is atomized into a compressed air stream, and the mixture is then expanded in a turbo-expander capable of handling multiple phases. Cooling of the expansion results in the production of salt crystals and ice crystals, which are then separated.
Research Triangle Institute, FOA-1238 & FOA-1095	Project 1: Low-Energy Water Recovery from Subsurface Brines (NETL, 2015a); Project 2: Fouling-Resistant Membranes for Treating Concentrated Brines for Water Reuse in Advanced Energy Systems (NETL, 2014a)	Project 1: Uses non-aqueous solvents to extract water from concentrated brine. Project 2: Carbon nanotubes are incorporated into a membrane for use in a membrane distillation process. The carbon nanotubes are electrically conductive, so application of an electrical potential results in the removal or prevention of scaling and fouling.
Southern Research Institute, FOA-1095	Treatment of Produced Water from Carbon Sequestration Sites for Water Reuse, Mineral Recovery, and Carbon Utilization (NETL, 2014b)	A system for evaporation–crystallization. Details are not available.
University of Illinois, FOA-1095	An Integrated Supercritical System for Efficient Produced Water Treatment and Power Generation (NETL, 2015c)	Brine is heated above the critical point (374 °C, 220 bar), resulting in the precipitation of most salts. Supercritical steam with only ~100 ppm of salt is polished by supercritical membrane distillation and used to generate power. Low-pressure steam is condensed as pure water. Continuous removal of precipitated salts allows for high water recovery.
University of Pittsburgh, FOA-1095	Development of Membrane Distillation Technology Utilizing Waste Heat for Treatment of High-Salinity Wastewaters (NETL, 2014c)	Direct contact membrane distillation with a low-grade heat source is used for desalination. Details are not available.

References

Ahmad, M., and P. Williams, 2012, Assessment of desalination technologies for high saline brine applications—Discussion Paper: Desalination and Water Treatment, v. 30, p. 22–36.

Aines, R.D., T.J. Wolery, W.L. Bourcier, T. Wolfe, and C. Hausmann, 2011, Fresh water generation from aquifer-pressured carbon storage: Feasibility of treating saline formation waters: Energy Procedia, v. 4, p. 2269–2276.

Al-Karaghouli, A., and L.L. Kazmerski, 2013, Energy consumption and water production cost of conventional and renewable-energy-powered desalination processes: Renewable and Sustainable Energy Reviews, v. 24, p. 343–356.

Al-Sahali, M., and H. Ettouney, 2007, Developments in thermal desalination processes: Design, energy, and costing aspects: Desalination, v. 214, p. 227–240.

Alspach, B., 2014, Produced water and salinity management: The desalination frontier: Journal of the American Water Works Association, v. 106, p. 47–52.

Aquaver, 2014, Membrane distillation: A low-cost breakthrough technology for water treatment: http://www.aquaver.com/knowledge-center-articles/membrane-distillation-a-low-costbreakthrough-technology-for-water-treatment-2/ (accessed December 10, 2015).

Awerbuch, L., and M.C. Weekes, 1990, Disposal of concentrates from brackish water desalting plants by means of evaporation technology: Desalination, v. 78, p. 71–76.

Bajpayee, A., D. Kraemer, A.J. Muto, G. Chen, J.H. Lienhard, and B.B. Mikic, 2012, Water desalination using directional solvent extraction: U.S. Patent Application 8119007 B2, February 21.

Bethke, C.M., 2008, Geochemical and biogeochemical reaction modeling: New York, Cambridge University Press.

Bourcier, W.L., T.J. Wolery, T. Wolfe, C. Haussmann, T.A. Buscheck, and R.D. Aines, 2011, A preliminary cost and engineering estimate for desalinating produced formation water associated with carbon dioxide capture and storage: International Journal of Greenhouse Gas Control, v. 5, p. 1319–1328.

Clesceri, L.S., A.E. Greenberg, A.D. Eaton, eds., 1998, Method 2540 C: Total dissolved solids dried at 180 °C, *in* Standard methods for the examination of water and wastewater, 20th ed.: American Public Health Association, American Water Works Association, and Water Environment Federation, p. 2-56–2-57.

Coday, B.D., L. Miller-Robbie, E.G. Beaudry, J. Munakata-Marr, and T.Y. Cath, 2015, Life cycle and economic assessments of engineered osmosis and osmotic dilution for desalination of Haynesville shale pit water: Desalination, v. 369, p. 188–200.

Coday, B.D., P. Xu, E.G. Beaudry, J. Herron, K. Lampi, N.T. Hancock, and T.Y. Cath, 2014, The sweet spot of forward osmosis: Treatment of produced water, drilling wastewater, and other complex and difficult liquid streams: Desalination, v. 333, p. 23–35.

Collares-Pereira, M., J.F. Mendes, and P. Horta, 2004, Advanced solar dryer for salt recovery from brine effluent of desalination MED plant: Freiburg, Germany, PSE GmbH, Proceedings of EuroSun2004—The 5th ISES Europe Solar Conference, p. 20–23.

Curcio, E., G.D. Profio, E. Fontananova, and E. Drioli, 2015, Membrane technologies for seawater desalination and brackish water treatment, *in* A. Basile and A.C.K. Rastogi, eds., Advances in membrane technologies for water treatment: Oxford, UK, Woodhead Publishing, p. 411–441.

Das, P.C., 2012, Selection of technology for produced water treatment, *in* North Africa Technical Conference and Exhibition 2012 (NATC 2012) Proceedings: Managing Hydrocarbon Resources in a Changing Environment, Cairo, p. 1122–1128.
Demirer, O.N., R.M. Naylor, C.A.R. Perez, E. Wilkes, and C. Hidrovo, 2013, Energetic performance optimization of a capacitive deionization system operating with transient cycles and brackish water: Desalination, v. 314, p. 130–138.
Desware, Encyclopedia of Desalination and Water Resources, 2002–2016, Energy requirements of desalination processes: Desware, http://www.desware.net/Energy-Requirements-Desalination-Processes.aspx (accessed November 9, 2016).
Drioli, E., A. Ali, and F. Macedonio, 2015, Membrane distillation: Recent developments and perspectives: Desalination v. 356, p. 56–84.
Dzombak, D.A., and F.F.M. Morel, 1990, Surface complexation modeling: Hydrous ferric oxide: New York, Wiley.
Elimelech, M., and W.A. Phillip, 2011, The future of seawater desalination: Energy, technology, and the environment: Science, v. 333, p. 712–717.
Ettouney, H., 2009, Conventional thermal processes, *in* A. Cipollina, G. Micale, and L. Rizzuti, eds., Seawater desalination: Conventional and renewable energy processes: Berlin, Springer-Verlag, p. 17–40.
Fakhru'l-Razi, A., A. Pendashteh, L.C. Abdullah, D.R.A. Biak, S.S. Madaeni, and Z.Z. Abidin, 2009, Review of technologies for oil and gas produced water treatment: Journal of Hazardous Materials, v. 170, p. 530–551.
Fath, H., Z. Abbas, and A. Khaled, 2011, Techno-economic assessment and environmental impacts of desalination technologies: Desalination, v. 266, p. 263–273.
Flury, K., N. Jungbluth, R. Frischknecht, and I. Muñoz, 2012, Recommendation for life cycle inventory analysis for water use and consumption: Working paper: Zurich, Switzerland, ESU-Services Ltd., 16 p.
Freiburg, J.T., and H.E. Leetaru, 2012, Controls on porosity development and the potential for CO_2 sequestration or wastewater disposal in the Cambrian Potosi Dolomite (Knox Group): Illinois Basin: 41st Annual Eastern Section AAPG Meeting, Cleveland, Ohio, September 22–26.
Fujioka, R., L.P. Wang, G. Dodbiba, and T. Fujita, 2013, Application of progressive freeze concentration for desalination: Desalination v. 319, p. 33–37.
Gao, P., Z. Guo, D. Zhang, X. Zhou, and G. Zhou, 2014, Performance analysis of evaporation–freezing desalination system by humidity differences: Desalination, v. 347, p. 215–223.
GE Global Research, 2015, Water desalination using multi-phase turbo-expander: Munich, Germany, GE Global Research, http://www.netl.doe.gov/File%20Library/Events/2015/crosscutting/Crosscutting_20150428_Poster23_GE.pdf (accessed February 29, 2016).
GE Power, 2016, Zero-liquid-discharge (ZLD) crystallizers: http://www.gewater.com/products/zero-liquid-discharge-zld-crystalizers.html (accessed November 20, 2016).
Ghaffour, N., T.M. Missimer, and G.L. Amy, 2013, Technical review and evaluation of the economics of water desalination: Current and future challenges for better water supply sustainability: Desalination, v. 309, p. 197–207.
Ghalavand, Y., M.S. Hatamipour, and A. Rahimi, 2014, Humidification compression desalination: Desalination, v. 341, p. 120–125.

Gradiant Corp., 2014, HDH tackles brine disposal challenge: Water Desalination Report, May 6, http://gradiant.com/hdh-tackles-brine-disposal-challenge/ (accessed November 18, 2016).
Greenlee, L.F., D.F. Lawler, B.D. Freeman, B. Marrot, and P. Moulin, 2009, Reverse osmosis desalination: Water sources, technology, and today's challenges: Water Research, v. 43, p. 2317–2348.
Guerra, K., K. Dahm, and S. Dundorf, 2011, Oil and gas produced water management and beneficial use in the western United States: U.S. Department of the Interior, Bureau of Reclamation.
Harvie, C.E., N. Moller, and J.H. Weare, 1984, The prediction of mineral solubilities in natural waters, the Na-K-Mg-Ca-H-Cl-SO_4-OH-HCO_3-CO_3-CO_2-H_2O system to high ionic strengths: Free energy minimization: Geochimica et Cosmochimica Acta, v. 51, p. 723–751.
Heist, J.A., and T. Barron, 1983, Freeze crystallization processes: Efficiency by flexibility: College Station, Texas A&M University, Energy Systems Laboratory, http://hdl.handle.net/1969.1/94528 (accessed November 18, 2016).
Ifelebuegu, A., S.M. Charlesworth, and C.A. Booth, 2014, Desalination, water resources in the built environment: Management issues and solutions: New York, Wiley Blackwell, p. 92–103.
Igunnu, E.T., and G.Z. Chen, 2014, Produced water treatment technologies: International Journal of Low-Carbon Technologies, v. 9, p. 157–177.
Illinois Emergency Management Agency, 2016, Title 32: Energy, Chapter II: Illinois Emergency Management Agency, Subchapter B: Radiation Protection, Part 330 Licensing of Radioactive Material: Springfield, Illinois Emergency Management Agency.
Juby, G., A. Zacheis, W. Shih, P. Ravishanker, and B. Morazavi, 2008, Evaluation and selection of available processes for a zero-liquid discharge system for the Perris, California, ground water basin: Washington, DC, U.S. Department of the Interior, Desalination and Water Purification Research and Development Program, Report No. 149, 198 p.
Knutson, C., S.A. Dastgheib, Y. Yang, A. Ashraf, C. Duckworth, and P. Sinata, 2012, Reuse of produced water from CO_2 enhanced oil recovery, coal-bed methane, and mine pool water by coal-based power plants: Champaign, Illinois State Geological Survey, Final Report, DOE Award DE-NT0005343.
Labotka, D.M., S.V. Panno, R.A. Locke, and J.T. Freiburg, 2015, Isotopic and geochemical characterization of fossil brines of the Cambrian Mt. Simon Sandstone and Ironton–Galesville Formation from the Illinois Basin, USA: Geochimica et Cosmochimica Acta, v. 165, p. 342–360.
Lean, M.H., J. Seo, and A.R. Volkel, 2012, Desalination using supercritical water and spiral separation: U.S. Patent Application US 2012/0205320 A1.
Lesico CleanTech, WAIV—Wind aided intensified evaporation: Holon, Israel, Lesico CleanTech, http://www.lesico-cleantech.com/?p=61 (accessed November 24, 2015).
Locke, R., D. Larssen, W. Salden, C. Patterson, J. Kirksey, A. Iranmanesh, B. Wimmer, and I. Krapac, 2013, Preinjection reservoir fluid characterization at a CCS demonstration site: Illinois Basin – Decatur Project, USA: Energy Procedia, v. 37, p. 6424–6433.
Lozier, J.C., U. Erdal, A. Lynch, and S. Schindler, 2007, Evaluating traditional and innovative concentrate treatment and disposal methods for water recycling at Big Bear Valley, California: Englewood, Colorado, CH2M HILL.

Macknick, J., R. Newmark, G. Heath, and K.C. Hallett, 2011, A review of operational water consumption and withdrawal factors for electricity generating technologies: Golden, Colorado, National Renewable Energy Laboratory, Technical Report NREL/TP-6A20-50900.

Mason, M.A., ed., 1958, Saline water conversion: Proceedings of a symposium, 4–6 November 1957: Washington, DC, U.S. Department of the Interior, National Academy of Sciences–National Research Council and Office of Saline Water.

McGinnis, R.L., and M. Elimelech, 2007, Energy requirements of ammonia–carbon dioxide forward osmosis desalination: Desalination, v. 207, p. 370–382.

McGinnis, R.L., N.T. Hancock, M. Nowosielski-Slepowron, and G.D. McGurgan, 2013, Pilot demonstration of the NH_3/CO_2 forward osmosis desalination process on high salinity brines: Desalination, v. 312, p. 67–74.

McGovern, R.K., A.M. Weiner, L. Sun, C.G. Chambers, S.M. Zubair, and J.H. Lienhard V, 2014, On the cost of electrodialysis for the desalination of high salinity feeds: Applied Energy, v. 136, p. 649–661.

Memsys, 2016, Technology of thermal membrane distillation: Munich, Germany, Memsys, http://www.memsys.eu/technology.html (accessed November 17, 2015).

Mezher, T., H. Fath, Z. Abbas, and A. Khaled, 2011, Techno-economic assessment and environmental impacts of desalination technologies: Desalination, v. 266, p. 263–273.

Mickley, M., 2008, Survey of high-recovery and zero liquid discharge technologies for water utilities: Alexandria, Virginia, Water Reuse Research Foundation.

Miller, S., H. Shemer, and R. Semiat, 2015, Energy and environmental issues in desalination: Desalination, v. 366, p. 2–8.

Minier-Matar, J., A. Hussain, A. Janson, F. Benyahia, and S. Adham, 2014, Field evaluation of membrane distillation technologies for desalination of highly saline brines: Desalination, v. 351, p. 101–108.

Minier-Matar, J., R. Sharma, A. Hussain, A. Janson, and S. Adham, 2016, Field evaluation of membrane distillation followed by humidification/dehumidification crystallizer for inland desalination of saline groundwater: Desalination v.398, p. 12–21.

Morillo, J., J. Usero, D. Rosado, H. El Bakouri, A. Riaza, and F.-J. Bernaola, 2014, Comparative study of brine management technologies for desalination plants: Desalination, v. 336, p. 32–49.

National Energy Technology Laboratory (NETL), 2015a, DOE selects twelve projects for crosscutting technology research funding: Pittsburgh, Pennsylvania, U.S. Department of Energy, National Energy Technology Laboratory, http://netl.doe.gov/newsroom/news-releases/news-details?id=96dc91c4-1ec4-4a18-97f1-d6c7b8d8013a (accessed February 29, 2016).

National Energy Technology Laboratory (NETL), 2015b, Water desalination using multi-phase turbo-expander: Pittsburgh, Pennsylvania, U.S. Department of Energy, National Energy Technology Laboratory, Award No. FE0024022, http://www.netl.doe.gov/research/coal/project-information/proj?k=FE0024022 (accessed February 29, 2016).

National Energy Technology Laboratory (NETL), 2014a, Fouling-resistant membranes for treating concentrated brines for water reuse in advanced energy systems: Pittsburgh, Pennsylvania, U.S. Department of Energy, National Energy Technology Laboratory,

Award No. FE0024074, http://www.netl.doe.gov/research/coal/project-information/proj?k=FE0024074 (accessed February 29, 2016).
National Energy Technology Laboratory (NETL), 2014b, Treatment of produced water from carbon sequestration sites for reuse, mineral recovery and carbon utilization: Pittsburgh, Pennsylvania, U.S. Department of Energy, National Energy Technology Laboratory, Award No. FE0024084, http://www.netl.doe.gov/research/coal/project-information/proj?k=FE0024084 (accessed February 29, 2016).
National Energy Technology Laboratory (NETL), 2015c, An integrated supercritical system for efficient produced water treatment and power generation: Pittsburgh, Pennsylvania, U.S. Department of Energy, National Energy Technology Laboratory, Award No. FE0024015, http://www.netl.doe.gov/research/coal/project-information/proj?k=FE0024015 (accessed February 29, 2016).
National Energy Technology Laboratory (NETL), 2014c, Development of membrane distillation technology utilizing waste heat for treatment of high salinity wastewaters: Pittsburgh, Pennsylvania, U.S. Department of Energy, National Energy Technology Laboratory, Award No. DE-FE002406, http://www.netl.doe.gov/research/coal/project-information/proj?k=FE0024061 (accessed February 29, 2016).
Odu, S.O., D.H. Van, S. Metz, and S.R.A. Kersten, 2015, Design of a process for supercritical water desalination with zero liquid discharge: Industrial & Engineering Chemistry Research, v. 54, p. 5527–5535.
Palandri, J.L., and Y.K. Kharaka, 2004, A compilation of rate parameters of water-mineral interaction kinetics for application to geochemical modeling: U.S. Geological Survey Open File Report 2004-106.8.
Parkhurst, D.L., and C.A.J. Appelo, 1999, User's guide to PHREEQC (Version 2): A computer program for speciation, batch-reaction, one-dimensional transport, and inverse geochemical calculations: Denver, Colorado, U.S. Geological Survey, Water-Resources Investigations Report 99-4259, 327 p.
PE International, 2016, GaBi software, system and databases for life cycle engineering: Leinfelden-Echterdingen, Germany, Thinkstep, GaBi Professional Database, http://www.gabi-software.com/ (accessed May 19, 2016).
Pereira, M.C., J.F. Mendes, P. Horta, and N. Korovessis, 2007, Final design of an advanced solar dryer for salt recovery from brine effluent of an MED desalination plant: Desalination, v. 211, p. 222–231.
Qasim, M., N.A. Darwish, S. Sarp, and N. Hilal, 2015, Water desalination by forward (direct) osmosis phenomenon: A comprehensive review: Desalination, v. 374, p. 47–69.
Qin, M., and Z. He, 2014, Self-supplied ammonium bicarbonate draw solute for achieving wastewater treatment and recovery in a microbial electrolysis cell-forward osmosis-coupled system: Environmental Science & Technology Letters, v. 1, p. 437–441.
Rahardianto, A., J. Gao, C.J. Gabelich, M.D. Williams, and Y. Cohen, 2007, High recovery membrane desalting of low-salinity brackish water: Integration of accelerated precipitation softening with membrane RO: Journal of Membrane Science, v. 289, p. 123–137.
Raluy, G., L. Serra, and J. Uche, 2006, Life cycle assessment of MSF, MED and RO desalination technologies: Energy, v. 31, p. 2361–2372.

Rane, M.V., and Y.S. Padiya, 2011, Heat pump operated freeze concentration system with tubular heat exchanger for seawater desalination: Energy for Sustainable Development, v. 15, p. 184–191.
Research Partnership to Secure Energy for America (RPSEA), 2011, Cost-effective treatment of flowback and produced waters via an integrated precipitative supercritical (IPSC) process: Sugar Land, Texas, Research Partnership to Secure Energy for America, http://www.rpsea.org/projects/11122-60/ (accessed November 15, 2016).
Roelofs, S.H., A. Van Den Berg, and M. Odijk, 2015, Microfluidic desalination techniques and their potential applications: Lab on a Chip—Miniaturisation for Chemistry, Physics, Biology, Materials Science and Bioengineering, v. 15, p. 3428–3438.
Saltworks Technologies, 2015a, ElectroChem advanced EDR: Richmond, BC, Saltworks, http://www.saltworkstech.com/wp-content/uploads/2015/03/Saltworks_ElectroChem_Product_Sheet_EN.pdf (accessed November 23, 2015).
Saltworks Technologies, 2015b, SaltMaker low temperature crystallizer: Richmond, BC, Saltworks, http://www.saltworkstech.com/wp-content/uploads/2015/03/Saltworks_SaltMaker_Product_Sheet_EN.pdf (accessed November 23, 2015).
Sethi, S., S. Walker, P. Xu, and J. Drewes, 2008, Comparison of an innovative approach for concentrate minimization with traditional approaches for zero liquid discharge. American Water Works Association Annual Conference and Exposition (ACE 2008), Atlanta, Georgia.
Shaffer, D.L., L.H. Arias Chavez, M. Ben-Sasson, S. Romero-Vargas Castrillón, N.Y. Yip, and M. Elimelech, 2013, Desalination and reuse of high-salinity shale gas produced water: Drivers, technologies, and future directions: Environmental Science and Technology, v. 47, p. 9569–9583.
Shaffer, D.L., J.R. Werber, H. Jaramillo, S. Lin, and M. Elimelech, 2015, Forward osmosis: Where are we now?: Desalination, v. 356, p. 271–284.
Shkolnikov, V., S.S. Bahga, and J.G. Santiago, 2012, Desalination and hydrogen, chlorine, and sodium hydroxide production via electrophoretic ion exchange and precipitation: Physical Chemistry Chemical Physics, v. 14, p. 11534–11545.
Sidem-Veolia, Desalination by distillation: Paris, Sidem-Veolia, http://www.sidem-desalination.com/en/Process/ (accessed January 19, 2016).
Standard Methods Online, Editorial Revisions, 2011, 5310 Total Organic Carbon (TOC) B. High Temperature Combustion Method, available at https://standardmethods.org/store/ProductView.cfm?ProductID=409 (accessed December 5, 2015).
Subramani, A., and J.G. Jacangelo, 2015, Emerging desalination technologies for water treatment: A critical review: Water Research, v. 75, p. 164–187.
Tarnacki, K., M. Meneses, T. Melin, J. van Medevoort, and A. Jansen, 2012, Environmental assessment of desalination processes: Reverse osmosis and Memstill®: Desalination, v. 296, p. 69–80.
TDA Research, Inc., 2004, Capacitive deionization: Denver, Colorado, TDA Research, Inc., http://www.tda.com/Research/capac_deion.htm (accessed November 17, 2015).

Thiel, G.P., E.W. Tow, L.D. Banchik, H.W. Chung, and J.H. Lienhard V, 2015, Energy consumption in desalinating produced water from shale oil and gas extraction: Desalination v. 366, p. 94–112.
U.S. Department of the Interior, Desalination and Water Purification Research and Development Program, 2003, Desalting handbook for planners, 3rd ed.: Washington, DC, U.S. Department of the Interior, Report No. 72, 310 p.
U.S. Environmental Protection Agency (USEPA), Office of Drinking Water, 1990, Suggested guidelines for the disposal of drinking water treatment wastes containing naturally occurring radionuclides: Washington, DC, U.S Environmental Protection Agency, Office of Drinking Water.
Voutchkov, N., 2011, Overview of seawater concentrate disposal alternatives: Desalination, v. 273, p. 205–219.
Water Desalination and Reuse Center, Adsorption Desalination (AD) and Adsorption Desalination with MED Pilot Facility: https://wdrc.kaust.edu.sa/Pages/Equipment-Pilot-AD-Plant.aspx (accessed December 13, 2016).
Wiegandt, H.F., and R.L. Von Berg, 1980, Myths about freeze desalting: Desalination, v. 33, p. 287–297.
Williams, P.M., M. Ahmad, and B.S. Connolly, 2013, Freeze desalination: An assessment of an ice maker machine for desalting brines: Desalination, v. 308, p. 219–224.
Williams, P.M., M. Ahmad, B.S. Connolly, and D.L. Oatley-Radcliffe, 2015, Technology for freeze concentration in the desalination industry: Desalination, v. 356, p. 314–327.
Wolery, T.J., 1992, EQ3NR, A computer program for geochemical aqueous speciation-solubility calculations: Theoretical manual, users' guide, and related documentation (version 7.0): Livermore, California, Lawrence Livermore National Laboratory, UCRL-MA-110662 PT III.
Xu, P., T.Y. Cath, A.P. Robertson, M. Reinhard, J.O. Leckie, and J.E. Drewes, 2013, Critical review of desalination concentrate management, treatment and beneficial use: Environ. Eng. Sci., v. 30, p. 502–514.
Zhou, J., V.W.-C. Chang, and A.G. Fane, 2014, Life cycle assessment for desalination: A review on methodology feasibility and reliability: Water Research, v. 61, p. 210–223.
Zijlema, T.G., R.M. Geertman, G. Witkamp, G.M. van Rosmalen, and J. de Graauw, 2000, Antisolvent crystallization as an alternative to evaporative crystallization for the production of sodium chloride: Industrial and Engineering Chemistry Research, v. 39, p. 1330–1337.
Zuback, R., L. Marchewka, and L. Herrmann, 2014, Industrial brine concentration using forward osmosis, *in* Proceedings of the Water Environment Federation, WEFTEC 2014: Alexandria, Virginia, Water Environment Federation, p. 2685–2690.

TASK 3-0 GEOLOGIC CHARACTERIZATION
Subtask 3-1 Review and Analyze New Geologic, Petrophysical, and Geophysical Data

The geologic, petrophysical, and geophysical data for six formations were reviewed and analyzed. These formations included the St. Peter Sandstone, Ironton Sandstone, Galesville Sandstone, Potosi Dolomite, Eau Claire, and Formation Mt. Simon Sandstone. Figure 3-1-1 shows the general stratigraphy of these formations.

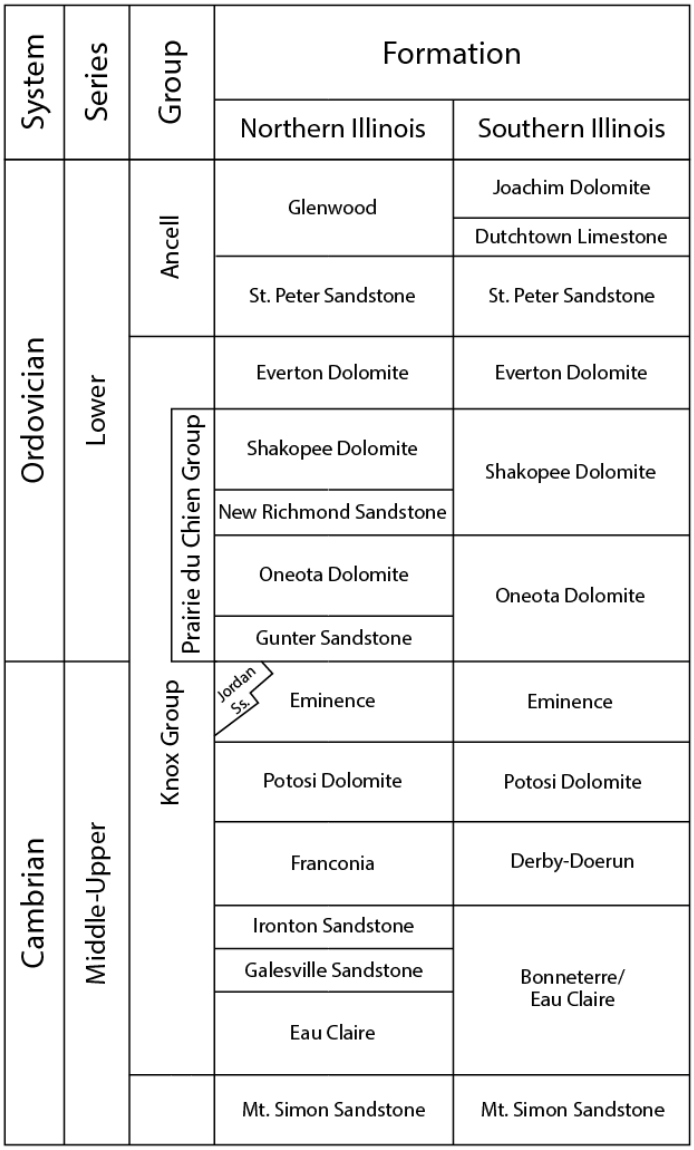

Figure 3-1-1 Stratigraphic classification of Cambrian through Ordovician rocks in Illinois (modified from Lasemi and Askari, 2014).

Ironton and Galesville Sandstones

The Cambrian Galesville and Ironton Sandstones cover the northern half of the state of Illinois, Indiana, Iowa, and southern parts of Minnesota, Wisconsin, and Michigan. They form the most extensive permeable and productive aquifer in northern Illinois (Buschbach, 1975) and

southern Wisconsin (Mossler, 1987). This study focuses on lithofacies analysis and stratigraphy of the succession using the available subsurface data.

Geologic and Stratigraphic Setting

The cratonic Illinois Basin (Figure 3-1-2) was formed during the Cambrian on the Laurentian continent (Kolata and Nelson, 1991) associated with the breakup of the Rodinia supercontinent during Late Precambrian to Early Cambrian (Bond et al., 1984; Meert and Torsvik, 2003). During the Late Cambrian, Illinois was covered by a very shallow sea (Figure 3-1-3); at times of sea level lowstands, the shoreline shifted southward, depositing siliciclastics sourced from the north. The Ironton and Galesville Sandstones occur in the Lower-Middle Cambrian boundary interval, the transition interval of Sauk II-III subsequences of Palmer (1981). The Sauk II-III unconformity appears to merge with a correlative conformity toward the south (Saltzman et al., 2004; Rukel et al., 2012).

The Ironton and the underlying Galesville Sandstone (Figure 3-1-4) are a part of the Knox Group (Kolata, 2010) and consist mainly of sandstone and sandy dolomite. The Galesville and Ironton Sandstones generally are fine- to coarse-grained quartz sandstones in the areas close to the paleoshoreline. The Ironton in Illinois is characterized by interlayered sandstone, dolomite or sandy dolomite, and can be easily distinguished in the subsurface. However, in the upper Mississippi valley region like Wisconsin and Minnesota, carbonate layers are absent and the Ironton and Galesville are very similar and not easily distinguishable. Because of their similarity in Wisconsin, both sandstones were demoted to member rank and assigned to Wonewoc Sandstone (Ostrom, 1966). In Minnesota, these units were classified as a formation (Mossler, 1987). However, they were assigned as members of the Wonewoc Sandstone by Mossler (2008). In Illinois, the Ironton contains dolomite layers that make it easily recognizable from the Galesville. Buschbach (1975), based on variation of grain size and dolomite content, divided the Ironton into four members, which from base to top, include the Buelter, Fox valley, Marywood, and Mooseheart members.

Lithofacies and Distribution of Galesville and Ironton Sandstones

The Galesville and Ironton Sandstones do not crop out in Illinois but are present in the subsurface in the northern half of Illinois. They are over 200 ft (61 m) thick in northern Illinois but their thickness decreases southwestward (Figure 3-1-5 and Figure 3-1-6). The zero thickness contour runs roughly along a northwest-southeast line connecting northern Adams County to southern Clark County.

Galesville Sandstone

The Galesville is up to 100 ft (30.5 m) thick and underlies, with a gradational contact, the dolomitic Ironton Sandstone. It overlies, with a sharp contact, the Eau Claire Formation (Figure 3-1-7). It is a white, porous, and commonly friable, fine-grained, mature quartzose sandstone (Figure 3-1-8). The average porosity of this unit is close to 18%. The net thickness of the porous interval in the Galesville Sandstone and its porosity is much greater than the overlying Ironton Sandstone (Figure 3-1-7). Exceptional mineralogical and textural maturity of the sandstone suggests the high-energy condition of a shoreface environment.

Ironton Sandstone

The Ironton Sandstone is nearly up to 150 ft (45.7 m) thick and is fine- to coarse-grained, commonly fossiliferous, porous quartzose sandstone that is interbedded with dolomite-cemented sandstone in the northern part of Illinois. Southward, the Ironton is interbedded with dense dolomitic sandstone or sandy dolomite (Figure 3-1-9). The average porosity of the sandstone is close to 12%. The Ironton overlies the Galesville Sandstone and underlies, with a sharp contact,

the glauconitic sandstone of the Franconia Formation (Figure 3-1-4 and 3-1-7). The fossiliferous dolomite of the Ironton indicates dolomitization of a limestone precursor and deposition in a shallow marine environment, though in a more distal setting compared to the sandstones.

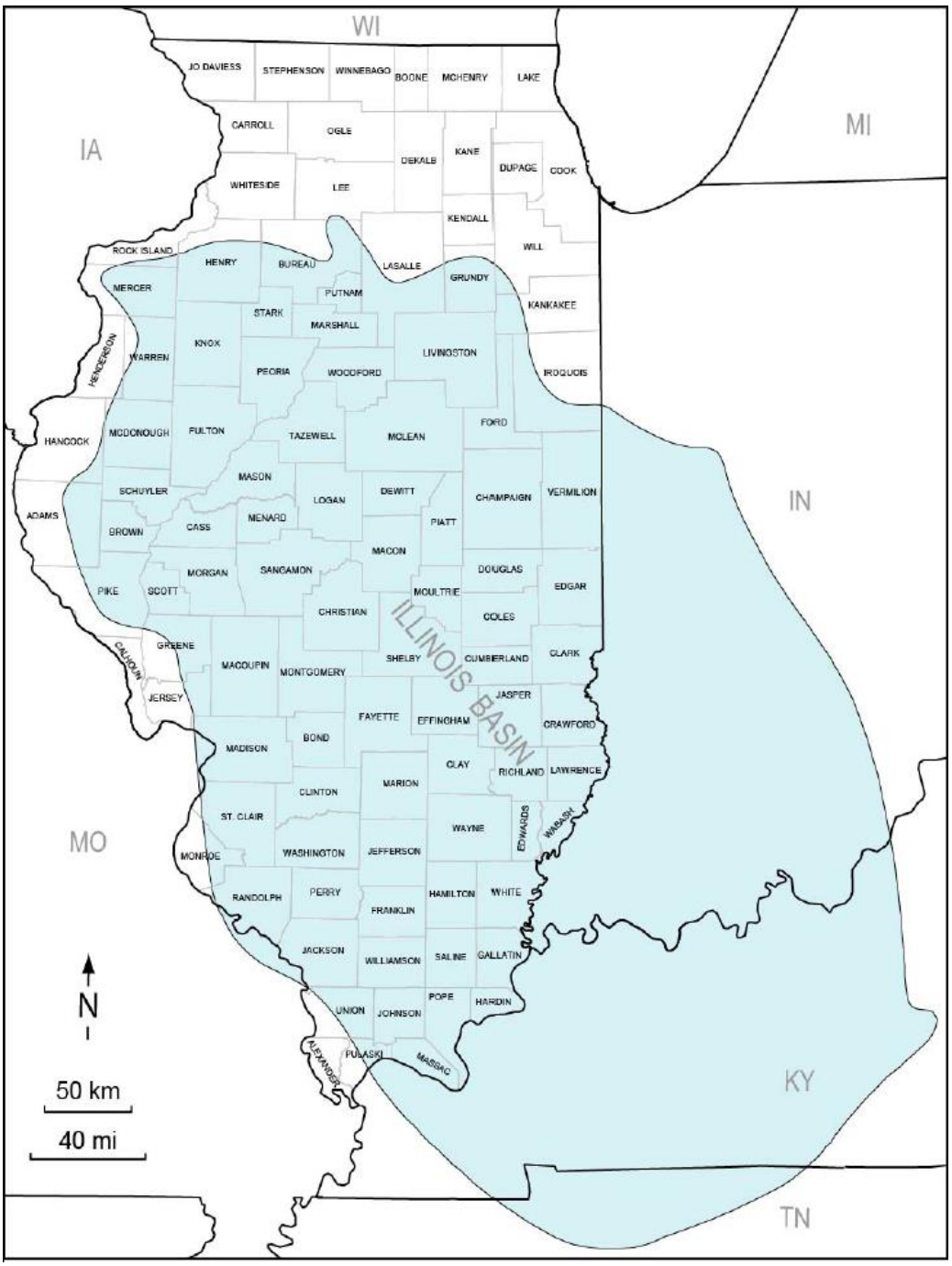

Figure 3-1-2 Illinois Basin in light blue (modified from Buschbach and Kolata, 1991; Lasemi and Askari, 2014). During the Middle and Upper Cambrian, a shallow sea covered all of Illinois during sea level highstands.

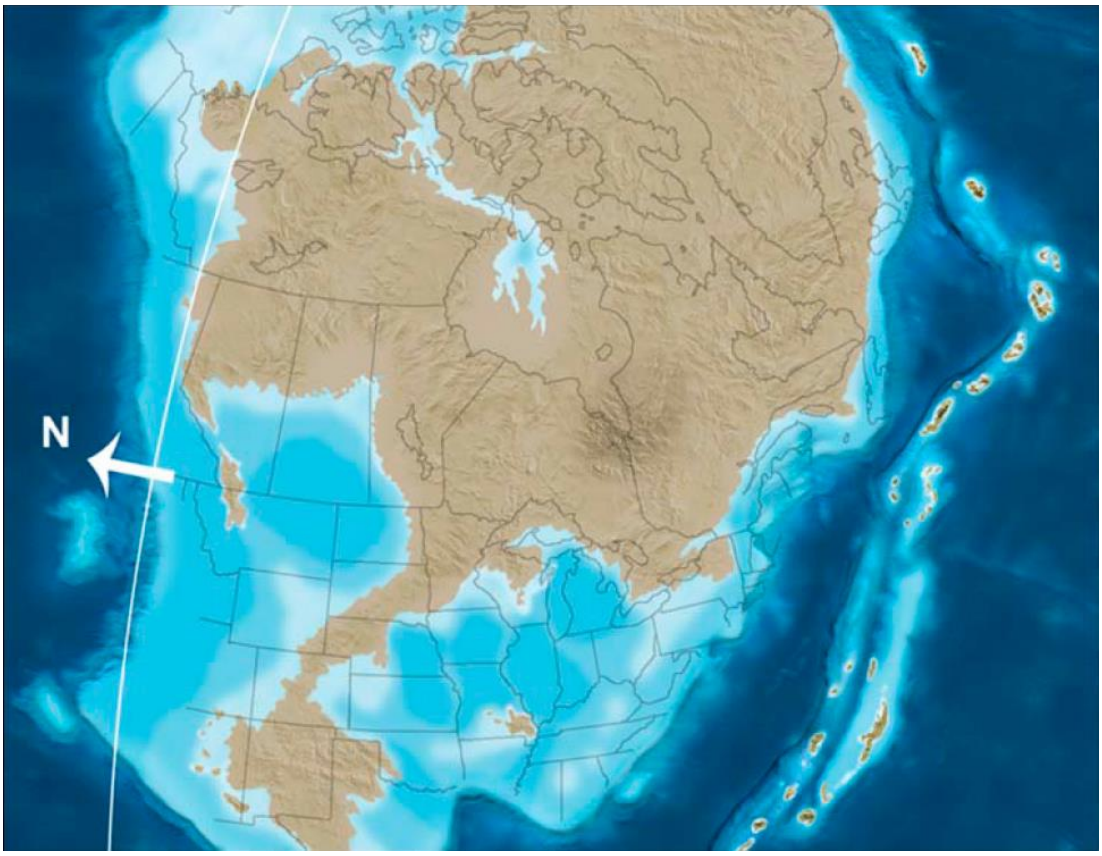

Figure 3-1-3 The paleogeography of Laurentia during the Late Cambrian. Used with permission Ron Blakey © Colorado Plateau Geosystems Inc 2010.

System	Series	Group	Formation	
			Northern Illinois	Southern Illinois
Cambrian	Middle-Upper	Knox Group	Franconia	Derby-Doerun
			Ironton Sandstone	Bonneterre
			Galesville Sandstone	
			Eau Claire	

Figure 3-1-4 Stratigraphic classification of a part of the Knox Group in Illinois (modified from Lasemi and Askari, 2014).

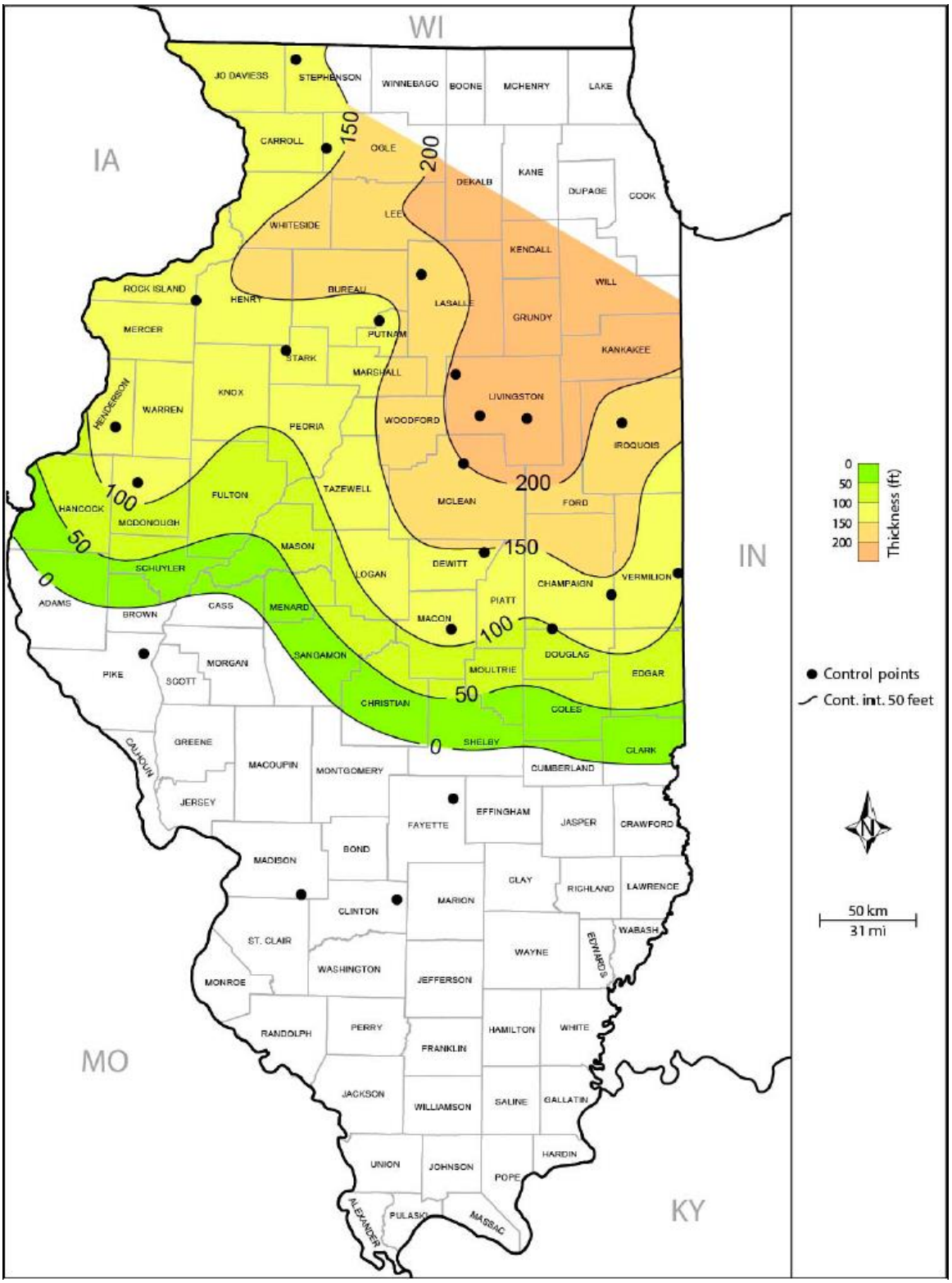

Figure 3-1-5 Isopach map of combined Galesville and Ironton Sandstones (modified from Lasemi and Askari, 2014).

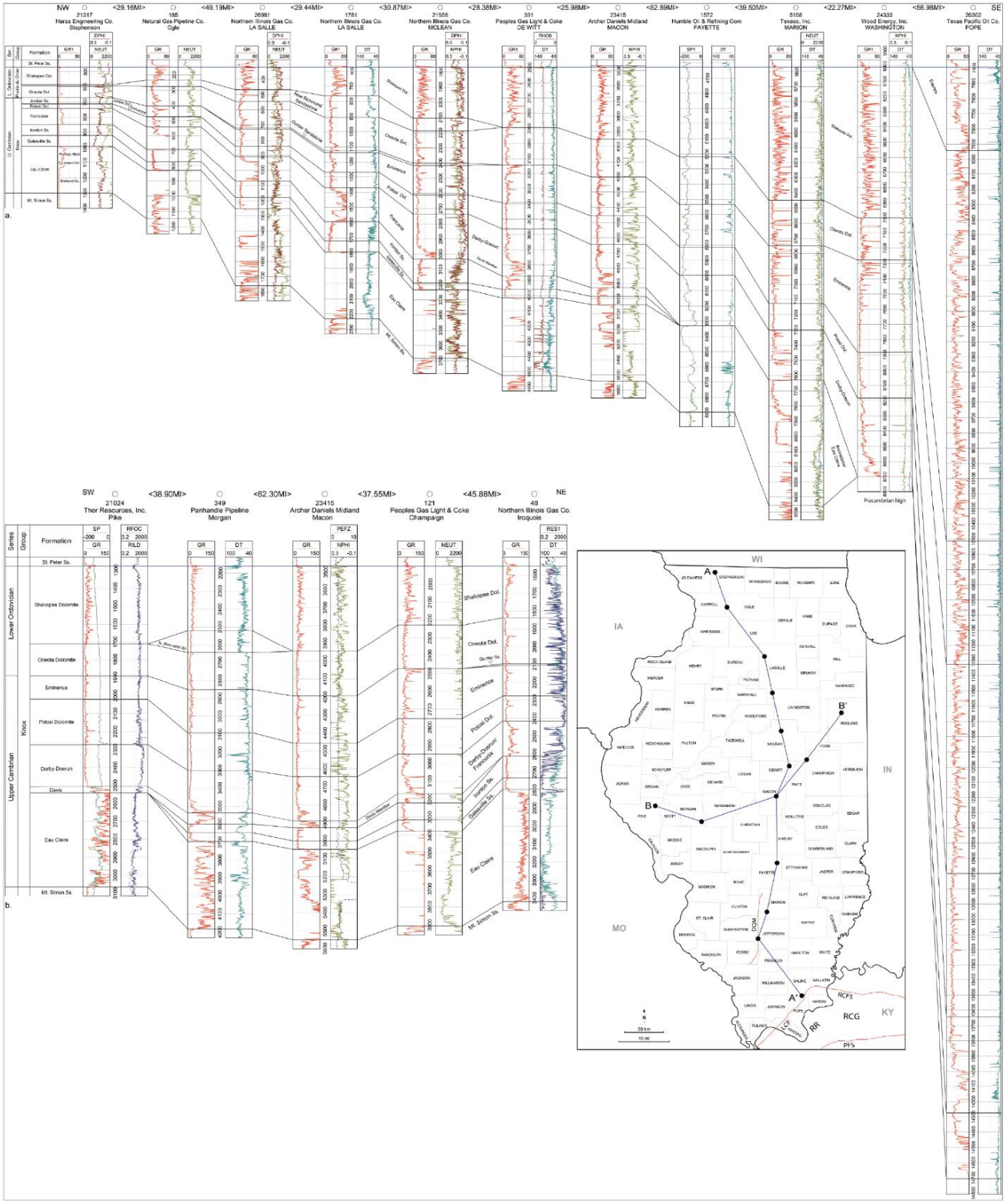

Figure 3-1-6 Stratigraphic cross sections of the Cambro-Ordovician Knox group showing lateral and vertical thickness variations through the Illinois Basin (Lasemi and Askari, 2014).

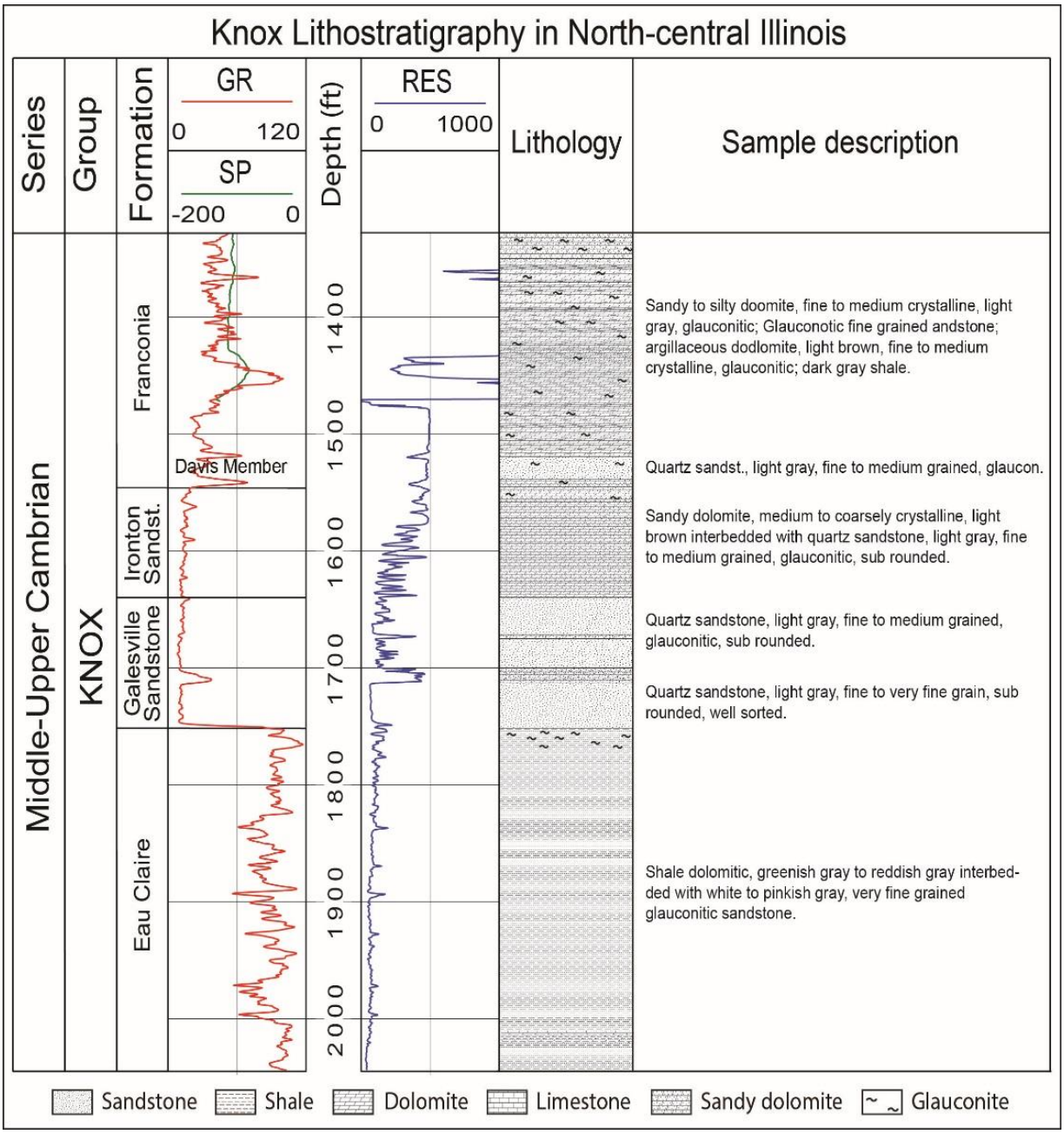

Figure 3-1-7 Type log of the Galesville and Ironton Sandstones in Northern Illinois, Gas Co. Fordyce No. 1, Livingston County (API number 121050026600; modified from Lasemi and Askari, 2014).

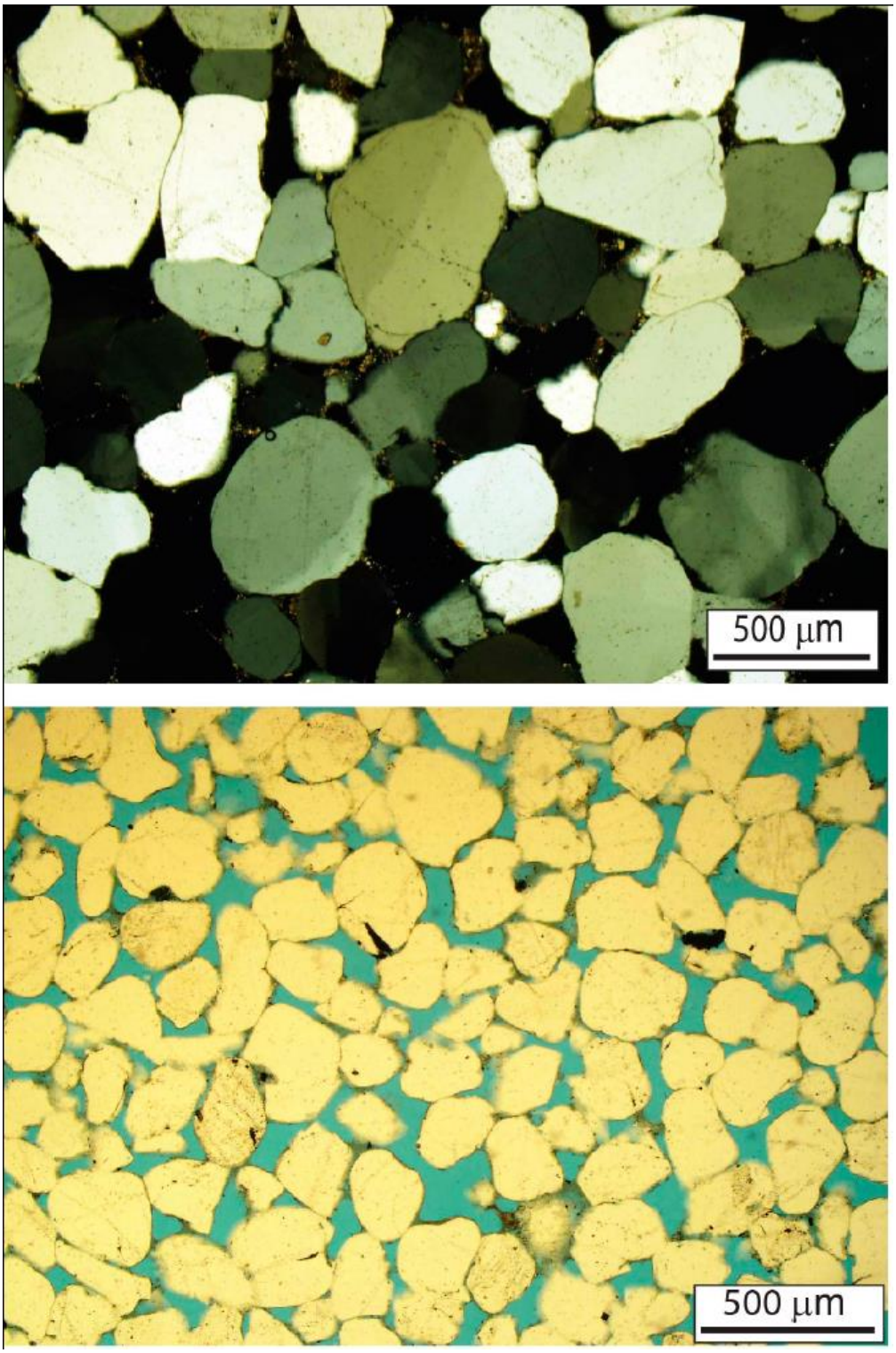

Figure 3-1-8 Photomicrographs of the Galesville Sandstone (from Lasemi and Askari, 2014). Top: Fine-grained quartz sandstone with quartz and dolomite cement under polarized light. Thin section photomicrograph from Peoples Gas Light & Coke Co., Lamb No.1, Dewitt County (depth 3,971 ft [1,210 m]; API number 120390039100). Bottom: Fine-grained porous quartz sandstone

under plane light. Photomicrograph from Northern Illinois Gas Co. Fordyce No. 1, Livingston County (depth 1,710–1,715 ft [521.2–522.7 m]; API number 121050026600).

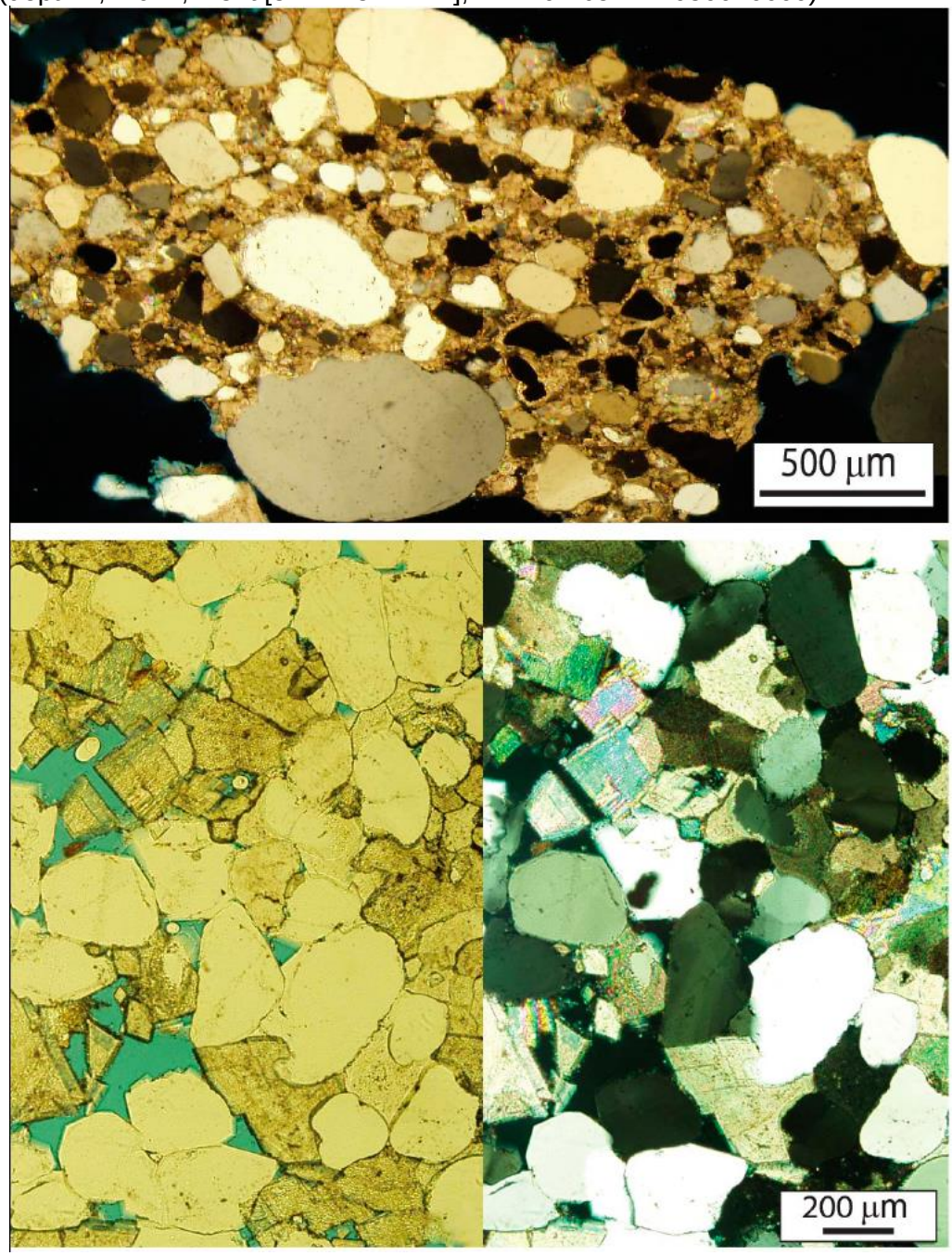

Figure 3-1-9 Photomicrographs of the Ironton Sandstone (from Lasemi and Askari, 2014). Top: Fine- to medium-grained quartz sandstone with dolomite cement under polarized light. Thin section photomicrograph from Vickery Drilling Co., Inc., Mathesius No.1, LaSalle County (depth 810–815 ft [246–248 m]; API number 120990103700). Bottom: Medium- to coarse-grained quartz sandstone under polarized and plane light. Note quartz cement and partial replacement of quarts by dolomite crystals. Thin section photomicrograph from ADM Co., CCS#1, Macon County (depth 4,970 ft [1,515 m]; API number 121152341500).

St. Peter Sandstone

The Middle Ordovician St. Peter Sandstone is an extensive quartz arenite unit that covers an area of 225,000 mi^2 (930,000 km^2; Figure 3-1-10) in the central part of the cratonic area of North America (Dapples, 1955). This widespread unit, exposed in northern Illinois, southern Wisconsin, and eastern Missouri, can be found in the subsurface through Ohio, western Kentucky, Illinois, Indiana, Kansas, and Nebraska (Droste et al., 1982; Hoholick et al., 1984). In the Michigan and Illinois Basins, the pure St. Peter Sandstone can be traced from few outcrops in the northern parts to depths below the surface in excess of 11,000 ft (3,350 m; Dapples, 1955; Willman et al., 1975; Catacosinos and Daniels, 1991; Barnes and Ellett, 2014).

Geologic and Stratigraphic Setting

The St. Peter Sandstone in the Illinois Basin is the basal part of the Ancell Group (Figure 3-1-11; Templeton and Willman, 1963) and Tippecanoe sequence (Sloss, 1963). Deposition of the Tippecanoe sequence began with a rise of sea level and a marine transgression of the Middle Ordovician siliciclastic rocks over Cambrian successions in the southern parts of the proto-Illinois Basin. During the Middle Ordovician, the Illinois Basin was situated near the equator, and sediments were exposed to both equatorial and arid climates (Kolata and Noger, 1991). The Ancell Group consists of siliciclastic rocks in the lower part, grading upward into an argillaceous and sandy limestone and dolomite formations (Figure 3-1-10; Collinson and Atherton, 1975; Droste et al., 1982; Kolata and Noger, 1991). The basal part of the St. Peter Sandstone predominantly consists of fine to coarse, uniformly well-sorted and well-rounded sandstones that are generally friable (Dapples, 1955; Collinson and Atherton, 1975; Hoholick et al., 1984; Barnes and Ellett, 2014) and was probably deposited by a northward advancing sea across the Illinois Basin (Dapples, 1955; Kolata and Noger, 1991). Except in some localities, the St. Peter Sandstone is very pure, free from carbonate and clay minerals (Collinson and Atherton, 1975).

The horizontal bedding is one of the most common sedimentary structures of the St. Peter Sandstone; however, some beds show low-angle cross-bedding (Lamar, 1928; Willman and Payne, 1943; Buschbach, 1964). The lower boundary of the St. Peter Sandstone is a major pronounced unconformity (Collinson and Atherton, 1975; Droste et al., 1982; Kolata and Noger, 1991) and is marked by a marine transgression over the Cambrian Franconia Formation (Collinson and Atherton, 1975). The St. Peter Sandstone is commonly overlain conformably by the Glenwood Shale in northern Illinois, by the Joachim Dolomite in central Illinois, and by the Duchtown Limestone in southern Illinois (Collinson and Atherton, 1975). In Indiana, evidence from sparse conodont fauna found in the St. Peter Sandstone suggests a Chazyan age (Droste et al., 1982).

The St. Peter Sandstone is divided into three members that includes, in ascending order (Figure 3-1-11), the Kress, the Tonti, and the Starved Rock members (Templeton and Willman, 1963). The Kress Member locally exists in some areas as a rubble or conglomerate of chert in a clay or sand matrix and at other places is mainly an argillaceous sandstone along with green and red shale (Buschbach, 1964). The Tonti Member is dominantly a fine-grained, well-sorted, friable, and highly porous sandstone and constitutes by far the greater part of the St. Peter Sandstone (Templeton and Willman, 1963). The Starved Rock Sandstone, the uppermost member, is dominantly a cross-bedded, medium-grained sandstone and not as thick as the Tonti Member (Templeton and Willman, 1963; Collinson and Atherton, 1975). The St. Peter Sandstone generally ranges from less than 100 to 200 ft (30.5 to 70 m) in thickness (Figure 3-1-12). Its maximum thickness occurs in northern Illinois where it locally thickens to more than 300 ft (91.4 m); however, the thickness of the formation decreases eastward and southward through the basin

(Dapples, 1955; Collinson and Atherton, 1975). Figure 3-1-13 shows a west-to-east cross section of the Cambro-Ordovician strata in the Illinois Basin.

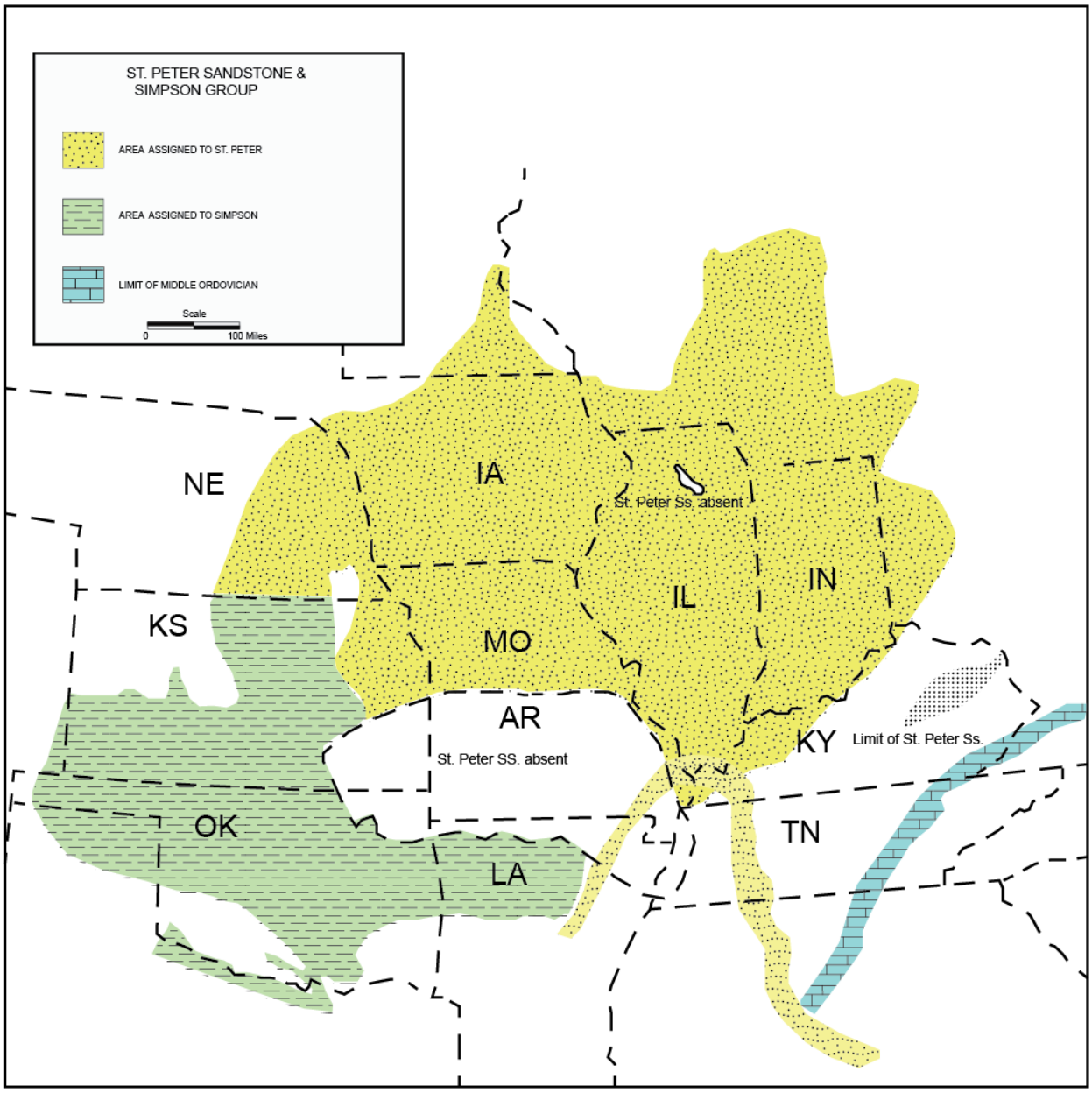

Figure 3-1-10 Areal distribution of St. Peter Sandstone and Simpson Group (modified from Dapples, 1955; AAPG©1963, reprinted by permission of the AAPG whose permission is required for further use).

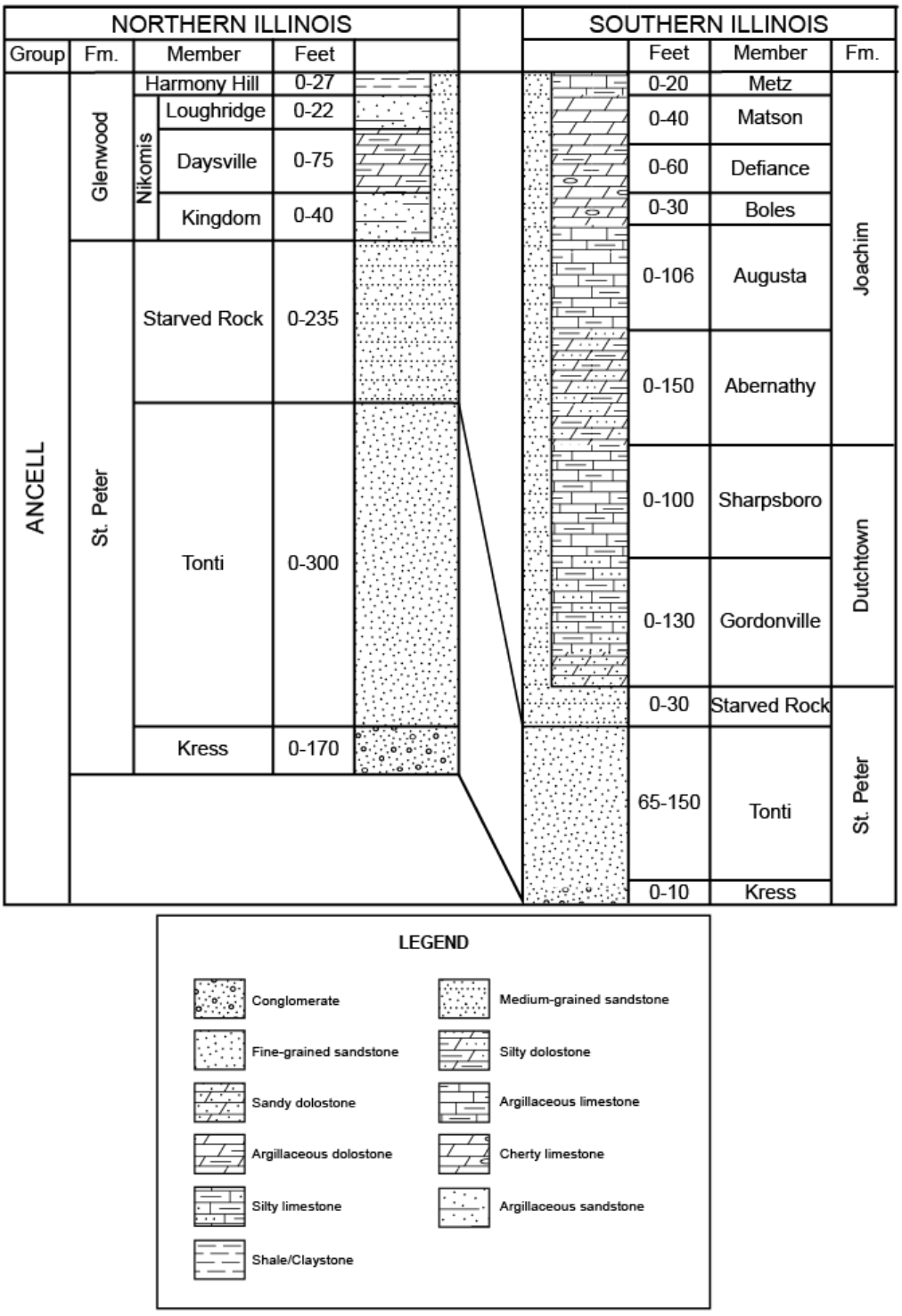

Figure 3-1-11 Columnar section of the Ancell Group (after Templeton and Willman [1963] in Willman and Buschbach [1975]; ©1975 University of Illinois Board of Trustees. Used by permission of the Illinois State Geological Survey).

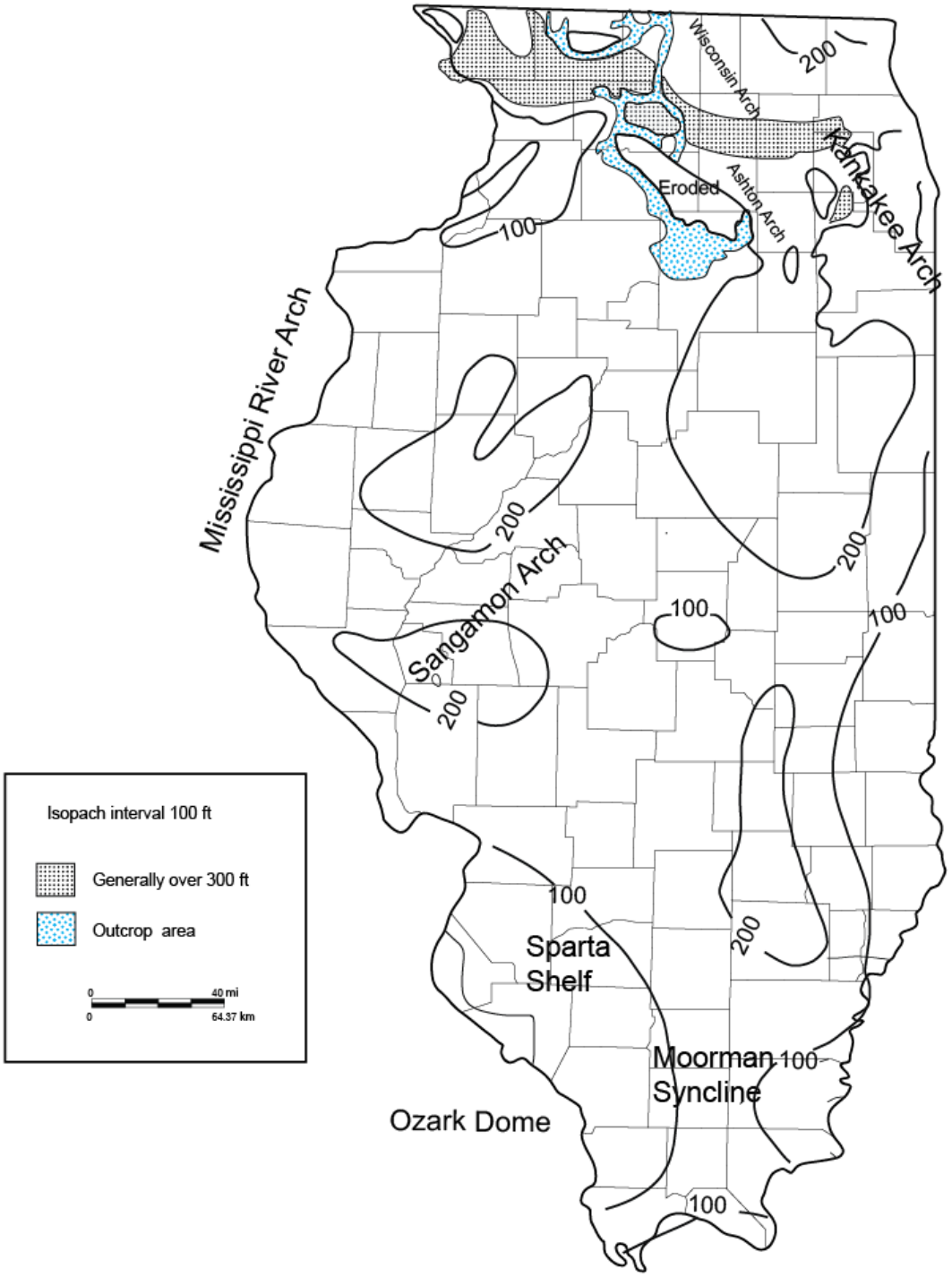

Figure 3-1-12 Thickness of St. Peter Sandstone in Illinois (modified from Collinson and Atherton, 1975; ©1975 University of Illinois Board of Trustees. Used by permission of the Illinois State Geological Survey).

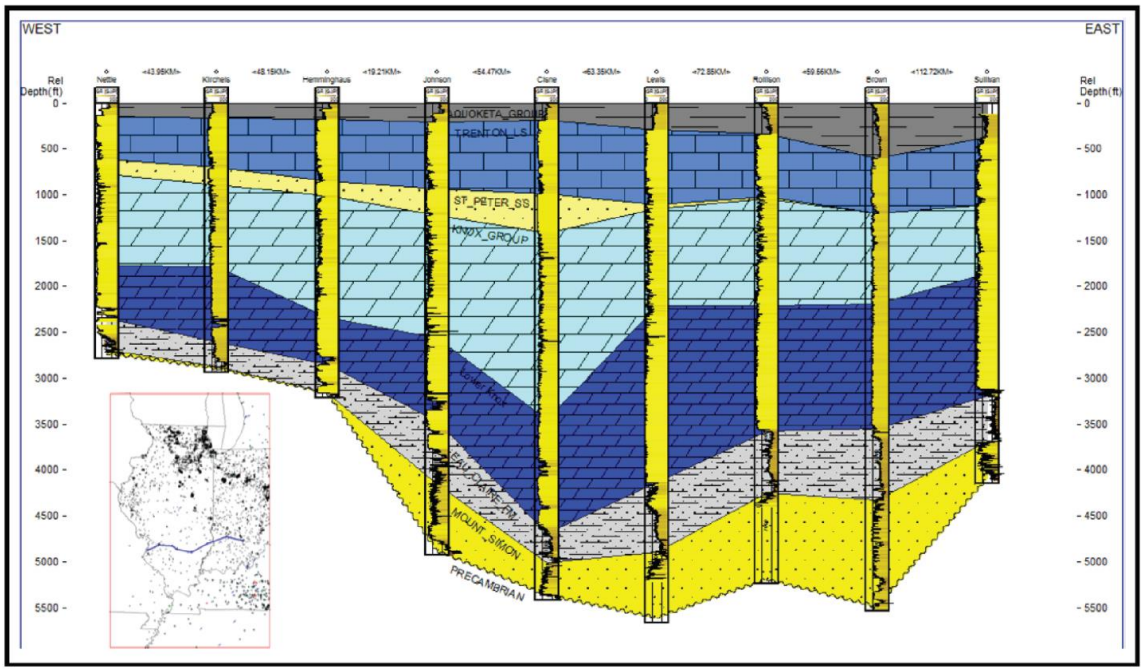

Figure 3-1-13 West-to-east cross section of the Cambro-Ordovician strata in the Illinois Basin (Barnes and Ellett, 2014).

Porosity Evolution and Regional Cement Variations

A sequence of diagenetic events has affected the deeply buried St. Peter Sandstone, resulting in development of secondary porosities and a variety of cement types. Primary porosity is dominant from outcrops to the deep subsurface at a depth of 4,000 ft (1,219 m), whereas secondary porosity generally occurs at depths greater than 4,000 ft (1,219 m). Primary porosity is the intergranular pore space preserved and retained after deposition of the sediments. The secondary porosities are in the form of dissolved authigenic cement and grain framework, fractures, and shrinkage cracks (Schmidt and McDonald, 1979; Hoholick et al., 1984).

The average porosity ranges from 14% to 18% and the permeability ranges from 150 to 400 mD (0.148–0.395 μm) in different fields within the basin (Leetaru, 2014). Successful natural gas storage projects and water production in the St. Peter Sandstone are reliable evidence supporting high reservoir quality (Leetaru, 2014). The St. Peter reservoir model for IBDP was updated in 2014 and utilized data from available geophysical logs and a three-dimensional seismic survey (Will et al., 2014). Reservoir simulations showed that the St. Peter may be capable of accommodating CO_2 at a rate of 3.5 million tons (3.2 million tonnes) per annum (MTPA) for 30 years (Leetaru, 2014).

Results of porosity and permeability measurements obtained from core analysis show a moderate correlation between porosity and permeability (Figure 3-1-14) in the Illinois Basin (Barnes and Ellett, 2014). The porosity values reveal a trend of considerable decrease with increasing depth. However, other factors, such as the depositional environment and type of diagenetic events, played a major role in increasing or decreasing reservoir properties (Barnes and Ellett, 2014).

The principal diagenetic cements observed in the St. Peter Sandstones are calcite, dolomite, anhydrite, chalcedony, chlorite, and quartz overgrowth. The distribution of cement types generally correlates with geographical regions and depth in the Illinois Basin (Hoholick et al., 1984).

Chalcedony cement is restricted to very shallow depths in northern Illinois. Calcite cementation considerably affected the St. Peter Sandstone in northern Illinois outcrops and in the subsurface, at shallow to moderate burial depths. Dolomite cement occurs in central parts of the region, separating the calcite cement zones in northern and southwestern Illinois. Anhydrite cement exists in deep burial depth in southern Illinois (Hoholick et al., 1984; Pitman et al., 1997).

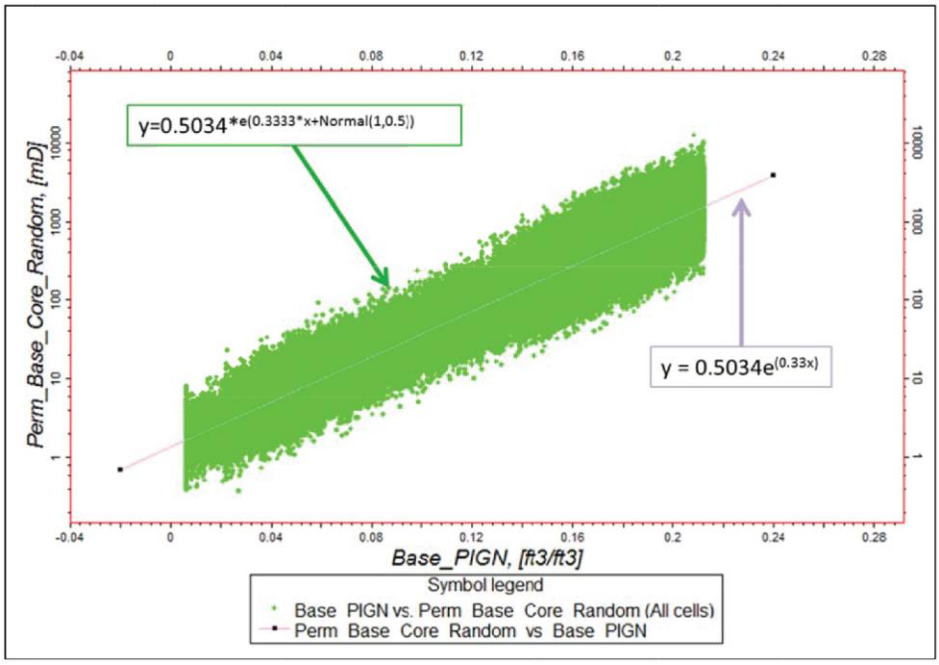

Figure 3-1-14 Relationship of porosity and permeability from core analysis (Will et al., 2014).

Potosi Dolomite

The Potosi Dolomite is a widespread unit in the subsurface of Illinois, except in the northern parts, where it was removed by sub-Tippecanoe erosion (Buschbach, 1975). It is a pure dolomite and regionally equivalent to the lower part of the Potosi in Indiana (Shaver et al., 1986), Trempealeau Formation of Michigan (Catacosinos et al., 1990), St. Lawrence Formation of Wisconsin and Minnesota (Mossler, 2008), and a portion of the Copper Ridge Dolomite in Kentucky and Ohio (Greb et al., 2012). The Potosi Dolomite is conformably underlain by the sandstone and sandy dolomite of the Franconia Formation and overlain by the Eminence Formation. The overlying Eminence Formation is composed principally of sandy, fine- to medium-grained dolomite that contains abundant chert and green clay and is interbedded with thin sandstone beds (Lasemi and Askari, 2014; Sargent, 1991).

Stratigraphic Setting

The deposition of the Potosi Dolomite occurred within the period of the upper Sauk Sequence (Sloss, 1963), as the relative sea level rose and the shoreline advanced across the Illinois Basin (Sargent, 1991). The boundary of the underlying Franconia Formation and the Potosi Dolomite is transitional and marked by a change in lithofacies from siliciclastics to carbonates (Buschbach, 1975). In general, the underlying Franconia Formation in northern Illinois is dominantly argillaceous sandstone and sandy dolomite, containing variable amounts of red and green shale (Buschbach, 1975). However, the Potosi overlies the Franconia equivalent, Derby-Doerun Formation in southern Illinois and consist mainly of dolomite.

The Potosi Dolomite is composed of thick to massively bedded, pure to slightly argillaceous dolostone intervals, characterized by fine- to medium-dolomite crystal sizes and large vugular porosity (Freiburg and Leetaru, 2012). The sedimentary facies of the Potosi Dolomite is dominated by subtidal and intertidal facies and the depositional setting differs from those of the underlying Franconia and overlaying Eminence Formations (Leetaru et. al., 2014). Because of its low reservoir quality, the dense dolomite intervals of the Knox Group would serve as one of the primary seals for the Potosi Dolomite, to effectively prevent horizontal and vertical migrations of injected carbon dioxide (Lasemi et. al., 2012).

Thickness Trend, Lithofacies, and Reservoir Properties

The thickness of the Potosi Dolomite is quite variable, ranging from 50 ft (15 m) in the northern parts of Illinois to over 900 ft (274 m) in the southern part (Lasemi and Askari, 2014) (see Figure 3-1-6 in the Ironton-Galesville section). In the northeast part of the Illinois Basin, the Potosi Dolomite was truncated by pre-Tippecanoe erosion along the Kankakee arch. Similar to other Phanerozoic dolomite successions, the original lithology of the Potosi Dolomite was limestone that was later replaced by secondary dolomite. All carbonate grains of the precursor limestone have been destroyed because of dolomitization. Only relics of original carbonate grains, including peloids, ooids, and bioclasts, are rarely recognized (Figure 3-1-15) suggesting deposition in a shallow marine environment. As a result of dolomitization of limestone, secondary intercrystaline and moldic porosity develops, leading to intercrystalline porosity enhancement and formation of reservoir rocks. In the Potosi Dolomite, however, intercrystalline and moldic porosity was later destroyed because of continuous dolomitization and crystal overgrowth (Figure 3-1-15). Secondary porosity in the Potosi Dolomite includes fracture, cavernous, and dissolution voids and development of pore-lining drusy quartz (Figure 3-1-15).

The principal diagenetic processes observed in the Potosi Dolomite, therefore, include replacement of limestone by secondary dolomite, extensive fracturing, dissolution, brecciation, and silica cementation. The precipitation of pore-lining dolomite cement, along with chalcedony and mega-quartz cements, inhibited pore-filling diagenetic cements and preserved the secondary porosities (Buschbach, 1975; Freiburg and Leetaru, 2012). In places, however, extensive silica cementation resulted in reduction or loss of porosity (Figure 3-1-15). In central and northern Illinois, accurate porosity data of some intervals of the Potosi Dolomite have not been acquired from wireline logs because of very large caves and the complete loss of drilling fluid circulation (Bell et al., 1964; Leetaru et al., 2014). More than a thousand barrels of fluid loss during drilling has been reported. Freiburg and Leetaru (2012) and Leetaru (2014) had proposed that the major porous zones in the Potosi Dolomite are related to regional Knox unconformity and vadose or phreatic karstification processes, which developed during subaerial exposure at the top of the Eminence Formation. This interpretation, however, is questionable because the upper boundary of the Eminence Formation lacks any evidence of karstification and, as indicated above, the contact between the Potosi and the overlying Eminence is conformable.

The lost circulation zones and formation micro-image (FMI) log confirm very porous and highly permeable intervals. Formation micro-image logs of a drilled well at the IBDP (Figure 3-1-16) reveal intervals up to 7 ft (2.1 m) thick with very large pore spaces (Adushita and Smith, 2014). The seismic inversion data also shows a lost circulation zone representing a high-permeability pathway between three wells at the IBDP (Adushita and Smith, 2014; Figure 3-1-17). The low-porosity Knox dolomite units overlie the Potosi Dolomite and may act as a flow barrier (Lasemi et. al., 2012; Lasemi and Askari, 2014). Locally, the overlying Knox dolomite units may have fractures and do not provide a reliable seal to underlying flow units. However, in this case,

the overlying Maquoketa Shale, which is commonly more than 100 ft (30.5 m) thick and present throughout the Illinois Basin, may serve as an effective seal for the injected fluids in the Potosi Dolomite. The high reservoir quality of the Potosi Dolomite has been established from a chemical waste disposal project at Tuscola, Illinois. This disposal project has already injected over 55 million tons (50 million tonnes) of CO_2 equivalent in liquid chemical waste into the Potosi Dolomite (Leetaru, 2014). Reservoir simulations conducted for the IBDP show that the Potosi Dolomite may be capable of accommodating CO_2 at a rate of 3.5 million tons (3.2 million tonnes) per annum (MTPA) for 30 years (Smith, 2014).

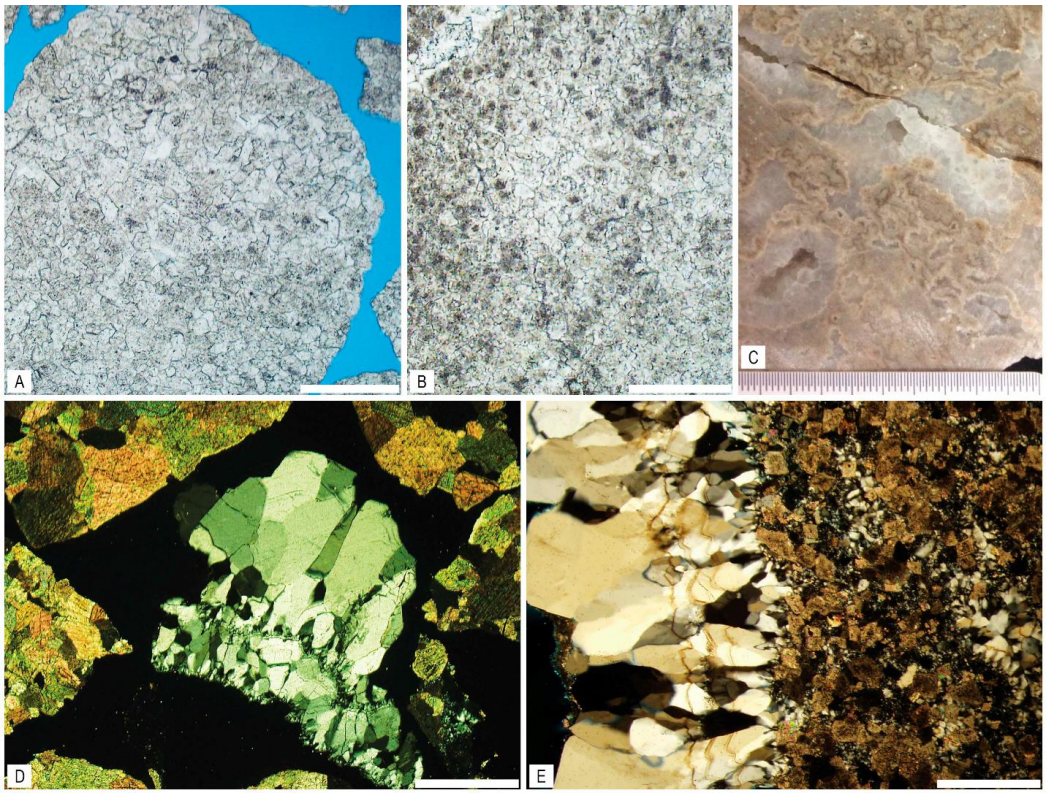

Figure 3-1-15 Photomicrographs of the Potosi Dolomite. (A and B): Photomicrographs under normal light showing dense medium to coarsely crystalline dolomite having no intercrystalline porosity (scale bars are 0.5 mm [0.02 in.]). The samples are from Layne Western Co., Inc. Dupage County (depth, 329.2 m [1,080 ft]; API number 120430135000). (C): Cavity filling fine to coarse quartz crystals (light color) and dolomite (light brown). Note that quartz cement (drusy quartz) in the cavities has resulted in loss of porosity. The core sample photograph is from Lanye Christensen, Exploratory Borehole #4, St. Louis County, MO (depth, 792.2 m [2,599 ft]; scale in millimeters). (D): Photomicrograph of well samples under plane polarized light showing chips of dolomite and drusy quartz (elongate fine to coarse crystals developed on dolomite) in the center of the photograph (scale bar 0.5 mm [0.02 in.]). The samples are from Layne Western Co., Inc. Dupage County (depth, 309.4 m [1,015 ft]; API number 120430135000). (E): Photomicrograph of well samples under plane polarized light showing enlarged chips of dolomite and drusy quartz (scale bar 0.5 mm [0.02 in.]). Note dolomite in the right side of the photomicrograph that is partially silicified, changing to elongate fine to coarse crystals of drusy quartz in the left. The samples are from the Northern Illinois Gas Co. Fordyce No. 1, Livingston County (depth, 382.5 m [1,255 ft]; API number 121050026600).

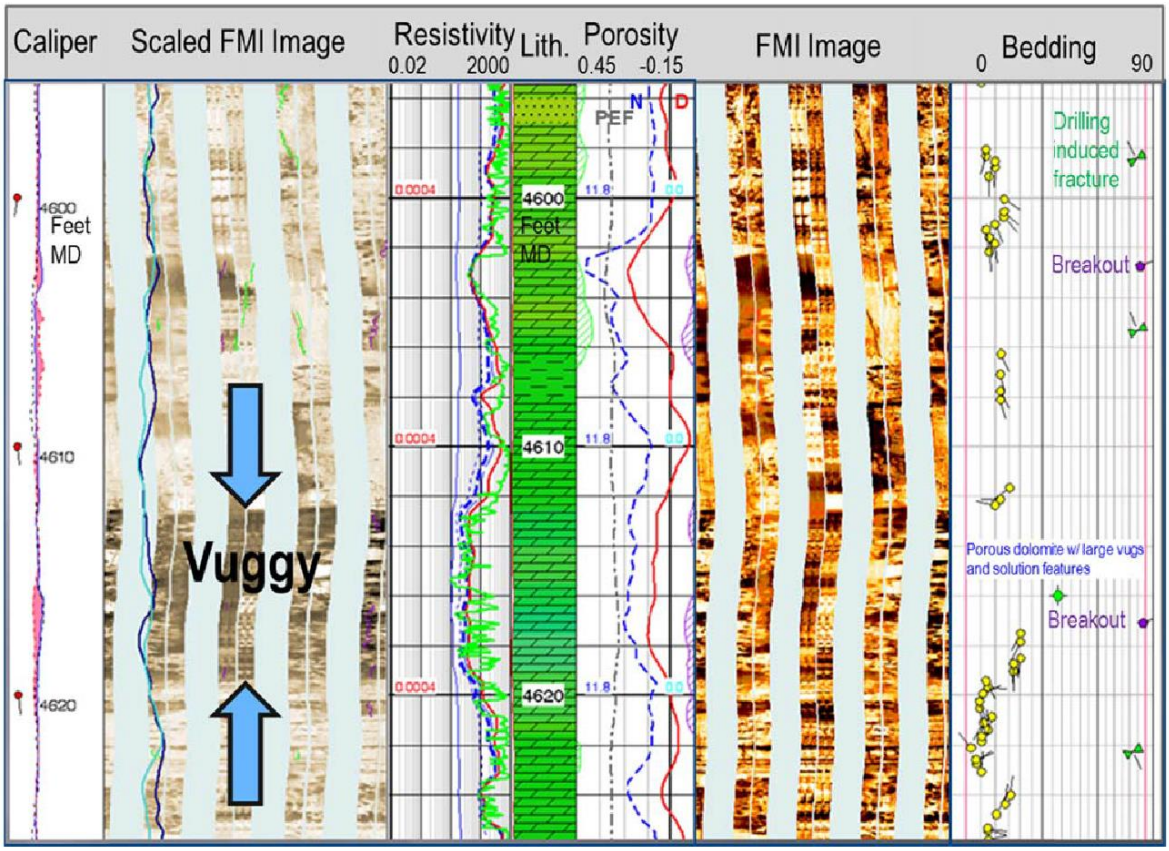

Figure 3-1-16 The FMI log of verification well #2 (VW#2) at the IBDP showing vuggy intervals within the Potosi Dolomite (Adushita and Smith, 2014).

Mt. Simon Sandstone and Eau Claire Formation

The Mt. Simon Sandstone is a distinctive unit in the subsurface of Illinois, Iowa, Indiana, Kentucky, Michigan, and Ohio (Figure 3-1-1; Barnes et al., 2009) and correlative units crop out in southeastern Missouri, southern Wisconsin, and southeastern Minnesota (Leetaru and McBride, 2009). The Mt. Simon Sandstone is conformably overlain by the Eau Claire Formation (Buschbach, 1975; Treworgy et al., 1997; Neufelder et al., 2012; Freiburg et al., 2014) that acts as barrier to flow throughout the Illinois Basin (Leetaru et al., 2009).

Geologic and Stratigraphic Setting

In the Illinois Basin, the Mt. Simon Sandstone and its overlaying Eau Claire Formation were deposited during Upper Cambrian time and constitute the lower part of the Sauk Sequence (Sloss, 1963).

The range and distribution of the Middle Cambrian sedimentary sequence of the Illinois Basin was associated with a rift system (Houseknecht and Weaverling, 1983). By late Cambrian time, the depositional setting of the Illinois Basin transformed from a rift system to a broad cratonic embayment (Kolata and Nelson, 1997). Simultaneously, the sea level began to rise and the bulk of the Mt. Simon Sandstone was deposited on Precambrian basement rocks (Sargent, 1991). As relative sea level continued to rise, the carbonates and mudstones of the Eau Claire Formation were deposited on the Mt. Simon Sandstone throughout the Illinois Basin and serve as a regional caprock zone to the more porous and permeable Mt. Simon (Leetaru et al., 2009; Person et al., 2010).

The Mt. Simon is predominately a submature to mature quartz arenite unit, interbedded with thin layers of feldspathic sandstone and shale, especially toward the top of the Mt. Simon. The grain size and the texture of Mt. Simon Sandstone varies from well sorted and rounded, coarse grained to poorly sorted, subangular, and fine to medium grained (Leetaru and Freiburg, 2014; Freiburg et al., 2014). The source of the basal part of the Mt. Simon Sandstone is believed to derive from Precambrian rocks of the Canadian Shield (Ojakangas, 1963; Buschbach, 1975; Houseknecht and Ethridge, 1978). The Mt. Simon Sandstone strata are dominated primarily by fluvial, eolian, and shallow subtidal marine deposits (Freiburg et al., 2014). The Mt. Simon Sandstone rests unconformably on the Precambrian granite-rhyolite basement (Morse and Leetaru, 2005; Sargent, 1991); the Eau Claire Formation conformably overlies the Mt. Simon.

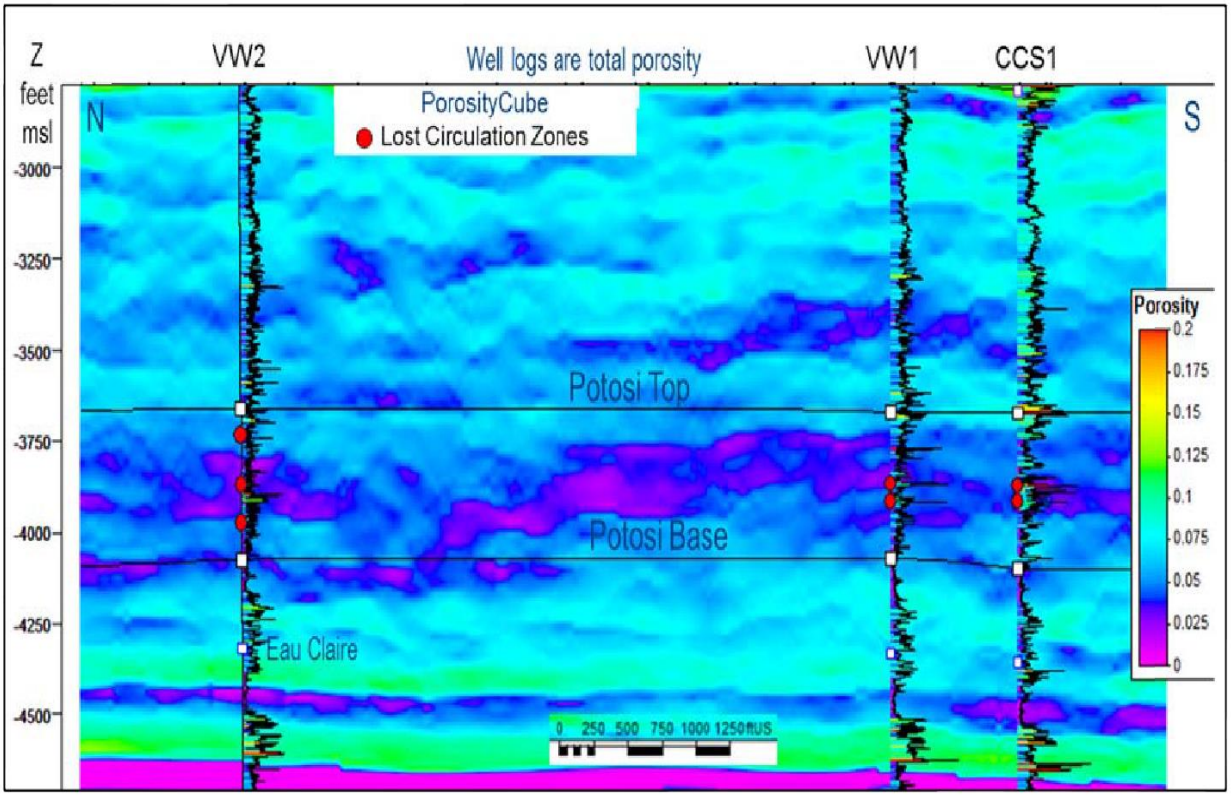

Figure 3-1-17 PorosityCube line through three wells at the IBDP. High-porosity trends within the PorosityCube correlate with lost circulation zones observed in wells (Adushita and Smith, 2014).

Deposition of the Eau Claire Formation occurred within a shallow marine to intertidal depositional setting (Palkovic, 2015). In the Illinois Basin, the basal part of the Eau Claire Formation consists primarily of a silty, argillaceous sandy dolomite or dolomitic sandstone in the northern part, changing to a siltstone or shale in the central part and a mixture of dolomite and limestone in the southern part (Leetaru and McBride, 2009). The basal portion of the Eau Claire Formation is a persistent shale in the central part of the Illinois Basin, where it acts as a caprock for the underlying strata. The Eau Claire Formation is overlain unconformably by upper Cambrian Ironton-Galesville sandstones (Kolata, 2010; Freiburg et al., 2014).

Thickness Trend, Lithofacies, and Reservoir Properties

The thickness of the Mt. Simon Sandstone is variable across the Illinois Basin, ranging from less than 500 ft (150 m) in southwestern Illinois to over 2,500 ft (762 m) in the northeast

(Buschbach, 1975; Morse and Leetaru, 2005; Figure 3-1-18). The Mt. Simon Sandstone does not exist south of the Rough Creek Graben, where it pinches out and grades to lithofacies consisting of deep marine shale and carbonates (Nelson, 1991). A structure contour map on the top of the Mt. Simon Sandstone (Figure 3-1-19; MGSC, 2005) shows that the formation dips to the south and southeast of the Illinois Basin.

The Mt. Simon Sandstone is overlain by dolomite and dolomitic sandstone of the Eau Claire Formation throughout all of Illinois. The thickness of the Eau Claire Formation generally ranges from 300 ft (91 m) in the western part to over 1,000 ft (304 m) in the southeast (Figure 3-1-20; Buschbach, 1975). The Eau Claire Formation acts as a regional caprock zone for the Mt. Simon Sandstone because of its low reservoir porosity and permeability (Leetaru et al., 2009; Person et al., 2010).

In north-central Illinois, the Mt. Simon Sandstone has been divided into seven members based on facies characteristics and the grain compositions (Templeton, 1950); however, just three upper members have been traced in northeastern Illinois (Buschbach, 1964). It has been proposed that the Mt. Simon Sandstone should be subdivided into three primary units, including Lower, Middle and Upper Mt. Simon Sandstone, reflecting different lithology, diagenetic events, log signatures, and eventually different reservoir qualities at the Illinois Basin–Decatur Project (Freiburg et al., 2014; Leetaru and Freiburg, 2014; Figure 3-1-21).

The pre-Mt. Simon has been identified as a confining zone between the Mt. Simon and Precambrian basement. It is characterized as a poorly-sorted sublithic arenite to quartz arenite (Figure 3-1-22) with 9% average porosity and 2.3 mD (0.002 μm) permeability.

The Lower Mt. Simon Sandstone primarily consists of fine- to coarse-grained feldspathic wacke to lithic wacke and conglomerate, and it contains the highest porosity and permeability of the Mt. Simon Sandstone. Most of the Lower Mt. Simon porosity is intergranular (Figure 3-1-22B). However, secondary porosity resulting from K-feldspar dissolution has been observed in the Lower Mt. Simon (Freiburg et al., 2014; Leetaru and Freiburg, 2014).

The Middle Mt. Simon Sandstone has been subdivided into two intervals: a lower and upper interval. The lower interval is composed of poorly sorted quartz arenite, quartz wacke, and feldspathic wacke (Figure 3-1-22) with thin interbedded mudstones. The upper interval is characterized by moderately well-sorted quartz arenite (Figure 3-1-22). Based on log evaluation and thin section studies, the porosity and permeability of the Middle Mt. Simon is moderately low (less than 10% porosity and 10 mD [0.010 μm] permeability) because of destructive diagenetic processes. High compaction and authigenic quartz cementation of the Middle Mt. Simon provide a moderate seal for the underlying Lower Mt. Simon Sandstone (Freiburg et al., 2014; Leetaru and Freiburg, 2014).

The Upper Mt. Simon Sandstone is composed of mudstone (Figure 3-1-22), poorly sorted arkose wacke, subarkose arenite, and well rounded, moderately sorted quartz arenite (Figure 3-1-22). The intergranular porosity is reduced to an average of 10% because of the filling of pores with authigenic cements, such as clay mineral, authigenic feldspar, and quartz overgrowth (Freiburg et al., 2014; Leetaru and Freiburg, 2014).

The Mt. Simon Sandstone has been targeted for a large-scale carbon capture and storage demonstration project, called the Illinois Basin–Decatur Project (IBDP). Three wells have been drilled at the storage site and the result shows that the Mt. Simon Sandstone has excellent reservoir quality and the ability to store carbon in the Illinois Basin. The Eau Claire Formation serves as a confining zone for the Mt. Simon Sandstone, and the overlaying Maquoketa Shale and New Albany Shale may provide additional seal intervals (Freiburg et al., 2014).

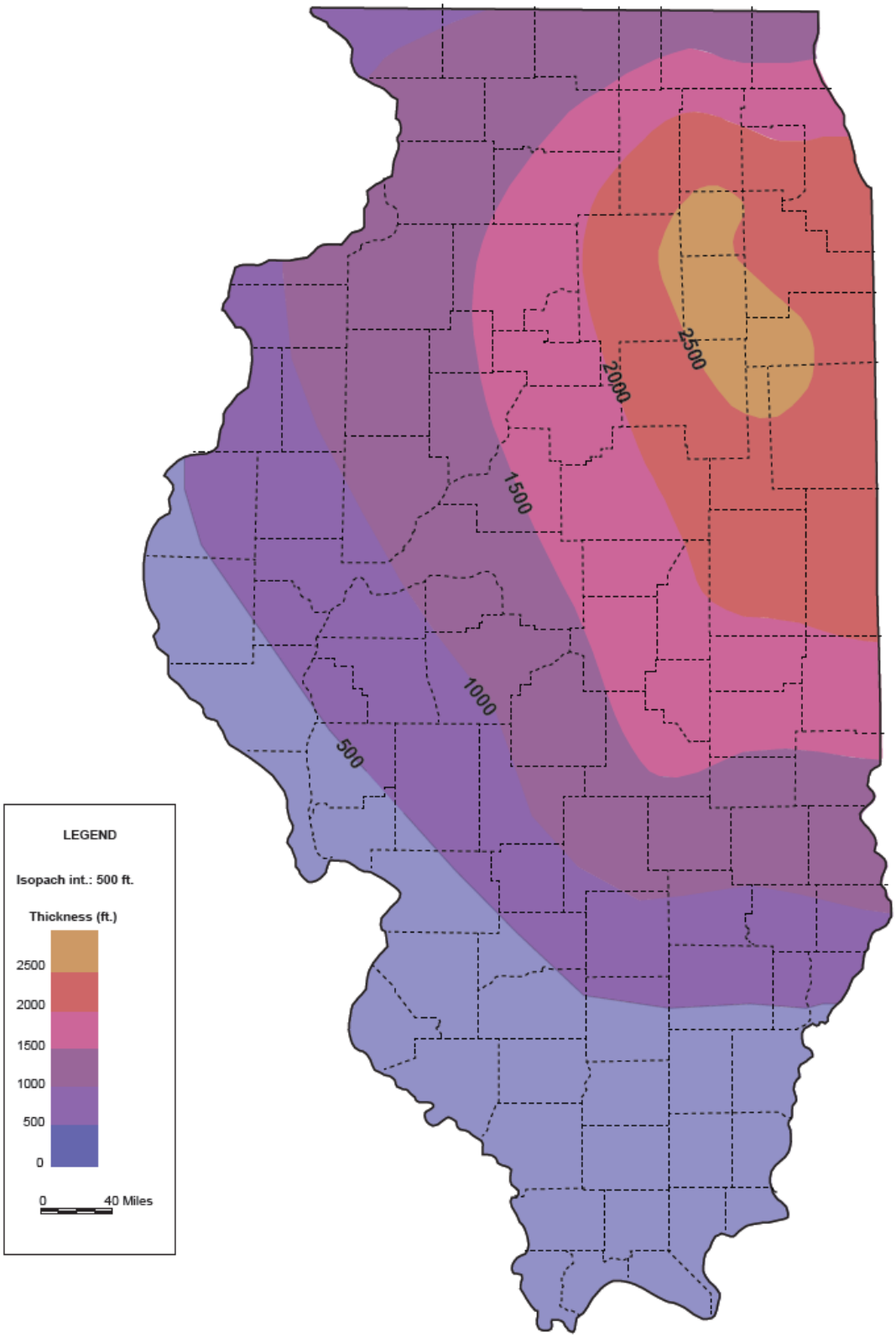

Figure 3-1-18 Thickness of the Mt. Simon Sandstone in the state of Illinois (modified from Buschbach, 1975; ©1975 University of Illinois Board of Trustees. Used by permission of the Illinois State Geological Survey).

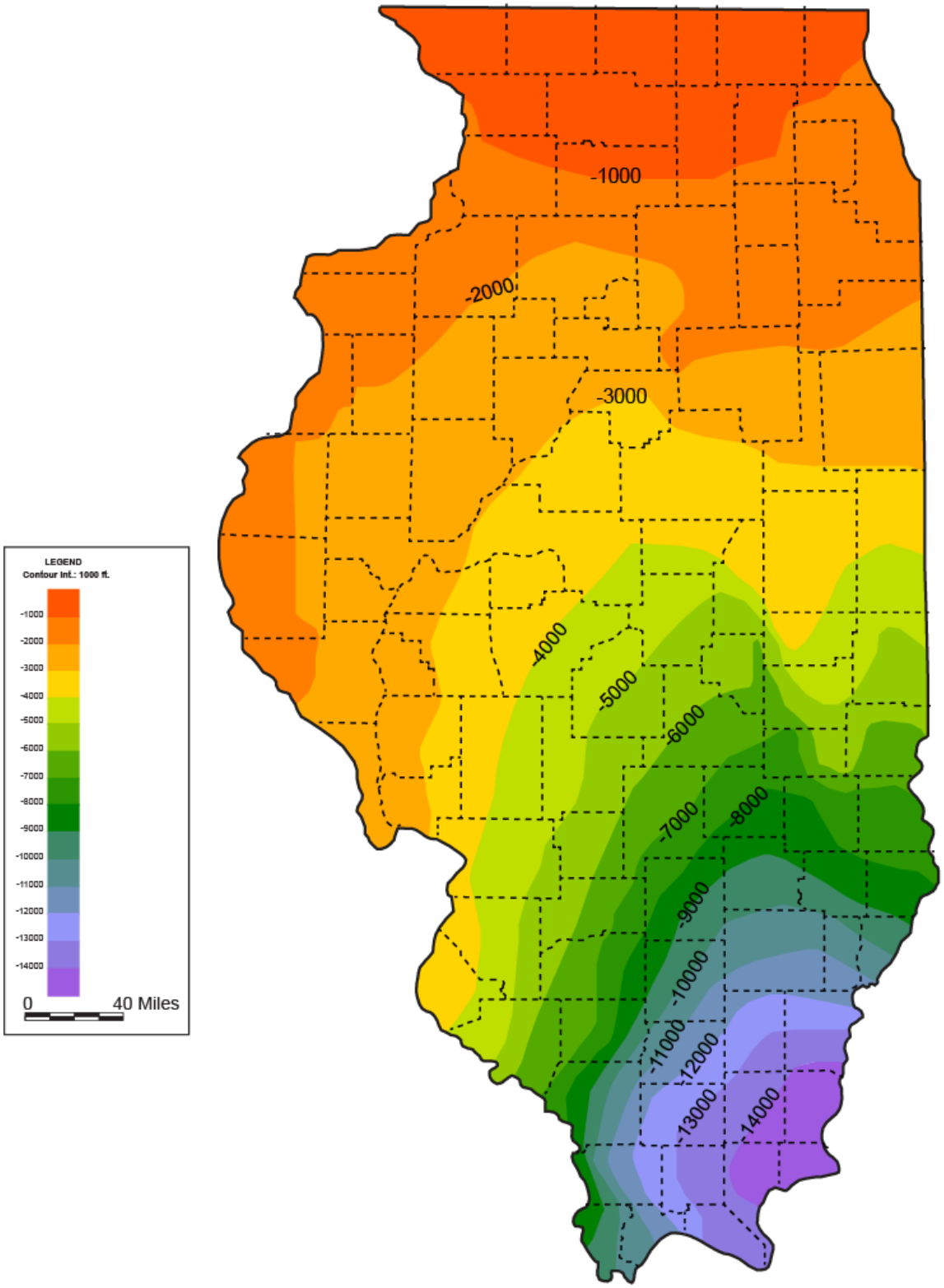

Figure 3-1-19 Structure map on the top of Mt. Simon Sandstone in the Illinois Basin (modified from MGSC, 2005).

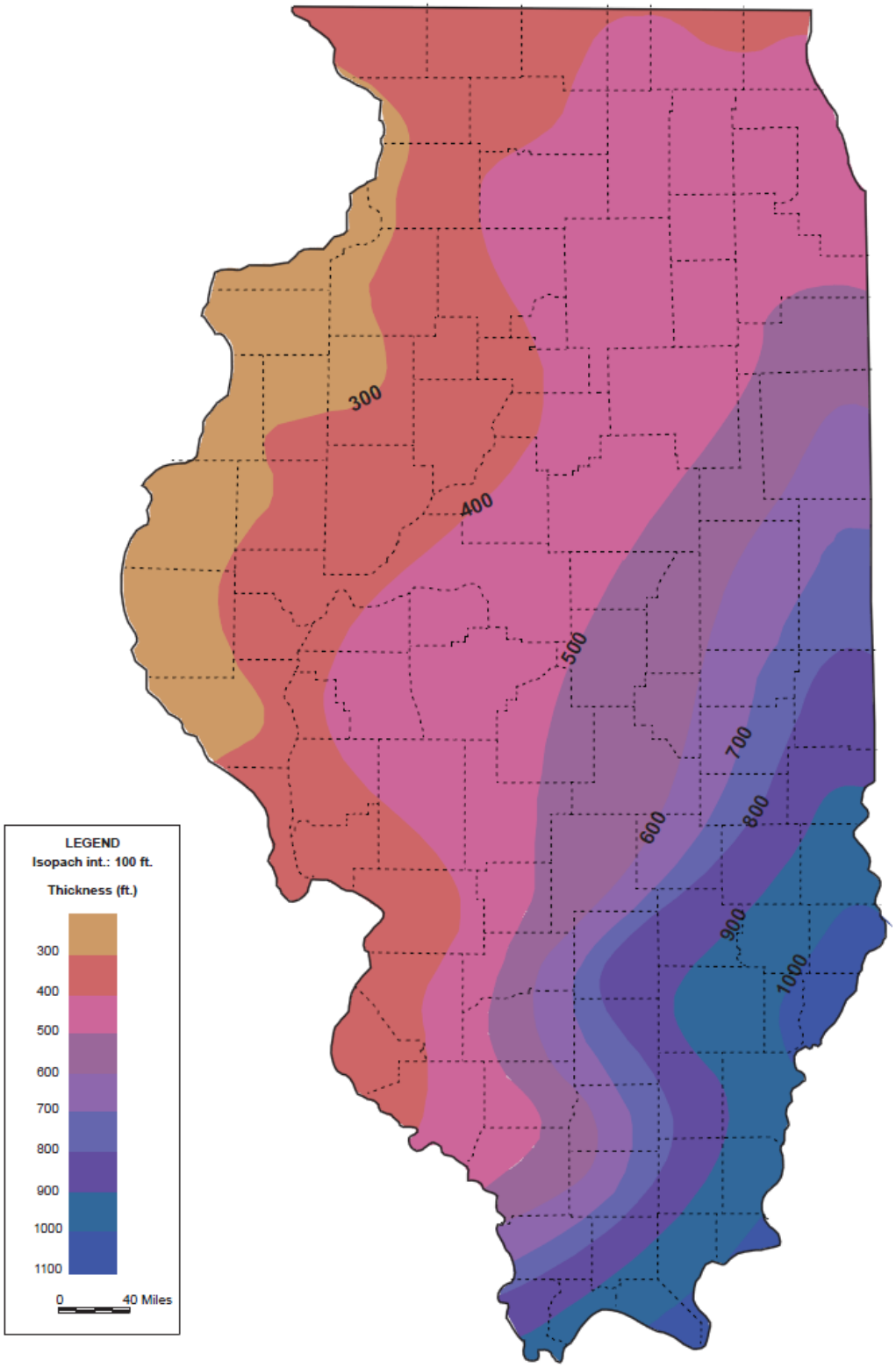

Figure 3-1-20 Thickness of the Eau Claire Formation in the state of Illinois (modified from Buschbach, 1975; ©1975 University of Illinois Board of Trustees. Used by permission of the Illinois State Geological Survey).

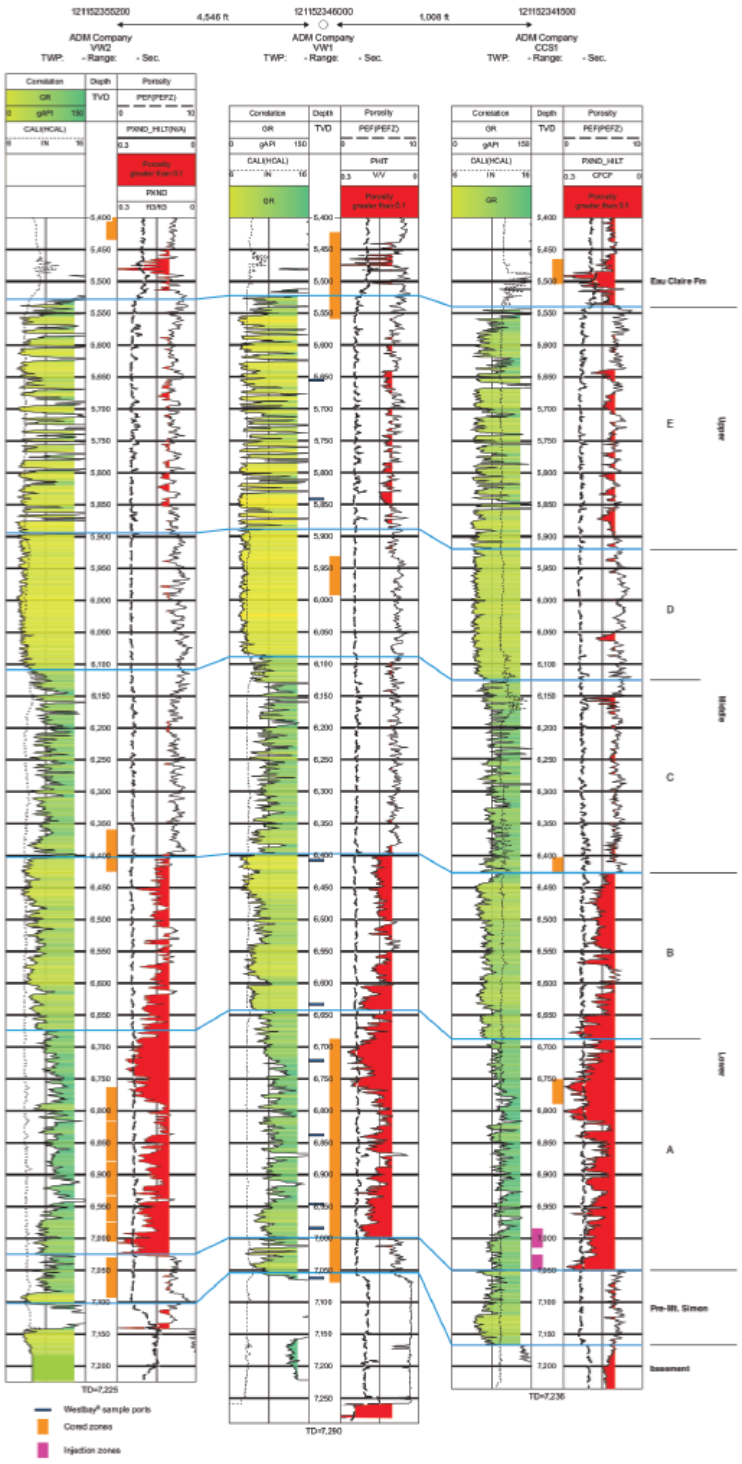

Figure 3-1-21 Geophysical logs from the CCS#1, VW#1, and VW#2 wells indicating the base of the Eau Claire Formation, the Mt. Simon Sandstone, the pre-Mt. Simon Sandstone, and the Precambrian basement (Freiburg et al., 2014; ©2014 University of Illinois Board of Trustees. Used by permission of the Illinois State Geological Survey).

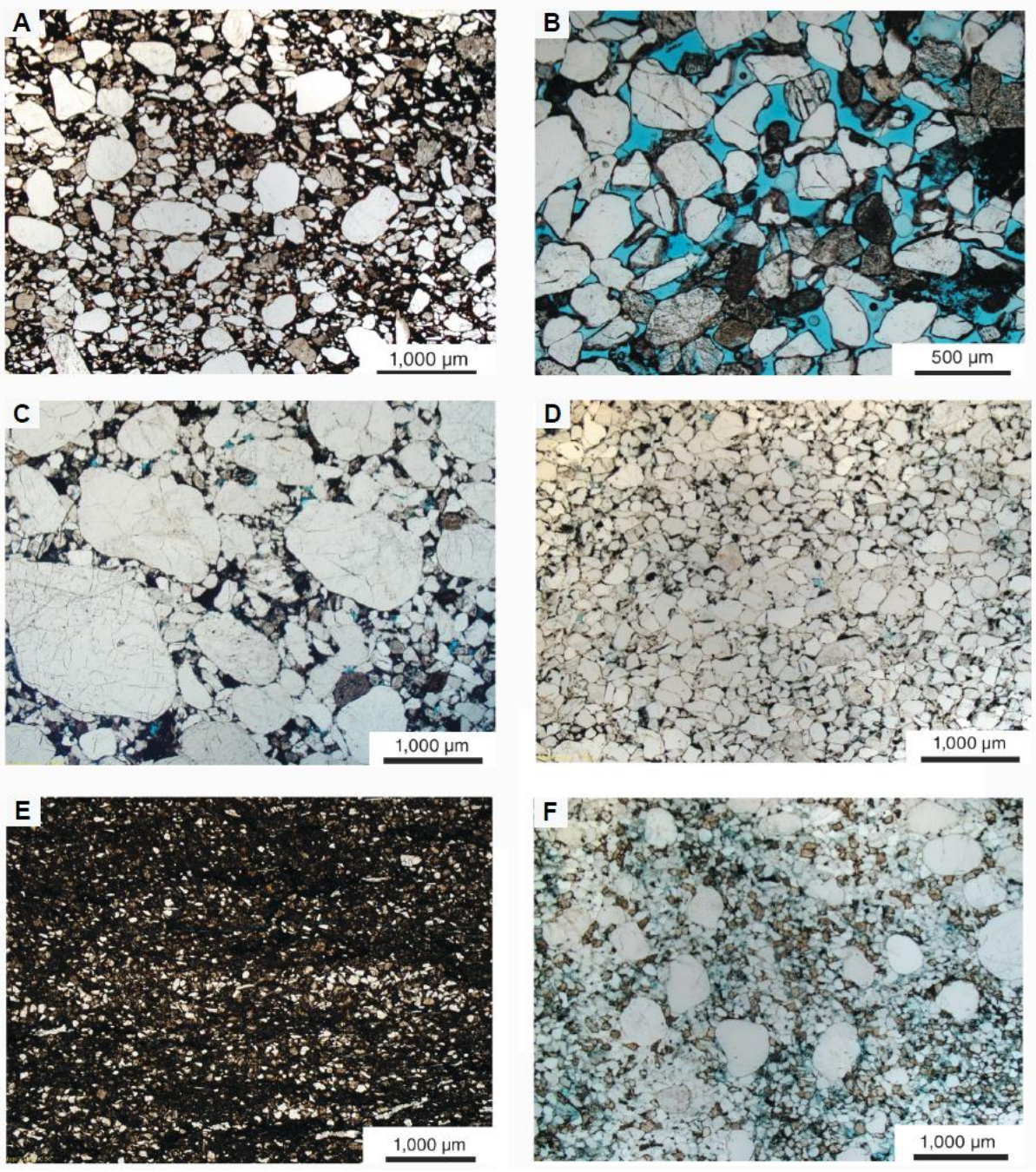

Figure 3-1-22 Thin section photographs of pre-Mt. Simon and Mt. Simon Sandstones. (A) A poorly sorted sublithic arenite with dense clay matrix of pre-Mt. Simon Sandstone. (B) A moderately well sorted subarkosic sandstone of Lower Mt. Simon Sandstone. (C) A poorly sorted bimodal quartz wacke of the lower portion of the Middle Mt. Simon Sandstone. (D) A moderately well sorted quartz arenite sandstone of the upper portion of the Middle Mt. Simon Sandstone. (E) A silty mudstone of the Upper Mt. Simon Sandstone. (F) A sandstone with bimodal quartz grains and abundant feldspar of the Upper Mt. Simon Sandstone (Freiburg et al., 2014; ©2014 University of Illinois Board of Trustees. Used by permission of the Illinois State Geological Survey.).

3-1 References

Adushita, Y., and V. Smith, 2014, The Potosi reservoir Model 2013: DOE contract DOE/FE0002068, 33 p.

Askari, Z., Y. Lasemi, Z. Lasemi, and H.E. Leetaru, 2011, Subsurface lithostratigraphy of the Cambro-Ordovician Knox Group in Illinois; regional correlation of potential reservoirs and seals for CO_2 sequestration, 40th Annual Eastern Section AAPG Meeting.

Barnes, D.A., D.H. Bacon, and S.R. Kelley, 2009, Geological sequestration of carbon dioxide in the Cambrian Mt. Simon Sandstone: regional storage capacity, site characterization, and large-scale injection feasibility, Michigan Basin: Environmental Geosciences, v. 16, no. 3, p. 163–183.

Barnes, D.A., and K.M. Ellett, 2014, Geological carbon sequestration storage resource estimate for the Ordovician St. Peter Sandstone, Illinois and Michigan Basins, USA: DOE contract DOE/FE0002068, 63 p.

Bell, A.H., E. Atherton, T.C. Buschbach, and D.H. Swann, 1964, Deep oil possibilities of the Illinois Basin: Illinois State Geological Survey, Circular 368, 38 p.

Bond, G.D., P.A. Nickeson, M.A. Kominz, 1984, Breakup of a supercontinent between 635 Ma and 555 Ma: New evidence and implications for continental histories: Earth and Planetary Science Letters, v. 70, p. 325–345.

Buschbach, T.C., 1964, Cambrian and Ordovician strata of northeastern Illinois: Illinois State Geological Survey, Report of Investigations 218, 90 p.

Buschbach, T.C., 1975, Cambrian System, *in* H.B. Willman, E. Atherton, T.C. Buschbach, C. Collinson, J.C. Frye, M.E. Hopkins, J.A. Lineback, and J.A. Simon, eds., Handbook of Illinois stratigraphy: Illinois State Geological Survey, Bulletin 95, p. 34–46.

Buschbach, T.C. and Kolata, D.R., 1991. Regional setting of Illinois Basin, *in* M.W. Leighton, D.R. Kolata, D.F. Oltz, and J.J. Eidel, eds., Interior cratonic basin: American Association of Petroleum Geologists, Memoir 51, p. 29–55.

Catacosinos, P.A., and P.A. Daniels, Jr., 1991, Stratigraphy of Middle Proterozoic to Middle Ordovician formations of the Michigan Basin, *in* P.A. Catacosinos, and P.A. Daniels, eds., Early sedimentary evolution of the Michigan Basin: Geological Society of America, Special Paper 256, p. 53–71.

Catacosinos, P.A., P.A. Daniels Jr., W.B. Harrison III, 1990, Structure, stratigraphy, and petroleum Geology of the Michigan Basin, *in* M.W. Leighton, D.R. Kolata, D.F. Oltz, and J.J. Eidel, eds., Interior cratonic basin: American Association of Petroleum Geologists, Memoir 51, p. 561–601.

Collinson, C., and E. Atherton, 1975, Devonian System, *in* H.B. Willman, E. Atherton, T.C. Buschbach, C. Collinson, J.C. Frye, M.E. Hopkins, J.A. Lineback, and J.A. Simon, eds., Handbook of Illinois stratigraphy: Illinois State Geological Survey, Bulletin 95, p. 104–123.

Dapples, E.C., 1955, General lithofacies relationship of St. Peter Sandstone and Simpson Group: American Association of Petroleum Geologists Bulletin, v. 39, no. 4, p, 444–467.

Droste, J.P., T.F. Abdulkareem, and J.B. Patton, 1982, Stratigraphy of the Ancell and Black River Groups (Ordovician) in Indiana: Indiana Geological Survey, Occasional Paper 36, 15 pp.

Freiburg, J.T., and H.E. Leetaru, 2012, Controls on porosity development and the potential for CO_2 sequestration or wastewater disposal in the Cambrian Potosi Dolomite (Knox Group): Illinois Basin: 41st Annual Eastern Section AAPG Meeting, Cleveland, Ohio, September 22–26.

Freiburg, J.T., D.G. Morse, H.E. Leetaru, R.P. Hoss, and Q. Yan, 2014, A depositional and diagenetic characterization of the Mt. Simon Sandstone at the Illinois Basin–Decatur Project carbon capture and storage site, Decatur, Illinois, USA: Illinois State Geological Survey, Circular 583, 62 p.

Greb, S.F., R.A. Riley, J.R. Bowersox, M.P. Solis, J.A. Rupp, M. Kelley, D.C. Harris, and N. Gupta, 2012, Ordovician Knox carbonates and sandstones of the eastern mid-continent: Potential geologic carbon storage reservoirs and seals, *in* J.R., Derby, R.D. Fritz, S.A. Longacre, W.A. Morgan, and C.A. Sternbach, eds., The great American carbonate bank: The geology and economic resources of the Cambrian–Ordovician Sauk megasequence of Laurentia: American Association of Petroleum Geologists, Memoir 98, p. 1,077–1,101.

Hoholick, J.D., T. Metarko, and P.E. Potter, 1984, Regional variations of porosity and cement: St. Peter and Mount Simon Sandstones in Illinois Basin: American Association of Petroleum Geologists, Bulletin, v. 68, p. 733–764.

Houseknecht, D.W., and F.G. Ethridge, 1978, Depositional history of the Lamotte Sandstone of southeast Missouri: Journal of Sedimentary Petrography, v. 48, p. 575–586.

Houseknecht, D.W., and P.H. Weaverling, 1983, Early Paleozoic sedimentation in Reelfoot rift: American Association of Petroleum Geologists Bulletin, v. 67, no. 9, p. 1456.

Kolata, D.R., 2010, Cambrian and Ordovician Systems (Sauk Sequence and Tippecanoe I Subsequence), *in* D.R. Kolata, and C.K. Nimz, eds., Geology of Illinois: Illinois State Geological Survey, p. 136–157.

Kolata, D.R. and Nelson, W.J., 1991. Tectonic history of the Illinois Basin, *in* M.W. Leighton, D.R. Kolata, D.F. Oltz, and J.J. Eidel, eds., Interior cratonic basin: American Association of Petroleum Geologists, Memoir 51, p. 263–285.

Kolata, D.R., and W.J. Nelson, 1997, Role of the Reelfoot Rift/Rough Creek Graben in the evolution of the Illinois Basin, *in* R.W. Ojakangas, A.B. Dickas, and J.C. Green, eds., Middle Proterozoic to Cambrian Rifting, Central North America: Geological Society of America, Special Paper 312, p. 287–298.

Kolata, D.R., and M.C. Noger, 1991, Tippecanoe I subsequence: Middle and Upper Ordovician Series, *in* M.W. Leighton, D.R. Kolata, D.F. Oltz, and J.J. Eidel, eds., Interior cratonic basin: American Association of Petroleum Geologists, Memoir 51, p. 89–99.

Lamar, J.E., 1928, Geology and economic resources of the St. Peter Sandstone of Illinois: Illinois State Geological Survey, Bulletin 53, 175 p.

Lasemi, Y., and Z. Askari, 2014, Stratigraphy of the Cambo-Ordovician succession in Illinois: DOE contract number DOE/FE0002068, 43 p.

Lasemi, Y., Z. Askari, and H.E. Leetaru, 2012, Potential of the Cambro-Ordovician Knox Carbonates of Illinois as combined reservoirs and seals for carbon sequestration: 41st Annual Eastern Section AAPG Meeting, Cleveland, Ohio, September 22–26.

Leetaru, H.E., 2014, An evaluation of the carbon sequestration potential of the Cambro-Ordovician strata of the Illinois and Michigan Basins: DOE contract DOE/FE0002068, 82 p.

Leetaru, H.E., and J.T. Freiburg, 2014, Litho-facies and reservoir characterization of the Mt. Simon sandstone at the Illinois Basin – Decatur Project: Greenhouse Gases: Science Technology, v. 4, no. 5, p. 580–595.

Leetaru, H.E., and J.H. McBride, 2009, Reservoir uncertainty, Precambrian topography, and carbon sequestration in the Mt. Simon Sandstone, Illinois Basin. Environmental Geosciences, v. 16, p. 235–243.

Leetaru, H.E., V. Smith, Y. Adushita, and J.T. Freiburg, 2014, An integrated approach to evaluating the suitability of the Potosi Dolomite as a carbon sequestration target: Interpretation, v. 2, no. 3, p. 125–133.

Leetaru, H.E., S. Frailey, D. Morse, R.J. Finley, J. Rupp, J.A. Drahozval, and J.H. McBride, 2009, Carbon sequestration in the Mt. Simon Sandstone saline reservoir, *in* Carbon dioxide sequestration in geological media: State of the science, M. Grobe, J.C. Pashin, and R.L. Dodge, eds., American Association of Petroleum Geologists Studies, v. 59, p. 261–277.

Meert, J.G. and T.H. Torsvik, 2003, The making and unmaking of a supercontinent: Rodinia revisited: Tectonophysics, v. 375, p. 261–288.

Midwest Geological Sequestration Consortium, (MGSC), 2005, An assessment of geological carbon sequestration options in the Illinois Basin: DOE contract DE-FC26-03NT41994, 581 pp.

Morse, D.G., and H.E. Leetaru, 2005, Reservoir characterization and three-dimensional models of Mt. Simon Gas Storage Fields in the Illinois Basin: Illinois State Geological Survey, Circular 567, 72 p.

Mossler, J.H., 1987, Paleozoic lithostratigraphic nomenclature for Minnesota: Minnesota Geological Survey, Report of Investigations 36, 36 p.

Mossler, J.H., 2008, Paleozoic stratigraphic nomenclature for Minnesota: Minnesota Geological Survey, Report of Investigations 65, 79 p.

Nelson,W. J., 1991, Structural styles of the Illinois Basin, *in* M.W. Leighton, D.R. Kolata, D.F. Oltz, and J.J. Eidel, eds., Interior cratonic basin: American Association of Petroleum Geologists, Memoir 51, p. 209–261.

Ostrom, M.E., 1966, Cambrian stratigraphy in western Wisconsin: Wisconsin Geological and Natural History Survey, Information Circular 7, 79 p.

Neufelder, R.J., B.B. Bowen, R.W. Lahann, and J.A. Rupp, 2012, Lithologic, mineralogical, and petrophysical characteristics of the Eau Claire Formation: Complexities of a carbon storage system seal: Environmental Geosciences, v. 19, no. 3, p. 81–104.

Ojakangas, R. W., 1963, Petrology and sedimentation of the Upper Cambrian Lamotte Sandstone in Missouri: Journal of Sedimentary Petrology, v. 33, no. 4, p. 860–873.

Palkovic, M.J., 2015, Depositional characterization of the Eau Claire Formation at the Illinois Basin–Decatur Project: Facies, mineralogy and geochemistry. M.S. thesis, University of Illinois at Urbana-Champaign, 84 p.

Palmer, A.R., 1981, Subdivision of the Sauk sequence, *in* M.E., Taylor, ed., Short papers for the Second International Symposium on the Cambrian System: US Geological Survey, Open-File Report 81–743, p. 160–162.

Person, M., A., Banerjee, J. Rupp, C. Medina, P. Lichtner, C. Gable, R. Pawar, M. Celia, J. McIntosh, and V. Bense, 2010, Assessment of basin-scale hydrologic impacts of CO_2 sequestration, Illinois Basin: International Journal of Greenhouse Gas Control, v. 4, p. 840–854.

Pitman, J.K., M.B. Goldhaber, and C. Spoetl, 1997. Regional diagenetic patterns in the St. Peter Sandstone: Implications for brine migration in the Illinois Basin: US Geological Survey, Bulletin 2094-A, 17 p.

Runkel, A.C., R.M. McKay, C.A. Cowan, J.F. Miller, and J.F. Taylor, 2012, The Sauk megasequence in the cratonic interior of North America: Interplay between a fully developed inner detrital belt and the central great American carbonate bank, *in* J.R. Derby, R.D. Fritz, S.A. Longacre, W.A. Morgan, and C.A. Sternbach, eds., The great American

carbonate bank: The geology and economic resources of the Cambrian–Ordovician Sauk megasequence of Laurentia: American Association of Petroleum Geologists, Memoir 98, p. 1,001–1,011.

Saltzman, M.R., C.A. Cowan, A.C. Runkel, B. Runnegar, M.C. Steward, and A.R. Palmer, 2004, The Late Cambrian SPICE 13C event and the Sauk II–III regression: New evidence from Laurentian basins in Utah, Iowa, and Newfoundland: Journal of Sedimentary Research, v. 74, p. 366–377.

Sargent, M.L., 1991, Sauk Sequence, Cambrian System through Lower Ordovician Series, *in* M.W. Leighton, D.R. Kolata, D.F. Oltz, and J.J. Eidel, eds., Interior cratonic basin: American Association of Petroleum Geologists, Memoir 51, p. 75–85.

Schmidt, V., and D.A. McDonald, 1979, The role of secondary porosity in the course of sandstone diagenesis, *in* Aspects of diagenesis, P.A. Scholle, and P.R. Schluger, eds, Society for Sedimentary Geology (SEPM), Special Publication 26, p. 175–207.

Shaver, R.H., C.H. Ault, A.M. Burger, D.D. Carr, J.B. Droste, D.L. Eggert, H.H. Gray, D. Harper, N.R. Hasenmueller, W.A. Hasenmueller, A.S. Horowitz, H.C. Hutchison, B.D. Keith, S.J. Keller, J.B. Patton, C.B. Rexroad, C.E. Wier, 1986, Compendium of Paleozoic rock-unit stratigraphy in Indiana—A revision: Indiana Geological Survey, Bulletin 59, 203 p.

Sloss, L.L., 1963, Sequences in the cratonic interior of North America: Geological Society of America Bulletin, v. 74, p. 93–114.

Smith, V., 2014, Potosi reservoir modeling; History and recommendations: DOE contract DOE/FE0002068, 21 p.

Templeton, J.S., 1950, Mt. Simon Sandstone in northern Illinois: Transactions of the Illinois State Academy of Science, v. 43, p. 151–159.

Templeton, J.S., and H.B. Willman, 1963, Champlainian Series (Middle Ordovician) in Illinois: Illinois State Geological Survey, Bulletin 89, 260 p.

Treworgy, J.D., S.T. Whitaker, and Z. Lasemi, 1997, Structural cross section of the Paleozoic rocks in Illinois, Wayne County to Stephenson County: Illinois State Geological Survey, Illinois, Map 7, 2 sheets.

Will, R., V.L. Smith, and H.E. Leetaru, 2014, Utilization of the St. Peter Sandstone in the Illinois Basin for CO_2 Sequestration: DOE contract DOE/FE0002068, 52 p.

Willman, H.B., and J.N. Payne, 1943, Early Ordovician strata along Fox River in northern Illinois: Journal of Geology, v. 51, no. 8, p. 531–541.

Willman, H.B., E. Atherton, T.C. Buschbach, C. Collinson, J.C. Frye, M.E. Hopkins, J.A. Lineback, and J.A. Simon, 1975, Handbook of Illinois stratigraphy: Illinois State Geological Survey, Bulletin 95, 261 p.

Subtask 3-2 Update and Enhancements of Geologic Models

Geologic models for the Mt. Simon Sandstone developed during the IBDP were built using surface seismic data, borehole geophysical logs, and routine core analysis results. The geologic models were used to address problems related to estimates of formation injectivity and the geometry (path) of subsurface CO_2 migration (Senel et al., 2014). At the time the geologic models were built, only two vertical wells, CCS#1 and VW#1, had been drilled at the IBDP site, and geophysical log data from these wells were incorporated with three-dimensional (3D) seismic data, side-wall core analysis, modular formation dynamic tester reservoir rock, and fluid analyses to build a second generation model (Senel et al., 2014). Additional data were acquired from two

newly drilled vertical wells, CCS#2 and VW#2, including geophysical log suites and rotary sidewall cores. Routine core analyses were also carried out on the sidewall cores.

In this subtask, geophysical log data from CCS#1, CCS#2, VW#1, and VW#2 have been used with 3D seismic data to update and enhance the geologic models for the Mt. Simon Sandstone. Geophysical data includes porosity logs from core tests, triple combo logs, and combined magnetic resonance (CMR) logs, as well as permeability data from core tests and CMR logs. The update to the geologic models reduced property uncertainty in the subsurface and enhanced coupled fluid flow and geomechanical modeling.

The geologic models discussed in this report were developed using Petrel (commercial software, Schlumberger, Houston, TX). To construct the geologic models, top and bottom surfaces were selected. The surface of the Eau Claire shale was selected as the top of the model because it represents the major upper confining unit. The surface of the Precambrian basement was selected as the base of the model, most importantly because injection occurs hundreds of feet above the basement and the basement is assumed to be a lower confining seal. The horizontal dimension of the constructed geologic model was limited by the coverage area of the 3D seismic data.

Input Data

Laboratory routine core analysis data, permeability data, and triple combo log data (Figure 3-2-1) consisting of porosity, density, gamma ray, electrical resistivity, and photoelectric index data were imported into Petrel. Permeability data were recorded in boreholes using the Schlumberger CMR logging tool, while the triple combo log data were recorded in boreholes using the Schlumberger platform express (PEX) wireline logging tool. Results from routine core analysis conducted on full diameter whole and rotary sidewall cores acquired at different depths in CCS#1 and VW#1 were available. Likewise, routine core analysis conducted on rotary sidewall cores acquired at different depths in VW#2 were also available. The core analysis performed on these cores includes laboratory measurement of petrophysical properties, such as porosity, permeability, and grain density.

Depth-converted litho-stratigraphic surfaces for the Precambrian basement, Pre-Mt. Simon Sandstone (informally known as the Argenta Formation), seven lithofacies of the Mt. Simon Sandstone, and Eau Claire shale were imported into Petrel to build the geologic model. The seven different lithofacies (from bottom to top) are Mt. Simon A lower, A-Ips (the letters "Ips" are used to denote a baffle zone), A upper, B, C, D, and E, based on geophysical log, stratigraphic, and petrographic analysis. In Leetaru and Freiburg (2014), the lithofacies Mt. Simon A lower, A-Ips, A upper, and B are collectively grouped as the Lower Mt. Simon Sandstone; Mt Simon C and D are grouped as the Middle Mt. Simon Sandstone; and Mt. Simon E is the Upper Mt. Simon Sandstone. These litho-stratigraphic surfaces served as key inputs for developing a structural framework for the Mt. Simon Sandstone in Petrel, and the structural framework was sequentially used for creating a property (i.e., porosity and permeability) model of the formation.

The available 3D seismic data covered an area of approximately 18 km^2 (7 mi^2), and this area represents the boundary limits to which geologic horizons (i.e., litho-stratigraphic surfaces) could be seismically mapped. However, to build a wider geologic model, surfaces were extrapolated beyond the boundary limit. Couëslan et al. (2014) provides a more detail discussion on the quality of the 3D seismic data, acquisition process, seismic data processing, and interpretation. Stochastic 3D seismic inversion data was also available and imported into Petrel.

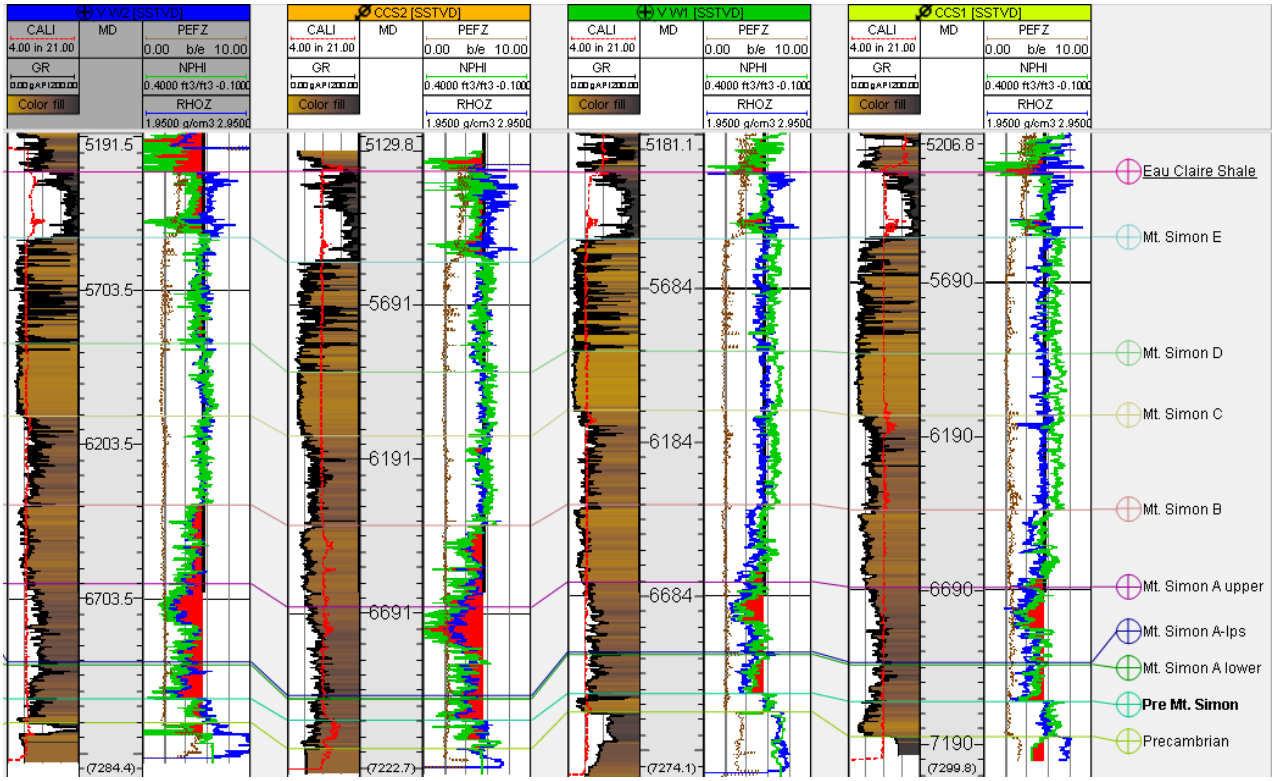

Figure 3-2-1 Interpreted traditional well log cross section between VW#2, CCS#2, VW#1, and CCS#1 that shows intervals of Eau Claire shale and different lithofacies of the Mt. Simon Sandstone (gamma ray [GR], neutron porosity [NPHI], bulk density [RHOZ], photoelectric factor [PEFZ]).

Development of Geologic Models

To create the updated geologic models, a small (i.e., 2.9 × 2.9 km [1.8 × 1.8 mi]) structural framework model was developed because of the area of the 3D seismic volume, as well as a large (i.e., 4.8 × 4.8 km [3 × 3 mi]) structural framework model because of fluid flow simulation requirement

Figure 3-2-2 and Figure **3-2-3** show the litho-stratigraphic surface (i.e., structure) map of each Mt. Simon Sandstone lithofacies. The litho-stratigraphic surfaces were useful in calculating a 3D stratigraphic thickness of each Mt. Simon Sandstone lithofacies. This calculation was carried out in Petrel, by a function that subtracts an underlying litho-stratigraphic surface from a referenced litho-stratigraphic surface. Figure 3-2-4 shows the derived thickness (isochore) for each Mt. Simon Sandstone lithofacies. Table 3-2-1 provides the minimum and maximum thickness of each lithofacies based on seismic interpretation and well log analysis.

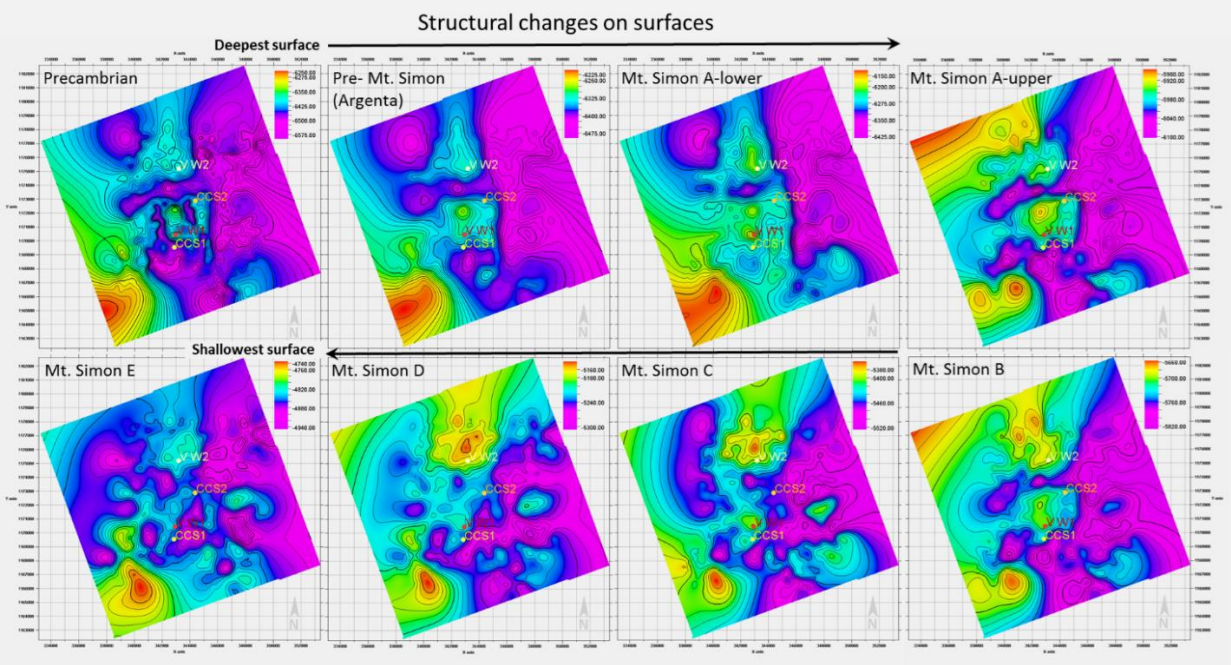

Figure 3-2-2 Gridded structural surfaces of the Precambrian basement, Pre- Mt. Simon Sandstone and the Mt. Simon Sandstone lithofacies (excluding A-Ips) shown from oldest (top left) to youngest (bottom left).

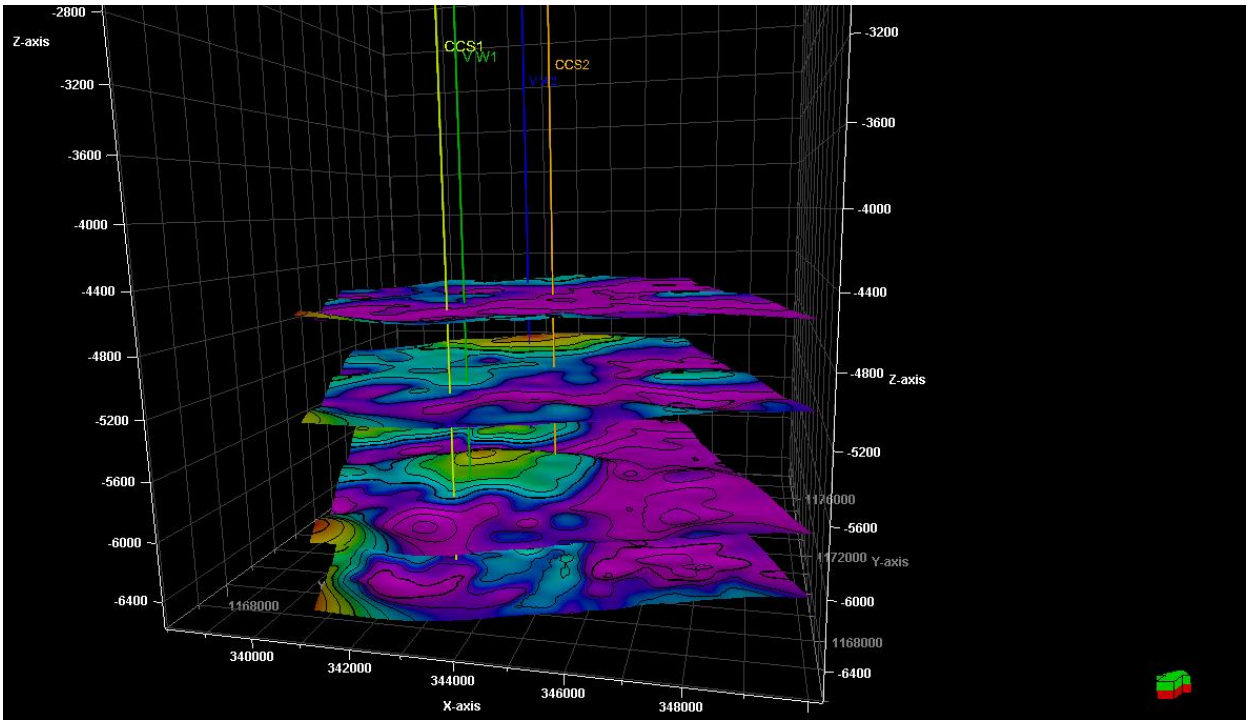

Figure 3-2-3 Three-dimensional view (from the southeast) of gridded Mt. Simon Sandstone lithofacies surfaces that illustrate subtle structural changes between each surface.

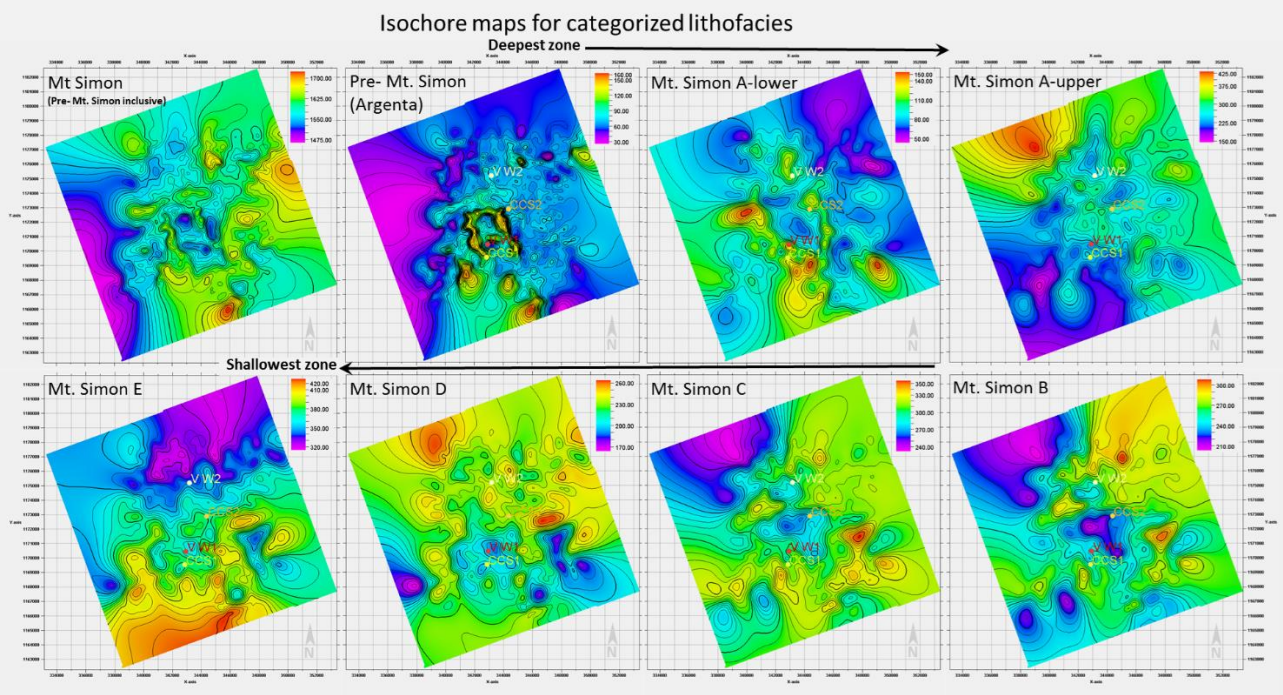

Figure 3-2-4 Isochore maps of the entire Mt. Simon Sandstone, Pre-Mt. Simon Sandstone and the Mt. Simon Sandstone lithofacies shown from oldest (top left) to youngest (bottom left).

Table 3-2-1 Minimum and maximum thickness of the various lithofacies based on well log and seismic data.

Zones (Lithofacies)	Seismic		Well log	
	Min. thickness m (ft)	Max. thickness m (ft)	Min. thickness m (ft)	Max. thickness m (ft)
Eau Claire Shale	46.656 (153.07)	87.027 (285.52)	64.843 (212.74)	90.126 (295.69)
Mt. Simon E	95.945 (314.78)	130.19 (427.13)	104.90 (344.17)	114.62 (376.05)
Mt. Simon D	49.929 (163.81)	80.440 (263.91)	58.5 (192)	71.881 (235.83)
Mt. Simon C	70.656 (231.88)	108.26 (355.19)	87.825 (288.14)	93.415 (306.48)
Mt. Simon B	61.978 (203.34)	93.958 (308.26)	76.663 (251.52)	80.827 (265.18)
Mt. Simon A upper	44.214 (145.06)	132.02 (433.14)	69.2 (227)	87.523 (287.15)
Mt. Simon A Ips	2 (7)	–	2.45 (8.05)	3.210 (10.53)
Mt. Simon A lower	13 (43)	46.893 (153.85)	21.21 (69.58)	38.274 (126.57)
Pre-Mt. Simon	7.763 (25.47)	49.670 (162.96)	18.11 (59.40)	34.644 (113.66)

Lateral thickness variations observed on the isochore maps are due to geologic factors such as pre-existing structural influence, local surface geomorphology (depositional setting), sediment source, sediment supply, and accommodation space at the time of deposition.

Based on seismically mapped litho-stratigraphic surfaces, the computed thickness of the Mt. Simon Sandstone with the pre-Mt. Simon Sandstone (Argenta) ranges between 346 and 643 m (1,134 and 2,111 ft), whereas the computed thickness of the Mt. Simon Sandstone without the pre-Mt. Simon Sandstone ranges between 250 and 513 m (819 and 1,684 ft).

Based on interpretation of well log data, the thickness of the Mt. Simon Sandstone (i.e., pre-Mt. Simon Sandstone inclusive) ranges between 439 and 524 m (1,439 and 1,721 ft). However,

if the pre-Mt. Simon is excluded from the Mt. Simon Sandstone, the thickness ranges between 421 and 490 m (1,380 ft and 1,607 ft).

The structural framework (Figure 3-2-5) of the geologic model for the Mt. Simon Sandstone comprised nine distinct zones, including the Eau Claire shale, the seven Mt. Simon Sandstone lithofacies, and the Pre-Mt. Simon Sandstone.

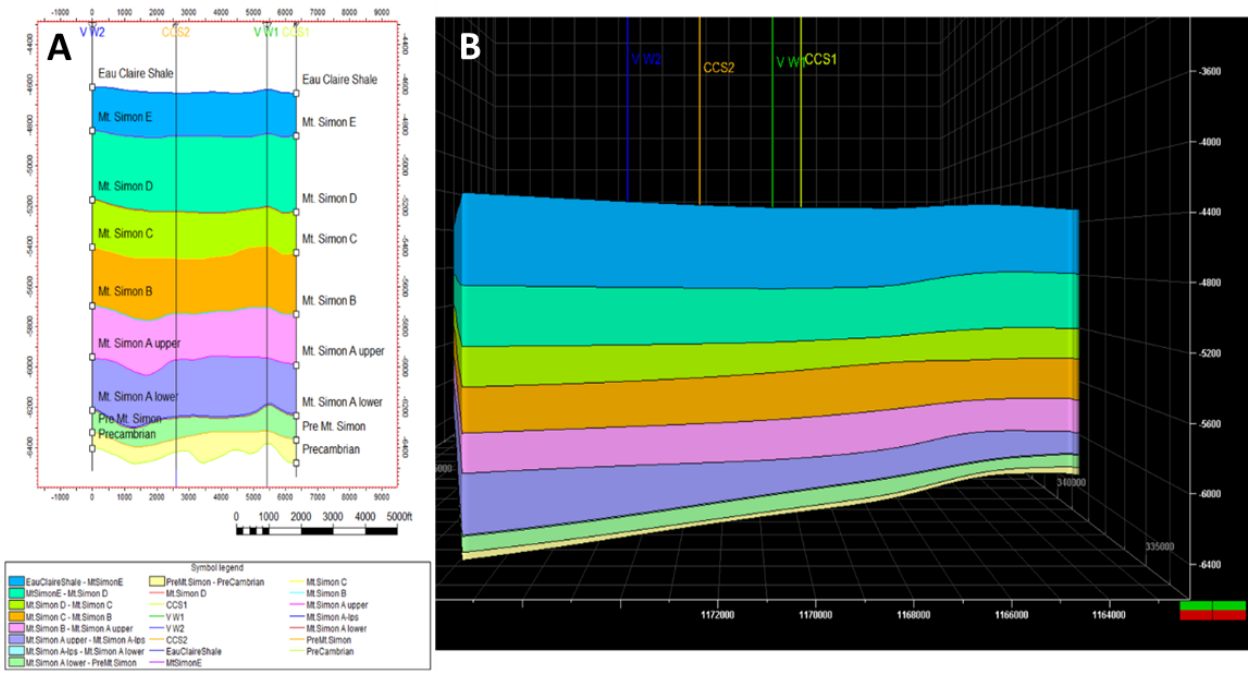

Figure 3-2-5 (A) Cross-sectional (north–south) and (B) 3D (from the west) views of zones used in the geologic model of the Mt. Simon Sandstone.

The nines zones were further divided into layers. To determine the optimum number of layers that would reproduce heterogeneity of the reservoir, data analysis was performed on pertrophysical data in each zone, specifically vertical variogram analysis for estimating the vertical range. The estimated range guided the process of assigning a number of layers to zones (Table 3-2-2).

Table 3-2-2 Number of assigned layers and vertical range estimated from data analysis.

Zones	No. of assigned layers	Vertical range m (ft)
Eau Claire shale	10	13.9 (45.7)
Mt. Simon E	20	4.438 (14.56)
Mt. Simon D	12	13.664 (44.83)
Mt. Simon C	15	18.611 (61.06)
Mt. Simon B	15	16.724 (54.87)
Mt. Simon A Upper	30	13.426 (44.05)
Mt. Simon A-Ips	4	1.408 (4.62)
Mt Simon A Lower	15	3.158 (10.36)
Pre-Mt. Simon (Argenta)	8	5.422 (17.79)

Petrophysical Analysis

Petrophysical analysis were carried out by evaluating correlations between geophysical logs and using theoretical relationships to quantify petrophysical properties. For example, apart from porosity logs recorded using PEX and CMR tool, density porosity logs were calculated using theoretical relationship. The average of the sum of both neutron and density porosity logs was used to approximate total porosity. However, the CMR tool also provide nuclear magnetic resonance (NMR) total and effective porosity. Both NMR total porosity and total porosity from averaging the sum of density and the neutron porosity logs were compared to find out how well they correlate.

Porosity modeling and static volumetric estimation require deriving effective porosity from the CMR measurement. Static volumetric estimation also requires the net-to-gross (N/G) reservoir ratio, which is normally derived from gamma-ray logs using a cut-off of 75 API to delineate sand from shale. In some of the Mt. Simon Sandstone zones, however, high feldspathic content (Freiburg et al., 2014) results in high gamma-ray readings, and so the gamma-ray cut-off method for estimating N/G ratio was deemed unreliable. As a result, N/G ratios of 0.6, 0.8, and 1 were assumed for volumetric estimation.

Two types of permeability models, a Schlumberger-Doll-Research (K_{SDR}) model and Timur-Coates (K_{Coates}) model, were used to estimate the permeability of the Mt. Simon Sandstone. The models use total and effective porosity measurements made by the CMR tool in boreholes to estimate permeability. Other forms of estimating permeability were also attempted, such as the porosity-permeability relationship method. However, the K_{SDR} and K_{Coates} logs were found most appropriate for this task because the CMR tool is a well-established technology in clastic reservoirs (Logan et al., 1997).

Additionally, geophysical and laboratory measurement of petrophysical properties were evaluated by plotting them on a vertical log cross section to determine if a good correlation existed between the two measurements. Figure 3-2-6shows an example of a vertical cross section plot of geophysical and laboratory measurement. In the well-to-well cross section plot, total porosity measurements showed good correlation at all depths, whereas permeability measurements showed poor correlation at most depths.

Grain density measurements from laboratory studies were used to estimate density porosity. Grain density measurements made on core samples from each well were compiled and statistically analyzed to derive grain density values for each zone. The grain density value for each zone was then assumed to be the mode (Figure 3-2-7) in the array of data that was analyzed. The modal value was used to estimate density porosity in each zone. The density porosity for each zone was estimated using Equation 3-2-1:

$$\phi_D = \frac{\rho_{ma} - \rho_{bulk}}{\rho_{ma} - \rho_{fl}}, \qquad \text{Eq. 3-2-1}$$

Where, ϕ_D represents density porosity; ρ_{ma} represents matrix density (assumed to be modal grain density rather than assumed grain density value of 2.65 g/cc); and ρfl represents fluid density (assumed to be 1.1 g/cc).

The derived density porosity and the neutron porosity values were averaged to estimate the total porosity. In general, the total porosity from the magnetic resonance log and averaging method showed a very good correlation.

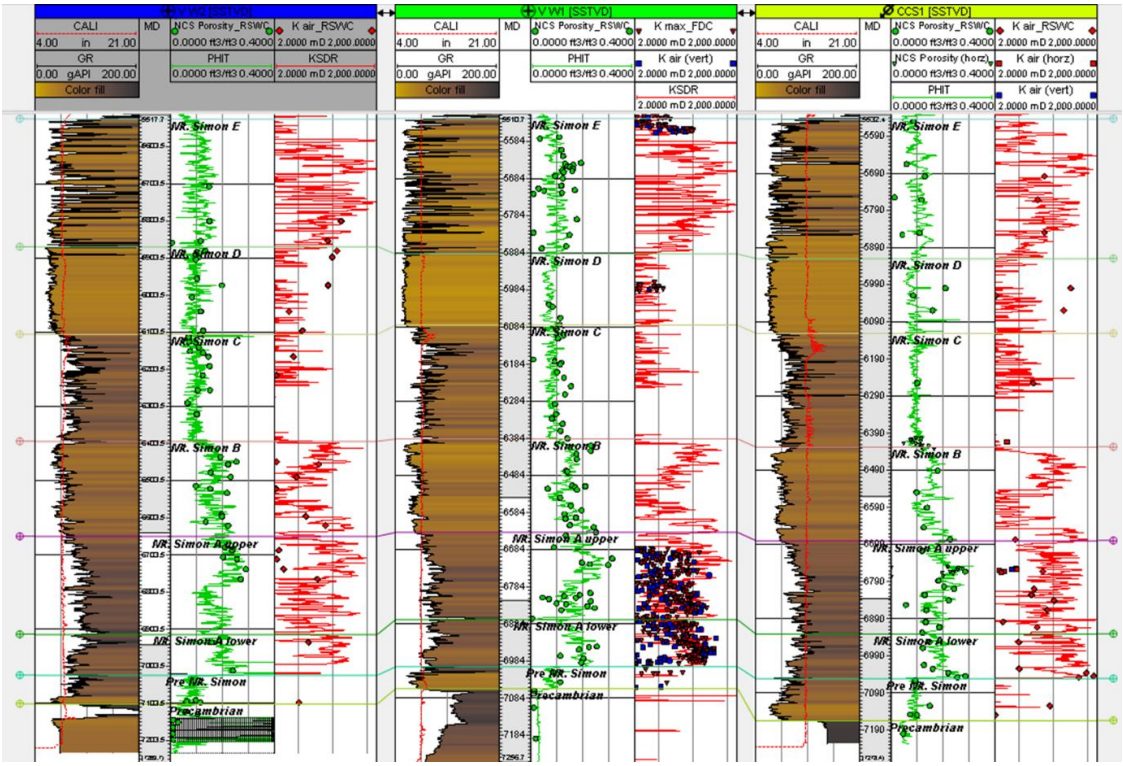

Figure 3-2-6 Well-to-well cross-section plot (Mt. Simon E used as datum) displaying geophysical log and laboratory measurements (discrete points represent porosity and permeability measurements carried out on sampled cores in the laboratory).

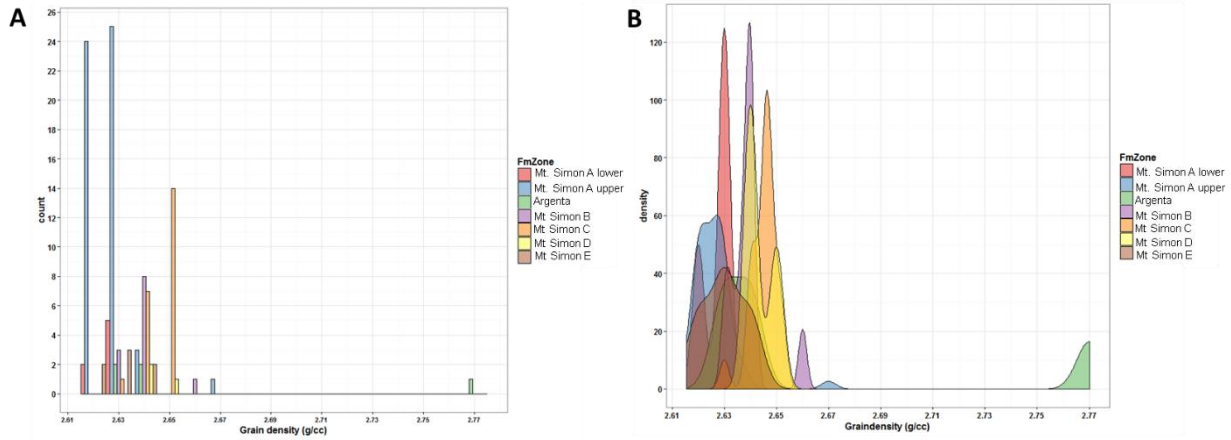

Figure 3-2-7 (A) Histogram and (B) Kernel density plot of static measurements of grain density for CCS#1.

The porosity logs were upscaled using the arithmetic averaging method, whereas permeability logs were upscaled using the geometric, arithmetic, and harmonic averaging methods. Figure 3-2-8 shows a cross section of the raw effective porosity (PIGN) log and corresponding upscaled cells. In general, the range of porosities were well represented by the upscaled cells, but some of the mid-range porosity values between 6% and 20% may have been slightly overrepresented (Figure 3-2-9) The three averaging methods used for the permeability logs were explored to determine a method that would be most suitable for averaging the input permeability

data (Figure 3-2-10). Based on the histogram plot, the geometric method better represented the well log data.

A porosity cube was created using the 3D seismic inversion results. Figure 3-2-11 illustrates how closely the inversion result matches the upscaled PIGN log. At the well locations, upscaled cells with porosity above 20% correlate fairly well with parallel zones on the seismic inversion line (i.e., zones that also have porosity above 20%). Similarly, upscaled cells with porosity below 15% also correlate with parallel zones on the seismic inversion line (i.e., indicating porosity below 15%). Overall, the seismic inversion results appear to be of good quality and show good correlation with upscaled well log data. This good correlation suggests that the seismic inversion data is a good secondary data for co-kriging with well log data during the geostatistical process to provide a better estimate of petrophysical property distribution in the geologic model.

Petrophysical Modeling

The coverage area for the geologic model depended mainly on available site characterization data (i.e., the seismic data and the geophysical log data) and minimally on fluid flow simulation requirements. The 3D seismic volume and seismic inversion results that were available for the study area covered a total area of 14.9 km^2 (5.76 mi^2). Hence, the lateral extent of the two geologic models were limited by the coverage area of the seismic data. The two geologic models varied in horizontal dimension but had similar vertical dimension.

The initial process involved building two separate structural framework models that differed in horizontal dimension. One structural framework model (called the small model) with a 2.9 × 2.9 km (1.8 × 1.8 mi) grid was built to match the horizontal dimension of the seismic inversion results, so that the petrophysical data could be co-krigged with those results. The second structural framework (called the large model) had a 4.8 × 4.8 km (3 × 3 mi) grid, and it was constructed with an area beyond that covered by the seismic inversion results to meet fluid flow simulation requirements. The small and large models had 63 × 63 × 115 and 104 × 105 × 115 grid cells, respectively. In both models, the horizontal grid cell size was 45.72 × 45.72 m (150 × 150 ft), and the vertical grid cell size varied within the geologic intervals and depended on the number of layers assigned to each zone. In total, the small model had approximately 0.46 million grid cells, whereas the large model had 1.2 million grid cells.

After generating the structural framework for each model, petrophysical modeling was carried out in both models. The upscaled porosity and permeability values were populated across both models using Sequential Gaussian Simulation (SGS). Before using the SGS to distribute the petrophysical data, horizontal and vertical variograms were computed to determine the spatial continuity of the reservoir properties. The horizontal variograms (major and minor) were computed separately for each zone by considering maximal and minimal continuity of data in the *x* and *y* directions. The vertical variograms were generated perpendicular to the *x* and *y* directions to display the continuity of datasets through the well paths. To determine the direction of major and minor anisotropy of the porosity distribution, variogram maps (Figure 3-2-12) for each zone were prepared in Petrel from seismic inversion results.

Within the small model, porosity logs were co-krigged with the porosity cube generated from seismic inversion results, and the resulting porosity model was later co-krigged with permeability log data to generate a permeability model. However, within the large model, porosity logs were not co-krigged with the porosity cube because the porosity cube did not cover the entire framework of the model. The process of modeling porosity and permeability in both models involved the use of variogram parameters, including the horizontal ranges (minor and major), sill, and nugget derived from variogram analysis of the seismic inversion results.

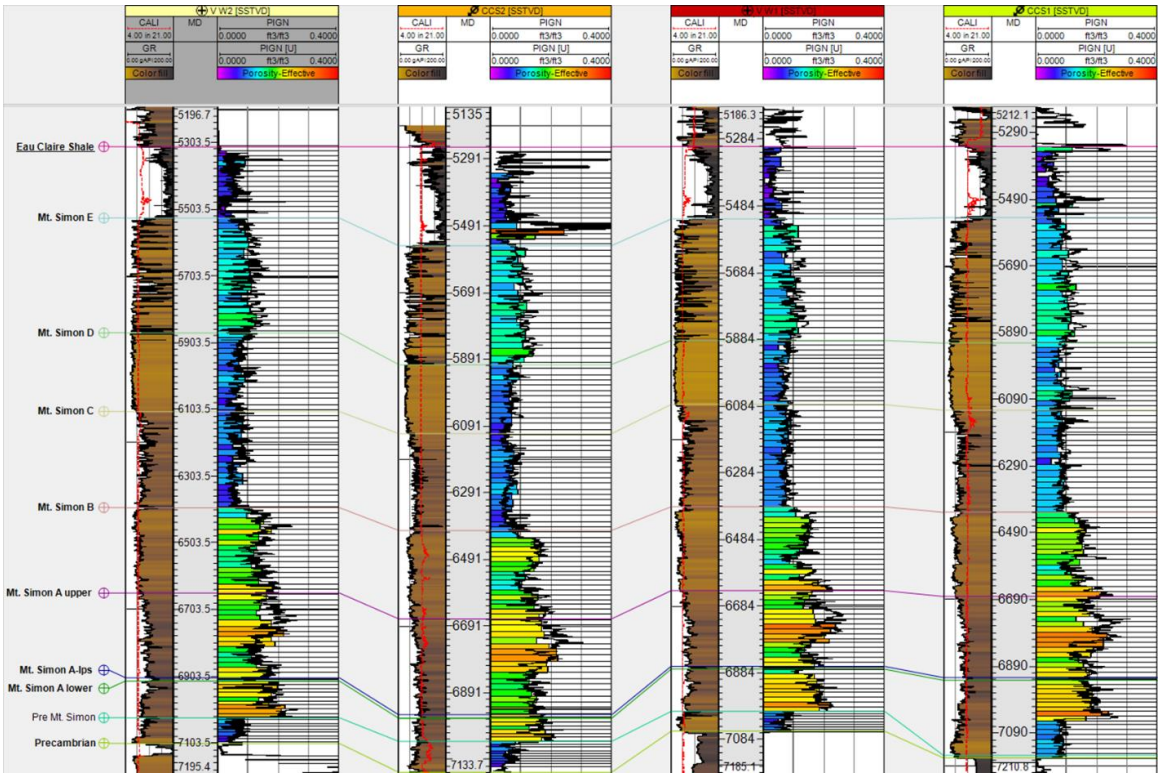

Figure 3-2-8 Well-to-well cross section of the studied wells showing upscaled PIGN and raw PIGN.

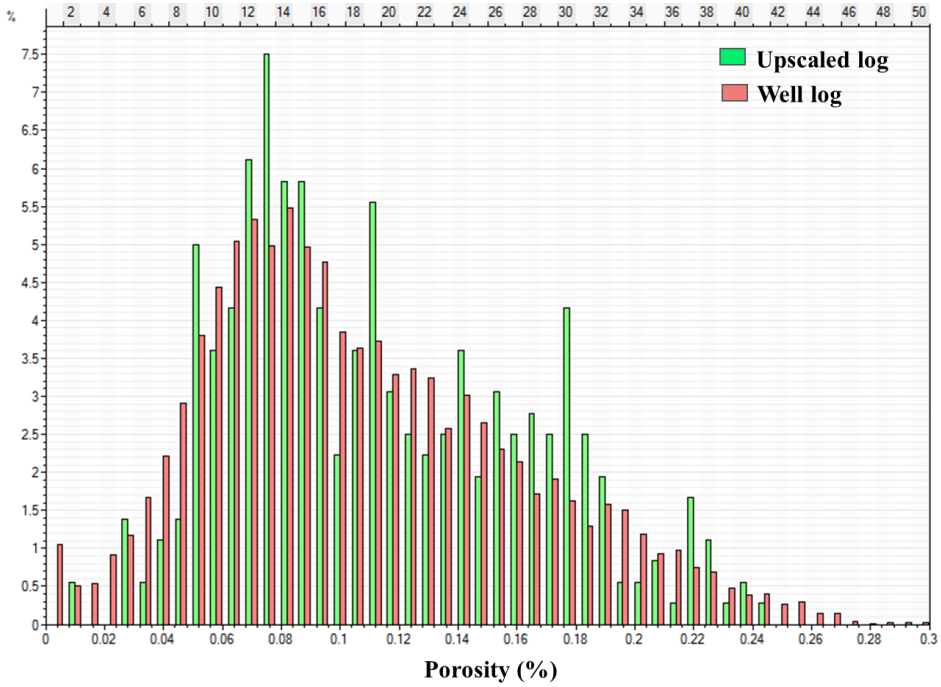

Figure 3-2-9 Histogram showing the upscaled log and raw (well) logs.

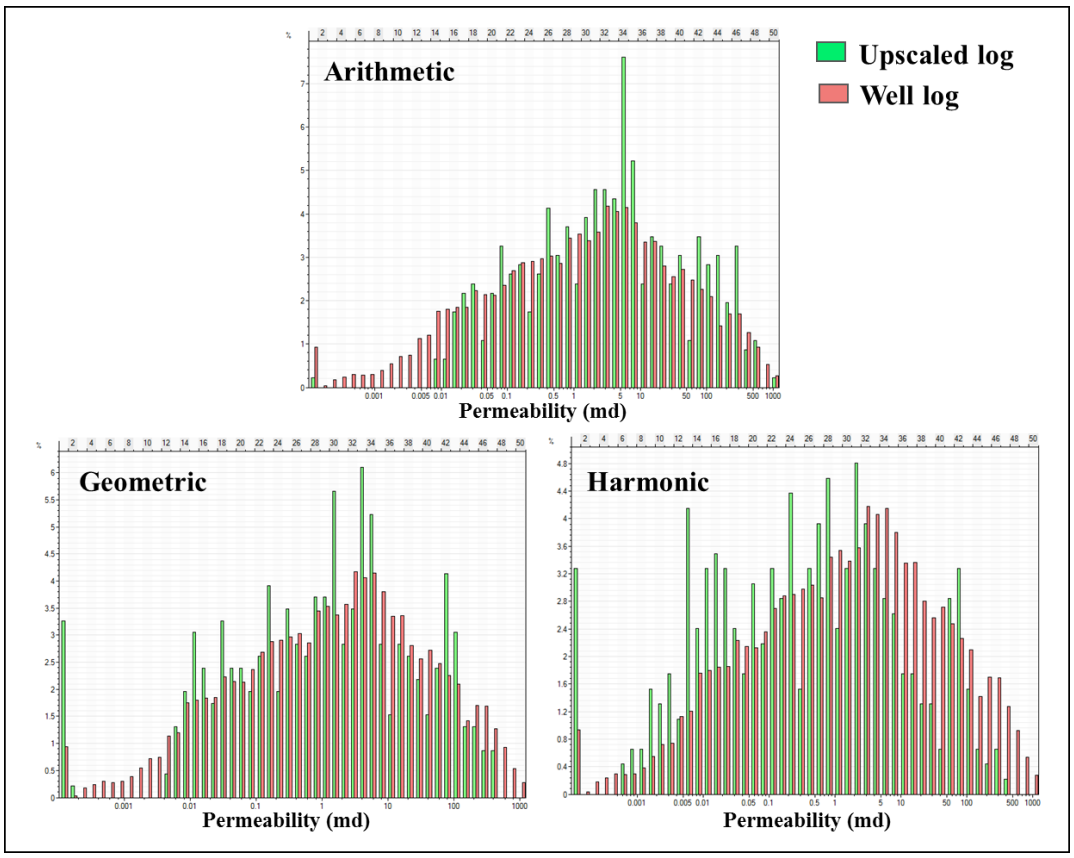

Figure 3-2-10 Histograms of each averaging method used for the permeability data.

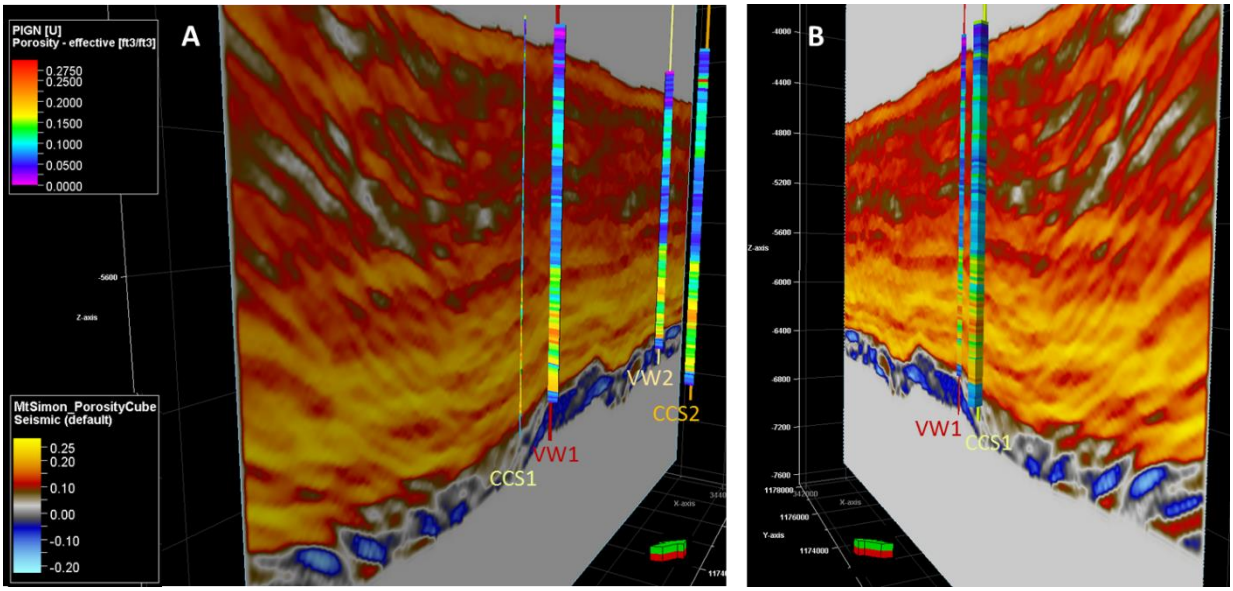

Figure 3-2-11 Comparison of seismic inversion results with upscaled porosity: (A) oblique view from the southeast showing the north–south seismic inversion line crossing CCS#1 and (B) oblique view from the southwest showing the north–south seismic inversion line crossing VW#1. The legend in the upper left corner is for the upscaled PIGN (well data), and the legend in the bottom left corner is for the seismic inversion result.

Final Geologic Models

The small and large models were reviewed to compare porosity and permeability values. In both models, the range of porosity and permeability values observed were similar, but the models showed differences in the property trends because of the different approaches used for petrophysical modeling. Table 3-2-3 and Table **3-2-4** show the range of effective porosity and permeability observed in each zone, respectively.

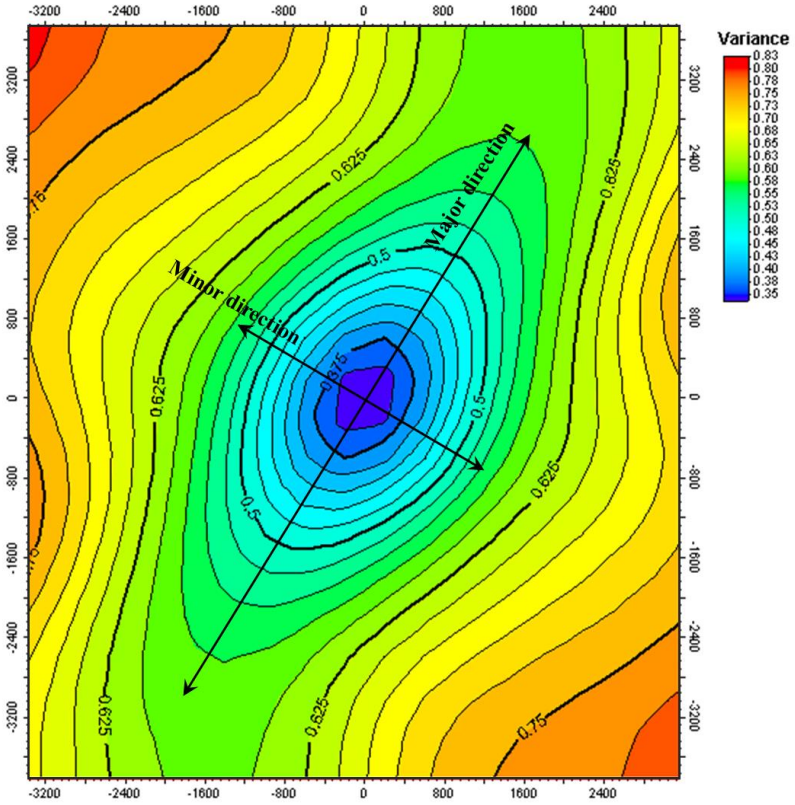

Figure 3-2-12 An example of one of the variogram maps computed for each zone of the Mt. Simon. This map shows the major and minor directions (black arrows) of anisotropy for the lower zone of the Mt. Simon A.

Table 3-2-3 Range of the effective porosity (PIGN) from the well log, upscaled log, and 3D model for the Eau Claire and Mt. Simon Sandstone.

Zones	PIGN Range (Well log) (ft^3/ ft^3)	PIGN Range (Upscaled and 3D Model) (ft^3/ ft^3)
Eau Claire shale	0.00001−0.5028	0.032−0.3115
Mt. Simon E	0.0053−0.1744	0.058−0.1407
Mt. Simon D	0.0122−0.2630	0.0421−0.1375
Mt. Simon C	0.02−0.1738	0.0452−0.1041
Mt. Simon B	0.0469−0.2354	0.0888−0.2185
Mt. Simon A Upper	0.04811−0.3127	0.1126−0.2432
Mt. Simon A-Ips (baffle)	0.0001−0.1812	0.0213−0.1921
Mt. Simon A Lower	0.0174−0.2697	0.0835−0.2373
Pre-Mt. Simon (Argenta)	0.0046−0.1894	0.0402−0.0925

Table 3-2-4 Range of the Schlumberger-Doll-Research permeability model (K_{SDR}) from the well log, upscaled log, and 3D model for the Eau Claire and Mt. Simon Sandstone.

Zones	K_{SDR} range (Well log) um^2 (md)	K_{SDR} range (Upscaled and 3D Model) Geometric um^2 (md)	K_{SDR} range (Upscaled and 3D Model) Harmonic um^2 (md)	K_{SDR} range (Upscaled and 3D Model) Arithmetic um^2 (md)
Eau Claire shale	9.869×10^{-8}–2.430 (0.0001−2,462)	9.869×10^{-8}–0.02 (0.0001−21)	9.869×10^{-8}–0.293 (0.0001−297)	9.869×10^{-8}– (0.0001−297)
Mt. Simon E	9.869×10^{-8}–7.444 (0.0001−7,543)	9.869×10^{-8}–0.350 (0.0001−355)	9.869×10^{-8}–0.324 (0.0001−936)	0.0003–0.917 (0.389−929)
Mt. Simon D	9.869×10^{-8}–0.115 (0.0001−117)	6.32×10^{-6}–0.009 (0.0064−9)	2.665×10^{-6}–0.01 (0.0027−15)	7.895×10^{-6}–0.01 (0.0080−15)
Mt. Simon C	1.97×10^{-7}–0.399 (0.0002−404)	7.90×10^{-6}–0.009 (0.008−9)	2.467×10^{-6}–0.03 (0.0025−35)	1.056×10^{-5}–0.04 (0.0107−37)
Mt. Simon B	3.85×10^{-6}–1.055 (0.0039−1,069)	0.0001–0.399 (0.1508−404)	5.714×10^{-5}–0.454 (0.0579−460)	0.0002–0.457 (0.2419−463)
Mt. Simon A Upper	7.797×10^{-6}–1.821 (0.0079−1,845)	0.0007–0.351 (0.7561−356)	0.0001–0.407 (0.1207−412)	0.0012–0.404 (1.179−409)
Mt. Simon A-Ips (baffle)	2.862×10^{-6}–0.232 (0.0029−235)	7.007×10^{-6}–0.07 (0.0071−73)	5.231×10^{-6}–0.112 (0.0053−113)	1.421×10^{-5}–0.100 (0.0144−101)
Mt. Simon A Lower	9.869×10^{-8}–1.165 (0.0001−1,180)	7.353×10^{-5}–0.389 (0.0745−394)	2.270×10^{-6}–0.463 (0.0023−469)	0.0004–0.463 (0.4264−469)
Pre-Mt. Simon (Argenta)	9.869×10^{-8}–0.04 (0.0001−41)	9.869×10^{-8}–0.0008 (0.0001−0.8136)	0–0.0083(0–8.413)	8.586×10^{-6}–0.008 (0.0087−8)

Maps of average PIGN and K_{SDR} for each zone were generated by vertically averaging PIGN and K_{SDR} values. Figure 3-2-13 and Figure **3-2-14** show the PIGN and K_{SDR} maps, respectively, for the small model. Figure 3-2-15 and Figure **3-2-16** show PIGN and K_{SDR} maps, respectively, for the large model. Note the differences in the average property trend in the corresponding maps. This is primarily because seismic inversion results were co-krigged with the small model and not with the large model.

The average property maps were also generated to capture locations within the study area that may have fair to good reservoir properties. The results of the generated average property maps could be used in planning locations to drill future wells, the well path, forecasting migration pathways, and estimating zonal properties. However, the maps heavily depend on the geologic data used for developing the petrophysical model and the geostatistical algorithm used for populating the petrophysical properties. Figure 3-2-17 and Figure **3-2-18** show a 3D view of porosity and permeability of the large model, respectively.

Finally, the bulk, net, and pore volumes of each zone were estimated for the large model (Table 3-2-5). However, the Mt. Simon Sandstone is known to extend beyond the large model, so the estimated volumes will be higher if a larger model is used or lower if a smaller model is used. The three assumed N/G were used to calculate the net and pore volume in each zone. The net and pore volume estimates in Table 3-2-5 represent the lower- and upper-bound values for the large model.

Table 3-2-5 Calculated volumes for zones of the Mt. Simon Sandstone in the large geologic model.

		Net to gross					
		0.6		**0.8**		**1**	
Zones	**Bulk Vol 10^6 m^3 ($\times 10^6$ ft^3)**	**Net Vol 10^6 m^3 ($\times 10^6$ ft^3)**	**Pore Vol 10^6 m^3 ($\times 10^6$ ft^3)**	**Net Vol 10^6 m^3 ($\times 10^6$ ft^3)**	**Pore Vol 10^6 m^3 ($\times 10^6$ ft^3)**	**Net Vol 10^6 m^3 ($\times 10^6$ ft^3)**	**Pore Vol 10^6 m^3 ($\times 10^6$ ft^3)**
Mt. Simon E	2,557.27 (90,309)	1,534.35 (54,185)	273.29 (9,651)	2,045.81 (72,247)	364.38 (12,868)	2,557.26 (90,309)	455.48 (16,085)
Mt. Simon D	1,571.16 (55,485)	942.70 (33,291)	167.89 (5,929)	1,256.93 (44,388)	223.87 (7,906)	1,571.16 (55,485)	279.83 (9,882)
Mt. Simon C	2,085.84 (73,661)	1,251.52 (44,197)	222.91 (7,872)	1,668.68 (58,929)	297.21 (10,496)	2,085.84 (73,661)	371.52 (13,120)
Mt. Simon B	1,783.17 (62,972)	1,069.89 (537,783)	190.54 (6,729)	1,426.54 (50,378)	254.09 (8,973)	1,783.17 (62,972)	317.60 (11,216)
Mt. Simon A upper	1,932.14 (68,233)	1,159.29 (240,940)	206.49 (7,292)	1,545.73 (54,587)	275.30 (9,722)	1,932.14 (68,233)	344.13 (12,153)
Mt. Simon A-lps	48.70 (1,720)	29.22 (1,032)	5.21 (184)	38.96 (1,376)	6.94 (245)	48.70 (1,720)	8.66 (306)
Mt. Simon A lower	618.13 (21,829)	370.87 (13,097)	66.06 (2,333)	494.50 (17,463)	88.07 (3,110)	618.13 (21,829)	110.10 (3,888)
Pre-Mt. Simon	452.45 (15,978)	271.47 (9,587)	48.34 (1,707)	361.95 (12,782)	64.48 (2,277)	452.45 (15,978)	80.59 (2,846)
Total	11,048.87 (390,187)	6,629.32 (234,112)	1,180.73 (41,697)	8,839.09 (312,150)	1,574.33 (55,597)	11,048.85 (390,187)	1,967.90 (69,496)

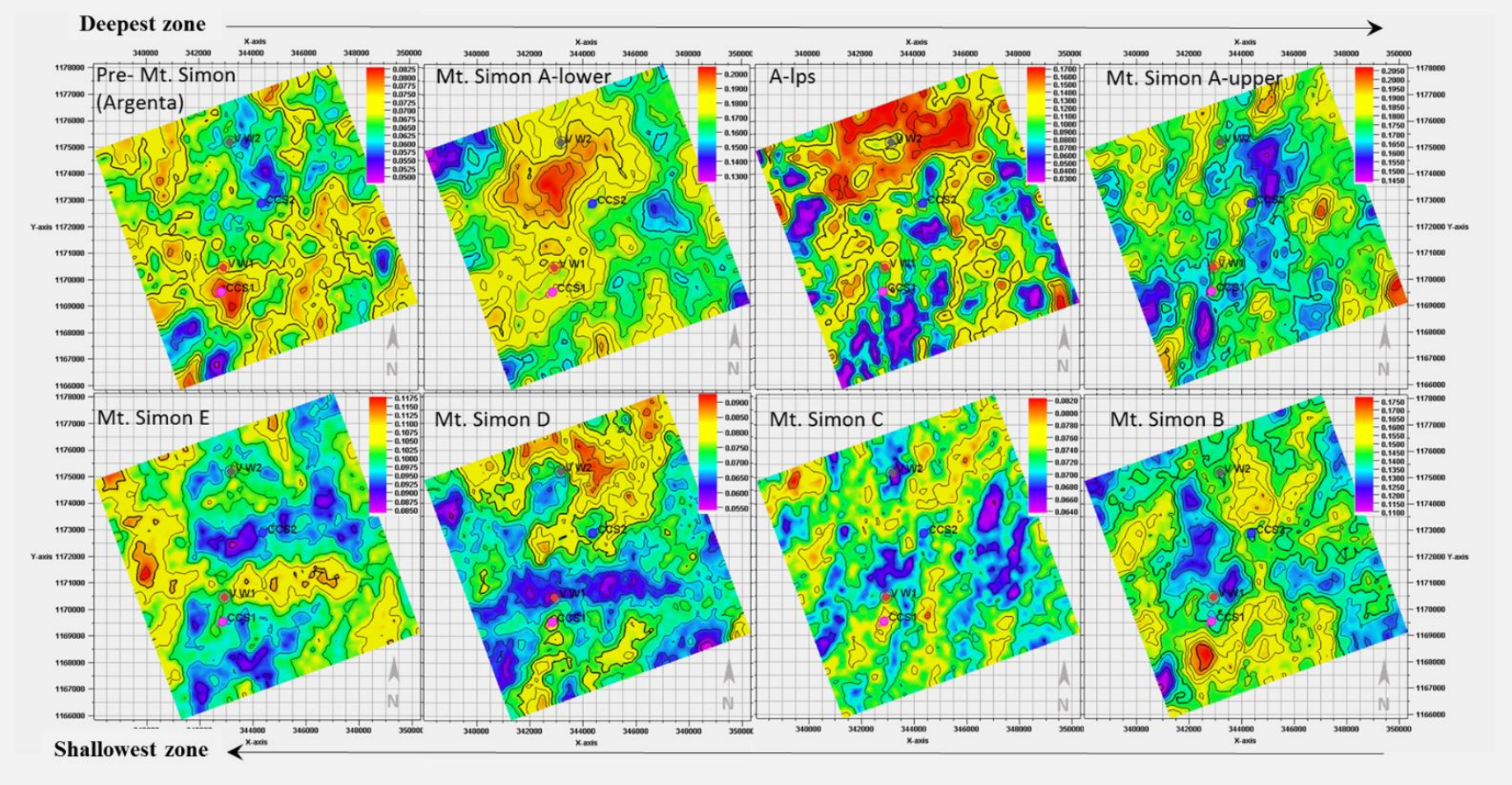

Figure 3-2-13 Average PIGN maps from the small model for the Mt. Simon Sandstone. Note that each property map is displayed with its color bar.

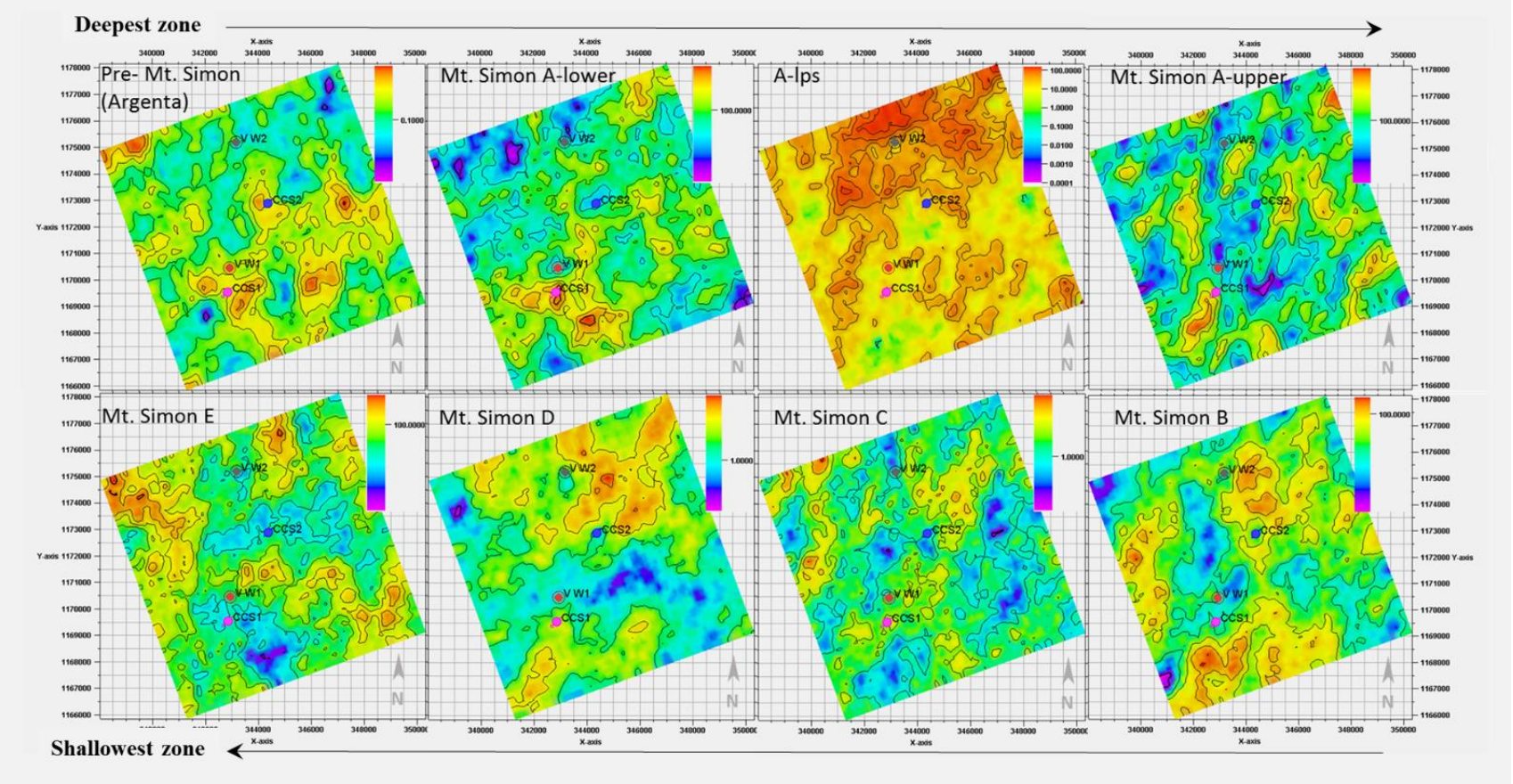

Figure 3-2-14 Average KSDR maps from the small model for the Mt. Simon Sandstone. Note that each property map is displayed with its color bar.

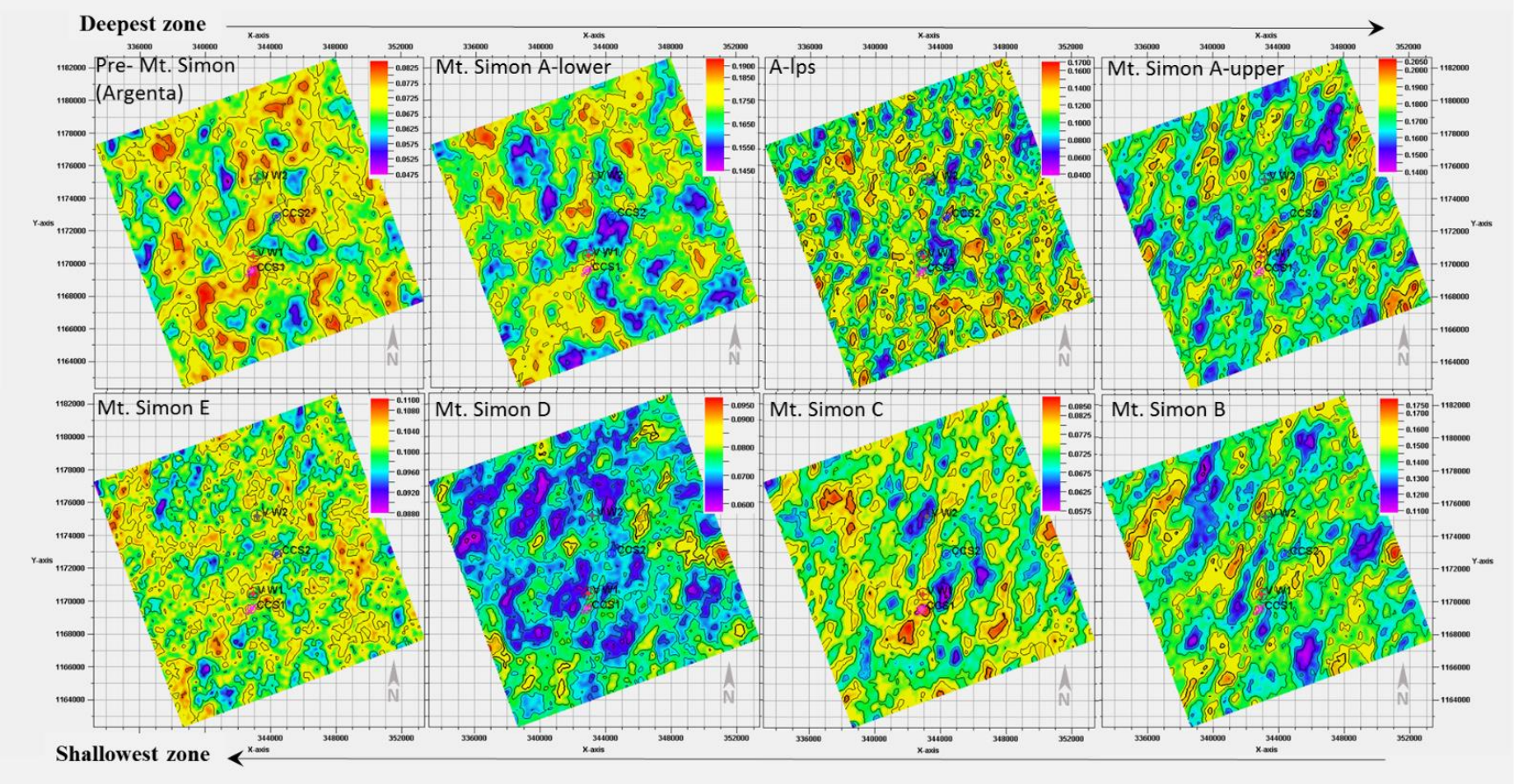

Figure 3-2-15 Average PIGN maps from the large model for the Mt. Simon Sandstone. Note that each property map is displayed with its color bar.

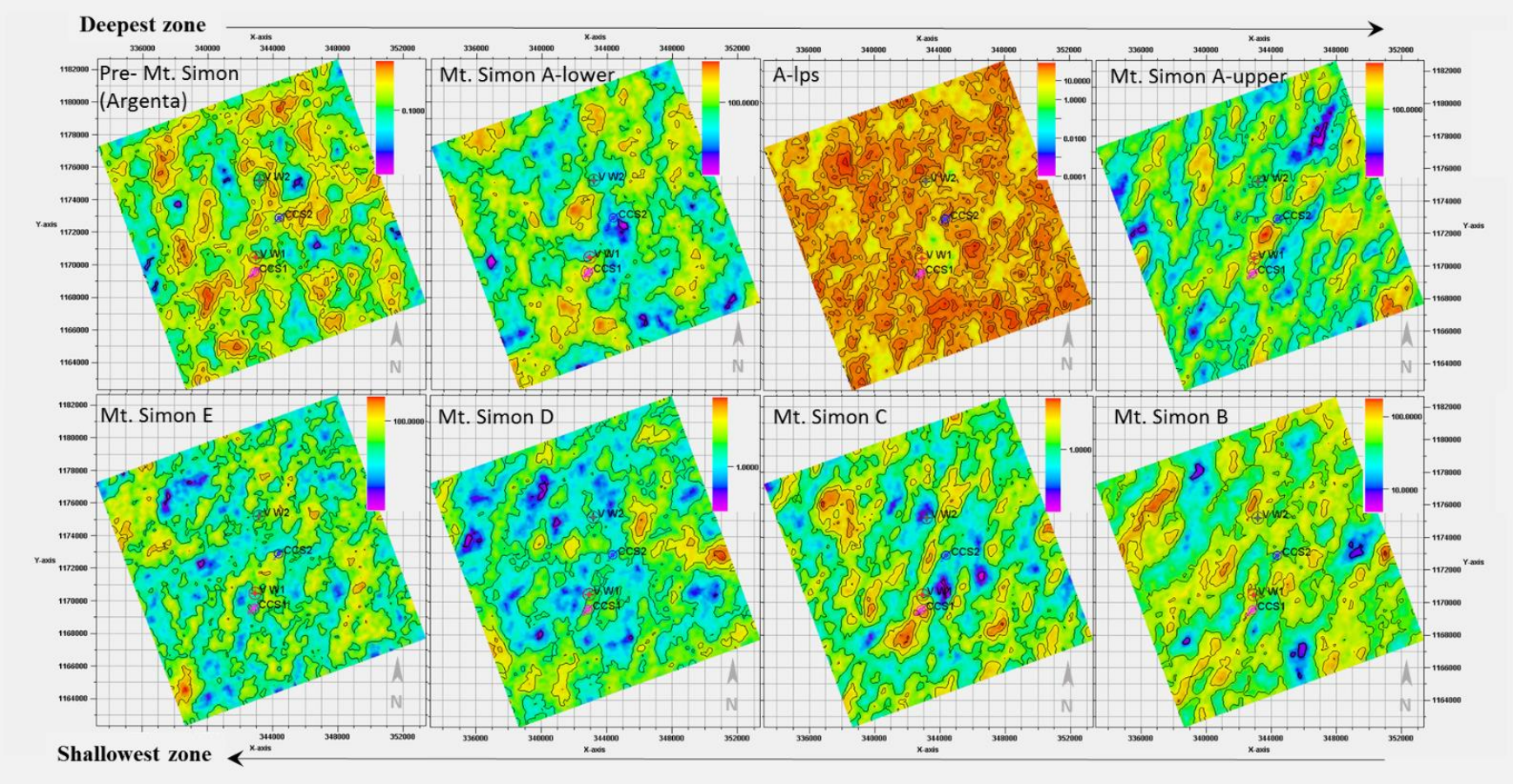

Figure 3-2-16 Average KSDR maps from the large model for the Mt. Simon Sandstone. Note that each property map is displayed with its color bar.

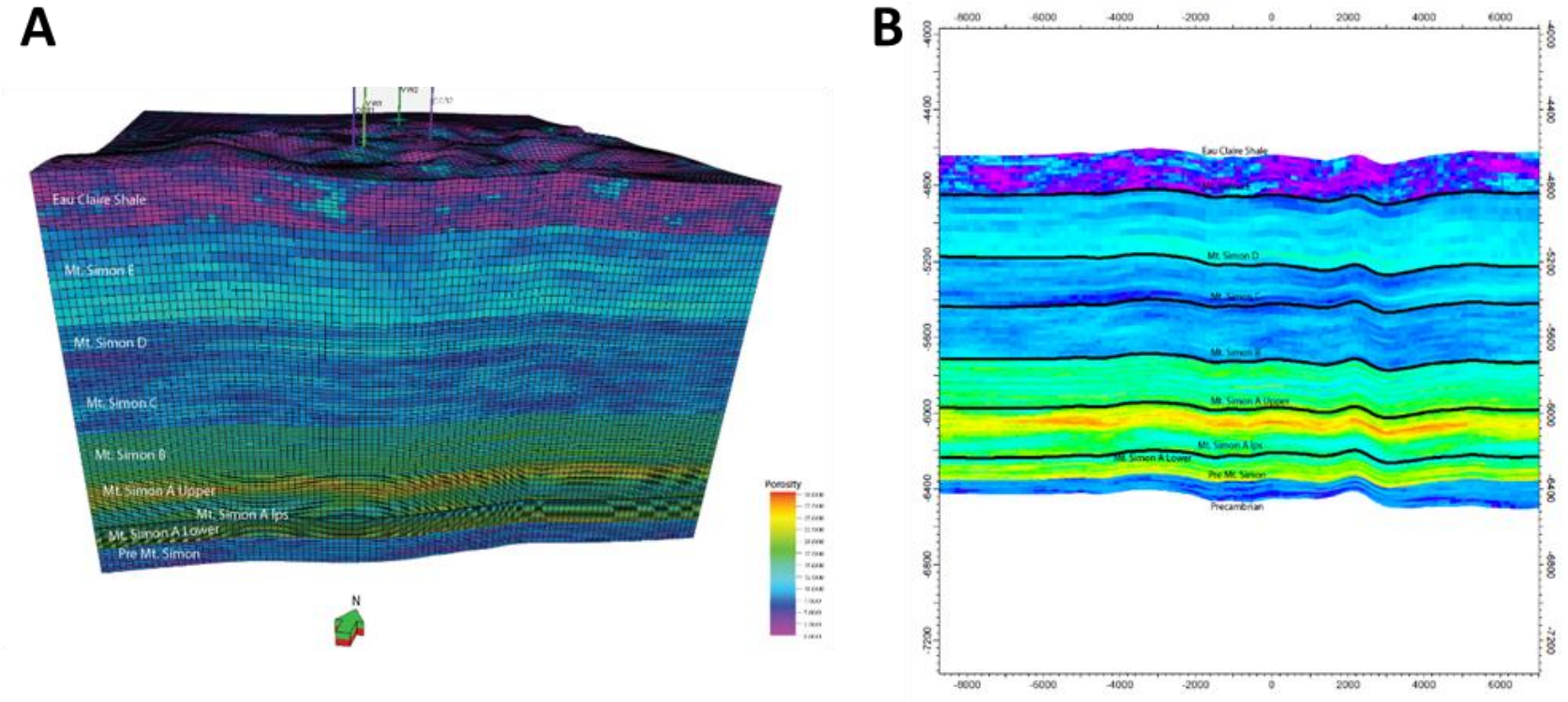

Figure 3-2-17 (A) Three-dimensional view (from the south) and (B) north-to-south cross section of porosity distribution in the Mt. Simon Sandstone, as determined from the large model.

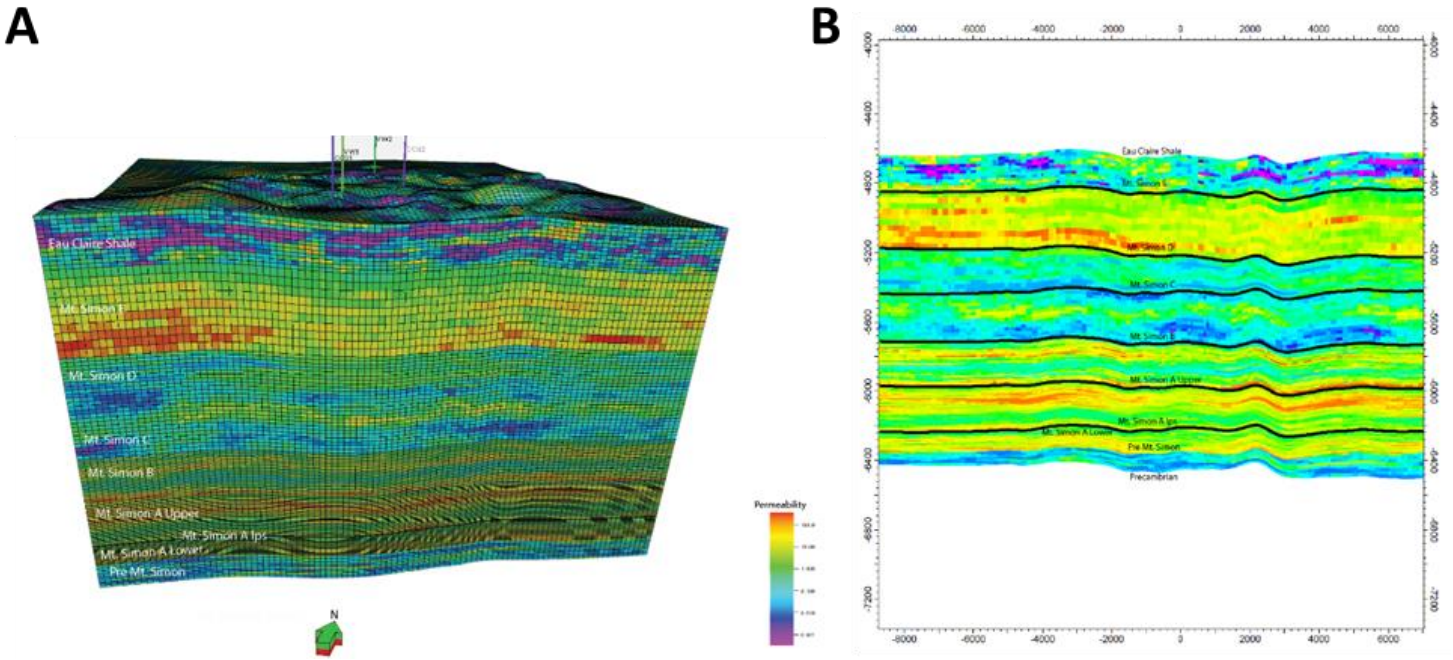

Figure 3-2-18 (A) Three-dimensional view (from the south) and (B) north-to-south cross section of permeability distribution in the Mt. Simon Sandstone, as determined from the large model.

3-2 Summary

The geologic models of the Mt. Simon Sandstone have been updated and enhanced by integrating additional geophysical log and routine core analyses data acquired from two newly drilled wells, CCS#2 and VW#2, with existing data at the IBDP site. The process involved building new structural models, carrying out petrophysical analysis on geophysical log data, upscaling formation properties, performing geostatistical data analysis, and distributing petrophysical properties using geostatistical algorithms. Results show spatial and lateral continuity of high effective porosity values (i.e., above 17%) within interwell spacing in certain Mt. Simon sandstone lithofacies (zones): A lower and A upper. Lateral continuity of moderate effective porosity values (between 10%–17%) were observed in Mt. Simon B and E, whereas lateral continuity of low effective porosity values (below 10%) were observed in other zones. However, Mt. Simon A lower, A upper, B, and E showed lateral continuity of high permeability values—that is, above 0.099 um^2 (100 md). These results suggest Mt. Simon A lower, A upper, B, and E have potential to show good injectivity when the geologic model is used for reservoir modeling.

3-2 References

Couëslan, M.L., V. Smith, G. El-Kaseeh, J. Gilbert, N. Preece, L. Zhang, and J. Gulati, 2014, Development and implementation of a seismic characterization and CO_2 monitoring program for the Illinois Basin – Decatur Project: Greenhouse Gases: Science and Technology, v. 4, no. 5, p. 626–644.

Freiburg, J.T., D.G. Morse, H.E. Leetaru, R.P. Hoss, and Q. Yan, 2014, A depositional and diagenetic characterization of the Mt. Simon Sandstone at the Illinois Basin–Decatur Project carbon capture and storage site, Decatur, Illinois, USA: Illinois State Geological Survey, Circular 583, 62 p.

Leetaru, H.E., and J.T. Freiburg, 2014, Litho-facies and reservoir characterization of the Mt. Simon sandstone at the Illinois Basin – Decatur Project: Greenhouse Gases: Science Technology, v. 4, no. 5, p. 580–595.

Logan, W.D., Horkowitz, J.P., Laronga, R. and Cromwell, D., 1997, January. Practical application of NMR logging in carbonate reservoirs. In *SPE Annual Technical Conference and Exhibition*. Society of Petroleum Engineers.

Senel, O., R. Will, and R. Butsch, 2014, Integrated reservoir modeling at the Illinois Basin–Decatur Project: Greenhouse Gases: Science and Technology, v. 4, p. 622–684.

Subtask 3-3 Geostatistical Analyses and Geocellular Modeling

Existing geocellular or reservoir models from the IBDP were reviewed and exported from Petrel to Landmark VIP (GridGen) for subsequent use as input in reservoir simulations for the Phase II application. The approach used in building the geocellular model, as described by Senel et al., 2014, is summarized below.

In building the geocellular model for Mt. Simon Sandstone, the Mt Simon Sandstone interval was classified into different geologic facies based on elastic properties output from seismic inversion work carried out on available 3D seismic data and correlation with petrophysical well log attributes. Afterward, a variogram model for different lithological types was produced in order to distribute facies over the structural model that was developed. Once this process was completed the porosity logs were interpolated over the interwell space using the geostatistical method known as co-kriging. The porosity logs was co-krigged with the facies model to generate a 3D porosity distribution. Subsequently, the geostatistical method was applied on the permeability logs and was co-krigged with the porosity model to create 3D permeability distribution. The final geological output model from this workflow was subsequently used in the reservoir flow modeling task.

The geocellular models were updated as described in Section 3-2.

3-3 References

Senel, O., R. Will, and R. Butsch, 2014, Integrated reservoir modeling at the Illinois Basin–Decatur Project: Greenhouse Gases: Science and Technology, v. 4, p. 622–684.

TASK 4-0 RESERVOIR FLOW MODELING
Subtask 4-1 Fluid Flow Simulations

Fluid flow simulations were conducted using the commercial software Nexus, version 5000.4.7, from Landmark, to predict changes in pressure (formation) and CO_2 saturation during brine extraction. The primary CO_2 trapping mechanisms modeled in the simulations were residual gas trapping (non-hysteretic) and CO_2 solubility. The geochemical reactions among CO_2, rock, and formation water were considered negligible because the target formation is predominantly composed of quartz and expected to be chemically inert for the duration of the simulated period (Yoksoulian et al., 2013).

A series of simulation scenarios were conducted to determine optimal brine extraction well types, well location(s), injection-to-extraction ratios, perforation intervals, and brine extraction and re-injection strategies to enhance pressure and CO_2 plume management in the subsurface. These scenarios were categorized into two groups based on well type: vertical well extraction and horizontal well extraction. For brine extraction via a vertical well, both brine extraction and re-injection were considered. Brine disposal into the Potosi Dolomite was also considered to evaluate the capacity and maximum allowable disposal rate.

Model Development

The geocellular model used in reservoir simulations covers an area of 2.7 × 2.7 mi (4.3 × 4.3 km) and consists of about one million gridblocks (96 × 96 × 113). Vertically, the model consists of the entire Mt. Simon, the Eau Claire shale (the upper confining formation), and the pre-Mt. Simon. Reservoir properties of the model are presented in Table 4-1-1.

Table 4-1-1 Reservoir model description.

Parameter	Value
Area	2.7 × 2.7 mi (4.3 × 4.3 km)
Grid cells	96 × 96 × 113
Lateral cell dimension	150 × 150 ft (45.7 × 45.7 m)
Vertical cell dimension	Averaging 16 ft (4.9 m)
Reference depth	5740 ft subsea (1750 m) or 6430 ft in measured depth (1960 m)
Average thickness	1816 ft (553.5 m)
Porosity	12.88%
Permeability	79.67 mD
k_v/k_h (cell)	0.1
Rock compressibility	3.88 e^{-6} 1/psi (5.63 e^{-7} 1/kPa)

*Permeability of the entire model, including Pre-Mt. Simon and Eau Claire

The areal cell dimensions are 150 × 150 ft (45.7 × 45.7 m), and the vertical cell dimensions range from 2.3 ft (0.71 m) to 36 ft (11 m), with an average of 16 ft (4.9 m). A high gridding resolution is maintained in the Lower Mt. Simon Sandstone to capture changes in pressure and CO_2 saturation in the sub-unit where the CO_2 is injected.

The relative permeability data set for Mt. Simon Units A and B is based on laboratory measurements by Schlumberger Reservoir Laboratories in 2015. Sidewall core samples were acquired from VW #2 at measured depths of 6877.6 and 6881.45 ft (2096 and 2097 m). The two cores were stacked to create a longer, composite core. Synthetic brine and supercritical CO_2 ($scCO_2$) were injected simultaneously at a constant rate of 2 cc/min at test conditions (2600 psi,

122°F or 17927 kPa, 50°C). The fractional flow rate of $scCO_2$ was increased 5 times to measure a single brine drainage saturation path. The constant flow rate was decreased to 1 cc/min and the fractional flow rate of $scCO_2$ was decreased 5 times to measure a single brine imbibition saturation path. For each measurement, 42 X-ray scans were taken at 0.24 cm intervals over the total 9.989 cm length of the composite core.

Table 4-1-2 summarizes data gathered from laboratory measurements of VW#2 core. Figure 4-1-1 shows the relative permeability curve that was fitted to the drainage data using Corey's function and used in simulations.

Table 4-1-2 Measurements of CO_2 and brine relative permeability in the Lower Mt. Simon (Schlumberger Reservoir Laboratories, 2015).

Parameter	Value
Average porosity for both cores	22.1%
Air permeability	529 mD (shallower core) 399 mD (deeper core)
Irreducible water saturation	0.326
Residual gas saturation	0.11
Minimum relative permeability of water in the drainage process	0 .000
Maximum relative permeability of water in the imbibition process	0.135
Maximum relative permeability of gas	0.86

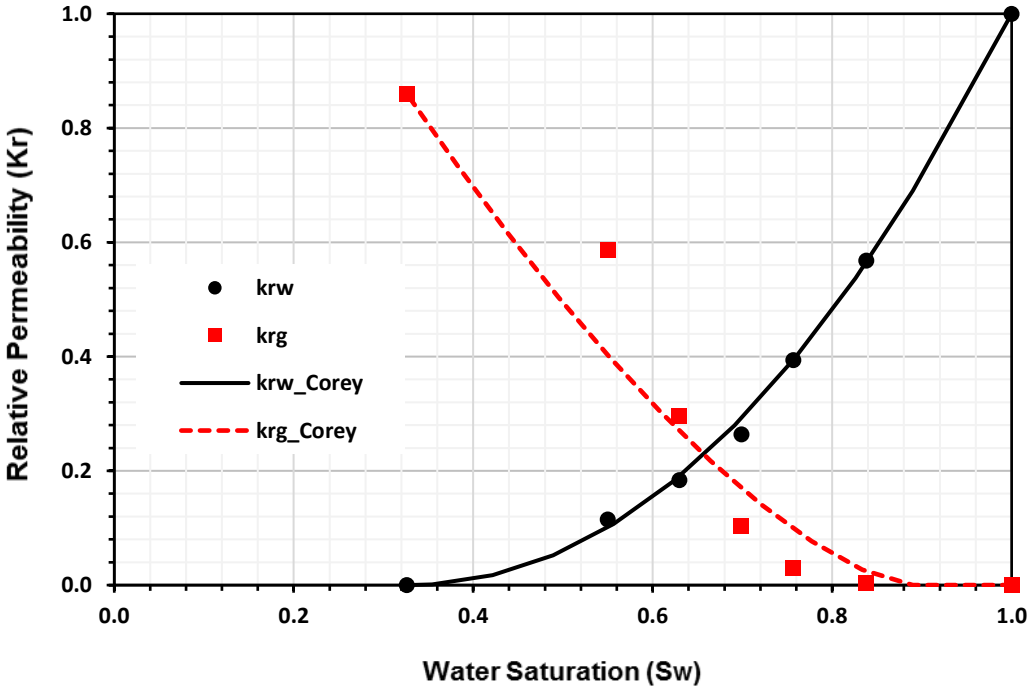

Figure 4-1-1 Drainage measurements of CO_2 and brine relative permeability, and the curve fitted using Corey's function for the Lower Mt. Simon.

Initial conditions and well data for the model are listed in Table 4-1-3. The initial pressure and temperature of the Mt. Simon Sandstone were sampled at 37 different depth intervals using a

modular formation dynamics tester (MFDT). The data were used to develop correlations (Figure 4-1-2 and Figure **4-1-3**) for estimating formation pressure and temperature as a function of depth.

Table 4-1-3 Reservoir model initial conditions and well data.

Parameter	Value
Reference depth	6430 ft (1960 m)/5740 ft subsea (1750 m)
Reference pressure	2911 psi (20,071 kPa)
Pressure gradient*	0.453 psi/ft (10.2 kPa/m)
Reference temperature*	122.6 °F (50.3 °C)
Temperature gradient	0.45 °F/100 ft (0.82 °C/100 m)
Brine salinity	200,000 ppm (lower), 150,000 ppm (middle), 100,000 ppm (upper)
Outer boundary	Infinite-acting
CCS#1 injection time	11/17/2011–11/26/2014
CCS#1 cumulative injection	999,232 tonnes
CCS#2 injection target rate	1 Mt/year

*gradients are internal to the Mt. Simon

The initial formation pressure and temperature at the top of the Lower Mt. Simon (6430 ft/1960 m) were estimated to be 2911 psi [20,071 kPa, following a gradient of 0.453 psi/ft (10.2 kPa/m)] and 122.6 °F [50.3 °C, following a gradient of 0.45 °F/100 ft (0.82 °C/100 m)]. (These gradients are within the Mt. Simon, and should not be used to project pressure or temperature from a surface datum.) The initial salinity of formation water was 200,000 ppm in Mt. Simon Units A and B, 150,000 ppm in Mt. Simon Units C and D, and 100,000 ppm in Mt. Simon Unit E.

Infinite-acting conditions were imposed on the outer boundaries of the reservoir model by attaching a Carter-Tracy analytical model to the edge gridblocks. The key input parameters for the Carter-Tracy model were the aquifer constant, *BAQ*, and a dimensionless time factor, t_c. The constant *BAQ* defines the aquifer strength and is measured in reservoir barrels per psi (rb/psi; Eq. 4-1); t_c is a measure of the conductivity of an aquifer (Eq. 4-2):

$$BAQ = \frac{\phi h c_t \theta r_o^2}{\alpha_1}, \quad \text{(Eq. 4-1)}$$

$$t_c = \frac{\alpha_2 k}{\phi \mu c_t r_o^2}, \quad \text{(Eq. 1-2)}$$

$$r_o = \sqrt{\frac{wl}{\pi}}, \quad \text{(Eq. 4-3)}$$

where w is the reservoir width (ft); l is the reservoir length (ft); ϕ is the average porosity; h is the aquifer thickness (ft); k is the aquifer permeability (md); μ is the fluid (brine) viscosity (cp); c_t is the aquifer total compressibility (psi^{-1}); θ is the angle subtended by the aquifer (0–2π); r_o is the equivalent reservoir radius (ft); and α_1 (5.61458 scf/rb) and α_2 (0.006328 cp-scf/md-psi/day) are unit-dependent constants. According to the reservoir properties, *BAQ* and t_c were calculated as 102,150.4225 rb/psi and 0.010223 1/day.

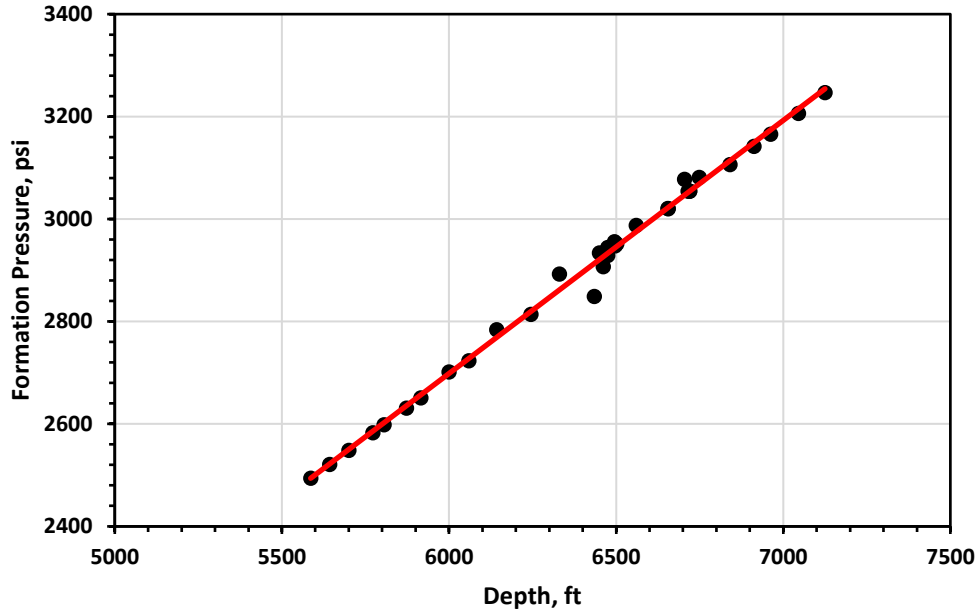

Figure 4-1-2 Measured pressure at various depths. A trend line was used to project pressure at any depth within the Mt. Simon Sandstone. The pressure at the top of the Lower Mt. Simon (6430 ft/1960 m) was estimated to be 2911 psi.

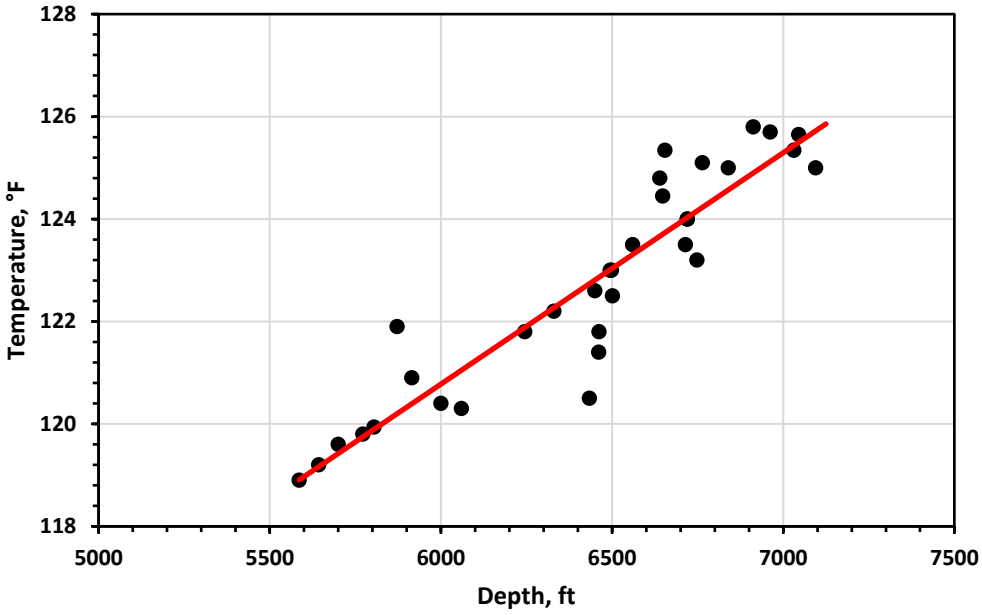

Figure 4-1-3 Measured temperature at various depths. A trend line was used to project temperature at any depth within the Mt. Simon Sandstone. The temperature at the top of the Lower Mt. Simon (6430 ft/1960 m) was estimated to be 122.6 °F (50.3 °C).

Four wells have been drilled at the storage site, including two injection wells (CCS#1 and CCS#2) and two verification wells (VW#1 and VW#2). The past and planned CO_2 injection schedules were used to project a baseline CO_2 injection scenario (BaseINJ). Approximately 1.1 million tons (1 million tonnes) of CO_2 have been injected into the Lower Mt. Simon Unit A via CCS#1 over 3 years. Another 3.3 million tons (3 million tonnes) of CO_2 will be injected via CCS#2 (perforated in the upper part of the Mt. Simon Unit A and the lower part of the Mt. Simon Unit B) over 3 years at a rate of 1.1 million tons (1 million tonnes) per annum (51,750.7 thousand standard cubic feet [Mscf]/day [1,465,580 m^3/day]). The injection of CO_2 at CCS#2 is anticipated to begin between April and June 2017.

Vertical Well Extraction

Brine Extraction

The brine extraction strategy that would predict significant and detectable pressure and CO_2 saturation changes was determined via comparison with baseline simulation results.

All simulated scenarios (Table 4-1-4) began with 3.3 million tons (3 million tonnes) of CO_2 injected via CCS#2 (from years 1 to 3), based on the historical 1.1 million tons (1 million tonnes) of CO_2 injection via CCS#1. Brine was extracted via BEST#1 for 1 year (from years 2 to 3) or until CO_2 breakthrough at BEST#1, followed by 2 years of post-extraction monitoring (from years 3 to 4). The CO_2 injection via CCS#2 was conducted in the same year of brine extraction via BEST#1.

Geologic heterogeneity, formation dip, and effective distance affect well location. Fluids have the tendency to flow through high permeability zones and bypass low permeability zones, resulting in low utilization of available pore volume or CO_2 breakthrough at an early time. The well should preferably be placed in a low permeability zone or perpendicular to the high permeability direction to direct the CO_2 plume toward the low permeability zone and increase sweep efficiency. Formation dip affects CO_2 flow via buoyancy. Improving sweep efficiency and preventing early CO_2 breakthrough can be achieved by placing a brine extraction well at a down-dip location. As for effective distance, Frailey and Finley (2011) found that a brine extraction well needs to be placed less than 0.5 mi (0.8 km) from the injection well to effectively control CO_2 plume movements.

The Mt. Simon Sandstone has relatively high permeability in the northeast to southwest direction and dips to the south and southeast of the Illinois Basin (MGSC, 2005). Therefore, a base brine extraction scenario (WellPerp) was modeled first, where BEST#1 was located 0.5 mi (0.8 km) southeast of CCS#2, in the low-connectivity down-dip direction (perpendicular to the high-connectivity direction) of the geocellular model. The location of BEST#1 was varied with respect to reservoir anisotropy, formation dip, and well spacing (the lateral distance between BEST#1 and CCS#2) to explore the effect on pressure and the CO_2 plume. Figure 4-1-4 shows location of BEST#1) in the scenarios.

The most favorable BEST#1 location (Table 4-1-4) was chosen to simulate the injection-to-extraction ratio scenarios. In the WellPerp scenario, brine was extracted at a 1:1 extraction-to-injection volumetric ratio (approximately a rate of 20,000 stb/day [3180 m^3/day]) to minimize pressure buildup, as recommended by Buscheck et al. (2011).

Two extreme ratios were studied: 10:1 (ratio with an extraction rate of 2,000 stb/day [318 m^3/day]) and 1:10 (Ratio01 with an extraction rate of 200,000 stb/day [31,800 m^3/day]). Additional ratio scenarios (Vert3k/Ratio7, Vert5k/Ratio4, and Vert10k/Ratio2) were studied to determine the minimum extraction rate required to make an effective and detectable effect on pressure and the CO_2 plume, which would minimize the volume of brine extraction and the cost of handling

extracted brine. The studied rates were 3,000, 5,000, and 10,000 stb/day (477, 795, and 1,590 m^3/day), corresponding to an injection-to-extraction ratio of 7:1, 4:1, and 2:1, respectively.

The WellPerp scenario was perforated through the entire Lower Mt. Simon. Perforation in the layers above was also considered to investigate whether the CO_2 plume can be controlled to prevent early CO_2 breakthrough. Three scenarios, PerfBtm (same as WellPerp), PerfMid, and PerfTop, were modeled with perforation intervals through the Lower (Units A and B), Middle (Units C and D), and Upper (Unit E) Mt. Simon, respectively.

Sequential extraction scenarios involved a dynamically perforated well in which the initial perforation is shut in once CO_2 breakthrough occurs, after which a shallower perforation interval is activated. In scenario PerfSeq1, the initial perforation was in the Lower Mt. Simon interval (Mt. Simon Units A and B), which was shut in once CO_2 breakthrough occurred, and then the Middle Mt. Simon (Mt. Simon Units C and D) was activated, followed by the Upper Mt. Simon (Mt. Simon Unit E) if CO_2 broke through the second perforation interval. In scenario PerfSeq2, the dynamic perforation was kept within the Lower Mt. Simon (Mt. Simon Units A and B). The three perforation intervals were a deeper portion of the Lower Mt. Simon Unit A, a shallower portion of the Lower Mt. Simon Unit A, and the Lower Mt. Simon Unit B, which was directly above Unit A.

Table 4-1-4 Vertical well brine extraction scenarios.

Scheme	Scenario	Scenario ID	Description
Well location	Reservoir anisotropy	WellPerp*	Perpendicular to high-connectivity direction
		WellPara	Paralell to high-connectivity direction
		WellDiag	Diagonal to high-connectivity direction
	Dip	DipPerp	Opposite direction of perpendicular scenario
		DipPara	Opposite direction of parallel scenario
		DipDiag	Opposite direction of diagonal scenario
	Well spacing	Spac025	0.25 mile away from injector
		Spac05	0.5 mile away from injector
		Spac075	0.75 mile away from injector
		Spac1	1 mile away from injector
Injection–extraction ratio	10:1	Ratio10	2,000 stb/day (318 m^3/day) extraction rate
	1:1	Ratio1	20,000 stb/day (3,180m^3/day) extraction rate
	0.1:1	Ratio01	200,000 stb/day (31,800 m^3/day) extraction rate
	7:1	Vert3k/Ratio7	3,000 stb/day (477 m^3/day) extraction rate
	4:1	Vert5k/Ratio4	5,000 stb/day (795 m^3/day) extraction rate
	2:1	Vert10k/Ratio2	10,000 stb/day (1,590 m^3/day) extraction rate
Perforation	Static	PerfBtm	Perforate Lower Mt. Simon
		PerfMid	Perforate Middle Mt. Simon
		PerfTop	Perforate Upper Mt. Simon
	Sequential	PerfSeq1	Perforate sequentially through entire Mt. Simon
		PerfSeq2	Perforate sequentially within Lower Mt. Simon

*Scenario WellPerp is the same as scenarios Spac05, Ratio1, and PerfBtm.

Brine Re-injection via WAG

To reduce the mobility of injected CO_2, the extracted brine can be used in a water-alternating-gas (WAG) process. Injecting CO_2 and water in alternative sequences improves contact

between CO_2 and the reservoir, i.e., sweep efficiency. It also increases the amount of CO_2 dissolved in the brine. The formation water in the Mt. Simon is close to a hypersaline brine; if treated to become a low-salinity brine, the CO_2 solubility could be doubled or even tripled (Benson and Cole 2008). The simulated brine re-injection scenarios are listed in Table 4-1-5.

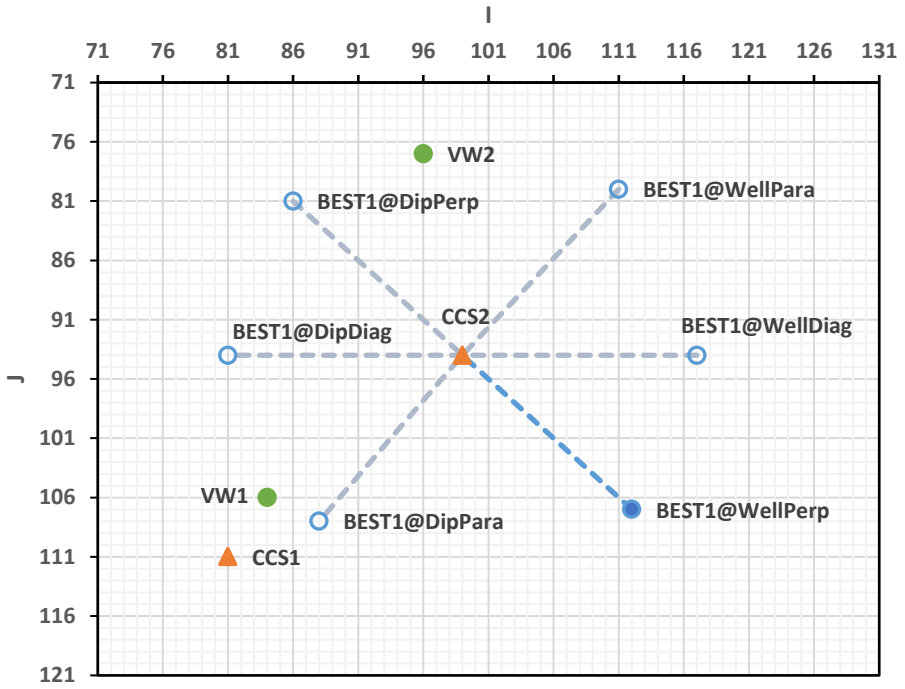

Figure 4-1-4 Brine extraction well locations of various scenarios in relation to the existing wells. For example, in scenario WellPerp, BEST#1 is one-half mile away from CCS#2 in a southeasterly direction, which is perpendicular to the high-connectivity direction based on the permeability distribution. The model is oriented in the I and J direction, which is at north 70° and north 160°, respectively (the orientation of the stress field).

Table 4-1-5 Brine re-injection scenarios.

Scenario	ScenarioID	Description
Initial slug size	Slug2	2 months of CO_2 injection initially
	Slug4	4 months of CO_2 injection initially
Water/gas ratio	WAG025	Water/gas reservoir volumetric ratio 0.25:1
	WAG05	Water/gas reservoir volumetric ratio 0.5:1
Salinity of formation water	SalHigh	200,000 ppm in Lower Mt. Simon
	SalLow	100,000 ppm in Lower Mt. Simon
Salinity of injection fluid	LMSW	Inject water extracted from Lower Mt. Simon, 200,000 ppm
	LMSWT	Inject treated Lower Mt. Simon water, 100,000 ppm

The WAG injection scenarios were conducted to evaluate the efficiency of WAG injection in controlling pressure and CO_2 plume movements and the effect of brine salinity on CO_2 dissolution. In the WAG process, an initial slug of CO_2 is injected, followed by water/CO_2 injection in cycles.

First, two scenarios were modeled to determine the proper initial slug size that would result in high CO_2 E: (1) Slug2: two months of initial CO_2 injection at 51,750.7 Mscf/day (1 million tonnes/year or 1,465,580 m^3/day) followed by WAG with a water-to-gas ratio (WGR) of 0.25:1 in one-month CO_2 injection increments (each cycle included one month of water injection and 1 month of CO_2 injection), and (2) Slug4: four months of initial CO_2 injection followed by WAG with a WGR of 0.25:1 in one-month CO_2 injection increments.

Next, a better WGR that would result in higher CO_2 *E* was determined by comparing these two scenarios: (1) WAG025: a WGR of 0.25:1 in one-month CO_2 injection increments (water injection rate of 5279.4 stb/day (839 m^3/day), gas injection rate 51,750.7 Mscf/day (1,465,580 m^3/day)), and (2) WAG05: a WGR of 0.5:1 in one-month CO_2 injection increments (water injection rate of 10,558.8 stb/day (1,864 m^3/day), same gas injection rate).

Finally, the effect of the salinity of the MT. Simon brine was studied by comparing a high-salinity scenario in the Lower Mt. Simon (SalHigh: 200,000 ppm formation water) with a low-salinity scenario (SalLow: 100,000 ppm formation water). In reality, it is unlikely that the brine salinity of the entire Lower Mt. Simon could be reduced to half its original value. Thus, two more practical scenarios, LMSW (200,000 ppm injection fluid) and LMSWT (100,000 ppm injection fluid), were added. These scenarios considered the injection fluid to be the untreated or treated Lower Mt. Simon brine.

All WAG scenarios have the same BEST#1 schedule, which is from year 2 to year 3. The CO_2 injection via CCS#2 continued year 3, until the 3 million tonnes injection goal was met. The LMSW scenario had a different schedule than the other WAG scenarios because it considered only the water source from the Lower Mt. Simon; the WAG cycle began and ended at the same time as brine extraction.

Horizontal Well Extraction

A horizontal extraction well was considered because of some potential advantages over a vertical extraction well. The advantages include (1) reducing risk of drilling into an existing CO_2 plume; (2) reducing distance between the extraction and injection wells, potentially allowing for a lower extraction rate to move CO_2 plume and resulting in more efficient pressure management; (3) providing greater certainty of reservoir geology because it is closer to the existing wells; and (4) eliminating the need for a third verification well at storage sites because the existing wells can be used to monitor pressure and CO_2 movement.

The horizontal extraction well, also referred to as BEST#1, was placed between CCS#1 and VW#1; the lateral section was located at the top of the Lower Mt. Simon at 6,450 ft (1,966 m), and it was perforated for 1,350 ft (411 m; Figure 4-1-5). Three injection-to-extraction ratio scenarios (Hori3k/Ratio7, Hori5k/Ratio4, and Hori10k/Ratio2) were considered with extraction rates of 3,000, 5,000, and 10,000 stb/day (477, 795, and 1,590 m^3/day), representing an injection-to-extraction ratio of 7:1, 4:1, and 2:1, respectively (

Table **4-1-5**). These rates are considerably less than the rates used in the vertical well scenarios, thus reducing the total cost of brine treatment.

Vertical permeability variation plays an important role in vertical CO_2 movement, and its effect was studied by conducting simulations with vertical-to-horizontal permeability ratios (kv/kh) of 0.1, 0.2, and 0.3.

A parallel study by Schlumberger conducted horizontal extraction well simulations based on a different geocellular and reservoir model, as described by Senel et al., (2014). Schlumberger

used the ECLIPSE reservoir simulator with the CO_2STORE module. Four extraction rates were considered: 5;000; 10,000; 15,000; and 20,000 stb/day (795, 1,590, 2,385, and 3,180 m^3/day).

Figure 4-1-5 Site map showing injector wells (CCS#1 and CCS#2), monitoring well (VW#1), and proposed horizontal brine extraction well (BEST#1), which is labeled as "HORIZ_MSB." The blue line is the lateral extent of the well.

Table 4-1-5 Horizontal well brine extraction scenarios.

Scheme	Scenario	Scenario ID	Description
Injection–extraction ratio	7:1	Hori3k/Ratio7	3,000 stb/day (477 m^3/day) extraction rate
	4:1	Hori5k/Ratio4	5,000 stb/day (795 m^3/day) extraction rate
	2:1	Hori10k/Ratio	10,000 stb/day (1,590 m^3/day) extraction
	Vk effect	HoriVk01	Vk=0.1 (kv/kh=0.1)

Scheme	Scenario	Scenario ID	Description
Vertical permeability		HoriVk02	Vk=0.2 (kv/kh=0.2)
		HoriVk03	Vk=0.3 (kv/kh=0.3)

Brine Disposal into the Potosi Dolomite

The Potosi Dolomite has been used for waste disposal in Tuscola, Illinois, since 1966, where three disposal wells have been used to inject 19.3 billion gal (73.1 L) of liquid into the Potosi as of October 31, 2016. The overall average injection rate ranges from 128 to 631 gal/min (485 to 2,398 L/min). The wells are currently operating at 60 to 350 gal/min (227 to 1,325 L/min; Brower et al., 1989; unpublished report, Illinois Environmental Protection Agency, Springfield, IL).

A reservoir model of the Potosi at the IBDP was constructed to evaluate the feasibility of disposing brine extracted from Lower Mt. Simon into the Potosi. The model covers an area of 2.7 × 2.7 mi (4.3 × 4.3 km) and consists of approximately 0.7 million gridblocks (96 × 96 × 71). The areal cell dimensions are 150 × 150 ft (45.7 × 45.7 m), and the vertical cell dimensions range from 1 ft (0.3 m) to 47 ft (14 m), with an average of 8 ft (2.4 m).

The total thickness of the Potosi Dolomite is 545 ft (166 m), and it is divided into two vugular zones that alternate with three low-permeability zones (see Task 3 for further description of the geology). The two vugular zones are about 10 ft (3 m) each and have a permeability up to 9,000 md, averaging 2,000 md. The three low-permeability zones have an average permeability of 2 md, 6 md, and 1 md, respectively, from top to bottom.

Infinite-acting conditions were assumed at the lateral boundaries of the model by attaching Carter-Tracy aquifers with average formation properties of corresponding zones. A no-flow boundary was assumed at the top and bottom of the model. The disposal well was placed close to the extraction well to minimize the cost of transporting brine.

Table 4-1-6 lists simulation scenarios conducted to determine the maximum brine injection rate and storage capacity of the Potosi Dolomite. To determine a maximum injection rate, the bottomhole pressure was constrained to be no greater than 3,044 psi (20,988 kPa), which was calculated based on a pressure gradient of 0.7 psi/ft (16 kPa/m). The disposal well was set to inject brine extracted from the Lower Mt. Simon without a rate constraint for 2 years, and then to be shut in. To determine the storage capacity, the disposal well was set to inject brine at 10,000 stb/day (1,590 m^3/day, or 290 gal/min) for 20 years, and the formation pressure variation was investigated.

Table 4-1-6 Scenarios of brine disposal into the Potosi .

Scenario	Scenario ID	Description
Maximum rate	PotoVQmax	Inject at maximum rate close to vertical extraction well
	PotoHQmax	Inject at maximum rate close to horizontal extraction well
Capacity	PotoV10k	Inject at 10,000 stb/day (1,590 m^3/day) close to vertical extraction well
	PotoH10k	Inject at 10,000 stb/day (1,590 m^3/day) close to horizontal extraction well

Subtask 4-2 Analyses and Interpretation of Flow Modeling Results

The flow modeling results were analyzed to evaluate the efficacy of and ability to monitor brine extraction for plume and pressure management. Reservoir simulation scenarios for brine extraction and re-injection were evaluated in terms of differential pressure (DP), differential

pressure index (DPI), storage efficiency (E), CO_2 plume distribution, well monitoring pressure, and seismic detectability. Geomechanical effects were also investigated to ensure formation and well integrity under injection and extraction operations. Analytical methods were used for vertical well scenarios, and coupled hydro-mechanical modeling analysis was used for horizontal well scenarios. Additionally, the Potosi was evaluated in terms of the maximum allowable brine injection rate and disposal capacity.

DP, DPI, and E

The performance metrics for comparing simulated scenarios with the baseline simulations are DP, DPI, and E. Differential pressure is defined for each grid cell as the pressure at any time, $p(t)$, minus the pressure at an initial time or a given point in time, $p(i)$;

$$DP = p(t) - p(i).$$

The DPI is defined as the ratio of pressure change at any time to the maximum allowable pressure change $[p(max) - p(i)]$:

$$DPI = \frac{p(t)-p(i)}{p(max)-p(i)},$$

where the maximum pressure of a gird cell, $p(max)$, is calculated as the product of the measured mid-depth of the cell and the maximum allowable pressure or fracture gradient, which is about 0.7 psi/ft for the Mt. Simon Sandstone.

The DPI can be viewed as a dimensionless differential pressure with regard to the maximum allowable pressure change of a formation. A negative value indicates the pressure dropped and a positive value indicates the pressure increased. A value of zero indicates no pressure change ($p[t]$ equals $p[i]$), and a value of one indicates the current pressure is at the maximum allowable pressure ($p[t]$ equals $p[max]$). In the latter case, formation damage could occur, and thus this indicates an ineffective pressure management strategy. A value of DPI close to zero indicates an effective pressure management strategy because it means that brine extraction has been able to reduce pressure buildup from CO_2 injection.

The geologic CO_2 storage efficiency is defined as the ratio of the injected volume of CO_2 (V_{CO2}) to the accessible pore volume (V_p):

$$E = \frac{V_{CO2}}{V_p}.$$

The accessible pore volume is dependent on the three-dimensional size and shape of the CO_2 plume, which varies through time. For this study, the rectangular geometry at each time was defined at the minimum and maximum I, J, and K cell coordinates with CO_2 saturation (S_g) greater than zero. Within this rectangular volume, the total CO_2 volume was divided by the total pore volume to obtain a value for E.

The overall effect of brine extraction can be evaluated in terms of DP by comparing selected brine extraction and re-injection scenarios with the baseline injection. Figure 4-2-1 compares the DP before and after extraction between BaseINJ and WellPerp. Whereas continuous injection increased formation pressure up to 20 psi (138 kPa), brine extraction decreased formation pressure within the entire mid-perforation layer of CCS#2, especially the area covering the two injectors and the extraction well, where the pressure drop was up to 300 psi (2069 kPa), indicating brine extraction greatly reduced the pressure buildup from injection. Figure 4-2-2 compares the DP in the first year of CO_2 injection between WellPerp and WAG05. The difference between these two scenarios during this period is that CO_2 was injected continuously in WellPerp and in a WAG process in WAG05. No brine was extracted in the first year, so the DP shows the effect of

continuous injection and WAG. Compared with continuous injection, the WAG process yielded higher DP around the injector and lower DP further out.

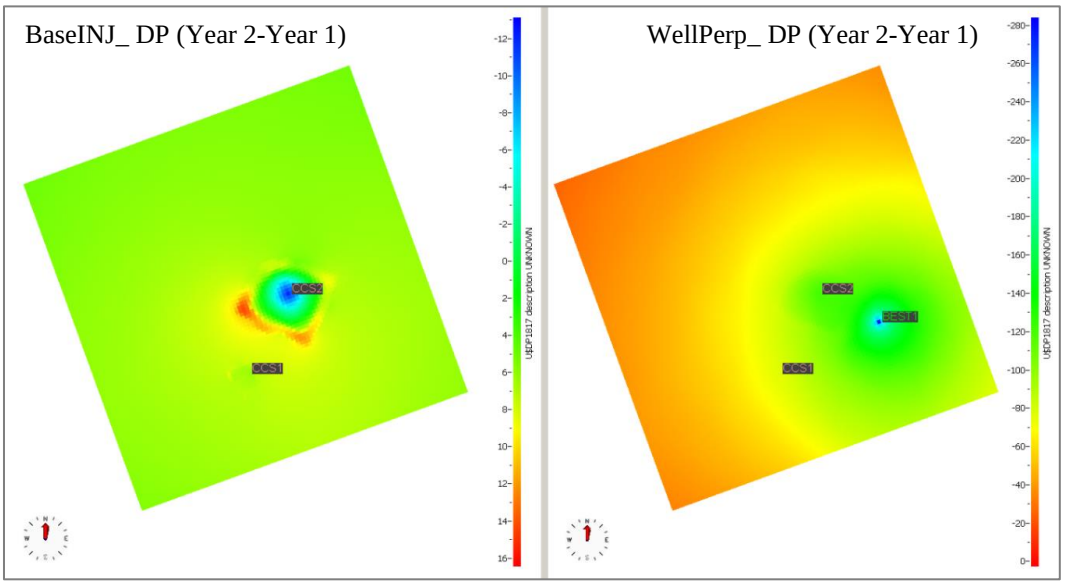

Figure 4-2-1 Differential pressure (DP) of BaseINJ and WellPerp before and after extraction (top view of the CCS#2 mid-perforation layer). The pressure drop from brine extraction was up to 300 psi around the wells. Cooler color indicates greater pressure drop.

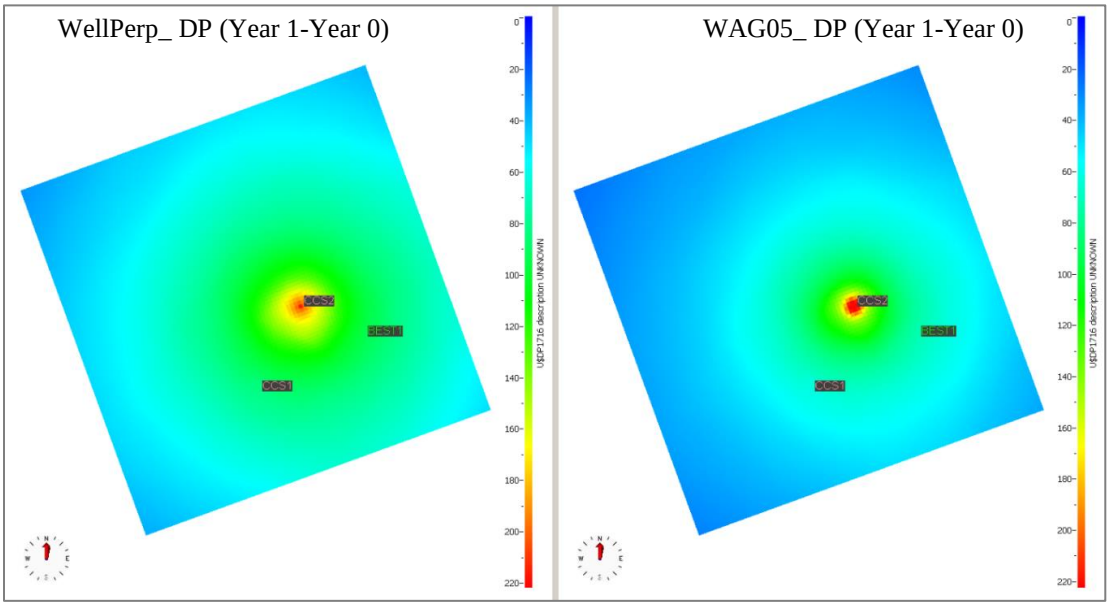

Figure 4-2-2 Differential pressure of WellPerp and WAG05 in the first year of injection (top view of the CCS#2 mid-perforation layer). The differential pressure was more restricted to wells in WAG than in continuous injection.

The DPI was used as a primary performance metric to determine the optimal extraction strategy to implement. The DPI distribution at the end of injection was summarized in terms of the relative frequency of DPI at various intervals, which is an overall effect of CO_2 injection and brine

extraction (Figures 4-2-3 through 4-2-10). The effect of brine extraction alone can be evaluated by comparing the DPI distribution to that of the baseline injection scenario.

In the brine extraction scenarios, early CO_2 breakthrough from BEST#1 was encountered for scenarios WellDiag, DipDiag, DipPara, and Spac025, suggesting the well locations are along fast flow paths from the injectors. Scenario Ratio01 also experienced early CO_2 breakthrough because of the high extraction rate. Scenario PerfMid was not able to extract brine at the desired rate because the perforated interval was within a low permeability zone, the Middle Mt. Simon (Units C and D). Both sequential perforation scenarios did not experience CO_2 breakthrough at the initial perforation interval, so other perforation intervals were not activated. As a result, PerfSeq1 and PerfSeq2 were the same as WellPerp and PerfBtm.

For all other brine extraction scenarios via either a vertical well or a horizontal well, the DPI at the end of injection since brine extraction (years 1–3) ranged from –0.019 to 0.019 (Figures 4-2-3 through 4-2-7). Within that range, most DPI values were between 0.003 and 0.009. This indicates effective pressure management because brine extraction decreased the rate of pressure buildup during CO_2 injection. Pressure buildup was less than 20% of the maximum allowable pressure change. Among all vertical brine extraction scenarios, WellPerp provided a noticeably favorable DPI distribution (most DPI values occurred from 0.003 to 0.005) because of the greater pressure drop compared with BaseINJ. This indicates that better pressure management can be expected when the extraction well is located 0.5 mi (0.8 km) away from the injector in the down-dip, low-connectivity direction; the perforation is in the injection zone; and brine is extracted at an injection-to-extraction ratio of 1:1. When the extraction rate is lower than 10,000 bbl/day (1,590 m^3/day), both the vertical and horizontal rate scenarios have a similar DPI distribution, suggesting the effect of extraction rate on the DPI becomes less significant once it drops below 10,000 bbl/day (1,590 m^3/day).

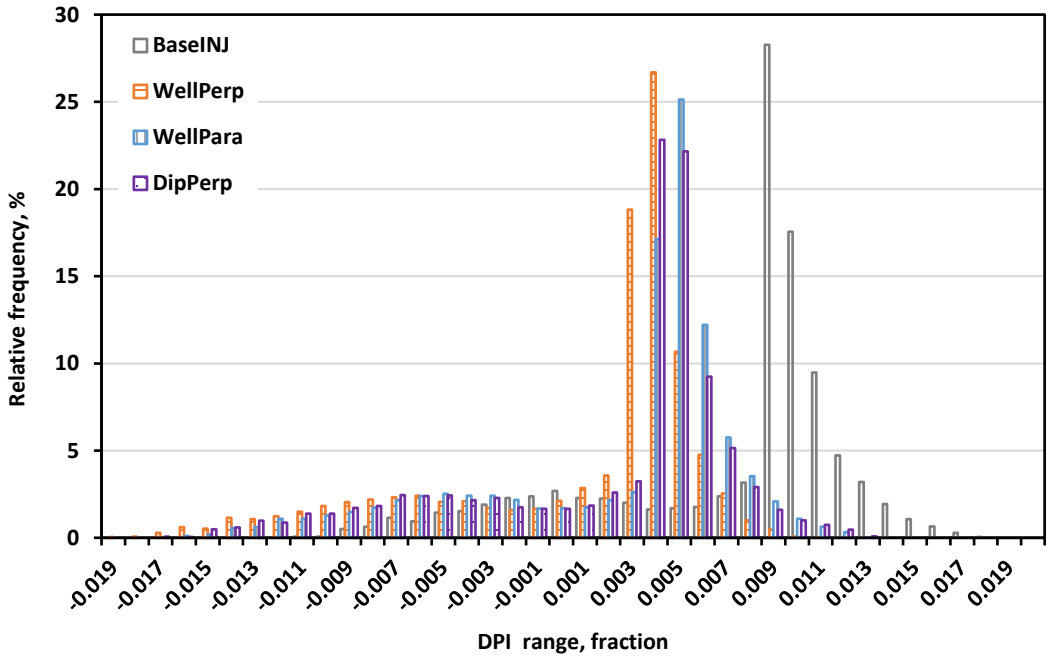

Figure 4-2-3 DPI of well location scenarios at the end of injection since brine extraction.

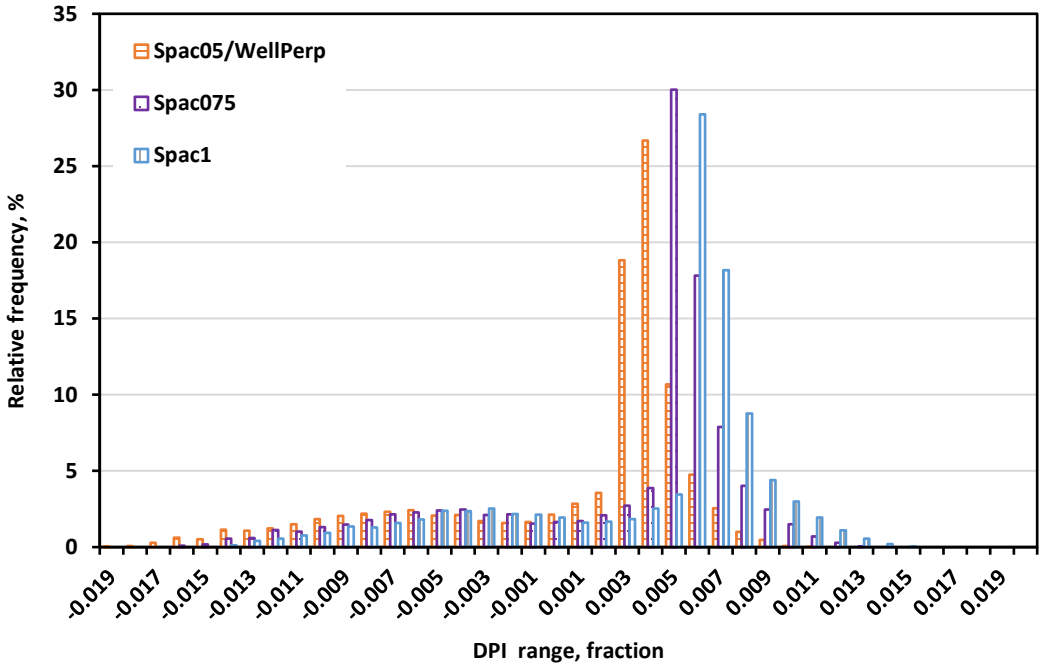

Figure 4-2-4 DPI of well spacing scenarios at the end of injection since brine extraction.

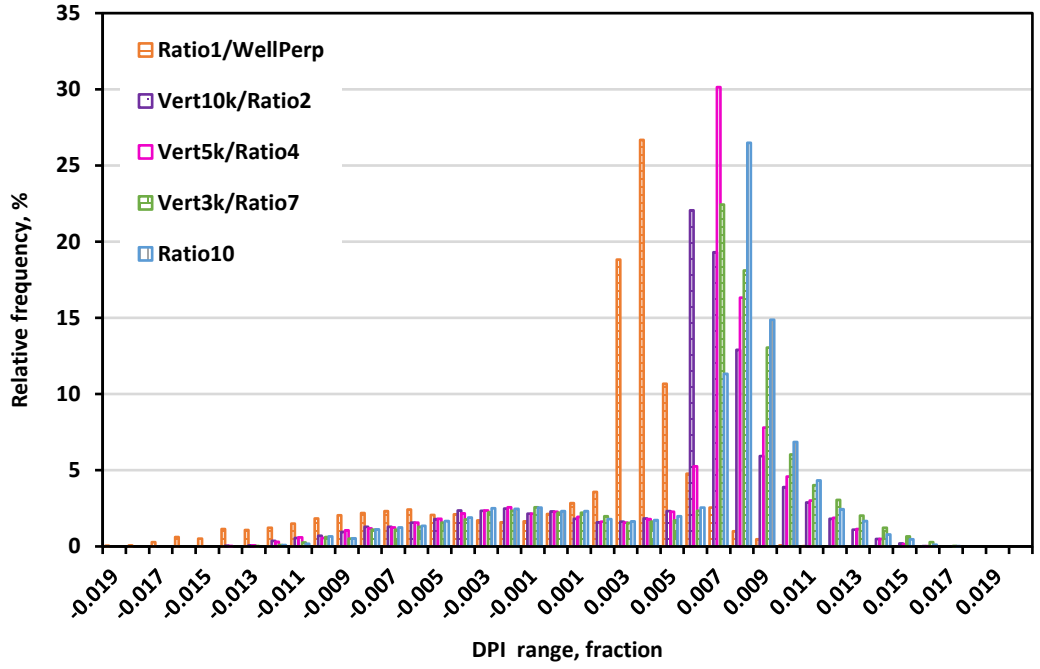

Figure 4-2-5 DPI of extraction ratio scenarios at the end of injection since brine extraction.

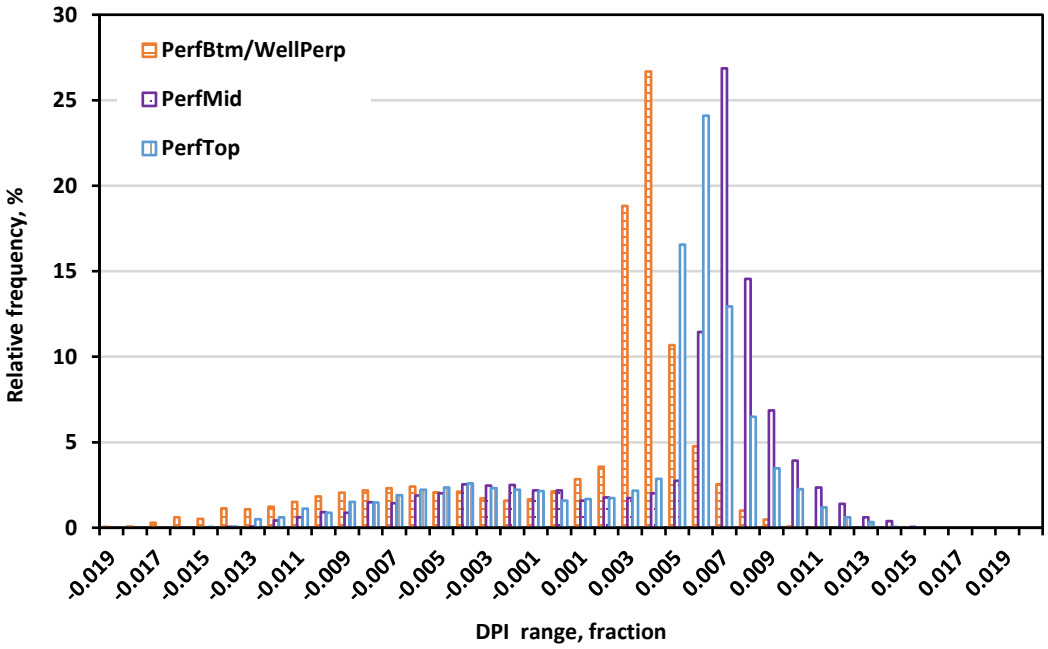

Figure 4-2-6 DPI of perforation scenarios at the end of injection since brine extraction.

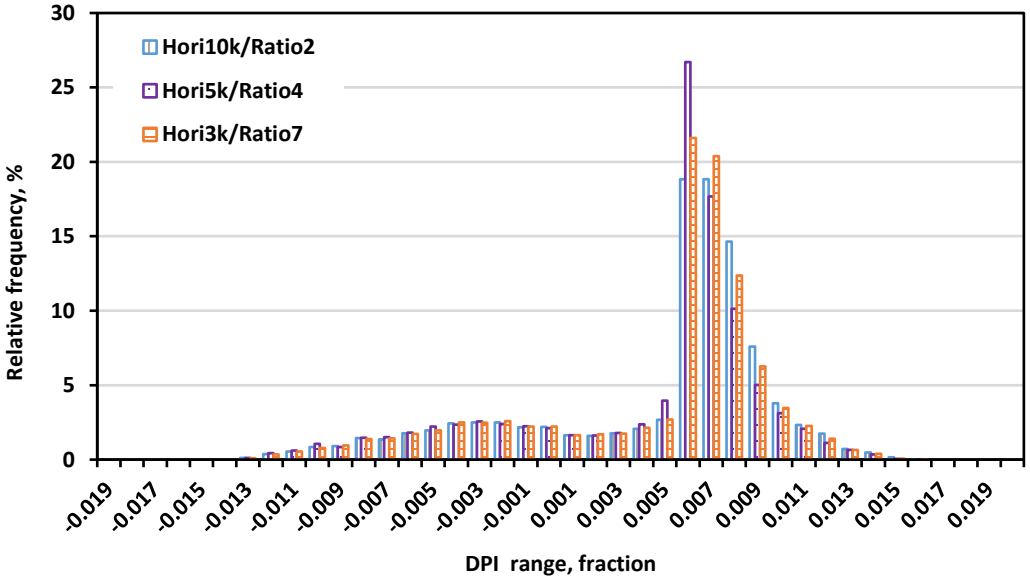

Figure 4-2-7 DPI of horizontal well scenarios at the end of injection since brine extraction.

In the brine re-injection scenarios, the DPI was calculated between pre- and post- injection (years 0–5) because the first-year injection schedule in the salinity scenarios was different from other WAG scenarios, and, for all WAG scenarios, the WAG injection time was longer than continuous injection given the same cumulative CO_2 injection target. A greater initial slug size yielded a greater pressure drop (Figure 4-2-8), so an initial slug of 4 months of CO_2 injection at 51,750.7 Mscf/day (1,465,580 m^3/day) was used in the following scenarios. With the same initial slug size, the scenario with the higher brine extraction rate (WAG05) yielded a slightly favorable

pressure drop (Figure 4-2-9). Additionally, the net cumulative water extraction of WAG05 was 56% of WAG025. This result suggests that less water needs to be disposed of in the WAG05 scenario. Therefore, a WGR of 0.5:1 was chosen for the salinity scenarios. SalHigh is the same as WAG05, where the salinity of the Lower Mt. Simon remains the same as its original value. Reducing the salinity of the Lower Mt. Simon in half (scenario SalLow) had little effect on DPI; however, beginning WAG in the second year instead of the first year and injecting brine extracted from Lower Mt. Simon (scenario LMSW) greatly reduced the pressure increase (Figure 4-2-10). The DPI distribution was the same for LMSW and LMSWT, which indicated that injecting extracted and treated (lower salinity) brine had no effect on pressure change. However, injecting the lower salinity brine could increase CO_2 solubility in the affected area (Figure 4-2-11). Overall, LMSWT is the optimal brine re-injection scenario. This indicates that better pressure management can be expected when the extracted brine is re-injected via WAG with simultaneous brine extraction.

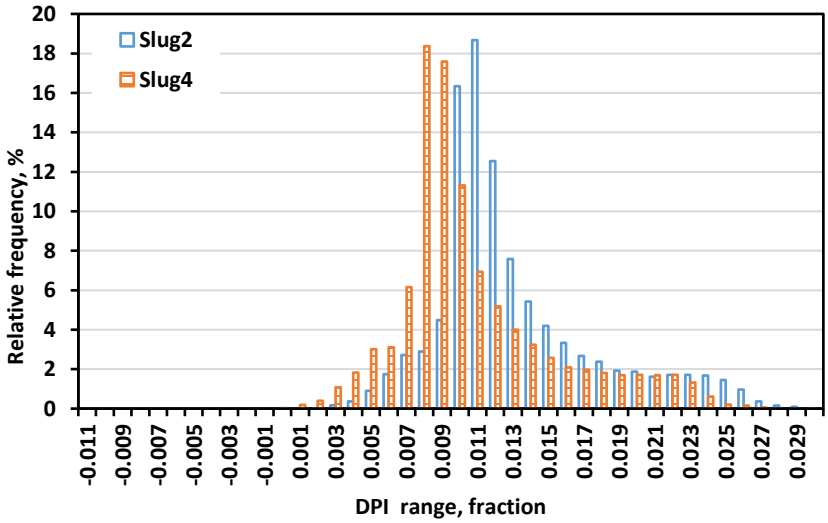

Figure 4-2-8 DPI of initial slug size scenarios between post- and pre- injection.

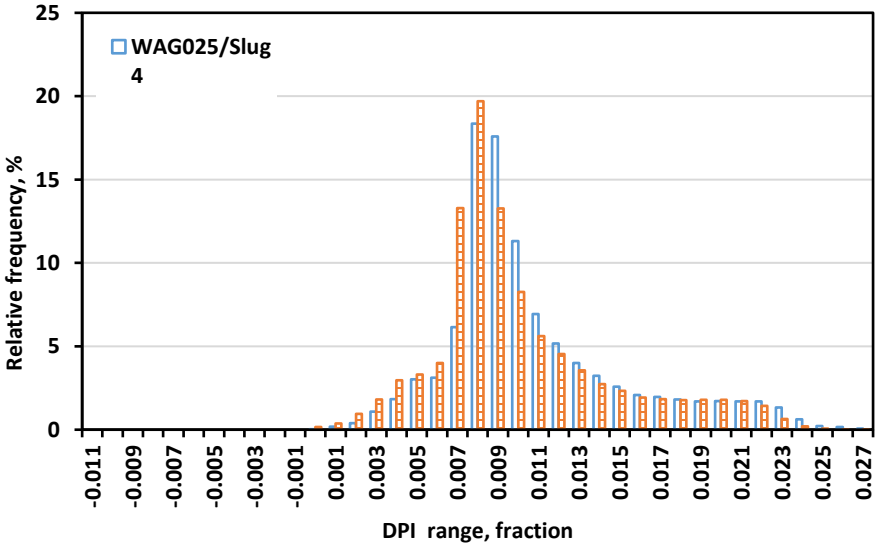

Figure 4-2-9 DPI of WGR scenarios between post- and pre- injection.

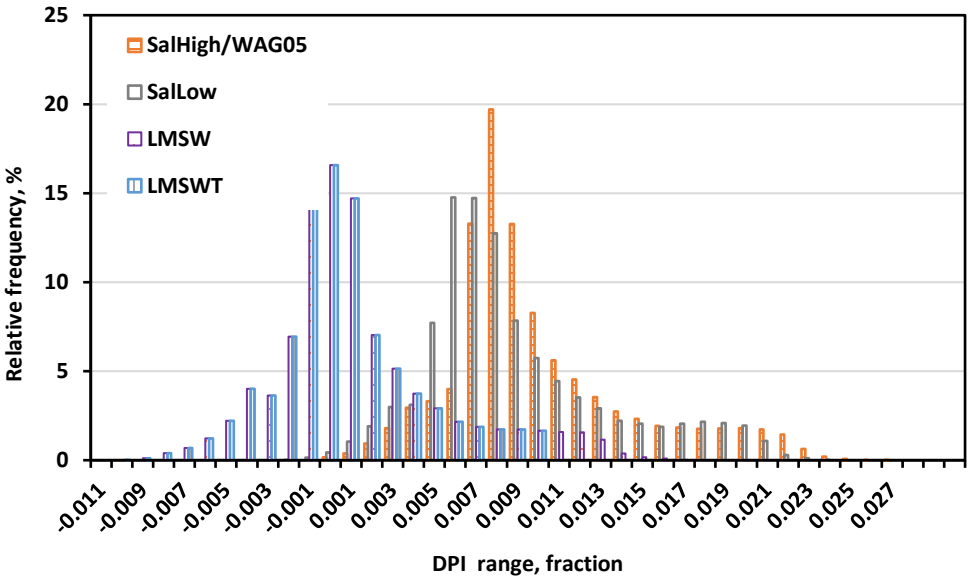

Figure 4-2-10 DPI of salinity scenarios between post- and pre- injection.

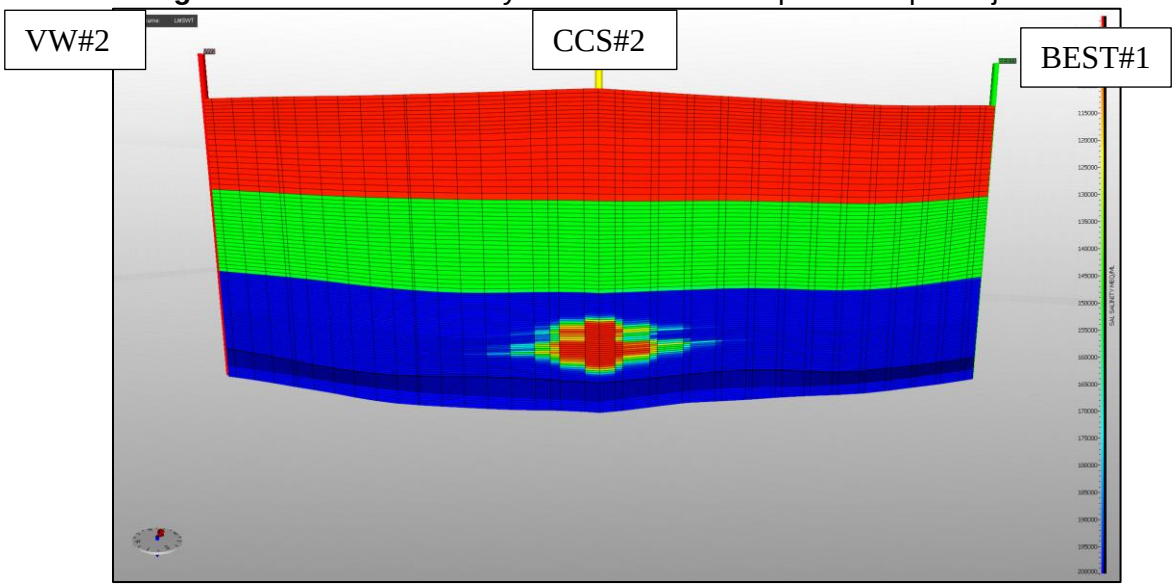

Figure 4-2-11 Cross sectional view of formation water salinity for scenario LMSWT. The injected lower salinity brine is shown in warmer colors (red and green) in the Lower Mt. Simon (in blue). A small, near-well area of the formation experienced a change in salinity (red and green area in the blue layer), which could increase the CO_2 solubility in that area.

Figure 4-2-12 compares the DPI of the optimal brine extraction and re-injection scenarios with the baseline between post- and pre-injection. The DPI of the baselines and LMSW ranged from –0.01 to 0.016 and were concentrated around 0, indicating the formation pressure was close to the pre-injection formation pressure in most parts of the reservoir. The DPI of WAG05 was concentrated around 0.008 and increased to 0.027, indicating an overall pressure increase. This result shows that water injection increased formation pressure more than did CO_2 injection, given that WAG05 was a 3-year WAG process; in contrast, LMSW included one year of WAG, and the

baselines had no water injection. However, the DPI values were small enough to maintain formation integrity.

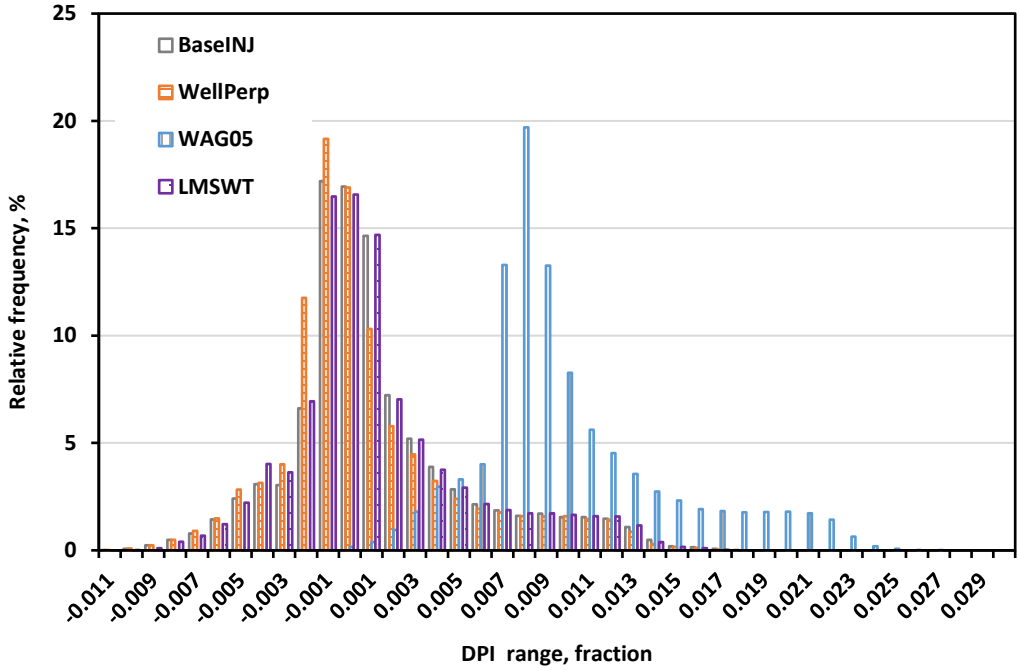

Figure 4-2-12 DPI of optimal scenarios and the baseline between post- and pre injection.

Storage efficiency was used as a secondary performance metric to assist performance evaluation. The E of all brine extraction and re-injection scenarios were compared with the baseline at the end of CO_2 injection (Tables 4-2-1 and 4-2-2). Most brine extraction scenarios yielded a higher E than the scenario without brine extraction, except the vertical extraction scenarios with an extraction rate of 5,000 bbl/day (795 m^3/day) and below. This indicates brine extraction with a vertical extraction well effectively improved E at only high rates (10,000 bbl/day [1,590 m^3/day]), whereas a horizontal extraction well effectively improved *E* at both high rates and low rates (as low as 3,000 bbl/day [3,000 m^3/day]). In the vertical extraction scenarios, WellPerp yielded the highest E, with a 7.32% increase over the baseline. In the horizontal extraction scenarios, Hori10k/Ratio2 yielded a 12.39% increase in E over the baseline and a 4.72% increase in E over WellPerp, suggesting higher extraction rates improve E and a horizontal well yields a more favorable E than a vertical well. However, lower rates should be considered to minimize the volume of brine extraction. Therefore, Hori5k is a better option because it provides similar increase in E with WellPerp with a low rate.

All re-injection scenarios had better E than did the baseline and WellPerp, which indicates brine re-injection in a WAG process improved E. Among all the WAG scenarios, the SalLow scenario had the highest E, suggesting that low-salinity formation water favors E and could be more effective at improving storage efficiency than other engineering measures. However, SalLow is a conceptual scenario that is not feasible. All other WAG scenarios had similar E, with a 6.96% to 9.90% increase in E over the baseline and a 2.19% to 4.93% increase in E over WellPerp.

Table 4-2-1 Storage efficiency of brine extraction scenarios at year 3.

Scenario	Efficiency, %	Increase over baseline, %
BaseINJ	3.55	N/A
WellPerp*	3.81	7.32
WellPara	3.70	4.23
DipPerp	3.62	1.97
Spac075	3.70	4.23
Spac1	3.70	4.23
Ratio10	3.55	0
Vert3k/Ratio7	3.55	0
Vert5k/Ratio4	3.55	0
Vert10k/Ratio2	3.63	2.25
PerfMid	3.61	1.69
PerfTop	3.70	4.23
Hori3k/Ratio7	3.72	4.79
Hori5k/Ratio4	3.81	7.32
Hori10k/Ratio2	3.99	12.39

*Scenario WellPerp is the same as scenarios Spac05, Ratio1, and PerfBtm.

Table 4-2-2 Storage efficiency of brine re-injection scenarios at year 5.

Scenario	Efficiency, %	Increase over baseline, %	Increase over WellPerp, %
BaseINJ	3.48	NA	N/A
WellPerp	3.65	4.62	N/A
Slug2	3.83	9.90	4.93
Slug4	3.83	9.86	4.93
WAG025	3.83	9.86	4.93
WAG05	3.82	9.54	4.66
SalHigh	3.82	9.54	4.66
SalLow	4.30	23.29	17.81
LMSW	3.73	6.96	2.19
LMSWT	3.73	6.96	2.19

The LMSW and LMSWT had lower E compared to other re-injection scenarios. To better understand the difference, the CO_2 plume distribution was investigated. Figure 4-2-13 and 4-2-14 show the CO_2 plume distributions of SalHigh and LMSWT at the end of injection. The CO_2 plume of SalHigh was further away from BEST#1 than was that of scenario LMSWT. This indicates that a longer period of WAG cycles in SalHigh reduced mobility of the CO_2 plume, resulting in higher *E* and suggesting a lower risk of CO_2 breakthrough.

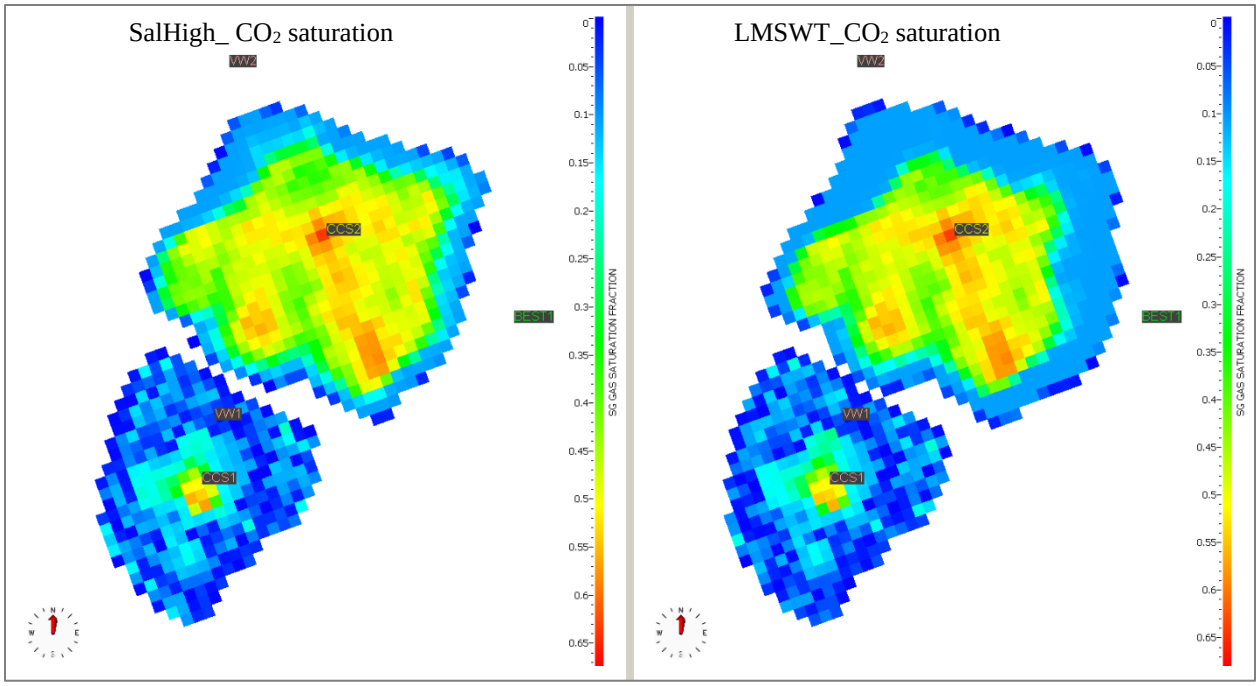

Figure 4-2-13 Map view of CO_2 plume distribution at the maximum extend layer of (left) SalHigh and (right) LMSW at the end of injection.

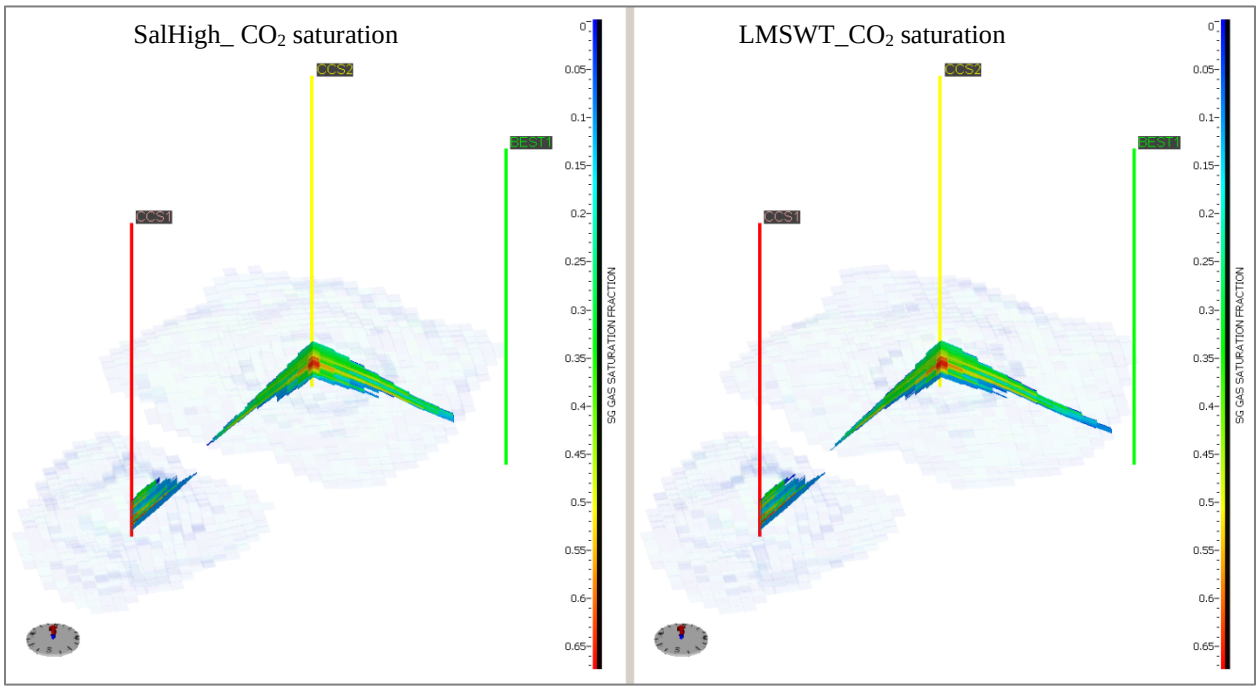

Figure 4-2-14 Cross sectional view of CO_2 plume distribution of (left) SalHigh and (right) LMSW at the end of injection.

In summary, continuous CO_2 injection is a better option than WAG because it provides better DPI, despite a less favorable E. The optimal location for a vertical brine extraction well was in a direction southeast of CCS#2 about 0.5 miles (805 m), perpendicular to high permeability direction. A blanketed perforation for BEST#1 within the Lower Mt. Simon Units A and B at a

1:1 volumetric ratio of surface injection to extraction rate is recommended for optimal DPI and E. Alternatively, a horizontal extraction well can be placed directly above the existing CO_2 plume. A 4:1 injection-to-extraction ratio is recommended for optimal DPI and E while minimizing the volume of brine extraction.

Low injection-to-extraction ratios benefited both DPI and E. The impact of brine extraction on DPI and E became unnoticeable at high injection-to-extraction ratios (4:1 and above, corresponding to an extraction rate no greater than 5,000 bbl/day [795 m^3/day]). However, a horizontal brine extraction well further increased E over the baseline scenario.

Low salinity formation water had little effect on DPI but greatly improved E; however, low salinity injection fluid had no effect on DPI or E because only the near-wellbore area was effected. Injecting treated Lower Mt. Simon water is not beneficial to DPI or E but can be used to improve CO_2 solubility rather than injecting untreated water.

CO_2 Plume Distribution

The CO_2 plume distribution was investigated as the most direct evidence of brine extraction. Generally, the CO_2 plume was oriented in the northeast–southwest direction, the high-connectivity direction based on the permeability distribution. The lateral extent of the plume at the end of injection was about 7,000 ft (2134 m) along the northeast direction and 4,300 ft (1311 m) in the perpendicular direction. The vertical extent of the plume was about 710 ft (216 m).

Without brine extraction, the CCS#1 plume was in a fan shape and the CCS#2 plume was in a rectangular shape. With brine extraction via a vertical well, the CCS#2 plume was directed toward the extraction well BEST#1, resulting in a more circular-shaped plume, whereas the CCS#1 plume was less affected by BEST#1. With brine extraction via a horizontal well, both plumes was less spreading plume than that of the vertical extraction scenario and the baseline injection scenario (Figure 4-2-15). The CO_2 plume in the horizontal scenario is more similar in shape with that of the baseline, while the plume moved laterally toward the extraction in the vertical well scenario. When brine was re-injected in the WAG process, the CCS#2 plume was less circular than that for the brine extraction scenario (Figure 4-2-13). This was because the pressure buildup from brine re-injection was more dominant than the pressure drop from brine extraction.

Figure 4-2-16 through 4-4-25 show the maximum distance between the CO_2 plume front and extraction well over time for the baselines and various brine extraction and re-injection scenarios using either a vertical well or a horizontal well. The distance attributed to brine extraction is the difference between the simulation scenarios and the baseline.

The CO_2 plume around CCS#1 (CCS#1 plume) existed before CCS#2 injection (year 0). With brine extraction in year 2, a vertical extraction well steered both the CCS#1 and CCS#2 plumes laterally because it was perforated in the injection zone. Moreover, the vertical extraction well had more impact on the CCS#2 plume than the CCS#1 plume because it was closer to CCS#2. A horizontal well steered the CCS#1 plume vertically and the CCS#2 plume laterally because it was located right above CCS#1 (therefore no lateral movement) and 2,758 ft (841 m) away from the CCS#2 plume, which led to nearly no vertical movement attributable to extraction.

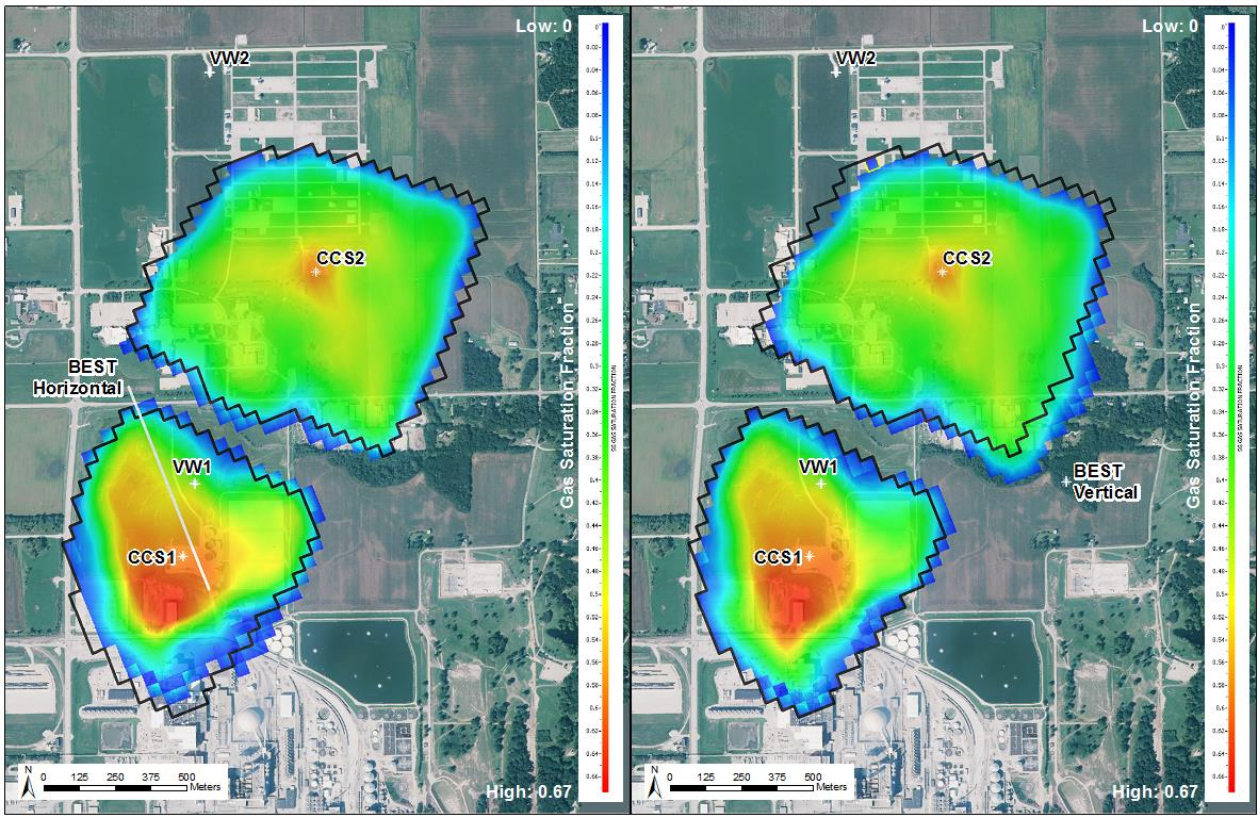

Figure 4-2-15 Map view of CO_2 plume distribution of scenario Hori10k (left) and a vertical scenario with the same rate at the end of extraction. The black outlines indicate the plume boundary of the baseline injection scenario. CCS#1 was perforated from 6976 ft (2126 m) to 7050 ft (2149 m) in MD, and CCS#2 was perforated from 6630 ft (2021 m) to 6825 ft (2080 m) in MD.

Perforation in the Middle and Upper Mt. Simon could not move the CO_2 plume, as indicated by the profile overlay of scenarios PerfMid, PerfTop, and BaseINJ (Figure 4-2-16 and Figure **4-2-17**). Increasing the extraction rate moved both the CCS#1 plume and the CCS#2 plume laterally up to 123 and 856 ft (37.5 and 261 m) (Figure 4-2-18 and Figure **4-2-19**). A higher extraction rate yielded a greater pressure decrease, thus greater lateral movement. However, too high a rate resulted in an early CO_2 breakthrough (in Ratio01). The minimum CCS#2 plume movement was 45 ft (14 m) from the baseline, with injection-to-extraction ratios of 10:1 and 7:1. When the injection-to-extraction ratio is higher than 2:1, brine extraction had no impact on the CCS#1 plume.

Compared with brine extraction alone (the WellPerp scenario), re-injection through WAG cycles allowed the CCS#2 plume to be up to 520 ft (158 m) further away from the extraction well (Figure 4-2-20 and Figure **4-2-21**). All the brine re-injection scenarios yielded similar plume movement; 670 ft (204 m) was the furthest distance from the extraction well (the LMSWT scenario). The CO_2 plume in scenario LMSW was 335 ft (102 m) away from the extraction well.

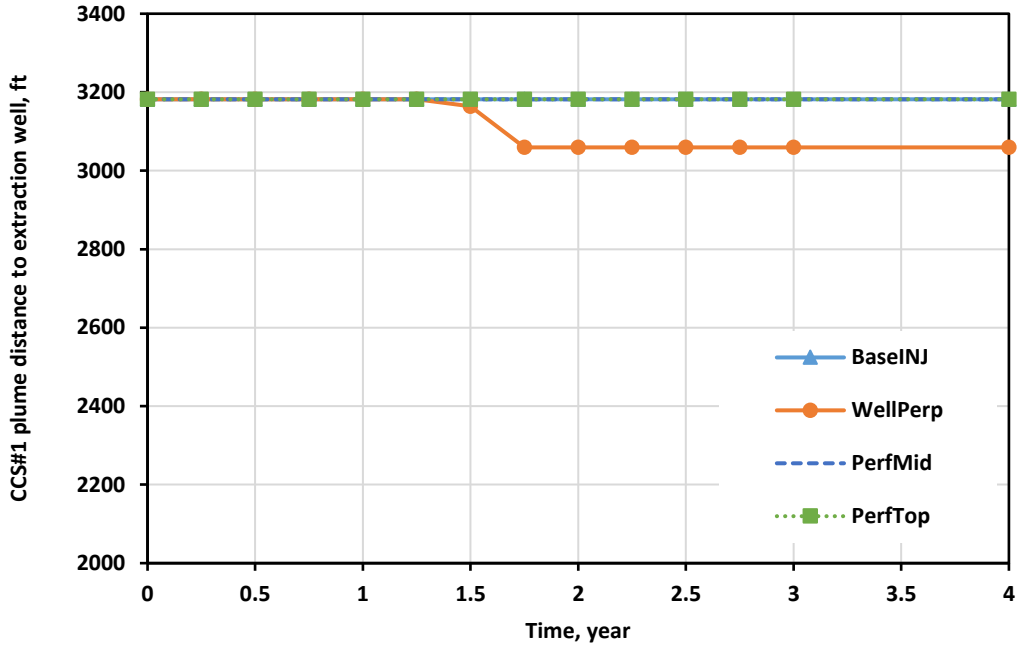

Figure 4-2-16 Distance between the CCS#1 plume front and BEST#1 with time for various perforation scenarios. The distance between CCS#1 and BEST#1 is 4689 ft (1429 m).

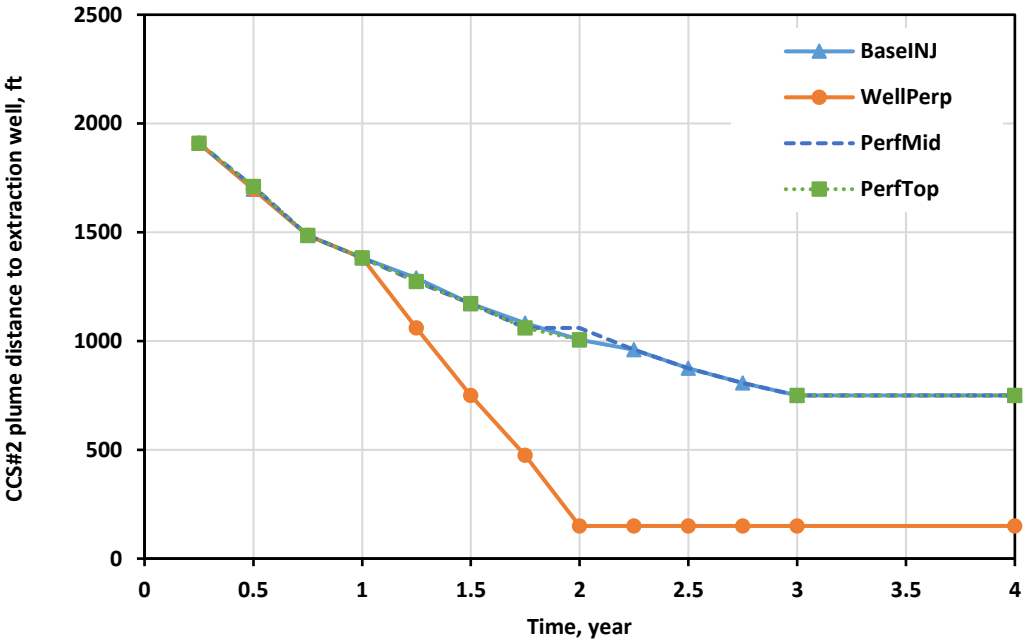

Figure 4-2-17 Distance between the CCS#2 plume front and BEST#1 with time for various perforation scenarios. The distance between CCS#2 and BEST#1 is 2758 ft (841 m).

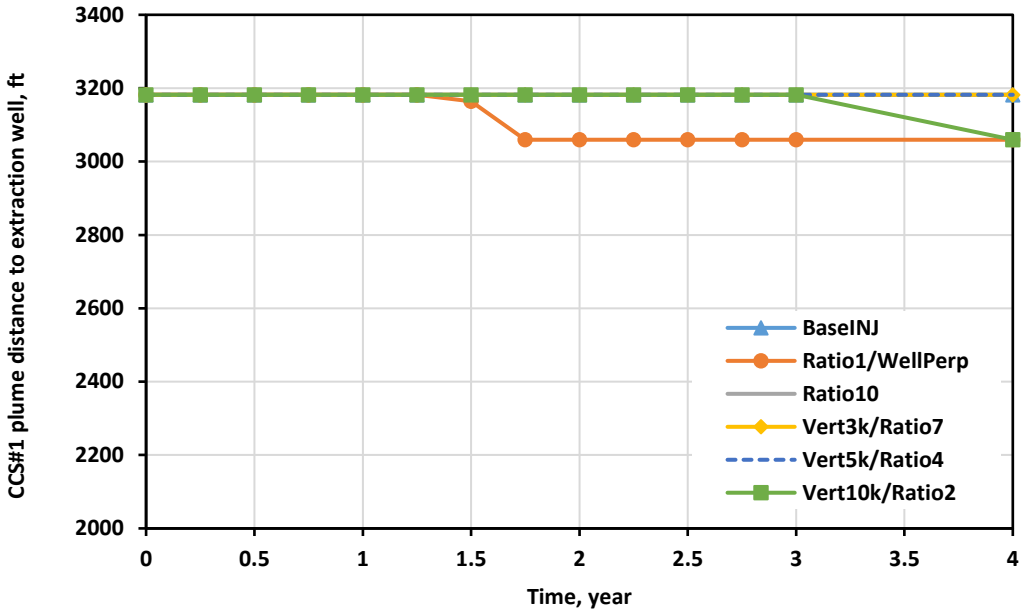

Figure 4-2-18 Distance between the CCS#1 plume front and BEST#1 with time for various extraction ratios scenarios. The distance between CCS#1 and BEST#1 is 4689 ft (1429 m).

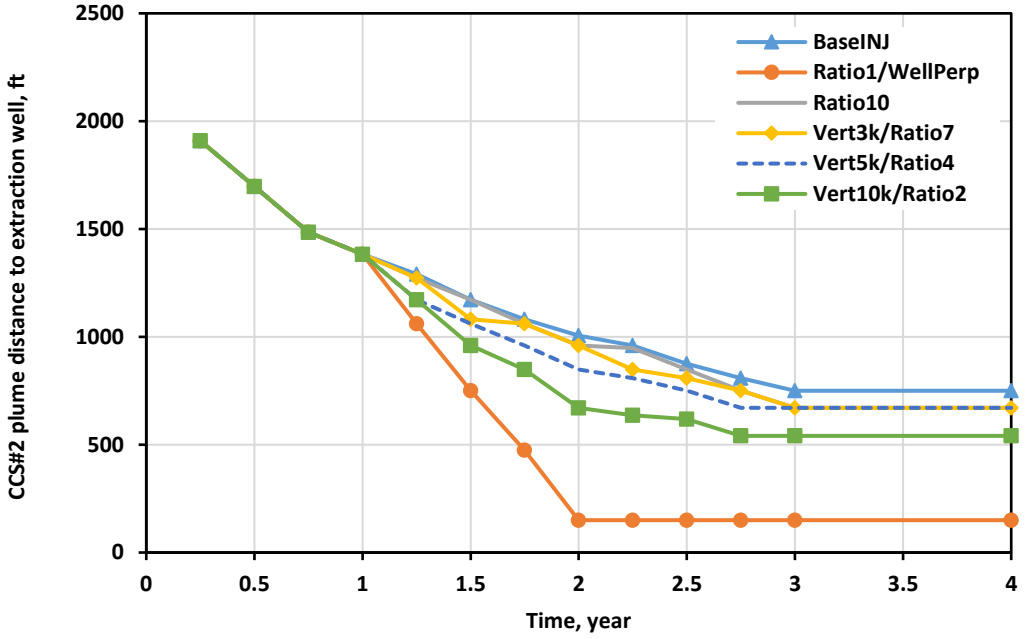

Figure 4-2-19 Distance between the CCS#2 plume front and BEST#1 with time for various extraction ratios scenarios. The distance between CCS#2 and BEST#1 is 2758 ft (841 m).

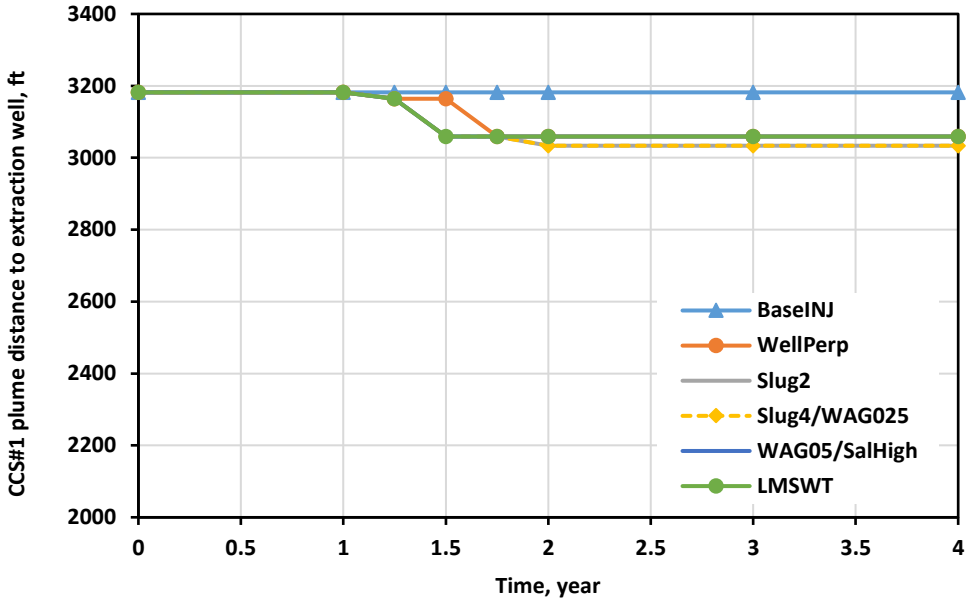

Figure 4-2-20 Distance between the CCS#1 plume front and BEST#1with time for various re-injection scenarios. The distance between CCS#1 and BEST#1 is 4689 ft (1429 m).

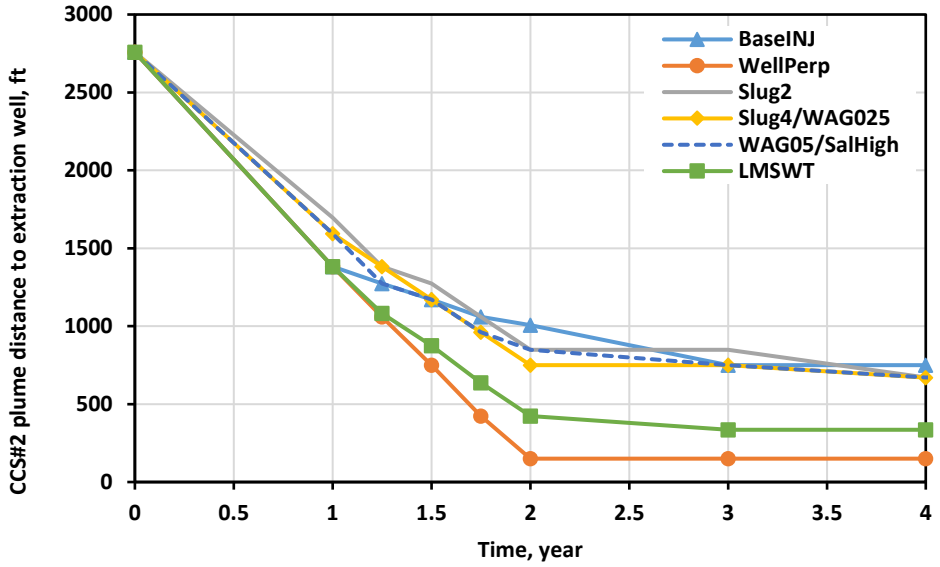

Figure 4-2-21 Distance between the CCS#2 plume front and BEST#1with time for various re-injection scenarios. The distance between CCS#2 and BEST#1 is 2758 ft (841 m).

A horizontal brine extraction well was able to move the CCS#1 plume vertically 38 ft (11 m; Figure 4-2-22) and the CCS#2 plume laterally 90 ft (27 m; Figure 4-2-23) with an injection-to-extraction ratio of 2:1. No plume movement was observed with an injection-to-extraction ratio of 7:1. The vertical distance between the CCS#1 plume and BEST#1 decreased with the brine

extraction rate. Increased brine extraction rates had no effect on the vertical distance, but they decreased the lateral distance between BEST#1 and the CCS#2 plume.

To effectively move both plumes, the maximum injection-to-extraction ratio was 2:1 for a vertical well and 4:1 for a horizontal well, corresponding to a minimum extraction rate of 10,000 bbl/day and 5,000 bbl/day (1,590 and 795 m^3/day). Note that the accuracy of the calculated plume movement distance depends on the reservoir grid resolution.

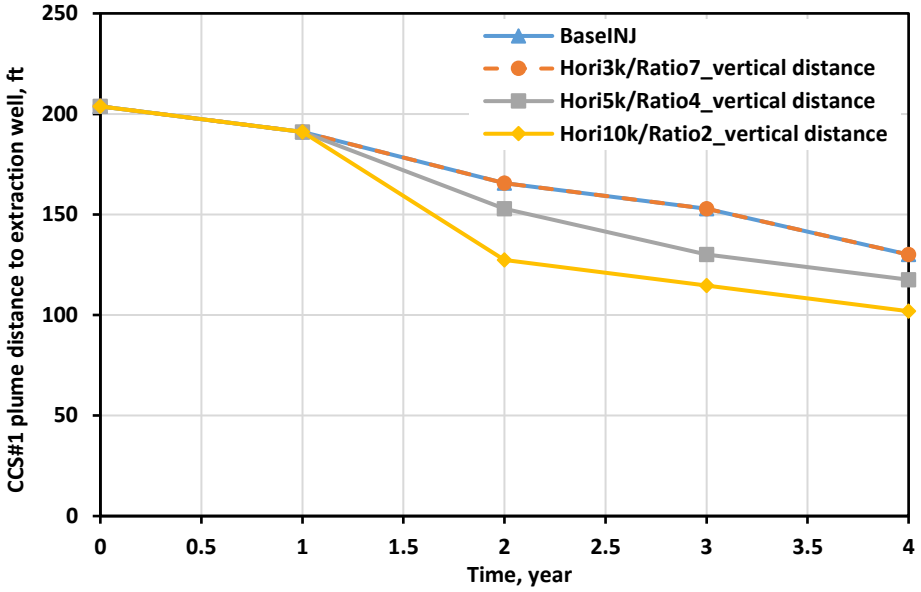

Figure 4-2-22 Distance between the CCS#1 plume front and BEST#1 with time for various horizontal well scenarios.

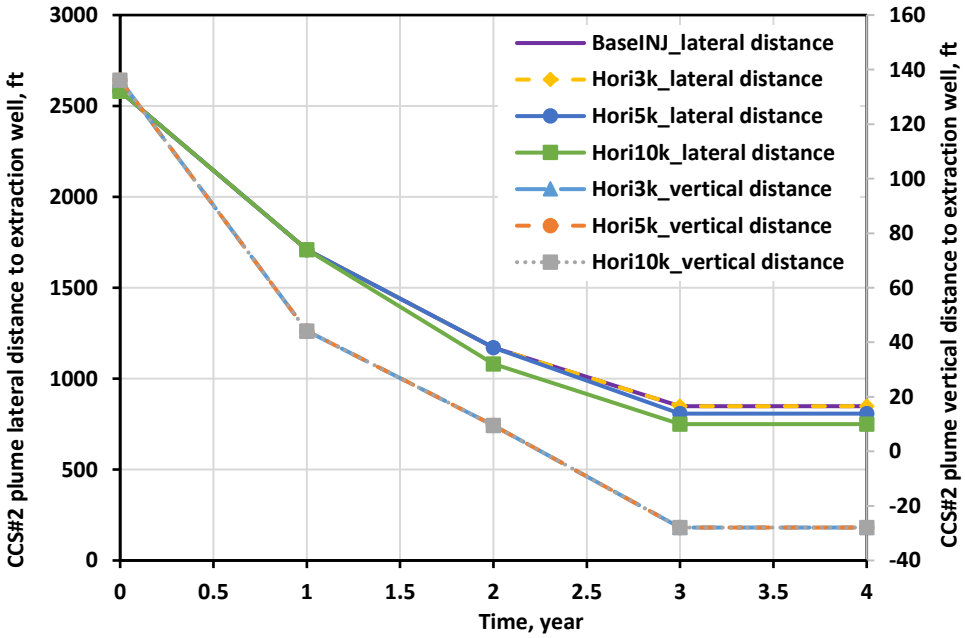

Figure 4-2-23 Distance between the CCS#2 plume front and BEST#1 with time for various horizontal well scenarios.

Figure 4-2-24 and 4-2-25 show how vertical permeability variation (kv/kh) affects plume distances from the extraction well for a horizontal extraction at a rate of 10,000 bbl/day (1,590 m^3/day). Increasing kv/kh accelerated the vertical movement of the CCS#1 plume and slowed the lateral movement of the CCS#2 plume. When kv/kh was greater than 0.1 (0.2 or 0.3), the CCS#1 plume reached BEST#1 after extraction (year 2); in addition, the CCS#2 plume was up to 20% further away from BEST#1 after extraction (year 2) and up to 31% further away at the end of injection (year 4).

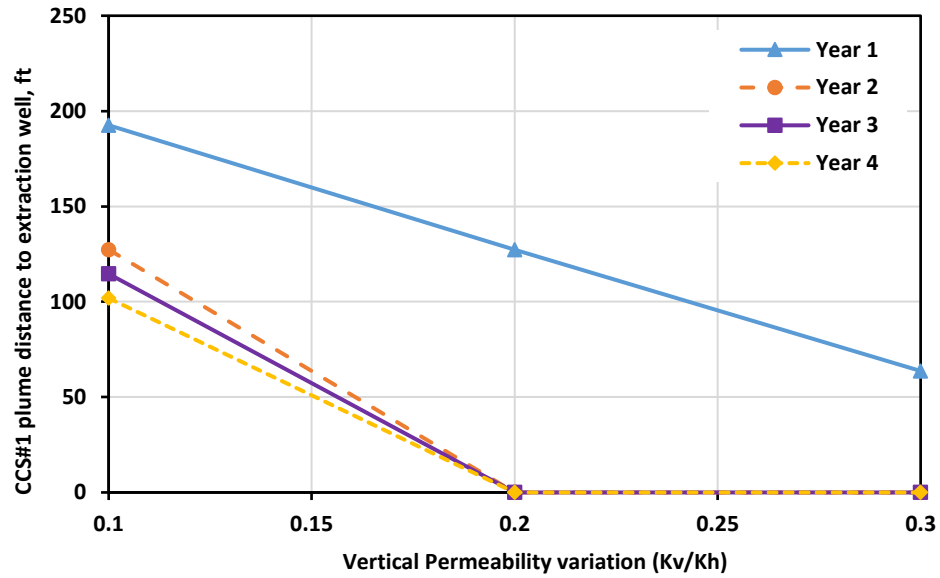

Figure 4-2-24 Vertical distance between the CCS#1 plume front and BEST#1 (horizontal well) with vertical permeability variation at various times.

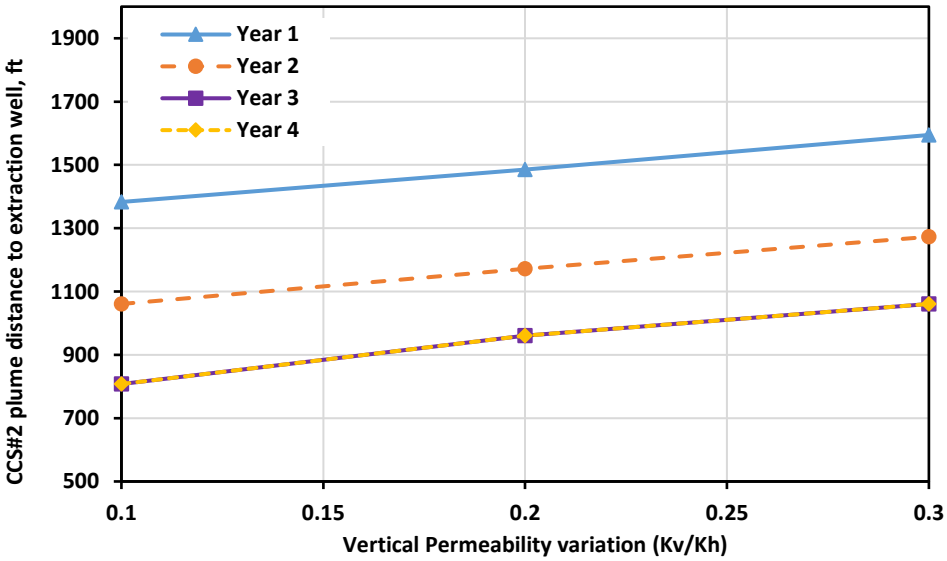

Figure 4-2-25 Lateral distance between the CCS#2 plume front and BEST#1 with vertical permeability variation at various times.

Well Monitoring Pressure

The formation pressure at CCS#1, VW#1, and VW#2 for the scenarios were analyzed to illustrate the detectability of brine extraction in managing pressure, using the existing wells and pressure gauge placement at the IBDP.

Table 4-2-3 lists the depths of pressure gauges in VW#1 and VW#2 and the corresponding formation units. The CCS#1 has one pressure gauge above the perforation intervals, and the monitoring pressure can be represented by the cell pressure at the mid-perforation layer in Mt. Simon Unit A.

Table 4-2-3 Monitoring well pressure gauge depths and corresponding formation units.

Well	Location	Depth (ft)	Formation Unit
VW#1	Zone 2	6982	Lower Mt. Simon Unit A
	Zone 4	6838	Lower Mt. Simon Unit A
	Zone 6	6632	Lower Mt. Simon Unit B
	Zone 7	6416	Lower Mt. Simon Unit B
	Zone 9	5654	Upper Mt. Simon Unit E
VW#2	Zone 1	7041	Pre-Mt. Simon
	Zone 2	6681	Lower Mt. Simon Unit A
	Zone 3	6524	Lower Mt. Simon Unit B
	Zone 4	5848	Upper Mt. Simon Unit E

Figure 4-2-26 through 4-2-29 show the pressure response at all the monitoring ports (a monitoring port is the location of a pressure gauge) for the representative brine extraction and re-injection scenarios. Pressure signatures for CCS#1 and CCS#2 injection are evident in most zones, as are effects of all extraction scenarios. VW#1 Zone 7 showed the greatest pressure drop from brine extraction. A pressure response from brine extraction was not observed at Mt. Simon Unit E monitoring ports (VW#1 Zone 9 and VW#2 Zone 4). This indicates pressure variations from all extraction scenarios should be detectable in the deeper monitoring ports.

Figure 4-2-30 to 4-2-33 show well pressure responses at two selected monitoring ports of VW#1 for the injection-to-extraction ratio scenarios in comparison to the baseline injection. One port was in zone 2, which is located in the Lower Mt. Simon (Unit A; CCS#1 injection zone), and the other port was in zone 7, which is located in the Lower Mt. Simon (Unit B; CCS#2 injection zone). The pressure variations can be detectable at both monitoring ports with an injection to extraction ratio as high as 10:1, corresponding to an extraction rate of 2,000 stb/day (318 m^3/day).

Similarly, Schlumberger modeled the pressure variations of all horizontal well extraction rate scenarios, 5,000 stb/day, 10,000 stb/day, 15,000 stb/day, and 20,000 stb/day (795, 1,590, 2,385, and 3,180 m^3/day), illustrating that the pressure variations of all rate scenarios are detectable at selected VW#1 monitoring zone 2 and zone 7 in Mt. Simon Unit A and B (Figure 4-2-34 and 4-2-35).

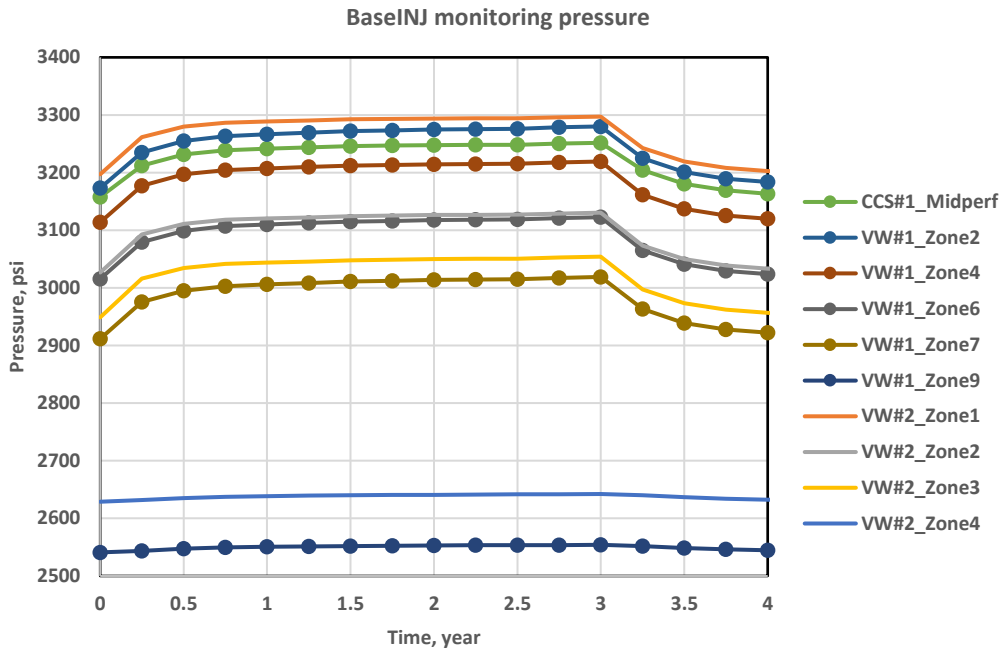

Figure 4-2-26 Pressure with time at various monitoring zones in the BaseINJ scenario.

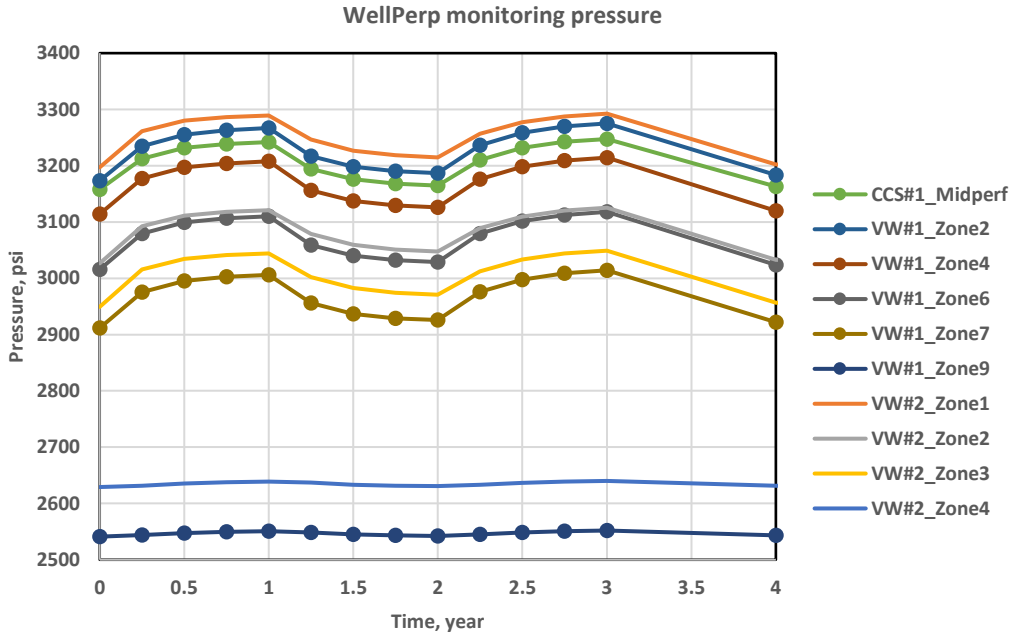

Figure 4-2-27 Pressure with time at various monitoring zones in the WellPerp scenario. A pressure drop of about 80 psi (552 kPa) due to brine extraction was observed in the deeper zones.

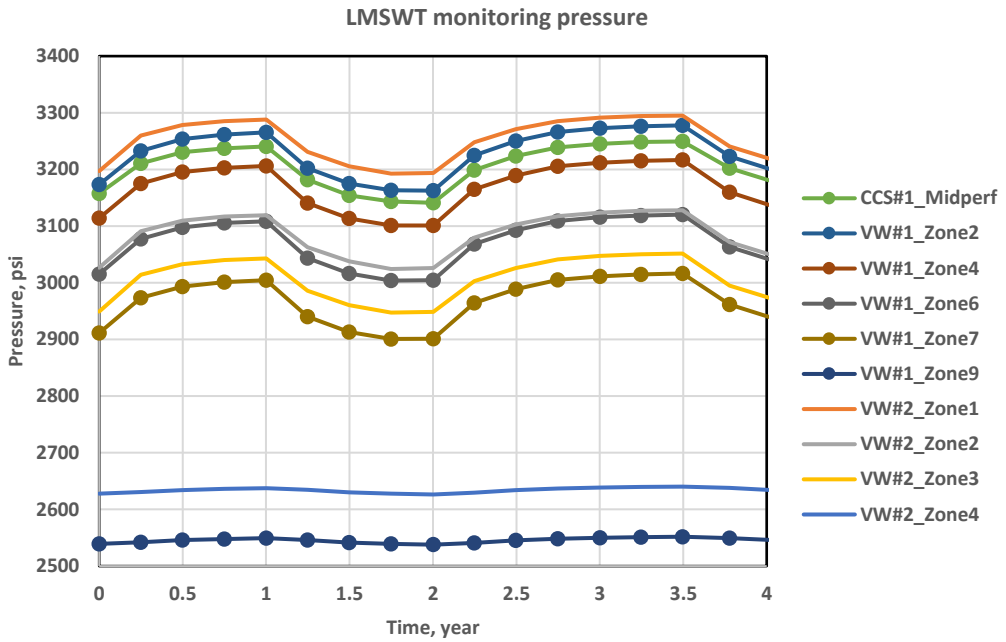

Figure 4-2-28 Pressure change with time at various monitoring zones in the LMSWT scenario. A pressure drop of about 100 psi (689 kPa) due to brine extraction was observed in the deeper zones.

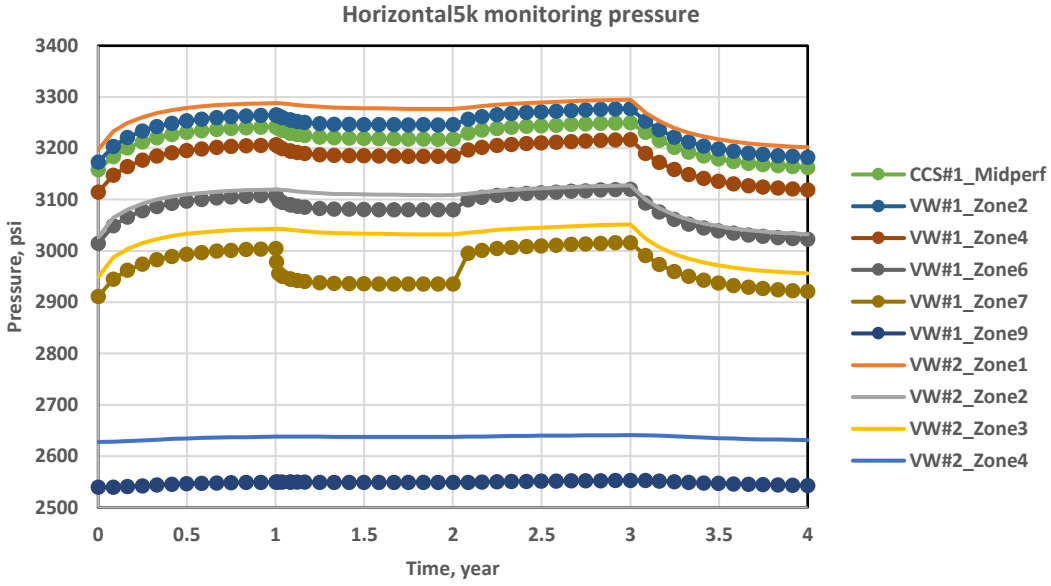

Figure 4-2-29 Pressure change with time at various monitoring zones in scenario Hori5k.

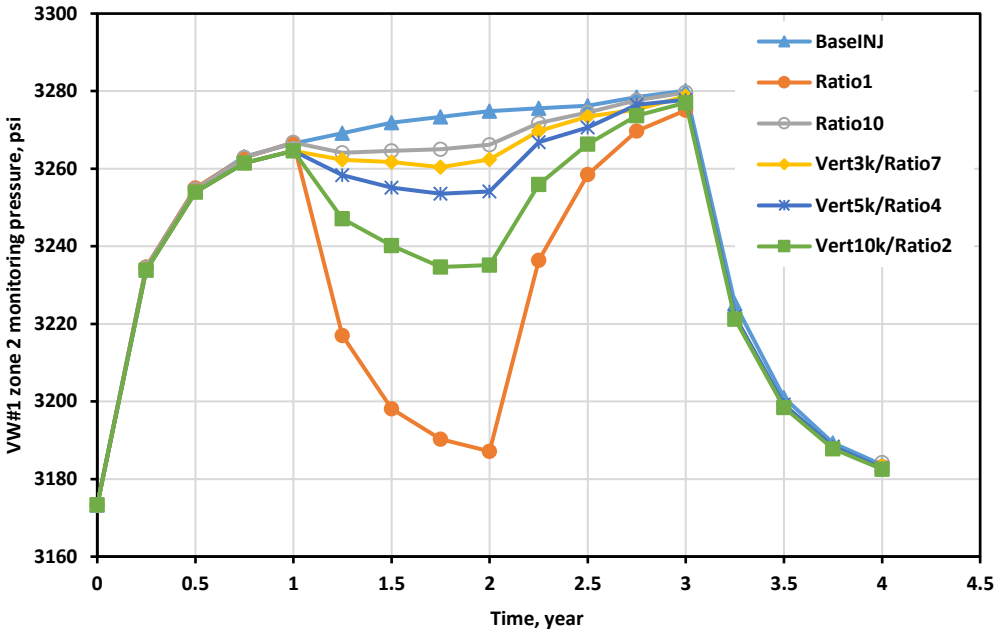

Figure 4-2-30 Pressure at VW#1 monitoring zone 2 (within the CCS#1 injection zone) for vertical extraction scenarios.

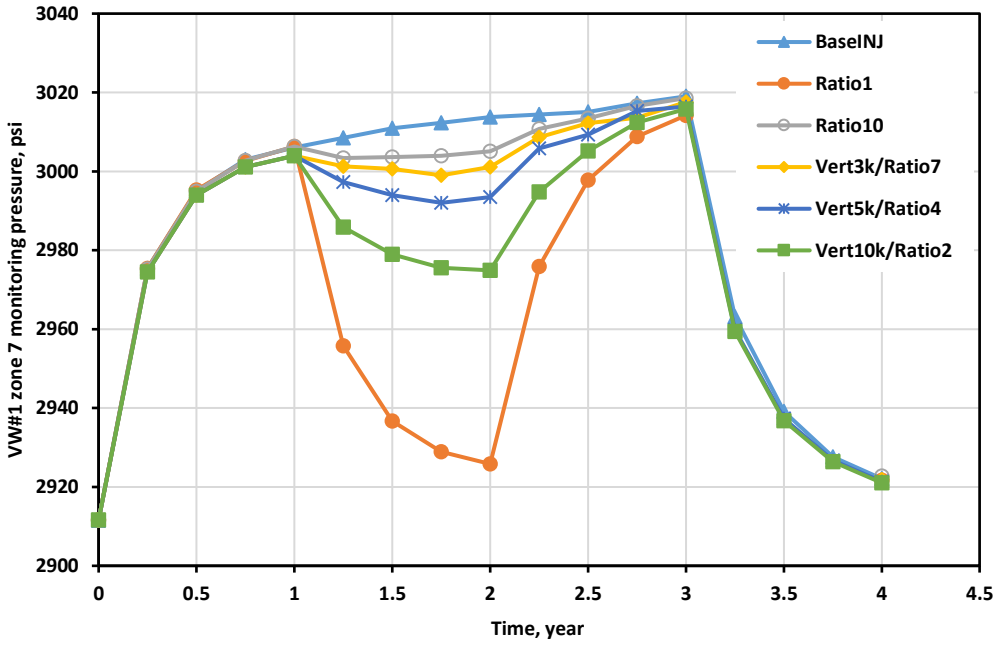

Figure 4-2-31 Pressure at VW#1 monitoring zone 7 (within the CCS#2 injection zone) for vertical extraction scenarios.

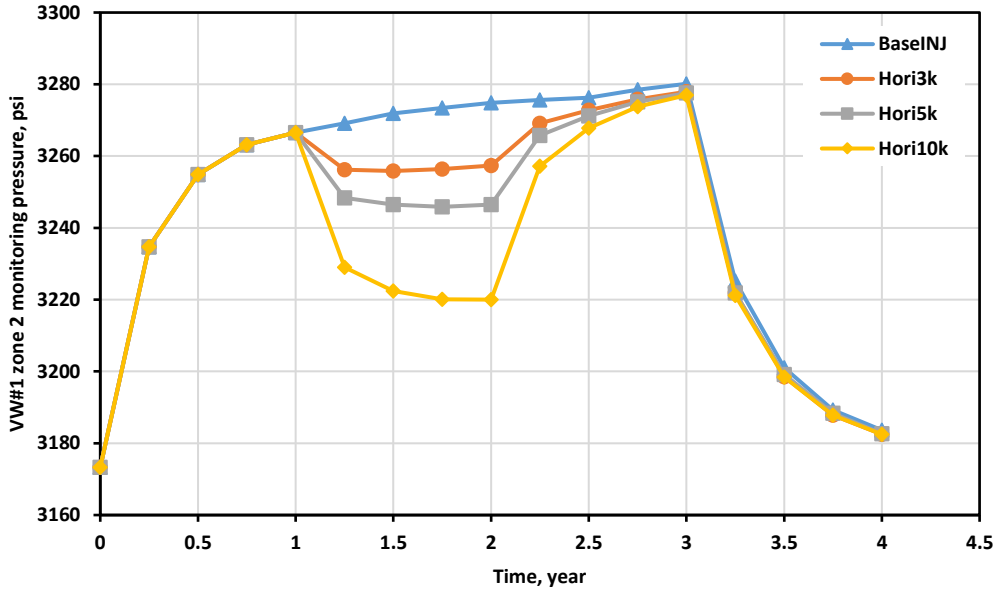

Figure 4-2-32 Pressure at VW#1 monitoring zone 2 (within the CCS#1 injection zone) for vertical extraction scenarios.

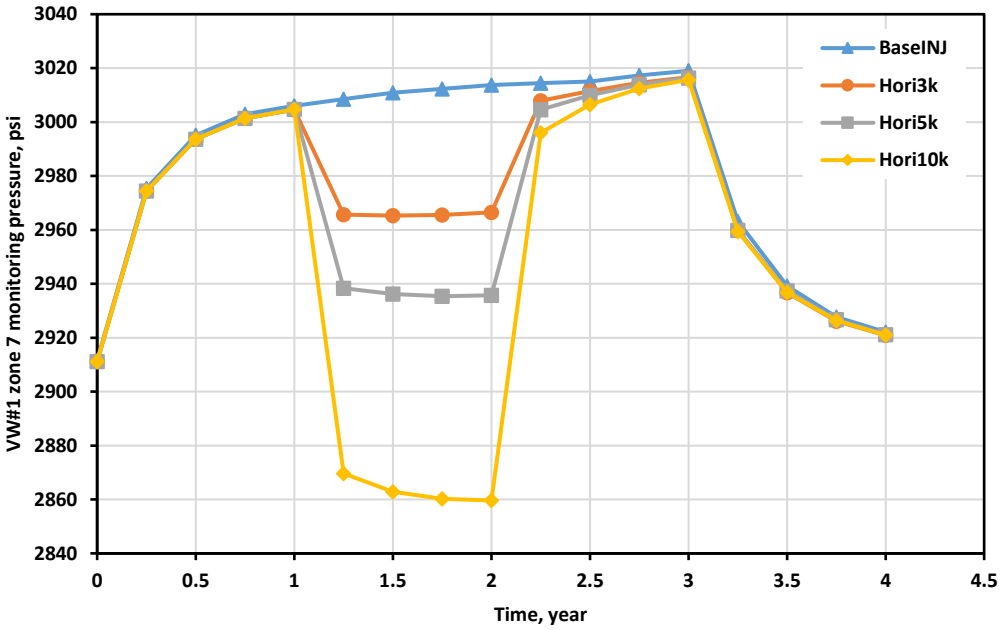

Figure 4-2-33 Pressure at VW#1 monitoring zone 7 (within the CCS#2 injection zone) for vertical extraction scenarios.

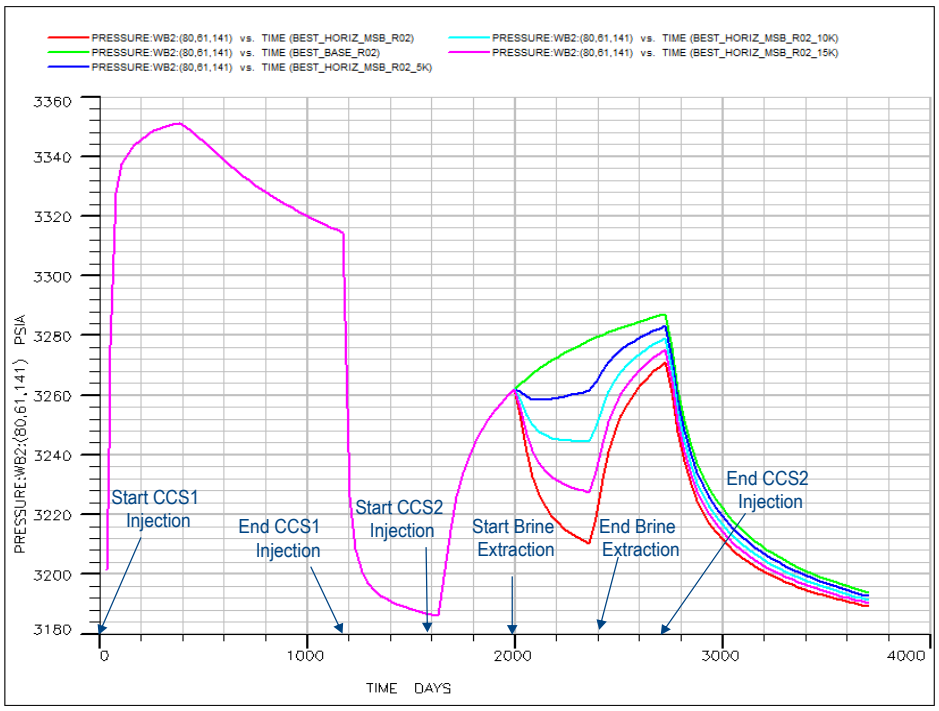

Figure 4-2-34 Pressure at VW1 monitoring zone 2 (within CCS#1 injection zone) for scenarios: Base (green), 5,000 stb/day (dark blue), 10,000 stb/day (light blue), 15,000 stb/day (magenta), and 20,000 stb/day (red) (795, 1,590, 2,385, and 3,180 m^3/day).

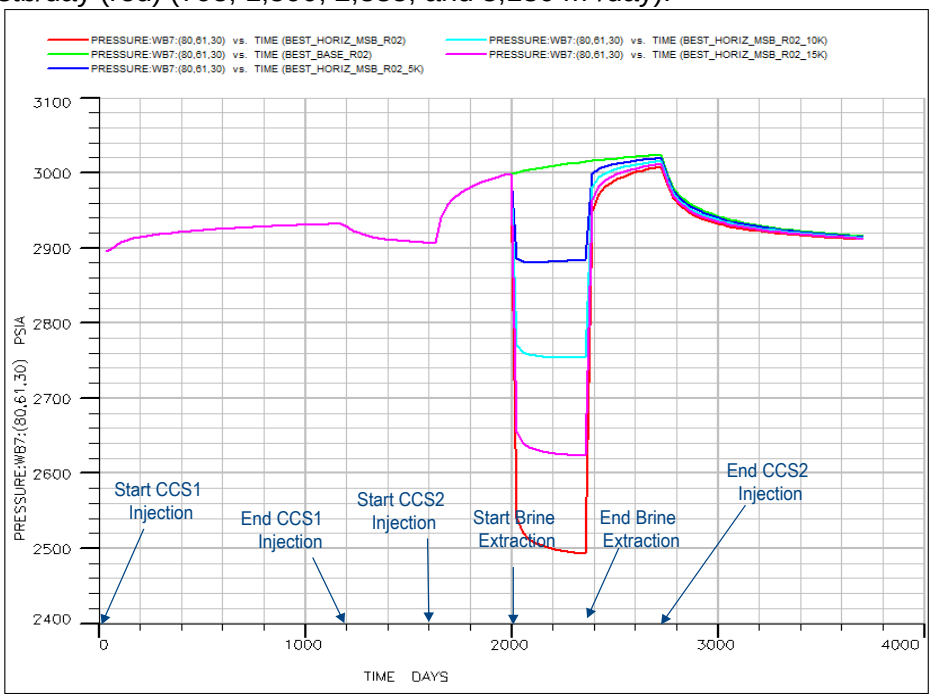

Figure 4-2-35 Pressure at VW1 monitoring zone 7 (within CCS#2 injection zone) for scenarios: Base (green), 5,000 stb/day (dark blue), 10,000 stb/day (light blue), 15,000 stb/day (magenta), and 20,000 stb/day (red) (795, 1,590, 2,385, and 3,180 m^3/day).

Seismic Detectability

Schlumberger evaluated seismic detectability via the modeling of elastic impedance differences between base scenario and brine extraction scenarios. Elastic properties for base scenario and extraction scenario reservoir conditions at the end of the extraction period were modeled using the Petrel* ESP. software platform ReSim2Seis plug-in. ReSim2Seis is equipped with accurate mathematical models for calculating thermodynamic properties of reservoir fluids. For brine properties, ReSim2Seis uses Batzle-Wang equations.

Properties for CO_2 were computed using new analytical expressions developed based on CO_2 data from the National Institute of Standards and Technology Reference Fluid Thermodynamic and Transport Properties Database (NIST-REFPROP) software. These expressions give less than 5% error in speed of sound calculations of CO_2. For this study, Hashin-Shtrikman (H-S) bounds were used to calculate the bulk and shear moduli and bulk density of solid rock.

Figure 4-2-36 shows an intersection along horizontal well path for Base Scenario CO_2 saturation (top), and predicted acoustic impedance (bottom). Similar acoustic impedance modeling was performed for the 20,000 stb/day (3,180 m^3/day) scenario.

Figure 4-2-37 shows the acoustic impedance difference (20,000 stb/day (3,180 m^3/day) minus Base Scenario) as percentage of Base Scenario. Impedance differences are due to both saturation reductions (positive change) in some cells and saturation increase (negative change) in other cells reflecting plume movement.

Figure 4-2-38 shows a map view of the 20,000 stb/day (3,180 m^3/day) minus Base Scenario acoustic impedance difference as percentage of Base Scenario exceeding -5% of Base Scenario (left) and +5% of Base Scenario (right). A 5% variation is being used as an estimate of detectability limit. This analysis illustrates the level of detectability required to monitor BEST efficacy with seismic observations and reinforces the need for high resolution measurements available with the cross well seismic method.

Geomechanical Effects

Vertical Well Extraction Effects

The primary areas of geomechanical investigation are the effects of stress redistribution and strain associated with brine extraction and CO_2 injection and caprock integrity. Emphasis is given here to assessing the effectiveness of simplified mechanics-based approaches to determining caprock integrity, the fracture gradient, and the maximum pressure drawdown as a secondary check to coupled geomechanical flow-modeling results.

To examine caprock integrity, several semiempirical methods and one finite element-based approach were applied (Fjaer 2008; Selvadurai 2009, 2013; Li et al. 2015) to determine vertical caprock displacement profiles (1-D- and 2-D-based approaches) from CO_2 injection or brine extraction. These simplified methods will serve as a check on the coupled geomechanical-flow simulation output performed in a coupled Petrel-Visage workflow. Vertical displacements of the caprock are of concern because this deformation has the potential to cause shear slip along preexisting fractures and faults or to cause brittle failure in the caprock, thereby initiating new fractures. These mechanisms may produce increased vertical permeability of the caprock and lead to leakage of the storage reservoir.

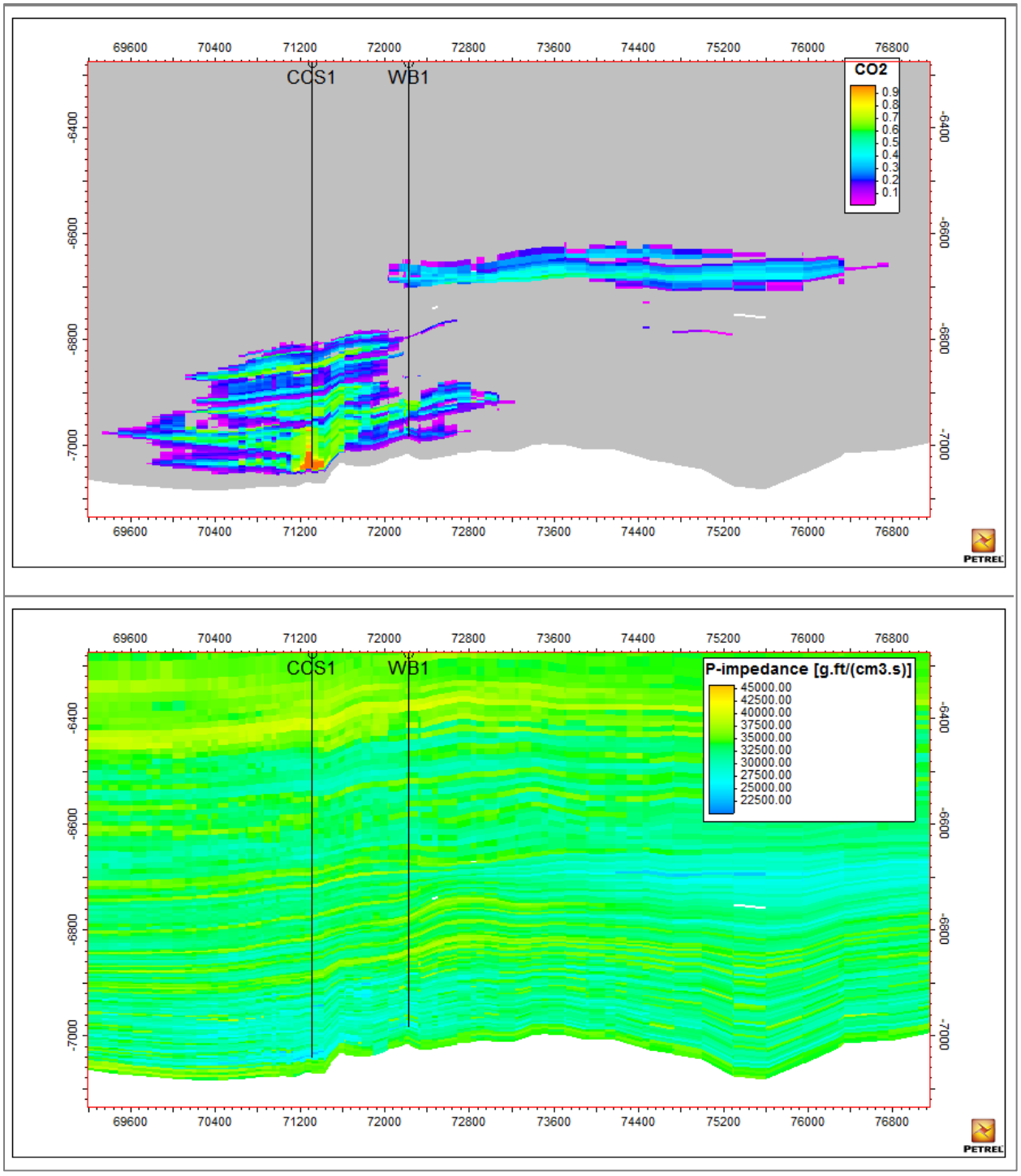

Figure 4-2-36 Intersection along horizontal well path for Base Scenario CO_2 saturation (top), and predicted acoustic impedance (bottom).

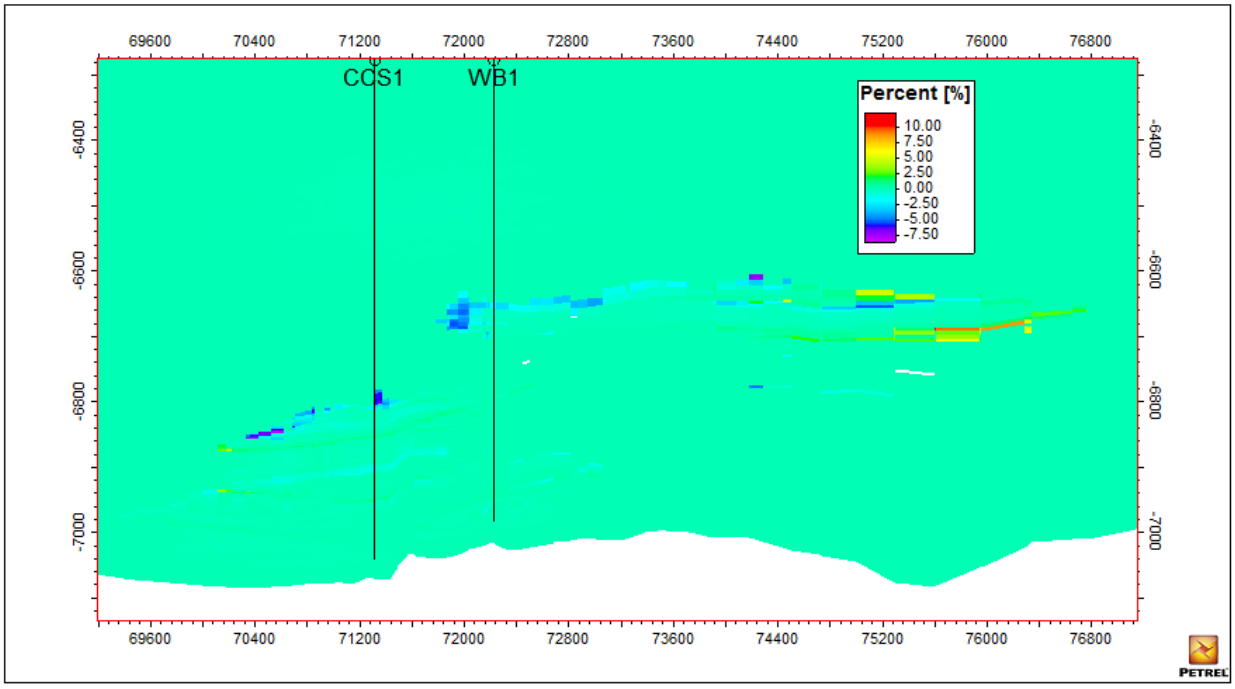

Figure 4-2-37 Intersection along horizontal well path for 20,000 stb/day (3,180 m^3/day) minus Base Scenario acoustic impedance difference as a percentage of Base Scenario.

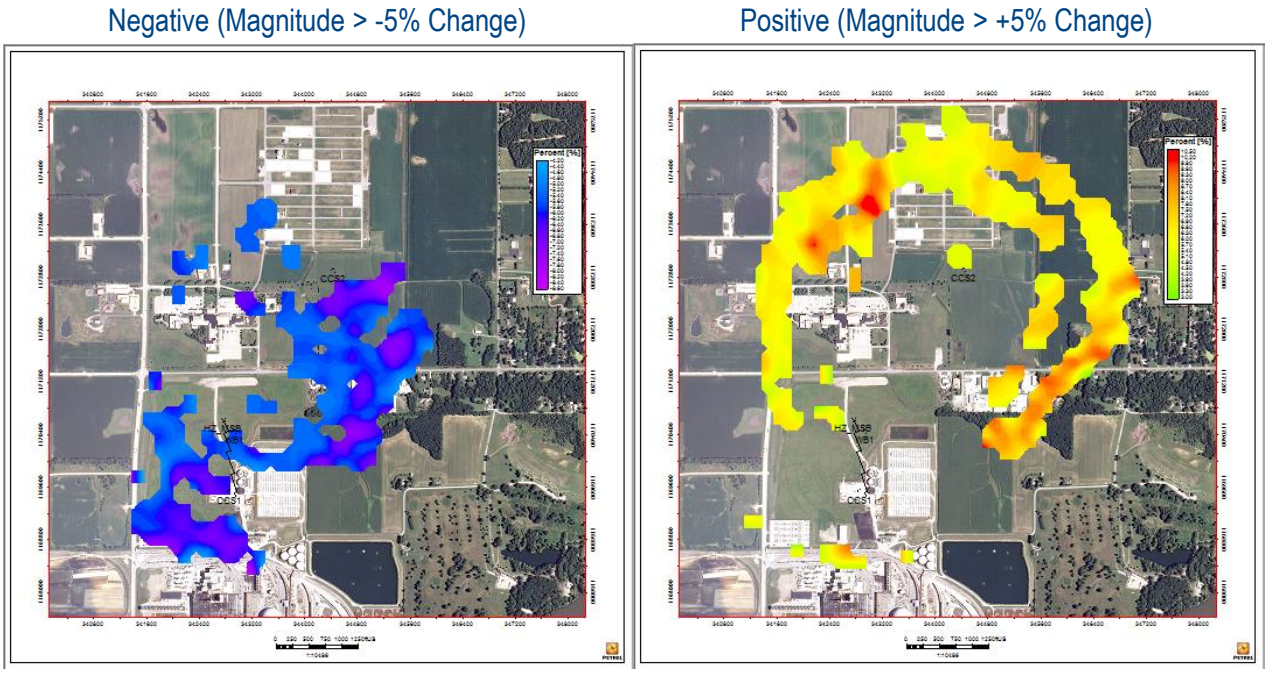

Figure 4-2-38 Map view of 20,000 stb/day (3,180 m^3/day) minus Base Scenario acoustic impedance difference as a percentage of Base Scenario exceeding -5% of Base Scenario (left) and +5% of Base Scenario (right).

Caprock Integrity: Caprock Deflection

Readily implementable semiempirical methods are evaluated here to determine vertical displacements from CO_2 injection or brine extraction on caprock integrity. Several semiempirical methods and one finite element-based approach were applied. These methods will serve as a check on coupled geomechanical-flow simulation output performed in a coupled Petrel-Visage workflow. Methods examined to determine vertical caprock displacement include (1) the method of Li et al. (2015; see Appendix A), and (2) a Mohr-Coulomb finite element simulation in Plaxis (http://www.plaxis.nl/plaxis3d/) with generalized pressure distributions (see Appendix B). Elevations of the three-layer model are shown in Table 4-2-2, and the geomechanical reservoir parameters are shown in Table 4-2-5. Three scenarios are considered for which we are interested in determining vertical caprock deflections: BaseInj, WellPerp, and WAG05.

Geomechanical strength parameters are not changed between well locations. (Thus, the constants Ω and φ used in the method of Li et al. [2013, 2014] are also unchanged.) Consequently, the differences between simulation scenarios for application to caprock flexure are the overpressure distribution (or drawdown pressure distribution, for BEST#1) for each well, the distance between the midpoint of the injection interval and the base of the caprock (l), and the caprock thickness (h). Pressure distributions are obtained from the Nexus reservoir model at the end of injection, and the method of Li et al. (2013, 2014) is applied.

Figure 4-2-39 shows that an equivalent radial distribution must be created from the 3-D formation pressure distribution. Differential pressures at the depth of the midpoint of the perforation interval are exported in the *i* and *j* directions. Figure 4-2-40 to Figure **4-2-44** show the differential pressure distribution, *i*, the *j* pressure slices, and the resulting deflections for the base of the caprock as calculated by Li et al. (2013, 2014).

Table 4-2-4 Depth for ground surface of model layers.

	Depth (ft)		
Layer	**CC#1**	**CC#2**	**BEST**
Caprock top	5048.0	5048.0	5042.5
Caprock bottom	5546.7	5545.5	5540.0
Perforated top	6622.5	6978.2	6455.0
Perforated bottom	6824.2	7051.5	7108.0

Table 4-2-5 Geomechanical reservoir input parameters and model dimensions.

			Well		
Parameter	**Unit**	**Layer**	**CCS#1**	**CCS#2**	**BEST**
G	Mpsi	Overburden	3	3	3
ν		Overburden	0.15	0.15	0.15
G	Mpsi	Caprock	2.78	2.78	2.78
ν		Caprock	0.15	0.15	0.15
G	Mpsi	Storage	2.45	2.45	2.45
ν		Storage	0.16	0.16	0.16
α	(Biot coeff)	Storage	0.88	0.88	0.88
h	Caprock thickness (ft)		497.0	498.7	497.5
l	Depth to injection from base of caprock (ft)		1681.4	1325.2	1241.5
m	Thickness of injection interval (perfed) (ft)		73.3	201.7	653
Δp	Overpressure (r), psi		Varies	Varies	Varies

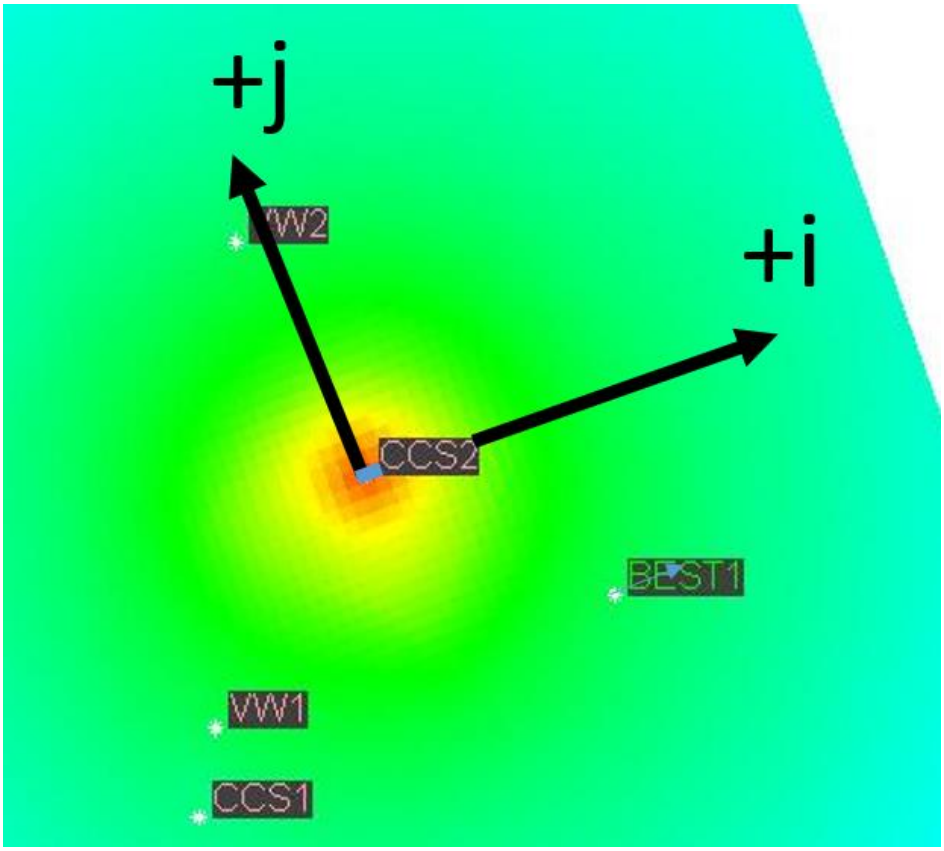

Figure 4-2-39 Critical pressure distribution from the +*i*, –*i*, +*j*, and –*j* directions for the CCS#2 well.

Table 4-2-6 presents a summary of vertical displacements calculated using the method of Li et al. (2013, 2014) with formation pressure distributions obtained from the Nexus reservoir simulation scenarios. The application of overpressures directly from a reservoir simulation, as was done here, differs from the approach used by Li et al. (2013, 2014), whereby the distribution of overpressures is estimated from the abrupt interface between the injected CO_2 and the host water, which are assumed to be immiscible. This interface is linked to vertically averaged overpressure expressions (Li et al. 2015) with models proposed by Vilarrasa et al. (2010) and others.

Table 4-2-6 Summary of maximum vertical displacements resulting from injection or extraction.

Simulation scenario	Direction	Maximum vertical deflection (in.)
CCS#2 BaseINJ	Upward	1.05×10^{-5}
CCS#2 WellPerp	Upward	1.04×10^{-5}
BEST#1 WellPerp	Downward	1.29×10^{-5}
CCS#2 WAG	Upward	1.78×10^{-5}
BEST#1 WAG	Downward	1.41×10^{-5}

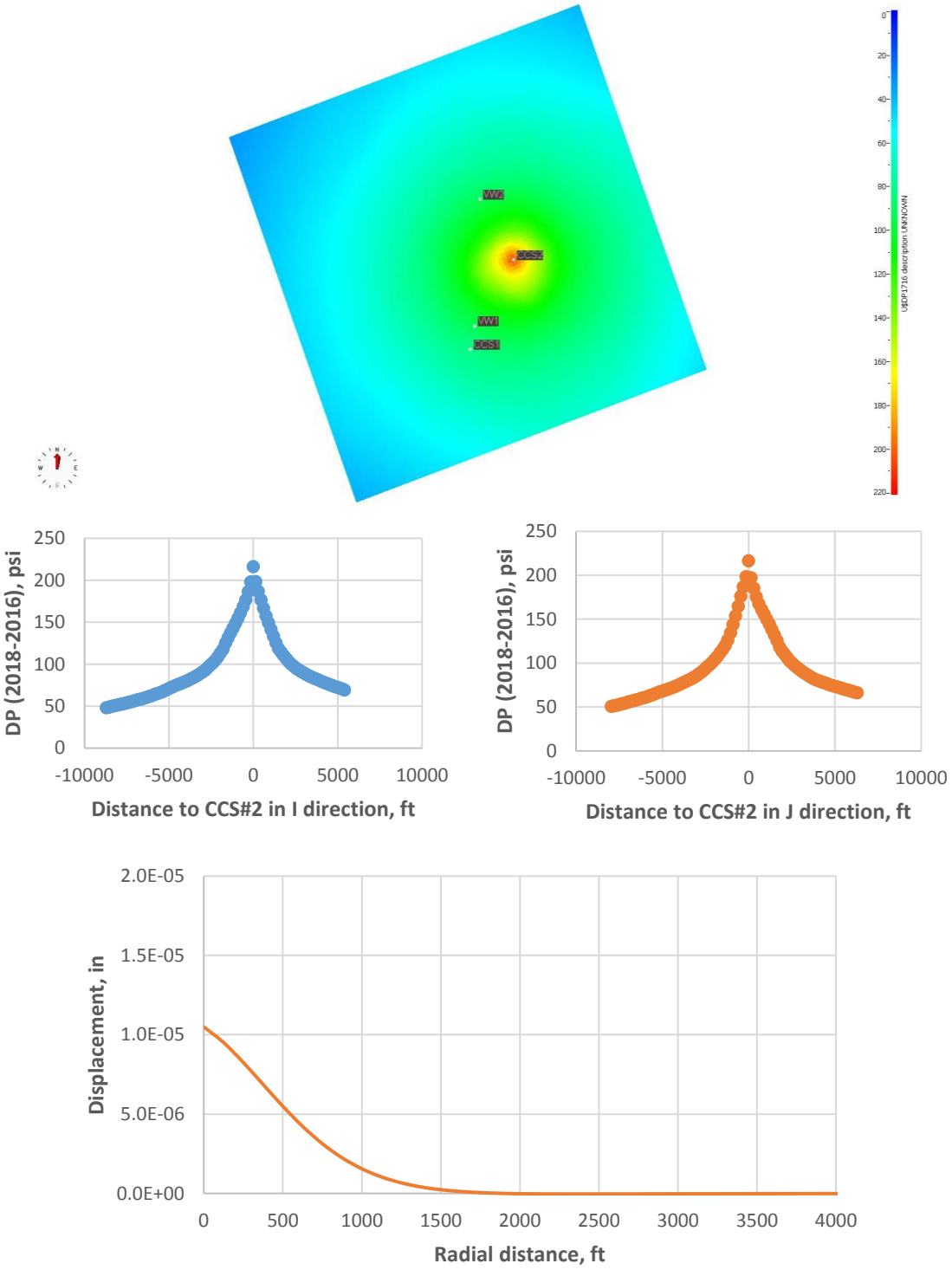

Figure 4-2-40 CCS#2 vertical displacement at the base of caprock at the end of injection in scenario BaseINJ.

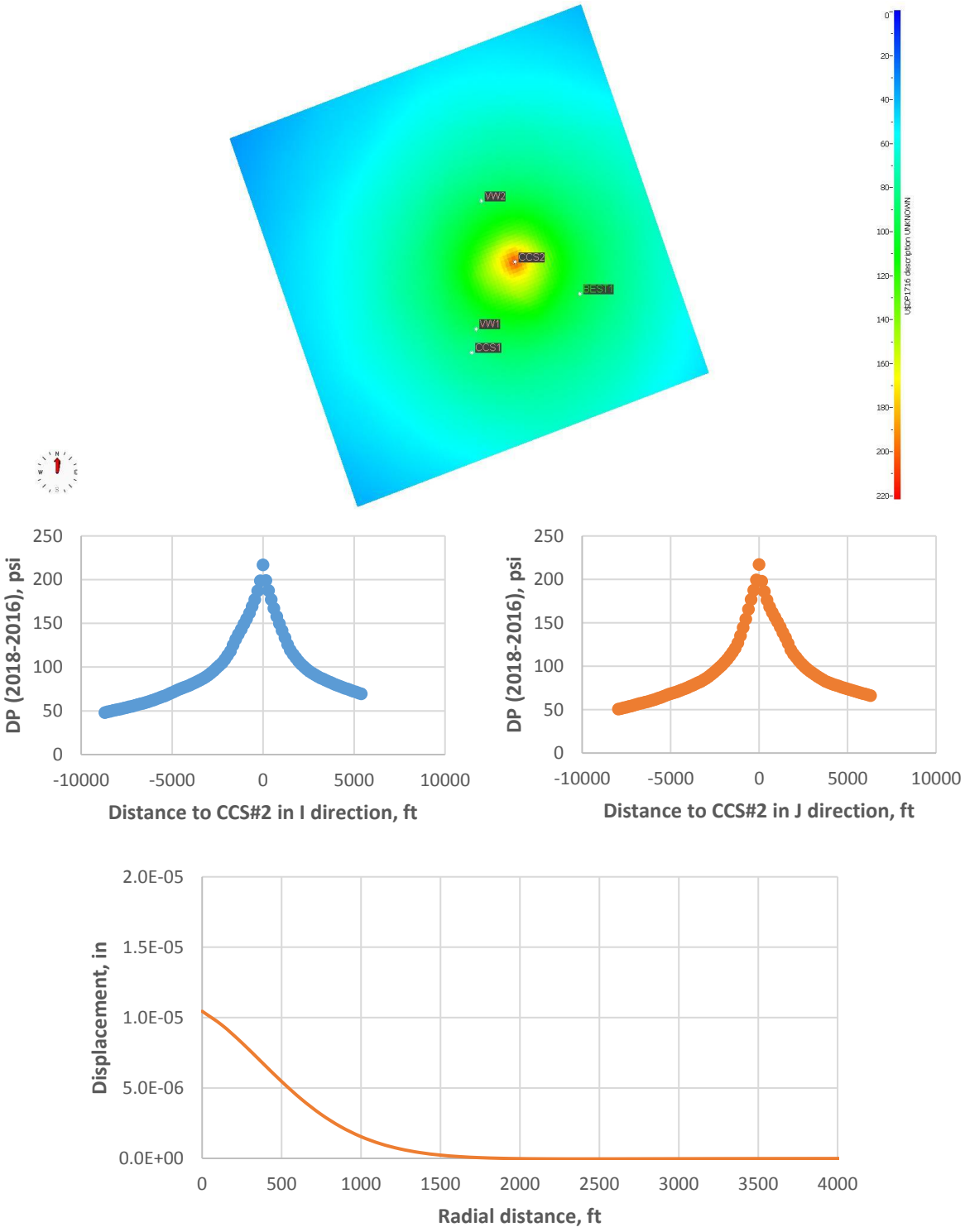

Figure 4-2-41 CCS#2 vertical displacement at the base of caprock at the end of injection in scenario WellPerp.

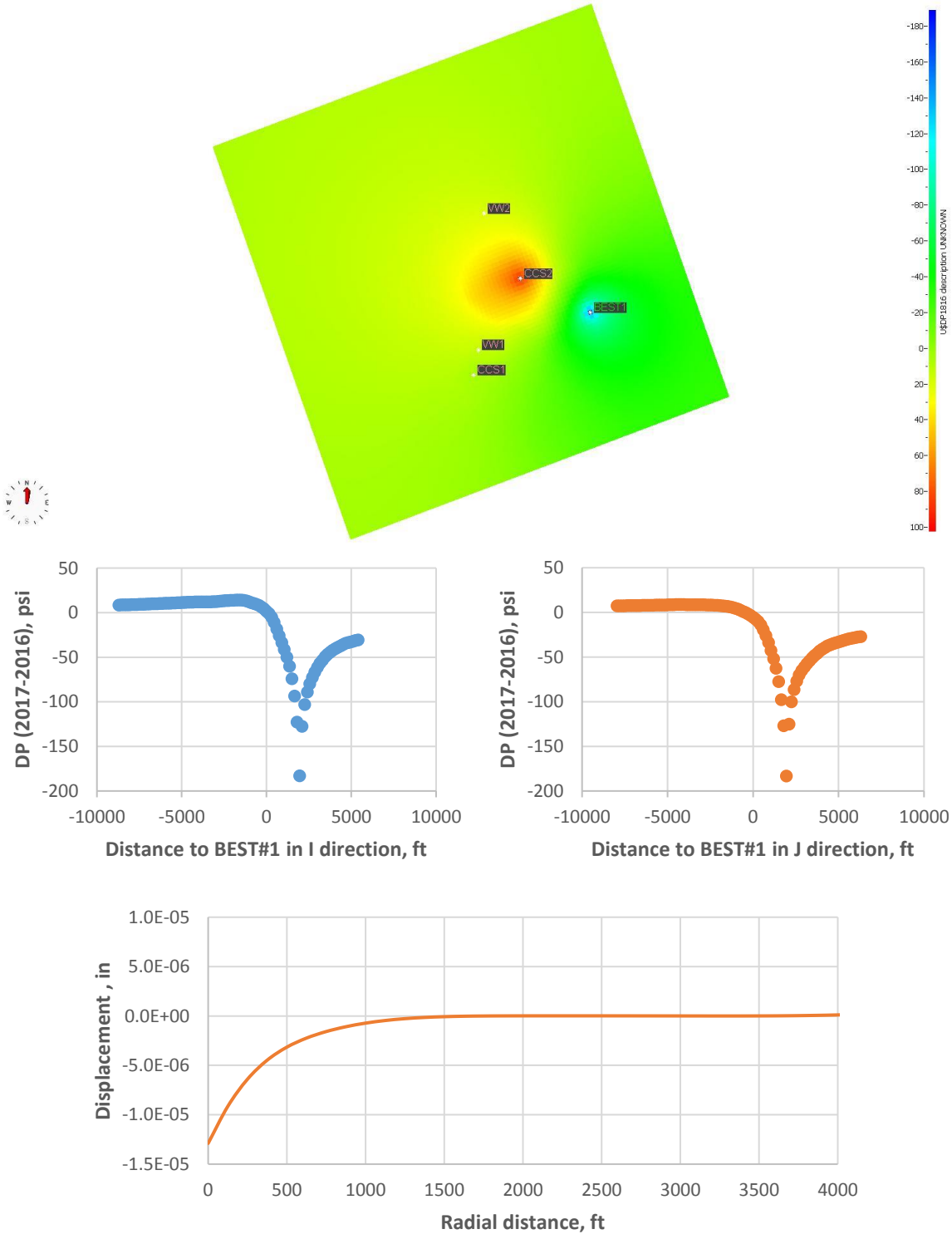

Figure 4-2-42 BEST#1 vertical displacement at the base of caprock at the end of injection in scenario WellPerp.

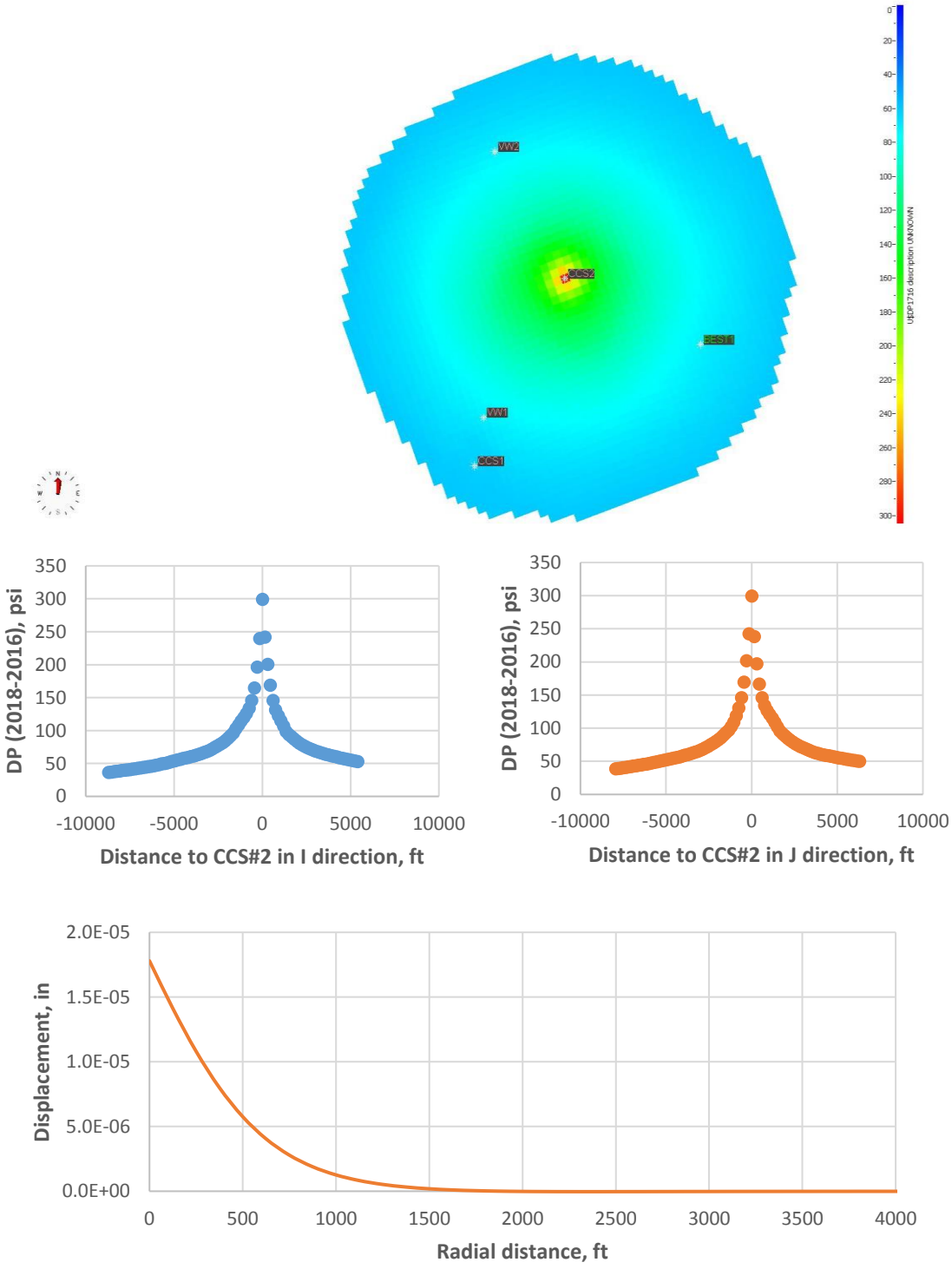

Figure 4-2-43 CCS#2 vertical displacement at the base of caprock at the end of injection in scenario WAG05.

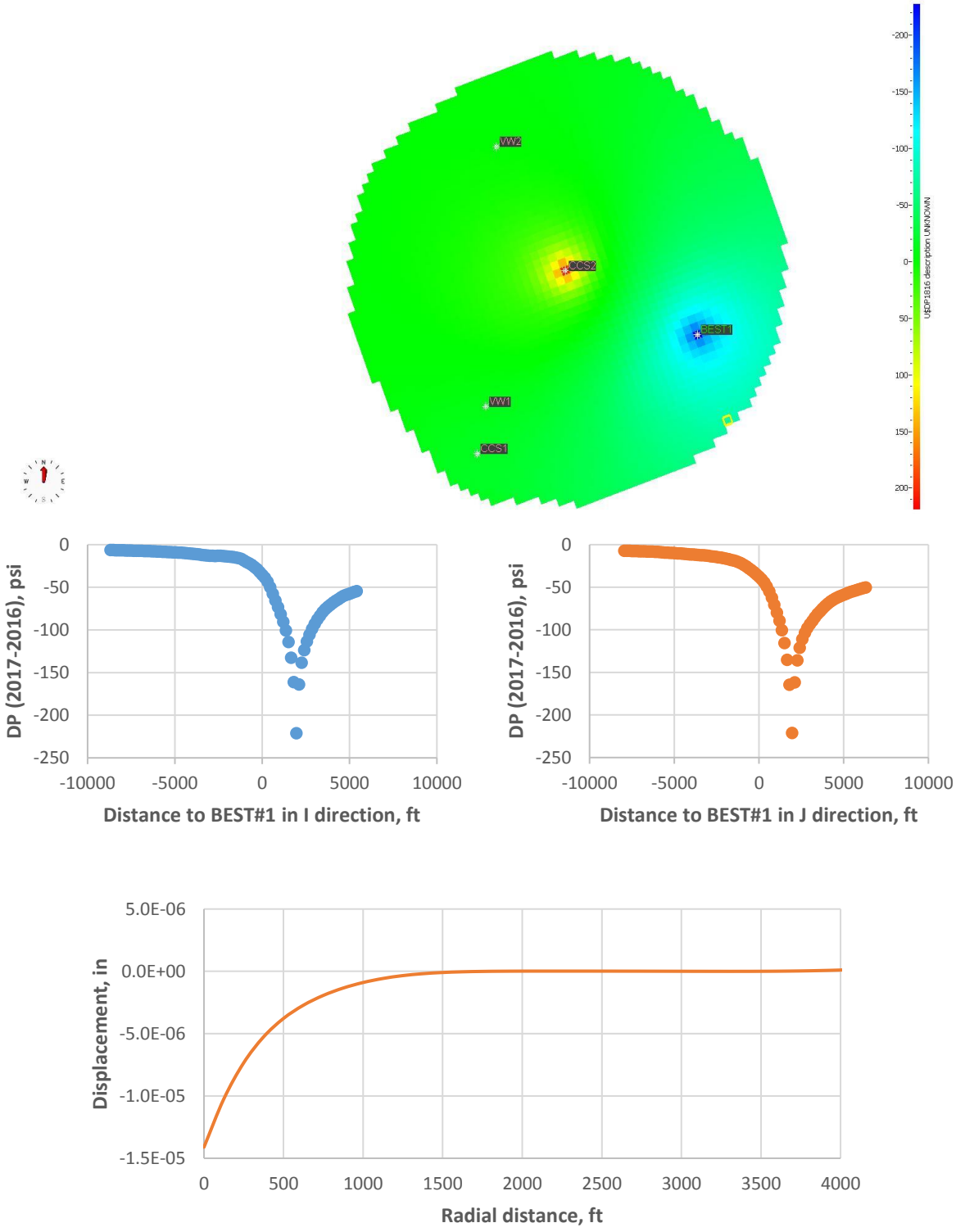

Figure 4-2-44 BEST#1 vertical displacement at the base of caprock at the end of injection in scenario WAG05.

The Plaxis model assumptions, input parameters, and boundary conditions are discussed in detail in Appendix B. Two scenarios were simulated to estimate vertical displacements in the caprock:

- Scenario 1: uniform distributed load = 150 psi (1,034 kPa).
- Scenario 2: linearly decreasing load with increasing distance from well, P_{max} = 150 psi (1,034 kPa), P_{min} = 10 psi (69 kPa) at 2500 ft (762 m).

Note that all maximum displacements occurred along the centerline of the model. A maximum upward displacement of 0.3 in. at the base of the caprock was observed when a uniform load of 150 psi (1,034 kPa) was applied over a radius of 2,500 ft (762 m; Scenario 1, Figure 4-2-45). Displacements decreased with increasing vertical distance from the applied load (base of caprock, top of caprock, surface). Similar behavior was observed for Scenario 2, which had a maximum upward displacement of 0.14 in (3.56 mm) at the base of the caprock (Figure 4-2-46). Scenario 1 was the most conservative because the pressure distribution surrounding the injection well decayed exponentially. Scenario 2 was a better approximation, although still conservative. Both scenarios showed small but nonzero surface displacements, whereas no detectable ground heave is expected during the BEST pilot, as suggested by InSAR monitoring for IBDP, which had detected no ground heave after injecting more than 1 million metric tons of CO_2. Because small ground deformations were predicted for both Scenario 1 and Scenario 2, this result may indicate that vertical caprock displacements (base and top) were also somewhat conservative.

The magnitude of vertical displacements is significantly smaller than the magnitudes predicted by the Plaxis simulation scenarios. The maximum upward vertical displacement at the base of the caprock for the most representative pressure distribution (linearly decreasing applied load) was 0.138 in (3.505 mm). As stated previously, displacements estimated from the coupled geomechanical flow modeling should provide the most representative estimates of vertical displacements as a result of the accurate characterization of constitutive behavior, and interdependent changes in stress states and stress paths as a result of the flow of CO_2 and brine.

Table 4-2-7 Maximum vertical upward displacement of caprock and the ground surface.

Scenario	Maximum upward vertical displacement (in.)		
	Base of caprock	Top of caprock	Ground surface
1	0.303	0.245	0.114
2	0.138	0.100	0.033

Note: The number of significant digits shown in Table 4-2-7 is for a relative comparison of displacements and does not denote the level of precision of the model in predicting vertical displacements.

Caprock Integrity: Potential Increase in Vertical Caprock Permeability

Selvadurai (2013) presented a model for increased caprock permeability caused by caprock flexure and associated fracture generation resulting from CO_2 injection. This model estimates the permeability of a single vertical, continuous elliptical fracture through the caprock. To determine the total change in vertical permeability, the frequency of such fractures must be estimated by a separate fracture model. The assumptions necessary to make a calculation of fracture-based vertical permeability by this or other semi-empirical equations combined with the level of available data for reservoir and mechanical behavior properties make performing such a calculation ill-advised and likely to produce erroneous results.

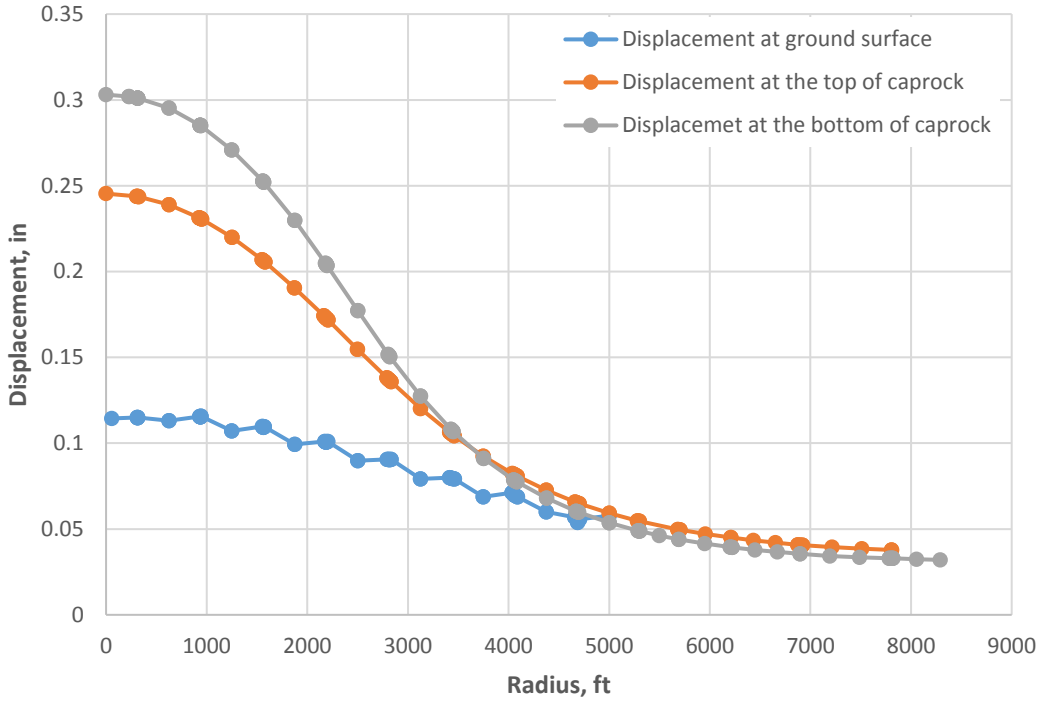

Figure 4-2-45 Scenario 1: vertical upward displacement (in.).

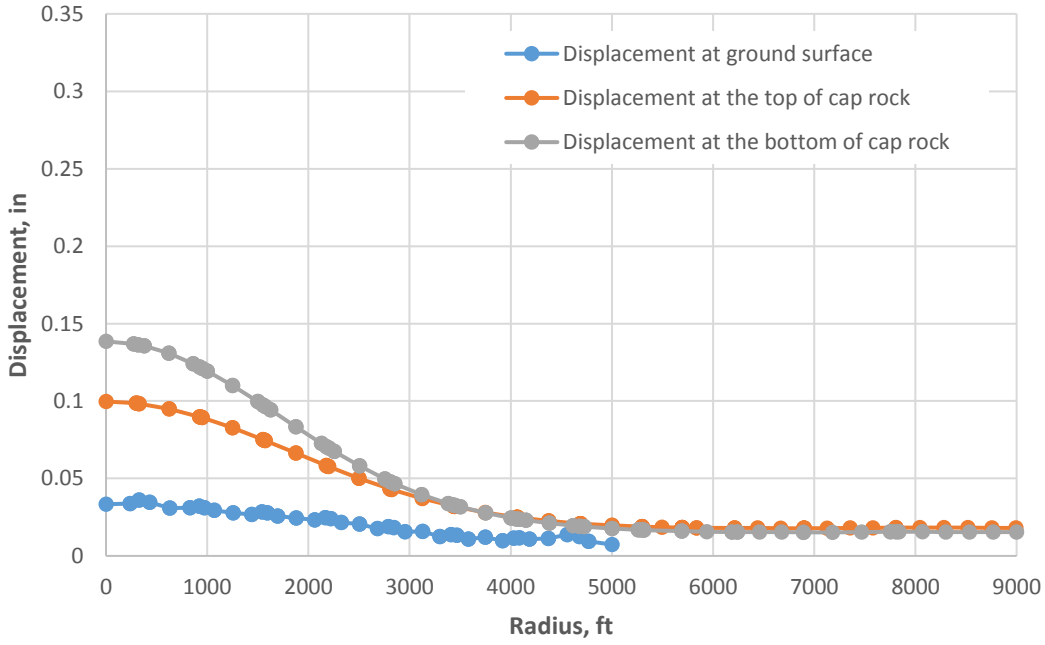

Figure 4-2-46 Scenario 2: vertical upward displacement (in.).

Additionally, the small vertical displacements calculated by the method of Li et al, 2015. and the Plaxis model scenarios, which correspond to relatively small shear forces and small radial flexural moments in the caprock, suggest that the caprock is below the tensile fracture threshold and below the shear slip reactivation threshold for existing fractures. Therefore, any increase in vertical permeability caused by the formation of new fractures or displacement and opening of existing fractures is likely minimal. These questions can be addressed through coupled geomechanical-flow modeling using commercial simulators as Petrel-Visage or CMG (as discussed in Rohmer and Seyedi 2010; Rutqvist 2002, 2007, 2008). From this output the detailed stress states and stress paths are known and can be used to determine risk of shear slip reactivation in existing fractures by using an approach similar to that by Rohmer and Seyedi (2010).

Fracture Gradient

The fracture gradient for the Eau Claire Shale was determined from mini-frac tests at CCS#1, which resulted in a fracture gradient of 0.93 to 0.98 psi/ft (21 to 22 kPa/m). The fracture gradient for the Mt. Simon Sandstone was determined from a step-rate injection test (Table 4-2-8).

Table 4-2-8 Fracture gradient for Eau Claire Shale and Mt. Simon Sandstone.

Borehole and formation	Depth (ft)	Minimum in situ stress (psi)	Fracture gradient (psi/ft)	Test type
CCS#1—Eau Claire shale	5435	5078 to 5324	0.93 to 0.98	Mini-frac
CCS#1—Mt. Simon	7025	5024	0.715	Step-rate injection

In summary, caprock flexure associated with CO_2 injection and brine extraction wells is the primary geomechanical effect examined. Simplified methods that include the effect of overburden, such as (1) the method of Li et al. (2014, 2015) and (2) the Mohr-Coulomb finite element Plaxis model, were examined to provide checks on coupled geomechanical flow modeling. These models are axisymmetric, with three layers (overburden, caprock, reservoir). Pressure distributions from the reservoir simulations at the end of injection (critical scenario, with a maximum differential pressure) were simplified to a 2-D axisymmetric distribution and used as inputs to the method of Li et al. (2014, 2015). Simplified pressure distributions (uniform 150 psi [1,034 kPa] pressure distribution, linearly decreasing pressure distribution from 150 to 10 psi [1,034 to 69 kPa] over a 2,500 ft [762 m] radius) are applied in the Plaxis model to provide a range of predicted displacements.

Pressure distributions are modeled as vertical upward (for injection well) or downward (for extraction well) applied loads. The maximum calculated displacements for the method of Li et al. (2014, 2015) are 1.04×10^{-5} to 1.78×10^{-5} in. (2.64×10^{-4} to 4.52×10^{-4} mm). Maximum displacements predicted from the Plaxis model at the base of the caprock are significantly larger at 0.14 to 0.3 in. (3.56 to 7.62 mm) for the linearly decreasing and uniform load distributions, respectively. Results from the simplified vertical deformation methods examined indicate vertical caprock displacements are sufficiently small, and the radius of curvature over which this deformation acts is sufficiently large, that the change in vertical permeability is not expected to be significant.

Horizontal Well Extraction Effects

Coupled Hydro-Mechanical Modeling

Schlumberger performed coupled hydro-mechanical modeling for geomechanical evaluation of extraction scenarios. As part of this workflow, pressures at selected times are output from the simulation for input to the coupled modeling process.

A geomechanical model was developed to examine the stress change due to CO_2 injection from CCS#1, CCS#2, and brine extraction from a horizontal well completed in Upper Mt Simon B. Model construction consisted of 60 × 60 ft (18 × 18 m) XY cell dimensions with varying cell thickness. The model included overburden, sideburden, and underburden cells that progressively coarsen outward from the focus interpretation area for a total of 8.2 million cells (Figure 4-2-47). Pressure time steps were chosen where large pressure changes occur during injection or extraction to determine associated stress changes.

Finite element properties examined included stress magnitude, stress orientation, rock displacement, and rock failure. Figure 4-2-48 through Figure **4-2-50** show stress magnitude at three depth slices at different times through the model. Figure 4-2-48 is at the CCS#1 injection depth/time, Figure 4-2-49 is at the CCS#2 injection depth/time, and Figure 4-2-50 is at the horizontal well depth brine extraction time.

Stress azimuth can rotate due to large pressure changes that occur during injection or production of reservoir fluids. Principal stress orientations were examined for rotation (Figure 4-2-51) but obvious rotation was not observed because of the small magnitude of pressure change.

Rock displacement was examined over the horizontal well brine extraction time period and is shown in Figure 4-2-52. Displacement is small (0.25 inch [6.35 mm]) around the wellbore and therefore not expected to cause any adverse effects.

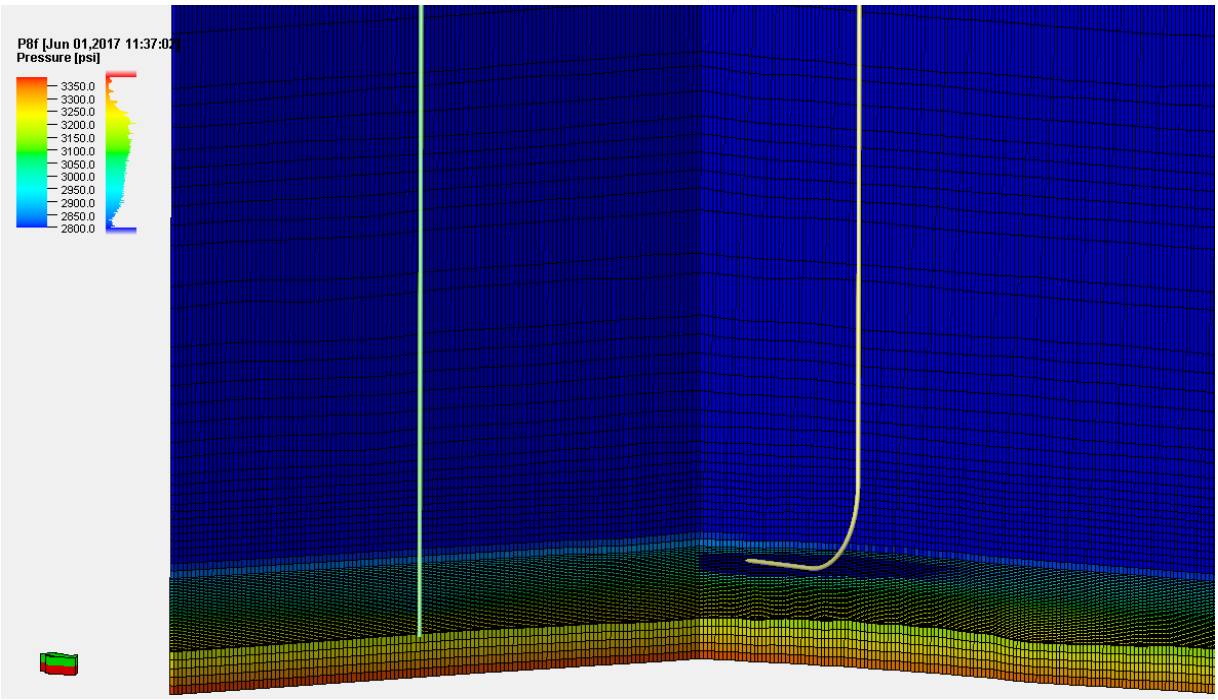

Figure 4-2-47 Geomechanical model showing cell size and variation. Pore pressure decrease is present around the horizontal well due to brine extraction.

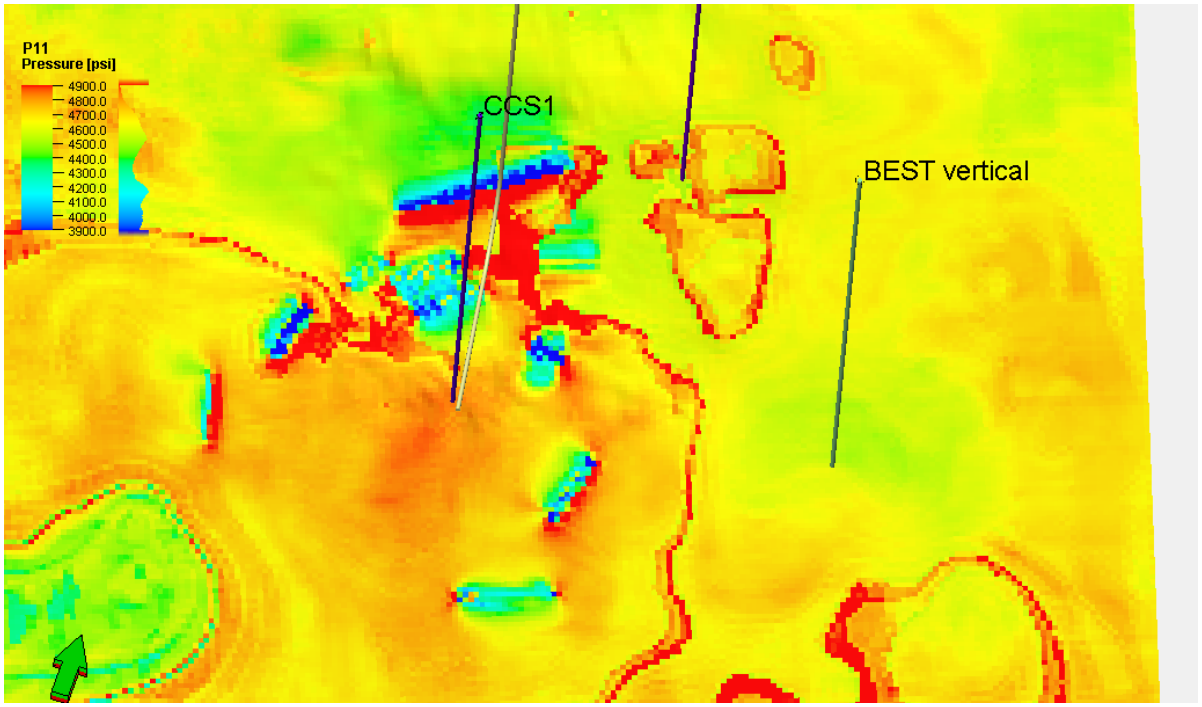

Figure 4-2-48 Minimum principal stress at the CCS#1 injection depth and time. The slight red color around CCS#1 shows a stress increase from CO_2 injection. At this, depth planes of weakness where microseismc events were measured in the field during injection are visible as blue lines. This is due to the stress contrast created by variation in mechanical properties between the weak planes and surrounding intact rock.

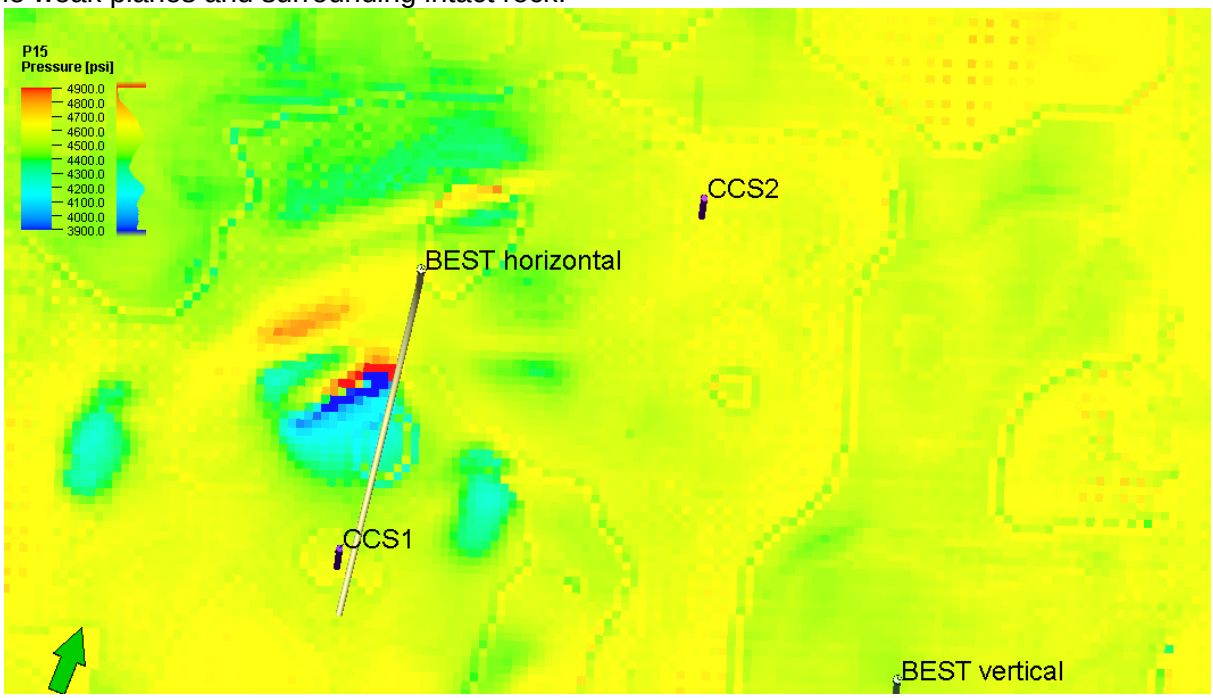

Figure 4-2-49 Minimum principal stress at the CCS#2 injection depth and time. A slight increase in stress is observed around CCS#2 from CO_2 injection.

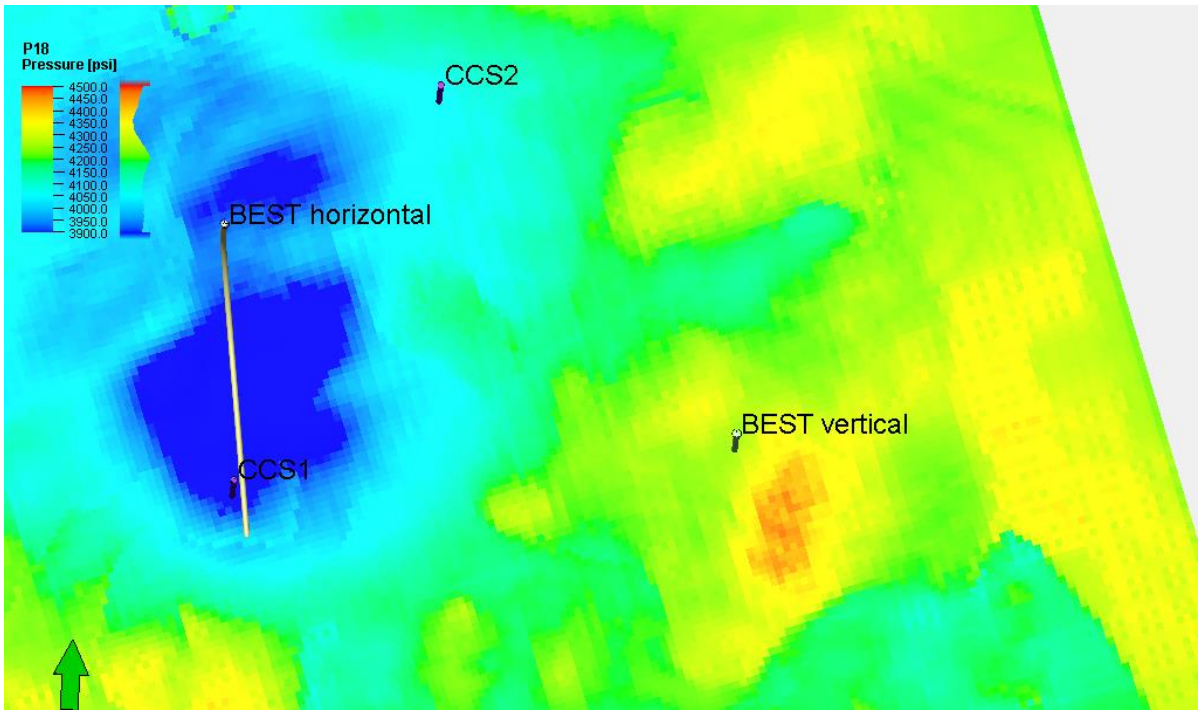

Figure 4-2-50 Minimum principal stress at the CCS#1 injection depth and time. A decrease in stress (blue) is observed along the horizontal well due to brine extraction.

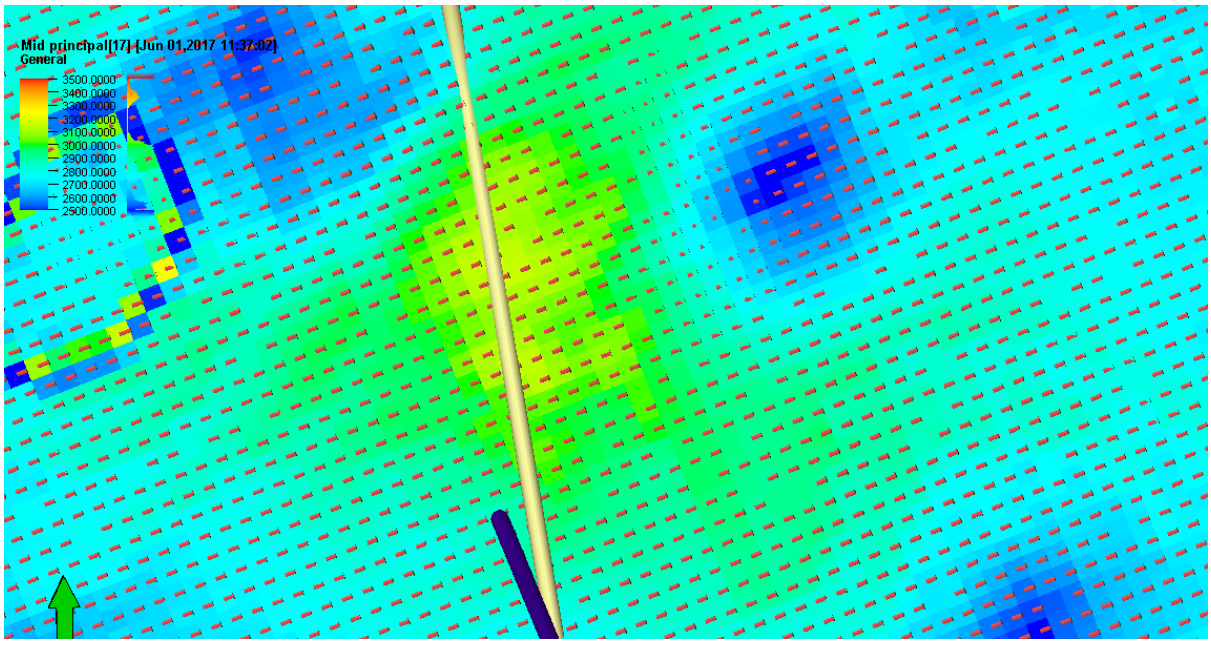

Figure 4-2-51 Medium principal stress orientation is shown as red body arrows with green tips in a northeast-southwest azimuth. Rotation was not observed during brine extraction.

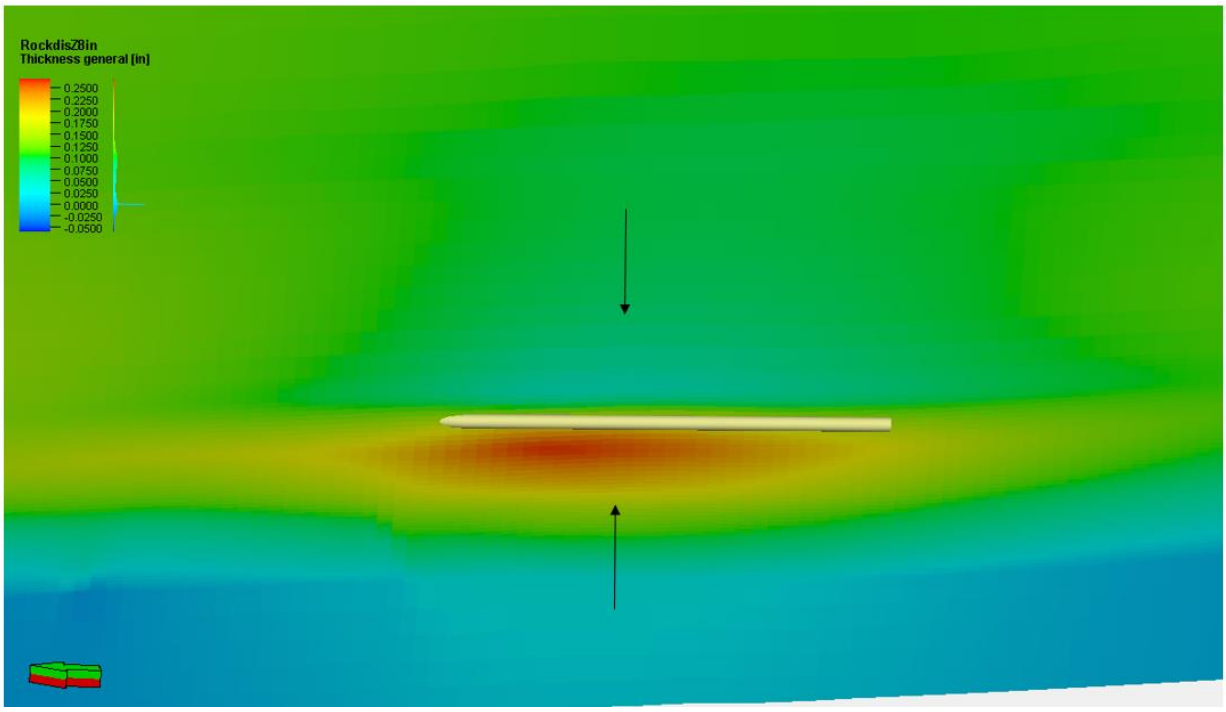

Figure 4-2-52 Rock displacement from brine extraction around the horizontal wellbore (white line) is shown as a decrease (blue) above the wellbore and increase (red) below the wellbore. This movement is typical in both directions when fluids are extracted from porous rock.

Stress Variation

Pressure depletion will occur during brine extraction and induces an associated stress change in the rock. The magnitude of stress change was investigated to check whether it can be detected using time-lapse shear slowness.

The minimum principal stress change from brine extraction was determined to be ~600 psi (4,137 kPa) decrease from pre-extraction conditions (Figure 4-2-53). Laboratory core test that measured velocity with stress change were examined to determine the range of stress and associated velocity change (Figure 4-2-54). The expected change in velocity is in the measurable range for wireline tools.

Sanding Prediction

Using the expected brine extraction pressure, stress, rock strength and other properties, sanding potential of the Upper Mt Simon B horizontal well interval was examined. Sand grain diameter range was determined from core thin section analysis. The borehole model was 8.5 in. (216 mm) diameter open hole. A single depth analysis was used to examine sensitivity of drawdown results to parameter selection (Figure 4-2-55). The main conclusion is that for this interval and expected pressure depletion, the rock strength is high, and dominates the interpretation results. This interval has low potential for sanding failure.

Potosi Dolomite Brine Disposal Rate and Capacity

Figure 4-2-56 shows the injection rate and average formation pressure of maximum rate scenarios. When the disposal well was close to the vertical extraction well, the brine disposal rate ranged from 20,561 to 41,765 stb/day (3,269 to 6,641 m^3/day), averaging approximately 21,000 stb/day (3,339 m^3/day). The formation pressure increased 135 psi (931 kPa) after 2-year injection. When the well was close to the horizontal extraction well, the brine disposal rate ranged from

14,384 to 26,072 stb/day (2,284.1 to 4,145.4 m^3/day), averaging approximately 15,000 stb/day (2,385 m^3/day). The formation pressure increased 119 psi (821 kPa) after 2-year injection. This indicates the maximum disposal rate is 15,000 to 20,000 stb/day (2,385 to 3,180 m^3/day), which is 435 to 580 gal/min (1,647 to 2,196 L/min). This rate is comparable to the historical long-term disposal rate of the Potosi (128 to 631 gal/min [485 to 2,389 L/min]) in Tuscola, IL.

Figure 4-2-57 shows the injection rate and average formation pressure of capacity scenarios. When the disposal well was operated at a constant rate of 10,000 stb/day (290 gal/min), the average formation pressure increased 133 psi (917 kPa) after 20-year injection for the vertical scenario and 160 psi (1,103 kPa) for the horizontal scenario. These pressure increases are about 11% to 13% of the maximum allowable pressure increase, suggesting the Potosi Dolomite has a large capacity for brine disposal in the long term with a relatively high disposal rate.

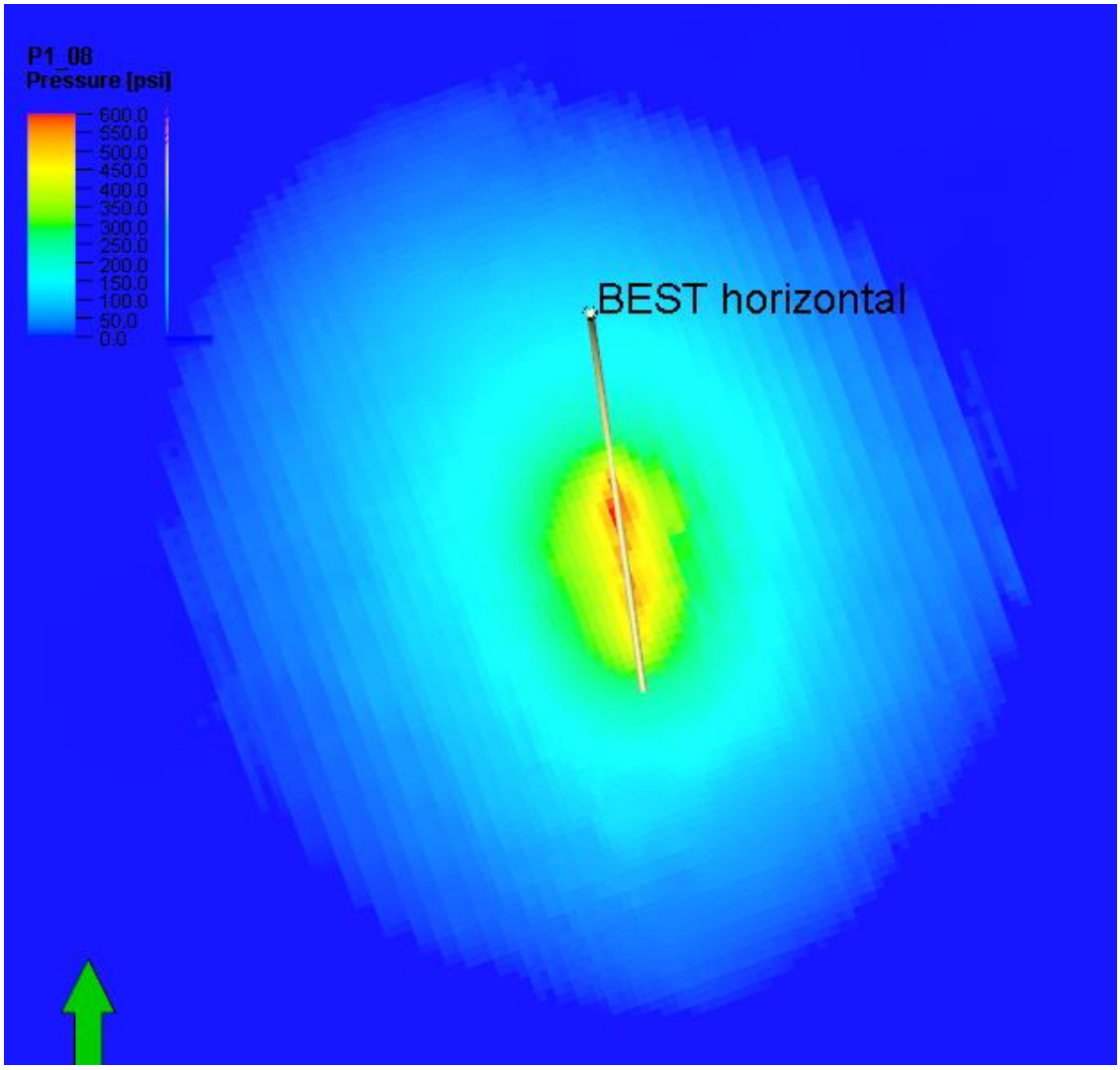

Figure 4-2-53 Minimum principal stress decrease from brine extraction.

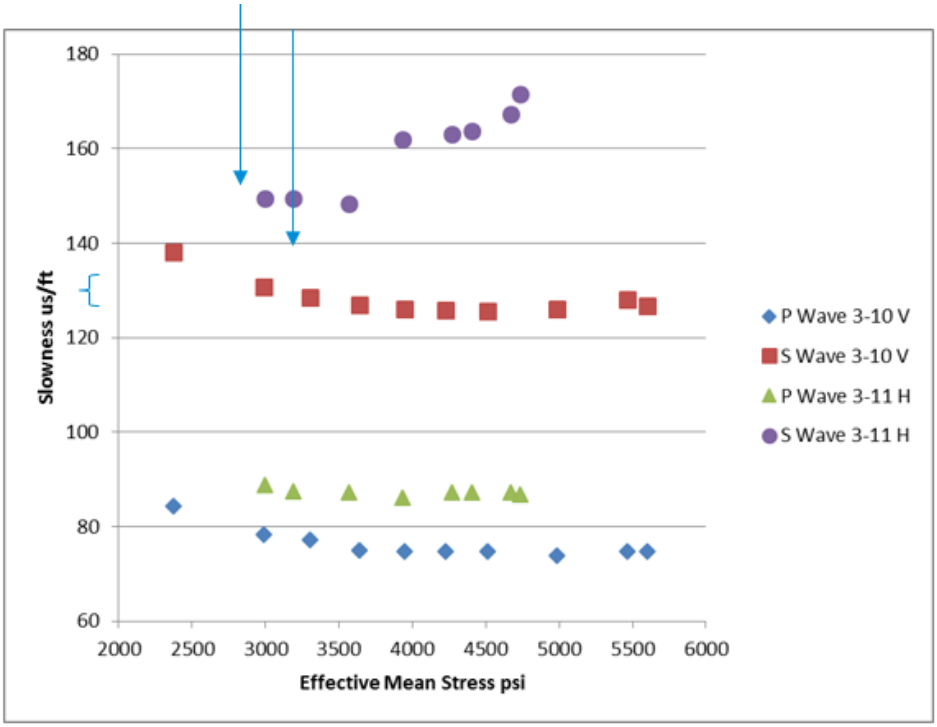

Figure 4-2-54 Points are slowness vs mean stress. The range of decrease from brine extraction is shown by the arrows and defines an expected change of slowness of 7-8 us/ft, which is measurable by time lapse, passes using wireline tools.

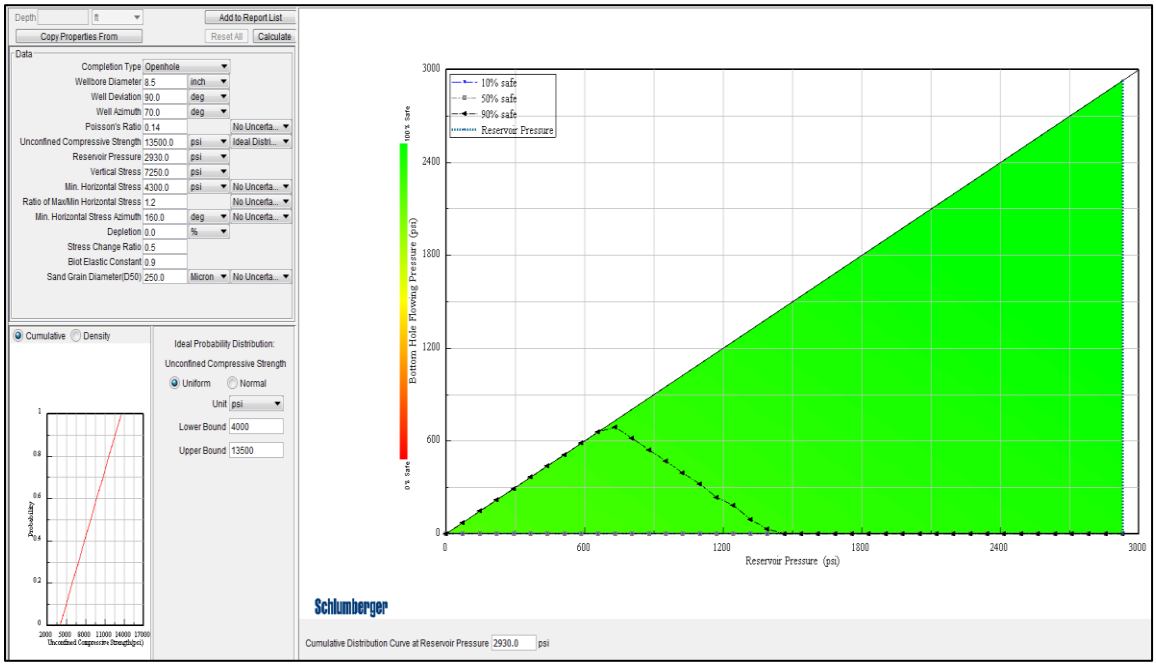

Figure 4-2-55 Single depth sanding sensitivity for UCS (unconfined compressive strength). Core UCS for this interval is ~13,500 psi (93,083 kPa), which shows no failure at any drawdown. Even reducing UCS to 4,000 psi (27,580 kPa), failure will not occur with the modeled brine extraction.

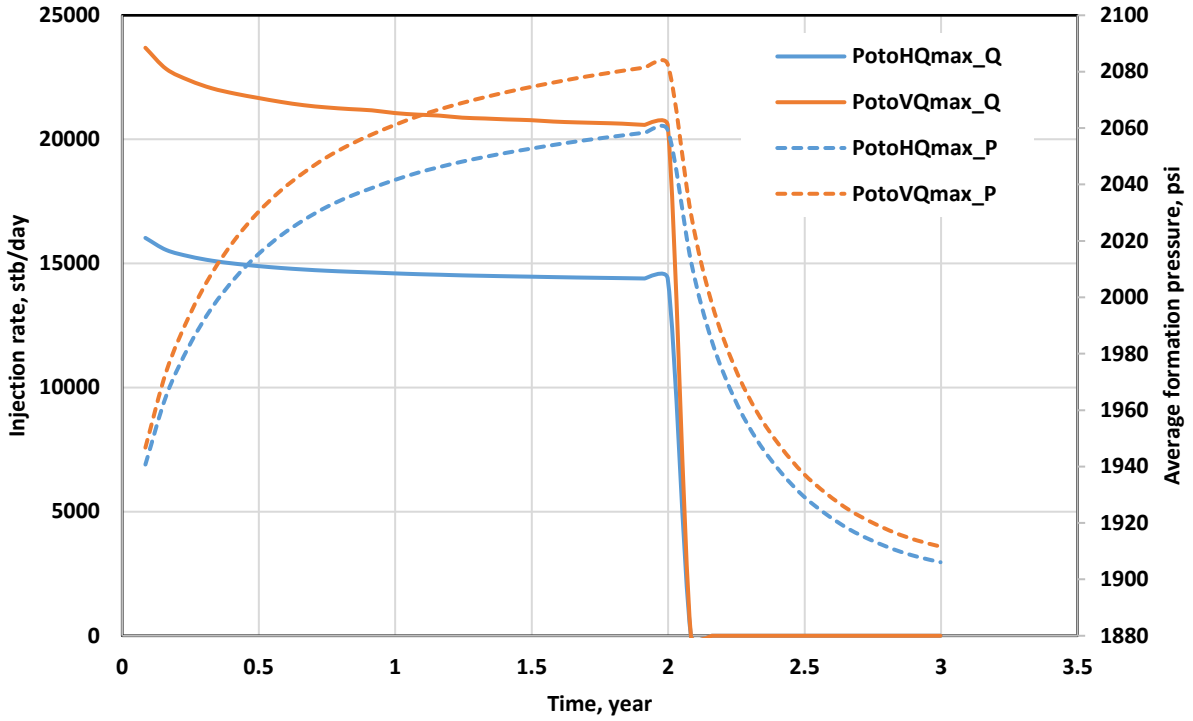

Figure 4-2-56 Injection rate and average formation pressure for maximum rate scenarios.

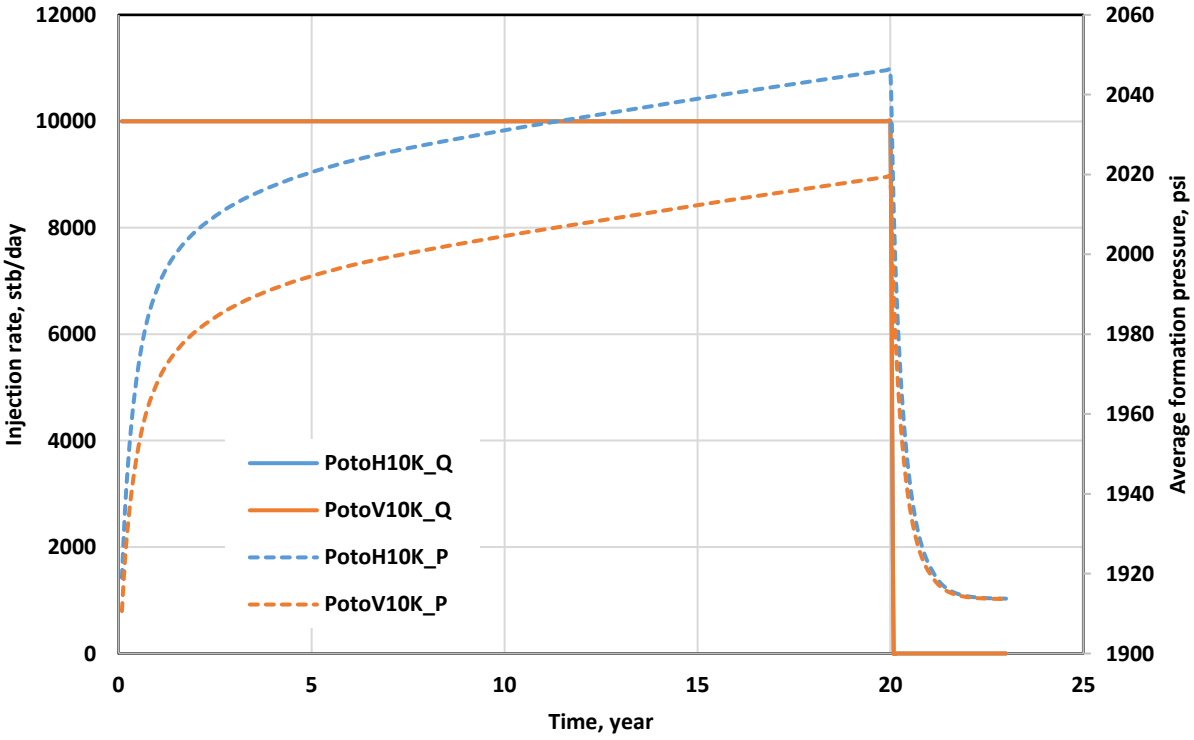

Figure 4-2-57 Injection rate and average formation pressure for capacity scenarios.

Summary

Reservoir simulation scenarios for brine extraction using either a vertical well or a horizontal well were considered, to evaluate the CO_2 plume distribution and whether or not extraction-induced changes in pressure can be detected at existing multi-level monitoring wells. Geomechanical effects were analyzed to evaluate wellbore integrity and the ability to monitor extraction-induced rock deformation. The disposal rate and capacity of the Potosi Dolomite to handle brine extracted from the Lower Mt. Simon was evaluated.

Generally, brine extraction can effectively manage pressure and control the CO_2 plume. The DPI values ranged from –0.019 to 0.029, indicating that variations in formation pressure induced by brine extraction were within 2.9% of the maximum allowable pressure change. The pressure variations should be of sufficient magnitude to be observed in multilevel monitoring for all modeled extraction rates.

Continuous CO_2 injection was a better option than WAG because it yielded a more favorable DPI than WAG, although a less favorable E. Reducing the salinity of the Lower Mt. Simon in half had little effect on DPI but greatly improved E; however, injecting treated lower salinity brine was not beneficial to either DPI or E.

To effectively release pressure and improve CO_2 efficiency, a vertical extraction well is recommended (1) 0.5 mi (0.8 km) away from the injector, (2) in a direction perpendicular to reservoir hydraulic connectivity, and (3) in the down-dip side with perforation(s) within the injection zone. A distance of 0.5 mi (0.8 km) is the optimal well spacing in this study, which is in agreement with Frailey and Finley (2011). However, this distance may not be applicable in other fields and can only be used as a starting point because it greatly depends on the injection and extraction rates and the geologic connectivity between wells. Studies to evaluate the sensitivity of well spacing are recommended for all brine extraction projects.

Alternatively, a horizontal extraction well can be placed directly above the existing CO_2 plume, decreasing the risk of drilling into an existing CO_2 plume and reducing uncertainty in the geology, as compared with a vertical extraction well. Before drilling a horizontal extraction well, reservoir saturation logs from the injection well must be analyzed and interpreted to determine the vertical location of the CO_2 plume. A horizontal extraction well increases E up to 12.39% over no brine extraction and up to 4.72% over brine extraction via a vertical well in an optimal location; in addition, a horizontal well can control the CO_2 plume and pressure at a lower extraction rate than a vertical extraction well. A horizontal extraction well has a significantly smaller impact on the lateral movement of a CO_2 plume than a vertical extraction well, which can be beneficial for maintaining the CO_2 plume within an area of review. In the simulated scenarios, the lateral movement of the CCS#2 plume attributable to brine extraction was 90 ft (27 m) by a horizontal well in comparison to 856 ft (261 m) by a vertical well. Note that the geocellular model assumed a low kv/kh of 0.1. Increasing kv/kh to 0.2 or 0.3 could greatly accelerate the vertical movement of the CCS#1 plume and slow lateral movement of the CCS#2 plume.

An injection-to-extraction ratio of 1:1 yields favorable pressure reduction, storage efficiency, and control of CO_2 plume. To minimize brine extraction and make a noticeable effect on pressure and the CO_2 plume, an injection-to-extraction ratio of 2:1 for a vertical well and an injection-to-extraction ratio of 4:1 for a horizontal well are recommended, which correspond to extraction rates of 10,000 and 5,000 bbl/day (1,590 and 795 m^3/day) when CO_2 is injected at 1.1 million tons per annum (1 million tonnes per annum).

The geomechanical effects examined by using the simplified vertical deformation methods indicate that the vertical caprock displacements would be negligible small and the radius of

curvature over which this deformation may act is very large such that the change in vertical permeability is not expected to be significant. Neither mechanical formation failure nor sanding in the extraction well are anticipated at a 20,000 stb/day (3,180 m^3/day) brine extraction rate. Extraction-induced rock deformation at a rate of 20,000 stb/day (3,180 m^3/day) will be of sufficient magnitude to be detected using repeat sonic measurements.

The Potosi Dolomite has a large capacity for brine disposal in the long term with a relatively high disposal rate. The maximum disposal rate was 435 to 580 gal/min (1,647 to 2,196 L/min). Simulation results predict pressure increase of about 160 psi (1,103 kPa) after 20 years at a brine disposal rate of 290 gal/min (1,098 L/min) into the Potosi Dolomite at the IBDP site.

4-1 and 4-2 References

Ali, A.H.A., T. Brown, R. Delgado, D. Lee, D. Plumb, N. Smirnov, R. Marsden, E. Prado-Velarde, L. Ramsey, D. Spooner, T. Stone, and T. Stouffer, 2003, Watching rocks change—Mechanical earth modeling: Oilfield Review, v. 15, no. 2, p. 22–39, https://www.slb.com/~/media/Files/resources/oilfield_review/ors03/sum03/p22_39.pdf (accessed March 21, 2016).

Benson, S.M., and D.R. Cole, 2008, CO_2 sequestration in deep sedimentary formations: Elements, v. 4, p. 325–331.

Brower, R.D., A.P. Visocky, I.G. Krapac, B.R. Hensel, G.R. Peyton, J.S. Nealon and M. Guthrie, 1989, Evaluation of underground injection of industrial waste in Illinois: Illinois State Geological Survey, Illinois Scientific Surveys Joint Report 2, 169.

Buscheck, T.A., Y. Sun, Y. Hao, T.J. Wolery, W. Bourcier, A.F.B. Tompson, and R.D. Aines , 2011, Combining brine extraction, desalination, and residual-brine reinjection with CO_2 storage in saline formations: implications for pressure management, capacity, and risk mitigation. Energy Procedia, 4, p. 4283–4290.

Fjaer, E., R.M. Holt, P. Horsrud, A.M. Raaen, and R. Risner, 2008, Petroleum Related Rock Mechanics, 2nd edition: Amsterdam, Elsevier, 491 p.

Frailey, S.M., and R.J. Finley, 2011, CO_2 plume management in saline reservoir sequestration: Energy Procedia, 4, p. 4238–4245.

Freiburg, J.T., and H.E. Leetaru, 2012, Controls on porosity development and the potential for CO_2 sequestration or wastewater disposal in the Cambrian Potosi Dolomite (Knox Group): Illinois Basin: 41st Annual Eastern Section AAPG Meeting, Cleveland, Ohio, USA, September 22–26.

Leetaru, H., 2014, Maquoketa Shale caprock integrity evaluation: Illinois State Geological Survey, U.S. Department of Energy Contract Number FE0002068, http://www.osti.gov/scitech/servlets/purl/1202275 (accessed March 21, 2016).

Li, C., P. Barès, and L. Laloui, 2013, Coupled semi-analytical solution for CO_2 injection-induced surface uplift and caprock deflection, *in* 47th US Rock Mechanics/Geomechanics Symposium: Alexandria, Virginia, American Rock Mechanics Association, p. 612–622.

Li, C., P. Barès, and L. Laloui, 2014, Coupled semi-analytical approach of CO_2 injection induced caprock deflection, *in* F. Oka, A. Murakami, R. Uzuoka, and S. Kimoto, eds., Computer Methods and Advances in Geomechanics: Leiden, The Netherlands, CRC Press/Balkema.

Li, C., P. Barès, and L. Laloui, 2015, A hydromechanical approach to assess CO_2 injection-induced surface uplift and caprock deflection: Geomechanics for Energy and the Environment, v. 4, p. 51–60.

Midwest Geological Sequestration Consortium (MGSC), 2005, An assessment of geological carbon sequestration options in the Illinois Basin. MGSC, U.S. Department of Energy contract DE-FC26-03NT41994, 581 pp.

Okwen, R., 2015, Brine extraction and treatment strategies to enhance pressure management and control of CO_2 plumes in deep geologic formations, *in* Developing and Validating Pressure Management and Plume Control Strategies through a Brine Extraction Test (BEST): Illinois State Geological Survey, U.S. Department of Energy Fit-for-Purpose Field Project DE-FOA-0001260.

Rohmer, J., and D.M. Seyedi, 2010, Coupled large scale hydromechanical modelling for caprock failure risk assessment of CO_2 storage in deep saline aquifers: Oil & Gas Science and Technology (Revue de l'Institut Français du Pétrole), v. 65, no. 3, p. 503–517.

Rutqvist, J., J.T. Birkholzer, C. Cappa, and C.-F. Tsang, 2007, Estimating maximum sustainable injection pressure during geological sequestration of CO_2 using coupled fluid flow and geomechanical fault-slip analysis: Energy Conversion and Management, v. 48, no. 6, p. 1798–1807.

Rutqvist, J., J.T. Birkholzer, and C.-F. Tsang, 2008, Coupled reservoir-geomechanical analysis of the potential for tensile and shear failure associated with CO_2 injection in multilayered reservoir-caprock systems: International Journal of Rock Mechanics and Mining Sciences, v. 45, no. 2, p. 132–143.

Rutqvist, J., and C.F. Tsang, 2002, A study of caprock hydromechanical changes associated with CO_2-injection into a brine formation: Environmental Geology, v. 42, no. 2–3, p. 296–305.

Selvadurai, A.P.S., 2009, Heave of a surficial rock layer due to pressures generated by injected fluids: Geophysical Research Letters, v. 36, no. 14, p. 1–5.

Selvadurai, A.P.S., 2013, Caprock breach: A potential threat to secure geologic sequestration of CO_2, *in* G. Pijaudier-Cabot and J.-M. Pereira, eds., Geomechanics in CO_2 Storage Facilities: New York, John Wiley & Sons, Ltd., p. 75–94.

Senel, O., R. Will, and R. Butsch, 2014, Integrated reservoir modeling at the Illinois Basin–Decatur Project: Greenhouse Gases: Science and Technology, v. 4, p. 622–684.

Vilarrasa, V., D. Bolster, M. Dentz, S. Olivella, and J. Carrera, 2010, Effects of CO_2 compressibility on CO_2 storage in deep saline aquifers: Transport in Porous Media, v. 85, p. 619–639.

Will, R., 2013, Geomechanical and flow modeling at the Illinois Basin–Decatur Project [PowerPoint slides]: Champaign, Illinois, Schlumberger Carbon Services, http://sequestration.org/resources/PAGOct2013Presentations/08-PAG_2013_GeoMech-Flow-Model-BobWill%20-%20FINALtrm.pdf (accessed October 2015).

Yi, X., P.P. Valko, and J.E. Russell, 2004, Predicting critical drawdown for the onset of sand production: SPE International Symposium and Exhibition on Formation Damage Control, Lafayette, Louisiana, USA, February 18–20, Paper SPE 86555.

Yoksoulian, L.E., J.T. Freiburg, S.K. Butler, P.M. Berger, and W.R. Roy, 2013, Mineralogical alterations during laboratory-scale carbon sequestration experiments for the Illinois Basin: Energy Procedia, 37, p. 5601–5611.

TASK 5-0 DEVELOPMENT OF PHASE II MONITORING PLAN AND PERMIT PREPARATION

Subtask 5-1 Phase II monitoring plan

Monitoring changes in the magnitude of pressure and position of a CO_2 plume in the subsurface underpins much of the requirements to assess the effectiveness of the BEST process, and the monitoring plan must consider aspects of the tools available and design of the test. In a recent survey of the state of the art monitoring practices for global carbon sequestration projects, Jenkins et al. (2015) organized the techniques into four major categories: containment, conformance, contingency, and environmental impact. Containment monitoring is designed to show that the stored CO_2 is securely retained within the storage site. Conformance monitoring provides data to measure the agreement between the simulated and observed CO_2 plumes. Contingency monitoring is a set of additional methods deployed if conformance is an issue. The final category, environmental impact monitoring, covers methods focused on near-surface environments and is often motivated by societal concerns. For this project involving brine extraction to investigate the effect of pressure management on CO_2 plume evolution monitoring purposes are mainly to address containment and conformance. Monitoring data is needed to both locate the CO_2 plume and changes in pressure resulting from brine extraction.

Descriptions of monitoring tools are available from a number of sources, including the IEAGHG On-line Monitoring and Verification Toolbox (http://ieaghg.org/ccs-resources/monitoring-selection-tool), the NETL Best Practice manual (NETL, 2012), the World Resources Institute Guidelines for Carbon Dioxide Capture, Transport and Storage (WRI, 2008) and CO2QUALSTORE guidelines (CO2QUALSTORE, 2010).

CO_2 Plume Tracking Methods

Active Seismic Methods

Of the monitoring methods used in CO_2 storage projects, three-dimensional (3D) surface seismic has been arguably the most effectively in mapping out the distribution of subsurface CO_2 plumes. Three-dimensional surface seismic is a sophisticated, deep echo-sounding technique utilizing multiple seismic sources and receivers to produce full volumetric images of subsurface structures in a reservoir, the overburden, and deeper sediments. Three-dimensional surface seismic is a set of numerous closely spaced seismic lines that provide a high spatially sampled measure of subsurface reflectivity (Figure 5-1-1). In a properly processed and imaged 3D seismic dataset, events are placed in their proper vertical and horizontal positions, which provides more accurate subsurface maps than can be constructed based on more widely spaced two-dimensional (2D) seismic lines. In particular, 3D seismic data provides detailed information about fault distribution and subsurface structures. Computer-based interpretation and display of 3D seismic data allows for more thorough analysis than 2D seismic data.

Acquisition hardware is the same for both 2D and 3D methods. Explosives or vibroseis are used as the energy source for onshore surveys. Geophones or accelerometers are used for receivers. In onshore acquisition geometry, a shot line consists of a number of shot points that are usually fired orthogonally to the receiver lines.

A key application of surface seismic for monitoring purposes is in time-lapse (4D) mode, in which a number of repeat surveys are acquired, enabling changes in fluid distribution to be mapped through time. In the time-lapse mode, 3D seismic provides a powerful leakage monitoring tool but provides data that is of modest value for demonstrating conformance (Jenkins et al., 2015).

Three-dimensional surface seismic has been used at the IBDP (Finley, 2014), with additional details about 2D and 3D seismic work at IBDP in Couëslan et al. (2014).

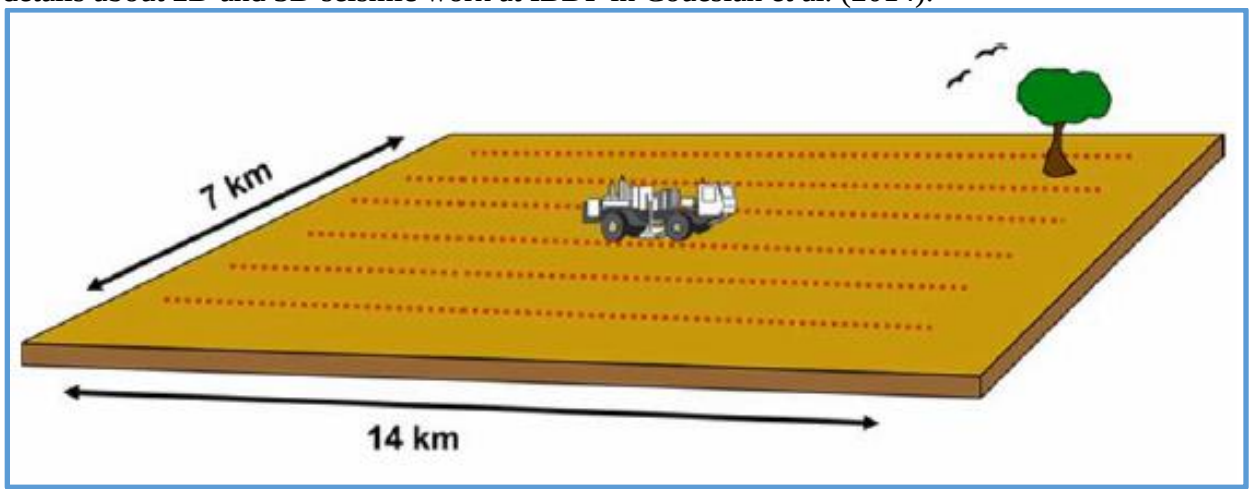

Figure 5-1-1 Three-dimensional seismic acquisition for onshore surveys (provided by G. El-kaseeh, Schlumberger Carbon Services).

Four-dimensional (4D) or time-lapse is two or more 3D surface seismic datasets acquired at different times over the same area. The datasets may be used to assess changes in a producing hydrocarbon reservoir with time or monitor plume development of injected CO_2. Changes may be observed in fluid location and saturation, pressure, and temperature. Four dimensional seismic data are used as the basis for indirect seismic monitoring of the CO_2 plume.

For a BEST project at the IBDP site, the high-density dataset that was acquired in 2015 (post-injection of 1.1 million tons [1 million tonnes] of CO_2 in Mt. Simon Sandstone) can be used as the baseline survey. A monitor survey (post-brine extraction), with the same acquisition geometry as the baseline survey, can be acquired. The two datasets will need to be simultaneously processed to reduce uncertainty in repeatability. Several attributes extracted during and post-processing can potentially provide information about plume movement.

Vertical Seismic Profiling (VSP) is a borehole seismic method where seismic receivers are placed in a wellbore and the seismic source is located on the ground surface. The advantages of VSP include having receivers permanently set, which boosts repeatability, and that detailed, high-resolution velocity and reflection images of the subsurface can be acquired while providing more freedom in imaging direction (versus cross-well seismic). Vertical Seismic Profiling was considered the principle seismic tool to monitor subsurface CO_2 movement at the IBDP (Couëslan et al., 2014). A 31-level geophone array was installed in GM#1 for conducting VSP surveys.

Cross-well seismic is a survey technique that measures the seismic signal transmitted from a source, located in one well, to a receiver array (geophones or hydrophones) in a neighboring well. An example of the configuration for gathering this data is shown in Figure 5-1-2. The resulting data are processed to create a reflection image or to map the acoustic velocity or other properties (velocities of compressional [P-] and shear [S-] waves, for example) of the area between the wells. Placement of the source and receiver array in adjacent wells not only enables the formation between wells to be surveyed, but also avoids seismic signal propagation through attenuative near-surface formations. Another advantage of the cross-well seismic method is that it places the source and receiver near the reservoir zone of interest, thereby obtaining better resolution than is possible with conventional surface seismic surveys. This technique is often used

for high-resolution reservoir characterization when surface seismic or VSP data lacks resolution, or for time-lapse monitoring of fluid movements (CO_2) in the reservoir. Acquisition hardware is dictated by several factors (e.g., distance between the two wells and size of the wells).

In the case of the ISGS-BEST project, the cross-well seismic method integrated with other measurements can potentially provide information on CO_2 plume movement within the injection zone (Mt. Simon) that might be caused by brine extraction from above the zone. Existing wells, CCS#1 and VW#1, could be used as source and receiver wells to conduct the baseline and subsequent monitoring surveys. Other options may be considered, e.g., using the proposed horizontal well as a source or receiver well, in combination with CCS#1 and/or VW#1. Survey planning and design is usually conducted to determine the optimal acquisition parameters for maximum coverage and generate an efficient acquisition plan. Forward modeling can also be performed to quantify any difference in seismic response between pre- and post-extraction.

Repeatable Wireline Tool Methods

Downhole geophysical logs can be obtained from tools that are lowered down the well on a cable known as a "wireline." These tools measure the in situ physical properties of the rocks that constitute the borehole walls, fluids in the rocks, and downhole conditions, such as pressure and temperature. Pulsed-neutron logs, also known through trade names as Reservoir Saturation Tool (RST) and Pulsed Neutron eXtreme (PNX) logs, are useful for determining CO_2 saturation in the near wellbore environment. Repeat surveys can be used to monitor CO_2 related changes. See Couëslan et al. (2014) for more information related to RST logging at IBDP.

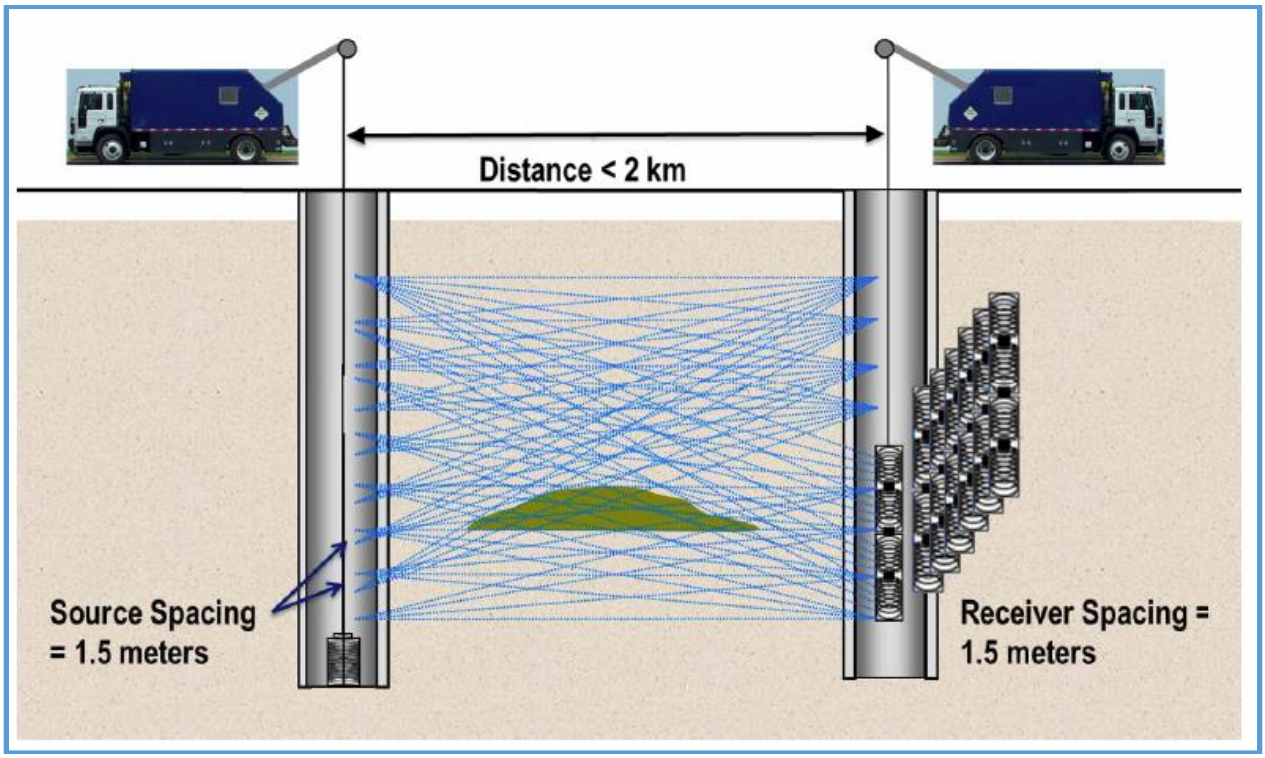

Figure 5-1-2 Schematic of cross-well seismic data acquisition, with the source in the left well and the receiver array in the right well (provided by G. El-kaseeh, Schlumberger Carbon Services).

The PNX is among the latest generation pulsed-neutron tools and has been optimized for gas, sigma, and neutron-porosity measurements (Figure 5-1-3), and includes a fast neutron cross

section measurement that is highly sensitive to CO_2 and gas volume and insensitive to water salinity and volume. A special pulse sequence used with the neutron generator allows borehole effects to be determined allowing formation capture cross section (SIGM) and neutron porosity (TPHI) to be self-compensated. Monitoring passes can be meaningfully compared even with changing borehole fluids and any change to the completion tubulars.

Pulsed Neutron Sigma ($\sum$) is the thermal neutron capture cross section, or the rate at which thermal neutrons are captured by the formation matrix and fluids. Pulsed Neutron Extreme has a pulsed-neutron generator that creates high-energy neutrons. These neutrons are slowed to a thermal velocity through elastic and inelastic collisions with the nuclei of the environment's elements, at which point they can be captured. Hydrogen, with the nuclei mass similar to the neutron, is the most effective element to slow the high-energy neutrons and chlorine is very good at capturing the thermal neutrons. Water has a capture cross section that depends largely on its salinity. Fresh water has a Sigma response of approximately 22 capture-units (cu) and salt-saturated water around 130 cu. Carbon dioxide has a very low ability to slow or capture neutrons and the Sigma response for CO_2 is near zero. Using the contrast in Sigma for water and CO_2, the water saturation (S_w) can be calculated from the Sigma measurement.

The neutron-porosity measurement is an inverse relationship of the slowing down length of high-energy neutrons emitted by the tool and responds primarily to the amount of hydrogen within the formation. Hydrogen is generally related to the fluids in the formation, (e.g., either water or oil). The carbon and oxygen nuclei of CO_2 have a much higher mass than a neutron, and interactions with high-energy neutrons are primarily elastic with the neutron losing very little energy similar to other formation elements. As CO_2 saturation increases, replacing formation water, the hydrogen density decreases, causing the neutron-porosity measurement to be lower than the true porosity.

Gas ratio (GRAT) and Fast Neutron Cross Section (FNXS) are new measurements based on the measurement of inelastic gamma rays, which are very sensitive to CO_2 and gas. Because inelastic gamma rays can only be induced by neutrons with energies at MeV levels, they respond to formation properties that are independent of neutron porosity and sigma.

The PNX neutron generator (minitron) burst contains a high flux of high-energy neutrons. The gamma rays resulting from the high-energy neutron interactions during the burst contain inelastic, epithermal, and thermal capture events, which are measured and normalized using a new compact neutron monitor (CNM) detector. By measuring the gamma ray events during and following a burst, the capture background can be determined and removed from the total measured gamma rays. Gas ratio is defined as the capture-background corrected-burst gamma-ray count rate normalized by the neutron-monitor count rate. In the presence CO_2 and/or gas in the formation, annulus, or wellbore, GRAT will increase. Characterizing GRAT for various formation conditions was done to obtain the fast-neutron cross section (FNXS) that provides an independent input to calculating the saturation of CO_2 and/or gas. Additional details about the PNX tool measurements can be found in Rose et al. (2015).

In the case of the ISGS-BEST project, pulsed-neutron measurements can be used to provide information about a CO_2 plume's vertical movement within the injection zone (Mt. Simon) that might be caused by the brine extraction.

Downhole gravity measurement offers the potential for higher resolution monitoring of CO_2 movement around the well, by measuring the gravity response of CO_2 layers in close proximity to the monitoring well. Jenkins et al. (2015) noted that well-based gravity was successfully tested at Cranfield in monitoring CO_2 movement.

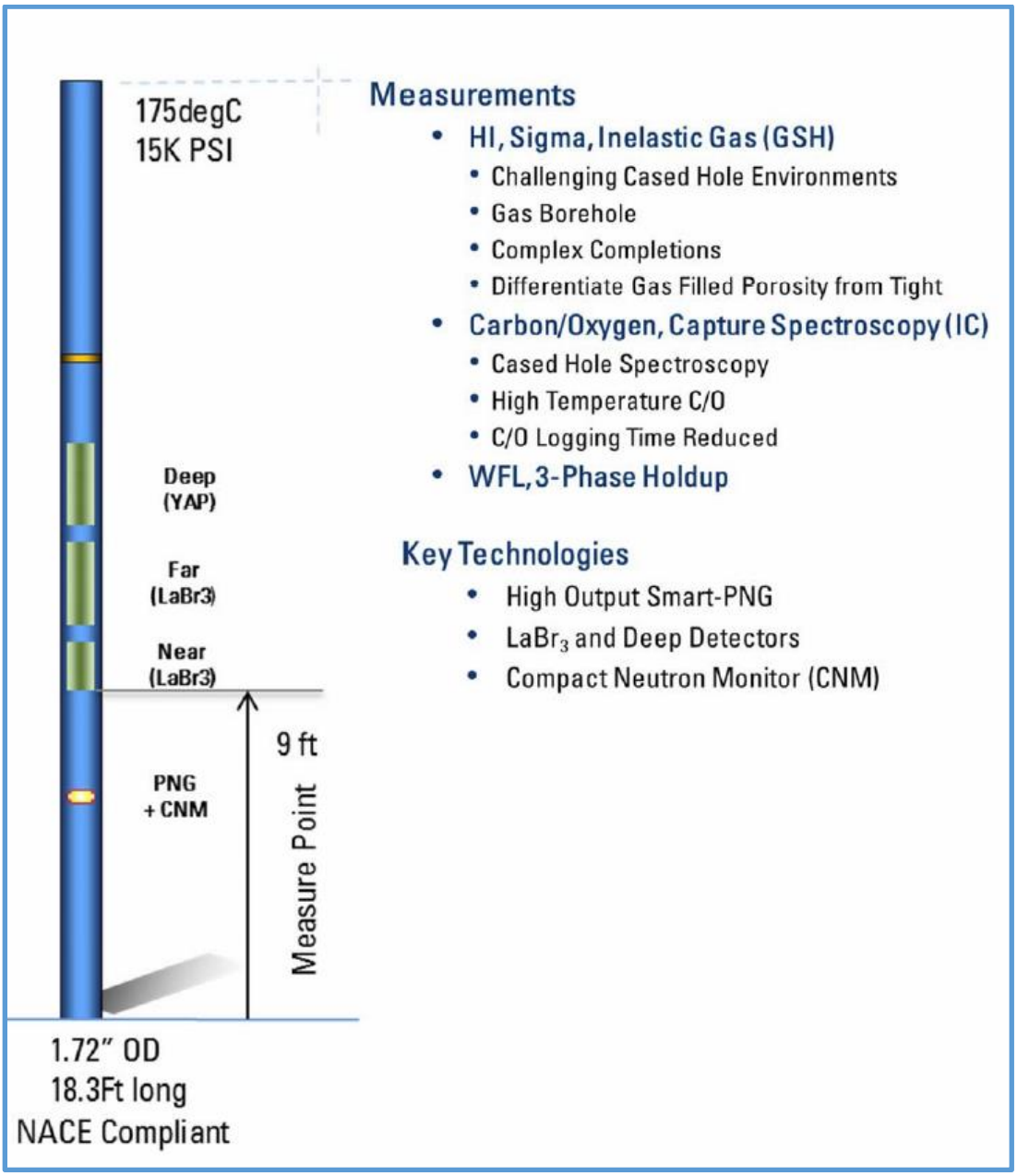

Figure 5-1-3 Pulsed Neutron eXtreme tool sketch and measurements (provided by G. El-kaseeh, Schlumberger Carbon Services).

Distributed Acoustic Sensing (DAS) is a recent fiber-optic sensing technology like Distributed Temperature Sensing (DTS) in which the fiber-optic cable itself is the sensor, but now the fiber senses the passage of elastic waves along its length becoming "geophones on a string." The success of DAS is based on the signal processing of backscattered optical signatures (Daley et al., 2013). Distributed Acoustic Sensing is also being used for monitoring in CO_2 sequestration projects (Daley et al., 2013, 2015; Worth et al., 2014). It is a prominent component of ADM's Intelligent Monitoring System (IMS) project at the Decatur site. In addition to active-source applications, ADM, Silixa, Lawrence Berkeley National Laboratory, and the United States

Geological Survey are incorporating DAS as part of a seismic network for locating induced microseismicity. Fiber-optic DAS cable may be emplaced in VW#1 or BEST#1 and 3 mi (5 km) may be laid horizontally on the surface above and parallel to the horizontal extraction well. On a monthly basis, time-lapse, seismic surveys may be conducted to monitor plume movement. The data can be used to image changes in seismic velocity associated with plume movement using active-source tomography (Lancelle et al., 2015). Two advantages of DAS for time-lapse seismic imaging are (1) fiber-optic cable is installed once for use in repeat surveys and (2) it can cover the entire length of a vertical well with a spatial resolution on the order of 33 ft (10 m). Two limitations of DAS are that (1) it is sensitive only to axial strain and (2) it has a lower signal-to-noise ratio (SNR) than traditional geophones. Usually sufficient signal strength is obtained to capture good first arrivals for active-source tomography. Signal stacking can also be used to increase the signal-to-noise ratio. Continuous recording also holds the potential for Ambient Noise Tomography (ANT) by using a combination of the surface DAS array and sensors in a vertical well and/or horizontal well. Noise Correlation Functions (NCF) are obtained by cross correlating the time series for pairs of DAS channels to image the intervening volume as if each channel at depth were a source and each channel at the surface were a receiver, or vice versa (Zeng et al., 2015). In addition to periodic active-source seismic surveys, the DAS cable can incorporate additional fibers into a single cable for temperature and/or fluid pressure monitoring (Becker et al., 2016).

Pressure and Temperature Methods

Dedicated downhole instrumentation for measuring pressure and temperature is strongly recommended. These parameters can be diagnostic of reservoir mechanical integrity, possible leakage from the reservoir or from a well, and of the physical properties of the injected CO_2. An inventory of available equipment (location, type of devices, and specifications) are listed in Table 5-2-1. Downhole pressure and temperature gauges are used to monitor formation pressure and temperature on a continuous basis. Some of these gauges use a sapphire sensor that can monitor pressure from atmospheric to 10,000 psi (68,950 kPa) and temperature from 77 to 212°F (25 to 100°C) at an accuracy of <±3 psi (20 kPa) and ± 33°F (0.5°C) and a resolution of 0.02 psi (0.14 kPa) and ± 32.01°F (0.004°C). Also, CCS#1 is equipped with downhole temperature sensors (DTS) for continuous temperature measurement from the ground surface to 6,300 ft (1,920 m).

Microseismicity Methods

An overview of microseismicity related to geologic carbon sequestration is provided by Pawar et al. (2015), while induced seismicity is described by Vilarrasa and Carrera (2015). Microseismic monitoring at the IBDP consists of two geophone arrays—the permanent geophone array in GM#1 and three WellWatcher PS3 passive seismic sensing levels in CCS#1 (Couëslan et al., 2014). The geophones in GM#1 are set at depths of 2,047 to 3,095 ft (623.9 to 943.4 m). The geophones in CCS#1 are set at 4,926, 5,743, and 6,137 ft (1,501, 1,750, and 1,871 m). As noted above, DAS may be employed as part of a seismic network for locating induced microseismicity at the IBDP.

In addition, the United States Geological Survey installed a seismic network around the IBDP using nine surface stations and three borehole stations and began monitoring in July 2013 (Kaven et al., 2014). The authors noted that their data indicates that the microseismic events occur in the Mt. Simon Sandstone and the Precambrian, not in the Eau Claire Formation (caprock).

Subtask 5-2 BEST permit preparation

A number of permits will be required for this project. The overall project requires a National Environmental Policy Act (NEPA) permit because federal funds will be used to complete

this work. Brine extraction and monitoring wells require permits before drilling. Brine injection wells also require permits as described below.

National Environmental Policy Act

The NEPA requires that all executive federal agencies prepare environmental assessments (EAs) and environmental impact statements (EISs) and all DOE-funded research projects are subject to this law. The Environmental Questionnaire (EQ) is required with the BEST Phase II application. The EQ is the first step in completing a NEPA application. The NEPA application could draw upon previous NEPA applications submitted for other DOE-funded projects, IBDP, and IL-ICCS.

Permitting for the Brine Extraction and Monitoring Wells

The brine extraction and associated monitoring well will require a permit from the Macon County Health Department, Environmental Health Division, as it manages permitting for the Illinois Department of Public Health. The application is two pages and costs $250 per well. These wells will not require a permit from the Illinois Department of Natural Resources (IDNR), Office of Oil and Gas Resource Management, based on discussions with Mr. Doug Shutt, permitting official with IDNR. Given the proximity of these proposed wells to the two Class VI injection wells, ADM will contact the United States Environmental Protection Agency (USEPA), Region 5, to determine permitting requirements under the UIC Class VI regulations.

In Illinois, high-capacity water wells need to be registered with the county soil and water conservation district (district) according to the Water Use Act of 1983 (525 Illinois Compiled Statutes 45/). A "high-capacity" well is defined as any well capable of pumping more than 100,000 gal/d (378,541 L/d; approximately 70 gal/min [265 L/min] or 2,380 bbl/d [378.4 m^3]). Anyone proposing the installation of a high-capacity well is required to notify the District before well construction and then participate in water-use reporting (Illinois Water Inventory Program) after the well is completed.

Permitting for a Brine Injection Well

A brine injection well may be needed for disposal of excess Mt. Simon brine. The Potosi Dolomite may be a suitable injection zone, as it has been a zone of lost circulation for several wells in Macon County. In addition, the Potosi Dolomite is used for injection wells in nearby Tuscola (Brower et al., 1989). This type of well is likely to be permitted as a UIC Class I well regulated by the Illinois Environmental Protection Agency (IEPA) under a primacy agreement with the USEPA. Given the proximity of this injection well to two Class VI injection wells, permitting this new well may require consultation with IEPA and USEPA Region 5 to determine which agency would handle permitting.

5-1 and 5-2 Summary

Subsurface monitoring at geologic carbon sequestration sites involves monitoring pressure, temperature, CO_2 saturation, and microseismicity. Monitoring pressure and temperature in the subsurface has some minor challenges but overall is a straightforward procedure. Monitoring CO_2 saturation is a more challenging and expensive process than monitoring pressure and temperature. Borehole methods, such as pulsed-neutron logs, can be very effective locating the injected CO_2, but offer data for a very small portion of the injection reservoir.

Areal methods such as 3D seismic and VSP can provide 2D and 3D maps of the injected CO_2. New methods such as DAS are being developed and provide promise. Borne out of the more publicized risk of induced seismicity (Pawar et al., 2015), monitoring microseismicity is a relatively new effort and is an emerging technology with many more challenges.

Table 5-2-1 Inventory of pressure and temperature sensors at the IBDP and Illinois Industrial Carbon Capture and Storage (IL-ICCS) sites.

Well	Location, ft (m)	Notes
IBDP CCS#1		
Wellhead P/T - Tubing	Wellhead	ADM Supplied
Wellhead P/T - Annulus	Wellhead	ADM Supplied
Downhole P/T	6,325 (1,928)	Schlumberger Sapphire Gauge (NDPG-CA, P/N 500897)
IBDP VW#1		
Wellhead P/T - Tubing	Wellhead	ADM Supplied
Wellhead P/T - Annulus	Wellhead	ADM Supplied
Westbay Eight downhole MOSDAX P/T MOSDAX probes	Zone 2 - 6,982.0 (2,128.1) Zone 4 - 6,837.8 (2,084.1) Zone 6 - 6,632.2 (2,021.5) Zone 7 - 6,416.1 (1,955.6) Zone 9 - 5,653.8 (1,723.3) Zone 10 - 5,000.6 (1,524.2) Zone 11 - 4,917.5 (1,498.9) Tubing - 4,849.2 (1,478.0)	1. Transducer Sensor: silicon strain gauge with electronic module for bi-directional communication of data and commands between the control circuitry and the surface control devices. The modules are individually addressable for “daisy-chain” operation of multiple MOSDAX probes on a single cable 2. On-Board digital converter: approximately 15-bit 3. Full Scale pressure range: 5,000 psia (34,475 kPa) 4. Specified accuracy: +/- 0.1% FS (+/- 5 psia [34 kPa]) 5. As-Calibrated accuracy (typical) +/- 0.025% FS (+/- 1.3 psia [9 kPa]) 6. Resolution (typical): 0.5 psia (3.4 kPa)
IBDP GM#1		
None	N/A	No pressure gauges installed in GM#1
IL-ICCS CCS#2		
Wellhead - Tubing	Wellhead	ADM Supplied
Wellhead - Annulus	Wellhead	ADM Supplied
Downhole P/T - Tubing	6,325 (1,928)	SLB Completions gauges/Quartz T-Gauge XPQG-16
Downhole P/T - Annulus	6,325 (1,928)	SLB Completions gauges/Quartz T-Gauge XPQG-16
IL-ICCS VW#2		
Wellhead - Tubing	Wellhead	ADM Supplied
Wellhead - Annulus	Wellhead	ADM Supplied
Five Intellizone Zones	Zone 1 - 7,041 (2,146) Zone 2 - 6,681 (2,036) Zone 3 - 6,524 (1,989) Zone 4 - 5,848 (1,782) Zone 5 - 5,027 (1,532)	SLB Completions gauges/Quartz Gauges XPQG-10
Dual Tubing/Annulus Gauge	4,901 (1,494)	SLB Completions gauges/Quartz T-Gauge XPQG-16
IL-ICCS GM#2		
Wellhead gauge - Annulus	Wellhead	ADM Supplied
Downhole P/T	3,399 (1,036)	GRC downhole gauge connected at bottom of Sercel string/QPG-820

Permitting requires interaction with county, state, and federal regulatory agencies. In Illinois, county government regulates water production wells and high-capacity wells. Underground injection wells for nonhazardous waste are classified as Class I wells and are regulated by the Illinois Environmental Protection Agency. Because of the existing Class VI permits at the proposed research site, the US Environmental Protection Agency will be consulted for any impact of this research project on those permits. Finally, any federally funded project is required to comply with NEPA.

5-1 and 5-2 References

Becker, M.W., M. Cole, C. Ciervo, T. Coleman, and M. Mondanos, 2016, Measuring hydraulic connection in fractured bedrock with periodic hydraulic tests and distributed acoustic sensing, Proceedings, 41st Workshop on Geothermal Reservoir Engineering, Stanford University, Stanford, California, February 22–24, 2016, SGP-TR-209.

Brower, R.D., A.P. Visocky, I.G. Krapac, B.R. Hensel, G.R. Peyton, J.S. Nealon, and M. Guthrie, 1989, Evaluation of underground injection of industrial waste in Illinois, Illinois Scientific Surveys Joint Report 2, 89 p.

CO2QUALSTORE, 2010, Guideline for selection and qualification of sites and projects for geological storage of CO_2, DNV Report No.2009-1425.

Couëslan, M.L., V. Smith, G. El-Kaseeh, J. Gilbert, N. Preece, L. Zhang, and J. Gulati, 2014, Development and implementation of a seismic characterization and CO_2 monitoring program for the Illinois Basin – Decatur Project: Greenhouse Gases: Science and Technology, v. 4, no. 5, p. 626–644.

Daley T.M., B.M., Freifield, J. Ajo-Franklin, S. Dou, R. Pevzner, V. Shulakova V., 2013, Field testing of fibre-optic distributed acoustic sensing (DAS) for subsurface seismic monitoring: The Leading Edge, v. 32, no. 6, p. 699–706.

Daley, T.M., D.E. Miller, K. Dodds, P. Cook, and B.M. Freifeld, 2015, Field testing of modular borehole monitoring with simultaneous distributed acoustic sensing and geophone vertical seismic profiles: Geophysical Prospecting, p. 1–17, doi: 10.1111/1365-2478.12324.

Finley, R.J., 2014. An overview of the Illinois Basin – Decatur Project: Greenhouse Gases: Science and Technology, v. 4, no. 5, p. 571–579.

Jenkins, C., A. Chadwick, and S.D. Hovorka, 2015, The state of the art in monitoring and verification - Ten years on: International Journal of Greenhouse Gas Control, v. 40, p. 312–349.

Kaven, J.O., S.H. Hickman, A.F. McGarr, S. Walter and W.L. Ellsworth, 2014, Seismic monitoring at the Decatur, IL, CO_2 sequestration demonstration site: Energy Procedia, v. 63, p. 4,264–4,272.

Lancelle, C., D. Fratta, N. Lord, H.F. Wang, and A. Chalari, 2015, Active travel-time tomography using a distributed acoustic sensing array: Paper No. NS41B-1933, Fall AGU Meeting, Dec. 14–18, https://agu.confex.com/agu/fm15/meetingapp.cgi/Paper/75676.

National Technology Energy Laboratory (NELT), 2012, Best practices for monitoring, verification, and accounting of CO_2 stored in deep geologic formations, second edition: The Energy Lab, National Energy Technology Laboratory, DOE/NETL-2012/1568.

Pawar, R.J., G.S. Bromhal, J.W. Carey, W. Foxall, A. Korre, P.S. Ringrose, O. Tucker, M.N. Watson, and J.A. White, 2015, Recent advances in risk assessment and risk management of geologic CO_2 storage: International Journal of Greenhouse Gas Control, v. 40, p. 292–311.

Rose, D., T. Zhou, S. Beekman, T. Quinlan, M. Delgadillo, G. Gonzalez, S. Fricke, J. Thornton, D. Clinton, F. Gicquel, I. Shestakova, K. Stephenson, C. Stoller, O. Philip, J.M. La Rotta Marin, S. Mainier, B. Perchonok, and J.-P. Bailly, 2015, An innovative slim pulsed neutron logging tool: Society of Petrophysicists and Well-Log Analysts 56th Annual Logging Symposium, Long Beach, California, USA, July 18–22.

Vilarrasa, V., and J. Carrera, 2015, Geologic carbon storage is unlikely to trigger large earthquakes and reactivate faults through which CO_2 could leak: Proceedings of the National Academy of Sciences, v. 112, no. 19, p. 5,938–5,943.

Worth, K., D. White, R. Chalaturnyk, J. Sorensen, C. Hawkes, B. Rostron, J. Johnson, and A. Young, 2014, Aquistore project measurement, monitoring, and verification: From concept to CO_2 injection: Energy Procedia 63, p. 3,202–3,208.

World Resources Institute (WRI), 2008, CCS guidelines: Guidelines for carbon dioxide capture, transport, and storage: Washington, DC: WRI, 144 p.

Zeng, X., C. Lancelle, C. Thurber, D. Fratta, H.F. Wang, A. Chalari, and A. Clarke, 2015, Properties of noise correlation functions obtained from a distributed acoustic sensing (DAS) Array at Garner Valley, California: Paper No. NS41B-2720, Fall AGU Meeting, Dec. 14–18, https://agu.confex.com/agu/fm15/meetingapp.cgi/Paper/74541.

TASK 6-0 BEST DESIGN AND IMPLEMENTATION PLAN (PHASE II)

The purpose of this task is to select field pilot infrastructure options and develop plans to demonstrate that brine extraction can manage pressure and control the CO_2 plume in the injection zone, and that this brine can be handled and treated for industrial use or safe and responsible disposal. The implementation plan must have flexibility for "real time" adjustments due to unforeseen challenges that are typically encountered during the deployment stage of all field demonstration projects.

The primary challenges identified for brine extraction at Decatur are as follows:

- drilling a brine extraction well that does not penetrate the CCS#1 and CCS#2 CO_2 plumes;
- extracting brine **without** extracting CO_2;
- timing the duration (start to end) of the brine extraction period with the CCS#2 CO_2 injection so that adequate CCS#2 plume is in situ to make a reliable brine extraction pressure and saturation baseline;
- measuring a definitive change in CO_2 saturation directly attributable to brine extraction;
- measuring a definitive change in pressure directly attributable to brine extraction;
- limiting number of caprock (Eau Claire) penetrations at the CO_2 storage site;
- handling and disposal of large volumes of brine.

Although these challenges are written specific to Decatur, every CO_2 storage site considering the use of brine extraction integrated with CO_2 storage will have similar technical and logistical challenges. Because the proposed BEST II site is at a site with CO_2 currently stored and additional CO_2 injection planned, every one of these challenges will be addressed, and will be part of the "lessons learned" documentation. Brine extraction and brine injection without CO_2 injection, in some cases, may not address any of these challenges and at most would address up to three of them.

Subtask 6-1 Scenarios

Based on the results of Tasks 2 through 5, several ideas were tested, simulated, and analyzed for effectiveness in extracting brine to positively impact CO_2 storage. To down-select and combine these ideas into a few brine extraction options, the following criteria were considered:

- magnitude of the change of formation pressure and movement of the CO_2 plume;
- measurement and quantification (at a field demonstration) of the pressure reduction and movement of CO_2 (change in saturation);
- control of costs within project budget and avoiding project delays;
- minimization of projected project risk; and
- requirement of straight-forward regulatory considerations (no unusual, atypical requests in the permit application).

The general design elements of BEST II project are

- brine extraction,
- brine handling and disposal,
- brine treatment,
- pressure monitoring, and
- saturation monitoring.

For brine extraction, the design elements are well location, well type, well orientation, perforated interval, and volumetric brine extraction rate. *The design goal* is to extract brine at a location in the injection zone (distance from CO_2 plume, CO_2 injection well, and depth-interval)

that minimizes the volume of brine extraction required (cumulative and daily rate) to cause a field-measureable pressure and saturation change at the current wells' gauge locations. Pressure and saturation measurements will be made before extraction to define a pressure trend for comparison to the period of brine extraction. The static CCS#1 plume and dynamic CCS#2 plumes were studied.

During the initial considerations for designing this pilot project, a vertical well was modeled to control the CCS#2 plume that was expected to begin in early 2016. Frailey et al. (2011) showed that brine extraction rates of similar volumetric magnitude to CO_2 injection rates were required to affect the distribution of CO_2. Furthermore, they found that the brine extraction well had to be relatively close to the CO_2 injection well (i.e., 0.5 mi [0.8 km]) in order to have an effect. Using brine extraction rates four-times greater than the CO_2 injection rate for brine extraction wells 1 mi (1.6 km) from the CO_2 injection well had no noticeable effect on the CO_2 plume distribution. (The modeling results in the Task 4 section of this report are in agreement with this earlier work.)

For impacting the expected CO_2 plume distribution at CCS#2, this meant a rate of about 20,000 bbl/d (3,180 m^3/d) was required from a brine extraction well located about 0.5 mi (0.8 km) from CCS#2. Based on existing infrastructure and accessibility to surface locations, a vertical brine extraction well location was limited to a southeast direction from CCS #2. Unfortunately, there were no existing monitoring wells in this general area, so the vertical brine extraction well option would require a new vertical monitoring well. An additional, very important consideration for this well location is the relative proximity to the CCS#1 plume, which, to date for this possible well location, can only be approximated via numerical flow modeling and surface seismic surveys. Presently, surface seismic interpretations of the plume extent are limited and have relatively low confidence. Also, reliability of a numerical model to project CO_2 distribution within +/–500 ft (+/–152 m) in any direction to drill a brine extraction well that would avoid the CCS#1 plume with confidence was very low.

Consequently, a new approach to the project design involving the CCS#1 plume was undertaken. From a research perspective, to design a brine extraction well to displace CO_2 and reduce pressure, measureable data must be collected that clearly indicates that brine extraction caused the observed outcome. In other words, it is necessary to know with certainty where the CO_2 will be and what the pressure *would have been if brine extraction had not occurred*. An established baseline is an absolute necessity to this project. A static plume is relatively well established in terms of CO_2 distribution and pressure, while a dynamic plume will have a three-dimensional (3D) pressure gradient that varies in space based on geologic heterogeneity and a moving CO_2 plume. Clearly, the induced movement of a static plume will be much more definitive than incremental movement of a dynamic plume.

The placement of a horizontal brine extraction well near a static plume has the same proximity issues that a vertical well placed near a dynamic plume with regards to the reliability of modeling and resolution of surface seismic. In comparison, the use of cased-hole logs to monitor CO_2 is much more reliable. The most recent cased-hole log (November/December 2014) indicated that CO_2 was present at depths of 6,750 and 6,921 ft (2,057 and 2,110 m) in CCS#1 and VW#1, respectively. To avoid the issue with placement of a vertical well, the design plan considered the use of a horizontal well placed above the CO_2 plume near two existing wells (CCS#1 and VW#1). The modeled horizontal well was placed at 6,400 ft (1,951 m), above the known depth of the plume and geologically near the boundary between the Middle and Lower Mt. Simon. Cross-well tomography between CCS#1 and VW#1 will provide much higher resolution of CO_2 plume distribution compared to surface seismic. (The cross-well seismic survey can be run before drilling

the horizontal brine extraction well to determine whether CO_2 is at shallower depths than noted in the cased-hole logs.) Because of the proximity of this horizontal well to CCS#1 and VW #1, no additional monitoring well (or Eau Claire penetration) is required.

The cost of a horizontal well at this depth is about 10–20% higher than a vertical well. However, if the cost of the vertical monitoring well that would be required for the vertical brine extraction well is included, the single horizontal well options is less expensive by 30–40% compared to the two-well option.

The horizontal well option has less risk in all of the design criteria. The brine extraction well will be oriented in the south-south east direction, extending 1,000 ft (304.8 m) from VW#1 and CCS#1 wells. In the remainder of Phase I and early Phase II, additional data will be available, including

- commencement of CCS#2 injection;
- reprocessing and interpretation of existing 3D surface and vertical seismic profile (VSP) seismic data;
- later cased hole logs at CCS#1 and VW#1;
- cross-well tomography; and
- updated well construction costs.

It is anticipated that this additional information will make the choice of well options clear. Table 6-1-1 summarizes the comparison between orientations for the brine extraction well.

Table 6-1-1 Comparison of vertical and horizontal brine extraction wells.

	Vertical Well	Horizontal Well
Extraction rates	10,000–30,000 bbl/d (1,590–4,770 m^3/d)	3,000–8,000 bbl/d (477–1,272 m^3/d)
Monitoring well required	Yes	No
Resolution of monitoring technique	Low (surface seismic)	High (cross well)
Risk of drilling CO_2 plume	Moderate to high	Very low to moderately low
Risk of producing CO_2	Moderate to high	Low to moderate
Certainty to measure pressure	Very low to moderate	Moderately high to very high
Certainty to measure CO_2	Very low to moderately low	Moderately high to very high
Timing with other ICCS	Necessary	Not required
Proximity to Archer Daniels Midland	Moderately close	Very close
Well construction expense	High to very high (with monitoring well)	High
Brine handling expense	High	Low to moderate

For brine handling and disposal, the design elements are volumetric brine rate, metering, temporary brine storage, surface distribution (manifolds, valves, and piping), and disposal (well, industrial/oilfield usage, and municipal). *The design goal* is to lift, meter, and characterize the brine from the extraction well at low unit cost (e.g., $/bbl) using readily available and tested pumping equipment, and transfer of the brine from the extraction well to the disposal well/facility while providing a relatively small slipstream and batch volume of brine for use in the brine treatment technologies on location (i.e., near the extraction well) and in the nearby laboratory facility (Richland Community College, National Sequestration Education Center [NSEC]).

Given the daily rates of extraction, potential for corrosion via high total dissolved solids (TDS) brine, brine extraction period up to 2 years, and budget, the only pumping option considered

was an electrical submersible pump commonly used in high-rate liquid wells in the oil and gas industry. These types of pumps are known for flexibility to pump moderate to very high liquid flow rates; the pumps' longevity ratings allow continuous usage for over 2 years without maintenance or a failure. The pressure at which the brine is extracted is anticipated to be adequately high to transfer the brine to the disposal well/facility without additional pressure (e.g., via a transfer pump).

At the surface, the extracted brine volume will be metered and periodically (i.e., weekly or bi-weekly) sampled for composition. A manifold will be built that allows up to two slipstreams provided simultaneously to pilot-scale brine technology treatments that will be set up on location near the extraction well. The extracted brine will likely be stored in 1,000 gal (3,785 L) tanks at atmospheric pressure. These tanks would be set in temporary surface reservoirs so that a brine spill would be completely contained.

The batch brine will be delivered periodically (e.g., weekly) via tank truck to the laboratory and stored locally in a 1,000 gal (3,785 L) storage tank with protective reservoir. A similar tank will be setup for temporary storage of treated brine and by-products.

The brine disposal option was decided to be one of three options: (1) UIC disposal well, (2) brine treatment and industrial use, and (3) brine pretreatment and discharge into municipal wastewater system. The primary design elements are budget and permitting requirements. The disposal well will likely be a vertical well drilled and completed into the Potosi. For the range of extraction rates anticipated, the cost of this well is relatively constant for various extraction scenarios. The cost of brine treatment is highly dependent on the extraction rate. If relatively high rates are required, the vertical disposal well option is more likely; for relatively lower rates, the two brine treatment options may be lower costs. Both brine disposal options using brine treatment will require removal of suspended solids for the entire extracted volume.

A small oilfield is within 6 mi (10 km) of the ADM facility. The operator was contacted for interest in using extracted brine in an oil reservoir waterflood operations. Unfortunately, the reservoir has relatively low flow properties, and 40–50 brine injection wells would be required, each requiring a UIC Class II permit. In addition to brine delivery logistics and costs, permitting, drilling, completing, or a combination of these for this number of wells was not a feasible option in a 4-year demonstration project.

A conceptual design and cost estimation for brine extraction, transportation, and handling (e.g., disposal) are detailed in Appendix 6-A. The conceptual design and cost estimation for development of the two test-bed types are in Appendix 6-B.

For brine treatment, the design elements are types of test-beds (continuous and batch), technology readiness (bench and pilot), pretreatment (suspended solids), and by-products (concentrated brine, salt solids, and sludge). *The design goal* is to provide infrastructure, space, brine, and by-product disposal for simultaneous testing up to two pilot-scale (~5 gpm [~19 L/m]) and several smaller bench-scale (<1 gpm [<4 L/m]) brine treatment technologies.

All brine treatment technologies that are being considered require pretreatment to remove suspended solids. This will require a low volume facility to separate solids for the brine treatment. A standard filtration system, which is readily available using proven technology will be part of the brine treatment design. Because of the technology readiness of each brine technology considered, both pilot (slipstream) and bench scales (batch) will be provided.

The partially treated brine (low TDS) and brine-treatment by-products (e.g., concentrated brine) would have similar on-site storage and containment (like the extracted brine) until they were disposed. Depending on the volume of by-product, local companies permitted to transfer and

dispose of these materials using standard and regulatory approved methods are available. If the brine disposal well option is used, then the by-product may be blended back into the main brine stream for on-site disposal.

Based on the evaluation and screening of brine treatment technologies performed in Task 2, pilot-scale testing of the multi-effect evaporation (MEE) system is recommended. A conceptual design and cost estimation for development of this technology for pilot-scale testing at the test-bed facility is presented in Appendix 6-C.

For pressure monitoring, the design elements are current wells (*x-y* location and depth), new wells, (*x-y* location and depth), proximity to the CO_2 plume, proximity to CO_2 injection, and brine extraction wells. *The design goal* is to measure pressure at existing wells' gauge depths by strategically locating the brine extraction well in proximity to the existing wells' gauges to ensure the pressure change is quantifiable and attributable to brine extraction.

Because brine is relatively incompressible, a pressure change due to brine extraction is expected to be measured. However, the magnitude of this change that is detectable from the baseline is the challenge and will be an even greater challenge in the case of a dynamic plume. Also, in the presence of CO_2, which has relatively high compressibility compared to brine, the pressure change will be dampened compared to that in the presence of brine only. A monitoring well closer to the brine extraction well will have a larger pressure change, but too close will have poor spatial representation of the pressure measurement. Placement of a monitoring well too far from the brine extraction well will have reduced or no pressure change measurement. To increase the ability to attribute a pressure response to brine extraction, a varied rate brine extraction schedule will be made so that a unique pressure pulse will be initiated from the brine extraction well. The detection of the unique pressure pulse at the monitoring well will confirm the pressure change is a consequence of brine extraction.

The use of the brine extraction well and an active CO_2 injection well will likely not provide pressure data that can be used to infer a pressure change in the CO_2 reservoir. This is primarily as a result of the fluctuations in pumps and compressors and back pressure created by surface pressure and temperature. In other words, the data will likely be too "noisy" and not offer a general trend that could be compared to the pre-brine extraction baseline. However, when these wells are shut-in for planned pressure transient testing or routine maintenance, a smooth and exponential pressure decrease will be recorded that can be analyzed for average formation pressure, which might be meaningful to understand longer term (e.g., annually) changes to pressure.

For CO_2 saturation monitoring, the design elements are surface seismic, vertical seismic profile, cross-well tomography, distributed acoustic sensing (DAS), distributed temperature sensing (DTS), and cased-hole logs (e.g., pulsed-neutron log). For those methods requiring wellbores or previously acquired baseline data, wellbore location and construction, surface considerations (e.g., buildings and lakes), and areal coverage of previous CO_2 saturation monitoring surveys were reviewed. *The design goal* is to measure saturation at existing wellbores and seismic surveys by strategically locating the brine extraction well in proximity to the existing wells to ensure the saturation change is quantifiable and attributable to brine extraction.

Cased-hole logs are the most direct monitoring method that indicate the presence of CO_2; however, this is limited to CO_2 that is very near the wellbore. CCS#1 and VW#1 have previously run cased-hole logs indicating the presence of CO_2. For the horizontal well option, increases in saturation at this depth or further up the wellbore within the Mt. Simon would be a relatively direct indication that CO_2 movement was induced by brine extraction. The high-resolution, cross-well tomography between two wells about 1,000 ft (300 m) apart would be definitive compared to

surface seismic, which would be nearly 14,000 ft (4,300 m) the distance between the surface energy source to the CO_2 plume and back to the surface detector, i.e., twice the depth of the plume.

The ability for surface seismic to detect lateral plume movements of less than 1,000 ft (300 m) is highly unlikely. The vertical brine extraction well placement must be about 0.5 mi (0.8 km); therefore, the maximum plume movement is limited.

Distributed temperature sensing in CCS#1 gave very high resolution changes to temperature, but CO_2 was not present around CCS#1 at the depth of the DTS, so a site-specific example is not possible. Likewise, DTS in the brine extraction well is likely going to be well above the CO_2 plume. (At this time, DTS is included because it is expected to be a requirement of the permit modification for the CO_2 storage permits.) Distributed acoustic sensing (DAS) may be deployed in VW#1, if the timing can be aligned with current plans to pull and replace the tubing in this well. DAS has the potential to be a relatively low-cost alternative to surface seismic surveys to monitor pressure; similar to the saturation represented by cased-hole logs, DAS is limited to the volume of reservoir represented by a single well, but would provide continuous measurement.

6-1 References

Frailey, S.M., and R.J. Finley, 2010, CO_2 plume management in saline reservoir sequestration: Energy Procedia, v. 4, p. 4,238–4,245. http://dx.doi.org/doi:10.1016/j.egypro.2011.02.372.

Subtask 6-2 Design

The current BEST Phase II design is an outcome of an iterative process that included the following:

- project requirements,
- technical specifications and requirements,
- safety,
- regulatory mandates,
- operational restrictions, and
- project management constraints (budgetary and timeline).

Presently, a horizontal brine extraction well between CCS#1 and VW#1 with a Potosi brine disposal well is the favored choice to meet all BEST objectives with the given budget and timeline. Two brine delivery options (i.e., test-bed types) will be provided for pilot and bench scale: slipstream and batch. The electrical submersible pump will have downhole pressure (and temperature) gauges; otherwise, no new pressure gauges will be required. Placing the horizontal well near two existing wells requires no additional monitoring wells. Previously run and analyzed cased-hole logs will provide the basis for the static CO_2 plume position. About halfway through the brine extraction period (0.5 to 1 years), cased-hole logs will be run to assess any CO_2 movement; cross-well tomography between two relatively close wells will further ensure that the most effective saturation monitoring technologies are deployed in relatively optimal placement and timing to quantify brine extraction effect on CO_2 storage.

To finalize the design, a rigorous review of each major component of the project will be completed by teams of engineers, technicians, and geoscientists as needed. The major components are well construction; surface site infrastructure; brine extraction, handling, and disposal; brine treatment; and pressure and CO_2 monitoring. The details of each major component will be finalized using a process hazard analysis to identify all critical components of the system and to determine if changes should be made to further ensure safe operations and longevity over the life of the project.

The final design will be complementary and synergistic to other projects at the site. This includes planned seismic surveys, well work, cased-hole logs, CO_2 injection schedules, and batch brine sampling events. Additionally, the options chosen will be projected to have the least impact on the permitting process so that minimal to no delays in the permit process occur.

Subtask 6-3 Implementation plan

To determine the existing wells and equipment that can be used in a BEST II pilot, an inventory and evaluation of existing infrastructure at the Decatur sites was completed. Following the final design described in Subtask 6.2, the BEST Phase II implementation plan includes the following elements:

- Project management and planning (year 1)
- Procurement (year 1)
- Site preparation (year 1)
- Monitoring (years 1-4)
- Operation (year 2-3)

In year 1, **the project management and planning** will be completed; it includes (1) the schedule and timeline, (2) risk management plan, (3) monitoring plan, and (4) operation plan. The 4-year stipulated duration of the BEST Phase II demonstration project requires that the injection permit application process begin immediately because it will have the most uncertainty in timing and impact on well construction. The three plans (risk management, monitoring, and operation) will be finalized in the latter part of the first year before brine extraction but following the final BEST II design.

In year 1, the **procurement** process will be completed; this includes (1) manufacturer selection, (2) procurement, and (3) delivery. The final design of BEST II is a requirement to initiate the procurement process. The process hazard analyses of the major elements of the design will be performed. Vendors and service providers have been identified and elements of bid packages completed. The bid process will start early in year 1.

Also in year 1, the **site preparation** will be completed; it includes (1) permitting, (2) well construction, and (3) site construction. The permit application is equal in importance to the BEST final design. The permit process includes the NEPA and UIC injection permits. All staff will be focused on the permit application until it is completed and submitted to the respective regulatory agency. Well construction for the brine extraction well is expected to last 60–90 days. Because the site is relatively well characterized, limited tests and samples will be necessary for this well, which is expected to reduce the budget and maintain the schedule. The surface site construction will require simple surface access permits, which have been approved for previous projects at this site. Surface site construction (e.g., test-bed infrastructure) can start immediately in Phase II and be completed following the placement of the wellhead on the brine extraction and disposal wells.

Monitoring using currently installed and new equipment will occur across *all four years*, and includes (1) pressure, (2) saturation, (3) microseismicity, and (4) data management. Because pressure and microseismicity are passive, continuous measurements that are already in place, there are no demands on the implementation plan. Data management (i.e., transmission, storage, and archiving) is active at the site because of the previous projects. The current system has the flexibility for additional data streams; consequently, BEST II data acquisition will be integrated into the existing system. Saturation measurements will be at discrete and specific times that are aligned with the brine extraction schedule, CCS#2 CO_2 injection schedule, the IL-ICCS monitoring requirements, and BEST II regulatory requirements.

In years 2 and 3, brine extraction and handling **operations** will include (1) brine extraction and handling, (2) test-bed operations, (3) permit compliance, and (4) site closure. The continued use of this site provides field staff, operators, and service providers that are familiar with the site and previous operations. Archer Daniels Midland monitored CCS#1 injection and related activities and real-time plant operations, including all logistics and routine maintenance involving compressor facilities, pipeline delivery, and the injection wellhead. The same infrastructure and operation control room will be used to monitor and operate the brine extraction and handling processes. The anticipated timing of CCS#2 overlaps with the scheduled brine extraction; so the same control room and staff are able to operate the brine extraction process with little extra effort.

In summary, *year 1* is to complete the BEST II design, procure services and equipment for subsurface and surface infrastructure, complete the permitting process, and construct and prepare the site. *Years 2 and 3* are planned for brine extraction and the subsequent brine handling and brine treatment tests. (The actual duration of extraction will be based on the timing of the permit issuance and the rate of extraction required to cause measurable pressure and saturation changes, which will be determined in real time.) Monitoring will occur across *all 4 years*. (The early year 1 monitoring will be from current ongoing monitoring from previous projects.) *Year 4* is to complete the final monitoring surveys and close the site.

The **budget** was an essential part of the design and implementation plan. Maintenance and permitting requirements were assessed to estimate costs for using existing infrastructure. New equipment and drilling and completion costs needed for implementation of the BEST pilot were estimated. The cost and time needed to meet the requirement for obtaining drilling permits and/or renewal or reclassification of existing permits were completed. These cost estimates are based on budgetary quotes (labeled as "drafts" in Appendix 6-D) for recent similar projects and cost estimation tools.

The major components of the budget (Table 6-3-1) are the well construction, brine treatment, monitoring and personnel. The wells' construction will require 30-40% of the total project budget (including cost-share). Brine handling and treatment is expected to be 10-20% of the total budget. The monitoring budget is 20–30% of the total budget. Personnel expenses that include all field staff preparing the site, scientific staff (geoscientists and engineers), and project managers are projected to be 15–25% of the total budget.

Table 6-3-1 Summary budget for the horizontal brine extraction wells option.

BEST II	
Brine Extraction Well Construction	$7.53 M
Brine Injection Well Construction	$2.93 M
Monitoring	$7.44 M
Brine Handling & Treatment	$4.11 M
Staff*	$6.16 M
Total**	$28.2 M

*Operators, project management, engineering, and geoscience staff.

**This represents costs that a commercial (non-research) company might have for a similar project.

Appendix 6-A Description of the Brine Extraction, Storage, and Transportation System

The drawing "Brine Extraction Schematic v0.pfd" is a schematic of a proposed system to produce and transfer 7,570 L/min (2,000 gpm, or nominally 70,000 bpd) of brine. Brine is produced from the well by an electrical submersible pump (ESP), P-4001, routed to a surge tank, T-4010, and then pumped to the Brine Pre-Treatment Unit. After pre-treatment, a small stream (30 L/min, or 8 gpm, average feed rate) is trucked to the Pilot Test Bed Facility (at the National Sequestration Education Center). The bulk of the stream (nominally 7,570 L/min) is pumped to ADM for disposal after pre-treatment.

The electrical submersible pump is designed to pump brine from a specified depth below the surface. The pump and motor are submerged, and controlled from the surface. Due to the corrosive environment, 316L stainless steel is the main wetted material of construction of the pump. The pump design and cost estimate were based on the following assumptions for the well design and reservoir:

- 7,570 L/min (2,000 gpm) brine production rate
- Pump set 305 m (1,000 ft) below surface
- Diameter for the motor and pumping equipment is 330 mm (13.0 inch) and will require minimum 346 mm (13 – 5/8 inch) diameter casing
- 221 bar (3,200 psig) well static pressure at 2,149 m (7,050 ft) was assumed, with a productivity index (PI) = 100

The very high brine production rate requires a specialized, non-standard design. It may be necessary to set the pump further below the surface depending on reservoir and well characteristics, which will increase the pump horsepower requirement and associated capital and operating costs. The Brine Surge Tank provides a capacity for 10 minutes of storage of the brine; the Brine Transfer Pump delivers brine at a rate of 7,570 L/min (2,000 gpm) to the Brine Pre-Treatment Unit.

The only utility requirement of this process is electrical power. Approximately 880 kW of power will be consumed, mostly by the ESP. The capital cost was estimated for this brine extraction system, and is shown in "Brine Extraction Costs v1.pdf." In addition to the ESP, the capital cost estimate only includes surface equipment – a surge tank, brine transfer pumps, and a power transformer to provide the substantial power load. No costs are included for any subsurface items such as well drilling, casings, etc.

GE Oil & Gas provided the design and cost estimate for the 7,570 L/min ESP. They also provided similar information for a 2,214 L/min (585 gpm, or 20,000 bpd) unit; however, the design basis for the 2,214 L/min unit was different from that of the 7,570 L/min unit – the 2,214 L/min unit was assumed to be set 2,000 ft below the surface, rather than 1,000 ft below the surface. Based on the purchase of the necessary equipment for the brine extraction, the capital and operating costs for the 2,000 gpm case are given in Table 6-A-1. Additionally, the design and cost information generated for the 2,000 gpm case were used to estimate the costs of three other cases: 500, 585, and 5,000 gpm feed. The cost information for these alternate cases are also shown in Table 6-A-1. In addition, Figure 6-A-1 through Figure **6-A-3** show conceptual costs and a block diagram for a brine extraction, storage, and transportation scheme.

Table 6-A-1 Capital and Operating Costs for Brine Extraction at 2,000 gpm Feed Rate, and Extrapolation to 500, 585, and 5,000 gpm Feed Cases.

Case	Capital Cost	Annual Operating Cost (including capital amortization)	Cost for Recovered Water ($ / 1000 gal)
2,000 gpm Base Case	$1,533,000	$795,000	$0.78
500 gpm Case	$667,000	$263,000	$1.03
585 gpm Case	$733,000	$295,000	$0.99
5,000 gpm Case	$2,656,000	$1,802,000	$0.70

PROJECT: ISGS BEST **Brine Extraction, Storage and Transportation Scheme**
Brine Extraction SECTION 4000 2,000 gpm, 20 wt. % brine
TRIMERIC CORPORATION 2/29/2016 Version 1.
Early Phase Conceptual Capital Cost Estimate

#	Item	Equipment Name	Tag #	Quantity	Purchased Equipment Cost (total)	Installed Cost (total)	Electric Power (kW)	Design Information
1	Pump	Electronic Submersible Pump	P-4001	1	$ 314,500	$ 471,750	850	7,570 L/min (2,000 gpm) at 482 m (1,582 ft) head, Electronic Submersible Pump (ESP). 745 kW (1,000 hp) with VFD. 316LSS.
2	Tank	Brine Surge Tank	T-4010	1.0	$ 81,100	$ 169,600	0	3.75 m (12.3 ft) diam x 6.85 m (22.5 ft). Low pressure (API-type) storage tank. 75.7 m3 (20,000 gal). 316LSS.
3	Pump	Brine Transfer Pump	P-4010 A/B/C	3 x 50%	$ 56,400	$ 203,300	30	3,785 L/min (1,000 gpm), at 18.1 m (60 ft), centrifugal pump. 15 kW (20 hp) drive. 316LSS.
4	Power	Power Transformer and Panel		1		$ 90,600		1125 kVA transformer with panel.

Major Equpiment Cost (MEC)	$ 452,000		
Installation Cost (IC)	$ 483,250		
Installed Equipment Cost (IEC)		$ 935,250	
Tax (8% of MEC + 2.5% of IC)	$ 48,200		
Freight (1.6% of MEC)	$ 7,200		
Construction OH, Contractor Fees (30% of IC)	$ 145,000		
Subtotal		$ 1,135,650	
Engineering & Procurement (15% of Subtotal)	$ 170,300		
Contingency (20% of Subtotal)	$ 227,100		
Early Phase Capital Cost Estimate		**$1,533,000**	*1Q15 basis*

NOTE: This estimate excludes all well-related costs, and brine pretreatment.

Figure 6-A-1 Early phase conceptual capital cost estimate for a brine extraction, storage, and transportation scheme.

PROJECT: ISGS BEST **Brine Extraction, Storage and Transportation Scheme**

Brine Extraction SECTION 4000 2,000 gpm, 20 wt. % brine

TRIMERIC CORPORATION 2/29/2016 Version 1.

Early Phase Conceptual Operating Cost Estimate

Operating Cost Factor	Usage Rate	Unit Cost	Cost (rate)	
			$/h	k$/y
Electrical Power	880 kW	0.08 $/kW-h	70.4	600
Labor	0.5 FTE	100 K$/FTE/y	5.9	50
Maintenance + G&A		4.5 % CAPEX/y	8.1	69
SUBTOTAL OPERATING COST			84.4	719
Capital Amortization		5 % CAPEX/y	9.0	77
TOTAL OPERATING COST INCLUDING CAPITAL AMORTIZATION			**93.4**	**795**
TOTAL UNIT COST FOR WATER TREATMENT		**0.78 $ / 1000 gal**		

Assumptions:

Operating days/year	355	
Flowrate	2,000	gpm (20 wt. % brine)
Capital Amortization	20	year, straight-line, no interest
Maintenance & G&A	4.5	pct of CAPEX/year

Figure 6-A-2 Early phase conceptual operating cost estimate for a brine extraction, storage, and transportation scheme.

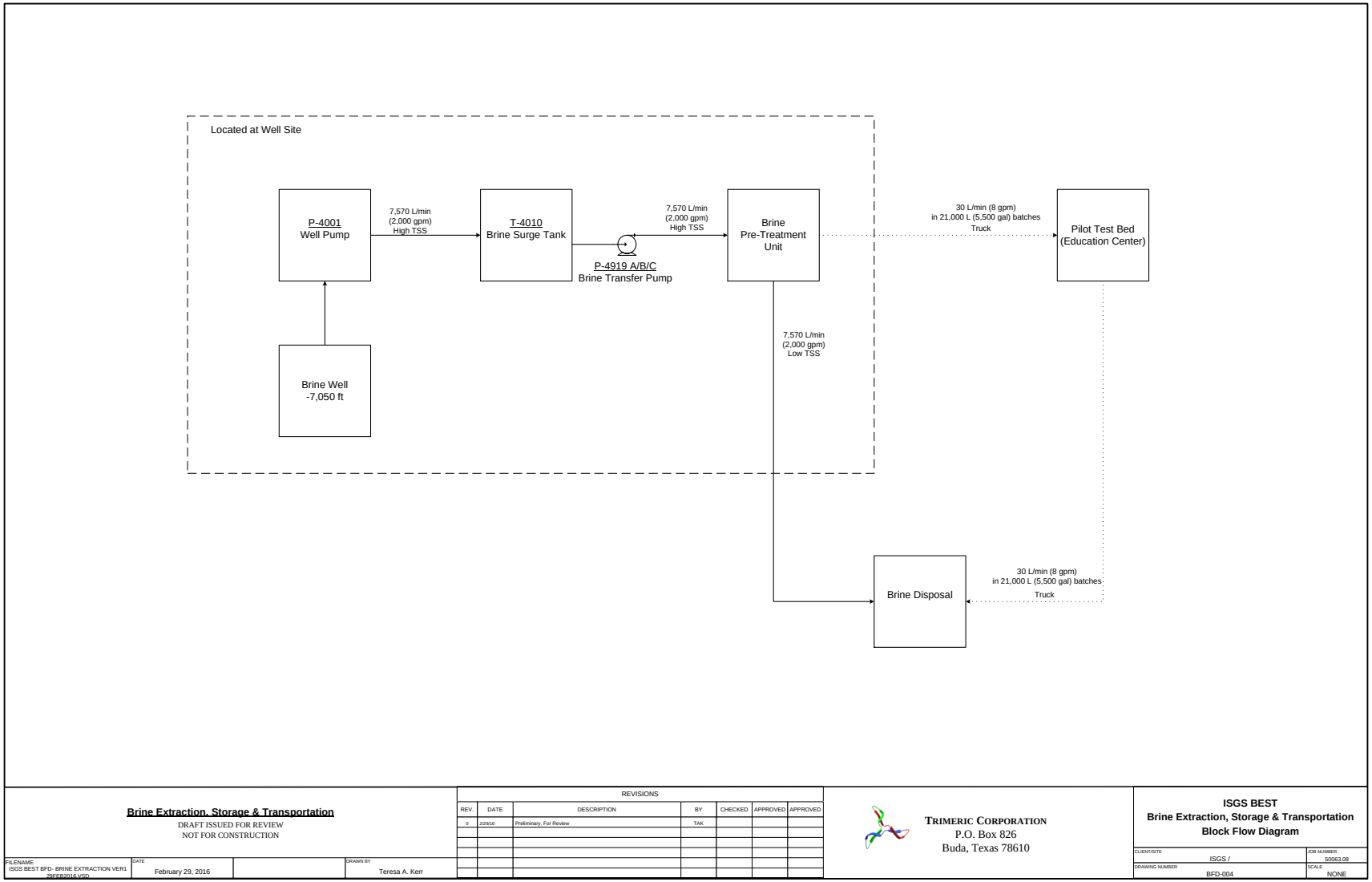

Figure 6-A-3 Block flow diagram for brine extraction, storage, and transportation.

Appendix 6-B Description of the ISGS BEST Pilot Plant Test Bed Facility: Options A and B

This is a revised version of the pilot plant test bed facility description; the original documentation was provided to ISGS on 24 February 2016. The ISGS had some concerns that the cost estimated for the originally-proposed systems was higher than desired. Based on those concerns, Trimeric decided to provide another option for the test bed wherein the pilot testing of significant size would be conducted at the ADM plant, instead of at the National Sequestration Education Center. This new version assumes that ISGS would have ready access to ADM's utilities, such as electrical power, steam, and instrument air, which could save a significant amount of capital cost, compared to conducting the tests at the Education Center.

In these documents, "Option A" refers to the original plan of conducting all of the pilot tests at the Education Center, and "Option B" refers to conducting the larger pilot tests at ADM while conducting smaller-scale tests (bench, mini-rig) tests at the Education Center. For Option B, it is assumed that a supply of pre-treated brine would be required at both testing locations; brine would still be provided by truck to the Education Center, but at ADM, the brine would instead be provided via pipe from the pre-treatment system.

Option A

The drawing "Pilot Test Bed v2 Option A Schematic.pdf" shows a schematic of the Option A pilot plant facility to be used for the testing of pilot-scale brine treatment technologies. ISGS's goal is to be able to run one or two brine treatment technologies concurrently, while having one two other spaces available for other technologies being installed or removed. The treatment technologies will be focused on recovering useful water from brine, and may result in precipitating and recovering solid salts. The brine treatment technologies are not part of this test bed facility design and cost estimate; they would be provided by other parties. The purpose of the test bed facility is to provide a location for the brine treatment tests to be carried out, provide the feed brine, handle disposition of the products, and provide utilities. The maximum capacity for any one of the brine treatment technologies is 5 gpm feed, with total brine handling at the test bed facility not exceeding an average of 8 gpm.

The Option A test bed facility is to be located at the National Sequestration Education Center at Richland Community College. It is assumed that some space (~2,000 ft^2) will be provided inside an existing lab building, and a similar or larger amount of space would be available outside for additional equipment.

Brine will be withdrawn from a well and treated for TSS reduction at another location and transported by tank truck to the test bed facility. The test bed facility will include a loading/unloading pump and three storage tanks; the three tanks could be used for feed brine, concentrated brine product, and recovered water. ISGS may wish to dispose of any solid salts produced in a brine treatment process by mixing them back into the recovered water; to facilitate such an operation, a mixing tank is also included in the design. Concentrated brine and recovered water would be transported off-site from the test bed facility by tank truck and disposed of at the ADM water treatment facility.

The utility requirements are estimated as follows:

- Electrical power – 530 kVA
- Nitrogen – from cylinder 6-pack
- Dry instrument/process air – 34 m^3/h (20 cfm) at 620 kPa (90 psi)
- Hot oil supply and return – nominally 400 °C (752 °F) supply, 290 kW electric heater
- Natural gas (assume existing supply is adequate)

- Potable water to be used for process water (assume existing supply is adequate)

A pipe header system would be provided to route the brine streams, water streams, and utilities to four process locations. Each of the process locations is assumed to require about 400 ft^2 (37 m^2). Two process locations would be located the inside the building and two would be located outside of the building on a new concrete pad.

The capital cost estimate given in the file "Pilot Test Bed v2 Option A Costs.pdf" must be considered to be early-phase and conceptual. The estimate includes the provision of the new process equipment (tanks, mixing tank, and pumps) and the provision of hot oil, electrical power, and compressed air. The new major equipment would be located on a new concrete pad outside of the building. The provision of the other utilities (natural gas, potable water, nitrogen) are considered to be inconsequential with respect to capital cost because natural gas and potable water are assumed to already available at the site of the test bed facility, and the provision of nitrogen (vendor-provided cylinders) does not represent a significant capital cost.

The cost for the complete system is estimated to be $1,400,000. The ISGS was also interested in potentially eliminating the mixing tank system from the design in order to save capital cost (which would result in having to dispose of solid salts in a different way); the cost of Option A without the mixing tank is also shown on the capital estimate document, and is estimated to be $1,300,000.

Figure 6- and 6-B-2 show the early phase conceptual capital cost estimate for the pilot plant test bed and a block flow diagram for pilot-scale support facility for Option A, respectively.

Option B

The drawing "Pilot Test Bed v2 Option B Schematic.pdf" shows a schematic of the Option B pilot plant facility to be used for the testing of pilot-scale brine treatment technologies. There are two locations at which tests would be run: at the Education Center, and at ADM (exact location at the plant is not known, but is assumed to be close to the ADM wastewater treatment area).

At the Education Center only small scale (< 1 gpm feed brine requirement) tests would be run, which might include bench and mini-rig scale work. The tests at the Education Center would use pretreated brine, which would be trucked to the site and stored in new storage tanks. Because the work is to be small scale, it is assumed that no significant changes in electrical power supply facilities at the Education Center would be required, and no central utilities (apart from utilities that are already available there, such as electrical power and water) need to be provided to the operators of the equipment being tested there. The only significant capital cost items to be required at the Education Center are two storage tanks (one for feed brine, and one for used brine that has been processed and is to be sent to the ADM water treatment facility), and pumps for feeding brine to users and for truck loading/unloading.

At the ADM pilot location, it is assumed that ISGS will be able to access major utilities, including electrical power, steam, process water, natural gas, and instrument air, from ADM without major cost (apart from some nominal costs for connection piping to the existing utility systems). The major costs of the ADM pilot location are primarily associated with providing concrete pads, piping headers, small holding tanks for the recovered water and concentrated brine, and pumps for sending the recovered water and concentrated brine to ADM's water treatment facility. The capital cost estimate given in the file "Pilot Test Bed v2 Option B Costs.pdf" must be considered to be early-phase and conceptual. The capital cost estimated for Option B is about $830,000.

Figures 6-B-3 and 6-B-4 show the early phase conceptual capital cost estimate for the pilot plant test bed and a block flow diagram for pilot-scale support facility for Option B, respectively.

PROJECT: ISGS BEST **Pilot Facility for Testing Brine Processing Technologies. Pilot Facilities at Education Center.**
Pilot Plant Test Bed, Option A. SECTION 9000
TRIMERIC CORPORATION 3/3/2016 Version 2.
Early Phase Conceptual Capital Cost Estimate

#	Item	Equipment Name	Tag #	Design Information	Purchased Equipment Cost	Installed Cost
1	Pump	Loading Pump	P-9100	316L SS. 6 L/s (96 gpm), 10 m (12 psi, 33 ft) head. 0.8 kW.	$ 5,600	$ 18,000
2	Tank	Pre-Treated Brine Feed Tank	T-9200	38 m3 (10,000 gal). 2.75 m (9 ft) diam x 6.4 m (21 ft). FRP.	$ 38,100	$ 88,700
3	Pump	Brine Feed Pump	P-9200	316L SS. 1 L/s (16 gpm), 42 m (50 psi, 139 ft) head. 1.1 kW.	$ 5,400	$ 19,900
4	Package	Hot Oil Package System	PKG-9300	400 C, 15 bar hot oil operating conditions (max). 290 kW.	$ 94,200	$ 152,300
5	Package	Air Compressor Package (Compressor, Bottle)	PKG-9700	34 m3/h (20 cfm) at 620 kPa (90 psi). 22 kW.	$ 42,800	$ 72,900
6	Package	Instrument Air Dryer	PKG-9700	35 m3/h (20 cfm) at 620 kPa (90 psi).	$ 10,800	$ 23,000
7	Tank	Concentrated Brine Tank	T-9400	19 m3 (500 gal). 2.5 m (8.2 ft) diam x 3.9 m (12.8 ft). 316L SS.	$ 40,800	$ 84,100
8	Tank	Recovered Water Tank	T-9500	38 m3 (10,000 gal). 2.75 m (9 ft) diam x 6.4 m (21 ft). FRP.	$ 38,100	$ 88,700
9	Mixing Tank	Mixing Tank	T-9501	316L SS. 250 gal (1 m3), 0.9 m (3 ft) diam x 1.75 m (5.75 ft). 4 kW.	$ 31,300	$ 95,300
10	Pump	Recovered Water Recirculation Pump	P-9500	316L SS. 2 L/s (32 gpm), 10 m (12 psi, 33 ft) head. 0.6 kW.	$ 5,200	$ 22,800
11	Power Supply	Power Transformer / Panel	misc	530 kVA power addition to site.		$ 56,200
12	Gravel	Truck In/ Out Loading Area (Gravel)	misc	7 m (23 ft) x 60 m (200 ft) gravel road.		$ 1,000
13	Concrete	Outside Pad, 2 skids	misc	93 m2 (1,000 ft2), 10" thickness, 24 m3 (31 yards) concrete.		$ 9,700
14	Piping	Misc Header Piping	misc	10 headers x 40 m (130 ft) each, 25.4 mm (1") pipe.		$ 64,500

Major Equpiment Cost (MEC)	$ 312,300		
Installation Cost (IC)	$ 484,800		
Installed Equipment Cost (IEC)		$ 797,100	
Tax (8% of MEC + 2.5% of IC)	$ 37,100		
Freight (1.6% of MEC)	$ 5,000		
Contractor Fees (30% of IC)	$ 145,400		
SUBTOTAL		$ 984,600	
Engineering & Procurement (15% of Subtotal)	$ 147,700		
Contingency (25% of Subtotal)	$ 246,200		
Early Phase Capital Cost Estimate		**$1,379,000**	*1st Quarter 2015 Basis*
Early Phase Capital Cost Estimate Without Mixing Tank		**$ 1,285,000**	*1st Quarter 2015 Basis*

Figure 6-B-1 Early phase conceptual capital cost estimate for pilot plant test bed, Option A.

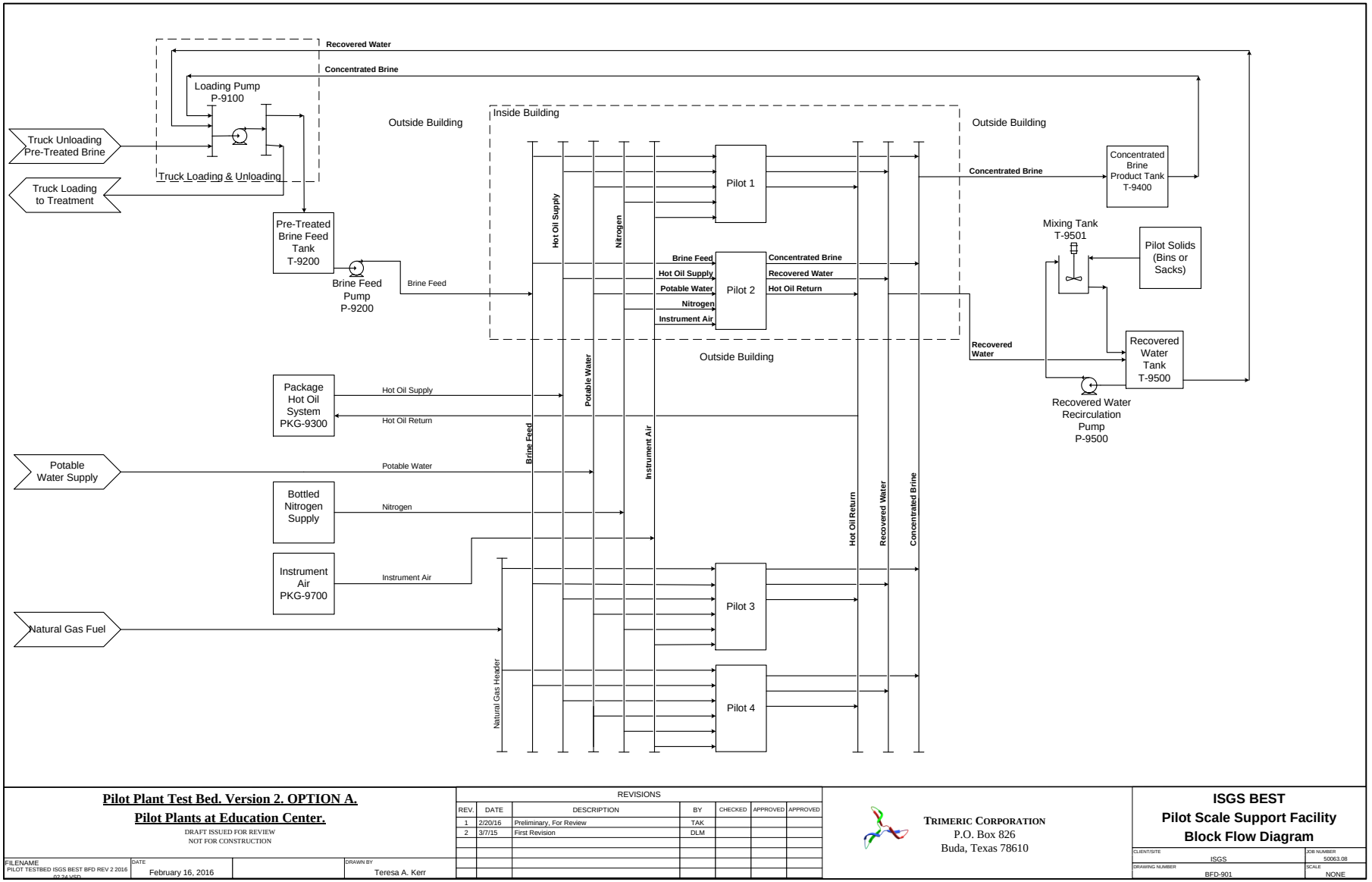

Pilot Plant Test Bed. Version 2. OPTION A.
Pilot Plants at Education Center.
DRAFT ISSUED FOR REVIEW
NOT FOR CONSTRUCTION

REVISIONS						
REV.	DATE	DESCRIPTION	BY	CHECKED	APPROVED	APPROVED
1	2/20/16	Preliminary, For Review	TAK			
2	3/7/15	First Revision	DLM			

FILENAME: PILOT TESTBED ISGS BEST BFD REV 2 2016 02.24.VSD
DATE: February 16, 2016
DRAWN BY: Teresa A. Kerr

TRIMERIC CORPORATION
P.O. Box 826
Buda, Texas 78610

ISGS BEST
Pilot Scale Support Facility
Block Flow Diagram

CLIENT/SITE: ISGS
JOB NUMBER: 50063.08
DRAWING NUMBER: BFD-901
SCALE: NONE

Figure 6-B-2 Block flow diagram for pilot-scale support facility, Option A.

PROJECT: ISGS BEST **Pilot Facility for Testing Brine Processing Technologies. Pilot Plants at ADM.**
Pilot Plant Test Bed, Option B. SECTION 9000
TRIMERIC CORPORATION 3/3/2016 Version 2.
Early Phase Conceptual Capital Cost Estimate

#	Item	Equipment Name	Tag #	Design Information	Purchased Equipment Cost	Installed Cost
1	Pump	Return Pump 1 (at ADM Pilot Facility)	P-9800	316L SS. 1 L/s (16 gpm), 42 m (50 psi, 139 ft) head. 1.1 kW.	$ 5,400	$ 19,900
2	Pump	Return Pump 2 (at ADM Pilot Facity)	P-9900	316L SS. 1 L/s (16 gpm), 42 m (50 psi, 139 ft) head. 1.1 kW.	$ 5,400	$ 19,900
3	Pump	Condensate Pump (at ADM Pilot Facility	P-9700	316L SS. 0.6 L/s (10 gpm), 42 m (50 psi, 139 ft) head. 0.75 kW.	$ 5,000	$ 17,000
4	Tank	Concentrated Brine Holding Tank (at ADM Pilot Facility)	T-9800	Fiberglass. 1,000 gal (3.8 m3), 1.25 m (4.1 ft) diam x 3 m (9.8 ft).	$ 10,900	$ 53,400
5	Tank	Recovered Water Holding Tank (at ADM Pilot Faciliity)	T-9900	Fiberglass. 1,000 gal (3.8 m3), 1.25 m (4.1 ft) diam x 3 m (9.8 ft).	$ 10,900	$ 53,400
6	Concrete	Concrete Pad, 4 skids (at ADM Pilot Facility)		186 m2 (2,000 ft2), 10" thickness, 48 m3 (62 yards) concrete.		$ 19,400
7	Piping	Connection to ADM Utilities (at ADM Pilot Facility)		400 m (1,300 ft) total length pipe assumed, various fittings. 25.4 mm (1") pipe. 316L SS.		$ 64,500
8	Piping	Misc Header Piping (at ADM Pilot Facility)		10 headers x 40 m (130 ft) each, various fittings. 25.4 mm (1") pipe. 316L SS.		$ 64,500
9	Pump	Loading Pump (at Education Center)	P-9100	316L SS. 6 L/s (96 gpm), 10 m (12 psi, 33 ft) head. 1.1 kW.	$ 5,600	$ 18,000
10	Tank	Pre-Treated Brine Feed Tank (at Education Center)	T-9200	Fiberglass. 1,000 gal (3.8 m3), 1.25 m (4.1 ft) diam x 3 m (9.8 ft).	$ 10,900	$ 53,400
11	Pump	Brine Feed Pump (at Education Center)	P-9200	316L SS. 1 L/s (16 gpm), 42 m (50 psi, 139 ft) head. 1.1 kW.	$ 5,400	$ 19,900
12	Tank	Used Brine Return Tank (at Education Center)	T-9400	Fiberglass. 1,000 gal (3.8 m3), 1.25 m (4.1 ft) diam x 3 m (9.8 ft)	$ 10,900	$ 53,400
13	Gravel	Truck In/ Out Loading Area (at Education Center)		7 m (23 ft) x 60 m (200 ft) gravel road.		$ 1,000

Major Equpiment Cost (MEC)	$ 70,400	
Installation Cost (IC)	$ 387,300	
Installed Equipment Cost (IEC)		$ 457,700
Tax (8% of MEC + 2.5% of IC)	$ 15,300	
Freight (1.6% of MEC)	$ 1,100	
Contractor Fees (30% of IC)	$ 116,200	
SUBTOTAL		$ 590,300
Engineering & Procurement (15% of Subtotal)	$ 88,500	
Contingency (25% of Subtotal)	$ 147,600	
Early Phase Capital Cost Estimate		**$ 826,000**

Figure 6-B-3 Early phase conceptual capital cost estimate for pilot plant test bed, Option B.

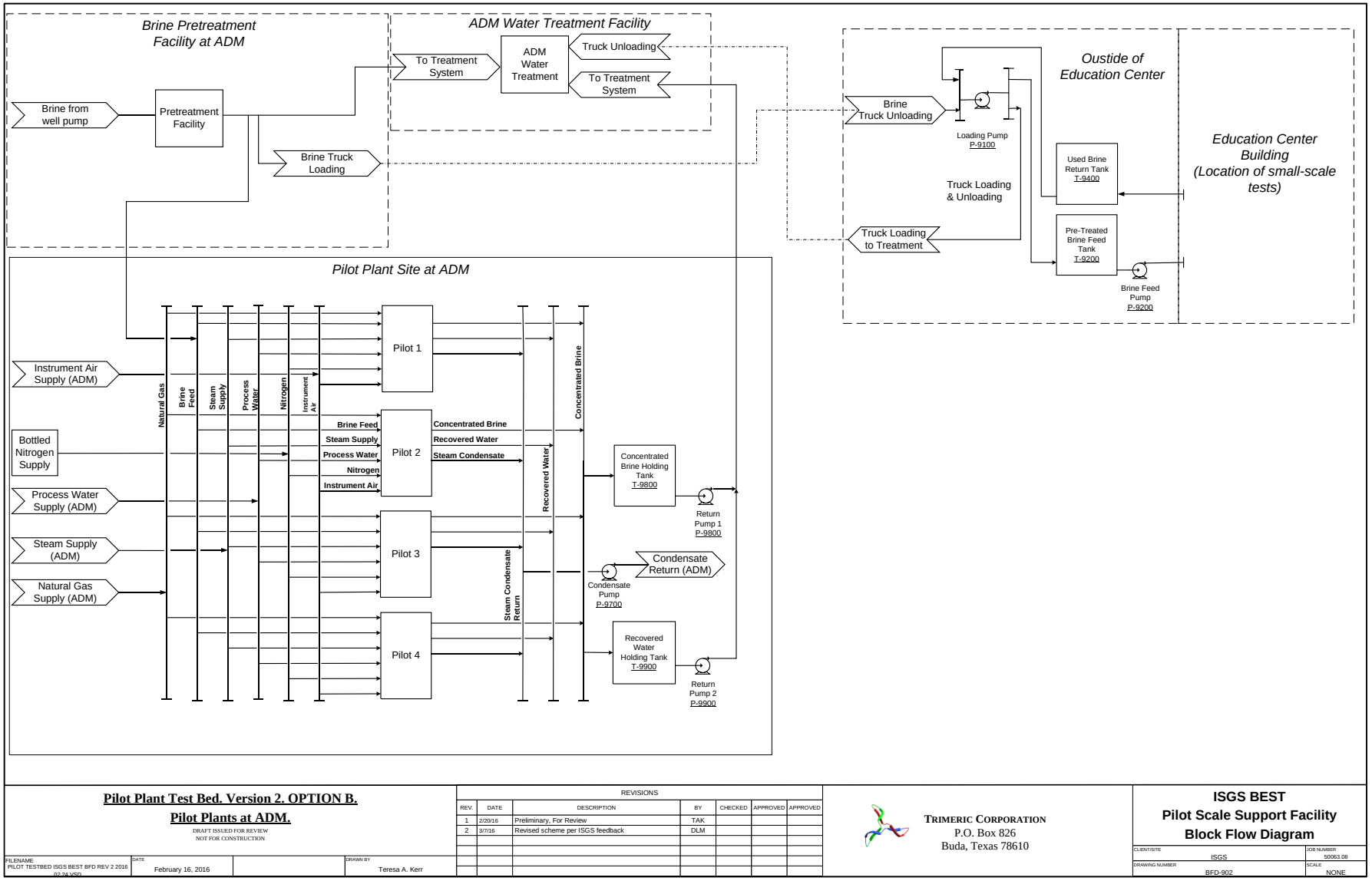

Figure 6-B-4 Block flow diagram for pilot-scale support facility, Option B.

Appendix 6-C Cost Estimate for Multi-Effect Evaporation Pilot Plant

The early-phase estimation of the cost of pilot plant systems tends to be difficult and is subject to a higher degree of uncertainty than full-scale process systems. Pilot plant cost estimates need to be further refined prior to budgeting the project. Better definition of the process equipment, possible reconsideration of the scale, and discussions with some vendors of some of these equipment items should be done in order to better define the costs.

The technology considered on the pilot plant scale is multi-effect evaporation (MEE). The pilot plant scale for MEE was defined by ISGS to be approximately 5 gpm. The potential cost of such a unit was discussed with Veolia, who stated that a legitimate estimate of the cost would require a significant engineering effort and some laboratory testing of the subject brine. Rather than expend a large effort in the estimation of the MEE pilot cost, a much simpler method was used. Although Veolia said that a large effort would be required to provide a good estimate for the pilot unit, they were able to provide a very rough likely range for such a pilot unit based on experience, and this cost range was compared to a scaled-down version of the estimated total cost of the 2,000 gpm MEE unit. This analysis resulted in an estimate for the installed MEE pilot plant (5 gpm) total cost being in the range of $1,500,000 to $3,000,000. It is probably possible to reduce the cost range of the system by only demonstrating parts of the system, rather than the entire process, on the pilot scale. Other options for demonstrating MEE, such as contracting with Veolia to carry out the tests at their laboratories should be considered.

Appendix 6-D Illinois State Geological Survey Brine Extraction and Storage Test Proposed Wells Design

Project Background

The Illinois State Geological Survey (ISGS) Brine Extraction and Storage Test (BEST) Project is funded by the U.S. Department of Energy's National Energy Technology Laboratory. The proposed project would expand on the existing carbon capture and storage (CCS) site that is on the property of Archer Daniels Midland Company (ADM) in Decatur, Illinois. The BEST Project is focused on developing subsurface engineering approaches that address research needs critical for advancing CCS to commercial scale.

Specifically, the project will determine if it is possible to manipulate and manage formation pressure for an existing carbon dioxide (CO_2) subsurface storage site by extracting brine from the CO_2 storage reservoir. The project is located in the immediate study area of the Midwest Geological Sequestration Consortium's (MGSC's) Phase III project, the Illinois Basin – Decatur Project (IBDP), and the Illinois Industrial Carbon Capture and Storage (ICCS) Project, and will attempt to influence the CO_2 already injected into the Mt Simon Sandstone by extracting brine from directly above the plume. Currently, IBDP is in the post-injection site care phase, and has completed the injection phase of the project by injecting ~one million tonnes of CO_2.

The wells are designed to accommodate the use of various monitoring techniques including cross-well seismic, pulsed neutron monitoring, pressure, and temperature monitoring to track how the plume evolves as brine is extracted.

Area Data, Location, Geology

The BEST project would be located inside the IBDP and ICCS immediate study areas on ADM land in Decatur, IL (Figure 6-).

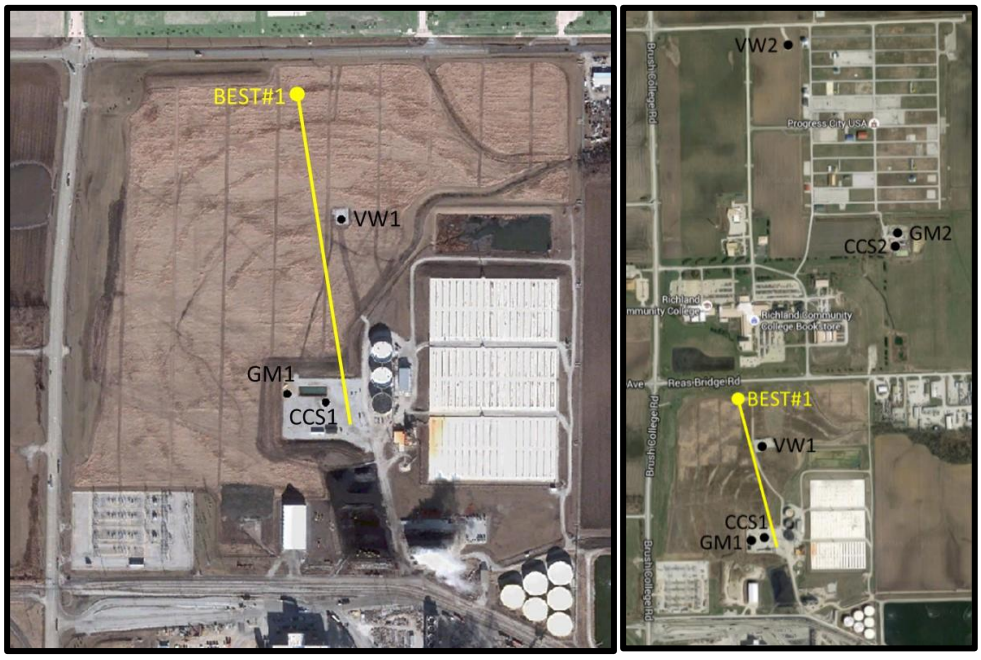

Figure 6-D-1 Site maps showing location of the BEST#1 well's trajectory in relation to (left) the IBDP wells (CCS1, VW1, and GM1) and (right) the ICCS Project wells (CCS2, VW2, and GM2), as well as the ADM plant, Richland Community College, and Progress City.

CCS1, VW1, CCS2, and VW2 of the IBDP and ICCS project have all been drilled beyond the 6,400 foot depth planned for the BEST#1 well. Both the IBDP and ICCS projects have collected core samples and

petrophysical logs, which have provided a wealth of geologic information. Figure 6- shows a stratigraphic column of the area. The most significant known drilling hazard is the under pressured Potosi Formation, which will be managed through the strategic spotting of cement plugs to control losses of drilling fluid.

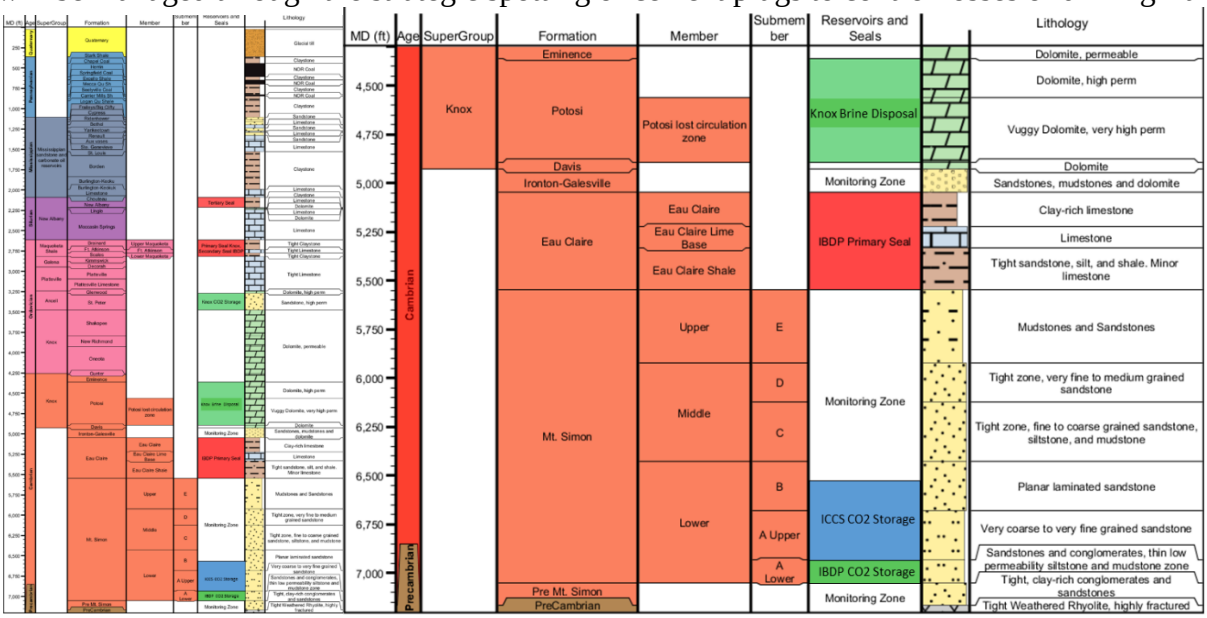

Figure 6-D-2 Stratigraphic column of the BEST project area.

Well Summary

Table 6-D-1 summarizes the basic well information and location. The BEST#1 is a brine production well (Figure 6- and 6-D-4), and will be drilled vertically to the Mt Simon E (~5,800 ft). The well will be kicked off from this point to the south south-west with a build rate of 15° every 100 feet (radius of 600 ft), eventually becoming horizontal in the Mt. Simon C (~6,400 ft), and continuing with approximately 1,000 ft horizontal component between the existing VW1 and CCS1 wells from the IBDP.

The vertical section of the BEST#1 well will contain an electric submersible pump (ESP), which will be designed to meet production rate requirements that will be optimized by reservoir engineering simulations. Preliminary reservoir engineering simulations indicate that a production rate of approximately 5,000 to 10,000 barrels/day will be sufficient to meet project objectives.

Plan is to deploy the ESP and packer to a depth of approximately 5,300 ft. Distributed temperature and/or distributed acoustic fiber optics are being considered as possible additions to the completion string. The ESP, a pressure/temperature gauge, and auto Y-tool will be placed beneath the packer in the production section. The Y-tool allows intervention or logging tools to pass below the ESP. The pressure/temperature gauges will allow for both pump and reservoir performance monitoring.

Table 6-D-1 Basic well information.

Well Name	BEST#1	**Lease Owner**	ADM Company
State	Illinois	**County**	Macon
TD/TVD	7,750 feet/6,400 feet	**Section/Township/Range**	32 / 17N / 3W
Latitude	39.881313	**Target Location Latitude**	39.876730
Longitude	-88.895100	**Target Location Longitude**	-88.892848
Elevation	~670 feet	**Anticipated BH Temperature:**	~120º F

Well Schematic

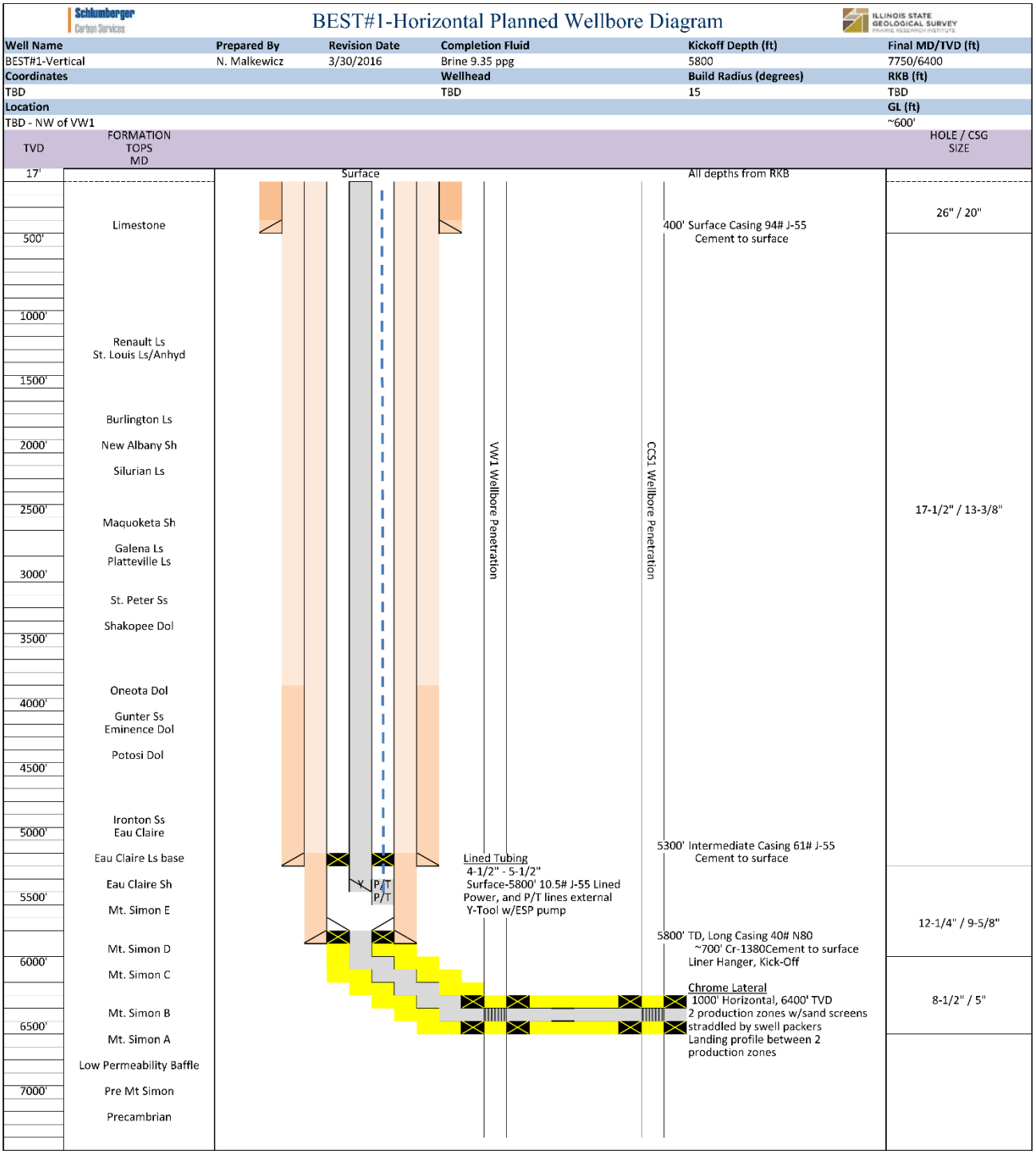

Figure 6-D-3 BEST#1 proposed well schematic.

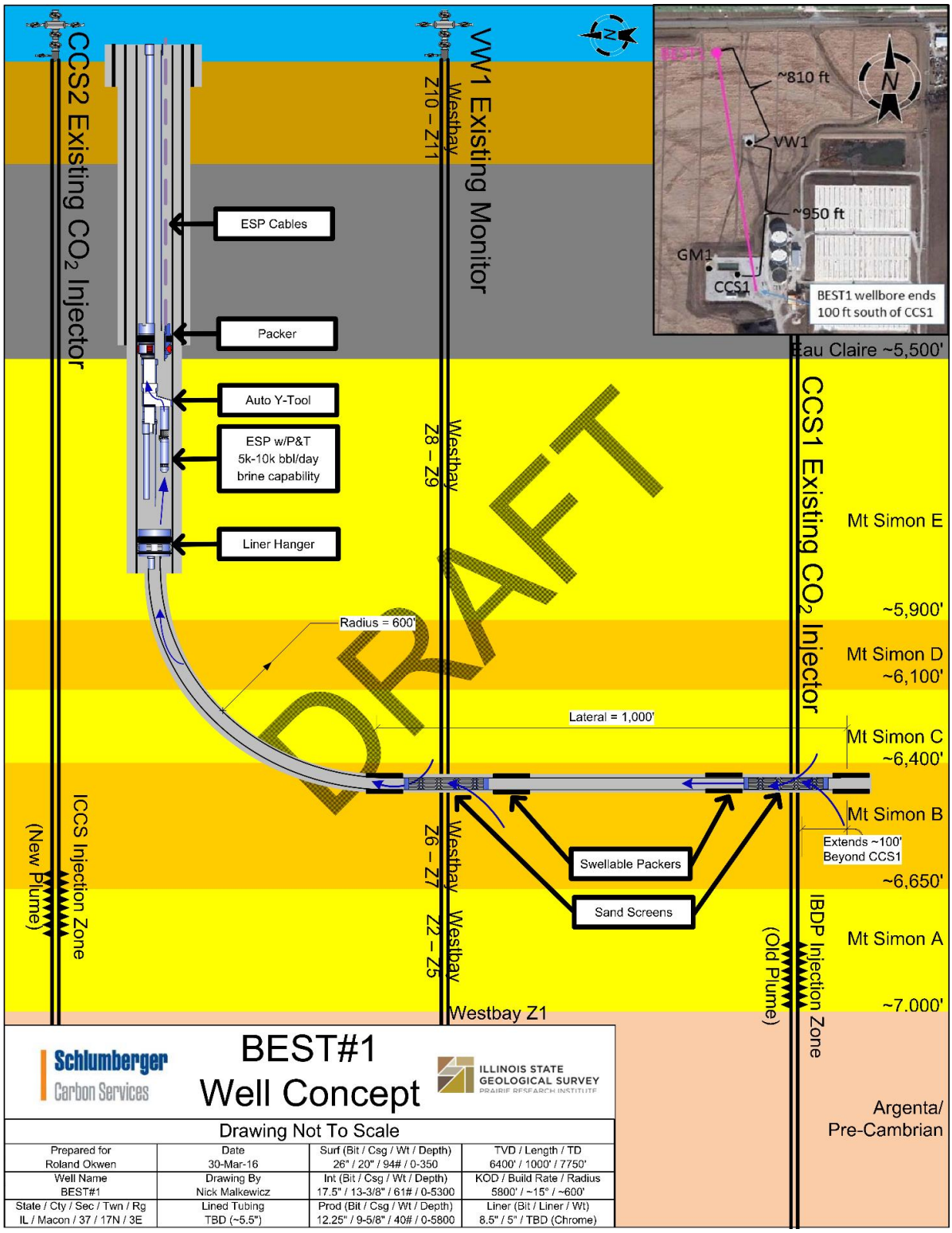

Figure 6-D-4 BEST#1 proposed well schematic.

Well Budget

Figure 6- shows the estimated cost of constructing a horizontal brine extraction wells.

Horizontal Brine Extraction Producing Well

AUTHORIZATION FOR EXPENDITURES - Est Cost

Schlumberger Carbon Services

In US $	$7,528,396	Project Type :	Brine Extraction		
Operator:	ADM/ISGS	Well Name :	BEST#1		
Project Manager:	Nick Malkewicz	Well Type :	Brine producer		
Client PI:	Roland Okwen	Platform/Tripod :	TBD	AFE #:	BEST-1
Prepared by	JMK	Field/Structure :	Decatur	Date:	28-Mar-16
		Basin :	Illinois		

Location	Decatur, IL	Surface Coordinate	Wellhead ~810' NW of VW1, Heel ~100' NW of VW1, Toe ~100' SE of CCS1
Surface Elev.	~600'	Elevation	TBD

	PROGRAM	ACTUAL
Spud Date	TBD	
Compl Days	10	
In Service	TBD	
Drilling Days	75	

	PROGRAM	ACTUAL
Rig Days	75	
Total Depth	7750	
Well Cost $/Ft.	$971.41	
Well Cost $/Day	$100,378.61	

Close Out Date: _____ Completion Type: H. Liner w/ESP Well Status: Planning

	Description	Dry Hole Budget	Completed Budget	Total Budget	Actual Expenditure	Remarks
1	**TANGIBLE COSTS**					
2	Casing	673,400	0	673,400	$0	20", 13 3/8", 9 5/8" (Cr) and 5" Liner (Cr)
3	Casing Accessories; Float Equip & Liners	180,637	0	180,637	$0	Cem. eqpt, Inr hanger, screens, swell pkr
4	Tubing		99,200	99,200	$0	4.5" Lined Tubing
5	Well Equipment - Surface	24,000	194,613	218,613	$0	Wellhead, hangers, spools
6	Well Equipment - Subsurface	0	305,500	305,500	$0	Packer, ESP package
7	Other Tangible Costs	0	0	0	$0	
8	Market Factor Tubulars	64,100	36,500	100,600	$0	
9	**Total Tangible Costs**	**$942,137**	**$635,813**	**$1,577,950**	**$0**	
10	**INTANGIBLE COSTS**					
11	**PREPARATION & TERMINATION**					
12	Surveys	6,000	0	6,000	$0	
13	Location Staking & Positioning	2,000	0	2,000	$0	
14	Wellsite & Access Road Preparation	166,000	0	166,000	$0	Grade and build out wellpad
15	Service Lines & Communications	63,750	0	63,750	$0	Pason during drilling
16	Water Systems	0	0	0	$0	
17	Rigging Up/Rigging Down/ Mob/Demob	100,000	0	100,000	$0	Rig move
19	**Total Preparations/MOB**	**$337,750**	**$0**	**$337,750**	**$0**	
20	**DRILLING - W/O OPERATIONS**					
21	Contract Rig	1,642,800	80,000	1,722,800	$0	Rig
22	Drlg Rig Crew/Contract Rig Crew/Catering	0	0	0	$0	
23	Mud, Chem & Engineering Servs	360,250	10,000	370,250	$0	Mud eng, solids control, packer fluid
24	Water	97,500	0	97,500	$0	
25	Bits, Reamers & Coreheads	142,500	0	142,500	$0	26", 17 1/2", 12 1/4", 8 1/2"
26	Equipment Rentals	267,614	75,000	342,614	$0	DH Equipment, Surface Equipment
27	Directional Drlg & Surveys	240,000	0	240,000	$0	Geosteering
28	Diving Services	0	0	0	$0	
29	Casing & Wellhead Installation & Inspection	88,500	23,000	111,500	$0	Casing crew
30	Cement, Cementing & Pump Fees	378,000	0	378,000	$0	Cement casing and lost circulation zone
31	Misc. H2S Services	0	0	0	$0	
32	**Total Drilling Operations**	**$3,217,164**	**$188,000**	**$3,405,164**	**$0**	
33	**FORMATION EVALUATION**					
34	Coring	0	0	0	$0	
35	Mud Logging Services	182,500	0	182,500	$0	
36	Drillstem Tests	0	0	0	$0	
37	Open Hole Elec Logging Services	664,372	0	664,372	$0	Logging all sections
39	**Total Formation Evaluation**	**$846,872**	**$0**	**$846,872**	**$0**	
40	**COMPLETION**					
41	Casing, Liner, Wellhead & Tubing Installation	0	50,000	50,000	$0	Completions support
42	Remedial Cementing and Fees	0	0	0	$0	
43	Cased Hole Elec Logging Services	50,000	45,000	95,000	$0	Cement logs
44	Perforating & Wireline Services	0	5,000	5,000	$0	
45	Stimulation Treatment	0	25,000	25,000	$0	Acid job
46	Production Tests	0	0	0	$0	
48	**Total Completion Costs**	**$50,000**	**$125,000**	**$175,000**	**$0**	
49	**GENERAL**					
50	Supervision	275,500	40,000	315,500	$0	Rig supervisor
51	Insurance	500,000	0	500,000	$0	Estimated cost for insurance and bond
52	Permits & Fees	0	0	0	$0	
53	Marine Rental & Charters	0	0	0	$0	
54	Helicopter & Aviation Charges	0	0	0	$0	
55	Land Transportation	40,800	0	40,800	$0	Trucking fees
56	Other Transportation	0	0	0	$0	
57	Fuel & Lubricants Non Rig	7,500	0	7,500	$0	
58	Camp Facilities	70,500	0	70,500	$0	Onsite shacks during drilling and compl.
59	Allocated Overhead - Field Office	0	0	0	$0	
60	Allocated Overhead - Main Office	0	0	0	$0	
61	Allocated Overhead - Overseas	0	0	0	$0	
62	Market Factor Other	233,710	17,650	251,360	$0	Market price change
64	**Total General Costs**	**$1,128,010**	**$57,650**	**$1,185,660**	**$0**	
65	**TOTAL INTANGIBLE COSTS**	**$5,579,796**	**$370,650**	**$5,950,446**	**$0**	
	TOTAL TANGIBLE COSTS	**$942,137**	**$635,813**	**$1,577,950**	**$0**	
66	**WELL COST**			**$7,528,396**		
67						
68	**TOTAL WELL COST**			**$7,528,396**		
69						
70						

Operator	Approved By:			**Remarks**
	Position			Market conditions are extremely depressed currently. Pricing may increase substantially with changes in market conditions.
	Date			
Operator Approval	Approved By;			Horizontal Well Parameters Kick-off depth - 5,800' TVD Lateral/well depth - 6,400' TVD Measured Depth - 7,750' MD
	Position			
	Date			

Figure 6-D-5 BEST#1 proposed well budget.

High Level Procedure for Well Construction

1. Build the location for the drilling rig and buildings, including a gravel wellpad, access road, and mud pit.
2. Move the drilling rig to location.
3. Set up the drilling rig and connect power/water/internet to the wellpad.
4. Drill the surface hole section.
5. Log the open hole surface section.
6. Run casing and cement the surface section casing.
7. Log the cased hole surface section.
8. Drill the intermediate hole section.
9. Log the open hole intermediate section.
10. Run intermediate casing and cement the intermediate section casing.
11. Log the cased hole intermediate section.
12. Drill the long string hole section.
13. Log the open hole of the long string section.
14. Run long string casing and cement the long string casing.
15. Log the cased hole long string section.
16. Drill the kickoff and lateral section using directional drilling tools.
17. Log the lateral section using ThruBit tools.
18. Complete the lateral section with sand screens straddled by swellable packers with liner hanger.
19. Run the injection, production, step-rate, and pressure fall-off tests
20. Complete the vertical section with an electronic subsurface pump, pressure/temperature gauges.
21. Install the surface wellhead and hook up completion systems to surface data acquisition systems.

Well construction days versus depth estimates for steps 4–19 are presented graphically in Figure 6-.

Well Construction and Completion Details

Table 6-D-2 describes the drilling, cementing, and drilling mud details for the BEST#1 well. BEST#1 will be drilled vertically to a depth of 5,800 ft, then the lateral section will be drilled to the south south-west with a build rate of 15° every 100 ft (radius of 600 ft), eventually becoming horizontal at true vertical depth of approximately 6,400 ft, and continuing with a 1,000 ft horizontal component. The well should be horizontal approximately 100 ft north-west of VW1 and with the horizontal section continuing approximately 100 ft south-east of CCS1.

Table 6-D-2 Drilling, cementing, and drilling mud details for BEST#1.

Section	Hole Depth (ft)	Bit Size (in)	Csg Size (in)	Csg Wt. (lb/ft)	Cement Type	Cement Density Lead/Tail (lb/gal)	Mud Type	Mud Weight (ppg)	Mud Funnel Vis (sec/qt)	Mud Salinity (ppm)
Surface	350	26	20	94	Conventional Class A	15.6	FW Spud Mud	8.4-9.3	70-90	500-1400
Intermed.	5,300	17.5	13.375	61	Conventional Class H	1st–15.6/16.4 2nd–13.0/16.1	FWND	8.33-9.3	40-44	500-1400
Product.	5,800	9.625	5	TBD	1st–35:65 Class A 2nd-EverCRETE	12.5/15.9	FWND	9.1-9.4	40-44	25,000-30,000
Lateral	+/- 7,250	12.25	8.5	40/47	N/A	N/A	2% KCl based LSND	9.1-9.4	40-44	25,000-30,000

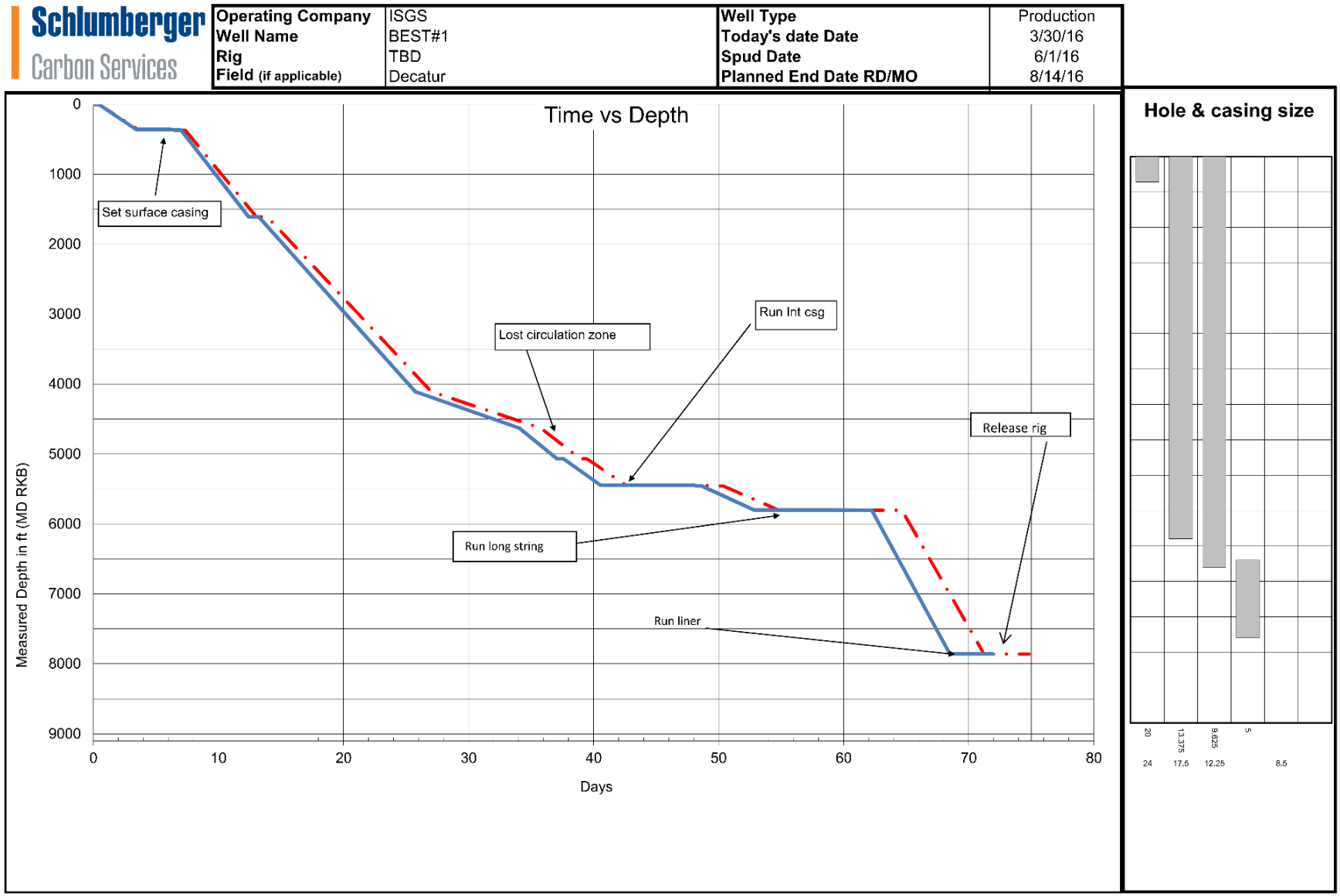

Figure 6-D-6 BEST#1 Horizontal well days versus depth.

Fiber optic distributed temperature and acoustic (DTS, DVS) are being consider for the BEST#1 completion. If deployed, the fiber optic cable would be mounted externally to the lined tubing. The lined tubing will have an automatic Y-Tool to allow for wireline logging beyond the ESP, which will be installed at a depth of approximately 5,800 ft. The ESP will us a REDA* electric submersible pump systems Maximus Motor, a REDA High-Efficiency Pump, and a monitoring system for the entire pump/motor assembly. The 5-inch liner completion will have two sand screens (Appendix C) for production in the immediate vicinities of CCS1 and VW1 to maximize the measureable effect on the reservoir near these two monitorable locations.

There will be a landing profile in the horizontal section between these two brine production zones to allow for isolated production to enable flow contribution profiling from each zone. Water swellable packers outside the 5-in. liner (in between the liner and the formation) will be used to isolate the two brine production zones in the liner/formation annular space. The wellhead will be a standard oil and gas tree that will be instrumented with annulus and lined tubing pressure/temperature gauges. Wellhead ports will accommodate downhole instrumentation.

The BEST#1 brine handling facilities will be instrumented to automate well control in case of earlier than expected CO_2 breakthrough or surging in the project production well. To do this, the BEST#1 brine production well will have an automatic actuated valve on the flow line, which will close in and simultaneously deactivate the ESP pump should an automated trigger be activated. The nature of the trigger will depend on final surface facility design. The two principal triggers being considered are:

1) Significant changes in ESP current amperage (gas laden fluid in either the suction or discharge of the pump causes wide variations of amperage), and/or
2) A CO_2 sensor in the gas vent line of a brine/gas separator in the surface facilities.

One or both of these can be tied to the automated ESP and wellhead valve equipment to assure the well operates within safe and expected parameters. The ESP will be managed through the Liftwatcher* real-time surveillance service, which allows for remote ESP monitoring and control (remote and onsite data monitoring and onsite control). LiftWatcher provides around-the-clock surveillance of all artificial lift systems, preventing or resolving ESP downtime, misuse, or failure. The service enables engineers to monitor and analyze data continuously 24 hours a day/365 days a year at one of many Schlumberger Artificial Lift Surveillance Centers (ALSCs). Further, data will be integrated into ADM's existing SCADA system. Motor temperature, flow rate, current, and input/output pressures are all monitored to identify potential performance issues, identify probable causes, and report remediation options.

The field data will be ported to the existing data acquisition and management systems for the IBDP, which has been in use since 2011. Currently data is aggregated into WellWatcher Connect* wellsite data transmission system. The WellWatcher Connect system is used for monitoring and control for the IBDP project where three wells are connected. WellWatcher Connect aggregates data inputs for a distributed temperature system (DTS), multiple surface and downhole pressure/temperature gauges, flowmeters, environmental measurements, and multiple geophones used for microseismic monitoring. WellWatcher Connect will be modified to include data inputs from the new wells constructed for the BEST project, which would potentially include additional fiber optics, pressure/temperature gauges (surface and downhole), and an ESP monitoring and control package. Project stakeholders can be granted access to interface with the data historian remotely and concurrently with other users. WellWatcher Connect would allow the BEST project scientists to acquire new data in addition to making comparisons with existing baseline datasets. Proposed integration into the existing architecture is shown in Figure 6-.

Alternative Well Configurations Considered

Additional well configurations reviewed for the proposal include a Knox/Potosi brine disposal well scenario (Figure 6-) and a vertical brine extraction well scenario Figure 6-. Also presented are the AFE's for these two well scenarios.

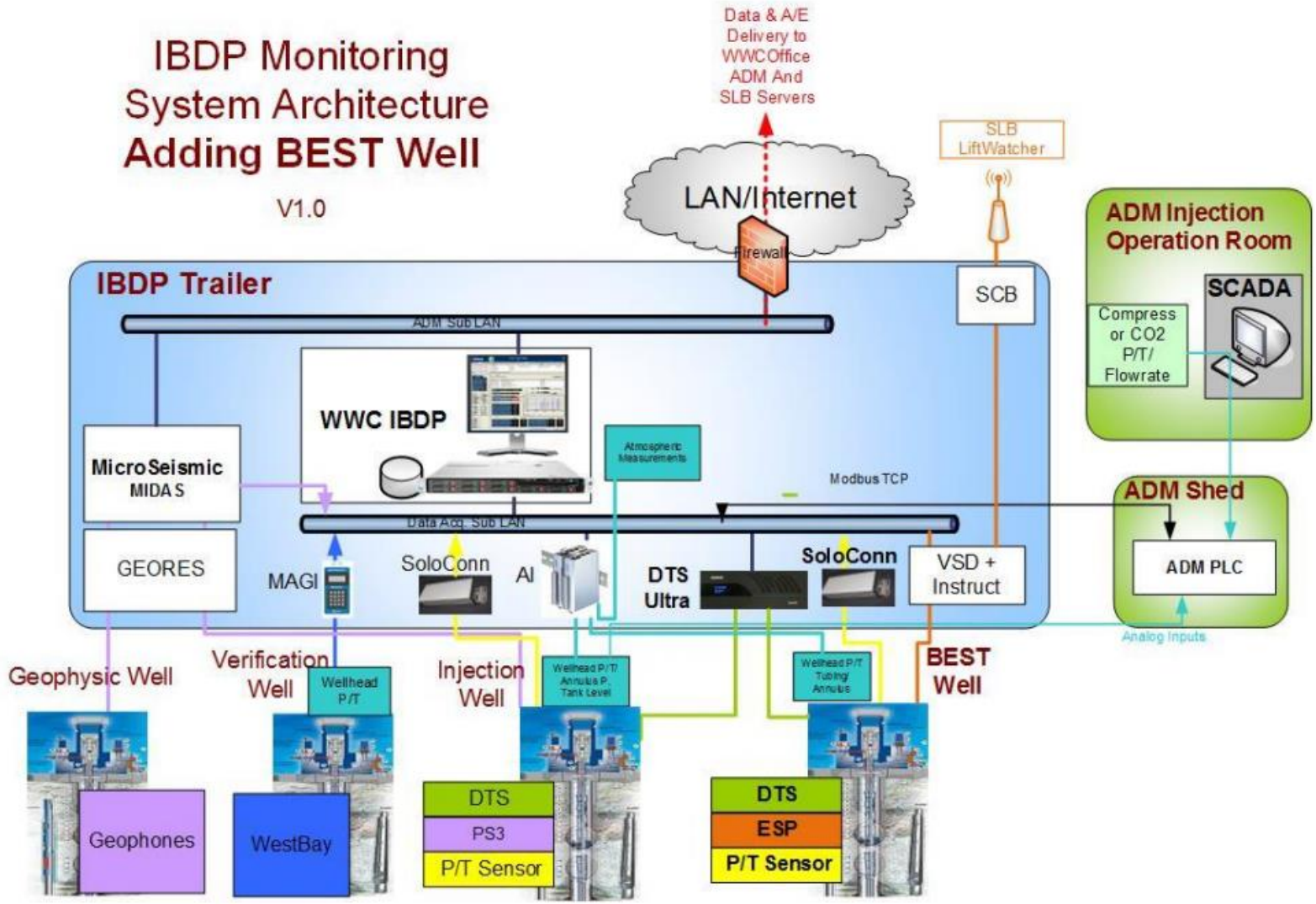

Figure 6-D-7 BEST#1 proposed data collection architecture modification from existing IBDP architecture

.

Planned Logging Program

Table 6-D-3 summarizes log program information.

Table 6-D-3 Information for different log programs.

Well Section	Open/Cased	Log	Log Information
Conductor	-	-	-
Surface	Open Hole	Platform Express / Gamma Ray Directional Survey Sonic	http://www.slb.com/~/media/Files/evaluation/brochures/wireline_open_hole/petrophysics/platform/platform_express_br.pdf http://www.slb.com/~/media/Files/rd/technology/product_sheets/gpit_general_purpose_inclinometry_tool1.pdf http://www.slb.com/~/media/Files/evaluation/brochures/wireline_open_hole/petrophysics/acoustic/sonic_scanner_br.pdf
	Cased Hole	Cement Bond Log	http://www.slb.com/~/media/Files/production/product_sheets/well_integrity/cement_bond_logging_tools.pdf
Intermediate	Open Hole	Platform Express / Gamma Ray Directional Survey Sonic Scanner Fullbore Formation Microimager Combinable Magnetic Resonance LithoScanner Mechanical Sidewall Coring Tool	http://www.slb.com/~/media/Files/evaluation/brochures/wireline_open_hole/petrophysics/platform/platform_express_br.pdf http://www.slb.com/~/media/Files/rd/technology/product_sheets/gpit_general_purpose_inclinometry_tool1.pdf http://www.slb.com/~/media/Files/evaluation/brochures/wireline_open_hole/petrophysics/acoustic/sonic_scanner_br.pdf http://www.slb.com/~/media/Files/evaluation/brochures/wireline_open_hole/geology/fmi_br.pdf http://www.slb.com/~/media/Files/evaluation/brochures/wireline_open_hole/petrophysics/nmr/cmrmdt_br.pdf http://www.slb.com/~/media/Files/evaluation/brochures/scanner_rock_fluid_character/litho_scanner2_brw.pdf http://www.slb.com/~/media/Files/evaluation/product_sheets/wireline_open_hole/insitu_fluid/msct_ps.pdf
	Cased Hole	Cement Bond Log Ultrasonic Imager	http://www.slb.com/~/media/Files/production/product_sheets/well_integrity/cement_bond_logging_tools.pdf http://www.slb.com/~/media/Files/production/product_sheets/well_integrity/usi.pdf
Production	Open Hole	Platform Express / Gamma Ray Directional Survey Sonic Scanner Fullbore Formation Microimager Combinable Magnetic Resonance LithoScanner Mechanical Sidewall Coring Tool	http://www.slb.com/~/media/Files/evaluation/brochures/wireline_open_hole/petrophysics/platform/platform_express_br.pdf http://www.slb.com/~/media/Files/rd/technology/product_sheets/gpit_general_purpose_inclinometry_tool1.pdf http://www.slb.com/~/media/Files/evaluation/brochures/wireline_open_hole/petrophysics/acoustic/sonic_scanner_br.pdf http://www.slb.com/~/media/Files/evaluation/brochures/wireline_open_hole/geology/fmi_br.pdf http://www.slb.com/~/media/Files/evaluation/brochures/wireline_open_hole/petrophysics/nmr/cmrmdt_br.pdf http://www.slb.com/~/media/Files/production/product_sheets/well_integrity/usi.pdf http://www.slb.com/~/media/Files/evaluation/product_sheets/wireline_open_hole/insitu_fluid/msct_ps.pdf
	Cased Hole	Cement Bond Log Ultrasonic Imager	http://www.slb.com/~/media/Files/production/product_sheets/well_integrity/cement_bond_logging_tools.pdf http://www.slb.com/~/media/Files/evaluation/brochures/wireline_open_hole/petrophysics/platform/platform_express_br.pdf
Lateral	Open Hole	Thru-Bit Triple Combo Thru-Bit Directional Thru-Bit Sonic Thru-Bit Formation Microimager	https://www.slb.com/~/media/Files/evaluation/brochures/wireline_open_hole/platform/thrubit_br.pdf http://www.slb.com/~/media/Files/rd/technology/product_sheets/gpit_general_purpose_inclinometry_tool1.pdf https://www.slb.com/~/media/Files/evaluation/brochures/wireline_open_hole/platform/thrubit_br.pdf http://www.slb.com/~/media/Files/evaluation/brochures/wireline_open_hole/geology/fmi_br.pdf

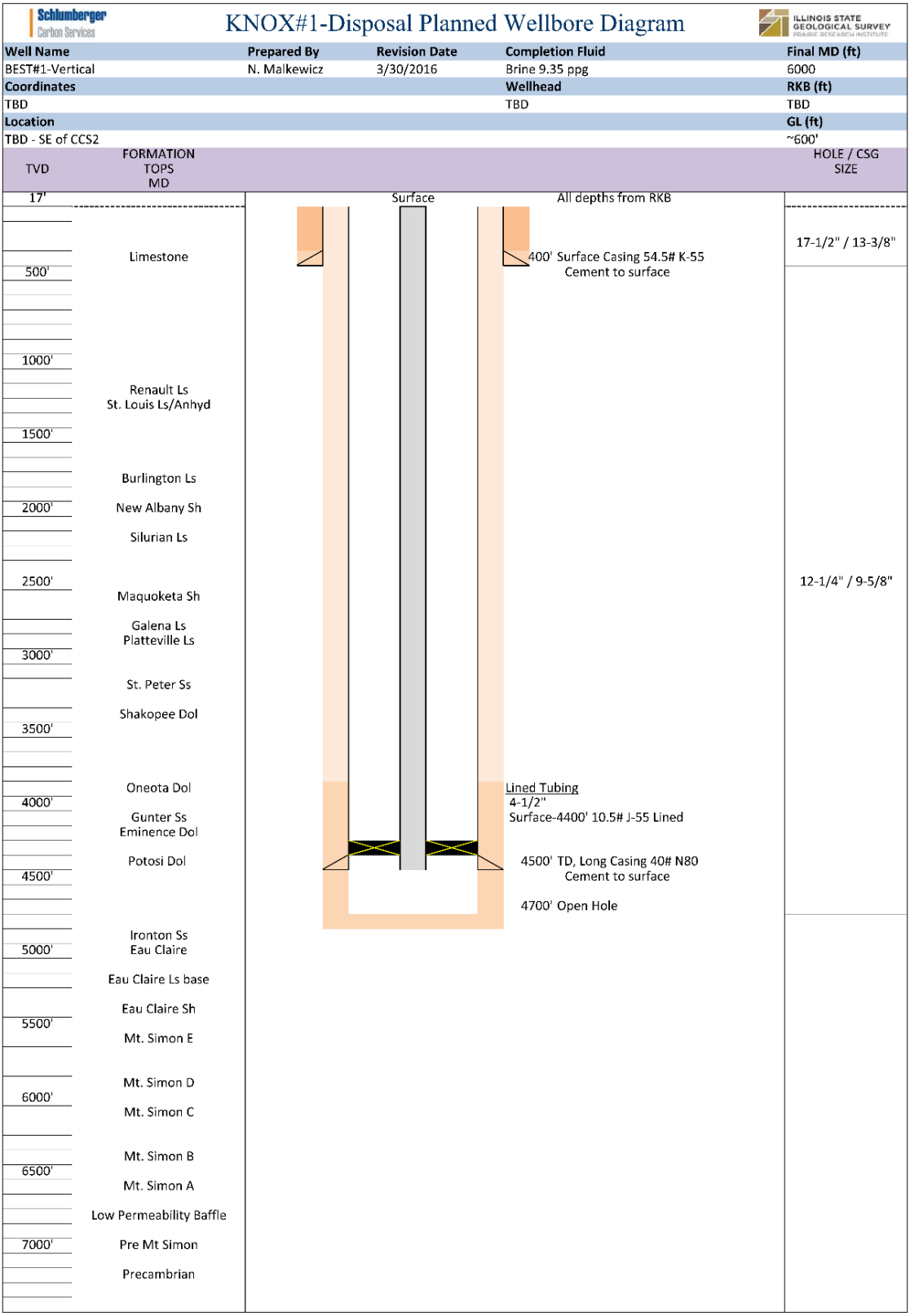

Figure 6-D-8 The KNOX#1 proposed brine disposal well.

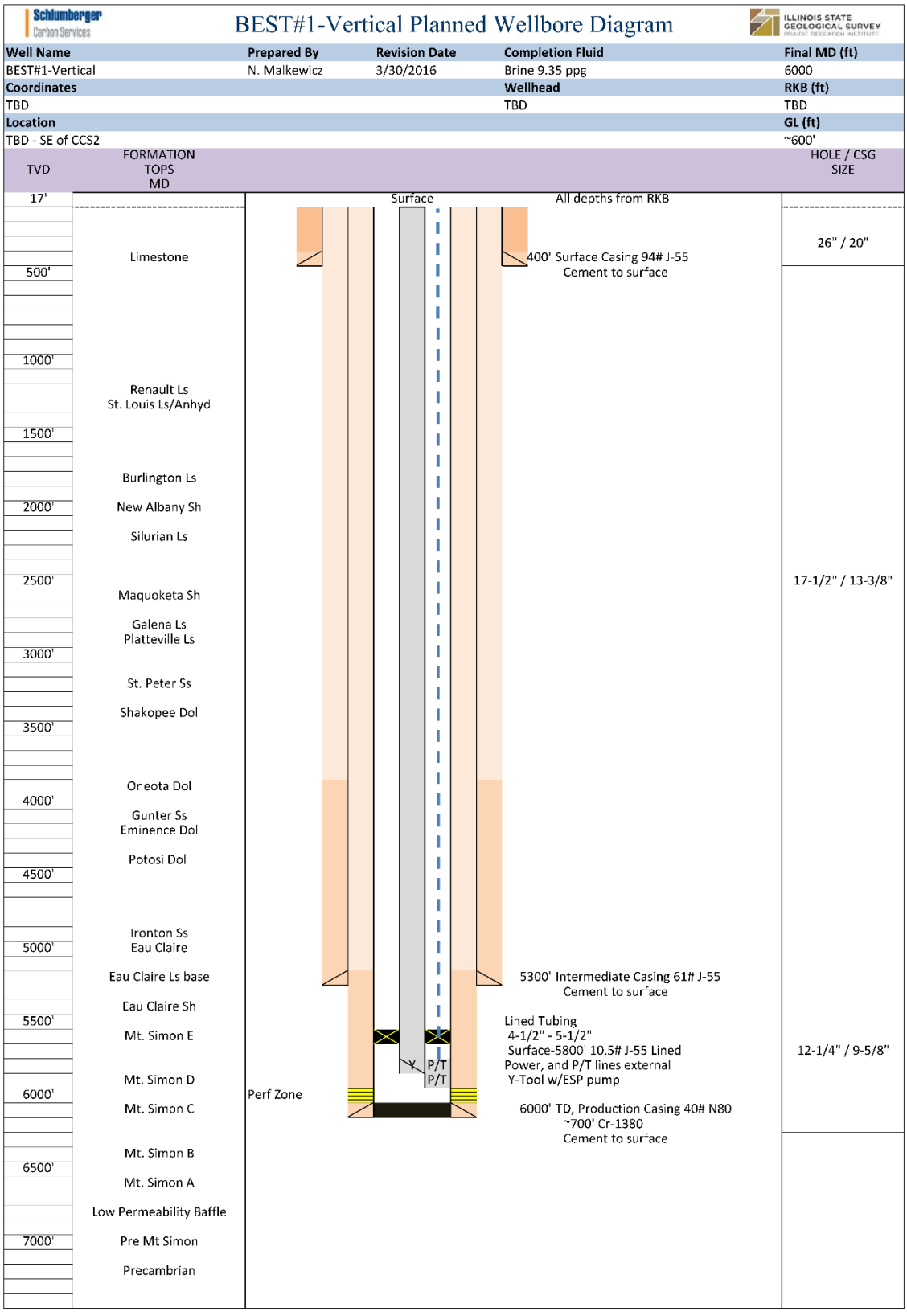

Figure 6-D-9 Proposed vertical brine production well.

AFE For Knox Disposal Well

Figure 6- shows an authorization for expenditures for a brine disposal drilled into the Knox.

Knox Brine Disposal Well

AUTHORIZATION FOR EXPENDITURES - Est Cost

Schlumberger Carbon Services

In US $	$2,934,774	Project Type :	Brine Disposal into Knox		
Operator:	ADM/ISGS	Well Name :	KNOX#1		
Project Manager:	Nick Malkewicz	Well Type :	Brine Disposal		
Client PI:	Roland Okwen	Platform/Tripod :	TBD	AFE #:	KNOX-1
Prepared by	JMK	Field/Structure :	Decatur	Date:	28-Mar-16
		Basin :	Illinois		

Location	Decatur, IL	Surface Coordinate	TBD
Surface Elev.	~600'	Elevation	TBD

	PROGRAM	ACTUAL
Spud Date	TBD	
Compl Days	10	
In Service	TBD	
Drilling Days	25	

	PROGRAM	ACTUAL
Rig Days	25	
Total Depth	4700	
Well Cost $/Ft	$624.42	
Well Cost $/Day	$117,390.94	

Close Out Date: TBD Completion Type: Standard Well Status: Planning

	Description	Dry Hole Budget	Completed Budget	Total Budget	Actual Expenditure	Remarks
1	**TANGIBLE COSTS**					
2	Casing	119,600	0	119,600	$0	13 3/8", 9 5/8"
3	Casing Accessories; Float Equip & Liners	21,168	0	21,168	$0	Cement equipment
4	Tubing		81,700	81,700	$0	4.5" Lined Tubing
5	Well Equipment - Surface	42,000	41,500	83,500	$0	Wellhead, hangers, spools
6	Well Equipment - Subsurface	0	35,000	35,000	$0	Packer
7	Other Tangible Costs	0	0	0	$0	
8	Market Factor Tubulars	27,415	23,730	51,145	$0	
9	**Total Tangible Costs**	**$210,184**	**$181,930**	**$392,114**	**$0**	
10	**INTANGIBLE COSTS**					
11	**PREPARATION & TERMINATION**					
12	Surveys	8,500	0	8,500	$0	
13	Location Staking & Positioning	5,000	0	5,000	$0	
14	Wellsite & Access Road Preparation	81,950	15,000	96,950	$0	Grade and build out wellpad
15	Service Lines & Communications	25,250	0	25,250	$0	Pason during drilling
16	Water Systems	0	0	0	$0	
17	Rigging Up/Rigging Down/ Mob/Demob	150,000	0	150,000	$0	Rig move
19	**Total Preparations/MOB**	**$270,700**	**$15,000**	**$285,700**	**$0**	
20	**DRILLING - W/O OPERATIONS**					
21	Contract Rig	502,500	75,000	577,500	$0	Rig with air package
22	Drlg Rig Crew/Contract Rig Crew/Catering	0	0	0	$0	
23	Mud, Chem & Engineering Servs	118,500	5,000	123,500	$0	Mud eng, packer fluid
24	Water	61,600	9,384	70,984	$0	
25	Bits, Reamers & Coreheads	77,000	0	77,000	$0	17 1/2", 12 1/4"
26	Equipment Rentals	102,710	8,000	110,710	$0	DH Equipment, Surface Equipment
27	Directional Drlg & Surveys	27,750	0	27,750	$0	Multishot
28	Diving Services	0	0	0	$0	
29	Casing & Wellhead Installation & Inspection	18,150	12,900	31,050	$0	Wellhead
30	Cement, Cementing & Pump Fees	144,216	0	144,216	$0	Cement casing
31	Misc. H2S Services	0	0	0	$0	
32	**Total Drilling Operations**	**$1,052,426**	**$110,284**	**$1,162,710**	**$0**	
33	**FORMATION EVALUATION**					
34	Coring	0	0	0	$0	
35	Mud Logging Services	40,000	0	40,000	$0	
36	Drillstem Tests	0	0	0	$0	
37	Open Hole Elec Logging Services	239,500	0	239,500	$0	Logging all sections
39	**Total Formation Evaluation**	**$279,500**	**$0**	**$279,500**	**$0**	
40	**COMPLETION**					
41	Casing, Liner, Wellhead & Tubing Installation	0	0	0	$0	
42	Cement, Cementing & Pump Fees	0	0	0	$0	
43	Cased Hole Elec Logging Services	51,000	0	51,000	$0	Cement logs
44	Perforating & Wireline Services	0	20,000	20,000	$0	
45	Stimulation Treatment	0	0	0	$0	
46	Production Tests	0	0	0	$0	
48	**Total Completion Costs**	**$51,000**	**$20,000**	**$71,000**	**$0**	
49	**GENERAL**					
50	Supervision	116,250	20,000	136,250	$0	Rig supervisor, 2 shifts
51	Insurance	500,000	0	500,000	$0	Estimated cost for insurance and bond
52	Permits & Fees	49,000	0	49,000	$0	Permit support
53	Marine Rental & Charters	0	0	0	$0	
54	Helicopter & Aviation Charges	0	0	0	$0	
55	Land Transportation	17,000	0	17,000	$0	Trucking fees
56	Other Transportation	0	0	0	$0	
57	Fuel & Lubricants	2,500	0	2,500	$0	
58	Camp Facilities	19,000	0	19,000	$0	Onsite shacks during drilling and compl.
59	Allocated Overhead - Field Office	0	0	0	$0	
60	Allocated Overhead - Main Office	10,000	10,000	20,000	$0	Engineering support
61	Allocated Overhead - Overseas	0	0	0	$0	
62	Technical Services From Abroad	0	0	0	$0	
64	**Total General Costs**	**$713,750**	**$30,000**	**$743,750**	**$0**	
65	**TOTAL INTANGIBLE COSTS**	**$2,367,376**	**$175,284**	**$2,542,660**	**$0**	
	TOTAL TANGIBLE COSTS	**$210,184**	**$181,930**	**$392,114**	**$0**	
66	**WELL COST**			**$2,934,774**	**$0**	
67						
68	**TOTAL WELL COST**			**$2,934,774**		
69	**-Future Years**					
70	**Total**					

Operator	Approved By:			**Remarks**
	Position			Market conditions are extremely depressed currently. Pricing may increase substantially with changes in market conditions.
	Date			
Operator Approval	Approved By;			
	Position			
	Date			

Figure 6-D-10 Authorization for expenditures for a Knox brine disposal well.

AFE For Vertical Production Well

Figure 6- shows an authorization for expenditures for a vertical brine extraction producing well.

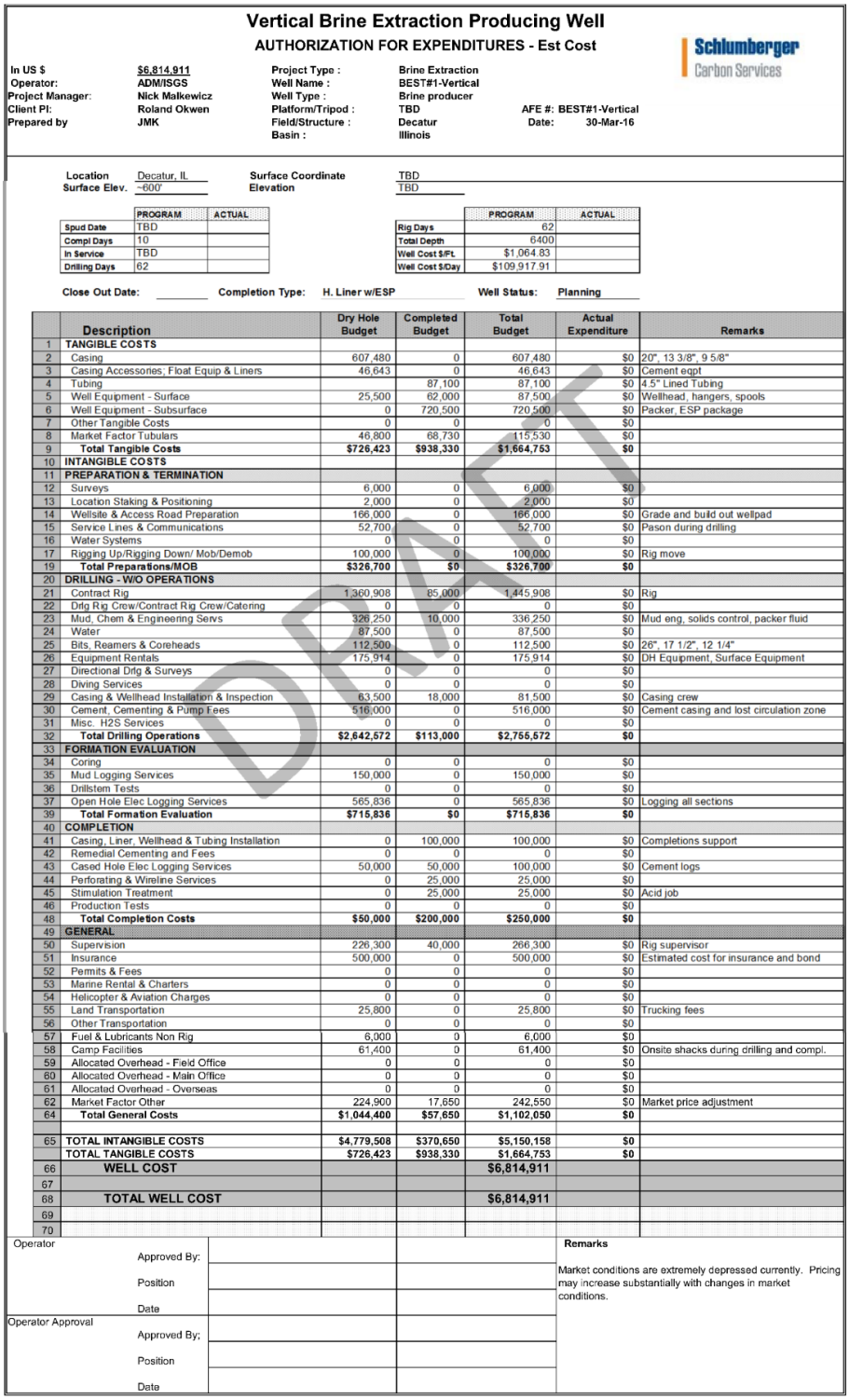

Vertical Brine Extraction Producing Well

AUTHORIZATION FOR EXPENDITURES - Est Cost

Schlumberger Carbon Services

In US $	$6,814,911	Project Type :	Brine Extraction		
Operator:	ADM/ISGS	Well Name :	BEST#1-Vertical		
Project Manager:	Nick Malkewicz	Well Type :	Brine producer		
Client PI:	Roland Okwen	Platform/Tripod :	TBD	AFE #:	BEST#1-Vertical
Prepared by	JMK	Field/Structure :	Decatur	Date:	30-Mar-16
		Basin :	Illinois		

Location: Decatur, IL — Surface Coordinate: TBD
Surface Elev.: ~600' — Elevation: TBD

	PROGRAM	ACTUAL
Spud Date	TBD	
Compl Days	10	
In Service	TBD	
Drilling Days	62	

	PROGRAM	ACTUAL
Rig Days	62	
Total Depth	6400	
Well Cost $/Ft	$1,064.83	
Well Cost $/Day	$109,917.91	

Close Out Date: — Completion Type: H. Liner w/ESP — Well Status: Planning

	Description	Dry Hole Budget	Completed Budget	Total Budget	Actual Expenditure	Remarks
1	**TANGIBLE COSTS**					
2	Casing	607,480	0	607,480	$0	20", 13 3/8", 9 5/8"
3	Casing Accessories, Float Equip & Liners	46,643	0	46,643	$0	Cement eqpt
4	Tubing		87,100	87,100	$0	4.5" Lined Tubing
5	Well Equipment - Surface	25,500	62,000	87,500	$0	Wellhead, hangers, spools
6	Well Equipment - Subsurface	0	720,500	720,500	$0	Packer, ESP package
7	Other Tangible Costs	0	0	0	$0	
8	Market Factor Tubulars	46,800	68,730	115,530	$0	
9	**Total Tangible Costs**	**$726,423**	**$938,330**	**$1,664,753**	**$0**	
10	**INTANGIBLE COSTS**					
11	**PREPARATION & TERMINATION**					
12	Surveys	6,000	0	6,000	$0	
13	Location Staking & Positioning	2,000	0	2,000	$0	
14	Wellsite & Access Road Preparation	166,000	0	166,000	$0	Grade and build out wellpad
15	Service Lines & Communications	52,700	0	52,700	$0	Pason during drilling
16	Water Systems	0	0	0	$0	
17	Rigging Up/Rigging Down/ Mob/Demob	100,000	0	100,000	$0	Rig move
19	**Total Preparations/MOB**	**$326,700**	**$0**	**$326,700**	**$0**	
20	**DRILLING - W/O OPERATIONS**					
21	Contract Rig	1,360,908	85,000	1,445,908	$0	Rig
22	Drlg Rig Crew/Contract Rig Crew/Catering	0	0	0	$0	
23	Mud, Chem & Engineering Servs	326,250	10,000	336,250	$0	Mud eng, solids control, packer fluid
24	Water	87,500	0	87,500	$0	
25	Bits, Reamers & Coreheads	112,500	0	112,500	$0	26", 17 1/2", 12 1/4"
26	Equipment Rentals	175,914	0	175,914	$0	DH Equipment, Surface Equipment
27	Directional Drlg & Surveys	0	0	0	$0	
28	Diving Services	0	0	0	$0	
29	Casing & Wellhead Installation & Inspection	63,500	18,000	81,500	$0	Casing crew
30	Cement, Cementing & Pump Fees	516,000	0	516,000	$0	Cement casing and lost circulation zone
31	Misc. H2S Services	0	0	0	$0	
32	**Total Drilling Operations**	**$2,642,572**	**$113,000**	**$2,755,572**	**$0**	
33	**FORMATION EVALUATION**					
34	Coring	0	0	0	$0	
35	Mud Logging Services	150,000	0	150,000	$0	
36	Drillstem Tests	0	0	0	$0	
37	Open Hole Elec Logging Services	565,836	0	565,836	$0	Logging all sections
39	**Total Formation Evaluation**	**$715,836**	**$0**	**$715,836**	**$0**	
40	**COMPLETION**					
41	Casing, Liner, Wellhead & Tubing Installation	0	100,000	100,000	$0	Completions support
42	Remedial Cementing and Fees	0	0	0	$0	
43	Cased Hole Elec Logging Services	50,000	50,000	100,000	$0	Cement logs
44	Perforating & Wireline Services	0	25,000	25,000	$0	
45	Stimulation Treatment	0	25,000	25,000	$0	Acid job
46	Production Tests	0	0	0	$0	
48	**Total Completion Costs**	**$50,000**	**$200,000**	**$250,000**	**$0**	
49	**GENERAL**					
50	Supervision	226,300	40,000	266,300	$0	Rig supervisor
51	Insurance	500,000	0	500,000	$0	Estimated cost for insurance and bond
52	Permits & Fees	0	0	0	$0	
53	Marine Rental & Charters	0	0	0	$0	
54	Helicopter & Aviation Charges	0	0	0	$0	
55	Land Transportation	25,800	0	25,800	$0	Trucking fees
56	Other Transportation	0	0	0	$0	
57	Fuel & Lubricants Non Rig	6,000	0	6,000	$0	
58	Camp Facilities	61,400	0	61,400	$0	Onsite shacks during drilling and compl.
59	Allocated Overhead - Field Office	0	0	0	$0	
60	Allocated Overhead - Main Office	0	0	0	$0	
61	Allocated Overhead - Overseas	0	0	0	$0	
62	Market Factor Other	224,900	17,650	242,550	$0	Market price adjustment
64	**Total General Costs**	**$1,044,400**	**$57,650**	**$1,102,050**	**$0**	
65	**TOTAL INTANGIBLE COSTS**	**$4,779,508**	**$370,650**	**$5,150,158**	**$0**	
	TOTAL TANGIBLE COSTS	**$726,423**	**$938,330**	**$1,664,753**	**$0**	
66	**WELL COST**			**$6,814,911**		
67						
68	**TOTAL WELL COST**			**$6,814,911**		
69						
70						

DRAFT

Operator	Approved By:			**Remarks**
	Position			Market conditions are extremely depressed currently. Pricing may increase substantially with changes in market conditions.
	Date			
Operator Approval	Approved By;			
	Position			
	Date			

Figure 6-D-11 Authorization for expenditures for a vertical brine extraction producing well.

DISCUSSION (LESSONS LEARNED FOR PHASE II)

Assessment of technologies and a general literature survey to evaluate and screen currently commercialized and emerging technologies for treating water with different total dissolved solids (TDS) values were performed. Pretreatment processes (for removal of suspended solids and scale-forming species) such as sand filtration, lime softening, coagulation, sedimentation, nanofiltration, and ion exchange, and core treatment processes (for removal of dissolved salts), such as membrane desalination and thermal distillation, were evaluated. Research gaps on brine treatment processes were identified and recommendations are provided.

Evaluation of a multitude of brine treatment technologies indicate that the evaporation/crystallization technology as the most suitable commercially available technology for the treatment of Mt. Simon brine because other existing desalination technologies are not well suited to treat high-TDS brines. However, energy consumption costs for evaporative crystallizers are expected to be high; as such, further research of emerging technologies at the test-bed facility is recommended. Pilot-scale testing of the evaporation/crystallization technology at the well-site test-bed facility to obtain baseline data for large-scale design and for comparison with the performance of emerging and innovative technologies is recommended. Invitation of all high-TDS treatment projects funded by the US Department of Energy through FOA-0001095 and FOA-0001238 to utilize the test-bed facility for testing different treatment technologies is recommended. The scale of operation to be tested would be determined by the readiness level of the technology.

Reservoir simulations were performed to evaluate the efficacy and ability to monitor pressure and CO_2 saturation changes due to brine extraction. Reservoir simulation scenarios for brine extraction using either a vertical well or a horizontal well were considered to evaluate the detectability of brine extraction-induced changes in pressure and CO_2 saturation distribution at existing multilevel monitoring wells. Geomechanical effects were analyzed to evaluate wellbore integrity and the ability to monitor extraction-induced rock deformation.

Generally, brine extraction can effectively manage pressure and control the CO_2 plume. Interpretations from geomechanical simulation results indicate that neither mechanical formation failure nor sanding are anticipated in the extraction well for brine extraction rates up to 20,000 stb/d (3,180 m^3/d). Extraction-induced rock deformation for the 20,000 stb/d (3,180 m^3/d) rate will be of sufficient magnitude to be detected using repeat sonic measurements.

The recommended brine extraction options include (1) a horizontal extraction well at the base of the Middle Mt. Simon, which is 350–520 ft (107–158 m) above the CO_2 plume at CCS#1 and VW#1; or (2) a vertical extraction well 0.5 mi (0.8 km) away from CCS#2 in a direction roughly southeast of CCS#2, perpendicular to the direction of high hydraulic connectivity. A horizontal extraction well has some advantages over a vertical extraction well, including less risk of drilling into an existing CO_2 plume and less uncertainty in the geology. Thus, it eliminates the need for a third verification well and allows for a lower extraction rate to control the CO_2 plume and pressure.

Subsurface monitoring at geologic carbon sequestration sites involves monitoring pressure, temperature, CO_2 saturation, and microseismicity. Monitoring pressure and temperature in the subsurface has some minor challenges but overall is a straightforward procedure. At some sequestration sites, the depth of the storage unit may lead to pressures and temperatures that exceed the limits of available sensors. The depth of the injection reservoir typically limits the number of locations where pressure and temperature can be monitored, due to high costs of monitoring wells. Multilevel well completions, such as the Westbay system (e.g., Locke et al., 2013), can provide

pressure and temperature data at multiple depths in a single well. In addition, the salinity of the brine in the injection reservoir may corrode the monitoring sensors and cause them to malfunction.

Monitoring CO_2 saturation is a more challenging and expensive process than monitoring pressure and temperature. Borehole methods, such as pulsed-neutron logs, can be very effective for locating the injected CO_2, but offer data for a very small portion of the storage reservoir. Areal methods, such as three-dimensional (3D) seismic can provide two-dimensional (2D) and 3D maps of the injected CO_2 in some storage reservoirs, such as Sleipner (Chadwick and Noy, 2015). For sites with deeper storage reservoirs and cultural complications (e.g., background noise at industrial sites and lack of access to land for seismic acquisition), 3D seismic has provided less conclusive maps of the injected CO_2 (Jenkins et al., 2015). The performance of vertical seismic profiling (VSP) has been similar to 3D seismic methods at the Illinois Basin–Decatur Project (IBDP; Couëslan et al., 2014). New methods are being developed and hold promise. Distributed acoustic sensing (DAS) is a recent fiber-optic sensing technology in which the fiber-optic cable itself is the sensor, but now the fiber senses the passage of elastic waves along its length becoming "geophones on a string." Distributed acoustic sensing has recently been used for monitoring in CO_2 sequestration projects (Daley et al., 2013, 2015; Worth et al., 2014).

Borne out of the more publicized risk of induced seismicity (Pawar et al., 2015), monitoring microseismicity is a relatively new effort. Microseismicity is defined as low-energy events ($M \leq 2$). Will et al. (2014) noted some of the challenges related to microseismic monitoring at the IBDP site. They noted that 10,123 microseismic events were detected but only 2,573 events were of sufficient quality to allow their location to be estimated. In addition, microseismic events appear to occur at areas of rock weakness that have not been identified by other methods.

Permitting requires interaction with county, state, and federal regulatory agencies. In Illinois, county government regulates water production wells and high-capacity wells. Underground injection wells for nonhazardous waste are classified as Class I wells and are regulated by the Illinois Environmental Protection Agency. Because of the existing Class VI permits at the proposed research site, the US Environmental Protection Agency will be consulted for any impact of this research project on those existing permits. Finally, any federally funded project is required to comply with the National Environmental Policy Act. Previous permitting experience by the proposal principals should allow the permitting process to proceed in an efficient manner.

SUMMARY

The main objective of this project was to develop and validate strategies that can be used to manage formation pressure and control of CO_2 plumes to address technical barriers to commercial deployment of CCS technologies. Computational (Phase I) work was completed for proposed field demonstration (Phase II) work at the Archer Daniels Midland Company (ADM) facility where the Illinois Basin–Decatur Project (IBDP) and the Illinois-Industrial Carbon Capture and Storage (IL-ICCS) projects are located.

Geologic and reservoir models of the Decatur sites were used to simulate brine extraction scenarios to predict changes in pressure and CO_2 saturation.

Options for brine handling and treatment were also evaluated. Brine treatment technologies were evaluated to determine those suitable for high-total dissolved solids brine. An evaporation/crystallization technology is the only commercially available technology. However, testing of the emerging high-TDS technologies is recommended. Life-Cycle-Analysis studies on extracted brine handling options suggest using a UIC well for brine disposal because it has the lowest total environmental impact score.

Subsurface monitoring at geologic carbon storage sites involves monitoring pressure, temperature, CO_2 saturation, and microseismicity. Minor challenges must be addressed when monitoring pressure and temperature in the subsurface, but overall, pressure and temperature monitoring are more straightforward than CO_2 saturation monitoring, which is more challenging and more expensive. Borehole methods such as pulsed neutron logs can be very effective locating the CO_2 plume but assess a very small portion of the storage unit. Areal methods such as 3D seismic and VSP can provide 2D and 3D maps of the injected CO_2.

Multiple regulatory agencies should be contacted in the event the site has an existing permit with an area of review that overlaps the area of review for the new permit application. In addition, if the project is federally funded, it will need to comply with the National Environmental Policy Act. The permitting application process should be started well in advance of a brine extraction project.

The results of geologic and reservoir modeling of the studied formations suggest the following features are optimal for a BEST project:

- A horizontal extraction well placed at the top of the Lower Mt. Simon (6,450 ft [1,966 m]) and passing between CCS#1 and VW#1.
- A vertical brine disposal well located near the extraction well that will inject pre-treated extracted brine into the Potosi Dolomite. Reservoir modeling results predict a maximum brine injection rate of 580 gal/min (about 26,500 bbl/day) is feasible for the Potosi Dolomite at the Decatur sites.
- A test bed located near the extraction well for testing pilot-scale brine treatment technologies, and another test-bed facility at the NSEC for testing bench-scale brine treatment technologies.

Discussion and Summary References

Daley, T.M., B.M. Freifield, J. Ajo-Franklin, S. Dou, R. Pevzner, V. Shulakova V., 2013, Field testing of fibre-optic distributed acoustic sensing (DAS) for subsurface seismic monitoring: The Leading Edge, v. 32, no. 6, p. 699–706.

Daley, T.M., D.E. Miller, K. Dodds, P. Cook, and B.M. Freifeld, 2015, Field testing of modular borehole monitoring with simultaneous distributed acoustic sensing and geophone vertical seismic profiles: Geophysical Prospecting, p. 1–17. http://dx.doi.org/doi:1111/1365-2478.12324.

Chadwick, R.A., and D.J. Noy, 2015, Underground CO_2 storage: demonstrating regulatory conformance by convergence of history-matched modeled and observed CO_2 plume behavior using Sleipner time-lapse seismics: Greenhouse Gases: Science and Technology, v. 5, no. 3, p. 305–322.

Couëslan, M.L., V. Smith, G. El-Kaseeh, J. Gilbert, N. Preece, L. Zhang, and J. Gulati, 2014, Development and implementation of a seismic characterization and CO_2 monitoring program for the Illinois Basin – Decatur Project: Greenhouse Gases: Science and Technology, v. 4, no. 5, p. 626–644.

Jenkins, C., A. Chadwick, and S.D. Hovorka, 2015, The state of the art in monitoring and verification - Ten years on: International Journal of Greenhouse Gas Control, v. 40, p. 312–349.

Locke II, R., D. Larssen, W. Salden, C. Patterson, J. Kirksey, A. Iranmanesh, B. Wimmer, and I. Krapac, 2013, Preinjection reservoir fluid characterization at a CCS demonstration site: Illinois Basin - Decatur Project, USA: Energy Procedia, v. 37, p. 6,424–6,433.

Pawar, R.J., G.S. Bromhal, J.W. Carey, W. Foxall, A. Korre, P.S. Ringrose, O. Tucker, M.N. Watson, and J.A. White, 2015, Recent advances in risk assessment and risk management of geologic CO_2 storage: International Journal of Greenhouse Gas Control, v. 40, p. 292–311.

Will, R., V. Smith, H.E. Leetaru, J.T. Freiburg and D.W. Lee, 2014, Microseismic monitoring, event occurrence, and the relationship to subsurface geology: Energy Procedia, v. 63, p. 4,424–4,436.

Worth, K., D. White, R. Chalaturnyk, J. Sorensen, C. Hawkes, B. Rostron, J. Johnson, and A. Young, 2014, Aquistore project measurement, monitoring, and verification: From concept to CO_2 injection: Energy Procedia 63, p. 3,202–3,208.

BIBLIOGRAPHY

Damico, J.R. and S.M. Frailey. 2012. Permeability Prediction for Geostatistical Characterization of a Deep Saline Reservoir. Geological Society of America North-Central Section Meeting, Dayton, OH, April 23–24, 2012. Oral presentation, April, 23, 2012. *Geological Society of America Abstracts with Programs*, 44 (5): p. 7.

Finley, R.J., S.M. Frailey, H.E. Leetaru, O. Senel, M.L. Couëslan, M. Scott, 2013, Early operational experience at a one-million tonne CCS demonstration project, Decatur, Illinois, USA: Energy Procedia, v. 37, p. 6,149–6,155 http://dx.doi.org/10.1016/j.egypro.2013.06.544.

Finley, R.J., S.E. Greenberg, S.M. Frailey, I.G. Krapac, HE. Leetaru, S. Marsteller, 2011, The path to a successful one-million tonne demonstration of geological sequestration: Characterization, cooperation, and collaboration: Energy Procedia, v. 4, p. 4,770–4,776. http://dx.doi.org/10.1016/j.egypro.2011.02.441.

Frailey, S.M., J. Damico, H.E. Leetaru, 2010, Reservoir characterization of the Mt. Simon Sandstone, Illinois Basin, USA: Proceedings of the 10th International Conference on Greenhouse Gas Control Technologies (GHGT-10), Amsterdam, September 19–23.

Frailey, S.M., and R.J. Finley, 2008, Overview of the Illinois Basin's sequestration pilots: SPE 113418, SPE/DOE Improved Oil Recovery, Tulsa, Oklahoma, April 19–23.

Frailey, S.M., and R.J. Finley, 2010, CO_2 plume management in saline reservoir sequestration: Energy Procedia, v. 4, p. 4,238–4,245. http://dx.doi.org/doi:10.1016/j.egypro.2011.02.372.

Frailey, S.M., and R.J. Finley, 2010, Overview of the Midwest Geologic Sequestration Consortium pilot projects: SPE 139746, SPE International Conference on CO_2 Capture, Storage, and Utilization held in New Orleans, Louisiana, USA, November 10–12.

Frailey, S.M., I.G. Krapac, J.R. Damico, R.T. Okwen, and R.W. McKaskle, 2012, Sequestration and enhanced oil recovery: Bald Unit test site, Mumford Hills Oil Field, Posey County, Indiana, J.H. Goodwin and C.C. Monson (eds.): Illinois State Geological Survey, Open File Series 2012-5, p. 173 p. http://library.isgs.uiuc.edu/Pubs/pdfs/ofs/2012/ofs2012-05.pdf

Frailey, S.M., T.M. Parris, J.R. Damico, R.T. Okwen, and R.W. McKaskle, 2012, Sequestration and enhanced oil recovery: Sugar Creek Oil Field test site, Hopkins County, Kentucky, C.C. Monson and J. H. Goodwin (eds.): Illinois State Geological Survey, Open File Series 2012-4, p. 234. http://library.isgs.uiuc.edu/Pubs/pdfs/ofs/2012/ofs2012-04.pdf.

Gershenzon, N.I., R.W. Ritzi, D.F. Dominic, M. Soltanian, E. Mehnert, and R.T. Okwen, 2015, Influence of small-scale fluvial architecture on CO_2 trapping processes in deep brine reservoirs, Water Resources Research, v. 51, http://dx.doi.org/10.1002/2015WR017638.

Leetaru, H.E., S.M. Frailey, J. Damico, E. Mehnert, J. Birkholzer, Q. Zhou, and P.D. Jordan, 2009, Understanding CO_2 plume behavior and basin-scale pressure changes during sequestration projects through the use of reservoir fluid modeling: Energy Procedia, v. 1, no.1, p. 1799–1806. http://dx.doi.org/10.1016/j.egypro.2009.01.235.

Mehnert, E., J.R. Damico, S.M. Frailey, H.E. Leetaru, R. Okwen, B. Storsved, and A. Valocchi, 2014, Basin-scale modeling for CO_2 sequestration in the basal sandstone reservoir of the Illinois Basin-Improving the geologic model: Energy Procedia, v. 63: p. 2,949–2,960.

Mehnert, E., J.R. Damico, S.M. Frailey, H.E. Leetaru, L. Yu-Feng, R. Okwen, N. Adams, B. Storsved, and A. Valocchi, 2013, Development of a basin-scale model for CO_2 sequestration in the basal sandstone reservoir of the Illinois Basin-issues, Approach and Preliminary Results: Energy Procedia, v. 37, p. 3,850–3,858.

Mehnert, E., and R.T. Okwen, 2013, Near-Well Pressure Distribution of CO_2-Injection in a Partially Penetrating Well, Proceedings of the TOUGH Symposium 2012, Lawrence Berkeley National Laboratory, Berkeley California, September 17–19, 2012. http://esd.lbl.gov/files/research/projects/tough/events/symposia/toughsymposium12/Proceedings_TOUGH-Symposium-2012.pdf

Mehnert E., and P.H. Weberling, 2014, Groundwater salinity within the Mt. Simon Sandstone in Illinois and Indiana: Illinois State Geological Survey, Circular 582, p. 19 + appendix.

Morse, D.G., and H.E. Leetaru, 2003, Reservoir characterization and 3-D models of Mt. Simon gas storage fields in the Illinois Basin: Illinois State Geological Survey, Open-File Series 2003-13, p. 96 plus 52 illustrations.

Okwen, R., Y. Fang, and S.M. Frailey, 2014, Effect of geologic depositional environment of CO_2 storage efficiency: Energy Procedia, v. 63, p. 5,247–5,257.

Okwen, R., R. Pu, and J. Cunningham, 2010, Remote sensing of temperature variations around major power plants as point sources of heat: International Journal of Remote Sensing, (in press).

Okwen, R.T., M. Stewart, J.A. Cunningham 2009, "Storage of CO_2 in deep saline aquifers via injection in horizontal wells." Proceedings of the TOUGH Symposium 2009, edited by G. Moridis, C. Doughty, S. Finsterle, and E. Sonnenthal, pp 102-107. Published by Lawrence Berkeley National Laboratory (LBNL-2790E), Berkeley, CA. Presented in Berkeley, CA, Sept 14–16.

Okwen, R., M. Stewart, and J. Cunningham, 2010, Analytical solution for estimating storage efficiency of geologic sequestration of CO_2: International Journal of Greenhouse Gas Control, v. 4, no. 1, p. 102–107. http://dx.doi.org/10.1016/j.ijggc.2009.11.002.

Okwen, R., M. Stewart, and J. Cunningham, 2010, Effect of well orientation (vertical vs. horizontal) and well length on the injection of CO_2 in deep saline aquifers: Transp Porous Med. http://dx.doi.org/10.1007/s11242-010-9686-5.

Okwen, R., M. Stewart, and J. Cunningham, 2011, Analytical model for screening potential CO_2 repositories: Computational Geosciences, v. 15, no. 4, p. 755–770. http://dx.doi.org/doi: 10.1007/s10596-011-9246-2.

Okwen, R., M. Thomas, M. Stewart, M. Trotz, and J. Cunningham, 2012, Conjunctive injection of CO_2 and wastewater in a heterogeneous porous formation: Technology and Innovation, vol.14, p. 143–151. http://dx.doi.org/10.3727/194898241X13462021397778.

Roy, W.R., E. Mehnert, P.M. Berger, J.R. Damico and R.T. Okwen, 2014, Transport modeling at multiple scales for the Illinois Basin – Decatur Project: *Greenhouse Gases: Science and Technology, v.* 4, no. 5, p. 645–661. http://dx.doi.org/doi:10.1002/ghg.1424.

Strandli, C.W., E. Mehnert, and S.M. Benson, 2015, Plume tracking and history matching using multilevel pressure monitoring at the Illinois Basin – Decatur Project: Energy Procedia, v. 63, p. 4,473–4,484.

Zhou, Q., J.T. Birkholzer, E. Mehnert, Y.-F. Lin, and K. Zhang, 2010, Modeling basin- and plume-scale processes of CO_2 Storage for full-scale deployment: Ground Water, v. 48, no. 4, p. 494–514 [published online Dec 2009].